Mono- and tri-nuclear ruthenium complexes incorporating N-heterocyclic carbene ligands

Saker, Olly

Award date:
2008

Awarding institution:
University of Bath

Mono- and tri-nuclear ruthenium complexes incorporating N-heterocyclic carbene ligands

Oliver John Saker

A thesis submitted in partial fulfilment of the requirements for the degree of

Doctor of Philosophy

UNIVERSITY OF BATH

University of Bath
Department of Chemistry

December 2008

Acknowledgements

I would foremost like to thank Dr Mike Whittlesey for giving me the opportunity to work in a fantastic laboratory environment for the past three years, and for always making time to answer the incessant number of questions I have supplied him with along the way. In addition, thanks must be given to Mike for providing an unrivalled selection of Whitesnake, Metallica, AC/DC and [insert generic 80's metal band here] albums to help combat the soul-destroying monotony of Jack Johnson and general Radio 1 natterings in the lab.

I would also like to thank Dr John 'Johnny DEPT' Lowe for his help with all my NMR enquiries, Dr Anneke Lubben for issues regarding mass spectrometry, and Dr Mary Mahon for solving the vast majority of my troublesome crystal structures. Additionally I would like to thank Dr Simon Brayshaw for being a great source of general chemical wisdom.

I have been really lucky to work with a great bunch of lab mates over the years, including Dr Suzanne Burling who helped me a great deal to get started and settled in the lab, Sarah Chatwin of course for always bringing happiness whenever there was a dull day and my MChem student Matt 'Ryan Sidebottom' Crittall. Of course I can't forget our current Whittlesey group members including Charlie, Tom, Minty, Elena and Mikey P (thanks especially for slaving over this thesis!). It's been great fun - especially all those 'cheeky' Thursdays! Thanks also to Stevo for being a great laugh, especially at the Barcelona conference - We'll have another drink won't we?!

I would however mostly like to thank my mum and sister for their encouragement and guidance, and my fiancée Hanny for her endless love, understanding and support...especially in having to try and sleep through a bombardment of tapping and clicking from the computer for the last two months till 1am most nights!

Abstract

This thesis describes the synthesis, stoichiometric and catalytic activity of trinuclear and mononuclear ruthenium-NHC complexes. The reactions of $Ru_3(CO)_{12}$ with NHCs possessing bulky N-^{t}Bu and N-adamantyl substituents results in abnormal binding of the free NHCs to give the complexes, $Ru_3(aNHC)(CO)_{11}$ (aNHC = I^{t}Bu$_2$ (**1A**), IAd$_2$ (**2A**)). Analogous chemistry was also found for $Os_3(aIAd_2)(CO)_{11}$ (**2C**). Subsequent thermolysis of these complexes facilitated C-H activation of the C5-imidazol protons to yield $Ru_3(\mu\text{-}H)(aNHC)'(CO)_9$ (aNHC = I^{t}Bu$_2$ (**1B**), IAd$_2$ (**2B**)) complexes, with the NHC in a novel binding mode. The reactions of $Ru_3(CO)_{12}$ with excess NHCs possessing smaller N-Et and N-^{i}Pr substituents resulted instead in degradation of the cluster to form the mononuclear complexes, $Ru(NHC)_2(CO)_3$ (NHC = IEt$_2$Me$_2$ (**3A**), I^{i}Pr$_2$Me$_2$ (**4A**), I^{i}Pr$_2$(**5A**)). The oxidation of Ru(0) and one CO ligand in these complexes under O_2 led to isolation of the Ru(II) carbonato complexes $Ru(NHC)_2(CO)_2(CO_3)$ (NHC = IEt$_2$Me$_2$ (**3B**), I^{i}Pr$_2$Me$_2$ (**4B**), I^{i}Pr$_2$(**5B**)).

A series of 16-electron *bis*-NHC complexes $Ru(NHC)_2(CO)HX$ (X = Cl; NHC = IPr (**6A**), SIPr (**7A**), BH_4; NHC = IPr (**6C**), SIPr (**7C**)) were also synthesised, and their ligand substitution and catalytic reactions investigated. The *bis*-CO $Ru(NHC)_2(CO)_2HCl$ (NHC = IPr (**6B**), SIPr (**7B**)) complexes were formed upon the addition of CO to $Ru(NHC)_2(CO)HCl$, with facile elimination of CO shown to occur from the SIPr complex under vacuum. Catalytic activity of the $Ru(NHC)_2(CO)HX$ complexes for the hydrogenation of acetophenone and 4-methoxyacetophenone followed the order IPr > SIPr in all cases, while X = BH_4 was more active than X = Cl for the hydrogenation of 4-methoxyacetophenone. The hydroxide complex $Ru(IPr)_2(CO)H(OH)$ (**6D**) was prepared and subsequently protonated with 1 equivalent of $HBF_4{\cdot}OEt_2$, which led to the formation of $[Ru(IPr)_2(CO)H(OH_2)]^+BF_4^-$ (**6E**) in THF. The addition of an extra equivalent of $HBF_4{\cdot}OEt_2$ in benzene gave loss of an NHC ligand and H_2O from the complex to yield $[Ru(IPr)(\eta^6\text{-}C_6H_6)(CO)H]^+BF_4^-$ (**6F**). Facile exchange of the η^6-C_6H_6 ligand occurred upon dissolution of the complex in other arene solvents.

Compound Labels and Abbreviations

Compound Labels

The compound labels used throughout this work for fully characterised new complexes consist of a number and a letter such as **1A**. The number relates explicitly to the specific NHC ligand found in the structure (listed in the table), and the letter identifies the particular complex. For example, $Ru(IPr)_2(CO)HCl$ is compound **6A** and $Ru(IPr)_2(CO)_2HCl$ is **6B** as both structures contain ligand number **6** (IPr) and compound **6A** is presented and discussed prior to compound **6B**.

Ligand Number	NHC
1	I^tBu_2
2	IAd_2
3	IEt_2Me_2
4	$I^iPr_2Me_2$
5	I^iPr_2
6	IPr
7	SIPr
8	SIMes

NHC ligand compound numbers

Abbreviations - Spectroscopic

NMR	Nuclear magnetic resonance
δ	NMR chemical shift
J_{YZ}	Coupling constant of Y to Z
HMQC	Heteronuclear multiple quantum coherence
HMBC	Heteronuclear multiple bond correlation
NOESY	Nuclear overhauser effect spectroscopy
COSY	Correlation spectroscopy
V.T.	Variable temperature
s	Singlet
d	Doublet
t	Triplet

q	Quartet
sept	Septet
m	Multiplet
br	Broad
IR	Infrared
$\nu_{(L)}$	IR shift of ligand L
ax	Axial
eq	Equatorial
MS	Mass spectrometry
GC	Gas chromatography
DFT	Density functional theory

Abbreviations - Unit

h	Hour
min	Minute
s	Second
K	Kelvin
°	Degree
ppm	Parts per million
Hz	Hertz
MHz	Megahertz
cm^{-1}	Wavenumber
kJ	Kilojoule
Å	Angstrom
g	Gram
mg	Milligram
mL	Millilitre
μL	Microlitre
mol	Mole
mmol	Millimol

Abbreviations - Chemical

NHC	N-heterocyclic carbene

aNHC	abnormally-bound N-heterocyclic carbene
(aNHC)'	N-heterocyclic carbene bound through both C4 and C5 positions
M	Metal
L	Ligand
μ-L	Bridging ligand
η^n-L	Ligand hapticity (of number, n)
5c-4e	5centre-4electron
X	Halide or heteroatom
R	Alkyl or aryl group
Ar	Aryl
Me	Methyl
Et	Ethyl
^{i}Pr	Isopropyl
^{t}Bu	*tert*-Butyl
Mes	Mesityl (2,4,6-trimethylphenyl)
Ad	Adamantyl
Ph	Phenyl
Cy	Cyclohexyl
i-	*Ipso*
o-	*Ortho*
m-	*Meta*
p-	*Para*
THF	Tetrahydrofuran
IPA	Isopropyl alcohol
pyr	Pyridine
Mesitylene	1,3,5-trimethylbenzene
p-cymene	1-isopropyl-4-methylbenzene
dppe	1,2-*bis*(diphenylphosphino)ethane
I^{t}Bu$_2$	1,3-*bis*(*tert*-butyl)imidazol-2-ylidene
IAd$_2$	1,3-*bis*(1-adamantyl)imidazol-2-ylidene
IEt$_2$Me$_2$	1,3-diethyl-4,5-dimethyl-imidazol-2-ylidene
I^{i}Pr$_2$Me$_2$	1,3-diisopropyl-4,5-dimethyl-imidazol-2-ylidene
I^{i}Pr$_2$	1,3-*bis*(isopropyl)imidazol-2-ylidene

IPr	1,3-*bis*(2,6-diisopropylphenyl)imidazol-2-ylidene
IMes	1,3-*bis*(2,4,6-trimethylphenyl)imidazol-2-ylidene
SIPr	1,3-*bis*(2,6-diisopropylphenyl)imidazolin-2-ylidene
SIMes	1,3-*bis*(2,4,6-trimethylphenyl)imidazolin-2-ylidene
SIPr.C_6F_5-H	1,3-*bis*(2,6-diisopropylphenyl)-2-(pentafluoro-phenyl)imidazolidene
SIMes.C_6F_5-H	1,3-*bis*(2,4,6-trimethylphenyl)-2-(pentafluoro-phenyl)imidazolidene

Contents

Chapter 1 Introduction

Chapter 2 Cluster Chemistry

Appendices

Chapter 1

Introduction

1.1 N-heterocyclic carbenes (NHCs)

1.1.1 Overview

The study of N-heterocyclic carbenes (NHCs) is an important and rapidly expanding field of organometallic chemistry. The first isolable NHC was prepared by Arduengo in 1991[1] in the form of the sterically bulky adamantyl carbene, IAd_2 (**Figure 1.1**).[2,3] Since Arduengo's report, the interest in NHCs has increased steadily and now encompasses a significant range of areas and topics. NHCs have been shown on many occasions to stabilise highly reactive organometallic fragments, which have often displayed a high degree of catalytic activity for a wide variety of important transformations.[4-8] However, due to the relatively recent development of NHCs, our understanding of their interactions within the coordination sphere of a metal complex is still in its relative infancy, with many interesting and unexpected results still being discovered right up until the present day.

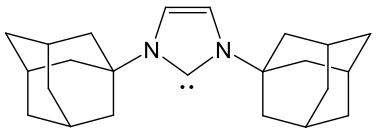

Figure 1.1 The first isolated free NHC, IAd_2

1.1.2 Structure and nomenclature

NHCs are a specific class of carbene compound in which a singlet carbenic carbon is flanked by two nitrogen atoms within a heterocyclic ring. The singlet nature of the carbenic carbon may draw initial similarities to the Fischer-class of carbenes, but unlike Fischer carbenes, the vacant p-orbital of the carbon is stabilised internally by the donation of π-electron density from the two adjacent nitrogen atoms. Therefore NHCs do not rely on metal backbonding to form stable metal complexes. In general, NHCs behave as strong, neutral 2-electron σ-donor ligands that form for the most part highly inert metal-carbon bonds with metals throughout the periodic table.[4,5]

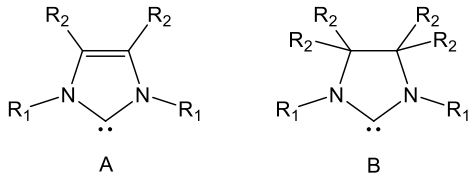

Figure 1.2 Illustration of an imidazol-2-ylidene (A) and an imidazolin-2-ylidene (B)

For this report, imidazol-2-ylidenes (Compound A, **Figure 1.2**) and imidazolin-2-ylidenes (Compound B, **Figure 1.2**) are the NHC types used, although variations of these are described in the next section. NHCs of these two kinds may be tuned in their electronic and steric properties by affecting the degree of saturation of the C4-C5 backbone and the nature of the R_1 and R_2 substituents. All of the NHCs contained in this study are symmetrical, with matching R_1 and R_2 groups. R_1 consists of alkyl or aryl moieties and R_2 are in most instances hydrogen atoms. For Compound A, methyl substituents have also been used at the R_2 position to improve their ease of synthesis by improving the crystallinity of the carbenes and their imidazolium precursors. The general nomenclature of these complexes that will be used throughout this work is fairly standard. Imidazol-2-ylidenes (Compound A) are prefixed with 'I' to denote the imidazol ring, with R_1 and R_2 groups abbreviated in that order and hydrogen groups remaining unlabelled. For example the imidazol-2-ylidene $I^iPr_2Me_2$ has R_1= isopropyl, and R_2= methyl. Similarly, the imidazolin-2-ylidenes (Compound B) are prefixed 'SI' to imply the saturated imidazol ring, with R-group abbreviations following the same order as above (e.g. SIMes has R_1= mesityl and R_2= hydrogen). Note that the numeric suffix for the number of aryl R-groups is usually omitted.

1.1.3 Related compounds

A wide range of related NHC motifs have also been described in the literature. For example NHCs with varying R_1 groups may be readily synthesised with either of the substituents often incorporating a second donor group that may coordinate to a metal centre.[9,10] A large variety of R_2 substituents have also been reported from electronegative chlorine atoms,[11] to a range of alkyl or aryl groups,[6-8,12] to complete 'benzannulation' of the backbone bond.[13]

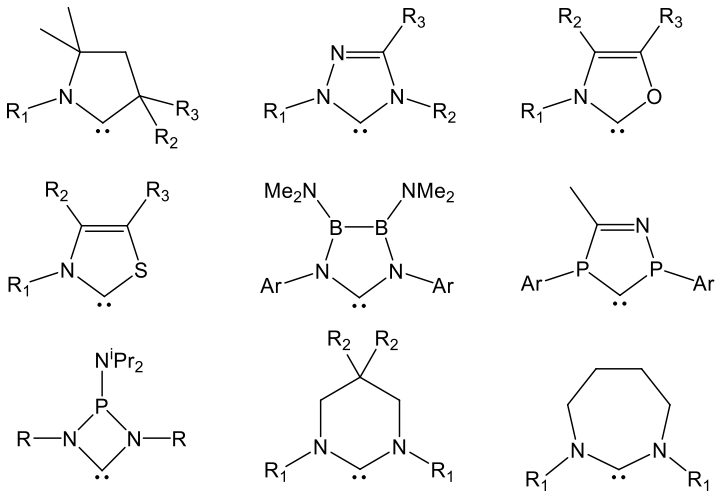

Figure 1.3 Examples of the diverse range of NHC ligands

In addition to the imidazol-derived carbenes described above, 5-membered NHCs exist which vary depending on the number, location and type of heteroatoms incorporated within the ring and a selection from this extensive range is shown in **Figure 1.3**,[14-20] in addition to examples of NHCs containing 4-[21], 6-[22] and 7-[23] membered rings. These various structural modifications have resulted in an enormous range of NHCs which display a wide diversity of steric and electronic properties.

1.1.4 General syntheses of free NHCs

There are a variety of different routes to free NHCs, the most typical involving the deprotonation of their corresponding imidazolium salts. A common method for the generation of imidazolium salts for symmetrical imidazol-2-ylidenes is the condensation of glyoxal with an amine, containing the desired N-substituent, in the presence of paraformaldehyde and hydrochloric acid (**Figure 1.4**).[24,25] To synthesise the saturated NHC imidazolinium salts, the resulting Schiff base formed from the glyoxal and amine condensation step is reduced using $NaBH_4$, subsequent addition of acid then triethyl orthoformate closes the ring to yield the desired product (**Figure 1.5**).[25] An interesting alternative route to saturated NHCs (including 6- and 7-membered rings) was recently reported by Cavell *et al*. Reaction of a diaryl amidine with a dihaloalkane in the presence of a base, followed by anion exchange with $NaBF_4$ is found to afford the imidazolinium species in high yield (**Figure 1.6**).[23]

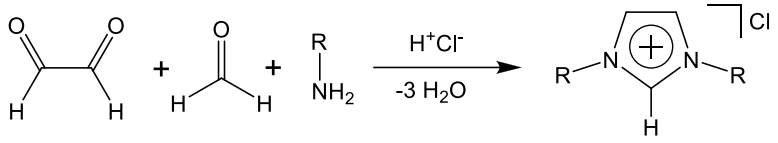

Figure 1.4 Standard imidazolium synthesis route

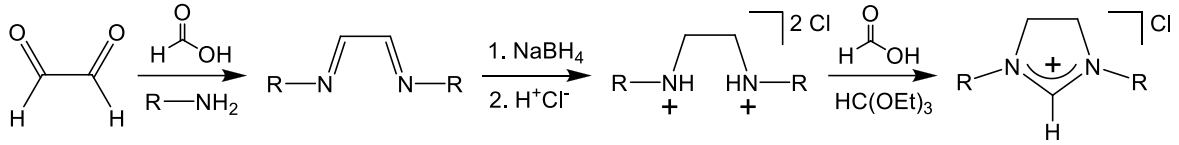

Figure 1.5 Standard imidazolinium synthesis route

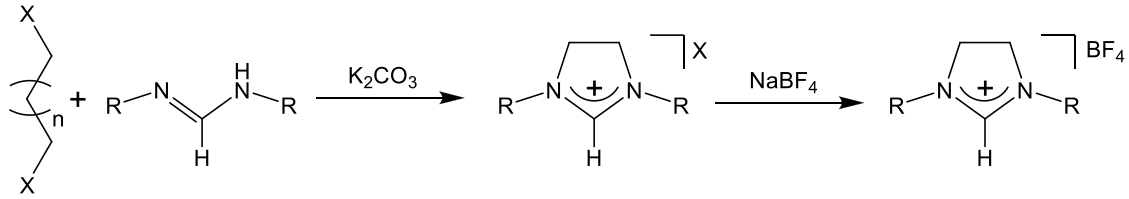

Figure 1.6 Recent imidazolinium synthesis route by Cavell

A wide variety of bases can then be used to deprotonate imidazolium salts to yield the free NHCs, from KO^{t}Bu for the imidazol-2-ylidenes to stronger bases such as KH which is often required for the deprotonation of the more basic imidazolinium salts. A useful non-coordinating base that can be used for a range of different NHC precursors is potassium trimethylsilylamide, $KN(SiMe_3)_2$ (**Figure 1.7**).[25]

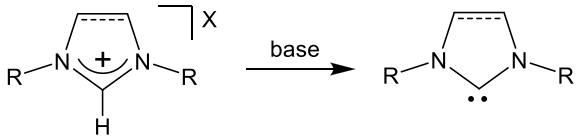

Figure 1.7 Deprotonation of an imidazolium salt

For alkyl NHCs containing methyl groups on the backbone positions, the habitual route is to generate the cyclic thiourea precursors which can then be reduced via reaction with potassium metal to leave free carbenes. Thiourea precursors are typically synthesised via condensation of the corresponding acyclic thiourea with hydroxybutanone (**Figure 1.8**).[26]

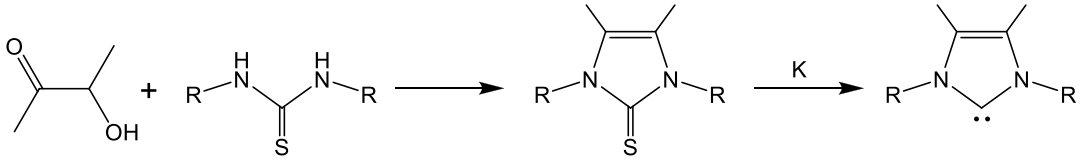

Figure 1.8 Synthesis of N-alkyl NHCs with C4/C5 methyl groups

1.2 NHC complexes

1.2.1 Overview

NHC complexes have been of primary interest to chemists as a result of the stability of the M-C_{NHC} bond. The strength of this bond acts as a thermodynamic driving force for the formation of NHC complexes as shown in **Figure 1.9**, with the equilibrium lying firmly to the right hand side.

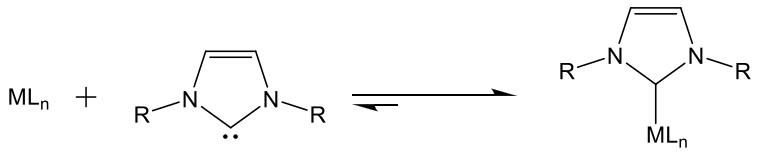

Figure 1.9 Equilibrium of NHC dissociation

The stability of NHC complexes gives access to a number of different routes into their generation, depending upon the metal and the desired NHC type. The reaction of free or 'bottle-able' NHCs detailed previously in **Section 1.1** with metal fragments may be employed, although in many cases isolation of the free carbene is often not practical or at all possible. In these instances, alternative methods of complex synthesis are required, the most common of which are now described herein.

1.2.2 General synthetic methods

A popular method that avoids the storing and handling of the reactive free carbene is generation of the complex from the imidazolium salt *in situ*, and this can be achieved in several ways. One of the first methods to be employed involved the use of basic ligand groups on the complex precursor. **Figure 1.10** shows the first two NHC complexes isolated by Öfele (Compound A)[27] and Wanzlick (Compound B)[28] in 1968 and in both cases the starting metal salts contained ligands that acted as bases to deprotonate the imidazolium salts in concerted reactions. Alternatively, the deprotonation step may be carried out using an external base, a method that is now very popular and has been utilised by Herrmann,[4] Cavell[10] and Nolan[29] among many others.[4,7,8]

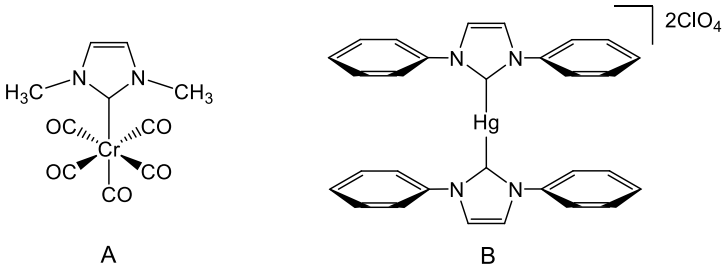

Figure 1.10 The first NHC complexes, by Öfele (A) and Wanzlick (B)

A second method for forming the NHC *in situ* was initially developed by Lappert *et al* who reacted NHC dimers (enetetramines)[3,30,31] with various metal fragments resulting in the metal inserting into the electron-rich alkenic bond to yield complexes with between 1 and 4 NHC ligands.[32] These enetetramines were initially detected by Wanzlick *et al* upon elimination of chloroform under thermal conditions from the NHC-adduct and "dimerisation" of the resulting unstable carbene shown in **Figure 1.11**.[3]

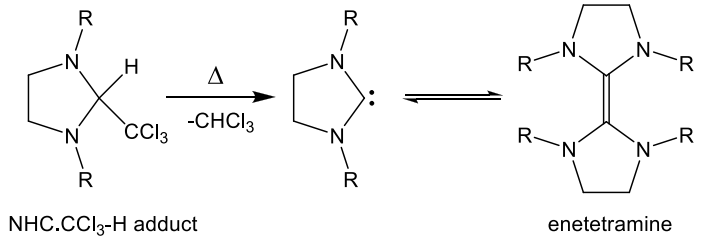

Figure 1.11 Enetetramine (Wanzlick dimer) formation from NHC.CCl_3-H adducts

A more recent method for the *in situ* generation of NHCs involves the addition of a metal fragment *directly* with the NHC-adducts (enetetramine precursors) from **Figure 1.11**.[33-36] These adducts can readily eliminate chloroform, methanol or other small molecules from the C2 position to leave the carbenic carbon,[37] although it is not clear if NHC-adducts when heated in the presence of a metal undergo direct reaction with it or conversion first to the enetetramine dimer (see **Figure 1.11**). An important detail with NHC-adducts is that in most instances they cannot be formed with unsaturated NHCs and so this route is essentially restricted to the saturated version. A related method recently developed by Crabtree *et al* found that imidazolium-2-carboxylates (Compound A, **Figure 1.12**) could yield a range of various NHC complexes in good yield via loss of CO_2.[38,39]

A method for the synthesis of NHC complexes was reported by Wang *et al* in 1998 who described the labile nature of silver-NHC bonds and their potential application as NHC transfer agents (Compound B, **Figure 1.12**).[40] Since then, this route has proved popular

through avoiding the necessities of strong bases, inert atmospheres and problematic workups. This method has been shown to give NHC complexes in good yield, especially when the starting metal species contain a halide group as it is the low solubility of the resulting silver halide which is one of the driving forces for reaction.[41,42] Unfortunately, saturated NHCs have been shown in most examples to be poor reagents for transmetallation when compared to their unsaturated analogues. Reasons given for these observations point towards the increased σ–donating ability of imidazolin-2-ylidenes and therefore an increase in the strength of the Ag-NHC bond, although there are also indications that sterics may play a role.[41]

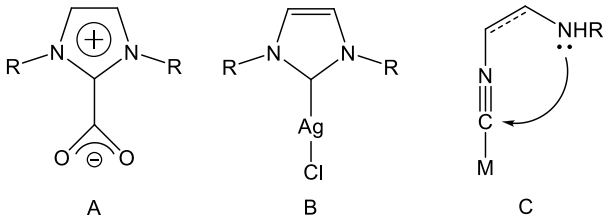

Figure 1.12 Methods of NHC complex generation including carboxylate (A) and silver (B) transfer agents and template synthesis (C) techniques

Another important method to generate NHC complexes involves the oxidative addition of the C2-X bond (X = H, halogen, Me) of imidazolium salts to low valent metal species.[43] The attraction of this method is that when X = H, the resulting metal hydride complex is generated in an atom-efficient manner and forms a potentially catalytically active compound, as has been shown by Cavell *et al*.[44,45] A final approach involves a 'template synthesis' technique, which negates the use of cyclic azoliums entirely. With this approach a coordinated amine functionalized isocyanide or carbonyl moiety is cyclised to generate the NHC ring on the metal centre (Compound C, **Figure 1.12**).[17,46,47]

1.2.3 Abnormal NHC (aNHC) complexes

Approximately 98% of NHC complexes thus far contain NHCs bound 'normally' to the metal through the C2 position (Compound A, **Figure 1.13**).[48] However, a growing number of reports have started to detail examples of a much rarer NHC binding type, through the C4 backbone position (Compound B, **Figure 1.13**).

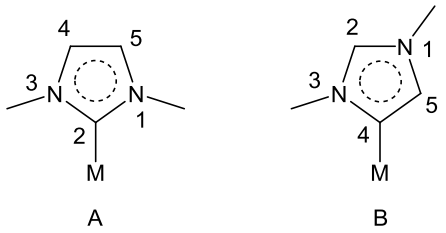

Figure 1.13 Normal (A) and abnormal (B) NHC binding modes

Compounds of this type are known as abnormal NHC (aNHC) complexes and were first discovered and isolated by Crabtree *et al* in 2001 upon addition of an iridium phosphine hydride complex to a pyridine-tethered imidazolium salt (**Figure 1.14**).[49] By modification of the anion and the R-group of the ligand, Crabtree showed that the abnormal or normal NHC product could be selected in preference to the other through either steric influences or hydrogen bonding to the anion.[50] DFT calculations have found that the free normal NHC is more stable than the free abnormal species by ca. 15 kcal/mol,[51] which helps explain the rarity of these compounds in the literature and the need for additional stabilisation of the aNHC complex by manipulation of sterics and electronics. Other aNHC complexes may be generated by substitution of the C2 proton with a phenyl group (thereby preventing oxidative addition at the C2 position and favouring reaction at the backbone), followed by reaction with a silver salt to act as a transfer agent from the C4 position.[52]

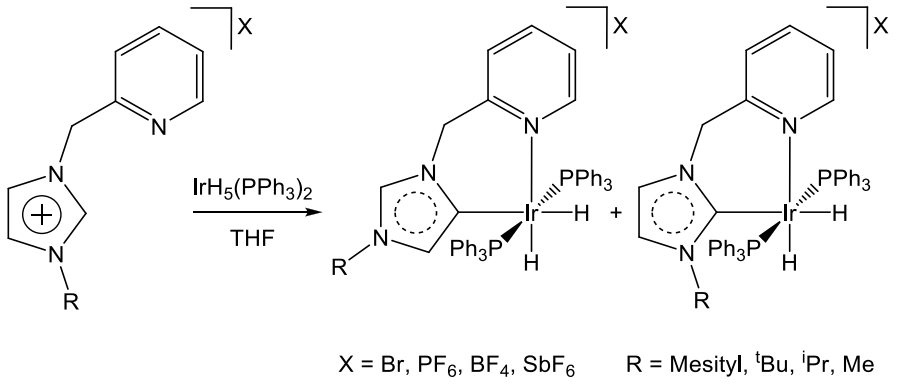

Figure 1.14 The first abnormal NHC (aNHC) complex synthesis by Crabtree

Complexes containing aNHC ligands are often generated unexpectedly due to the prevalence of *in situ* deprotonation of imidazolium salts, especially in the fabrication of NHC containing catalysts. For example, Nolan *et al* have shown that by varying the quantity of base used in the *in situ* reaction of $Pd(OAc)_2$ with 2 equivalents of $IMesH^+Cl^-$, the resulting $Pd(IMes)_2Cl_2$ product consists of both the expected $Pd(IMes)(IMes)Cl_2$ (Compound A, **Figure 1.15**) and the aNHC compound Pd(**a**IMes)$(IMes)Cl_2$ (Compound B,

Figure 1.15).[29] Interestingly, only Compound B is catalytically active for the Suzuki-Miyaura and Heck cross-coupling reactions, a factor which may have to be taken into account in catalyst design.

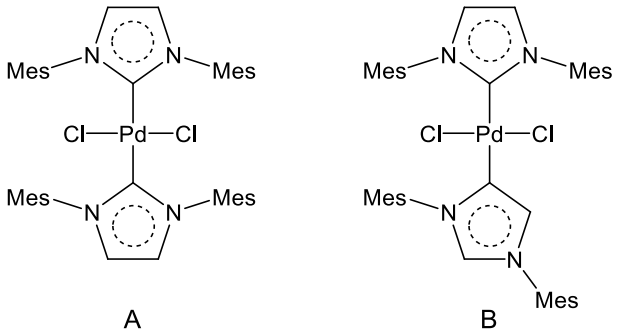

Figure 1.15 Pd(IMes)(IMes)Cl_2 (A) and Pd(aIMes)(IMes)Cl_2 (B)

Abnormal NHCs display different steric and electronic properties to their C2-bound congeners. In aNHC complexes, only the N-substituent at N3 impinges into the metal coordination sphere as opposed to both N-substituents for the normal NHC complex, thus reducing steric bulk at the metal centre. Abnormal NHCs are found also to offer significantly increased σ-donation to a metal centre as a result of the proximity of C4 to only one nitrogen atom in the heterocycle, a similar deduction to that made by Bertrand to explain the high basicity of the cyclic alkyl(amino) class of carbene complexes.[14,15] The effects of this increased σ-donation can be seen in examples by Crabtree in the IR bands for CO ligands of $Ir(CO)_2Cl(L)$ containing the normal NHC (2050 cm^{-1}) and the abnormal NHC (2039 cm^{-1}),[53] and by Albrecht in the increased trans influence of aNHCs on palladium-chloride bond distances of 2.404(4) Å (average) for Compound A (**Figure 1.16**) and 2.357(2) Å (average) for Compound B (**Figure 1.16**).[54]

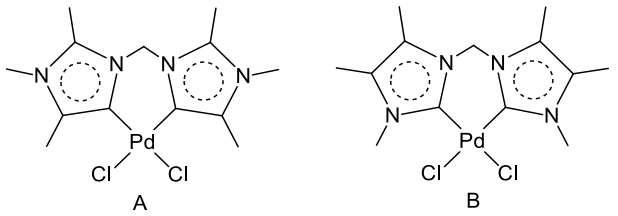

Figure 1.16 Compounds by Albrecht demonstrating the trans influence of aNHC (A) and normal NHC (B) ligands

1.3 Comparisons of NHCs and phosphines

1.3.1 Overview

NHCs have classically been compared with the ubiquitous triaryl and trialkyl phosphine ligand class, owing to the neutral 2-electron donating properties and *generally* inert nature of both ligands within the coordination sphere of a metal. However upon closer examination, considerable differences in the steric and electronic properties of NHCs cause these ligands to behave very differently to phosphines in terms of their coordination chemistry.

1.3.2 Structure and sterics

The structures of NHCs and phosphines are very different as shown in **Figure 1.17**. NHCs encompass an additional bond to phosphines between the metal and the R-substituent, which alters the geometry of the ligand from the 'cone-shape' of a phosphine to a 'fence-like' NHC.

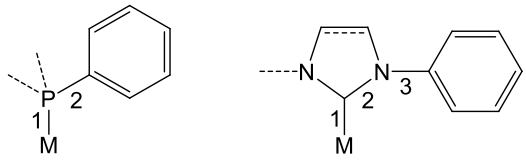

Figure 1.17 Illustrations of structural differences between phosphines and NHCs

It is often useful to quantify the steric contribution of both ligands and whereas the Tolman cone angle is useful for phosphines,[55] this model is not appropriate for NHCs due to the different orientation of the R-groups. To quantify the sterics of NHCs, the percentage buried volume (%V_{Bur}) model was developed by Nolan *et al*.[56] The %V_{Bur} model describes the percentage volume of a spherical space (of 3 Å radius) around the metal which is occupied by the substituents of a coordinated ligand (**Figure 1.18**). The greater the %V_{Bur} of a ligand, the more sterically encumbered the metal centre.

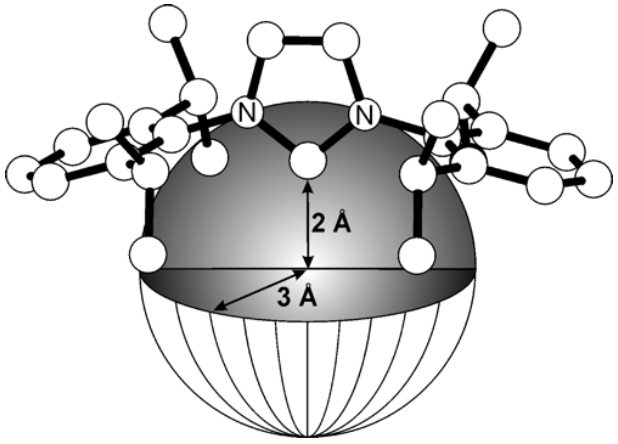

Figure 1.18 The %V_{Bur} model by Nolan

In addition to allowing the steric influences of NHCs to be quantified, the %V_{Bur} model allows a direct comparison of the sterics between phosphines and NHCs. A list of %V_{Bur} values for important NHCs and phosphines is displayed in **Table 1.1**.[56,57] The %V_{Bur} values show how some commonly used NHCs generally give a more congested profile at the metal centre than triphenyl phosphine. **Table 1.1** also shows that SIPr bestows slightly more steric congestion around a metal than IPr, due to the increase in length of the C4-C5 backbone that forces the N-substituents closer in towards the metal. However, a drawback of this model is that it does not take into account the anisotropy of the NHC ligand as it may twist along the M-C2 bond axis to minimise steric interactions, which may affect various other subtle electronic and steric parameters in different systems. Nevertheless, the general trend is useful to help explain observations and discussions later.

Ligand	%V_{Bur}
I^{t}Bu$_2$, IAd$_2$	37
SIPr	30
IPr	29
IMes	26
PPh$_3$	22

Table 1.1 %V_{Bur} values of selected NHC and phosphine ligands

1.3.3 Electronics

The electron donating qualities of NHCs have been measured using a variety of experimental data such as pK_a values, CO stretching frequencies and bond dissociation

energies, which are detailed below. These results reveal the same general trend that the least electron donating NHC is a better σ-donor than the most electron donating phosphine.

Cavell *et al* have determined the theoretical pK_a values of various NHC and phosphine ligands in an effort to describe their relative basicities (**Table 1.2**).[58] The data in **Table 1.2** indicates that phosphines are considerably weaker σ-donors than NHCs. Another important observation is that the σ-donor ability of an NHC is highly dependant on the backbone substituents, as shown by IMe_2Me_2 > IMe_2 > IMe_2Cl_2.

Ligand	pK_a (H_2O)
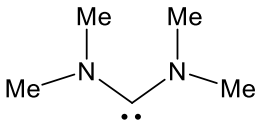	34.0 ± 0.3
***bis*(dimethylamino carbene)**	
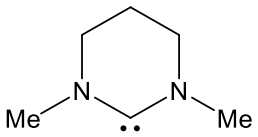	33.7 ± 0.3
SI-6-Me_2	
IMe_2Me_2	29.5 ± 0.3
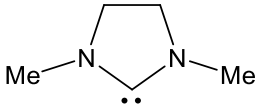	28.5 ± 0.4
$SIMe_2$	
IMe_2	27.4 ± 0.4
IMe_2Cl_2	23.4 ± 0.2
P^tBu_3	11.40
PPh_3	2.73

Table 1.2 Theoretical pK_a values of selected NHC and phosphine ligands by Cavell

An interesting observation is the difference between saturated and unsaturated NHCs. $SIMe_2$ is slightly more σ-donating than IMe_2 as other studies have shown, however Cavell portrays this to be due to differences in NCN bond angles, not differences in electron delocalisation. This can be concluded by comparing the pK_a values of $SIMe_2$ (28.5 ± 0.4), the 6-membered version, SI-6-Me_2 (33.7 ± 0.3) and the acyclic *bis*(dimethylamino carbene) (34.0 ± 0.3). The difference in electron delocalisation between $SIMe_2$ and SI-6-Me_2 should

not be substantial as both are saturated systems, yet the difference in pK_a is very large. Also, SI-6-Me_2 and *bis*(dimethylamino carbene) have NCN bond angles that are similar to each other (ca. 116˚ and ca. 119˚ respectively, compared with $SIMe_2$ at ca. 106˚) and their pK_a values are very close also. Cavell therefore states that "in the absence of other factors, such as electron-donating or withdrawing substituents, the NCN angle has the most dramatic effect on basicity, with an increase in valence angle leading to a rise in the pK_a". This finding is supported in work by Alder *et al*, where acyclic *bis*(amino carbenes) are found to be among the most basic neutral ligands available.[59] A last important note is that these studies by Cavell look only at the ligands individually, not their properties once inside the coordination sphere of a metal.

IR data from NHC and phosphine carbonyl complexes provides a useful measure of the σ-donation from these different ligands. CO stretching frequencies are inversely proportional to the amount of electron density at the metal centre, which itself is affected by the degree of σ-donation from the other ligands. Nolan *et al* have compared a variety of NHC and phosphine ligands using the $Ni(CO)_3(L)$ scaffold and as with Cavell's results in **Table 1.2** find NHCs (IPr; SIPr; IMes; SIMes) to be more electron donating than the phosphines, PPh_3 and PCy_3 (**Table 1.3**).[60] Interestingly this data implies that imidazol-2-ylidenes are marginally more donating than imidazolin-2-ylidenes.[60]

L	$\nu_{(CO)}$ (cm^{-1})	$\nu_{(CO)}$ (cm^{-1})
IMes	2050.7	1969.8
SIMes	2051.5	1970.6
IPr	2051.5	1970.0
SIPr	2052.2	1971.3
PCy_3	2056.4	1973.0
PPh_3	2068.9	1990.0

Table 1.3 IR bands (CH_2Cl_2) for $Ni(CO)_3L$ (L = NHC, PR_3)

Nolan has also measured bond dissociation enthalpies (BDEs) for the reaction in **Figure 1.19** as a means of comparing electron donor ability.[56]

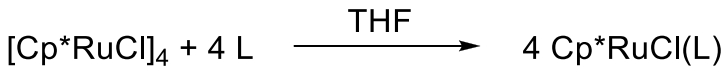

Figure 1.19 Ligand substitution reaction demonstrating differences in BDEs for NHC and phosphine ligands (L)

Through calorimetric studies (results in **Table 1.4**), Nolan found NHCs to be better donors than phosphines, except in the case of IAd_2. A plot of BDEs for the NHC ligands in **Table 1.4** versus their steric parameter ($\%V_{Bur}$) finds a linear relationship, suggesting that steric bulk is inversely proportional to the orbital overlap between the NHC and the metal. Therefore in the case of IAd_2, the steric effects of the adamantyl groups act to hinder the overlap of the metal and carbenic carbon orbitals to give the low BDE of 6.8 kcal/mol. Additionally, these results implied that saturated NHCs formed more stable species than their unsaturated analogues, but that the difference in energy was very small, at only 1 kcal/mol.

L	BDE (kcal/mol)
SIMes	16.8
IMes	15.6
SIPr	12.1
IPr	11.1
PCy_3	10.5
IAd_2	6.8

Table 1.4 BDEs of NHC and phosphine ligands in Cp*Ru(L)Cl

1.3.4 NHC binding: Sterics vs. electronics

The formation of NHC complexes has been shown to be a competition between the thermodynamic sink of the strong electronic σ-donation (relative to phosphines) versus the kinetic barrier of the sterically demanding N-substituents. In some examples, NHCs may be in equilibrium with phosphines if the metal is too sterically encumbered to give good M-NHC orbital overlap, such as that seen for the cobalt complex shown in **Figure 1.20**.[61]

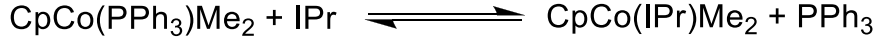

Figure 1.20 Reaction describing the equilibrium of IPr with PPh_3

A good illustration that NHC stability cannot be guaranteed is in work by Crudden *et al* involving the NHC derivative of Wilkinson's catalyst, $Rh(IMes)(PPh_3)_2Cl$ which was

demonstrated to be a hydrogenation catalyst of near equal activity to Wilkinson's original catalyst, but only upon addition of PPh_3 to the reaction mixture.[62] In further work it transpired that elimination of the NHC occurred through reaction with the dichloroethane solvent to leave Wilkinson's catalyst ($Rh(PPh_3)_3Cl$) as the only active species.[63] In other instances, the steric bulk of the N-substituents of NHCs may weaken other surrounding ligands, such as in the reaction of $Ni(CO)_4$ with IAd_2 and I^tBu_2 which produces the rare three coordinate species $Ni(CO)_2(IAd_2)$ and $Ni(CO)_2(I^tBu_2)$ upon loss of a CO ligand.[56]

1.4 NHC complexes: Applications

1.4.1 Overview

Complexes of late transition metals such as palladium and ruthenium display a wide range of activity for such catalytic processes as cross-coupling, metathesis and hydrogenation.[4,5] The combination of these metals with NHCs has led to the generation of complexes with unrivalled levels of activity, where the superior σ-donating abilities and increased steric bulk compared with phosphines ligands has proved the raison d'être.

1.4.2 Cross-coupling reactions

An insight into how useful NHC complexes could be in catalytic transformations first came in 1995 when Herrmann *et al* showed *bis*-NHC palladium species to be highly active in the Heck reaction (**Figure 1.21**).[4,8,64]

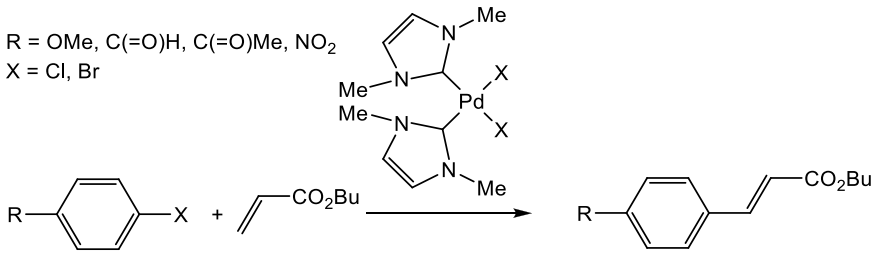

Figure 1.21 Heck reaction with a *bis*-NHC palladium catalyst

This activity was attributed directly to the increased thermal and hydrolytic stability of the catalyst resulting from the strength of the metal-NHC bond, a trend that is echoed in numerous studies including a report by Peris *et al* in which a *bis*-NHC palladium catalyst maintains activity at over 180 ˚C in air.[65] Although a significant amount of research has detailed the use of NHC complexes in the Heck reaction,[4,5] this is by no means their limitation. The coupling of aryl halides with phenyl boronic acids to give substituted

biphenyls, also known as the Suzuki-Miyaura reaction, has also been greatly influenced since the introduction of NHC-palladium complexes which have shown significant improvements in activity over other known systems.[4,8,66] An example of the high catalytic activity of NHC containing complexes comes from Cavell *et al* using the catalyst shown in **Figure 1.22**[10] to give turnover numbers (TONs) of 1.7 x 10^6 in the Heck reaction and 1.1 x 10^5 in the Suzuki reaction.

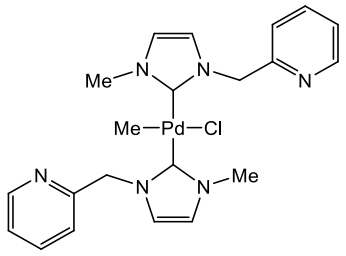

Figure 1.22 Highly active NHC-palladium catalyst for Heck and Suzuki reactions

Other important C-C bond formation cross-coupling reactions in which NHC complexes have excelled include the α-arylation of ketones,[66,67] the Sonogashira coupling of aryl halides to terminal alkynes[68] and the Kumada coupling of aryl halides directly with Grignard reagents.[69] There are also applications in the C-N bond forming reaction of aryl amination, with NHC complexes proving to be useful in activating the more difficult but cheaper aryl chlorides (as opposed to aryl bromides) and their activity is not affected by the presence of water or air.[66,67,70]

1.4.3 Metathesis

One section of catalysis that has been revolutionised by the incorporation of NHCs is the area of alkene metathesis.[71,72] Alkene metathesis is the redistribution of two alkenic bonds in the presence of a metal and is an especially useful reaction due to the prevalence of this functional group.

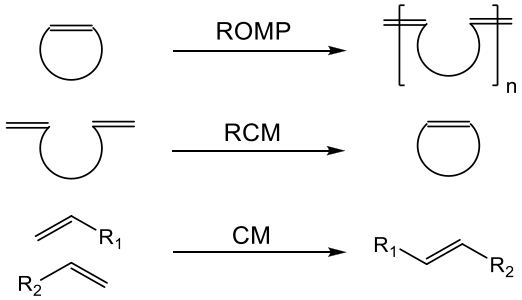

Figure 1.23 Common metathesis reaction schemes

The general schemes of metathesis include cross metathesis (CM), ring closing metathesis (RCM) and ring opening metathesis polymerisation (ROMP), shown in **Figure 1.23**. In the early 90's the most active catalysts for these reactions were based on molybdenum (Compound A, **Figure 1.24**)[12,73] and ruthenium (Compound B, **Figure 1.24**),[74] and each catalyst had its advantages and disadvantages. Whereas Schrock's molybdenum system was the most active it suffered from poor functional group tolerance and although Grubbs' ruthenium species (Grubbs I catalyst) was far more tolerant to other functionality and was much less air/moisture sensitive, it unfortunately had significantly reduced activity.

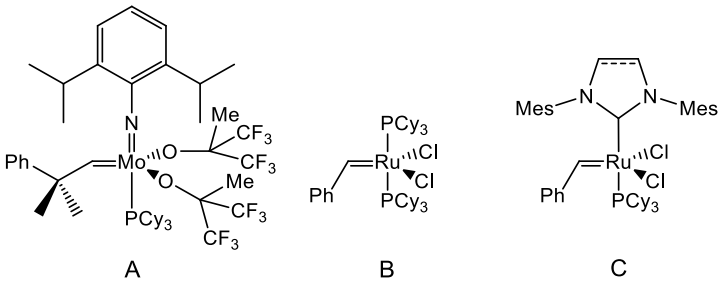

Figure 1.24 Metathesis catalysts by Schrock and Grubbs

This changed in 1999 when the groups of Nolan, Herrmann and Grubbs reported the synthesis of a variety of NHC containing analogues of the Grubbs I catalyst, the most successful of which featured IMes or SIMes ligands in place of one of the phosphines (Compound C, **Figure 1.24**).[75-79] Compound C (Grubbs II catalyst) was found to be highly active for CM, RCM and ROMP reactions, sometimes more even than Complex A,[80] all whilst retaining an inertness to air and moisture. The success of the Grubbs II catalyst lies in the stabilisation of the 14-electron reactive intermediate by the NHC when the phosphine dissociates. In addition, the strong Ru-NHC bond allows significantly higher temperatures to be employed without catalyst decomposition and therefore access to more highly substituted organic molecules can result. A good example of the use of this species can be seen in the total synthesis of Epothilones by Sinha *et al*, where an RCM reaction was sought to close a heterocycle of 16 atoms.[80] This reaction was unachievable using the molybdenum and Grubbs I systems but worked to give the product in 89% yield in the case of the Grubbs II catalyst.

Catalyst	RCM (*k*)	ROMP (*k*)
Ru(**PCy_3**)$_2Cl_2$=CHPh	1	1
Ru(**IMes**)(PCy_3)Cl_2=CHPh	53	8
Ru(**SIMes**)(PCy_3)Cl_2=CHPh	138	27

Table 1.5 Comparison of RCM/ROMP activities upon changing a PCy_3 ligand for IMes or SIMes for RCM (of 4,4-dicarboethoxy-2-methyl-1,6-heptadiene) and ROMP (of 1,5-cycloactadiene)

The difference in activity for various RCM and ROMP reactions when moving from IMes to SIMes in the Grubbs II catalyst system is significant, as shown by the results in **Table 1.5**.[36] This is interesting as Nolan has shown above that the difference in these two ligands with respect to steric and electronic properties is not very substantial and therefore subtle changes can obviously make large differences to the activity of these species.[56] Recent improvements to the Grubbs II catalyst have involved bringing about chirality to the NHC N-substituents for asymmetric transformations,[81-84] mounting on various polymer[85-87] or ionic liquid[88] supports to aid catalyst recyclability and reduce metal contamination in the products and the introduction of polarity to the ligands to make the catalyst water soluble.[89]

1.5 NHC complexes: Bond activation and catalysis

Two areas of immense interest for our research group centre on bond activation and catalysis studies of NHC complexes. NHCs act as spectator ligands in most instances, however our group has reported a number of examples showing that under certain circumstances C-H, C-C and even C-N bond activation of an NHC can occur and some of these reactions can be exploited towards catalytic transformations of their own.

The reactions that initially established our group's interest in the field of NHC complexes were those shown in **Figure 1.25**. Treatment of Ru(PPh_3)$_3$(CO)H_2 with IMes gave Ru(IMes)(PPh_3)$_2$(CO)H_2 (Compound A), which was found to induce C-H activation of one of the mesityl CH_3 groups upon loss of H_2 in the presence of a hydrogen acceptor to give Compound B. Even more interesting was that heating of Compound A at elevated temperature in the presence of excess IMes resulted in the unprecedented C-C activation of an unstrained carbon-carbon single bond of a mesityl CH_3 group (Compound C) and its release as methane.[90,91] Reaction of excess IMes with Compound A initially gave Ru(IMes)$_2$(PPh_3)(CO)H_2, although dissociation of one of the IMes ligands with respect to

PPh_3 (see **Section 1.3.4**) was observed and was attributed to the steric bulk of IMes.[91] C-H activation of Compound A with trimethylvinylsilane to make Compound B was found to be reversible in the presence of H_2, which opened up possibilities for catalytic hydrogenation reactions, whereas Compound C proved to be inert to all gases and reagents.

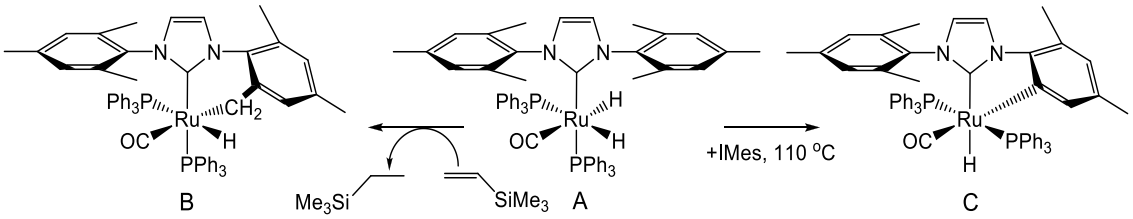

Figure 1.25 Reactions of $Ru(IMes)(PPh_3)_2(CO)H_2$ (A) with a hydrogen acceptor to form B and with excess IMes to form C

In subsequent work, the C-H activation of an NHC ligand was again found to occur in systems containing bidentate phosphine and mixed phosphine-arsine ligands,[92] and in mono dentate phosphine systems containing N-alkyl NHCs (IEt_2Me_2, $I^iPr_2Me_2$, I^iPr_2).[93,94] N-alkyl containing NHC complexes of the type, $Ru(NHC)(PPh_3)_2(CO)H_2$ have proved useful for the hydrogenation of ketones and alkenes,[95] and in collaboration with Professor Jonathan Williams at the University of Bath, their use was also investigated for the hydrogen storage-and-release potential in the one-pot indirect Wittig reaction of alcohols (**Figure 1.26**).[94,96] The indirect Wittig reaction permits C-C bond formation from alcohol precursors through their oxidation to aldehydes and then their reaction with Wittig reagents to give alkenes that are finally hydrogenated using the hydrogen 'stored' by the metal species.[97] This reaction demonstrated the use of NHC C-H activation in a catalytic cycle and the reaction was found to proceed under considerably milder conditions than previous catalysts.[97] By far the most active species for this reaction was $Ru(I^iPr_2Me_2)(PPh_3)_2(CO)H_2$, which in fact is the only species that directly forms the C-H activated product without the presence of a hydrogen acceptor.[94]

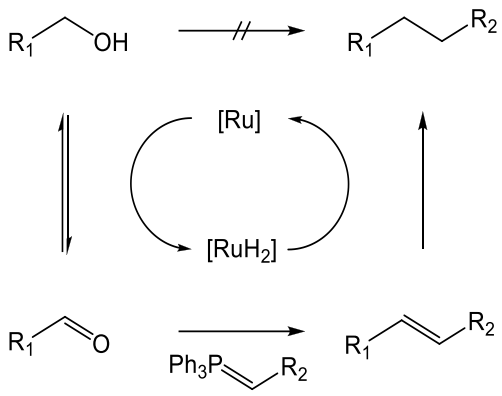

Figure 1.26 Schematic of the indirect Wittig reaction

Another example of how $I^iPr_2Me_2$ has proved to be unusual in the field of bond activation chemistry is the reaction with $Ru(PPh_3)_3(CO)HCl$. The expected substitution product, $Ru(I^iPr_2Me_2)(PPh_3)_2(CO)HCl$, was not observed (as it was with IEt_2Me_2), but instead the reaction yielded the products shown in **Figure 1.27**.[98] Compound A is the C-H activated complex $Ru(I^iPr_2Me_2)(PPh_3)_2(CO)H$ as generated previously, although in this case through loss of HCl instead of H_2. The other generated complexes are Compounds B and C, which are tautomers resulting from the C-N activation of an isopropyl arm. Compound B can be converted to Compound C via heating with excess NHC.

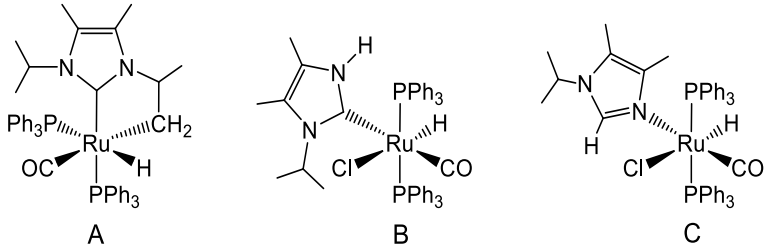

Figure 1.27 Products from the reaction of $Ru(PPh_3)_3(CO)HCl$ with $I^iPr_2Me_2$

1.6 Study prologue

1.6.1 Overview

Our group's interest in the fields of bond activation and catalysis chemistry provide the foundation for this study. Background to the two main results chapters entitled 'Cluster Chemistry' and 'Ruthenium Hydride Chemistry' are presented below.

1.6.2 Ru/Os cluster chemistry

$Ru_3(CO)_{12}$ has been shown to catalyse interesting and important organic transformations, such as those demonstrated by Murai and co-workers involving the chelation-assisted regioselective activation of sp^2 and sp^3 hybridised C-H bonds.[99-101] Although the landmark method first demonstrated in 1993[102] (**Figure 1.28**) was shown to be better suited towards mono-ruthenium catalysts such as $Ru(PPh_3)_3(CO)H_2$ instead of $Ru_3(CO)_{12}$, it was found subsequently that related processes involving the use of nitrogen instead of oxygen directing groups and/or the presence of CO for carbonyl incorporation revealed $Ru_3(CO)_{12}$ to be considerably more active than mono-ruthenium alternatives.[100,101]

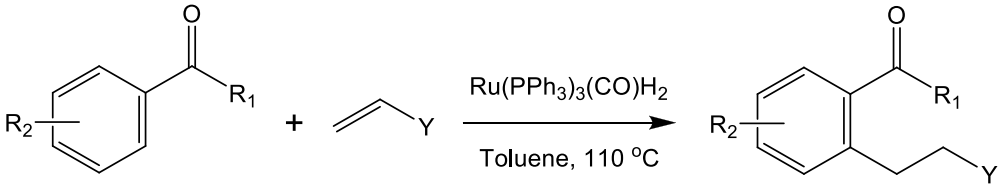

Figure 1.28 Regioselective addition of alkenes to aromatic ketones - Murai reaction

For the intermolecular [2+2+1] cyclocoupling of ketones, alkenes or alkynes and CO (**Figure 1.29**), $Ru_3(CO)_{12}$ was found to be an active species, although the addition of additive phosphine ligands was shown to increase activity considerably.[103] This demonstrates that there may be a part to play by the presence of various donor ligands, including potentially NHCs in reactions such as those described.

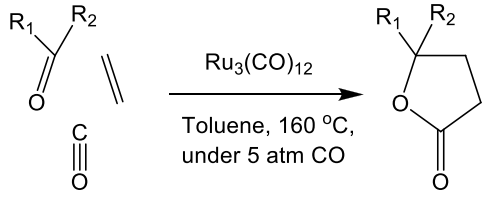

Figure 1.29 [2+2+1] Cyclocoupling reaction with $Ru_3(CO)_{12}$ catalyst

A number of examples exist in the literature of the substitution of a carbonyl ligand in $Ru_3(CO)_{12}$ for phosphine, arsine and acetonitrile ligands although there have been considerably fewer examples of this occurring with NHCs.[104] The earliest example was from Lappert and co-workers who reacted $Ru_3(CO)_{12}$ with an enetetramine to give the mono-substituted NHC product, $Ru_3(SIEt_2)(CO)_{11}$.[105] 28 years later, Cabeza *et al* reacted the Ru_3 cluster at room temperature with the *in situ* prepared IMe_2 to give $Ru_3(IMe_2)(CO)_{11}$. Upon heating in THF there followed a double C-H activation of a methyl arm on the NHC, a reaction that was reversed upon slow bubbling of CO through the solution at room temperature.[106] In addition, it was later found that heating of $Ru_3(IMe_2)(CO)_{11}$ in a higher boiling solvent such as toluene permitted the formation of novel carbyne and carbide complexes, via a number of bond activation processes (**Figure 1.30**).[107]

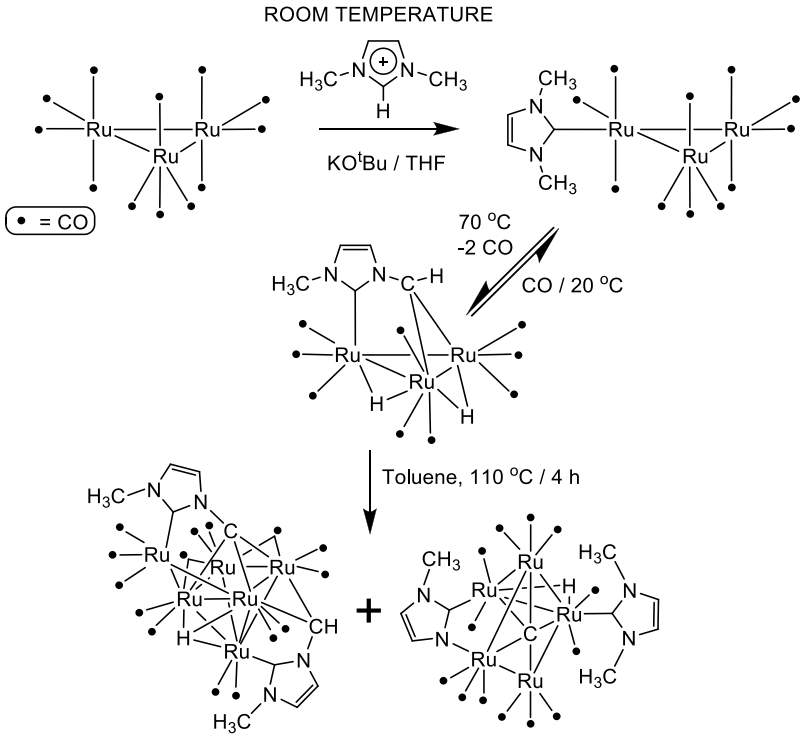

Figure 1.30 Formation of $Ru_3(IMe_2)(CO)_{11}$ and subsequent bond activation reactions upon heating

In other work, Cabeza showed that IMes reacted with $Ru_3(CO)_{12}$ to give $Ru_3(IMes)(CO)_{11}$, although no reaction was observed, even at elevated temperatures, with free IPr. Subsequent DFT calculations showed that a kinetic barrier to $Ru_3(IPr)(CO)_{11}$ must exist as a result of considerable steric hindrance.[108] Conversely, studies into this same reaction by Bruce *et al* found that reaction of excess free IMes and IPr with $Ru_3(CO)_{12}$ resulted in

cleavage of the cluster to give the air stable tetracarbonyl complexes, $Ru(NHC)(CO)_4$.[109] It is known that osmium forms complexes that are often analogous to those of ruthenium, albeit in reactions that typically require higher temperatures due to the increased strength of the Os-Os and Os-L bonds.[104] Cabeza *et al* have shown that $Os_3(IMe_2)(CO)_{11}$ can be prepared and that heating at 110 ˚C in toluene results first in the single-activation of one of the methyl C-H bonds and then on further heating, activation of the second C-H bond (**Figure 1.31**).[110]

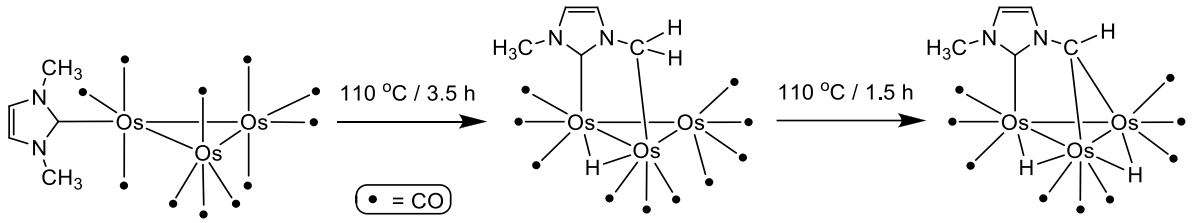

Figure 1.31 Formation of $Os_3(IMe_2)(CO)_{11}$ and following bond activation products

Osmium-NHC complexes were also investigated by Clyburne *et al* who showed that IMes can transfer to the hydride bridged tetranuclear osmium cluster, $Os_4(\mu\text{-}H)_4(CO)_{12}$ via transmetallation from silver to give the substitution product, $Os_4(\mu\text{-}H)_4(IMes)(CO)_{11}$. Upon heating of this complex inside a pressure tube in benzene at 200 ˚C for 72 hours, there is formation of two unforeseen products. The first is an isomer of the starting material where the IMes ligand is now bound *abnormally*, $Os_4(\mu\text{-}H)_4(aIMes)(CO)_{11}$ and the second product is a triply C-H activated IMes-CH_3 group that is coupled to a partially dehydrogenated benzene molecule (**Figure 1.32**).[111]

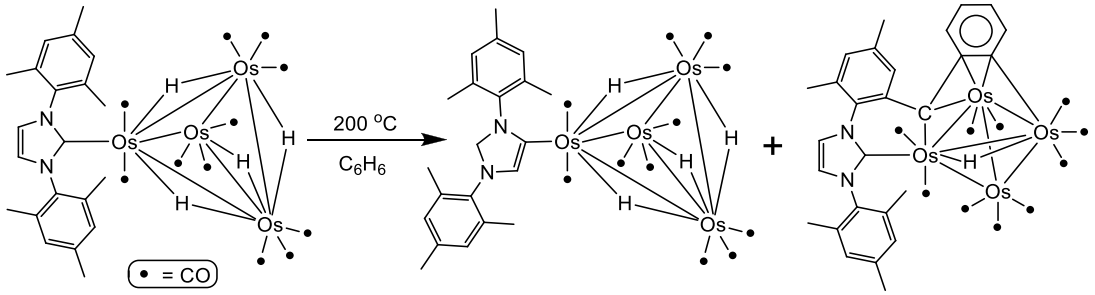

Figure 1.32 Bond activation products of $Os_4(\mu\text{-}H)_4(IMes)(CO)_{11}$ on heating

In a recent report, DFT studies by Cabeza *et al* have detailed a number of reasons for the ability of metal clusters to easily activate NHC ligands. The first is a result of the proximity of the N-substituents due to the sterically bulky nature of the ligands themselves, and the second is that thermal decarbonylation can occur in ruthenium/osmium cluster compounds, facilitating C-H activation to remove the unsaturation. A third reason states

that although the reactions are in most cases endothermic, any loss of CO gas makes the reaction essentially irreversible, allowing it to be driven to completion.[112]

1.6.3 *bis*-NHC ruthenium hydride chemistry

Hydrogenation is an important transformation in many chemical systems. It involves the reduction of a multiple bond by the addition of hydrogen in the presence of a catalyst. Direct hydrogenation occurs by the addition of molecular H_2, although hydrogen may also be derived from the oxidation of sacrificial donor molecules such as alcohols (typically isopropyl alcohol), the process being referred to as transfer hydrogenation (general scheme, **Figure 1.33**).

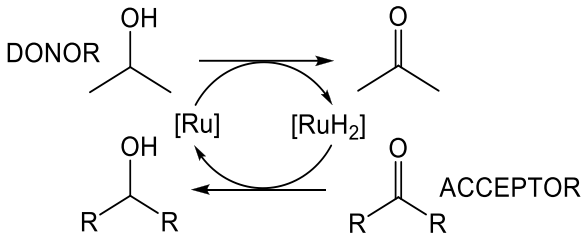

Figure 1.33 Transfer hydrogenation scheme

Ruthenium has been used as a transfer hydrogenation catalyst by Bäckvall among many others,[113] and he has shown that the dihydride complex $Ru(PPh_3)_3H_2$ proves to be substantially more active than the corresponding dichloride species $Ru(PPh_3)_3Cl_2$, clearly demonstrating that hydride ligands increase catalyst activity for hydrogenation reactions, especially in the absence of a base.[114] The incorporation of hydride ligands and/or vacant sites onto active homogenous hydrogenation catalysts acts to aid the fundamental steps for hydrogenation, which include the binding and insertion of the substrate. Our group has recently been utilising the steric properties and thermal stability of the IMes ligand to effectively stabilise ruthenium complexes containing both hydride and vacant site moieties.

The formation of 16-electron *bis*-IMes complexes has been shown to proceed through the reaction of IMes with $Ru(AsPh_3)_3(CO)H_2$. $Ru(AsPh_3)_3(CO)H_2$ is used in preference to $Ru(PPh_3)_3(CO)H_2$ as the more labile (less σ-donating) $AsPh_3$ ligand readily dissociates from the metal to yield the desired 16-electron *bis*-NHC complexes, whereas $Ru(PPh_3)_3(CO)H_2$ instead yields mono-NHC phosphine or *bis*-NHC phosphine complexes under the same conditions.[90] It was our group's initial intention to try to isolate the 16-electron dihydride complex, $Ru(IMes)_2(CO)H_2$ as shown in **Figure 1.34** (X = -H) on the

basis that it would be a highly active hydrogenation catalyst. However, at no point was $Ru(IMes)_2(CO)H_2$ observed by ^1H NMR spectroscopy throughout the reaction, although the 18-electron species $Ru(IMes)_2(AsPh_3)(CO)H_2$ was detected as two doublets at δ -5.71 and -8.93.[115] Unfortunately, $Ru(IMes)_2(AsPh_3)(CO)H_2$ was found to be inherently unstable and reacts readily with solvents (e.g. EtOH) or residual water to yield a range of 16-electron $Ru(IMes)_2(CO)HX$ (**Figure 1.34**) complexes (X = -OH, -OEt, -Cl, -F, -SH, etc).[115,116] X is typically a π-donor that forms a stable species presumably through π-push-pull interactions with the CO ligand *trans*- to it. A selection of characterised $Ru(IMes)_2(CO)HX$ species have been shown to react stoichiometrically with a range of small molecules.[117,118]

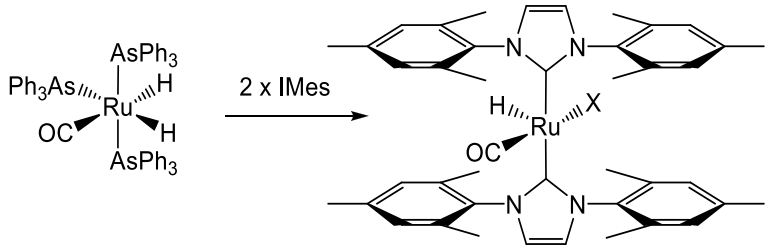

Figure 1.34 Formation of $Ru(IMes)_2(CO)HX$

A number of analogous 16-electron *bis*-phosphine complexes exist in the literature and offer good opportunities for comparisons of various spectroscopic and crystallographic data to the NHC complexes. Species containing alkyl phosphine ligands that are both strongly σ-donating and bulky (e.g. P^iPr_3, P^tBu_2Me) form 16-electron species of the type, $Ru(PR_3)_2(CO)HX$,[119-121] whereas those containing phosphines that are not strongly coordinating (such as PPh_3) or not especially bulky (such as P^iPr_2Me) typically form 18-electron complexes of the type, $Ru(PR_3)_3(CO)HX$.[122]

$Ru(IMes)_2(CO)HCl$ can be reduced with loss of NaCl by $NaBH_4$, although instead of producing $Ru(IMes)_2(CO)H_2$, there is retention of the borohydride ligand to give $Ru(IMes)_2(CO)H(\eta^2\text{-}BH_4)$ (**Figure 1.35**), which can be isolated.[118,123]

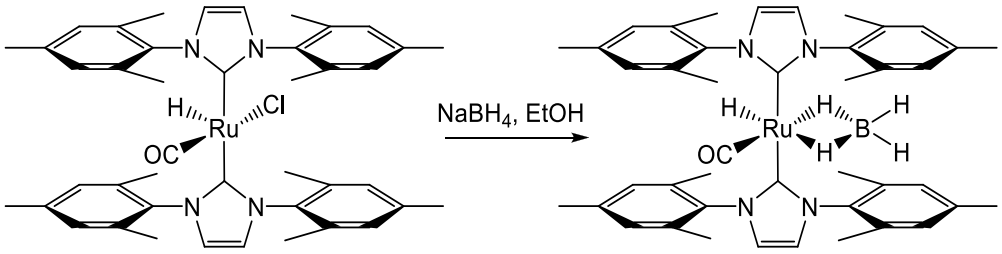

Figure 1.35 Formation of $Ru(IMes)_2(CO)H(\eta^2\text{-}BH_4)$

Marks and Kolb have described the η^2-BH_4 moiety to act as a 'gate-keeper' and have speculated that it could play an important role in catalysis by stabilising coordinatively unsaturated complexes, whilst opening up and permitting reaction of the metal with certain small molecules.[124] Indeed, the geometry of $Ru(L)_2(CO)H(\eta^2\text{-}BH_4)$ complexes is typically pseudo-octahedral 18-electron (η^2-BH_4) but can open to the 16-electron type (η^1-BH_4) in a facile manner. Preliminary results of $Ru(IMes)_2(CO)H(\eta^2\text{-}BH_4)$ compared with the parent complex $Ru(IMes)_2(CO)HCl$ in hydrogenation reactions have indicated higher levels of activity from the borohydride species.[123] Esteruelas *et al* have shown that the activity of $Ru(PR_3)_2(CO)HCl$ complexes (where R = ^{i}Pr$_3$ or ^{t}Bu$_2$Me) in ketone and alkene hydrogenation reactions is significantly enhanced by the addition of $NaBH_4$. This suggests that $Ru(L)_2(CO)H(\eta^2\text{-}BH_4)$ species may be more active catalysts than $Ru(L)_2(CO)HCl$ complexes in the absence of strong nucleophiles.[125,126]

The reaction of $Ru(PR_3)_2(CO)H(\eta^2\text{-}BH_4)$ complexes with strong nucleophiles such as phosphines or CO have been shown to degrade the complex though donation of the nucleophile into the Lewis-acidic BH_3 and then occupation by the nucleophile of the resulting vacant site of the metal. For example, reaction of $Ru(PMe_2Ph)_2(CO)H(\eta^2\text{-}BH_4)$ with a nucleophile (N) is shown to yield the product, $Ru(PMe_2Ph)_2(N)(CO)H_2$,[127,128] where N = CO, 4-methylpyridine or phosphine. This was shown to occur also by our group for $Ru(IMes)_2(CO)H(\eta^2\text{-}BH_4)$, where the addition of 1 atm CO leaves the 18e$^-$ *bis*-IMes dicarbonyl dihydride complex $Ru(IMes)_2(CO)_2H_2$, upon loss of BH_3. Mechanistic studies utilising variable temperature ^{1}H NMR and ^{13}CO labeling have shown that the addition of CO is preceded by dissociation of one bridging hydride to give an η^1-BH_4 complex with a vacant site, into which the carbonyl adds. The vacant site is shown to open *trans*- to the Ru-H bond as opposed to *cis*-.[118]

The search for more active catalysts has led some research groups to combine already effective catalysts with reagents designed to remove specific ligands from the complexes. Processes of protonation,[129,130] dehydrohalogenation[131] and halide extraction[132-136] have in some cases led to the isolation of highly electron-deficient species, such as that by Caulton *et al* in **Figure 1.36**, while in others has been utilised to improve a complex's catalytic activity *in situ*.

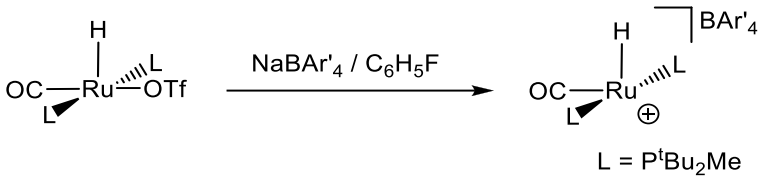

Figure 1.36 Formation of a 14-electron ruthenium hydride by Caulton

Studies by Yi *et al* have shown that the addition of 1.2 equivalents of $HBF_4 \cdot OEt_2$ to solutions of $Ru(PCy_3)_2(CO)HCl$ increases the activity of this complex for catalytic transformations such as the hydrogenation of cyclooctene, possibly through generation of highly reactive 14-electron intermediates.[137] Yi proposed that loss of phosphine (as $Cy_3PH^+BF_4^-$) gave rise to "$Ru(PCy_3)(CO)HCl$" which can be observed as a solvent adduct in CH_3CN by variable temperature ^1H NMR spectroscopy at 228 K, but could not be isolated. Gradual degradation of this complex in benzene was shown to lead to the formation of the tetrameric ruthenium species in **Figure 1.37**, containing bridging chloride ligands. With these results, comparisons may be made with analogous 16-electron NHC systems to monitor any divergence in results.

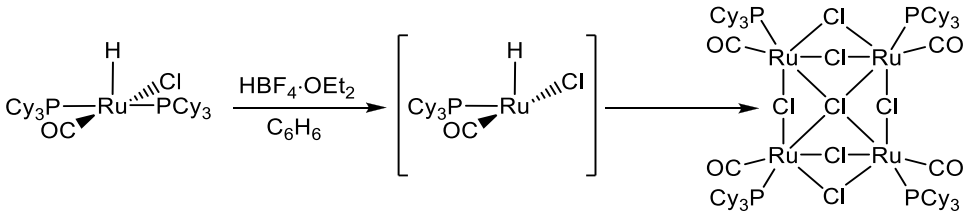

Figure 1.37 Formation of the tetrameric ruthenium complex from degradation of a 14-electron intermediate in C_6H_6 by Yi

1.6.4 Thesis synopsis

This thesis describes the use of N-heterocyclic carbenes for the stabilisation of ruthenium (and osmium) complexes for catalytic and novel bond activation processes.

Chapter 2 illustrates the reactions of a selection of N-alkyl NHCs with $Ru_3(CO)_{12}$ and $Os_3(CO)_{12}$ to investigate the effects that steric bulk has on the nature of the products. First, the formation of $M_3(aNHC)(CO)_{11}$ (M = Ru, Os) and $Ru_3(\mu\text{-}H)(aNHC)'(CO)_9$ complexes are described and their structural and spectroscopic characteristics are compared to each other and other related species where appropriate. The second part of Chapter 2 explains the formation of cluster degradation products, $Ru(NHC)_2(CO)_3$ and their subsequent

oxidation to $Ru(NHC)_2(CO)(L)(CO_3)$ (L = CO, C_5H_5N). All species are characterised and compared with each other and previously reported phosphine and NHC congeners.

Chapter 3 explains the processes involved in the formation and characterisation of 16-electron *bis*-NHC complexes of the type, $Ru(NHC)_2(CO)HCl$ (NHC = IPr, SIPr). Stoichiometric reactions of these complexes with CO and $NaBH_4$ are shown to give the complexes; $Ru(NHC)_2(CO)_2HCl$ and $Ru(NHC)_2(CO)H(\eta^2\text{-}BH_4)$ (NHC = IPr, SIPr). The $Ru(NHC)_2(CO)HX$ (NHC = IPr, SIPr and X = -Cl, $-BH_4$) complexes were then investigated for their catalytic activity for ketone hydrogenation reactions involving two substrates. Spectroscopic data is compared in these complexes and with analogous IMes and phosphine systems in an effort to demonstrate the differences in σ-donor ability of NHCs vs. phosphines and of saturated vs. unsaturated NHCs. Later, Chapter 3 describes the synthesis of $Ru(IPr)_2(CO)H(OH)$, and then investigates the reactions of $Ru(IPr)_2(CO)HX$ (X = -Cl, -OH) complexes with $HBF_4{\cdot}OEt_2$. The investigation provides insights into the competing ligand-loss pathways upon protonation of these complexes, and presents characterisation details relating to the isolated cationic ruthenium-NHC complexes containing aqua and η^6-arene ligands.

Chapter 4 contains the experimental section and characterisation data for all complexes described in this work.

1.7 References

1 Arduengo, A. J.; Harlow, R. L.; Kline, M., *J. Am. Chem. Soc.* **1991**, *113*, 361-363.

2 Wanzlick, H. W.; Schikora, E., *Angew. Chem.* **1960**, *72*, 494.

3 Wanzlick, H. W., *Angew. Chem., Int. Ed.* **1962**, *1*, 75-80.

4 *N-Heterocyclic Carbenes in Synthesis*. Nolan, S. P., Wiley-VCH, Weinheim, Germany; **2006**.

5 *N-Heterocyclic Carbenes in Transition Metal Catalysis*. Glorius, F., Springer-Verlag Berlin, Heidelberg, Germany; **2007**.

6 Crudden, C. M.; Allen, D. P., *Coord. Chem. Rev.* **2004**, *248*, 2247-2273.

7 Hahn, F. E.; Jahnke, M. C., *Angew. Chem., Int. Ed.* **2008**, *47*, 3122-3172.

8 Herrmann, W. A., *Angew. Chem., Int. Ed.* **2002**, *41*, 1290-1309.

9 Nielsen, D. J.; Cavell, K. J.; Skelton, B. W.; White, A. H., *Inorg. Chim. Acta.* **2002**, *327*, 116-125.

10 McGuinness, D. S.; Cavell, K. J., *Organometallics* **2000**, *19*, 741-748.

11 Arduengo, A. J.; Davidson, F.; Dias, H. V. R.; Goerlich, J. R.; Krafczyk, R.; Marshall, W. J.; Prakasha, T. K., *J. Am. Chem. Soc.* **1997**, *119*, 12742-12749.

12 Bazan, G. C.; Khosravi, E.; Schrock, R. R.; Feast, W. J.; Gibson, V. C.; O'Regan, M. B.; Thomas, J. K.; Davis, W. M., *J. Am. Chem. Soc.* **1990**, *112*, 8378-8387.

13 Hahn, F. E.; Wittenbecher, L.; Boese, R.; Blaser, D., *Chem. Eur. J.* **1999**, *5*, 1931-1935.

14 Lavallo, V.; Canac, Y.; Prasang, C.; Donnadieu, B.; Bertrand, G., *Angew. Chem., Int. Ed.* **2005**, *44*, 5705-5709.

15 Lavallo, V.; Canac, Y.; DeHope, A.; Donnadieu, B.; Bertrand, G., *Angew. Chem., Int. Ed.* **2005**, *44*, 7236-7239.

16 Enders, D.; Breuer, K.; Raabe, G.; Runsink, J.; Teles, J. H.; Melder, J.-P.; Ebel, K.; Brode, S., *Angew. Chem., Int. Ed.* **1995**, *34*, 1021-1023.

17 Ruiz, J.; Garcia, G.; Mosquera, M. E. G.; Perandones, B. F.; Gonzalo, M. P.; Vivanco, M., *J. Am. Chem. Soc.* **2005**, *127*, 8584-8585.

18 Alder, R. W.; Blake, M. E.; Chaker, L.; Harvey, J. N.; Paolini, F.; Schutz, J., *Angew. Chem., Int. Ed.* **2004**, *43*, 5896-5911.

19 Krahulic, K. E.; Enright, G. D.; Parvez, M.; Roesler, R., *J. Am. Chem. Soc.* **2005**, *127*, 4142-4143.

20 Martin, D.; Baceiredo, A.; Gornitzka, H.; Schoeller, W. W.; Bertrand, G., *Angew. Chem., Int. Ed.* **2005**, *44*, 1700-1703.

21 Despagnet-Ayoub, E.; Grubbs, R. H., *J. Am. Chem. Soc.* **2004**, *126*, 10198-10199.

22 Alder, R. W.; Blake, M. E.; Bortolotti, C.; Bufali, S.; Butts, C. P.; Linehan, E.; Oliva, J. M.; Orpen, A. G.; Quayle, M. J., *Chem. Commun.* **1999**, 241-242.

23 Iglesias, M.; Beetstra, D. J.; Knight, J. C.; Ooi, L.-L.; Stasch, A.; Coles, S.; Male, L.; Hursthouse, M. B.; Cavell, K. J.; Dervisi, A.; Fallis, I. A., *Organometallics* **2008**, *27*, 3279-3289.

24 Arduengo, A. J., *Patent: 5,077,414* **1991**.

25 Arduengo, A. J.; Krafczyk, R.; Schmutzler, R., *Tetrahedron* **1999**, *55*, 14523-14534.

26 Kuhn, N.; Kratz, T., *Synthesis* **1993**, 561-562.

27 Öfele, K., *J. Organomet. Chem.* **1968**, *12*, 42-43.

28 Wanzlick, H. W.; Schonherr, H. J., *Angew. Chem., Int. Ed.* **1968**, *7*, 141-142.

29 Lebel, H.; Janes, M. K.; Charette, A. B.; Nolan, S. P., *J. Am. Chem. Soc.* **2004**, *126*, 5046-5047.

30 Wanzlick, H. W.; Kleiner, H. J., *Angew. Chem.* **1961**, *73*, 493.

31 Wanzlick, H. W.; Kleiner, H. J.; Esser, F., *Chem. Ber.* **1963**, *96*, 1208-1212.

32 Lappert, M. F., *J. Organomet. Chem.* **1988**, *358*, 185-213.

33 Scholl, M.; Ding, S.; Lee, C. W.; Grubbs, R. H., *Org. Lett.* **1999**, *1*, 953-956.

34 Bedford, R. B.; Betham, M.; Blake, M. E.; Frost, R. M.; Horton, P. N.; Hursthouse, M. B.; Lopez-Nicolas, R. M., *Dalton Trans.* **2005**, 2774-2779.

35 Nyce, G. W.; Csihony, S.; Waymouth, R. M.; Hendrick, J. L., *Chem. Eur. J.* **2004**, *10*, 4073-4079.

36 Trnka, T. M.; Morgan, J. P.; Sanford, M. S.; Wilhelm, T. E.; Scholl, M.; Choi, T.; Ding, S.; Day, M. W.; Grubbs, R. H., *J. Am. Chem. Soc.* **2003**, *125*, 2546-2558.

37 Arduengo, A. J.; Calabrese, J. C.; Davidson, F.; Dias, H. V. R.; Goerlich, J. R.; Krafczyk, R.; Marshall, W. J.; Tamm, M.; Schmutzler, R., *Helv. Chim. Acta* **1999**, *82*, 2348-2364.

38 Voutchkova, A. M.; Appelhans, L. N.; Chinaese, A. R.; Crabtree, R. H., *J. Am. Chem. Soc.* **2005**, *127*, 17624-17625.

39 Voutchkova, A. M.; Feliz, M.; Clot, E.; Eisenstein, O.; Crabtree, R. H., *J. Am. Chem. Soc.* **2007**, *129*, 12834-12846.

40 Wang, H. M. J.; Lin, I. J. B., *Organometallics* **1998**, *17*, 972-975.

41 Garrison, J. C.; Youngs, W. J., *Chem. Rev.* **2005**, *105*, 3978-4008.

42 Lin, I. J. B.; Vasam, C. S., *Coord. Chem. Rev.* **2007**, *251*, 642-670.

43 Cavell, K. J.; McGuinness, D. S., *Coord. Chem. Rev.* **2004**, *248*, 671-681.

44 Druin, M. A.; Clement, N. D.; Cavell, K. J.; Elsevier, C. J., *Chem. Commun.* **2003**, 400-401.

45 Clement, N. D.; Cavell, K. J.; Jones, C.; Elsevier, C. J., *Angew. Chem., Int. Ed.* **2004**, *43*, 1277-1279.

46 Motschi, H.; Angelici, R. J., *Organometallics* **1982**, *1*, 343-349.

47 Ito, Y.; Hirao, T.; Tsubata, K.; Saegusa, T., *Tetrahedron Lett.* **1978**, *19*, 1535-1538.

48 Arnold, P. L.; Pearson, S., *Coord. Chem. Rev.* **2007**, *251*, 596-609.

49 Grundemann, S.; Kovacevic, A.; Albrecht, M.; Faller, J. W.; Crabtree, R. H., *Chem. Commun.* **2001**, 2274-2275.

50 Grundemann, S.; Kovacevic, A.; Albrecht, M.; Faller, J. W.; Crabtree, R. H., *J. Am. Chem. Soc.* **2002**, *124*, 10473-10481.

51 Appelhans, L. N.; Zuccaccia, D.; Kovacevic, A.; Chianese, A. R.; Miecznikowski, J. R.; Macchioni, A.; Clot, E.; Eisenstein, O.; Crabtree, R. H., *J. Am. Chem. Soc.* **2005**, *127*, 16299-16311.

52 Alcarazo, M.; Roseblade, S. J.; Cowley, A. R.; Fernandez, R.; Brown, J. M.; Lassaletta, J. M., *J. Am. Chem. Soc.* **2005**, *127*, 3290-3291.

53 Chianese, A. R.; Kovacevic, A.; Zeglis, B. M.; Faller, J. W.; Crabtree, R. H., *Organometallics* **2004**, *23*, 2461-2468.

54 Albrecht, M., *Chem. Commun.* **2008**, 3601-3610.

55 Tolman, C. A., *Chem. Rev.* **1977**, *77*, 313-348.

56 Hillier, A. C.; Sommer, W. J.; Yong, B. S.; Petersen, J. L.; Cavallo, L.; Nolan, S. P., *Organometallics* **2003**, *22*, 4322-4326.

57 Gonzalez, S. D.-.; Nolan, S. P., *Coord. Chem. Rev.* **2007**, *251*, 874-883.

58 Magill, A. M.; Cavell, K. J.; Yates, B. F., *J. Am. Chem. Soc.* **2004**, *126*, 8717-8724.

59 Alder, R. W.; Blake, M. E.; Oliva, J. M., *J. Phys. Chem. A* **1999**, *103*, 11200-11211.

60 Dorta, R.; Stevens, E. D.; Scott, N. M.; Costabile, C.; Cavallo, L.; Hoff, C. D.; Nolan, S. P., *J. Am. Chem. Soc.* **2005**, *127*, 2485-2495.

61 Simms, R. W.; Drewitt, M. J.; Baird, M. C., *Organometallics* **2002**, *21*, 2958-2963.

62 Chen, A. C.; Ren, L.; Decken, A.; Crudden, C. M., *Organometallics* **2000**, *19*, 3459-3461.

63 Allen, D. P.; Crudden, C. M.; Calhoun, L. A.; Wang, R., *J. Organomet. Chem.* **2004**, *689*, 3203-3209.

64 Herrmann, W. A.; Elison, M.; Fischer, J.; Kocher, C.; Artus, G. R. J., *Angew. Chem., Int. Ed.* **1995**, *34*, 2371-2374.

65 Peris, E.; Loch, J. A.; Mata, J.; Crabtree, R. H., *Chem. Commun.* **2001**, 201-202.

66 Viciu, M. S.; Germaneau, R. F.; Fernandez, O. N.-.; Stevens, E. D.; Nolan, S. P., *Organometallics* **2002**, *21*, 5470-5472.

67 Marion, N.; Ecarnot, E. C.; Navarro, O.; Amoroso, D.; Bell, A.; Nolan, S. P., *J. Org. Chem.* **2006**, *71*, 3816-3821.

68 Ma, Y.; Song, C.; Jiang, W.; Wu, Q.; Wang, Y.; Liu, X.; Andrus, M. B., *Org. Lett.* **2003**, *5*, 3317-3319.

69 Huang, J.; Nolan, S. P., *J. Am. Chem. Soc.* **1999**, *121*, 9889-9890.

70 Viciu, M. S.; Kelly, R. A.; Stevens, E. D.; Naud, F.; Studer, M.; Nolan, S. P., *Org. Lett.* **2003**, *5*, 1479-1482.

71 Trnka, T. M.; Grubbs, R. H., *Acc. Chem. Res.* **2001**, *34*, 18-29.

72 Grubbs, R. H.; Chang, S., *Tetrahedron* **1998**, *54*, 4413-4450.

73 Bazan, G. C.; Oskam, J. H.; Cho, H.-N.; Park, L. Y.; Schrock, R. R., *J. Am. Chem. Soc.* **1991**, *113*, 6899-6907.

74 Schwab, P.; Grubbs, R. H.; Ziller, R. H., *J. Am. Chem. Soc.* **1996**, *118*, 100-110.

75 Yet, L., *Chem. Rev.* **2000**, *100*, 2963-3007.

76 Heck, M.-P.; Baylon, C.; Nolan, S. P.; Mioskowski, C., *Org. Lett.* **2001**, *3*, 1989-1991.

77 Hamilton, J. G.; Frenzel, U.; Kohl, F. J.; Weskamp, T.; Rooney, J. J.; Herrmann, W. A.; Nuyken, O. J., *J. Am. Chem. Soc.* **2000**, *606*, 8-12.

78 Bielawski, C. W.; Grubbs, R. H., *Angew. Chem., Int. Ed.* **2000**, *39*, 2903-2906.

79 Choi, T.; Chatterjee, A. K.; Grubbs, R. H., *Angew. Chem., Int. Ed.* **2001**, *40*, 1277-1279.

80 Sun, J.; Sinha, S. C., *Angew. Chem., Int. Ed.* **2002**, *41*, 1381-1383.

81 Seiders, T. J.; Ward, D. W.; Grubbs, R. H., *Org. Lett.* **2001**, *3*, 3225-3228.

82 Veldhuizen, J. J. V.; Garber, S. B.; Kingsbury, J. S.; Hoveyda, A. H., *J. Am. Chem. Soc.* **2002**, *124*, 4954-4955.

83 Veldhuizen, J. J. V.; Campbell, J. E.; Giudici, R. E.; Hoveyda, A. H., *J. Am. Chem. Soc.* **2005**, *127*, 6877.

84 Fournier, P.-A.; Collins, S. K., *Organometallics* **2007**, *26*, 2945-2949.

85 Clavier, H.; K., G.; Kirschning, A.; Mauduit, M.; Nolan, S. P., *Angew. Chem., Int. Ed.* **2007**, *46*, 6786-6801.

86 Schurer, S. C.; Gessler, S.; Buschmann, N.; Blechert, S., *Angew. Chem., Int. Ed.* **2000**, *39*, 3898-3901.

87 Jafarpour, L.; Heck, M.-P.; Baylon, C.; Lee, H. M.; Mioskowski, C.; Nolan, S. P., *Organometallics* **2002**, *21*, 671-679.

88 Clavier, H.; Nolan, S. P.; Mauduit, M., *Organometallics* **2008**, *27*, 2287-2292.

89 Jordan, J. P.; Grubbs, R. H., *Angew. Chem., Int. Ed.* **2007**, *46*, 5152-5155.

90 Jazzar, R. F. R.; Macgregor, S. A.; Mahon, M. F.; Richards, S. P.; Whittlesey, M. K., *J. Am. Chem. Soc.* **2002**, *124*, 4944-4945.

91 Diggle, R. A.; Macgregor, S. A.; Whittlesey, M. K., *Organometallics* **2008**, *27*, 617-625.

92 Chilvers, M. J.; Jazzar, R. F. R.; Mahon, M. F.; Whittlesey, M. K., *Adv. Synth. Catal.* **2003**, *345*, 1111-1114.

93 Burling, S.; Mahon, M. F.; Paine, B. M.; Whittlesey, M. K.; Williams, J. M. J., *Organometallics* **2004**, *23*, 4537-4539.

94 Burling, S.; Paine, B. M.; Nama, D.; Brown, V. S.; Mahon, M. F.; Prior, T. J.; Pregosin, P. S.; Whittlesey, M. K.; Williams, J. M. J., *J. Am. Chem. Soc.* **2007**, *129*, 1987-1995.

95 Burling, S.; Whittlesey, M. K.; Williams, J. M. J., *Adv. Synth. Catal.* **2005**, *347*, 591-594.

96 Edwards, M. G.; Jazzar, R. F. R.; Paine, B. M.; Shermer, D. J.; Whittlesey, M. K.; Williams, J. M. J.; Edney, D. D., *Chem. Commun.* **2004**, 90-91.

97 Edwards, M. G.; Williams, J. M. J., *Angew. Chem., Int. Ed.* **2002**, *41*, 4740-4743.

98 Burling, S.; Mahon, M. F.; Powell, R. E.; Whittlesey, M. K.; Williams, J. M. J., *J. Am. Chem. Soc.* **2006**, *128*, 13702-13703.

99 Kakiuchi, F.; Matsumoto, M.; Tsuchiya, K.; Igi, K.; Hayamizu, T.; Chatani, N.; Murai, S., *J. Organomet. Chem.* **2003**, *686*, 134-144.

100 Asaumi, T.; Chatani, N.; Matsuo, T.; Kakiuchi, F.; Murai, S., *J. Org. Chem.* **2003**, *68*, 7538-7540.

101 Chatani, N.; Asaumi, T.; Yorimitsu, S.; Ikeda, T.; Kakiuchi, F.; Murai, S., *J. Am. Chem. Soc.* **2001**, *123*, 10935-10941.

102 Murai, S.; Kakiuchi, F.; Sekine, S.; Tanaka, Y.; Kamatani, A.; Sonoda, M.; Chatani, N., *Nature* **1993**, *366*, 529-531.

103 Tobisu, M.; Chatani, N.; Asaumi, T.; Amako, K.; Ie, Y.; Fukumoto, Y.; Murai, S., *J. Am. Chem. Soc.* **2000**, *122*, 12663-12674.

104 *Comprehensive Organometallic Chemistry III*. Crabtree, R. H.; Mingos, M. P.; Bruce, M., Elsevier, Oxford, UK; **2007**.

105 Lappert, M. F.; Pye, P. L., *Dalton Trans.* **1977**, 2172-2180.

106 Cabeza, J. A.; Rio, I.; Miguel, D.; Sanchez-Vega, M. G., *Chem. Commun.* **2005**, 3956-3958.

107 Cabeza, J. A.; Rio, I.; Miguel, D.; Sanchez-Vega, M. G., *Angew. Chem., Int. Ed.* **2008**, *47*, 1920-1922.

108 Cabeza, J. A.; Rio, I.; Miguel, D.; Perez-Carreno, E.; Sanchez-Vega, M. G., *Organometallics* **2008**, *27*, 211-217.

109 Bruce, M. I.; Cole, M. L.; Fung, R. S. C.; Forsyth, C. M.; Hilder, M.; Junk, P. C.; Konstas, K., *Dalton Trans.* **2008**, 4118-4128.

110 Cabeza, J. A.; Rio, I.; Miguel, D.; Perez-Carreno, E.; Sanchez-Vega, M. G., *Dalton Trans.* **2008**, 1937-1942.

111 Cooke, C. E.; Jennings, M. C.; Pomeroy, R. K.; Clyburne, J. A. C., *Organometallics* **2007**, *26*, 6059-6062.

112 Cabeza, J. A.; Perez-Carreno, E., *Organometallics* **2008**, *27*, 4697-4702.

113 Backvall, J. E., *J. Organomet. Chem.* **2002**, *652*, 105-111.

114 Aranyos, A.; Csjernyik, G.; Szabo, K. J.; Backvall, J. E., *Chem. Commun.* **1999**, 351-352.

115 Jazzar, R. F. R.; Bhatia, P. H.; Mahon, M. F.; Whittlesey, M. K., *Organometallics* **2003**, *22*, 670-683.

116 Chatwin, S. L.; Davidson, M. G.; Doherty, C.; Donald, S. M.; Jazzar, R. F. R.; Macgregor, S. A.; McIntyre, G.; Mahon, M. F.; Whittlesey, M. K., *Organometallics* **2006**, *25*, 99-110.

117 Chatwin, S. L.; Diggle, R. A.; Jazzar, R. F. R.; Macgregor, S. A.; Mahon, M. F.; Whittlesey, M. K., *Inorg. Chem.* **2003**, *42*, 7695-7697.

118 Chantler, V. L.; Chatwin, S. L.; Jazzar, R. F. R.; Mahon, M. F.; Saker, O.; Whittlesey, M. K., *Dalton Trans.* **2008**, 2603-2614.

119 Poulton, J. T.; Sigalas, M. P.; Folting, K.; Streib, W. E.; Eisenstein, O.; Caulton, K. G., *Inorg. Chem.* **1994**, *33*, 1476-1485.

120 Huang, D.; Streib, W.; Bollinger, J. C.; Caulton, K. G.; Winter, R. F.; Scheiring, T., *J. Am. Chem. Soc.* **1999**, *121*, 8087-8097.

121 Esteruelas, M. A.; Werner, H., *J. Organomet. Chem.* **1986**, *303*, 221-231.

122 Marchenko, A. V.; Huffman, J. C.; Valerga, P.; Jimenez, M.; Tenorio, J.; Puerta, M. C.; Caulton, K. G., *Inorg. Chem.* **2001**, *40*, 6444-6450.

123 Chatwin, S. L., *Ph.D. Thesis, University of Bath.* **2007**.

124 Marks, T. J.; Kolb, J. R., *Chem. Rev.* **1977**, *77*, 263-293.

125 Esteruelas, M. A.; Sola, E.; Oro, L. A., *J. Mol. Catal.* **1988**, *45*, 1-5.

126 Esteruelas, M. A.; Sola, E.; Oro, L. A., *J. Mol. Catal.* **1989**, *53*, 43-52.

127 Chamberlain, B.; Duckett, S. B.; Lowe, J. P.; Mawby, R. J.; Stott, C. J., *Dalton Trans.* **2003**, 2603-2614.

128 Duckett, S. B.; Lowe, J. P.; Mawby, R. J., *Dalton Trans.* **2006**, 2661-2670.

129 Kranenburg, M.; Kamer, P. C. J.; van Leeuwen, P. W. N. M.; Chaudret, B., *Chem. Commun.* **1997**, 373-374.

130 Sanchez-Delgado, R. A.; Thewalt, U.; Valencia, N.; Andriollo, A.; Marquez-Silva, R.-L.; Puga, J.; Schollhorn, H.; Klein, H.-P.; Fontal, B., *Inorg. Chem.* **1986**, *25*, 1097-1106.

131 Coalter, J. N.; Bollinger, J. C.; Huffman, J. C.; Werner-Zwanziger, U.; Caulton, K. G.; Davidson, E. R.; Gerard, H.; Clot, E.; Eisenstein, O., *New J. Chem.* **2000**, *24*, 9-26.

132 Huang, D.; Bollinger, J. C.; Streib, W. E.; Folting, K.; Young, V.; Eisenstein, O.; Caulton, K. G., *Organometallics* **2000**, *19*, 2281-2290.

133 Scott, N. M.; Dorta, R.; Stevens, E. D.; Correa, A.; Cavallo, L.; Nolan, S. P., *J. Am. Chem. Soc.* **2005**, *127*, 3516-3526.

134 Huang, D.; Huffman, J. C.; Bollinger, J. C.; Eisenstein, O.; Caulton, K. G., *J. Am. Chem. Soc.* **1997**, *119*, 7398-7399.

135 Baratta, W.; Mealli, C.; Herdtweck, E.; Lenco, A.; Mason, S. A.; Rigo, P., *J. Am. Chem. Soc.* **2004**, *126*, 5549-5562.

136 Huang, D.; Streib, W. E.; Eisenstein, O.; Caulton, K. G., *Angew. Chem., Int. Ed.* **1997**, *36*, 2004-2006.

137 Yi, C. S.; Lee, D. W.; He, Z.; Rheingold, A. L.; Lam, K.-C.; Concolino, T. E., *Organometallics* **2000**, *19*, 2909-2915.

Chapter 2

Cluster Chemistry

2.1 Preface

Our group's interest in reactions of cluster complexes of the type $M_3(CO)_{12}$ (M = Ru, Os) began with a report by Cabeza and co-workers in 2005.[1] In this work, $Ru_3(CO)_{12}$ was reacted at room temperature with IMe_2 (formed via *in situ* deprotonation of the corresponding imidazolium salt with KO^tBu) to give the mono-NHC substituted product $Ru_3(IMe_2)(CO)_{11}$, shown in **Figure 2.1**. This was only the second Ru_3-NHC cluster reported up to that point, the first being $Ru_3(SIEt_2)(CO)_{11}$ from the group of Lappert, 28 years earlier.[2]

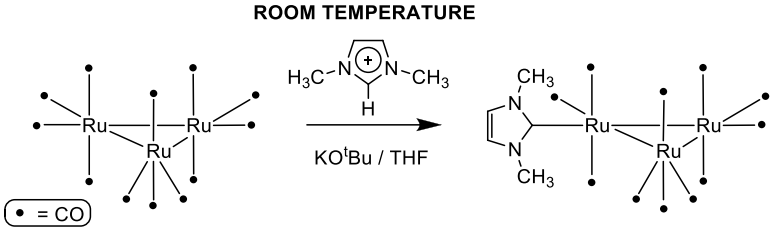

Figure 2.1 Formation of $Ru_3(IMe_2)(CO)_{11}$ by Cabeza

We therefore concluded that this represented a relatively unexplored area of chemistry, and one that showed potential in the topics of bond activation chemistry (see the effect of heating $Ru_3(IMe_2)(CO)_{11}$ in **Figure 1.30**, **Section 1.6.2**) and catalysis (see the use of $Ru_3(CO)_{12}$ by Murai, **Section 1.6.2**), both of which are spheres of interest for our group.

2.2 Formation of $M_3(aNHC)(CO)_{11}$ complexes

2.2.1 Introduction

Bond activation involving a C-H bond of an IMe_2 ligand had never previously been revealed until Cabeza's reaction (**Figure 1.30**, **Section 1.6.2**). We realised from this result that $Ru_3(CO)_{12}$ therefore displayed the potential to activate NHCs that were not thus far known to activate, such as I^tBu_2. As stated previously in **Section 1.5**, our group has formerly shown examples of C-H bond activation for IEt_2Me_2, $I^iPr_2Me_2$ and I^iPr_2[3-5] and the reactions of these ligands with $Ru_3(CO)_{12}$ are discussed in **Section 2.4**.

2.2.2 $Ru_3(al^tBu_2)(CO)_{11}$ (1A)

Upon addition of d_8-THF to a J. Young's NMR tube containing $Ru_3(CO)_{12}$ and I^tBu_2 (1:1.2 ratio) there was spontaneous evolution of CO gas observed at room temperature

which ceased after 30-60 minutes. The solution turned from an initial dark red to a pale orange colour containing a small amount of orange precipitate.

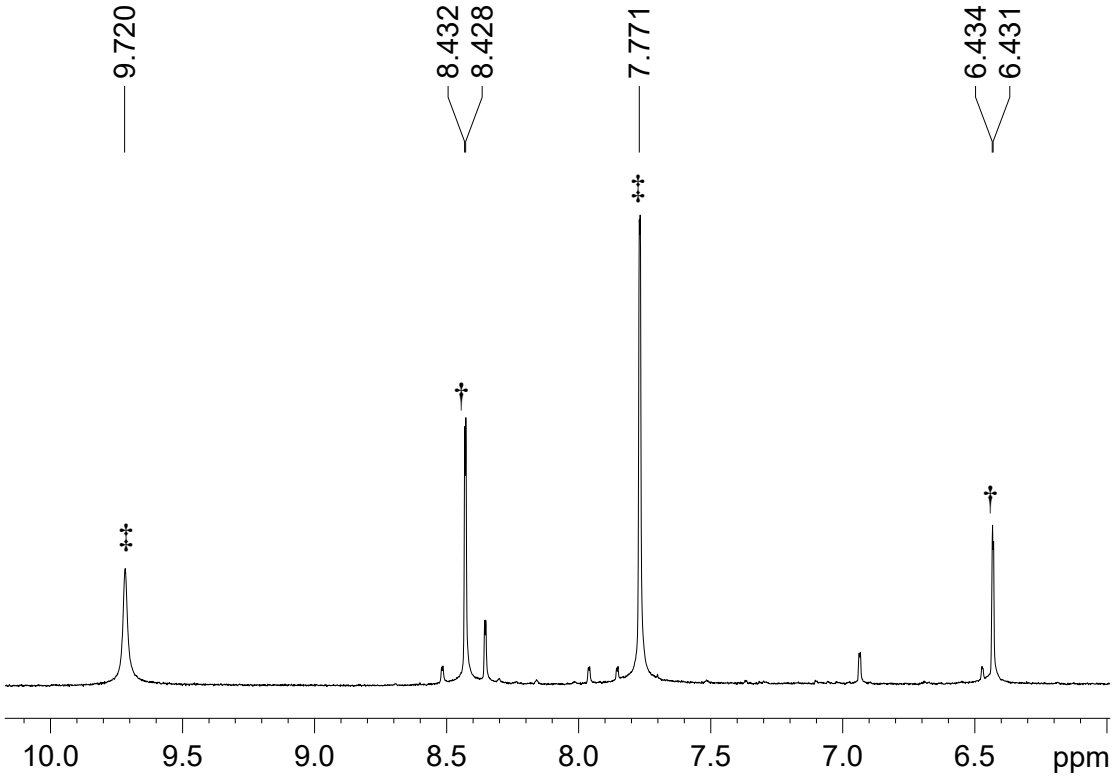

Figure 2.2 ^{1}H NMR spectrum of 1A and imidazolium by-product (d_8-THF, 298 K, 400 MHz)

^{1}H NMR spectroscopy of the crude reaction mixture (high frequency region shown in **Figure 2.2**) showed the evolution of two doublets for a new product, **1A** (†) at δ 8.43 and 6.43 in 1:1 ratio, with each doublet separately integrating in a 1:9 ratio with two new singlets at δ 1.86 and 1.54. The presence of additional signals characteristic of imidazolium salts (‡) were also observed as a broad singlet (δ 9.72) and a broad doublet (δ 7.77) in 1:2 ratio. ^{1}H NMR spectroscopy of subsequent reactions involving the use of 2, 3 or greater excesses of I^{t}Bu$_2$ to $Ru_3(CO)_{12}$ resulted in no additional products to those in **Figure 2.2**. The IR spectrum of **1A** showed eight CO bands. Similarities in these frequencies to other $Ru_3(L)(CO)_{11}$ products, shown in **Table 2.1**, indicated a possible substitution product had formed.

Compound	$\nu_{(CO)}$ / cm^{-1}
$Ru_3(CO)_{12}$[6]	2059, 2027, 2007
Product (1A)	2085, 2034, 2013, 1996, 1984, 1977, 1962, 1943
$Ru_3(PPh_3)(CO)_{11}$[7]	2097, 2046, 2030, 2023, 2014, 1996, 1986, 1972, 1960
$Ru_3(PMe_2Ph)(CO)_{11}$[7]	2092, 2039, 2026, 2010, 1998, 1991, 1980, 1973, 1956
$Ru_3(MeCN)(CO)_{11}$[6]	2098, 2045, 2037, 2021, 2001, 1994, 1972

Table 2.1 IR data for 1A and other Ru_3 compounds

Extraction of **1A** in toluene from the imidazolium salts was followed by recrystallisation from a saturated THF solution layered with hexane to produce dark red X-ray quality crystals which proved to be $Ru_3(aI^tBu_2)(CO)_{11}$ (**Figure 2.3**),[8] which demonstrated the first example of abnormal NHC (aNHC) binding in a ruthenium complex. Structural data for **1A** is discussed separately in **Section 2.2.5**.

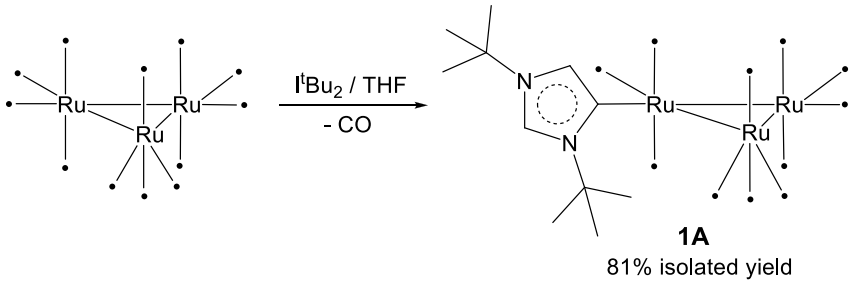

Figure 2.3 Formation of $Ru_3(aI^tBu_2)(CO)_{11}$ (1A)

The ^{1}H NMR spectrum of a crystalline sample of **1A** (**Figure 2.4**) features different proton environments for each imidazol proton and ^{t}Bu group, with the observed coupling (J_{HH} = 1.50 Hz) between the protons at C2 and C5 over four bonds aided by the aromaticity of the ring. Full assignment of ^{1}H NMR resonances was deduced through the use of NOE spectroscopy. As the model in **Figure 2.5** demonstrates, the imidazol proton at the C2-position (H_A) shows a through-space correlation to both ^{t}Bu groups (at N1 and N3), whereas the imidazol proton at the C5-position (H_B) is only in close proximity to the ^{t}Bu group at N1. This is shown in the NOESY spectrum in **Figure 2.5** that displays the correlation of signals between H_A with both sets of ^{t}Bu groups and H_B with only one.

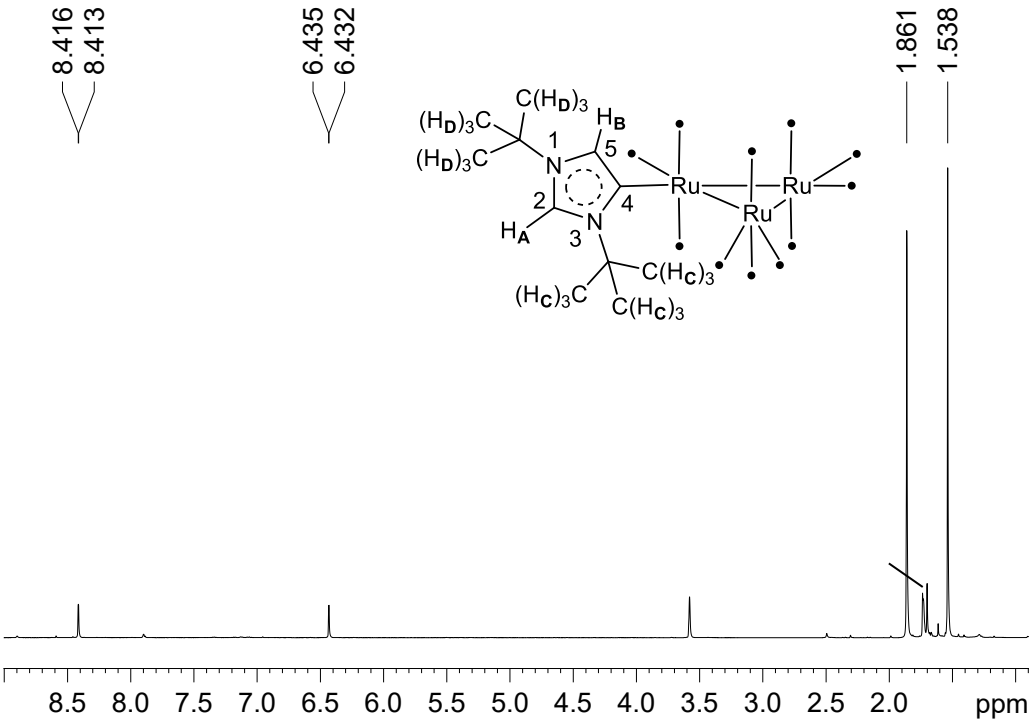

Figure 2.4 ^{1}H NMR spectrum of crystalline 1A (*d*$_8$-THF, 298 K, 500 MHz)

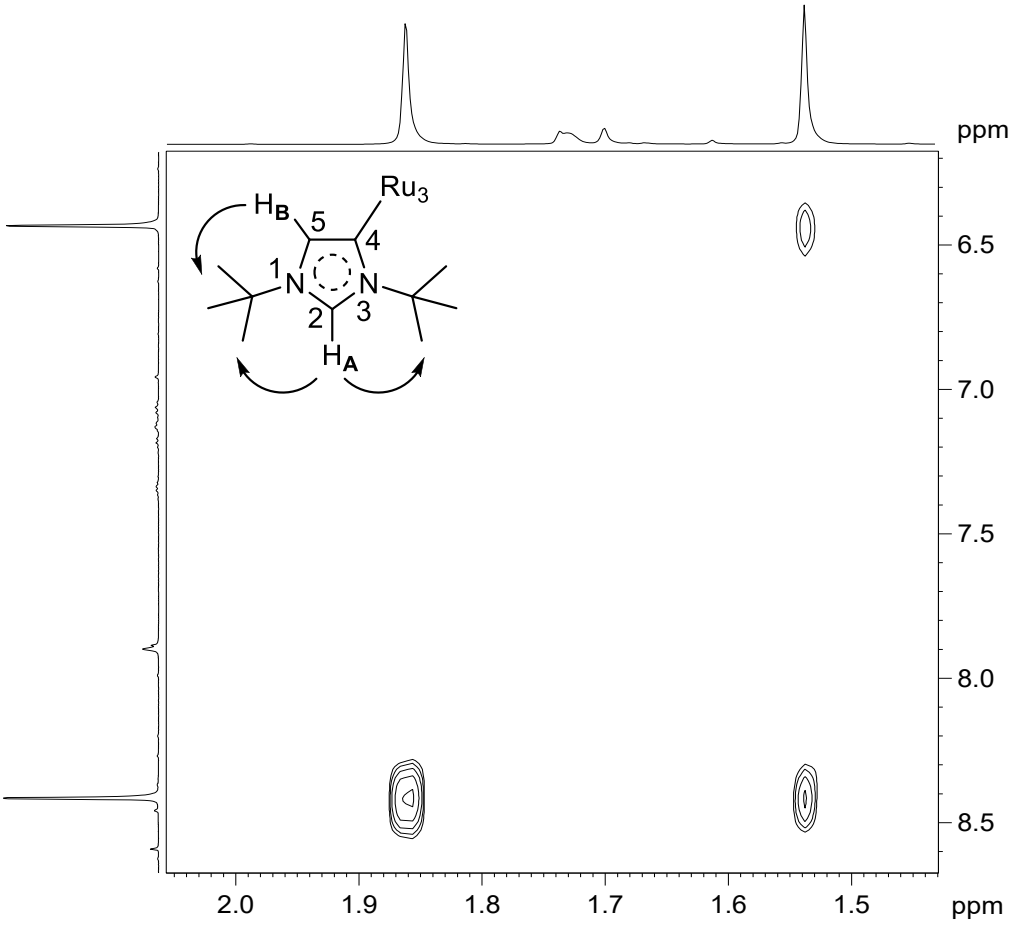

Figure 2.5 NOESY spectrum of 1A (*d*$_8$-THF, 298 K, 500 MHz)

^{13}C NMR resonances of **1A** were assigned through the use of ^{1}H-^{13}C HMQC and HMBC experiments with notable resonances for the imidazol carbons at 134.1 (Ru-*C*4), 132.5 (*C*2) and 130.5 (*C*5). Further to X-ray evidence for the formation of the aNHC structure of **1A**, a ^{13}C NMR chemical shift of δ 134.1 for Ru-C_{NHC} is characteristic of an aNHC complex. As stated in a review by Arnold *et al* where M-C_{NHC} of aNHC complexes are typically located at ca. 140 ppm, normal-NHC complexes are typically located at a higher frequency of ca. 170 ppm.[8]

Compound	Ru-C_{NHC} (δ)	$\nu_{(CO)}$ / cm^{-1}
1A	134.1	2085-1943
$Ru_3(IMe_2)(CO)_{11}$[1]	204.9	2093-1949
$Ru_3(SIEt_2)(CO)_{11}$[2]	198.6	2096-1950

Table 2.2 Ru-C_{NHC} and IR bands of Ru_3-NHC complexes

IR and ^{13}C NMR data for **1A** and normal-NHC Ru_3 cluster compounds from Cabeza and Lappert are presented in **Table 2.2**. The Ru-C_{NHC} resonance for **1A** is located at considerably lower frequency than in both $Ru_3(IMe_2)(CO)_{11}$ and $Ru_3(SIEt_2)(CO)_{11}$ as expected, and IR bands of **1A** are found at lower wavenumber than both normal-NHC compounds which is consistent with the aNHC acting as a stronger σ-donor.[8,9] A comparison of M-C_{NHC} ^{13}C NMR resonances for a variety of related aNHC complexes is shown in **Table 2.3**. In addition the aNHC complexes from the groups of Esteruelas[10] and Nolan[11] show C2/C5 imidazol proton resonances at similar ^{1}H NMR chemical shifts and with similar J_{HH} couplings to **1A**.

Compound	M-$C4_{NHC}$ (δ)	^{1}H of imidazol C2/C5 protons (δ)
1A	134.1	8.42 (d, J_{HH} = 1.50 Hz), 6.43 (d, J_{HH} = 1.50 Hz)
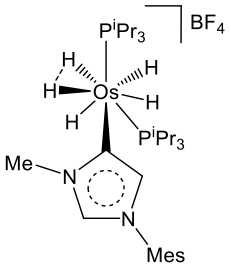	136.3	7.17 (d, J_{HH} = 1.70 Hz), 6.33 (d, J_{HH} = 1.70 Hz).[10]
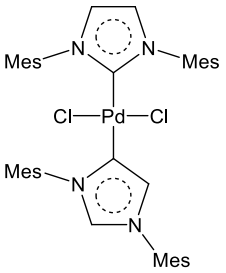	150.7	7.47 (d, J_{HH} = 1.70 Hz), 6.57 (d, J_{HH} = 1.70 Hz).[11]
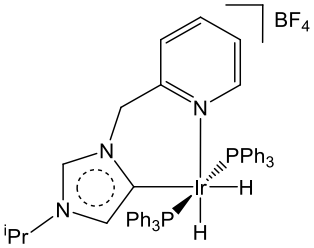	141.1	8.72 (s), 5.17 (s)[12,13]
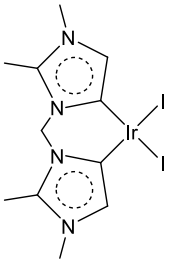	123.1	7.06 (s)[14]
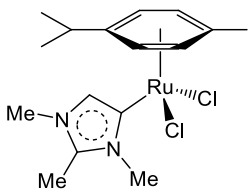	152.2	6.59 (s)[15]

Table 2.3 ^{1}H and ^{13}C NMR resonances for M-aNHC complexes in the literature

2.2.3 $Ru_3(aIAd_2)(CO)_{11}$ (2A)

The reaction of $Ru_3(CO)_{12}$ with I^tBu_2 to form **1A**, coupled with results obtained from the reactions of $Ru_3(CO)_{12}$ with IEt_2Me_2 and $I^iPr_2Me_2$ (see **Section 2.4**) led us to believe that steric bulk of the N-alkyl substituent could be a principle factor for abnormal-NHC binding in this system. $Ru_3(CO)_{12}$ was consequently reacted with IAd_2 to investigate whether $Ru_3(aIAd_2)(CO)_{11}$ could be formed. The choice of IAd_2 was based on its high $\%V_{Bur}$ value (see Nolan's $\%V_{Bur}$ values, **Table 1.1**, **Section 1.3.2**) which was the same as that of I^tBu_2, and a number of literature examples detailing similar behaviour of these two NHCs.[16,17] For example, Nolan *et al* have shown that in the attempted preparation of $Ni(NHC)(CO)_3$ from $Ni(CO)_4$, IAd_2 and I^tBu_2 were the *only* NHCs to generate the sterically encumbered $Ni(NHC)(CO)_2$ complexes instead.[18-20]

Reaction of $Ru_3(CO)_{12}$ with IAd_2 (1:1) in THF led again to the spontaneous evolution of gas, and ^1H NMR spectroscopy of the reaction mixture after 1 hour displayed resonances that were characteristic of the aNHC-complex, $Ru_3(aIAd_2)(CO)_{11}$. Excess IAd_2 again did not lead to the formation of any additional products. Scale-up of the reaction (with extraction in toluene and washing with hexane) and crystallisation from THF/hexane led to the isolation of $Ru_3(IAd_2)(CO)_{11}$ (**2A**) as shown in **Figure 2.6**, which was characterised by X-ray crystallography (structural data discussed in **Section 2.2.5**).

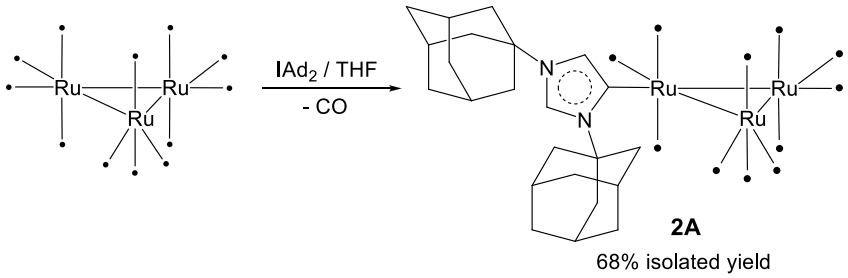

Figure 2.6 Formation of $Ru_3(aIAd_2)(CO)_{11}$ (2A)

The N-adamantyl groups (in the absence of additional inequivalent environments) display three proton environments, expanding outwards from the *ipso*- carbon atom (**Figure 2.7**). The closest are the 2,8,9 positions shown in red for the first $-CH_2$ groups, followed by the 3,5,7 set of -CH groups shown in green and then the furthest 4,6,10 set from the second $-CH_2$ groups shown in blue.

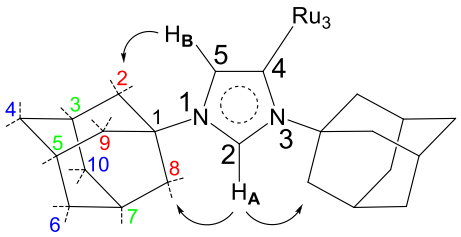

Figure 2.7 Illustration of observed NOESY signals for 2A and assignments of adamantyl protons

As with **1A**, NOE spectroscopy (**Figure 2.8**) was instrumental in assigning the imidazol protons at the C2 (H_A) (δ 2.46) and C5 (H_B) (δ 2.01) positions through correlation to the two closest -CH_2 groups (the $Ad_{2,8,9}$ set).

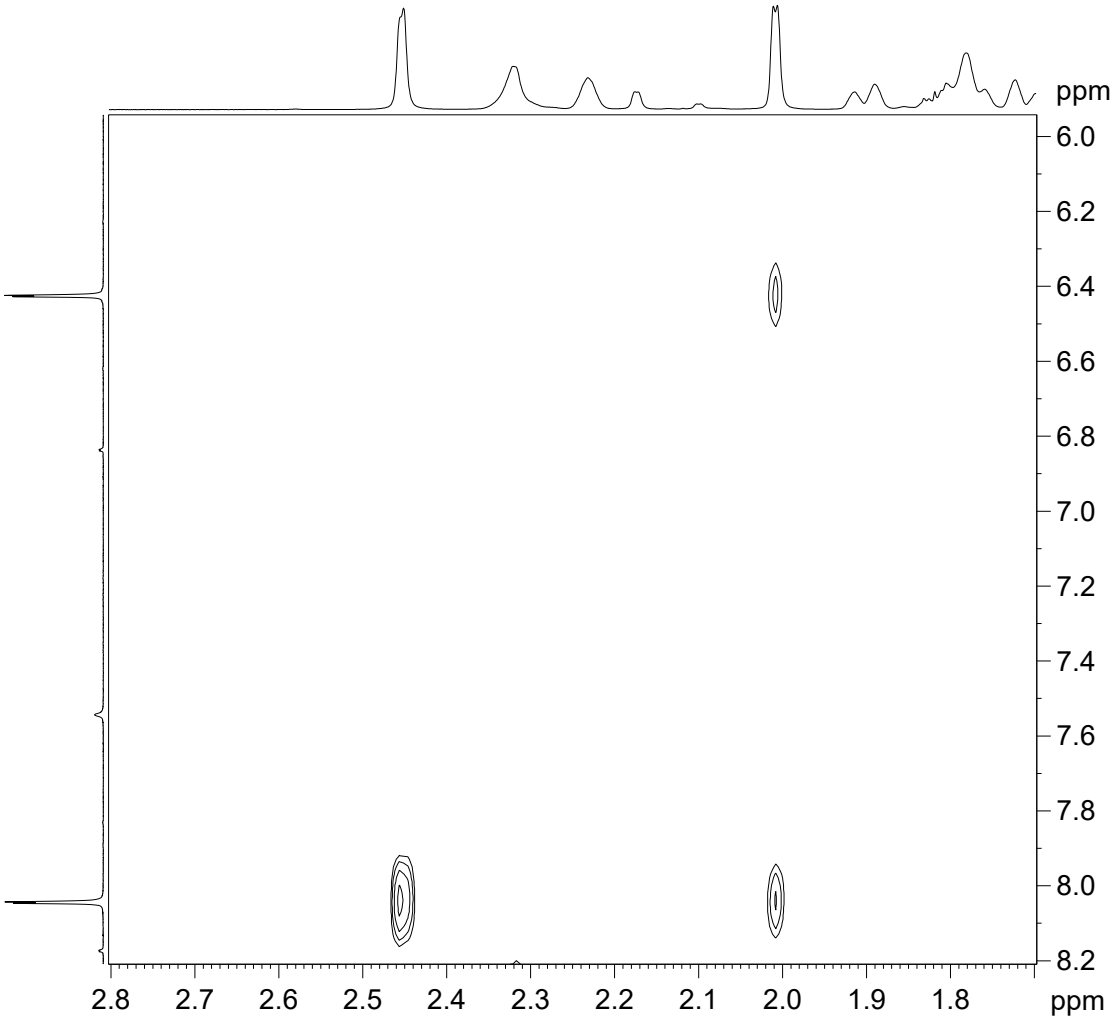

Figure 2.8 NOESY spectrum of 2A (CD_2Cl_2, 298 K, 500 MHz)[21]

Assignment of the $Ad_{3,5,7}$ set of -CH groups was elucidated from $^{13}C\{^1H\}$ PENDANT NMR spectroscopy which showed -CH carbons in a different phase to -CH_2 carbons, and through subsequent use of ^1H-^{13}C HMQC to deduce the corresponding

protons. Remaining proton environments are then represented by the $Ad_{4,6,10}$ set of -CH_2 groups and are shown to be inequivalent, possibly as a result of proximity to the metal centre (**Figure 2.9**). Characteristic ^{13}C NMR resonances for **2A** are located at δ 132.8 (Ru-$C4_{NHC}$) and 130.3 (imidazol $C2/C5$ carbons) which are similar to those found for **1A** and comparable with the literature examples in **Table 2.3**. IR bands for **2A** appear between 2085-1947 cm^{-1} and are essentially identical to those for **1A** (2085-1943 cm^{-1}).

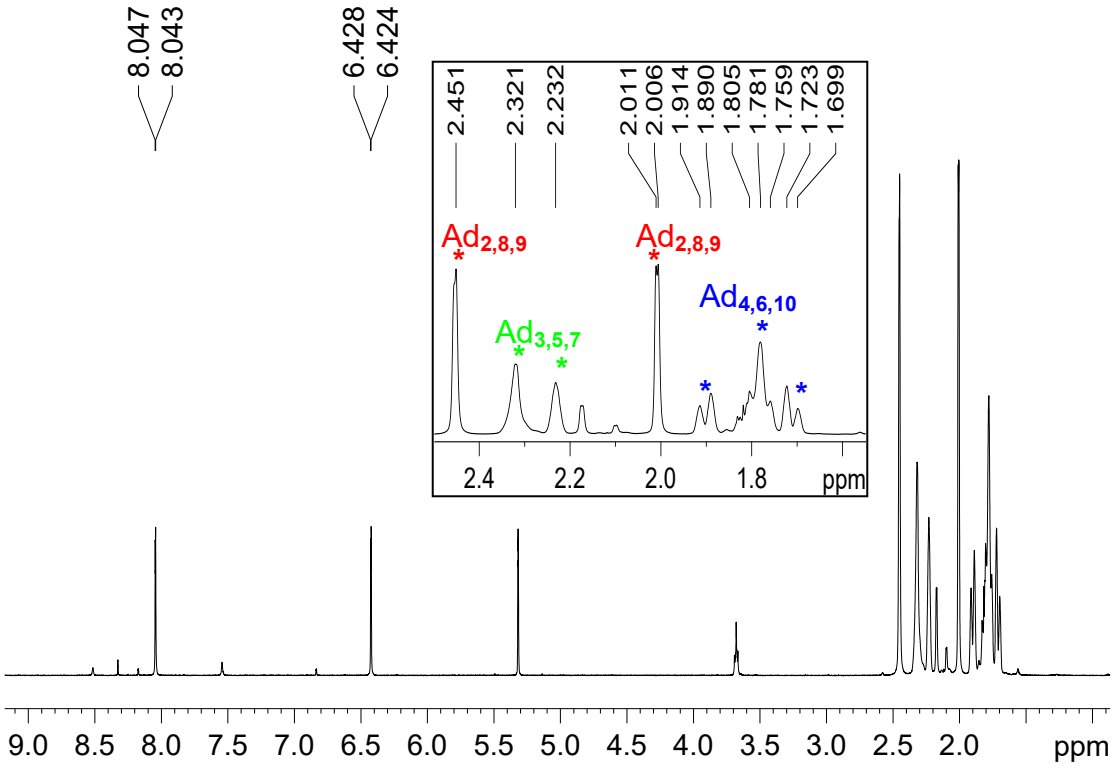

Figure 2.9 ^{1}H NMR spectrum of 2A, with expanded adamantyl signals shown in insert (CD_2Cl_2, 298 K, 500 MHz)

2.2.4 $Os_3(aIAd_2)(CO)_{11}$ (2C)

Following the formation of **1A** and **2A** we sought to investigate if $M_3(aNHC)(CO)_{11}$ complexes were purely restricted to ruthenium, or would also occur with osmium. Unlike in the ruthenium cases, addition of d_8-THF to a J. Youngs NMR tube containing a 1:1 ratio of $Os_3(CO)_{12}$ and IAd_2 did not lead to immediate gas evolution and indeed a ^{1}H NMR spectrum recorded after 2 hours at room temperature confirmed that no reaction had taken place. Subsequent heating at 70 ˚C (3 hours) led to the appearance of two doublets at δ 8.34 and 6.77 attributed to the C4/C5 protons of the aNHC-complex, $Os_3(aIAd_2)(CO)_{11}$ (**2C**). Imidazolium salt was observed (as with **1A** and **2A**), although the low solubility of **2C** in THF at room temperature allowed for the facile removal of imidazolium salts through

washing with THF. Subsequent dissolution of the remaining residue in THF at 70 ˚C[22] and layering with hexane afforded X-ray quality crystals that confirmed the structure (discussed in **Section 2.2.5**) as $Os_3(aIAd_2)(CO)_{11}$ shown in **Figure 2.10**.

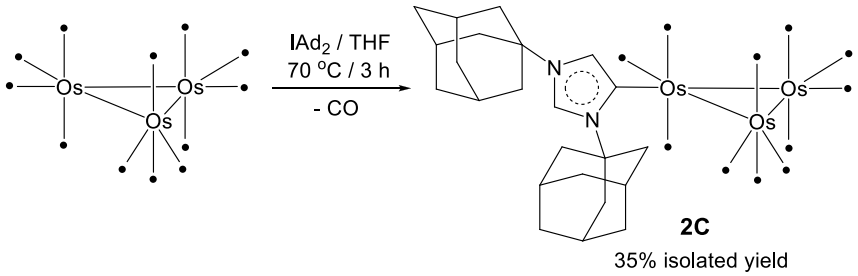

Figure 2.10 Formation of $Os_3(aIAd_2)(CO)_{11}$ (2C)

Subsequent investigations to optimise the yield of **2C** established that heating $Os_3(CO)_{12}/IAd_2$ under argon led to increased imidazolium salt formation compared with reaction in a degassed solution. This led us to deduce that the evolved CO in solution was recombining with **2C** to generate the imidazolium by-product when the mixture was heated (not observed in the synthesis of **1A** and **2A** to the same extent, as no heating was required). The general synthesis of **2C** therefore incorporates an argon purge to remove liberated CO and increase product yield. $Os_3(CO)_{12}$ is known to be less soluble and contain stronger M-CO bonds than $Ru_3(CO)_{12}$,[23] although it is not clear if heating is required to overcome the energy barrier to reaction or to permit the solvation of $Os_3(CO)_{12}$.

^1H NMR assignment was completed as for **2A**, with NOE spectroscopy used to assign imidazol protons at the C2 (H_A) and C5 (H_B) positions through correlation with $Ad_{2,8,9}$ doublets at δ 2.55 and 2.10 (**Figure 2.11**). $^{13}C\{^1H\}$ PENDANT spectroscopy distinguished the $Ad_{3,5,7}$ set through difference in phase polarisation by the use of a ^1H-^{13}C HMQC correlation experiment, with remaining ^1H NMR signals therefore attributed to $Ad_{4,6,10}$ protons.

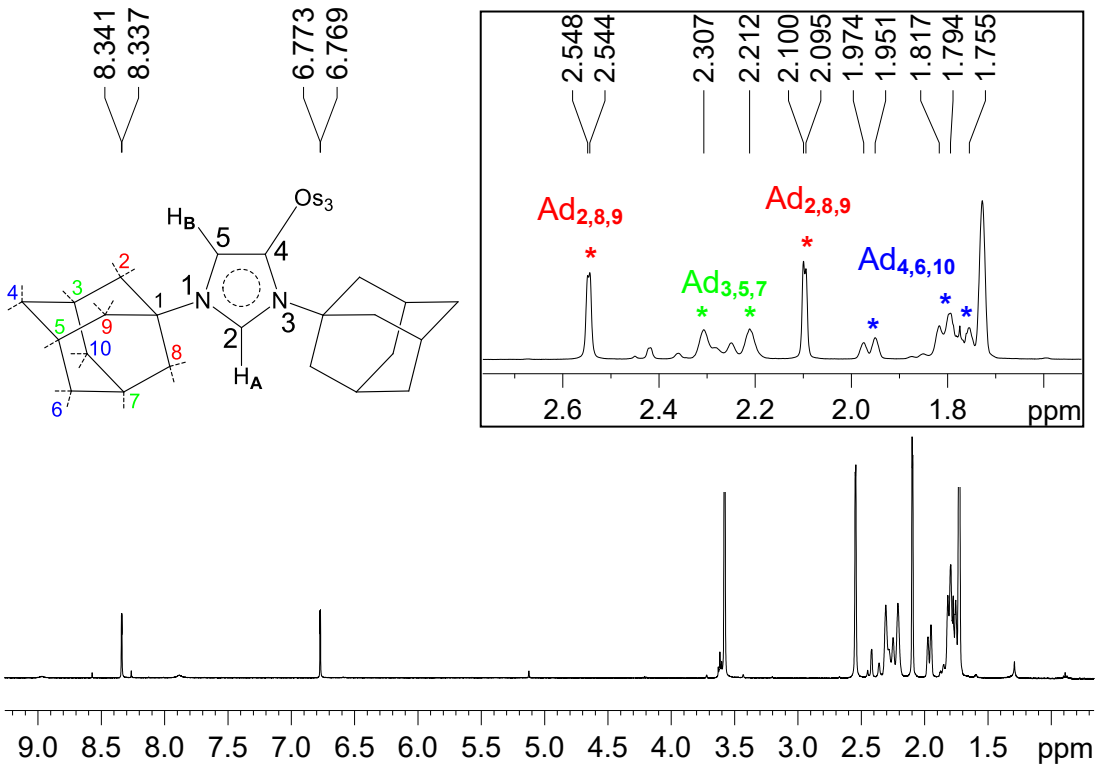

Figure 2.11 ^{1}H NMR spectrum of 2C, with expanded adamantyl signals shown in insert (d_8-THF, 298 K, 500 MHz)

The ^{13}C NMR resonances of **2C** were assigned by ^{1}H-^{13}C HMQC/HMBC spectroscopy, with the relevant NHC resonances located at δ 135.8 (*C*5), 131.4 (*C*2) and 111.6 (Os-*C*4). The ^{13}C NMR signal of the coordinated carbenic carbon (Os-*C*4) at δ 111.6 was significantly lower than the values of ca. δ 130 found for **1A** and **2A**. This value was established by ^{1}H-^{13}C HMBC spectroscopy, shown in **Figure 2.12** which correlates this signal with the imidazol proton at C2 (H_A). In addition, there is correlation between imidazol C2(H_B) and C5(H_A) positions shown in **Figure 2.12**, demonstrated by two doublets (J_{HC} = 140 Hz) resulting from the one bond (C-H) coupling. During the course of this work, the analogous complex $Os_3(aI^tBu_2)(CO)_{11}$ was synthesised by Ellul in the Whittlesey group. This was also found to display a very low Os-*C*4 ^{13}C NMR resonance, at δ 113.5.

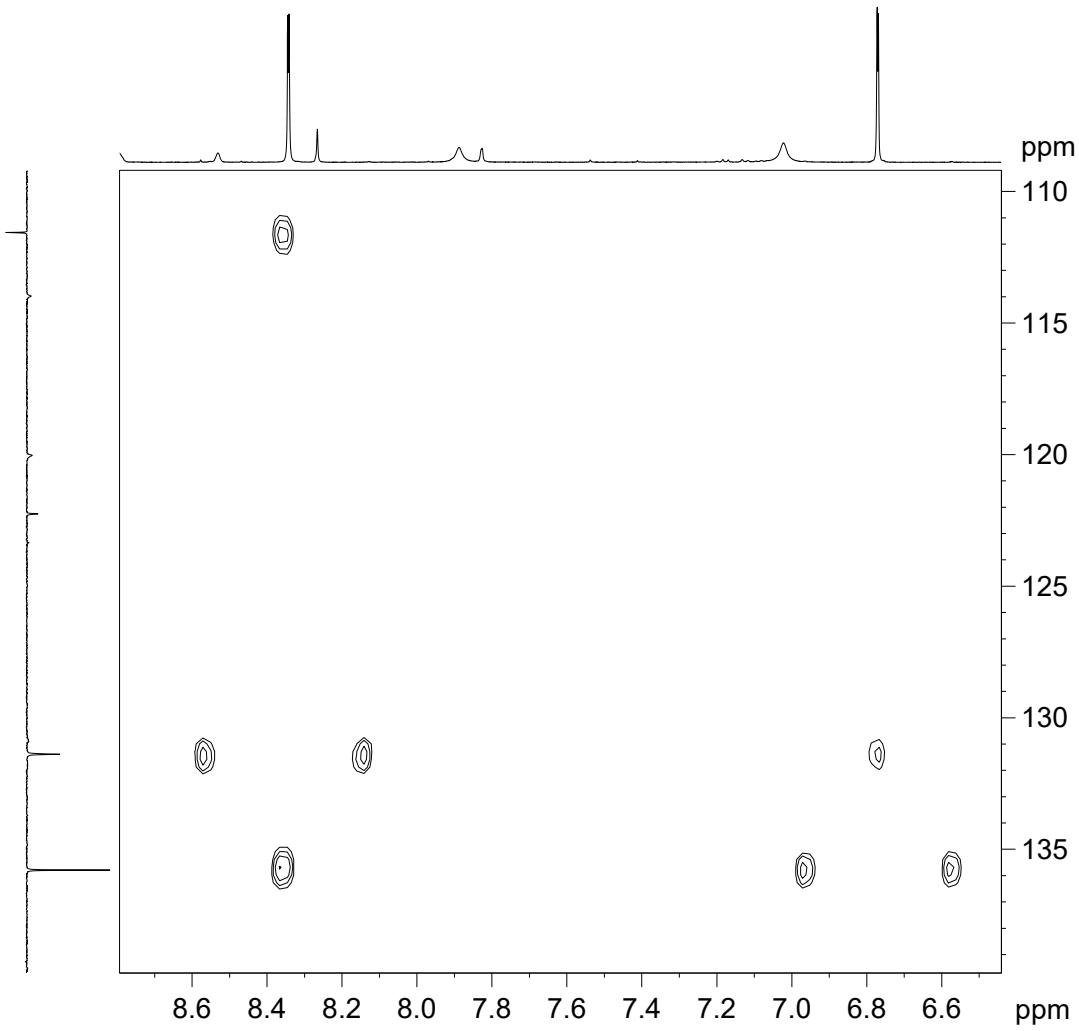

Figure 2.12 ^{1}H-^{13}C HMBC spectrum of 2C (d_8-THF, 298 K, 500/126 MHz)

$Os_3(aI^tBu_2)(CO)_{11}$ and **2C** display IR bands over a slightly wider frequency range than those of **1A** and **2A** (**Table 2.4**) in addition to lower wavenumbers than for phosphine and normal-NHC containing congeners.

Compound	M-C_{NHC} (δ)	$\nu_{(CO)}$ / cm^{-1}
$Ru_3(aI^tBu_2)(CO)_{11}$ (1A)	134.1	2085-1943
$Ru_3(aIAd_2)(CO)_{11}$ (2A)	132.8	2085-1947
$Os_3(aIAd_2)(CO)_{11}$ (2C)	111.6	2094-1927
$Os_3(aI^tBu_2)(CO)_{11}$[24]	113.5	2093-1923
$Os_3(IMe_2)(CO)_{11}$[25]	- [a]	2102-1941
$Os_3(PPh_3)(CO)_{11}$[6]	n/a	2108-1956

[a] M-C_{NHC} not quoted.

Table 2.4 M-C_{NHC} ^{13}C NMR and IR bands of $M_3(L)(CO)_{11}$ complexes (L = NHC, aNHC, PR_3)

2.2.5 Structural comparisons of 1A, 2A and 2C

This section compares the crystal structures of **1A**, **2A** and **2C** with each other and related complexes. $M_3(aNHC)(CO)_{11}$ complexes throughout this section are orientated as shown in **Figure 2.13**, with atom labelling following the order shown. M_1 is the metal atom (Ru or Os) directly bonded to C_{NHC}, with M_{TRANS} and M_{CIS} representing the metal atoms *trans*- and *cis*- to the main C_{NHC}-M_1 bond.

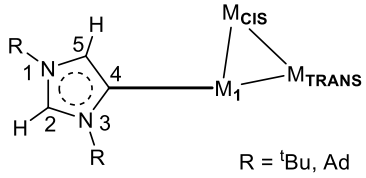

Figure 2.13 Numbering model used for X-ray structural descriptions

Most references to atoms (C4 or N3 for example) are exclusively mentioned with respect to the model in **Figure 2.13**, whereas atom references containing a number in brackets, i.e. 'C(7)' are with reference to crystallographic labelling as in the structures in **Figure 2.14**, **2.15** and **2.16**, with complete bond lengths and angles for these given in the **Appendices**.

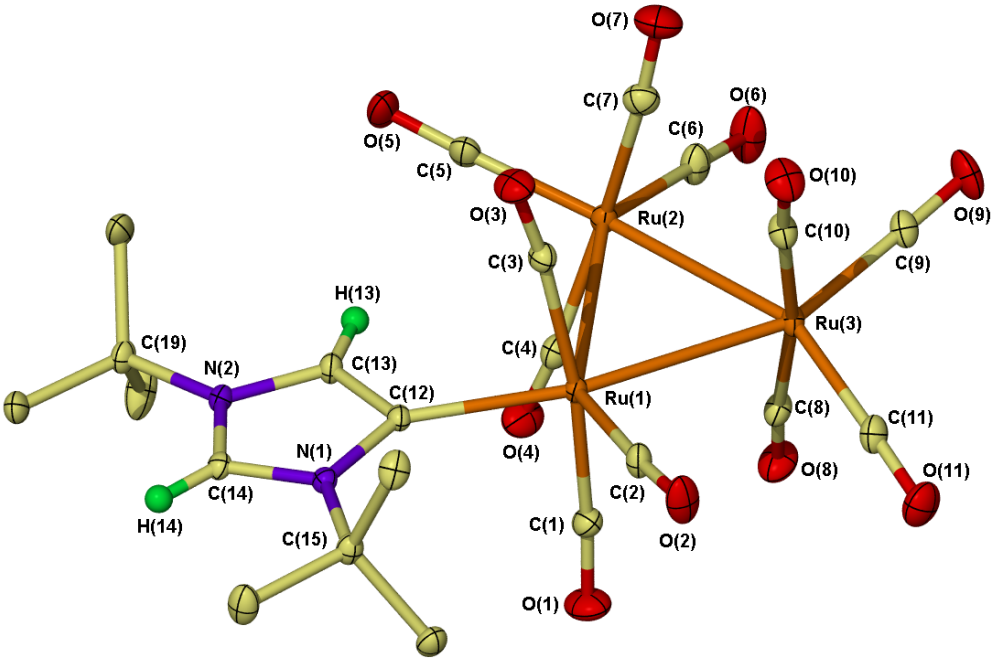

Figure 2.14 Crystal structure of $Ru_3(aI^tBu_2)(CO)_{11}$ (1A) with thermal ellipsoids set to 30% probability and hydrogen atoms (except those on the imidazol ring) removed for clarity

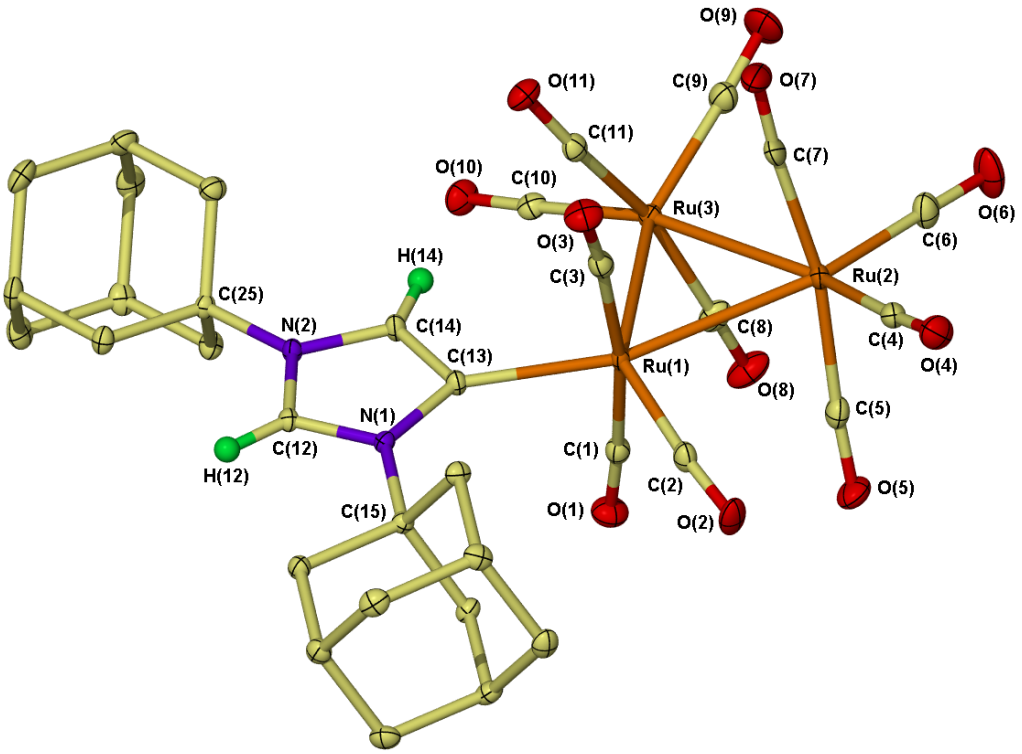

Figure 2.15 Crystal structure of $Ru_3(aIAd_2)(CO)_{11}$ (2A) with thermal ellipsoids set to 30% probability and hydrogen atoms (except those on the imidazol ring) removed for clarity

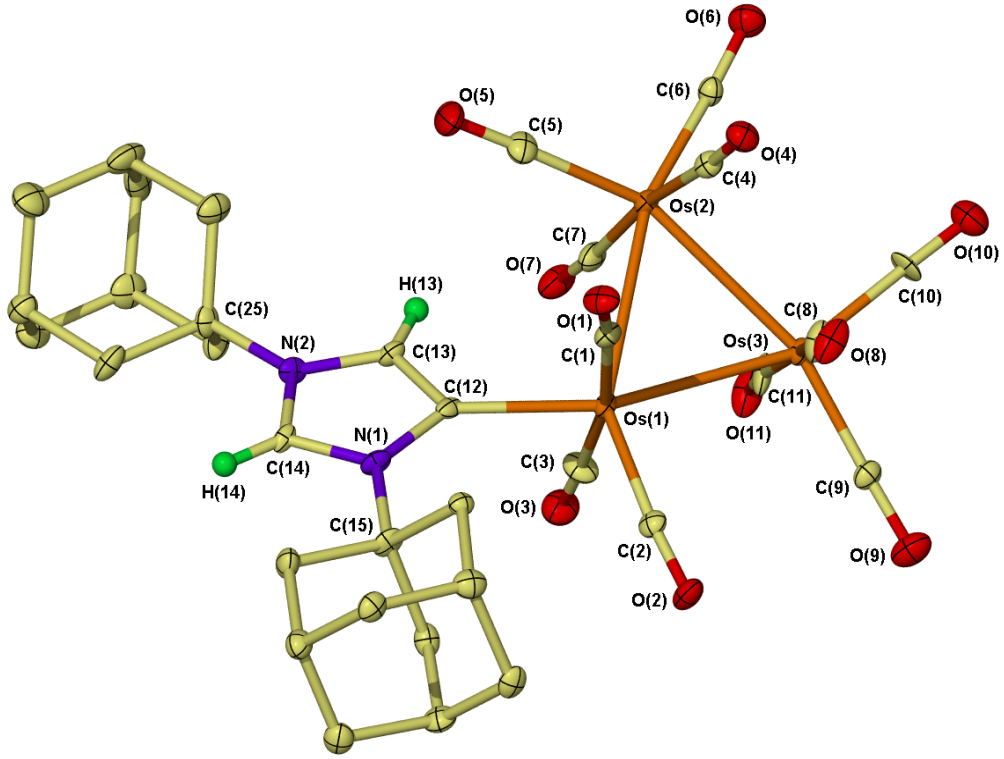

Figure 2.16 Crystal structure of $Os_3(aIAd_2)(CO)_{11}$ (2C) with thermal ellipsoids set to 30% probability and hydrogen atoms (except those on the imidazol ring) removed for clarity

The crystal structures of **1A**, **2A** and **2C** are shown in **Figures 2.14**, **2.15** and **2.16** respectively, with the aNHC ligand occupying in each case an equatorial site on the M_3 ring. This geometry is expected for generic $M_3(L)(CO)_{11}$ complexes, as steric interactions are minimised.[26] The angle between the plane of the M_3 core and the imidazol ring represents the most salient difference between complexes **1A**, **2A** and **2C** as the acute angles of 9.8˚ (**1A**) and 8.5˚ (**2A**) contrast with the appreciably larger value of 36.7˚ for **2C** (**Figure 2.17**). These angles contrast with the value of 9.1˚ for $Os_3(aI^tBu_2)(CO)_{11}$, indicating that the angle in **2C** is not a phenomenon only associated with osmium. The substantial twisting of the heterocycle with respect to the M_3 ring in **2C** stems from the relative orientation of the axial carbonyl ligands on M_1 and M_{CIS}, where a torsion angle for **2C** of +27˚ (O(1)-Os(1)-Os(2)-O(4)) compares with a torsion angle of -24˚ for **2A** (O(3)-Ru(1)- Ru(3)-O(11)).

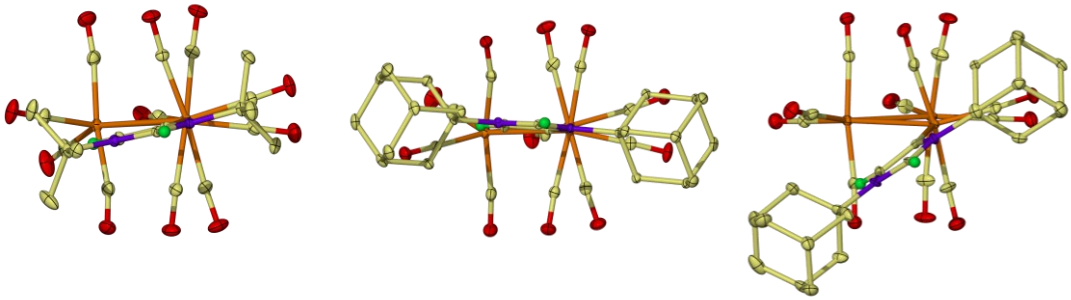

Figure 2.17 M_3-imidazol twist as viewed along the C_{NHC}-M_1 bond for 1A, 2A and 2C

Pertinent bond lengths and angles for **1A**, **2A** and **2C** (as well as $Os_3(aI^tBu_2)(CO)_{11}$)[24] are shown in **Table 2.5**. The Ru_1-C_{NHC} bond lengths in **1A** and **2A** are indistinguishable and are found to be comparable with the distance of 2.144(3) Å reported in the normal-NHC complex $Ru_3(IMes)(CO)_{11}$,[25] but longer than that for $Ru_3(IMe_2)(CO)_{11}$ (2.115(4) Å).[1] It appears the reduced steric bulk in moving from IMes to IMe_2 induces a closer interaction with the Ru_3 core. The Os_1-C_{NHC} bond lengths of **2C** and $Os_3(aI^tBu_2)(CO)_{11}$ are the same and are comparable with values of 2.116(9) Å in $Os_3(IMe_2)(CO)_{11}$[25] and aNHC osmium compounds synthesised by Esteruelas (2.120(4) and 2.123(6) Å)[10,27] and Clyburne (2.121(12) Å).[28]

Bond Lengths (Å) / Angles (˚)	**1A**	**2A**	**2C**	**$Os_3(aI^tBu_2)(CO)_{11}$[24]**
M_1-C_{NHC}	2.151(2)	2.150(2)	2.128(12)	2.161(6)
M_1-M_{TRANS}	2.8456(3)	2.8384(3)	2.8831(8)	2.8658(3)
M_1-M_{CIS}	2.8835(3)	2.8989(3)	2.9051(8)	2.9054(3)
M_{CIS}-M_{TRANS}	2.8504(3)	2.8613(3)	2.8911(5)	2.8773(3)
C_{NHC}-M_1-C_{CO}(eq)	108.12(10)	109.68(10)	107.7(5)	108.0(3)
C_{NHC}-M_1-M_{TRANS}	162.97(7)	162.76(6)	159.6(3)	161.53(16)
C_{NHC}-M_1-M_{CIS}	104.03(7)	103.51(6)	102.9(3)	102.59(16)
M-M_1-M	59.670(7)	59.818(6)	59.930(13)	59.806(8)
M-M_{TRANS}-M	60.825(7)	61.141(6)	60.41(2)	60.781(8)
M-M_{CIS}-M	59.505(7)	59.041(6)	59.66(2)	59.413(8)

Table 2.5 Bond lengths (Å) and angles (˚) for 1A, 2A, 2C and $Os_3(aI^tBu_2)(CO)_{11}$

The aNHC ligands in complexes **1A**, **2A**, **2C** and $Os_3(aI^tBu_2)(CO)_{11}$ are located in approximately the same position as the CO ligand of the parent $M_3(CO)_{12}$ structures. This is demonstrated by C_{NHC}-M_1-M_{TRANS} and C_{NHC}-M_1-M_{CIS} angles of ca. 161˚ and 102˚ respectively for all compounds in **Table 2.5**, that closely match angles for the equivalent CO ligand in $Ru_3(CO)_{12}$ (159˚ and 99˚)[29] and $Os_3(CO)_{12}$ (159˚ and 100˚).[30] It is therefore clear that the steric influence of the aNHC ligand acts to push the geminal equatorial CO ligand of M_1 to a C_{NHC}-M_1-C_{CO}(eq) angle of around 108˚, which is greater than those found in $Ru_3(CO)_{12}$ (ca. 104˚) and $Os_3(CO)_{12}$ (ca. 103˚) and also the related PPh_3 complexes; $Ru_3(PPh_3)(CO)_{11}$ (102.6(8)˚)[31] and $Os_3(PPh_3)(CO)_{11}$ (101.8(3)˚).[32]

The M_1-M_{CIS} distances for all complexes in **Table 2.5** are generally longer than the two M_1-M_{TRANS} and M_{CIS}-M_{TRANS} bond lengths due to steric interactions between the aNHC ligand and the closest CO group on the adjacent metal atom (M_{CIS}). As a consequence, the M-M_{TRANS}-M angle is slightly greater than the M-M_1-M and M-M_{CIS}-M angles in these complexes, resulting from elongation of the M_1-M_{CIS} bond (**Figure 2.18**). For example, in **1A** a distance of 2.8835(3) Å for M_1-M_{CIS} is longer than those of M_1-M_{TRANS} (2.8456(3) Å) and M_{CIS}-M_{TRANS} (2.8504(3) Å). In addition, an angle of 60.825(7)˚ for M-M_{TRANS}-M represents the largest angle of the three (M-M_1-M = 59.670(7)˚, M-M_{CIS}-M = 59.505(7))˚ in the Ru_3 ring. This comparison can be demonstrated against the more uniform M-M bond

lengths found in $Ru_3(CO)_{12}$ at 2.8595(4), 2.8518(4) and 2.8512(4) Å with M-M-M angles of 59.92(1), 59.90(1) and 60.18(1)°[29] and for $Os_3(CO)_{12}$ (2.8824(5), 2.8752(5) and 2.8737(5) Å with angles of 59.88(1), 59.93(1) and 60.18(1)°).[30]

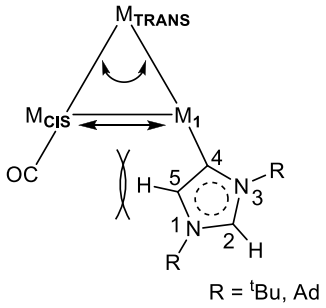

Figure 2.18 Model showing the lengthening of the M_1-M_{CIS} bond and widening of the M-M_{TRANS}-M angle with the sterically bulky aNHC ligand

2.3 Formation of $M_3(\mu\text{-H})(aNHC)'(CO)_9$ complexes

2.3.1 Introduction

The formation of complexes **1A** and **2A** at room temperature led us to investigate if bond activation of I^tBu_2 and/or IAd_2 ligands would occur upon heating as was seen by Cabeza for $Ru_3(IMe_2)(CO)_{11}$ (**Figure 2.19**)[1]

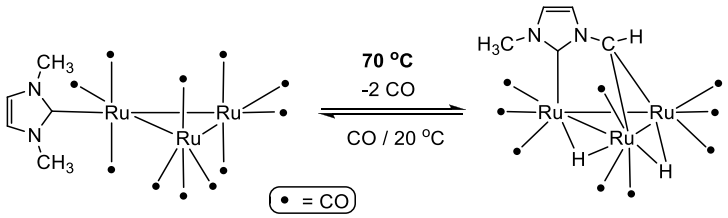

Figure 2.19 Double C-H bond activation of $Ru_3(IMe_2)(CO)_{11}$ upon heating

2.3.2 $Ru_3(\mu\text{-H})(al^tBu_2)'(CO)_9$ (1B)

Heating of a d_8-THF solution of **1A** at 50 ˚C led to a gradual decrease in the resonances (***** in **Figure 2.20**) by ^{1}H NMR spectroscopy, until only a trace amount was detectable after approximately 11 hours. Simultaneously the evolution of signals attributed to a new compound (**1B**, † in **Figure 2.20**) and imidazolium salt (‡ in **Figure 2.20**) were observed.

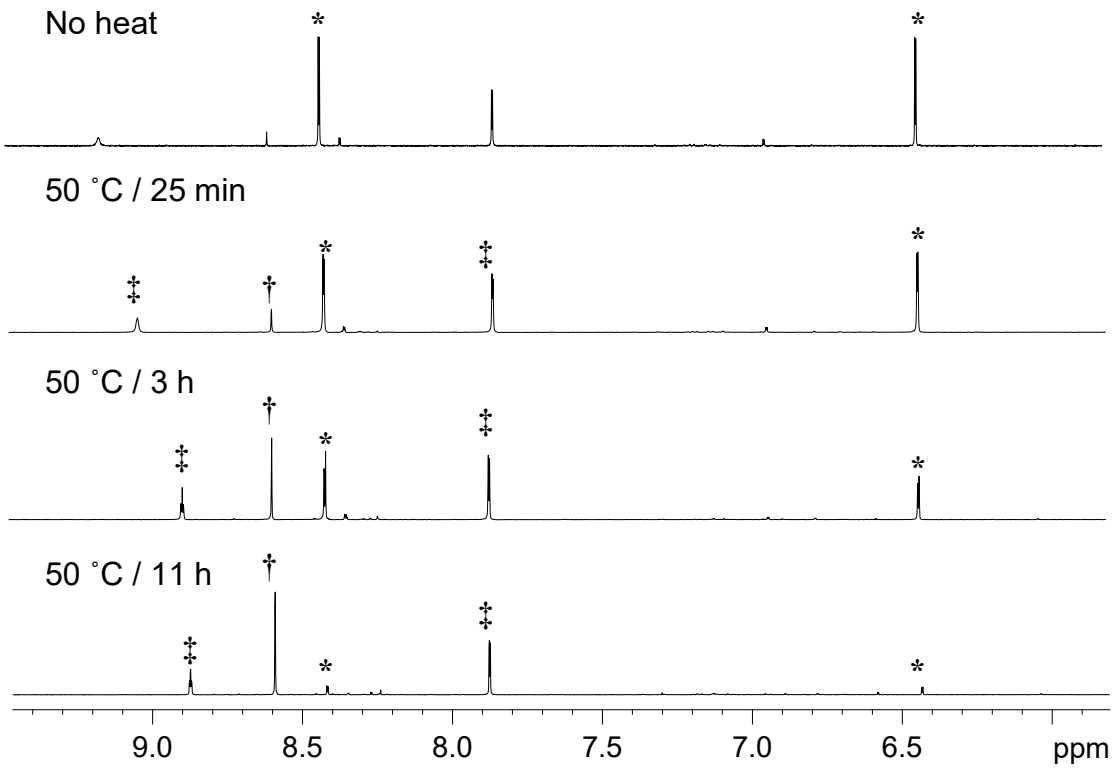

Figure 2.20 ^{1}H NMR spectra demonstrating the effects of heating 1A at 50 ˚C in THF over 11 hours (d_8-THF, 298 K, 500 MHz)

Singlet resonances for **1B** at δ 8.59, 1.74 and -17.85 integrated in a 1:18:1 ratio, with the signal at δ -17.85 characteristic for a hydridic proton environment. Indeed, subsequent separation of **1B** by toluene extraction from imidazolium salts, washing with hexane and laying from THF/hexane yielded X-ray quality crystals revealed through crystallographic studies to be $Ru_3(\mu\text{-}H)(aI^tBu_2)'(CO)_9$ (**1B**, **Figure 2.21**). $Ru_3(\mu\text{-}H)(aI^tBu_2)'(CO)_9$ was formed from **1A** upon thermally induced C-H activation of the C5 imidazol proton, with the loss of two CO molecules. This represents the first example in the literature of this binding mode for an NHC.

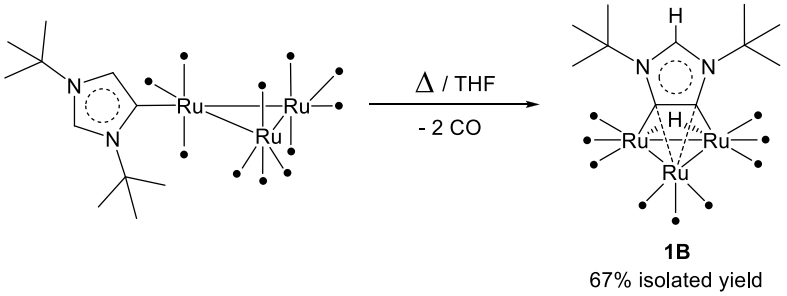

Figure 2.21 Formation of $Ru_3(\mu\text{-}H)(aI^tBu_2)'(CO)_9$ (1B)

The ^{1}H NMR spectrum of a crystalline sample of **1B** (**Figure 2.22**) shows equivalent environments for the ^{t}Bu protons at 298 K, with no changes observed upon cooling to 223 K. $^{13}C\{^{1}H\}$ PENDANT NMR spectroscopy of **1B** was used to assign resonances for *C*2 and *C*4/*C*5 imidazol positions at δ 144.0 and 139.4 respectively.

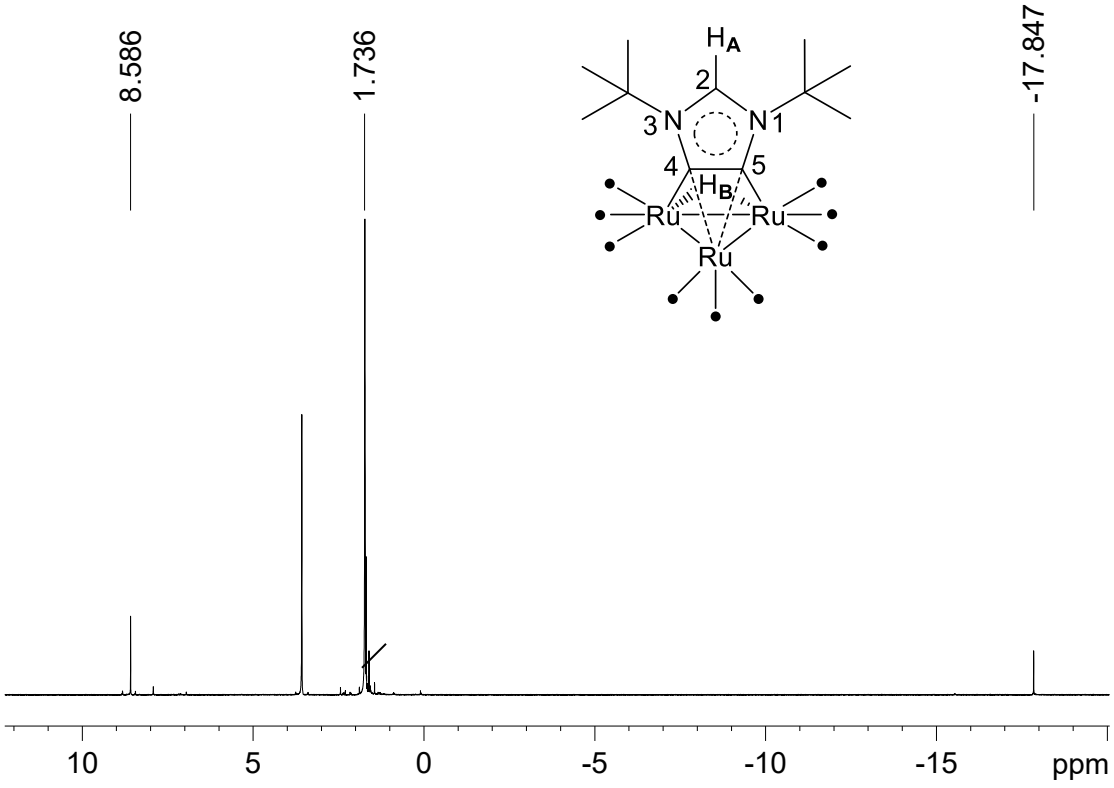

Figure 2.22 ^{1}H NMR spectrum of 1B (d_8-THF, 298 K, 400 MHz)

The structure of **1B** (**Figure 2.23**) can be described as zwitterionic with an overall electron count of 48. The bonding motif of the aI^{t}Bu$_2$' ligand consists of two main types of interaction. Firstly, the heterocyclic ring bridges over two Ru atoms, with imidazol C4 and C5 atoms forming two σ-bonds with the two Ru atoms. Secondly, a π-interaction from the C4-C5 multiple-bond toward the remaining apical Ru atom relays a substantial tilt of the heterocyclic ring over the Ru$_3$ core of 73.2˚. Overall the C4 and C5 carbon atoms of the activated aI^{t}Bu$_2$ ligand occupy axial sites above all three ruthenium atoms, exhibiting a 5centre-4electron (5c-4e) binding mode with the Ru$_3$ ring, the metrics of which are discussed in more detail in **Section 2.3.3**.

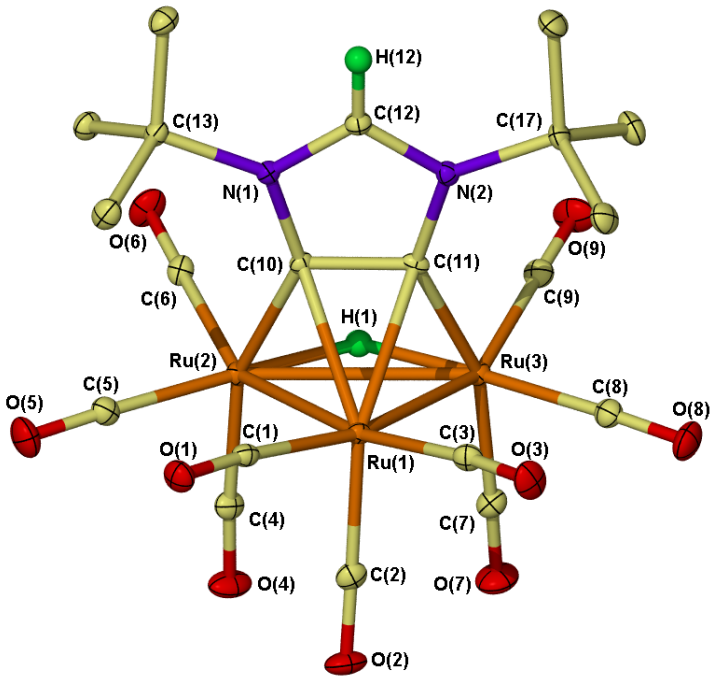

Figure 2.23 Crystal structure of $Ru_3(\mu\text{-}H)(aI^tBu_2)'(CO)_9$ (1B) with thermal ellipsoids set to 30% probability and hydrogen atoms (except at C2 and the bridging hydride) removed for clarity

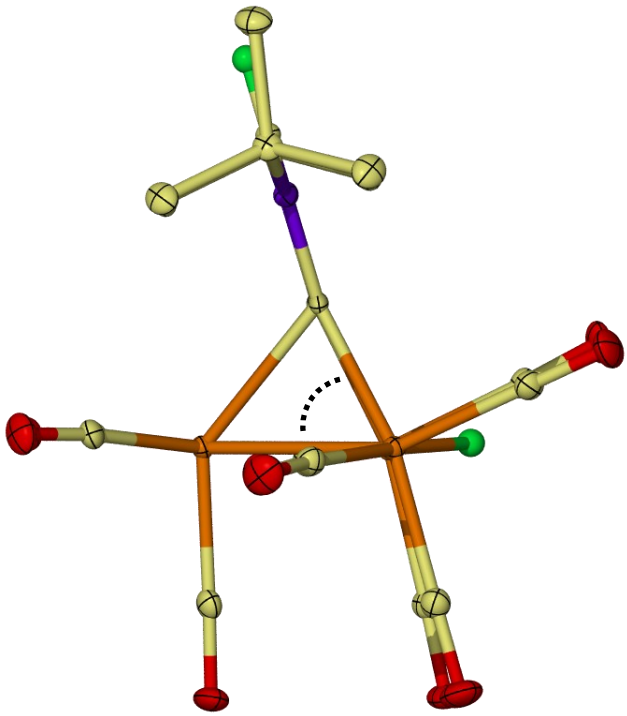

Figure 2.24 Profile of $Ru_3(\mu\text{-}H)(aI^tBu_2)'(CO)_9$ (1B) crystal structure demonstrating tilting of the imidazol ring towards the apical Ru atom (thermal ellipsoids set to 30% probability)

Addition of 1 atm CO to a degassed solution of **1B** in d_8-THF resulted in no reformation of **1A** at ambient or elevated (70 ˚C) temperatures over a number of days. ^{1}H NMR spectroscopy instead revealed a gradual reduction in resonances for **1B** and an increase in signals for imidazolium salts upon heating of the solution. The reformation of Ru_3 clusters into higher nuclearity complexes in the presence of NHC ligands has been described in detail by Cabeza, and this process was found to be accelerated with heating. In one example[25] Cabeza describes formation of $[Ru_6(\mu_3\text{-}CO)_2(\mu\text{-}CO)_2(CO)_{14}]^{2-}[IPrH]_2^+$ from heating $Ru_3(CO)_{12}$ with IPr, which led us to propose that a similar species may explain the existence of imidazolium signals observed by ^{1}H NMR spectroscopy when heating **1B** under CO. As two molecules of CO are evolved when **1A** is heated to form **1B**, reinvestigation of this method allowed us to optimise the route through use of an argon purge to remove evolved CO, which led to an increased yield of **1B** (now in 5 hours at 70 ˚C) with a simultaneous decrease in imidazolium salt formation.

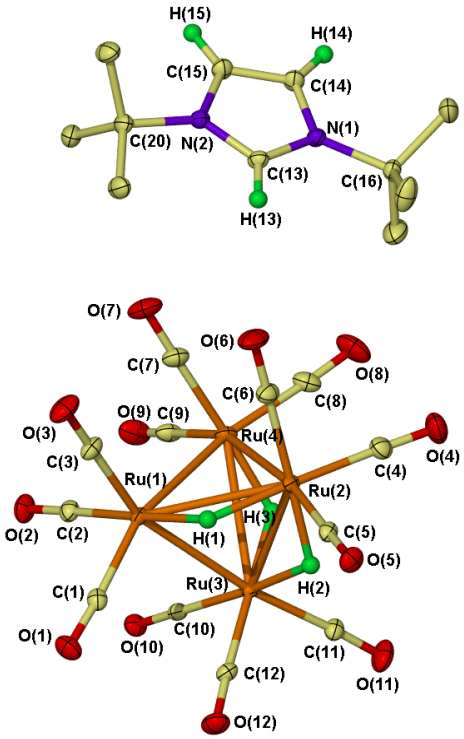

Figure 2.25 Crystal structure of $[Ru_4(\mu\text{-}H)_3(CO)_{12}]^-[I^tBu_2H]^+$ with thermal ellipsoids set to 30% probability and hydrogen atoms (except hydrides and imidazol protons) omitted for clarity

Thermolysis of **1B** with 1 atm H_2 generated significant amounts of imidazolium salts as observed by ^{1}H NMR spectroscopy, in addition to new hydride resonances at δ -12.5 and -17.0. Upon crystallisation of the solution from THF/hexane after 40 hours at 50 ˚C the cluster compound $[Ru_4(\mu\text{-}H)_3(CO)_{12}]^-[I^tBu_2H]^+$ was structurally characterised

(**Figure 2.25**). This anionic tetraruthenium complex contains three bridging hydride ligands and an imidazolium cation resulting from the elimination of aI^{t}Bu$_2$' by the addition of two molecules of H_2 overall. Formation of the Ru_4 core must result from a cluster condensation reaction similar to that observed by Cabeza,[25] and would explain why integration of imidazolium salts against hydride signals never led to a correlation, as other proton-silent cluster products must be present.

2.3.3 $Ru_3(\mu\text{-}H)(aIAd_2)'(CO)_9$ (2B)

Thermolysis of **2A** at 70 ˚C in THF for 5 hours under an argon purge led to the observation of one major product by ^{1}H NMR spectroscopy with resonances (δ 8.55 and -17.77 in 1:1 ratio) characteristic of those for $Ru_3(\mu\text{-}H)(aIAd_2)'(CO)_9$. The product (**2B**) was extracted from trace imidazolium salts in toluene and recrystallised by the slow evaporation of a concentrated CH_2Cl_2 solution[33] to yield X-ray quality crystals that confirmed the structure as $Ru_3(\mu\text{-}H)(aIAd_2)'(CO)_9$. Assignment of three adamantyl environments for $Ad_{2,8,9}(H_B)$, $Ad_{3,5,7}(H_C)$ and $Ad_{4,6,10}(H_D)$ (**Figure 2.26**) was completed by NOE spectroscopy. Pertinent ^{13}C NMR resonances of **2B** were located at δ 143.1 (*C*2) and 137.8 (*C*4/*C*5), with adamantyl protons assigned through the use of ^{1}H-^{13}C HMBC/HMQC spectroscopy.

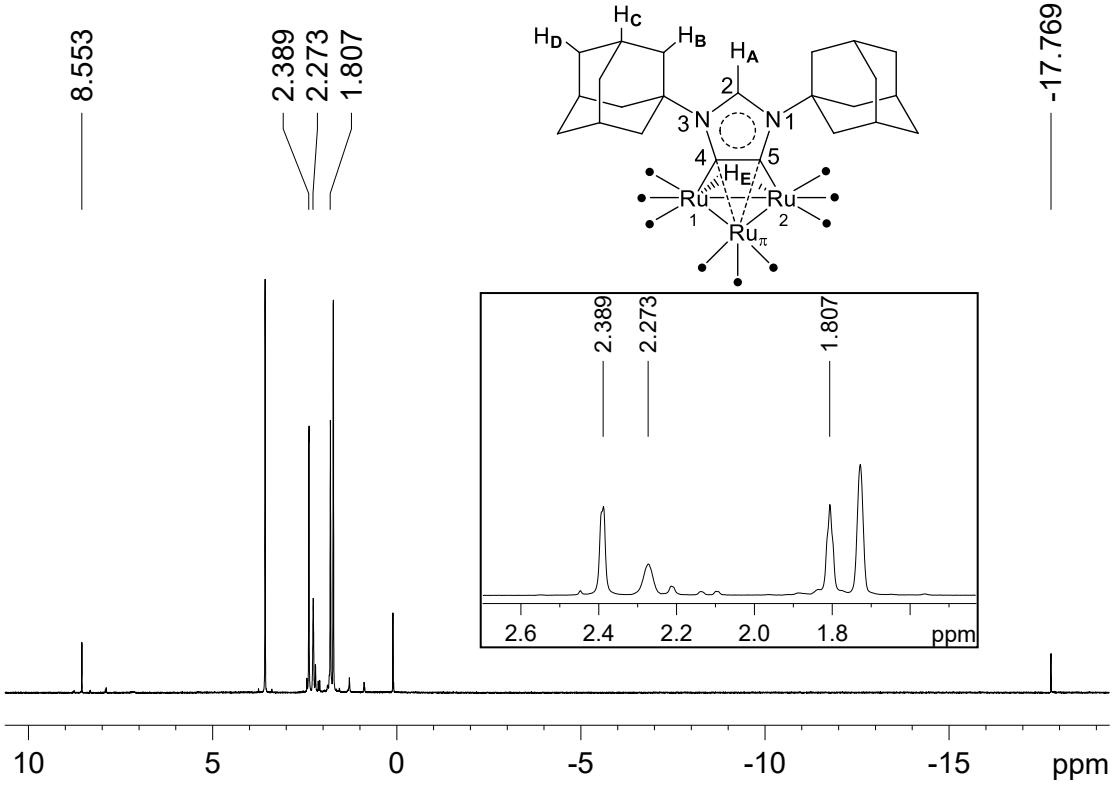

Figure 2.26 ^{1}H NMR spectrum of crystalline 2B (d_8-THF, 298 K, 400 MHz)

The crystal structure of **2B** (**Figure 2.27**) displays many similarities to that of **1B**, the most palpable of which is a tilt angle of the NHC ring over the Ru_3 core of 73.1˚ and 73.2˚ respectively. Pertinent bond lengths and angles of the two compounds are presented in **Table 2.6**, with atom labelling following the model shown. The 5c-4e bonding interaction is very similar for both complexes, for example C4-Ru_1/C5-Ru_2 σ-bonds for **1B** (2.102(3) / 2.109(3) Å) and **2B** (2.111(2) / 2.096(2) Å) are the same, as are the C4-Ru_π/C5-Ru_π bond lengths for the π-interaction (**1B** = 2.339(2) / 2.324(3) Å, **2B** = 2.338(2) / 2.326(2) Å). C_4-Ru_1-Ru_π/C_5-Ru_2-Ru_π bond angles for **1B** (56.31(7) / 55.76(7)˚) and **2B** (56.06(6) / 56.07(6)˚) also affirm the similarities between the two complexes. Comparison with the ideal angle for axial CO ligands in $Ru_3(CO)_{12}$ (87.70(13)-90.57(14)˚),[29] demonstrates the significance of the π-interactions in **1B** and **2B**. Overall these bond lengths/angles demonstrate that the 5c-4e bonding motif appears to be essentially independent of the nature of the aNHC' N-substituents. A substantial lengthening is observed in the Ru_3 core of the Ru_1-Ru_2 bond in **1B** (2.9739(3) Å) and **2B** (2.9639(2) Å) compared with the distances for Ru_1-Ru_π (**1B** = 2.7183(3) Å, **2B** = 2.7270(2) Å) and Ru_2-Ru_π (**1B** = 2.7235(3) Å, **2B** = 2.7137(2) Å) as a result of the bridging imidazol and hydride ligands across this bond.

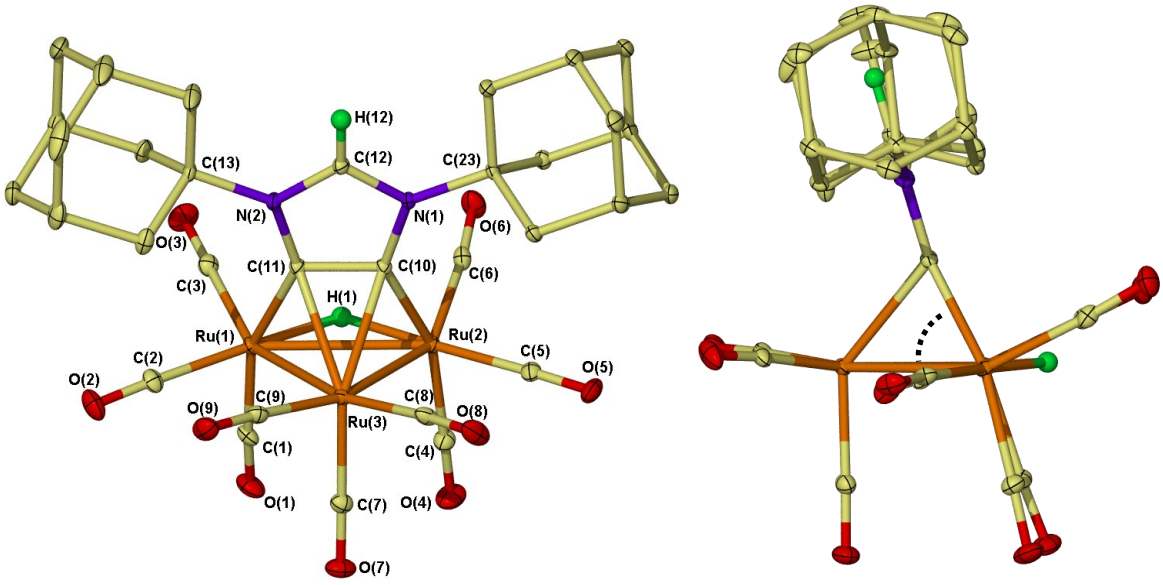

Figure 2.27 Crystal structure of $Ru_3(\mu\text{-}H)(aIAd_2)'(CO)_9$ (2B) with thermal ellipsoids set to 30% probability and hydrogen atoms (except at C2 and the bridging hydride) removed for clarity

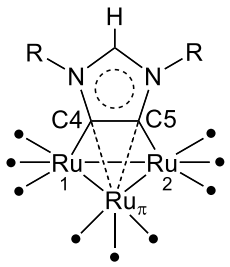

R = ^{t}Bu, Ad

Bond Lengths (Å) / Angles (˚)	$Ru_3(\mu\text{-}H)(aI^tBu_2)'(CO)_9$ (1B)	$Ru_3(\mu\text{-}H)(aIAd_2)'(CO)_9$ (2B)
C4-Ru$_1$ / C5-Ru$_2$	2.102(3) / 2.109(3)	2.111(2) / 2.096(2)
C4-Ru$_\pi$ / C5-Ru$_\pi$	2.339(2) / 2.324(3)	2.338(2) / 2.326(2)
Ru$_1$-Ru$_2$	2.9739(3)	2.9639(2)
Ru$_1$-Ru$_\pi$ / Ru$_2$-Ru$_\pi$	2.7183(3) / 2.7235(3)	2.7270(2) / 2.7137(2)
C$_4$-Ru$_1$-Ru$_\pi$	56.31(7)	56.06(6)
C$_5$-Ru$_2$-Ru$_\pi$	55.76(7)	56.07(6)
C$_4$-Ru$_1$-Ru$_2$	68.37(7)	68.34(6)
C$_5$-Ru$_2$-Ru$_1$	67.92(7)	68.32(6)

Table 2.6 Bond lengths (Å) and angles (˚) for 1B and 2B

The 5c-4e bonding mode of **1B** and **2B** draw structural similarities to a class of 48 electron, 5c-5e compounds involving bridging μ_3-η^2 imino groups over $Ru_3(CO)_9$ clusters with a bridging hydride ligand. Two examples (metrics presented in **Table 2.7**) include those developed by the groups of Rosenberg (Imino-A)[34-36] and Süss-Fink (Imino-B), [37] which contain a localised C=N double bond that binds in a similar manner to the C4-C5 bond of the delocalised imidazol ring in **1B** and **2B**. The C=N bond bridges over Ru_1-Ru_2 forming σ-bonds between C-Ru_1 and N-Ru_2 (with a hydride ligand bridging Ru_1-Ru_2 also) and with π-donation towards Ru_π. The μ_3-η^2 imino groups in Imino-A and Imino-B are generally found to exhibit comparable, but slightly shorter bond distances for σ-bonds (2.038(5)-2.093(4) Å) and π-interactions (2.230(4)-2.275(6) Å) with the Ru_3 core, than in **1B**/**2B** (σ: 2.096(2)-2.111(2) Å; π: 2.324(3)-2.339(2) Å). These shorter bond lengths result in the C=N bond lying slightly closer to the Ru_3 plane as C/N-Ru_1-Ru_π angles of 53.7(1)-54.2(2)˚ compared with 55.76(7)-56.31(7)˚ in **1B**/**2B** suggest. These results indicate an increased σ- and π-contribution from the imino ligands to the Ru_3 ring which may result from the more localised π-bond in the imino group compared with the aNHC'

ligand. The Ru_1-Ru_2 bonds of Imino-A and Imino-B are significantly longer than the Ru_1-Ru_π and Ru_2-Ru_π distances, as was observed also for **1B** and **2B**.

Bond Lengths (Å) / Angles (˚)	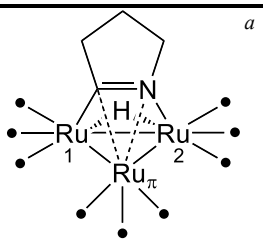 Imino-A [a]	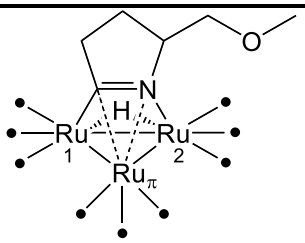 Imino-B
C-Ru₁ / N-Ru₂	2.07(1) / 2.07(1)	2.038(5) / 2.093(4)
C-Ruπ / N-Ruπ	2.26(1) / 2.26(1)	2.275(6) / 2.230(4)
Ru₁-Ru₂	3.018(1)	2.971(1)
Ru₁-Ruπ / Ru₂-Ruπ	2.709(1) / 2.709(1)	2.754(1) / 2.698(1)
C-Ru₁-Ruπ	54.43	54.2(2)
N-Ru₂-Ruπ	54.43	53.7(1)

[a] Refinement based on equal populations of C and N in the C=N bond.[34]

Table 2.7 Bond lengths (Å) and angles (˚) of Ru_3-μ_3-η^2 imino groups from Rosenberg and Süss-Fink

The IR bands of **1B**/**2B** and Imino-A/B are shown in **Table 2.8** and indicate a larger concentration of electron density on the Ru_3 clusters in **1B** and **2B**.

Compound	$\nu_{(CO)}$ / **cm^{-1}**
1B	2072, 2042, 2024, 2002, 1981, 1968, 1944, 1932
2B	2070, 2044, 2013, 1994, 1966, 1944
Imino-A	2092, 2066, 2061, 2037, 2022, 2010, 2006, 1999, 1981, 1975
Imino-B	2090, 2060, 2032, 2010, 2002, 2000, 1998, 1971

Table 2.8 IR bands of 1B, 2B, Imino-A and Imino-B

2.3.4 Attempted isolation of $Os_3(\mu\text{-}H)(aIAd_2)'(CO)_9$

Heating of **2C** at 70 ˚C in d_8-THF for three hours resulted in no new hydride signals observed by ^{1}H NMR spectroscopy, indicating no formation of $Os_3(\mu\text{-}H)(aIAd_2)'(CO)_9$. Heating of the same solution at 120 ˚C for 1 hour saw evolution of a hydride signal at δ -18.29 which integrated in a 1:1 ratio with a new resonance at δ 8.58 which may be attributed to $Os_3(\mu\text{-}H)(aIAd_2)'(CO)_9$ († in **Figure 2.28**). This compound is however always formed as a trace product, with the majority of **2C** forming imidazolium salts which are suspected to be cluster condensation compounds analogous to

$[Ru_6(\mu_3\text{-}CO)_2(\mu\text{-}CO)_2(CO)_{14}]_2^-[ImH]_2^+$ or $[Ru_4(\mu\text{-}H)_3(CO)_{12}]^-[ImH]^+$ explained in **Section 2.3.2**. Similar results were observed by Ellul in the Whittlesey group, on thermolysis of $Os_3(aI^tBu_2)(CO)_{11}$.

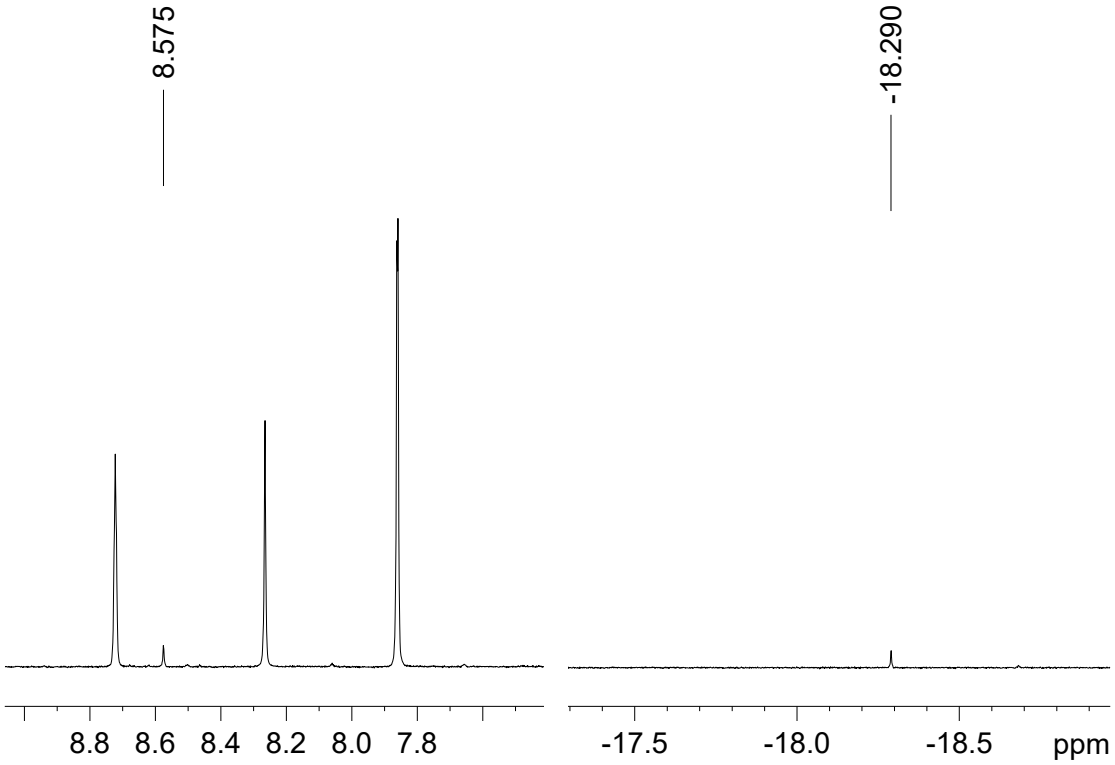

Figure 2.28 ^{1}H NMR spectrum of 2C heated at 120 ˚C in THF for 1 hour (d_8-THF, 298 K, 500 MHz)

Rosenberg *et al* have described the isolation of a 5c-5e Os_3-imino complex[38] analogous to the imino complexes discussed in **Section 2.3.3**, which display similar binding motifs to those of **1B** and **2B**. We propose therefore that a 5c-4e binding mode would be stable for osmium as well as for ruthenium and that $Os_3(\mu\text{-}H)(aIAd_2)'(CO)_9$ was likely to be the product observed in **Figure 2.28**. Unequivocal confirmation of $Os_3(\mu\text{-}H)(aIAd_2)'(CO)_9$ will however require an alternative higher yielding synthetic route.

2.4 Formation of $Ru(NHC)_2(CO)_3$ complexes

2.4.1 Introduction

We have shown from the reactions of $Ru_3(CO)_{12}$ with I^tBu_2 and IAd_2 that NHCs may bind abnormally if the N-substituents are sufficiently large. Cabeza has shown on the other hand that normal NHC binding will occur if N-substituents are small, such as in IMe_2.[1] In this section, the reactions of $Ru_3(CO)_{12}$ with IEt_2Me_2, $I^iPr_2Me_2$ and I^iPr_2 ligands are described to

investigate the effects of NHCs containing N-substituents of a size between those described by Cabeza and ourselves (**Figure 2.29**).[24,39] In addition, both IEt_2Me_2 and $I^iPr_2Me_2$ contain methyl groups at the C4/C5 positions which should prevent abnormal binding, whereas I^iPr_2 is used to directly compare the effects of steric bulk of the N-substituents with I^tBu_2.

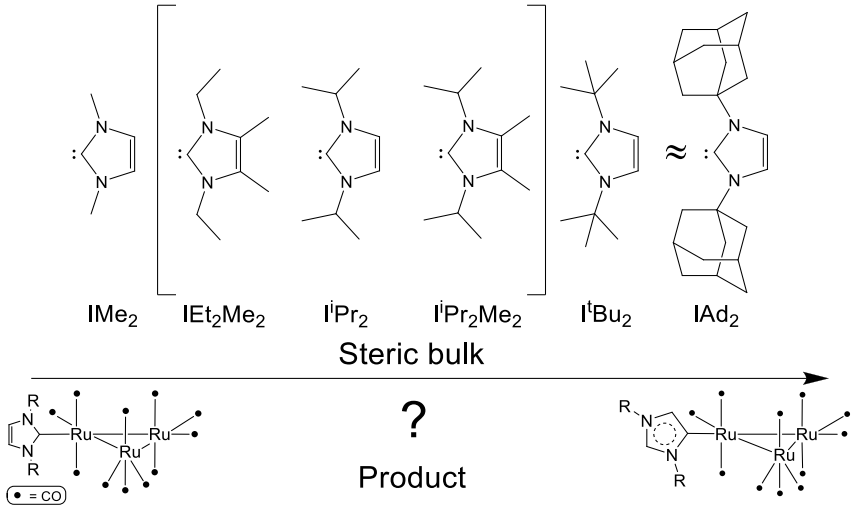

Figure 2.29 Schematic relating steric bulk of NHCs with observed products thus far

2.4.2 $Ru(IEt_2Me_2)_2(CO)_3$ (3A)

The addition of d_8-THF to two J. Youngs NMR tubes containing IEt_2Me_2 and $Ru_3(CO)_{12}$ in 1:1 and 1:5 ratios resulted in the spontaneous evolution of gas for ca. 30 minutes. On cessation of bubbling, ^{1}H NMR spectroscopy revealed an absence of free IEt_2Me_2 signals in each case and the presence of one new set of resonances attributed to a product, **3A**. Subsequent reaction of 1:6 $Ru_3(CO)_{12}$ to IEt_2Me_2 in a J. Youngs ampoule followed by washing with hexane and recrystallisation from THF/hexane afforded crystals of **3A** that were characterised by crystallographic studies to be *trans*-$Ru(IEt_2Me_2)_2(CO)_3$ (**Figure 2.30**). This cluster-degradation product is of the expected *trans*-NHC geometry for $Ru(NHC)_2(CO)_3$ complexes[40] and is comparable in structure to *trans*-$Ru(IMes)_2(CO)_3$ and *trans*-$Ru(ICy_2)_2(CO)_3$ previously isolated by our group upon addition of CO to $Ru(IMes)_2(CO)H(OH)$ and $Ru(ICy_2)_2(PPh_3)(CO)H_2$ respectively.[41,42] Crystallographic details of the structure of **3A** are discussed in **Section 2.4.6**.

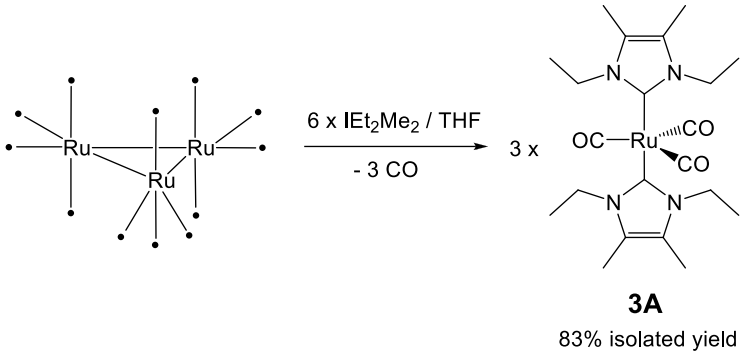

Figure 2.30 Formation of *trans*-Ru(IEt$_2$Me$_2$)$_2$(CO)$_3$ (3A)

The ^{1}H NMR spectrum for **3A** in d_8-THF (**Figure 2.31**) contains resonances located at δ 4.43 (H_A), 2.17 (H_B) and 1.22 (H_C) which indicated equivalent proton environments at ambient temperature for both NHC ligands.

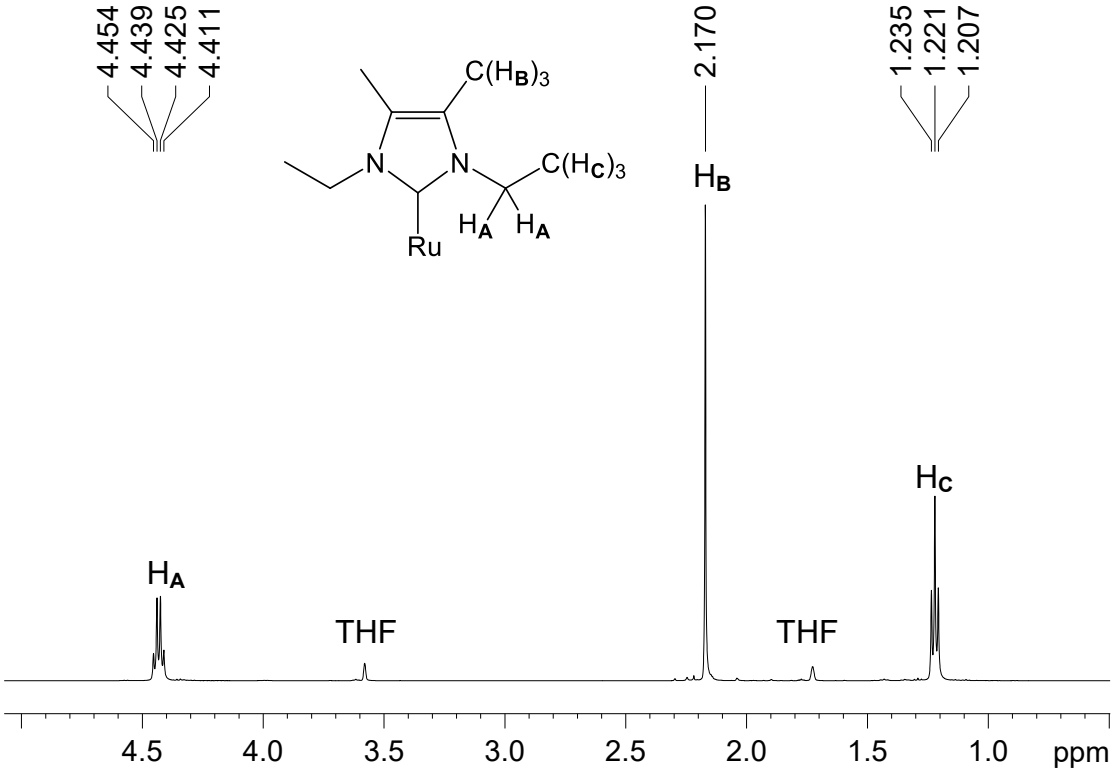

Figure 2.31 ^{1}H NMR spectrum of crystalline 3A (d_8-THF, 298 K, 500 MHz)

Upon cooling a d_8-THF solution of **3A**, these signals broadened and then split into two separate signals below ca. 230 K (**Figure 2.32**). Integration of the two H_C resonances at all temperatures failed to suggest inequivalent NHCs or restricted rotation of only one conformer, as whole integers were not observed. For example, the integration was 1:1.7 at 210 K, and this suggested the presence of different conformers of **3A** in solution. NOE spectroscopy at 200 K showed exchange between the split signals, indicating the

complex was still fluxional at this temperature. The addition of 1 atm of CO to the sample at 210 K in an attempt to impede this fluxionality resulted in no change to the spectrum. Interestingly, further variable temperature ^{1}H NMR spectroscopic studies in d_8-toluene (**Figure 2.32**) resulted in broadening but no splitting of the proton resonances, implying that the solution behaviour of **3A** in d_8-THF may be a solvent based effect. Further variable temperature studies were undertaken in d_5-pyridine to study the effects of **3A** in a more Lewis-basic solvent (**Figure 2.33**). Splitting of ^{1}H NMR resonances was observed again for the quartet (H_A) and triplet (H_C) signals in d_5-pyridine, although the singlet of the back-bone CH_3 groups (H_B) did not appear to broaden or split.

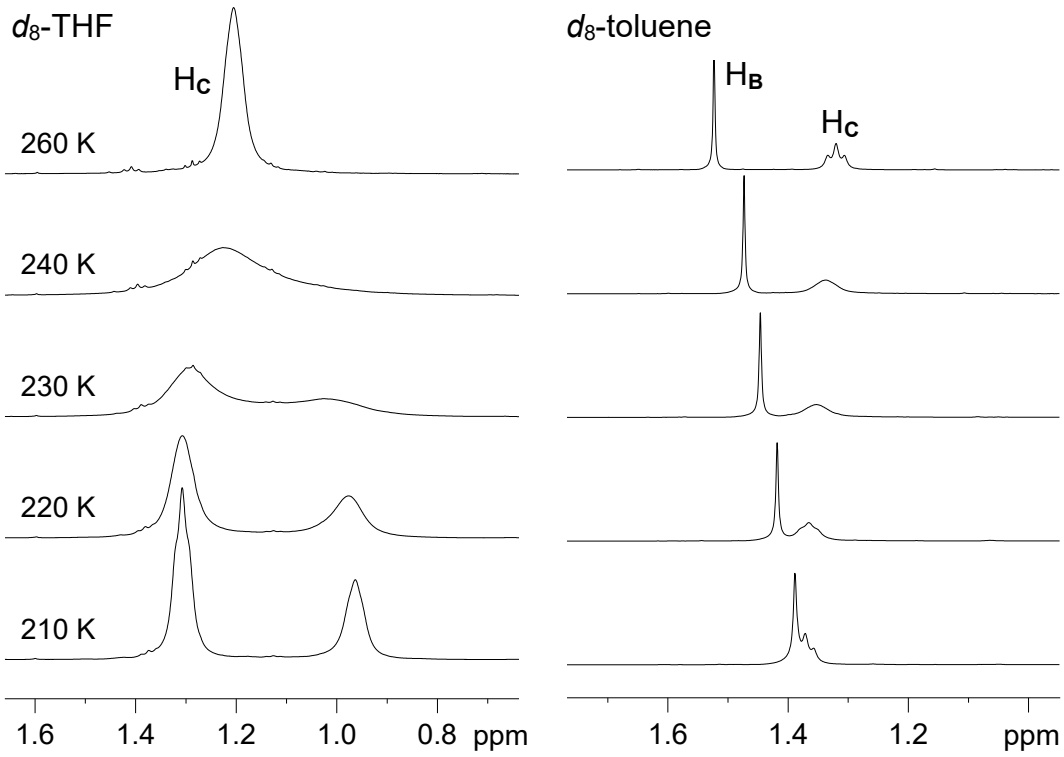

Figure 2.32 Variable temperature ^{1}H NMR spectra of 3A in d_8-THF and d_8-toluene (500 MHz)

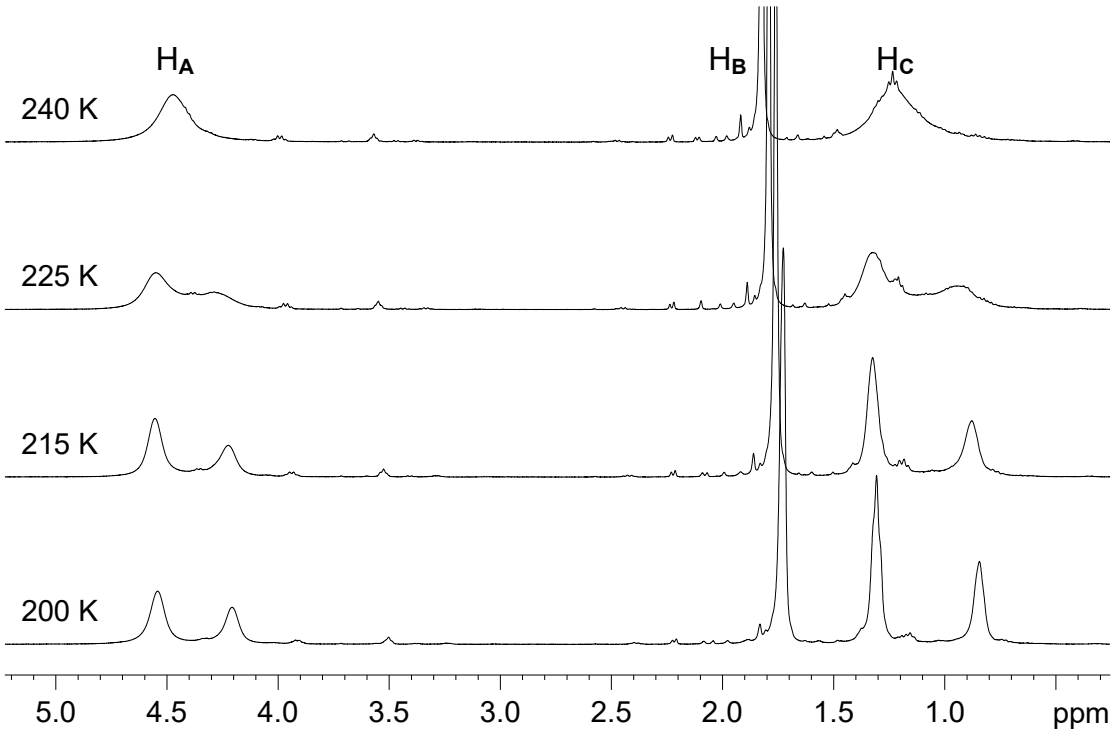

Figure 2.33 Variable temperature ^{1}H NMR spectra of 3A in d_5-pyridine (400 MHz)

The $^{13}C\{^{1}H\}$ NMR spectrum of **3A** in d_8-THF at 298 K showed six resonances in total which were assigned through ^{1}H-^{13}C HMQC/HMBC spectroscopy. Pertinent resonances appear at δ 218.6 (*C*O) and δ 181.6 (Ru-C_{NHC}) (**Figure 2.34**). Upon cooling to 210 K, splitting of both the *C*O (δ 219.9 and 218.0) and Ru-C_{NHC} (δ 183.2 and 178.2) resonances occurred as shown in **Figure 2.34**. Each of the N-ethyl *C*H$_2$ (δ 44.8) and *C*H$_3$ (δ 15.7) signals were also observed to split at 210 K into two sets of peaks at δ 45.0 and 44.9 and at δ 16.1 and 15.4 respectively.

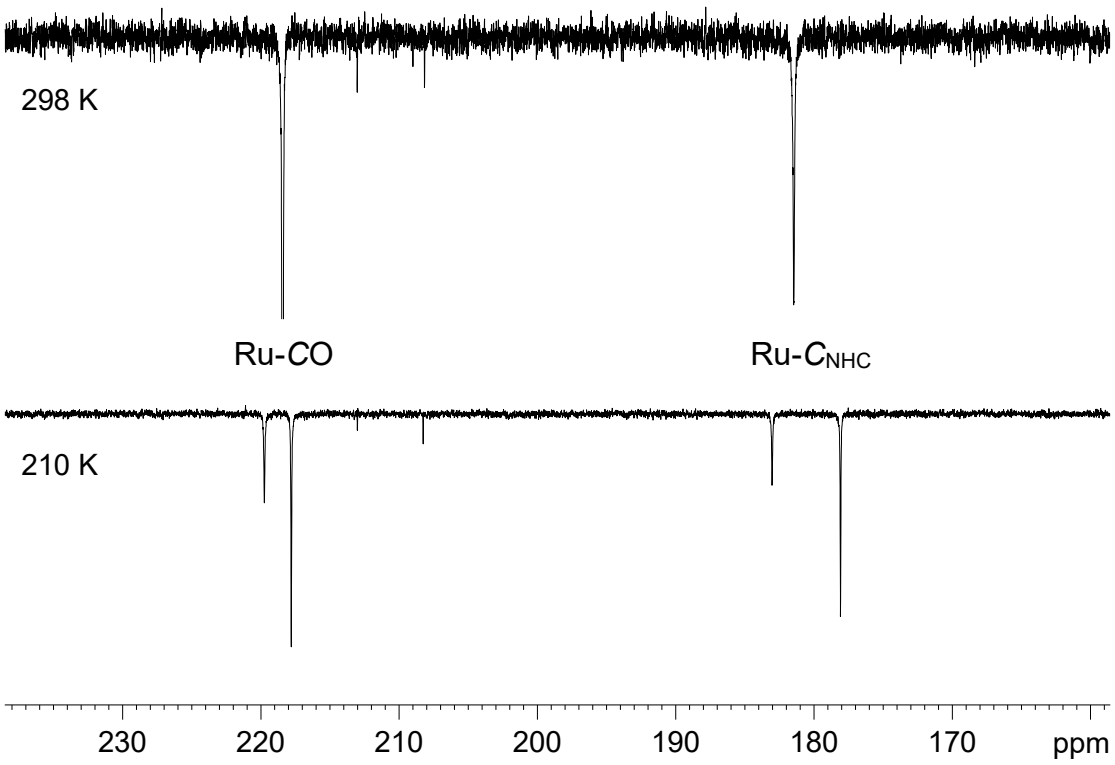

Figure 2.34 Variable temperature $^{13}C\{^1H\}$ PENDANT NMR spectrum of 3A (*d*$_8$-THF, 126 MHz)

Samples of **3A** were sent to the EPSRC solid-state NMR service at Durham University to deduce if these inequivalencies persisted in the solid-state structure. $^{13}C\{^1H\}$ solid-state NMR data of **3A** at 303 K showed three discrete *C*O signals at δ 224.3, 214.3, and 212.6; two Ru-C_{NHC} signals at δ 178.0 and 177.3; two broad CH_2 signals at δ 45.0 and 43.4 and eight CH_3 signals. Cooling to 206 K produced no significant changes to the spectrum. **Figure 2.35** shows the high degree of inequivalence of **3A** from the solid-state ^1H NMR resonances for the methyl and N-ethyl environments at 206 K. In addition, ^{15}N NMR studies at both 303 K and 206 K both showed four resonances for NHC nitrogen environments. These findings indicate substantial ligand asymmetry in solution and in the solid-state for **3A**. Consistent with ligand asymmetry was the IR spectrum of **3A**, which displayed four CO bands at 1967, 1937, 1849 and 1839 cm^{-1}, with this data explained and compared with other related *trans*- and *cis*-$Ru(L)_2(CO)_3$ complexes in **Section 2.4.5**.

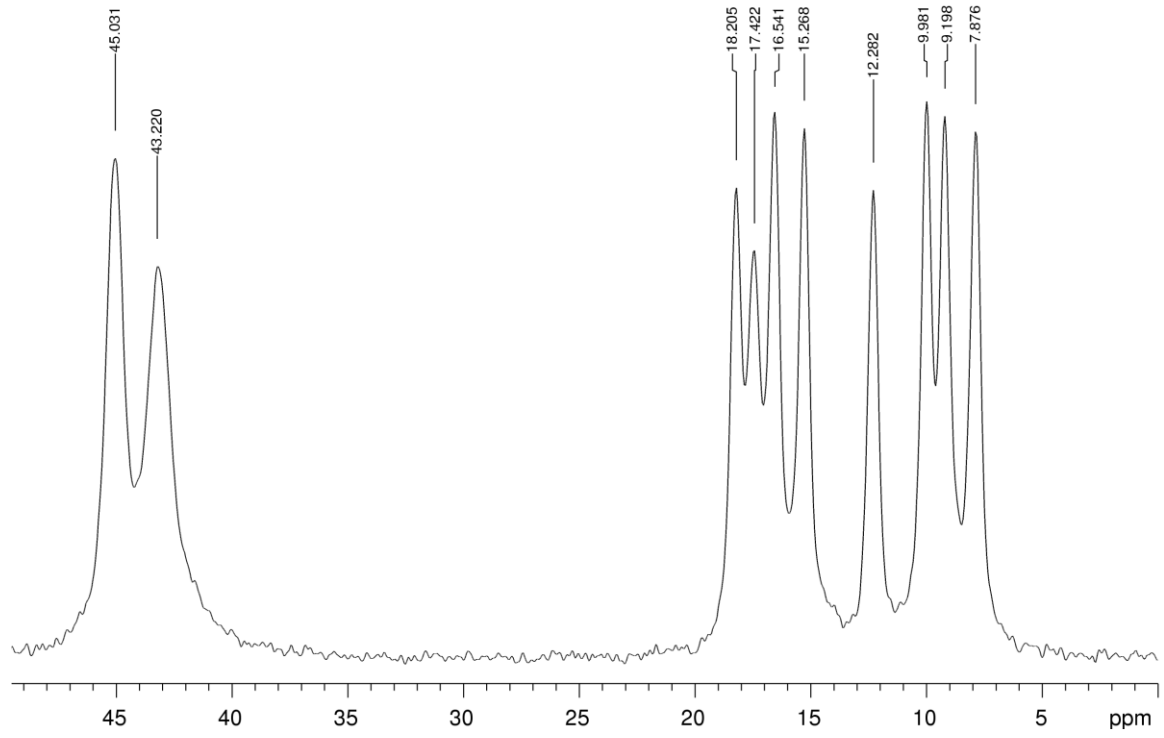

Figure 2.35 Solid-state $^{13}C\{^1H\}$ NMR spectrum (methyl region) of 3A (206 K, 101 MHz)

2.4.3 $Ru(I^iPr_2Me_2)_2(CO)_3$ (4A)

Upon addition of THF to a 1:6 mixture of $Ru_3(CO)_{12}$ and $I^iPr_2Me_2$ there was spontaneous evolution of gas, which ceased after 30-60 minutes. ^1H NMR showed the formation of one product (**4A**) with no additional products observed upon varying the $Ru_3(CO)_{12}$ to $I^iPr_2Me_2$ ratio. The orange/red product was washed with hexane and a small quantity of THF and recrystallised from THF/hexane to give X-ray quality crystals which were crystallographically characterised as *cis*-$Ru(I^iPr_2Me_2)_2(CO)_3$ (**4A**, **Figure 2.36**). Structural details are discussed in **Section 2.4.6**.

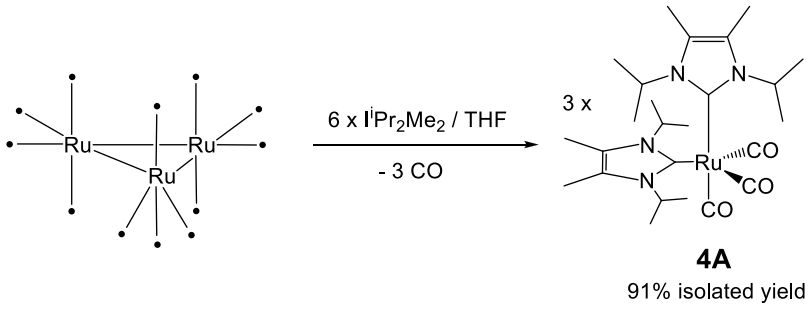

Figure 2.36 Formation of *cis*-$Ru(I^iPr_2Me_2)_2(CO)_3$ (4A)

The ^1H NMR spectrum of **4A** at ambient temperature in d_8-THF is shown in **Figure 2.37**, with resonances at δ 6.00 (H_A), 2.23 (H_B) and 1.26 (H_C). The spectrum is simplistic and

shows equivalent proton environments for both NHCs, similar to those of **3A** which is surprising considering the arrangement of the *cis*-NHC ligands.

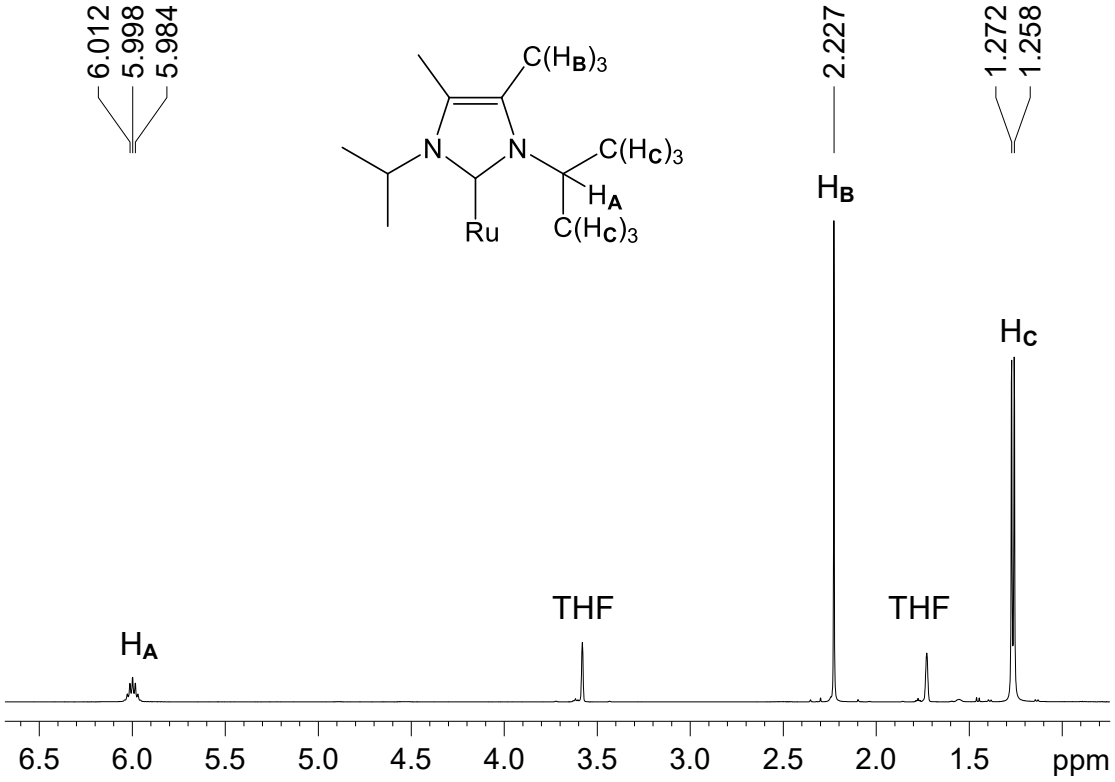

Figure 2.37 ^{1}H NMR spectrum of crystalline 4A (*d*$_8$-THF, 298 K, 500 MHz)

The $^{13}C\{^1H\}$ NMR spectrum of **4A** at 298 K (**Figure 2.38**) mirrors the ^{1}H NMR spectrum in its simplicity. Six resonances were observed in total, including one *C*O signal (δ 217.7), one Ru-C_{NHC} signal (δ 187.3) and four resonances for the I^{i}Pr$_2$Me$_2$ ligands, which were assigned by ^{1}H-^{13}C HMQC/HMBC experiments. Variable temperature NMR studies in solution and the solid-state were not conducted for **4A** due to extensive studies being undertaken for the related *cis*-NHC compound **5A**, presented in **Section 2.4.4**. IR data for **4A** indicated ligand asymmetry by the presence of four CO bands at 1967, 1867, 1845 and 1836 cm^{-1}, as was observed also for **3A**. **Section 2.4.5** compares and explains the IR bands of **3A** and **4A** from comparisons with related complexes.

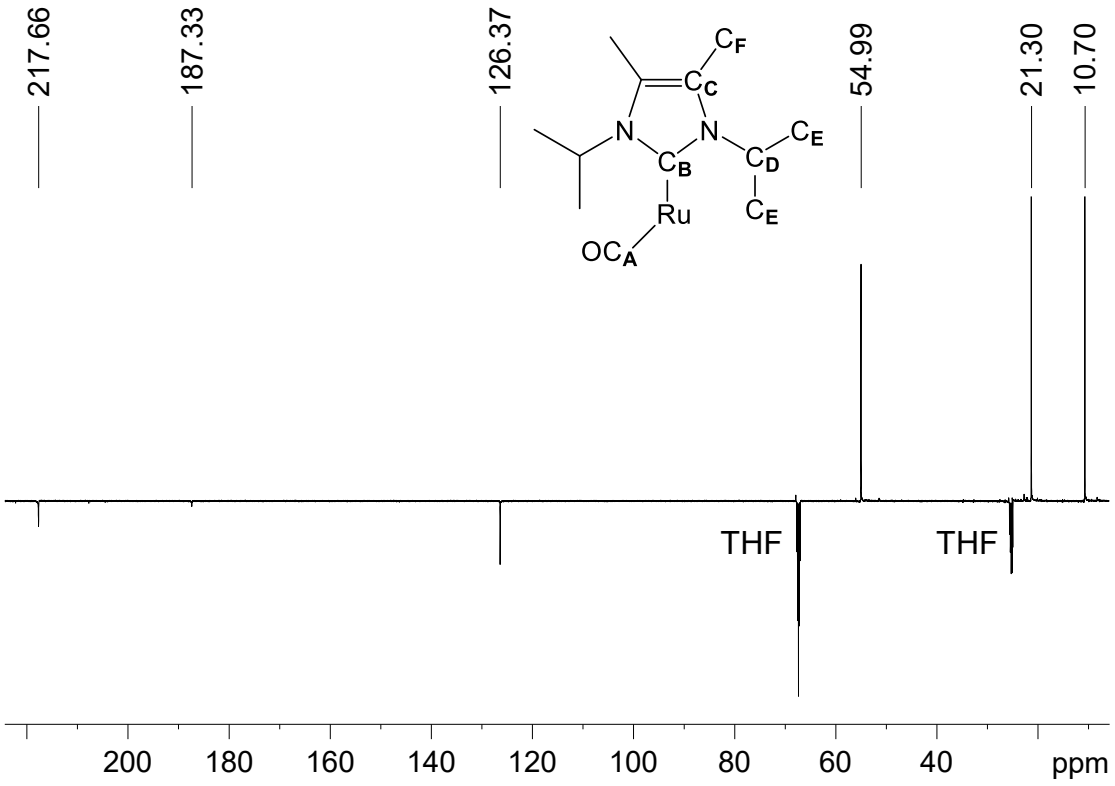

Figure 2.38 $^{13}C\{^{1}H\}$ PENDANT NMR spectrum of 4A (*d*8-THF, 298 K, 126 MHz)

The influence of CO addition to a toluene solution of **4A** was investigated, with the ^{1}H NMR spectrum shown in **Figure 2.39**. After 3 hours at room temperature, the formation of a new $I^{i}Pr_2Me_2$-containing product (‡) was observed alongside free $I^{i}Pr_2Me_2$ (†) and the original signals for **4A** (*). The observation of free $I^{i}Pr_2Me_2$ implied the new product (^{1}H NMR resonances at δ 6.39, 1.81 and 1.20) was the CO-substitution product, $Ru(I^{i}Pr_2Me_2)(CO)_4$. A NOESY spectrum at room temperature (insert in **Figure 2.39**) displayed exchange peaks between the $I^{i}Pr_2Me_2$ ligands of $Ru(I^{i}Pr_2Me_2)_2(CO)_3$ and $Ru(I^{i}Pr_2Me_2)(CO)_4$ indicating that these species interconvert. Evidence for the proposed complex $Ru(I^{i}Pr_2Me_2)(CO)_4$ was reinforced by freeze-pump-thaw-degassing the solution, which resulted in signals for free $I^{i}Pr_2Me_2$ and the new product disappearing, indicating re-association of $I^{i}Pr_2Me_2$. Although $Ru(I^{i}Pr_2Me_2)(CO)_4$ was not isolable from this reaction, $Ru(NHC)(CO)_4$ complexes (NHC = IMes and IPr) have recently been isolated in a report by Bruce and co-workers, demonstrating their existence.[43]

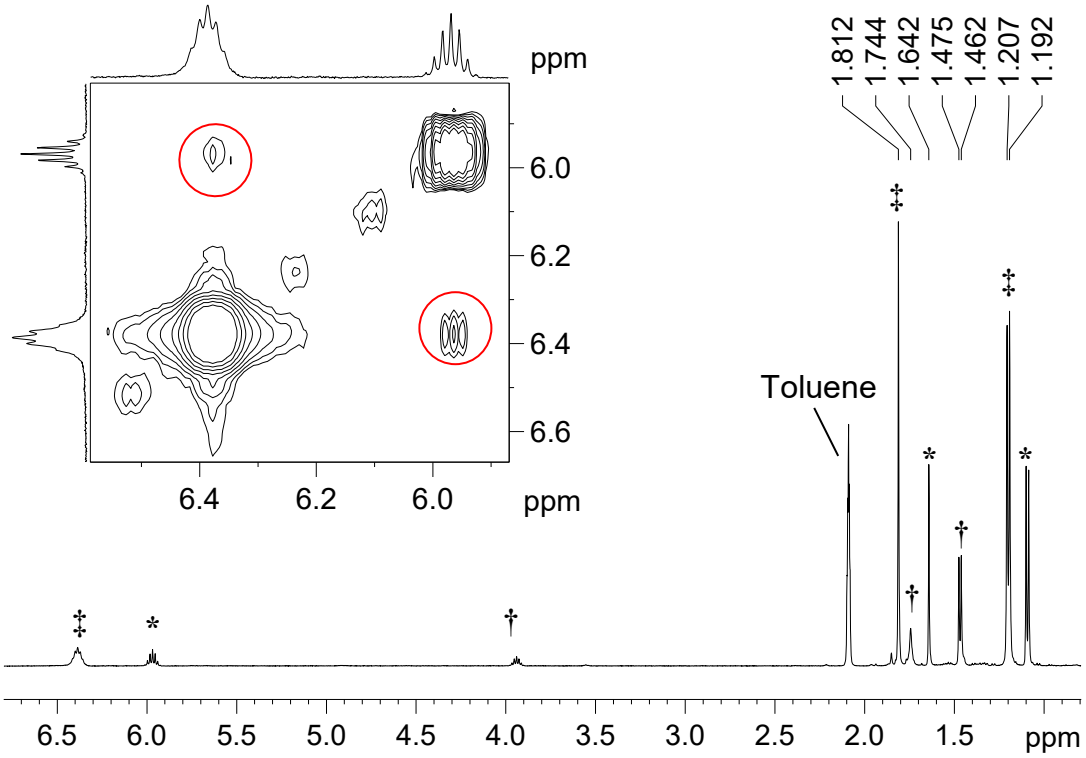

Figure 2.39 ^{1}H NMR spectrum of 4A + CO (1 atm) with NOESY spectrum in insert (d_8-toluene, 298 K, 500 MHz)

The fluxional nature of the I^{i}Pr$_2$Me$_2$ ligands in complex **4A** is evident from their exchange with CO. To affirm however that the *cis*-I^{i}Pr$_2$Me$_2$ geometry in **4A** was the thermodynamic product (not merely a kinetic phenomenon resulting from Ru$_3$(CO)$_{12}$ degradation), Ru(PPh$_3$)$_2$(CO)$_3$ was heated in THF with a 5:1 excess of I^{i}Pr$_2$Me$_2$ in a ligand substitution reaction. After 80 hours at 80 ˚C, distinct signals representing **4A** were observed by ^{1}H NMR spectroscopy, with no other products witnessed, which confirmed that this is indeed the thermodynamically favoured species.

2.4.4 Ru(I^{i}Pr$_2$)$_2$(CO)$_3$ (5A)

Reaction of I^{i}Pr$_2$ with Ru$_3$(CO)$_{12}$ was investigated to observe if an NHC ligand with protons at the C4/C5 positions but with less bulky N-substituents than I^{t}Bu$_2$ or IAd$_2$ would result in the cluster-degradation complex Ru(NHC)$_2$(CO)$_3$ or formation of the abnormal-NHC complex, Ru$_3$(aNHC)(CO)$_{11}$. The addition of d_8-THF to J. Youngs NMR tubes containing Ru$_3$(CO)$_{12}$ and I^{i}Pr$_2$ in ratios of 1:1, 1:6 and 1:10 resulted in vigorous bubbling of all solutions at ambient temperature for ca. 30 minutes. ^{1}H NMR spectroscopy showed in all cases the evolution of a new set of I^{i}Pr$_2$ resonances (**5A**), although at no point

were high frequency doublets characteristic of $Ru_3(aNHC)(CO)_{11}$ complexes **1A** and **2A** observed. The product was washed with hexane and recrystallised from THF/hexane to yield crystals which were structurally characterised as *cis*-$Ru(I^iPr_2)_2(CO)_3$ (**5A**, **Figure 2.40**).

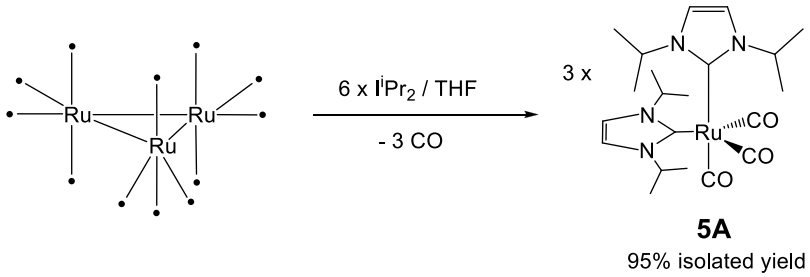

Figure 2.40 Formation of *cis*-$Ru(I^iPr_2)_2(CO)_3$ (5A)

The room temperature ^1H NMR spectrum of **5A** displayed resonances at δ 7.24 (s), 5.57 (sept) and 1.26 (d) in d_8-THF. The simplicity of this spectrum (as in **4A**) was surprising due to the close proximity of the NHC ligands in the solid-state structure, which could be envisaged to lead to inequivalent proton environments in solution through restricted rotation of the Ru-C_{NHC} bonds. Variable temperature ^1H NMR studies in d_8-THF showed splitting of all resonances below 215 K as observed for **3A**, but with no signal splitting detected in d_8-toluene (N-isopropyl septet region shown in **Figure 2.41**). Doping of a d_8-toluene solution of **5A** with ca. 15 equivalents of THF did not lead to splitting in any signals at low temperature, nor did cooling of **5A** in pure d_3-acetonitrile. Further attempts to elucidate the cause of this fluxionality using d_3-methanol and d_8-isopropanol as solvents resulted in rapid decomposition of the compound.

The $^{13}C\{^1H\}$ NMR spectrum of **5A** (in d_8-THF) is unremarkable at 298 K, with notable resonances at δ 217.8 (*C*O) and δ 184.4 (Ru-C_{NHC}). Upon cooling to 210 K, there was no palpable splitting of the ^{13}C NMR resonances, although signal splitting was observed in the ^1H NMR spectrum at the same temperature. A ^1H-^{13}C HMBC spectrum (**Figure 2.42**) at 210 K in d_8-THF indicated that in addition to the correlation for the major CH_3 resonances (†), there was also correlation of the minor proton CH_3 signal (*) to a very small new carbon signal (*). This suggested a degree of inequivalence was present in the ^{13}C NMR spectrum of **5A** at this temperature, although further cooling was unable to resolve the resonances completely.

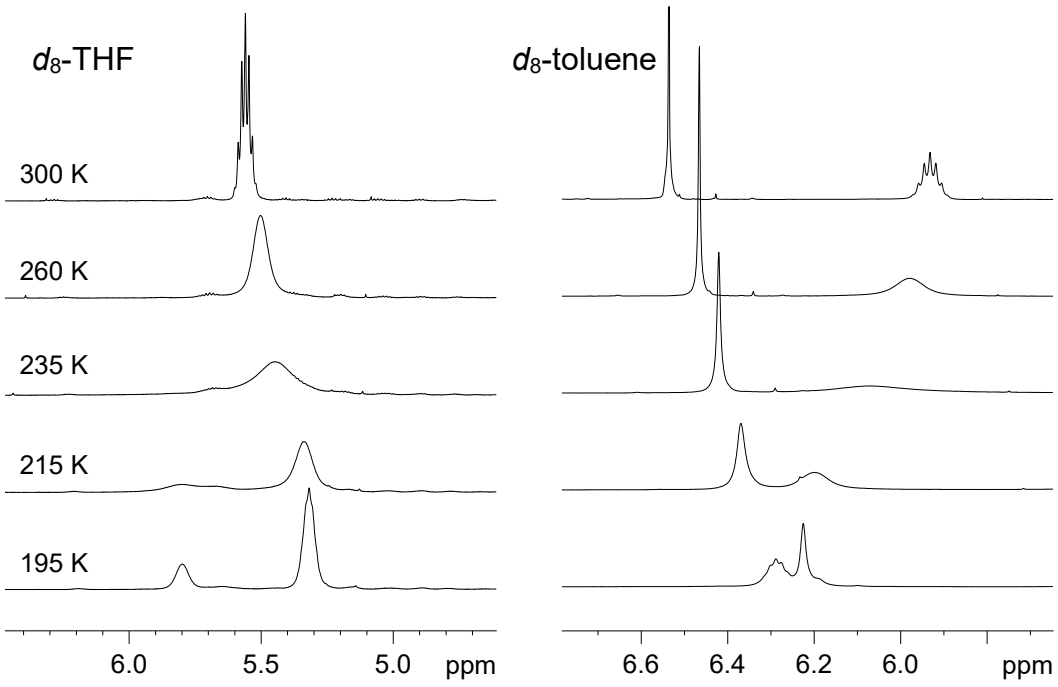

Figure 2.41 Variable temperature ^{1}H NMR spectrum of 5A in d_8-THF and d_8-toluene (500 MHz)

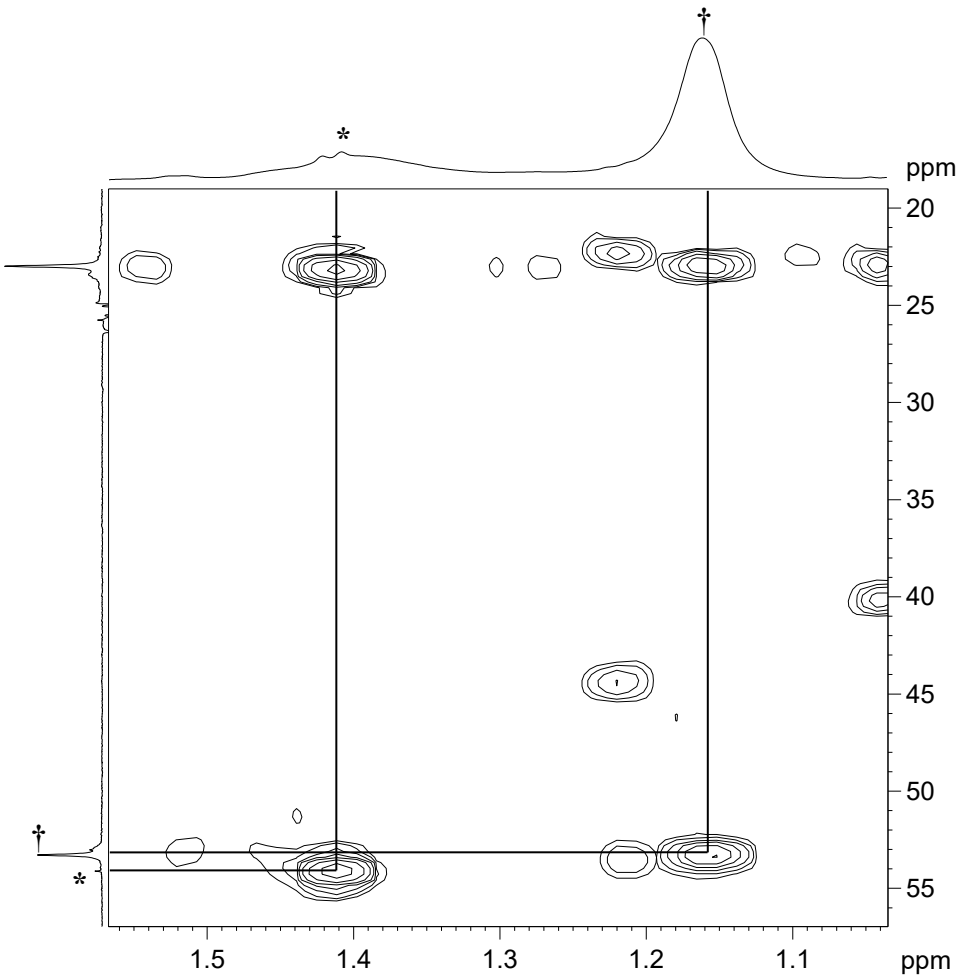

Figure 2.42 ^{1}H-^{13}C HMBC spectrum of 5A (d_8-THF, 210 K, 500/126 MHz)

Solid-state NMR studies of **5A** gave very similar spectra to that observed for **3A**, with inequivalent environments in both NHC and CO ligands at ambient temperature. Two ^{13}C NMR signals were recorded for Ru-C_{NHC} carbon atoms at δ 184.5 and 181.1 which demonstrated a larger difference in chemical shift (δ 3.4) than that observed in the *trans*-NHC complex, **3A** (δ 178.0 and 177.3) of only δ 0.7. This suggested a greater inequivalence between the NHC ligands in **5A** as might be expected from restricted rotation around the two *cis*-Ru-C_{NHC} bonds. There were three *C*O resonances at δ 227.5, 216.0 and 213.6 at 303 K that were not prominent but sharpened upon cooling to 206 K. The solid-state ^{15}N NMR spectrum displayed four signals for the imidazol nitrogen atoms clearly at both temperatures, shown in **Figure 2.43**.

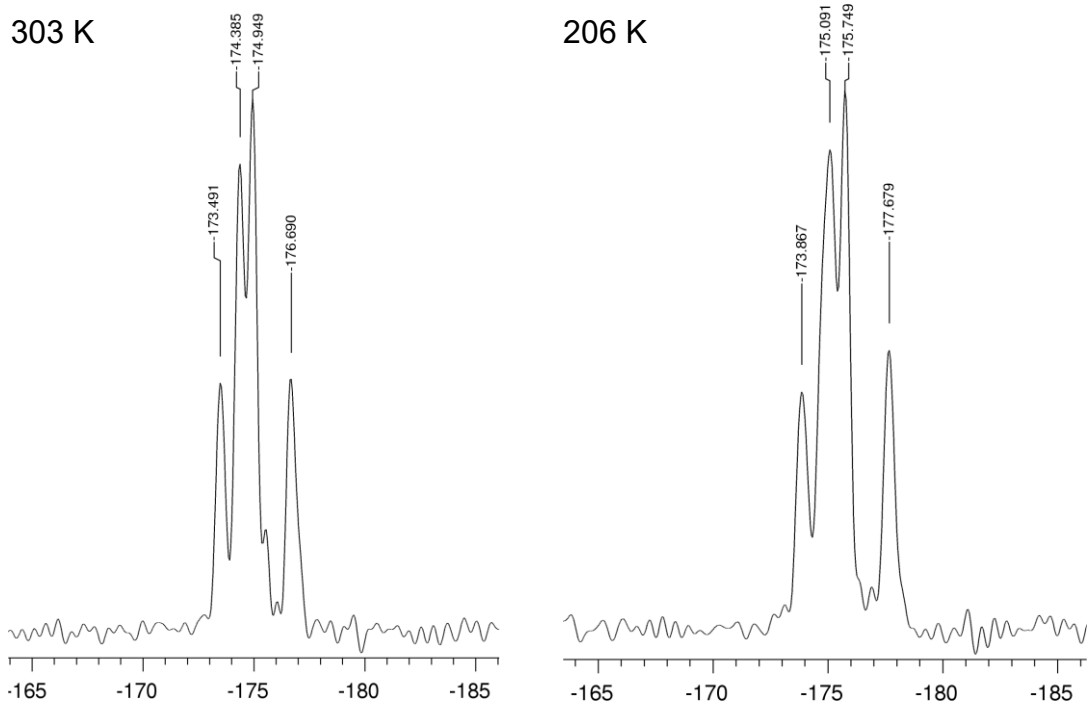

Figure 2.43 Solid-state ^{15}N NMR spectrum of 5A at 303 and 206 K (41 MHz)

2.4.5 Summary

In summary, the data gained through solution NMR spectroscopy for **3A**, **4A** and **5A** are indicative of highly dynamic systems that appear independent of the *cis*- or *trans*- nature of the NHC ligand geometries in the solid-state. In solution, variable temperature ^{1}H NMR studies have shown **3A** and **5A** to exhibit very similar behaviour, whilst in the solid-state the high number of signals observed in both compounds suggests highly inequivalent environments, regardless of the *cis*- or *trans*-NHC geometries of their crystal structures.

IR and ^{13}C NMR data for **3A**, **4A** and **5A** is presented in **Table 2.9** and shows close comparisons with related $Ru(L)_2(CO)_3$ literature compounds. Comparisons of ^{13}C NMR data show overall that *C*O resonances for $Ru(NHC)_2(CO)_3$ complexes occur at similar frequencies (δ 216.0-218.6), and are typically ca. 5 ppm higher in frequency than phosphine-containing systems such as $Ru(IMes)(PPh_3)(CO)_3$ (δ 211.4). Ru-C_{NHC} chemical shifts for **3A**, **4A** and **5A** (δ 181.6-187.3) match values found for $Ru(IMes)_2(CO)_3$ (δ 186.8) and $Ru(ICy_2)_2(CO)_3$ **(**δ 181.9**)**. In addition, the Ru-C_{NHC} chemical shift for **4A** (δ 187.3) is at higher frequency than that in **5A** (δ 184.4). IR bands for **3A**, **4A** and **5A** are essentially the same and comparable to related phosphine and NHC systems, with NHC systems typically leading to lower wavenumbers as a result of increased σ-donation and therefore increased π-backbonding into the CO π*-orbital. Generally for $M(L)_2(CO)_3$ complexes, the number of IR bands observed is typically one (for *trans*-L groups (D_{3h} symmetry)) or three (for *cis*-L groups (C_S symmetry)),[44] so the presence of four bands for **3A** and **4A** suggests that two conformers are present, indicative of the highly dynamic system outlined by ^1H NMR spectroscopy. In comparison, four bands are also observed in the N-alkyl NHC compound, *trans*-$Ru(ICy_2)_2(CO)_3$.[41]

Compound	^{13}C *C*O (δ)	^{13}C Ru-C_{NHC} (δ)	$\nu_{(CO)}$ cm^{-1}
3A	218.6	181.6	1967, 1937, 1849, 1836
4A	217.7	187.3	1967, 1867, 1845, 1836
5A	217.8	184.4	1970, 1852, 1841
$Ru(ICy_2)_2(CO)_3$[41]	216.0	181.9	2009, 1930, 1870, 1839
$Ru(IMes)_2(CO)_3$[42]	217.6	186.8	1950, 1879, 1830
$Ru(IMes)(PPh_3)(CO)_3$[45]	211.4	-[a]	1965, 1885, 1850
$Ru(dmpe)(CO)_3$[46]	212.7	-	2005, 1934, 1915

[a] Ru-C_{NHC} not quoted. dmpe = $Me_2PCH_2CH_2PMe_2$.

Table 2.9 IR bands and ^{13}C NMR data for 3A, 4A, 5A and related compounds

2.4.6 Structural comparisons of 3A, 4A and 5A

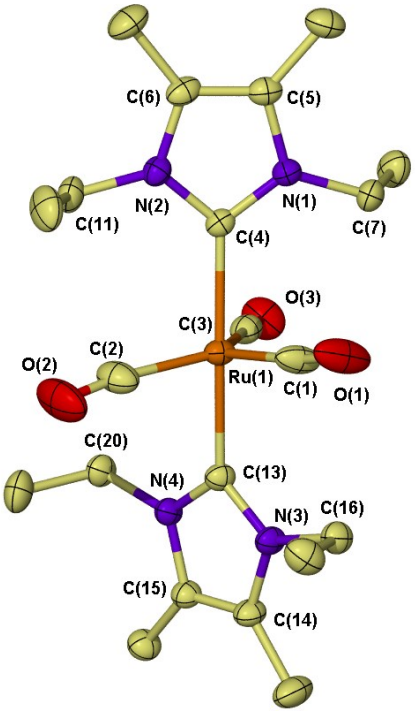

Figure 2.44 Crystal structure of $Ru(IEt_2Me_2)_2(CO)_3$ (3A) with thermal ellipsoids set to 30% probability and hydrogen atoms omitted for clarity

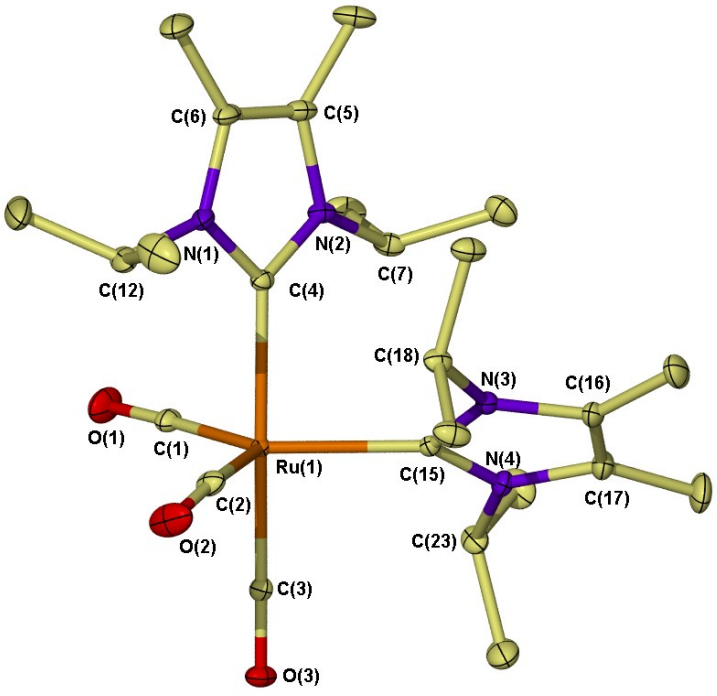

Figure 2.45 Crystal structure of $Ru(I^iPr_2Me_2)_2(CO)_3$ (4A) with thermal ellipsoids set to 30% probability and hydrogen atoms omitted for clarity

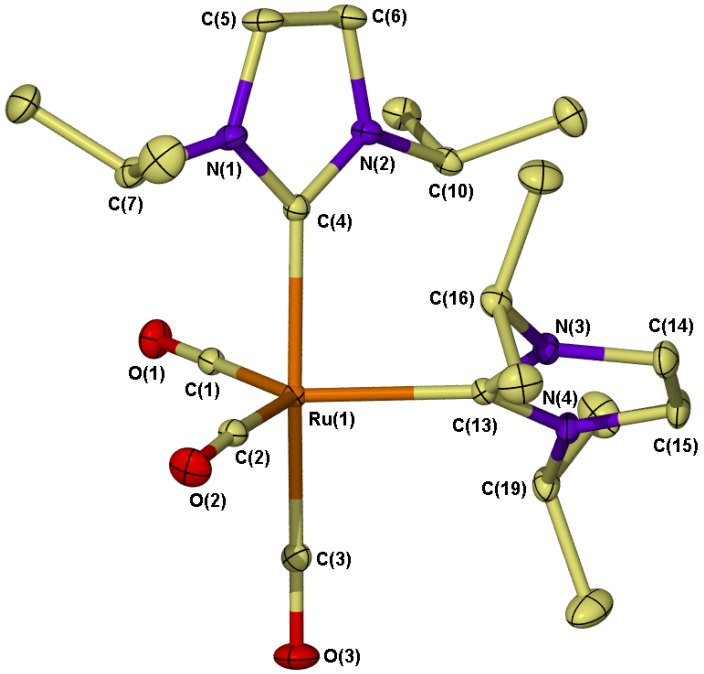

Figure 2.46 Crystal structure of $Ru(I^iPr_2)_2(CO)_3$ (5A) with thermal ellipsoids set to 30% probability and hydrogen atoms omitted for clarity

The crystal structures of **3A**, **4A** and **5A** are shown in **Figures 2.44**, **2.45** and **2.46** respectively, with complete tables of bond lengths and angles given in the **Appendices**. All three complexes exhibit distorted trigonal bipyramidal structures, with the most substantial difference in the structures relating to the unusual *cis*-NHC geometries of **4A** and **5A** compared with *trans*-NHC geometry in **3A**. Archetypal trigonal bipyramidal $Ru(L)_2(CO)_3$ complexes (L = PR_3, NHC) in the literature feature *trans*- axial ligands on electronic and steric grounds,[40] with *cis*- ligands typically featured only for complexes containing bidentate ligands such as dmpe ($Me_2PCH_2CH_2PMe_2$)[46] or d^{t}bpe ($^tBu_2PCH_2CH_2P^tBu_2$).[47] Complexes **3A**, **4A** and **5A** contain strong σ-donating NHCs of similar basicity and the observation of *cis*-NHCs occurring with the bulkier N-^{i}Pr compounds **4A** and **5A** compared with N-Et compound **3A** is surprising. A summary of important bond lengths (Å) and angles (˚) of these complexes are presented in **Table 2.10**.

	3A	4A	5A
Ru-C_{NHC}	2.142(2)	2.178(2) (ax)	2.153(2) (ax)
	2.133(2)	2.2019(17) (eq)	2.177(2) (eq)
Ru-C_{CO}	1.905(3)	1.880(2) (ax)	1.888(2) (ax)
	1.916(3)	1.8851(15) (eq)	1.884(2) (eq)
	1.915(3)	1.9055(19) (eq)	1.916(2) (eq)
L_{ax}-Ru-L_{ax}	172.24(9)[a]	174.02(7)	174.34(9)
C_{NHC}-Ru-C_{NHC}	172.24(9)[a]	88.52(7)	87.55(8)
C_{NHC}-Ru-C_{CO}	103.64(14)[b]	133.70(7) (eq-eq)	125.96(9) (eq-eq)
	124.34(13)[b]	105.73(8) (eq-eq)	105.90(9) (eq-eq)
C_{CO}-Ru-C_{CO}	131.98(13)[b]	120.57(8) (eq-eq)	128.07(9) (eq-eq)

[a] Same value due to *trans*-NHC ligands. [b] All values for equatorial C_{CO}-Ru-C_{CO} angles.

Table 2.10 Bond lengths (Å) and angles (˚) for 3A, 4A and 5A

The axial NHC ligands in **3A** are positioned at a C_{NHC}-Ru-C_{NHC} angle of 172.24(9)˚, with a twist of the two imidazol rings of 46.1˚ between the least-squares planes. The C_{NHC}-Ru-C_{NHC} bond angles for **4A** (88.52(7)˚) and **5A** (87.55(8)˚) are similar to each other, as are the dihedral angles of the least-squares NHC planes, with angles of 67.5˚ and 67.2˚ respectively, indicating no significant steric influence from the methyl C4/C5 backbone groups in **4A**. For **3A**, both Ru-C_{NHC} bonds (axial) are considerably shorter at 2.142(2) Å and 2.133(2) Å than those in **4A** (2.178(2) Å (ax) and 2.2019(17) Å (eq)) and **5A** (2.153(2) Å (ax) and 2.177(2) Å (eq)), and furthermore the equatorial Ru-C_{NHC} bonds in **4A** and **5A** are significantly longer than those in the axial positions. In all three complexes there is a degree of tilting of the NHC ligands (angle X = in **Figure 2.47**) (for example Ru-C_{NHC}-$N(1)_{NHC}$ = 131.11(17)˚ and Ru-C_{NHC}-$N(3)_{NHC}$ = 126.09(17)˚ for an IEt_2Me_2 ligand in **3A**) which allows one methylene α-hydrogen to increase in proximity towards the ruthenium (e.g. **3A**, Ru(1)-αH(20B) = 2.988 Å vs. Ru(1)-αH(16A) = 3.231 Å) (**Figure 2.47**). This tilting is observed for all NHC ligands to varying extents in compounds **3A**, **4A** and **5A** regardless of axial or equatorial position.

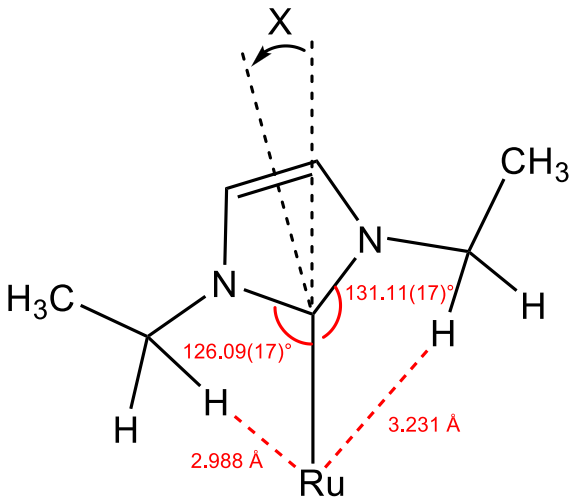

Figure 2.47 Model demonstrating the tilting of the NHC ligands in $Ru(NHC)_2(CO)_3$ complexes (example values for 3A)

The three equatorial ligands in each complex display one acute angle of between 103.64(14)-105.90(9)˚, allowing expansion of the other two L_{eq}-Ru-L_{eq} angles (from 120.57(8)-133.70(7)°) which coincide with the positions of the closest NHC methylene α-hydrogen atom locations. The L_{ax}-Ru-L_{ax} angle between the axial CO and NHC ligands is very similar for **4A** (174.02(7)˚) and **5A** (174.34(9)˚), although is reduced when the two NHCs are *trans*- to each other as in **3A** (172.24(9)˚). Each complex contains one CO ligand with a nearly linear Ru-C-O bond angle (CO(ax) in **4A** and **5A**) and two others which display significant deviation from 180°, for example Ru-C-O angles in **3A** of 177.1(2) vs. 171.2(3) and 172.9(3)˚ and in **4A** of 179.5(2) vs. 167.24(19) and 174.55(16)˚. Ru-C_{CO} bonds in **3A** (equatorial COs) are the same distance, whereas there is lengthening of one equatorial Ru-C_{CO} bond in both **4A** (1.9055(19) vs. 1.8851(15), 1.880 Å) and **5A** (1.916(2) vs. 1.884(2), 1.888(2) Å).

In comparison to other literature examples, Ru-C_{NHC} bonds for **3A** (2.142(2), 2.133(2) Å) are longer than those of $Ru(IMes)_2(CO)_3$ (2.1125(19), 2.1093(19) Å)[48] and the same as in *trans*-$Ru(IMes)(PPh_3)(CO)_3$ (2.12(2) Å).[45] $Ru(IMes)(PPh_3)(CO)_3$ contains a L_{ax}-Ru-L_{ax} angle of 171.4(3)° that is the same as in **3A**, **4A** and **5A**, as is the fact that one angle between the equatorial ligands is significantly more acute than the others (110.1(4) vs. 122.9(5) and 126.8(5)°). The equatorial Ru-C_{CO} bonds in **3A** (1.905(3), 1.916(3), 1.915(3) Å) compare well with those determined for $Ru(IMes)(PPh_3)(CO)_3$ (1.91(2), 1.92(2), 1.93(2) Å)[45] and $Ru(PPh_3)_2(CO)_3$ (1.917, 1.911 and 1.911 Å).[49]

2.5 Formation of $Ru(NHC)_2(CO)(L)(CO_3)$ complexes (L = CO, C_5H_5N)

2.5.1 Introduction

During characterisation of the $Ru(NHC)_2(CO)_3$ complexes it was evident by IR spectroscopy that additional bands were present in the KBr samples compared to those recorded in degassed C_6D_6. The additional bands (1590-1650 cm^{-1}) led us to deduce that oxidation of $Ru(IEt_2Me_2)_2(CO)_3$ (**3A**), $Ru(I^iPr_2Me_2)_2(CO)_3$ (**4A**) and $Ru(I^iPr_2)_2(CO)_3$ (**5A**) was taking place in air. The reaction of these compounds with O_2 was subsequently investigated and is presented in this section.

2.5.2 $Ru(IEt_2Me_2)_2(CO)_2(CO_3)$ (3B)

Exposure of powdered $Ru(IEt_2Me_2)_2(CO)_3$ (**3A**) to air led to a gradual colour change from red/orange to black. The solid was shown by ^1H NMR spectroscopy (**Figure 2.48**) after 3 days to contain residual **3A** (†) and a new product, **3B** (‡). Similar observations in colour change and speed of reaction were noted by Collman *et al* for the oxidation of $Ru(PPh_3)_2(CO)_3$ to $Ru(PPh_3)_2(CO)_2(CO_3)$.[50]

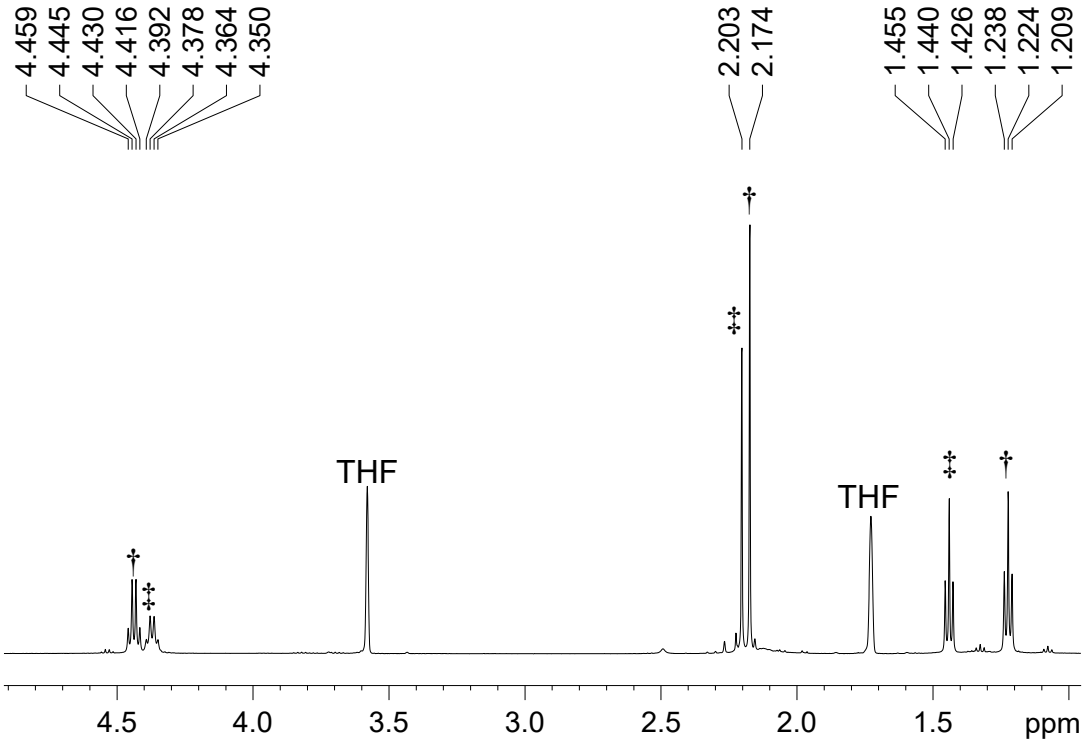

Figure 2.48 ^1H NMR spectrum for oxidation (in air) of 3A to 3B in the solid-state (d_8-THF, 298 K, 500 MHz)

Low yields (typically < 10%) of **3B** were obtained and the reaction took around 7 days to complete, with the dark colour implying that the majority of the residue was over-oxidised. This necessitated a higher yielding route which was achieved by charging a J. Youngs ampoule with **3A** under 1 atm O_2 and heating at 70 ˚C for 14 hours. Crystallisation from CH_2Cl_2/hexane gave X-ray quality crystals in 48% yield which were characterised as *trans*-Ru(IEt_2Me_2)$_2$(CO)$_2$(CO_3) (**3B**), as shown in **Figure 2.49**. The structure of **3B** is discussed in **Section 2.5.7**.

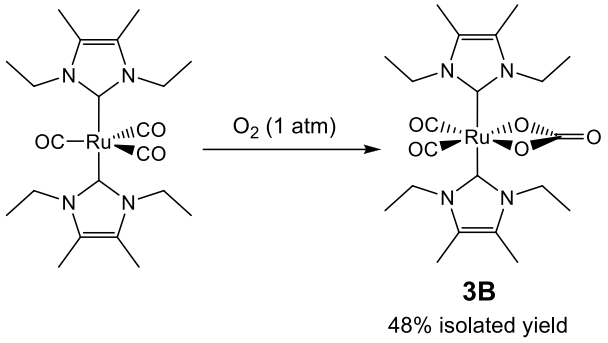

Figure 2.49 Formation of *trans*-Ru(IEt_2Me_2)$_2$(CO)$_2$(CO_3) (3B)

^{1}H NMR resonances for **3B** in d_8-THF at δ 4.37 (q), 2.20 (s) and 1.44 (t) are characteristic for equivalent *trans*-NHC ligands. The ^{13}C NMR spectrum displayed the same simplicity as the ^{1}H NMR spectrum, with notable resonances at δ 201.9 (*C*O), 174.5 (Ru-C_{NHC}) and 164.4 (CO_3), with their assignments deduced by ^{1}H-^{13}C HMBC correlation experiments. IR bands were located at 2024 and 1947 cm^{-1} (CO) and 1612 cm^{-1} (CO_3).

2.5.3 Ru($I^iPr_2Me_2$)$_2$(CO)$_2$(CO_3) (4B)

Exposure of powdered **4A** to air resulted in rapid darkening of the solid in less than one minute, and led to the formation of **4B** in low yields due to facile over-oxidation. Further investigation proved that dissolution of **4A** in pyridine with exposure to 1 atm O_2 for ca. 30 seconds and its removal *in vacuo* led to the formation of two products, **4B** and **4C**. ^{1}H NMR of the crude material (**Figure 2.51**) showed that the major product **4B** forms initially, with **4C** resonances increasing steadily over time. Extraction of **4C** (see **Section 2.5.4**) in THF allowed the two complexes to be isolated, with the pale yellow residue recrystallised from CH_2Cl_2/hexane to determine its structure as *cis*-Ru($I^iPr_2Me_2$)$_2$(CO)$_2$(CO_3) (**4B**, **Figure 2.50**) (structure discussed in **Section 2.5.7**). Pyridine was used in this procedure as it was found to solvate both Ru($I^iPr_2Me_2$)$_2$(CO)$_3$ and Ru($I^iPr_2Me_2$)$_2$(CO)$_2$(CO_3), whereas alternative solvents such as CH_2Cl_2 (which led to facile

degradation of $Ru(I^iPr_2Me_2)_2(CO)_3$) and THF (in which $Ru(I^iPr_2Me_2)_2(CO)_2(CO_3)$ is sparingly soluble) were less useful.

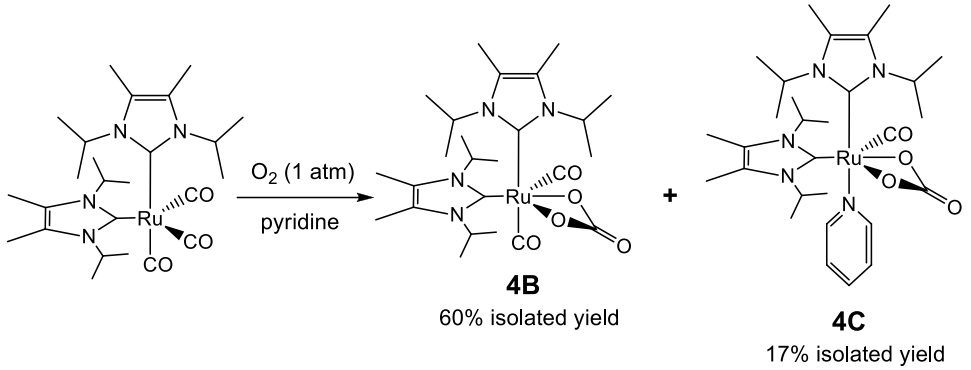

Figure 2.50 Formation of *cis*-$Ru(I^iPr_2Me_2)_2(CO)_2(CO_3)$ (4B) and *cis*-$Ru(I^iPr_2Me_2)_2(CO)(C_5H_5N)(CO_3)$ (4C)

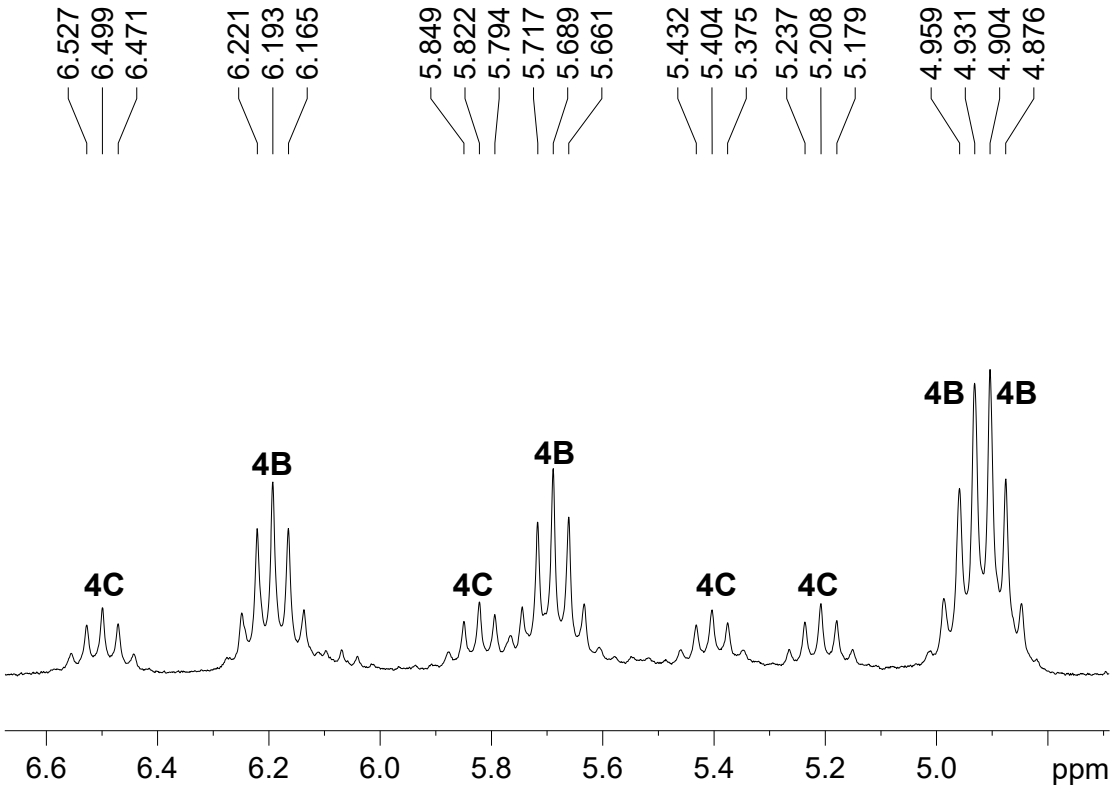

Figure 2.51 ^{1}H NMR spectrum of 4B and 4C, expansion of isopropyl septet region (*d*$_5$-pyridine, 298 K, 250 MHz)

Unlike the parent complex **4A** and the related *trans*-NHC carbonate complex **3B**, both ^{1}H and ^{13}C NMR spectra of crystalline **4B** showed virtually all proton and carbon environments to be inequivalent at ambient temperature. The ^{1}H NMR spectrum (**Figure 2.52**) displays eight proton signals for isopropyl-C*H*$_3$ groups, four isopropyl-C*H* groups and four C*H*$_3$ backbone resonances. Four of the eight isopropyl-C*H*$_3$ doublet

resonances are however closely overlying, indicating relatively similar environments for these protons.

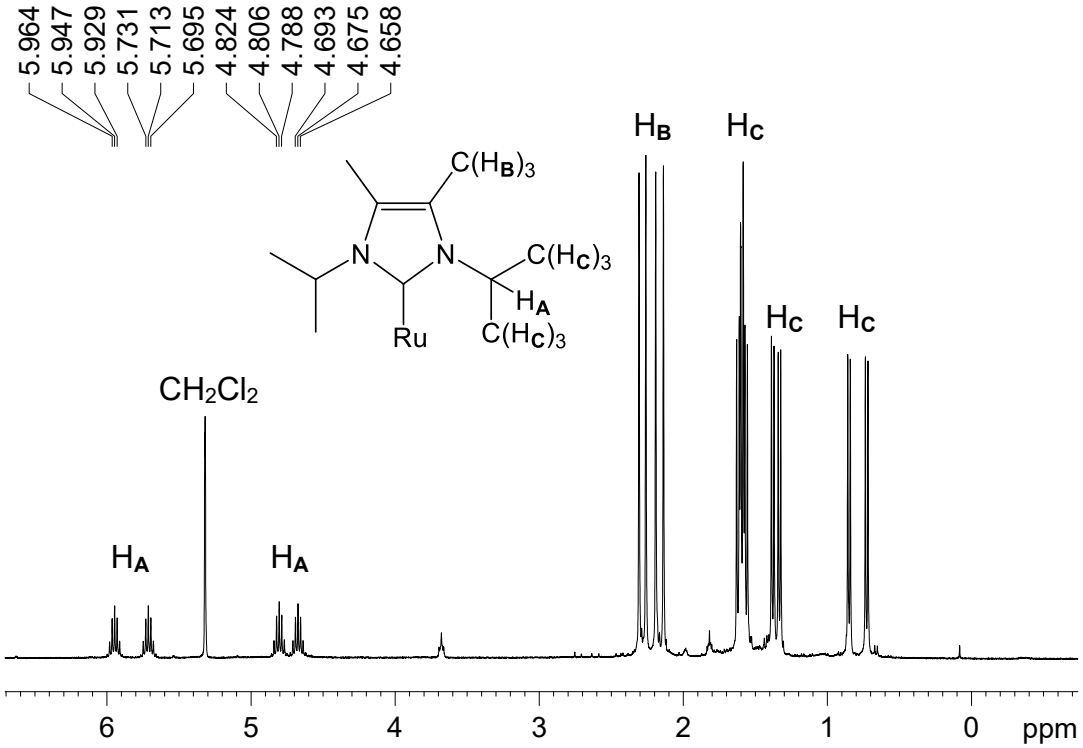

Figure 2.52 ^{1}H NMR spectrum of 4B (CD_2Cl_2, 298 K, 400 MHz)

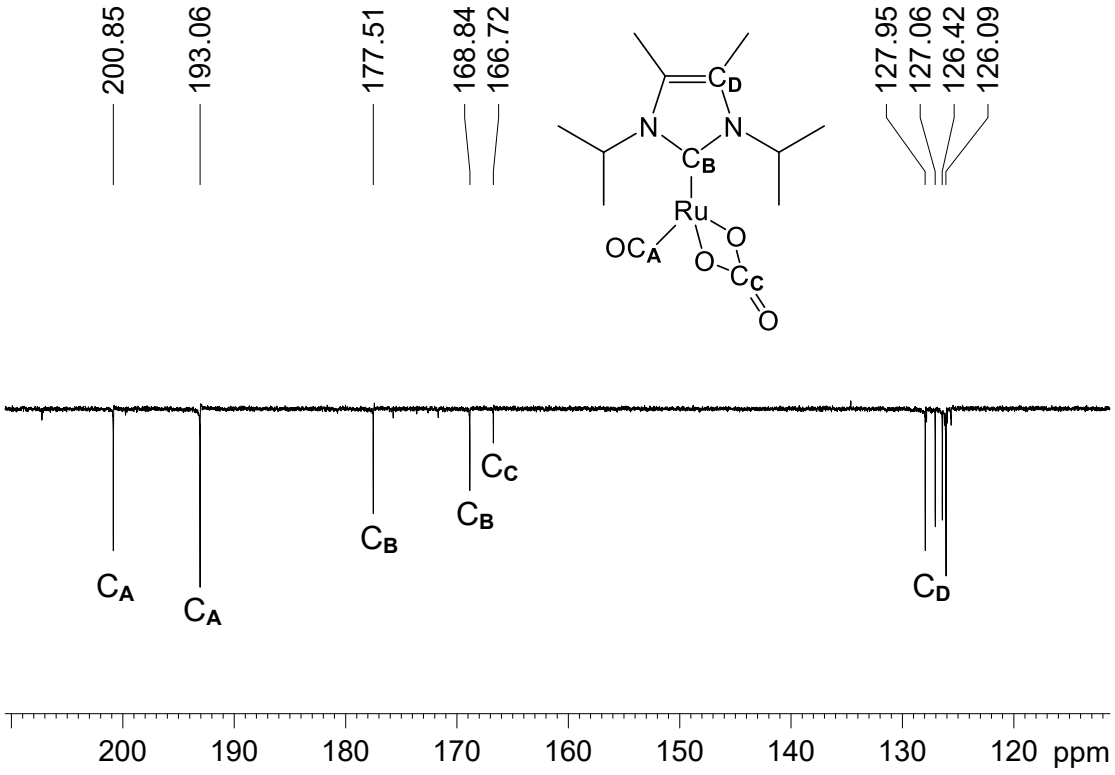

Figure 2.53 ^{13}C{^{1}H} PENDANT NMR spectrum of 4B, high frequency region (CD_2Cl_2, 298 K, 126 MHz)

The ^{13}C NMR spectrum in **Figure 2.53** shows each carbon resonance to be inequivalent, with large chemical shifts between resonances for the *C*O ligands (δ 200.9 and 193.1) and Ru-C_{NHC} atoms (δ 177.5 and 168.8). The CO_3 resonance is situated at δ 166.7. IR bands for **4B** were located at 2034 and 1945 cm^{-1} for the CO ligands and 1593 cm^{-1} for the CO_3, essentially the same as those for **3B**.

Caulton *et al* have described the formation of $Ru(\eta^2\text{-}O_2)(PR_3)_2(CO)_2$ complexes on addition of O_2 to ruthenium phosphine carbonyl species.[51] On addition of O_2 to a d_5-pyridine solution of **4A** at 238 K, there was no observation of intermediate species (such as a η^2-O_2 complex) by ^1H NMR spectroscopy. Gradual warming of the solution over 30 minutes until ca. 273 K saw the slow evolution of proton resonances for **4B**. Above 273 K there was more rapid formation of **4B**, with **4C** resonances also detected and no additional products observed.

The complex **4B** is an air-stable 18-electron species, however on thermolysis in CD_2Cl_2 it was shown by ^1H NMR spectroscopy to give rise to a number of degradation products. The recrystallisation of a sample following heating for 24 hours at 50 ˚C led to the formation of X-ray quality crystals which characterised the structure of one product as $Ru(I^iPr_2Me_2)_2(CO)_2Cl_2$, which was further confirmed by mass spectrometry (ESI-TOF MS: $[M - Cl]^+$ m/z = 553.1878, theoretical m/z = 553.1881). The complex contains *trans*-$I^iPr_2Me_2$ NHCs which are in axial positions, and these are separated by equatorial π-donor/π-acceptor chloride and carbonyl ligands (**Figure 2.54**).[40]

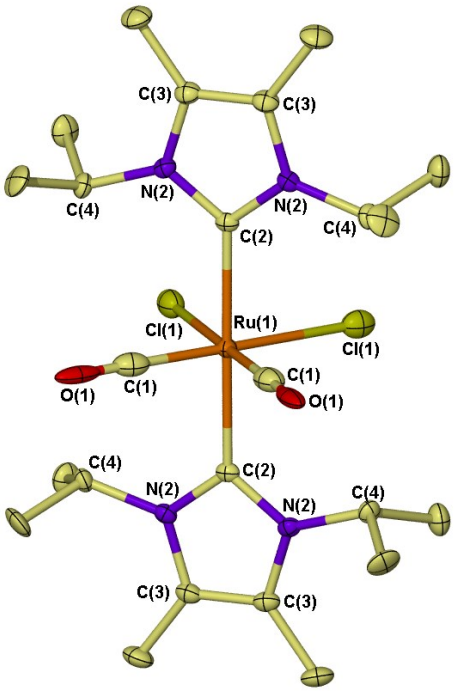

Figure 2.54 Crystal structure of Ru(I^{i}Pr$_2$Me$_2$)$_2$(CO)$_2$Cl$_2$ with thermal ellipsoids set to 30% probability and hydrogen atoms omitted for clarity

2.5.4 Ru(I^{i}Pr$_2$Me$_2$)$_2$(CO)(C$_5$H$_5$N)(CO$_3$) (4C)

The isolation of **4C** as a minor product from formation of **4B** (**Figure 2.50**, see **Section 2.5.3**) occurred from recrystallisation of THF washings which led to determination of its crystal structure as *cis*-Ru(I^{i}Pr$_2$Me$_2$)$_2$(CO)(C$_5$H$_5$N)(CO$_3$) (discussed in **Section 2.5.7**). ^{1}H NMR spectroscopy of **4C** reveals inequivalent environments for all protons at ambient temperature (**Figure 2.55**), as expected from the *cis*-NHC geometry. Multiplets representing the coordinated pyridine ligand are observed at high frequency in CD_2Cl_2 and are inequivalent due to restricted rotation around the Ru-N bond (see insert in **Figure 2.55**). The ^{13}C NMR spectrum displays one *C*O resonance at δ 208.3, with inequivalent Ru-C_{NHC} resonances at δ 179.7 and 176.8 and a signal at δ 168.7 for CO_3. The ^{13}C NMR resonances for the I^{i}Pr$_2$Me$_2$ ligands are all inequivalent (as seen for **4B**), with a selection shown in **Figure 2.56**. IR bands for **4C** were located at 1905 cm^{-1} for the CO ligand and 1643 cm^{-1} for the CO_3.

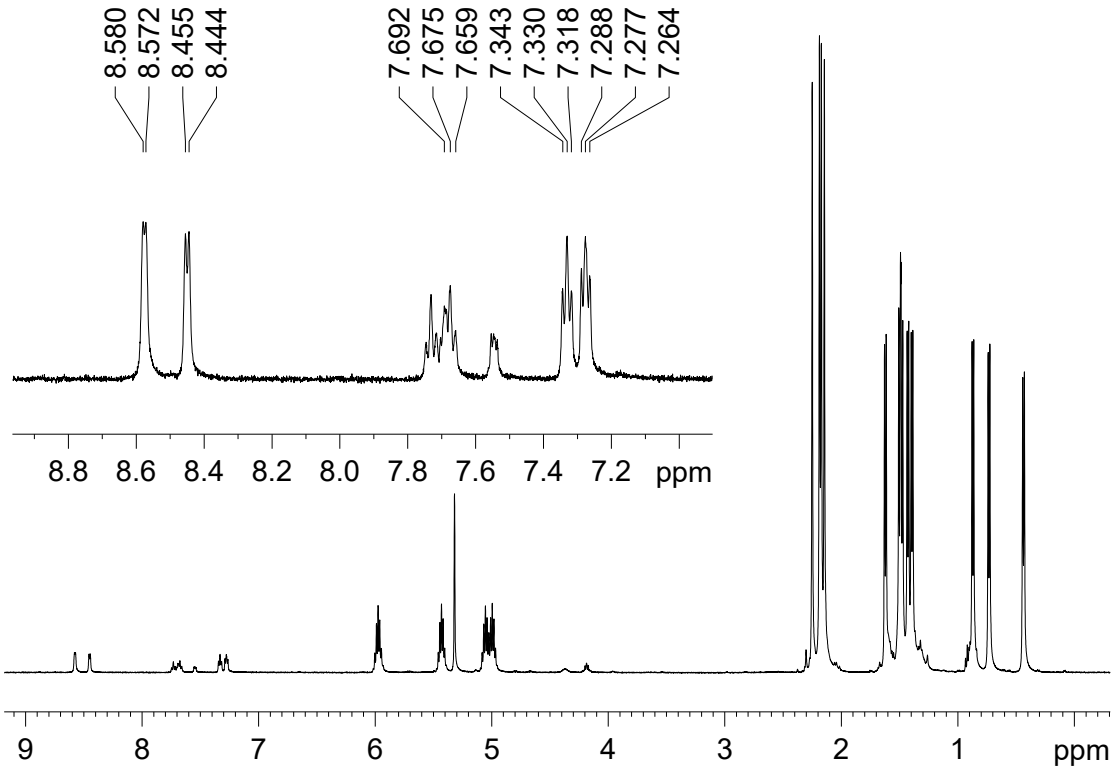

Figure 2.55 ^{1}H NMR spectrum of 4C, with coordinated pyridine resonances expanded in insert (CD_2Cl_2, 298 K, 500 MHz)

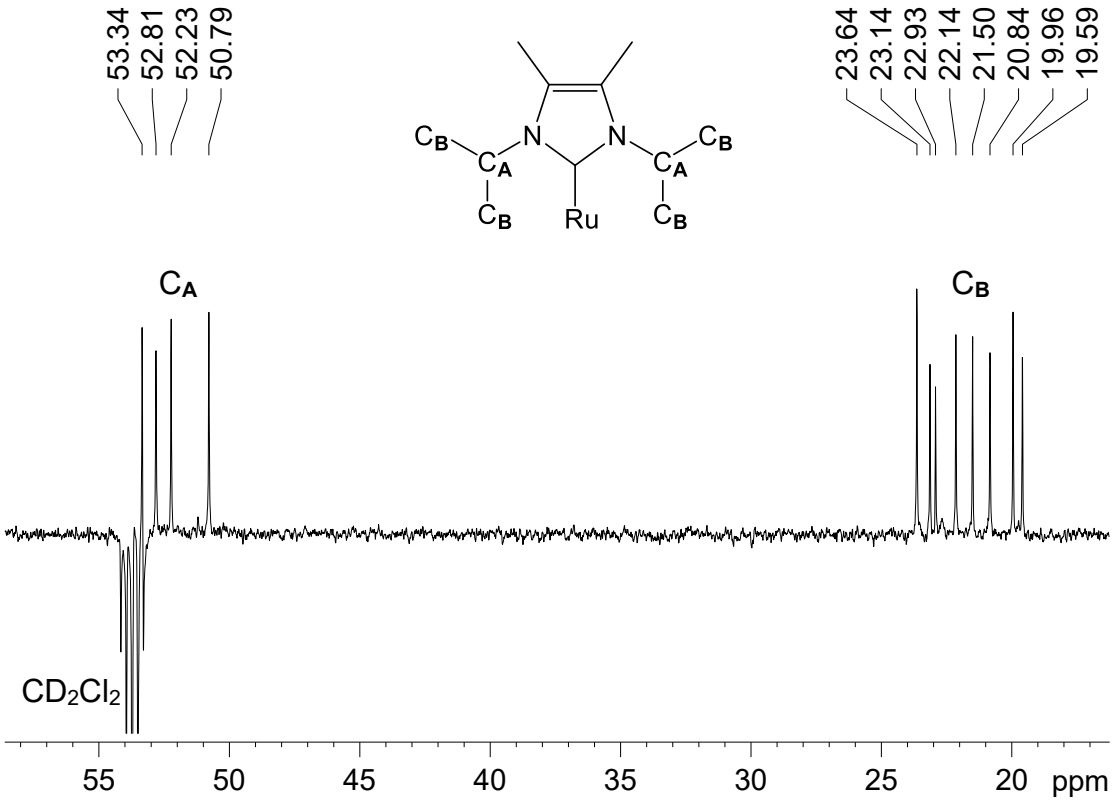

Figure 2.56 $^{13}C\{^{1}H\}$ PENDANT NMR spectrum of 4C, isopropyl region (CD_2Cl_2, 298 K, 126 MHz)

2.5.5 Ru(I^{i}Pr$_2$)$_2$(CO)$_2$(CO$_3$) (5B)

Dissolution of **5A** in pyridine in a J. Youngs ampoule with freeze-pump-thaw-degassing of the solvent was followed by exposure to O_2 (1 atm) for 30 seconds with agitation. Subsequent removal of the gas and solvent *in vacuo* afforded a yellow product. ^{1}H NMR spectroscopy of the crude material revealed signals for a new major product (**5B**) and a minor product, likely to be Ru(I^{i}Pr$_2$)$_2$(CO)(C$_5$H$_5$N)(CO$_3$), analogous to **4C**. Washing with THF removed the minor product, and recrystallisation from CH_2Cl_2/hexane afforded crystals which allowed **5B** to be structurally characterised as *cis*-Ru(I^{i}Pr$_2$)$_2$(CO)$_2$(CO$_3$) (**Figure 2.57**) (structure discussed in **Section 2.5.7**).

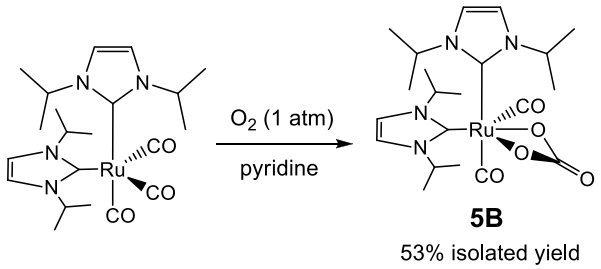

Figure 2.57 Formation of *cis*-Ru(I^{i}Pr$_2$)$_2$(CO)$_2$(CO$_3$) (5B)

In the ^{1}H NMR spectrum of pure **5B**, sixteen resonances were seen for the inequivalent proton environments of the two *cis*-I^{i}Pr$_2$ ligands. At 298 K, eight of these resonances were broad, but sharpened upon cooling to 262 K (**Figure 2.58**). ^{13}C NMR spectroscopy showed inequivalent environments for all carbon atoms, with notable resonances at δ 201.3 and 192.9 (*C*O), at δ 176.5 and 169.0 (Ru-C_{NHC}) and at δ 166.8 (*C*O$_3$) derived from a ^{1}H-^{13}C HMBC correlation experiment at 262 K (**Figure 2.59**). This spectrum provides correlation of C4(*H*)/C5(*H*) and isopropyl-C*H* protons of the I^{i}Pr$_2$ ligands with the Ru-C_{NHC} resonances, whereas no coupling is observed to the *C*O$_3$ ligand signal.

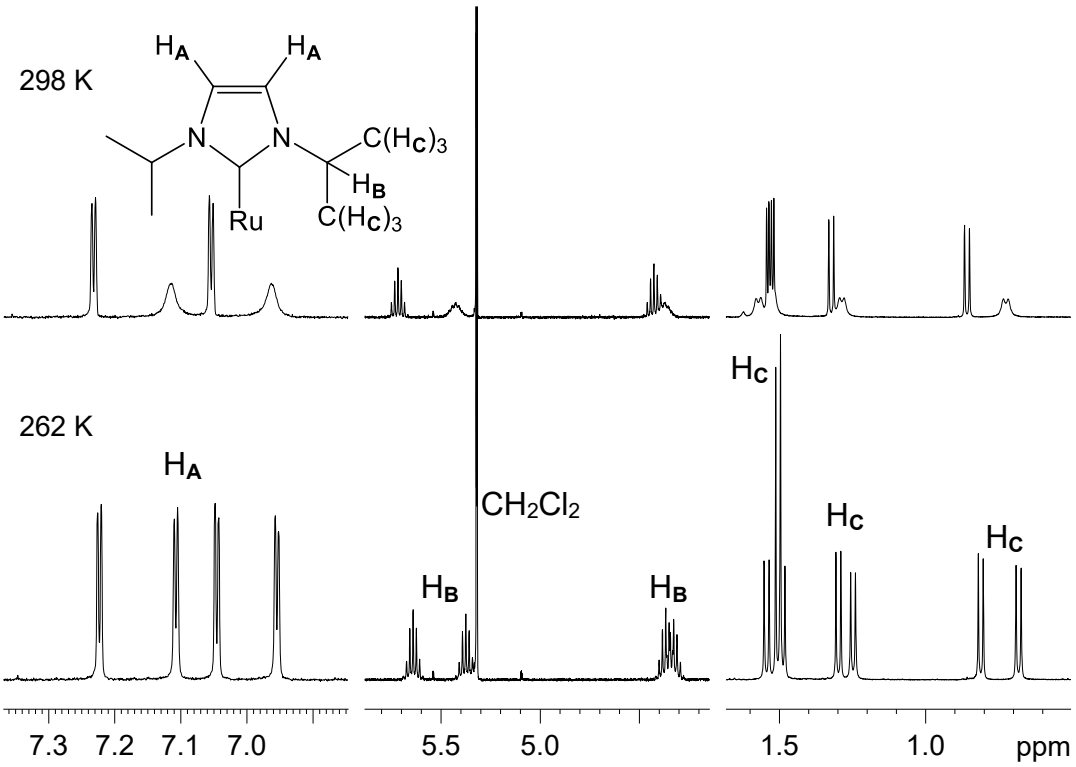

Figure 2.58 Variable temperature ^{1}H NMR spectra of 5B (CD_2Cl_2, 400 MHz)

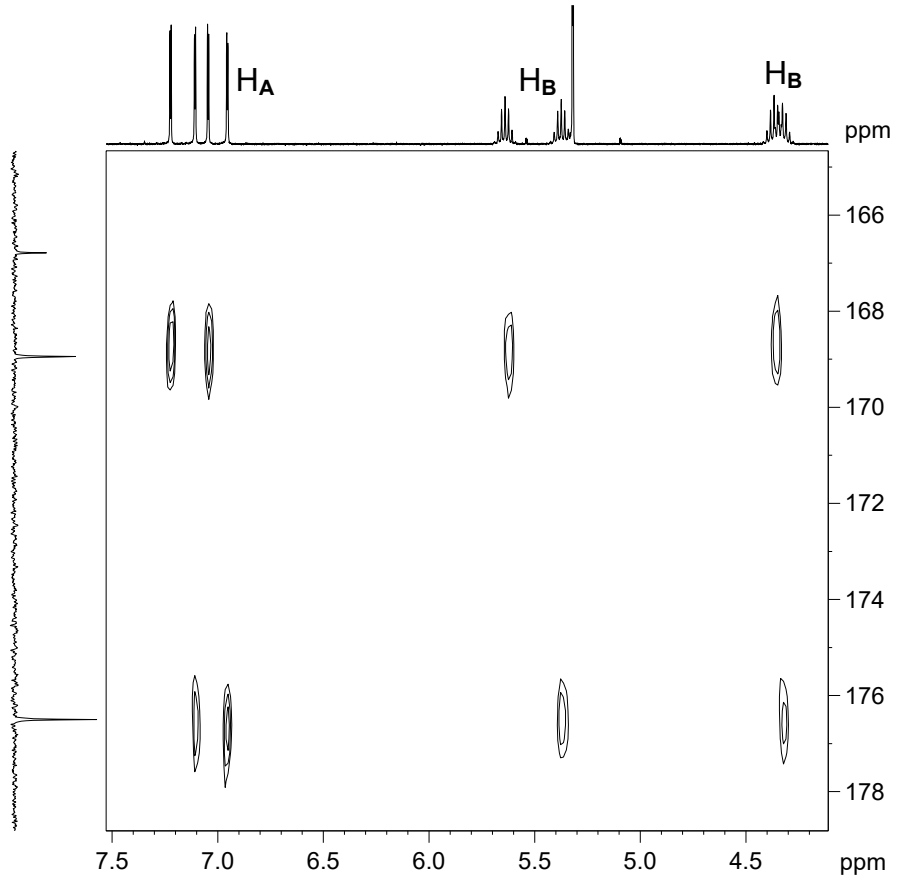

Figure 2.59 ^{1}H-^{13}C HMBC spectrum of 5B (CD_2Cl_2, 262 K, 400 MHz)

2.5.6 Summary

Complexes **3B**, **4B** and **5B** display two IR bands for each CO ligand, and **4C** has only one CO band. Carbonato bands are comparable in all cases to those of literature compounds, $Ru(PPh_3)_2(CO)_2(CO_3)$, $Ru(PEt_3)_3(CO)(CO_3)$ and $CpMo(CO)_2(CO_3)$ (**Table 2.11**). In summary, the rates of oxidation for $Ru(NHC)_2(CO)_3$ complexes was of the order **4A** ≈ **5A** >> **3A** and took place in solution and in the solid-state. The *trans*-NHC ligands in **3A** appear to help slow the rate of oxidation (1 week), whereas the *cis*-NHC ligands in **4A** and **5A** cause the oxidation reaction to be considerably more facile (< 1 minute). In comparison, Morris *et al* finds the related complex, *trans*-$Ru(IMes)(PPh_3)(CO)_3$ to be stable indefinitely in air.[45] **4B** and **5B** were best prepared by addition of 1 atm O_2 to pyridine solutions of **4A** and **5A**, although minor by-products from CO/pyridine exchange in solution did lead also to the isolation of **4C**. **3A** generated a range of products on addition of O_2 in solution and consequently heating in the solid-state under 1 atm of O_2 was preferred to form **3B**. In each complex, retention of NHC stereochemistry was maintained. Insertion of O_2 into the Ru-C bond of a CO ligand has been shown previously in separate studies by Caulton[51] and Valentine,[50] although not until now in the presence of NHC ligands.

Compound	$\nu_{(CO)}$ cm^{-1}	$\nu_{(OCO)}$ cm^{-1}
3B	2024, 1947	1612
4B	2034, 2945	1593
4C	1905	1643
5B	2044, 1954	1586
$Ru(PPh_3)_2(CO)_2(CO_3)$[50]	2045, 1980, 1950	1675, 1635
$Ru(PEt_3)_3(CO)(CO_3)$[51]	1917	1669
$CpMo(CO)_2(CO_3)$[52]	-	1615

Table 2.11 IR bands for 3B, 4B, 4C, 5C and related compounds

2.5.7 Structural comparisons of 3B, 4B, 4C and 5B

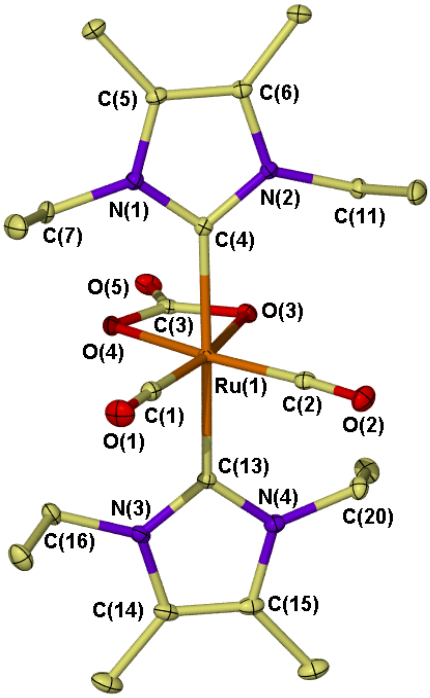

Figure 2.60 Crystal structure of $Ru(IEt_2Me_2)_2(CO)_2(CO_3)$ (3B) with thermal ellipsoids set to 30% probability and hydrogen atoms omitted for clarity

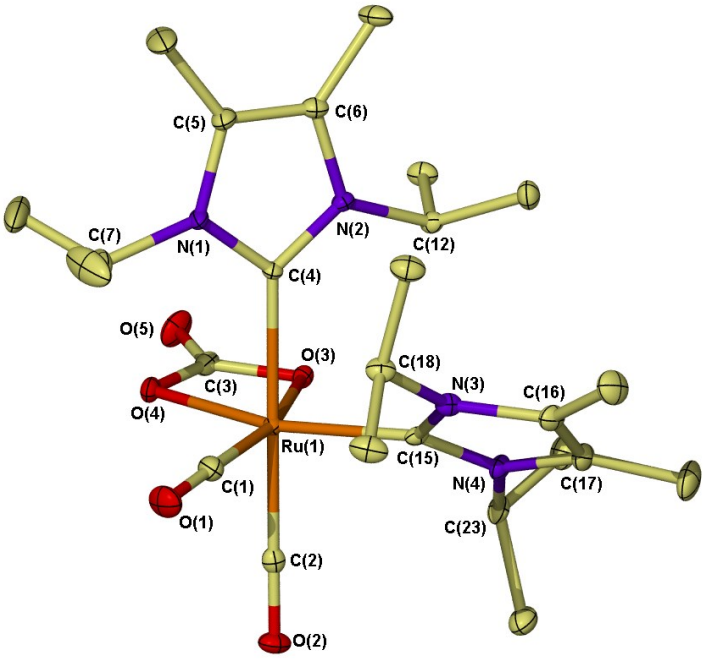

Figure 2.61 Crystal structure of $Ru(I^iPr_2Me_2)_2(CO)_2(CO_3)$ (4B) with thermal ellipsoids set to 30% probability and hydrogen atoms omitted for clarity

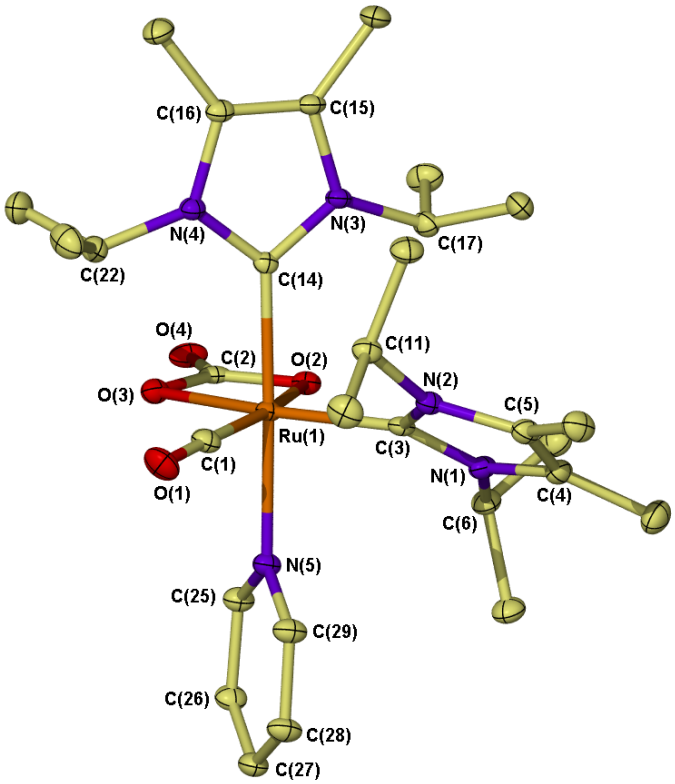

Figure 2.62 Crystal structure of Ru(I^{i}Pr$_2$Me$_2$)$_2$(CO)(C$_5$H$_5$N)(CO$_3$) (4C) with thermal ellipsoids set to 30% probability and hydrogen atoms omitted for clarity

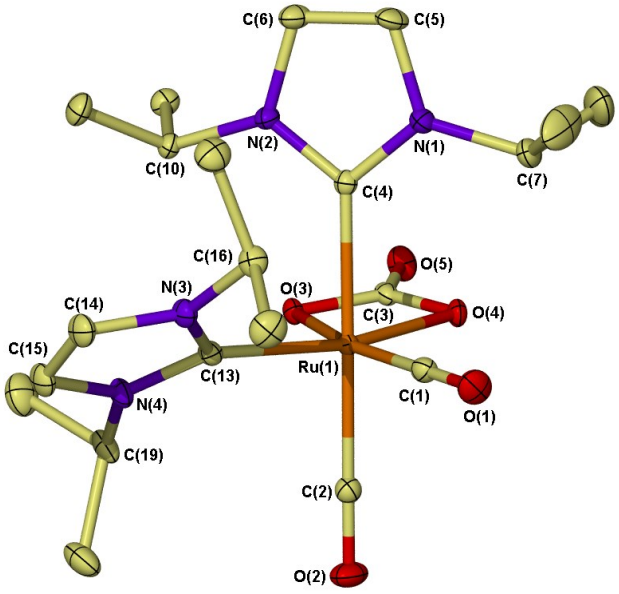

Figure 2.63 Crystal structure of Ru(I^{i}Pr$_2$)$_2$(CO)$_2$(CO$_3$) (5B) with thermal ellipsoids set to 30% probability and hydrogen atoms omitted for clarity

Crystal structures of **3B**, **4B**, **4C** and **5B** are shown in **Figures 2.60**, **2.61**, **2.62** and **2.63** respectively. **3B** crystallised as two similar but independent structures, only one of which

(Ru(1)) is shown in **Figure 2.60**. Pertinent bond lengths (Å) and angles (˚) are presented in **Table 2.12** (**4B**, **4C**, **5B**) and **Table 2.13** (**3B**), with complete tables of bond lengths and angles given in the **Appendices**. All complexes exhibit a distorted octahedral geometry, with retention of NHC stereochemistry from the parent compounds **3A**, **4A** and **5A**. The deviation from octahedral geometry is apparent in the L_{ax}-Ru-L_{ax} angles of 177.17(8)-170.37(7)˚, which follow the order **4B** > **4C** > **5B** > **3B**. Carboxylate ligand O-C and O=C bond lengths are identical for each compound at 1.310(3)-1.332(2) Å and 1.231(4)-1.236(3) Å respectively, and are comparable with literature examples such as 1.300(5)-1.307(5) Å (O-C) and 1.229(5) Å (O=C) for $CpMo(CO)_2(CO_3)$.[52]

	4B	**4C**	**5B**
Ru-C_{NHC}	2.151(3) (ax)	2.066(2) (ax)	2.121(3) (ax)
	2.109(2) (eq)	2.081(2) (eq)	2.083(3) (eq)
Ru-C_{CO}	1.901(4) (ax)	2.174(2) (ax)[a]	1.937(3) (ax)
	1.845(2) (eq)	1.820(3) (eq)	1.861(3) (eq)
Ru-O[b]	2.1003(12)	2.1132(16)	2.1165(19)
Ru-O[c]	2.0975(13)	2.1211(16)	2.0992(19)
O-C (CO_3)	1.332(2), 1.310(3)	1.327(3), 1.316(3)	1.328(3), 1.314(3)
O=C (CO_3)	1.233(3)	1.236(3)	1.231(4)
C_{NHC}-Ru-C_{NHC}	88.76(10)	92.47(9)	89.21(11)
L_{ax}-Ru-L_{ax}	177.17(8)	176.24(8)	175.46(12)

[a] value for Ru-N(C_5H_5N). [b] Trans to NHC. [c] Trans to CO.

Table 2.12 Bond lengths (Å) and angles (˚) for 4B, 4C and 5B

Dihedral angles between NHC rings in **4B** (64.1˚) and **5B** (66.1˚) are reduced on formation of the carbonato species compared with the tri-carbonyls **4A** (67.5˚) and **5A** (67.2˚), whereas a significantly greater angle is found in **4C** (70.7˚). The structure of **4C** also appears divergent to those of **4B**/**5B** by the enlarged C_{NHC}-Ru-C_{NHC} bond angle of 92.47(9)˚ compared with the identical values for **4B** and **5B** (88.76(10)-89.21(11)˚). In *cis*-NHC complexes **4A** and **5A**, equatorial ligands (both CO and NHCs) boast shorter Ru-L bond lengths than axial equivalents, such as the Ru-C_{NHC} bond lengths in **4A** which are 2.178(2) Å (axial) and 2.2019(17) Å (equatorial). Interestingly, for the related *cis*-phosphine compound $Ru(dppe)(CO)_3$ (also trigonal bipyramidal in structure), showed no difference in Ru-L bond lengths between axial (2.3555(10) Å) and equatorial

(2.3583(11) Å) phosphine ligands, or any of the CO ligands.[53] The overall trend in Ru-C_{NHC} bond lengths in *cis*-NHC carbonato complexes follows the order **4B** > **5B** > **4C**, although Ru-C_{CO} distances are longer in **5B** than both **4B** and **4C**. Complexes **4B** and **5B** display shorter Ru-C_{NHC} bond lengths than their parent complexes **4A** and **5A**, possibly as a result of a decrease in electron density around the metal centre when going from a neutral Ru(0) complex to a Ru(II) one, requiring greater Ru-C_{NHC} orbital overlap.

	3B, Ru(1)	**3B, Ru(2)**
Ru-C_{NHC}	2.1290(18)	2.1213(18)
	2.1318(17)	2.1264(19)
Ru-C_{CO}	1.8606(19)	1.864(2)
	1.8681(19)	1.866(2)
Ru-O	2.0945(12)	2.0955(12)
	2.1045(12)	2.1036(12)
O-C (CO_3)	1.326(2), 1.326(2)	1.328(2), 1.322(2)
O=C (CO_3)	1.228(2)	1.228(2)
C_{NHC}-Ru-C_{NHC}	172.94(6)	170.37(7)

Table 2.13 Bond lengths (Å) and angles (˚) for 3B (Ru1 and Ru2)

Tilting of NHC ligands (as shown in **Figure 2.47**) is maintained for *cis*-NHC compounds **4B**, **4C** and **5B**, (representative values in **4B**, N(2)-C(4)-Ru(1) 128.46(19)˚; N(1)-C(4)-Ru(1) 126.95(19)˚(ax); N(4)-C(15)-Ru(1) 126.69(15)˚; N(3)-C(15)-Ru(1) 127.68(17)˚(eq)) although is observed for only one NHC ligand (out of the four present over two structures in the asymmetric unit) in **3B**. A summary of important bond lengths (Å) and angles (˚) for both structures of **3B** is presented in **Table 2.13**. Due to the resulting high level of symmetry from *trans*-NHC ligands, bond lengths and angles in **3B** are unremarkable. Ru-C_{NHC} bond lengths are the same as for the parent complex **3A**, whereas Ru-C_{CO} distances are shorter (1.905(3)-1.916(3) Å (**3A**); 1.8606(19)-1.8681(19) Å (**3B**)). C_{NHC}-Ru-C_{NHC} bond angles are the same for **3A** and **3B**, although a significant reduction is observed in the dihedral twist angles of the NHC rings from **3A** (46.1˚) to **3B** (6.8˚ Ru(1) and 23.1˚ Ru(2)). The disparity in dihedral angles of **3B** for Ru(1) and Ru(2) may source from differences in conformations of the β-ethyl carbon atoms, which in Ru(2) both align along the CO vectors but in Ru(1) one pair are staggered, as shown in **Figure 2.64**.

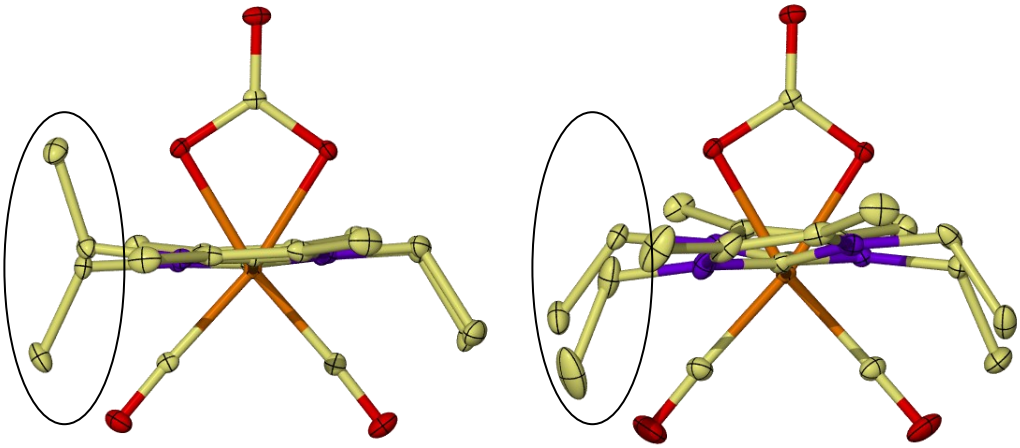

Figure 2.64 Crystal structures of 3B (Ru(1) (left) and Ru(2) (right)) viewed down the C_{NHC}-Ru-C_{NHC} axis and demonstrating the staggered and parallel β-ethyl carbon atoms

2.6 Summary and outlook

This work has sought to expand the range of reactions involving $M_3(CO)_{12}$ (M = Ru, Os) complexes with NHCs, in order to gain an improved understanding of how the steric and electronic factors of NHCs can affect the outcome of products. A summary of all isolated compounds in this chapter is shown in schematic form in **Figure 2.65**.

The reactions of $M_3(CO)_{12}$ with NHCs possessing extremely bulky N-substituents such as in I^tBu_2 and IAd_2 has been shown in this work to invoke abnormal binding from free NHCs for the first time. Of the resulting complexes, $Ru_3(aI^tBu_2)(CO)_{11}$ was the first known example of aNHC binding to ruthenium in the literature, with the related complexes $Ru_3(aIAd_2)(CO)_{11}$ and $Os_3(aIAd_2)(CO)_{11}$ joining a small but expanding class of Group VIII - aNHC compounds. Thermolysis of the $Ru_3(aNHC)(CO)_{11}$ complexes was then shown to facilitate thermally induced C-H activation of the C5-imidazol protons to yield complexes of the type, $Ru_3(\mu\text{-}H)(aNHC)'(CO)_9$. In these species the NHC is bound via a highly unusual 5centre-4electron binding mode which, to date, remains unprecedented for an NHC ligand.

Reactions of $Ru_3(CO)_{12}$ with NHCs possessing small to medium sized N-substituents such as those in IEt_2Me_2, $I^iPr_2Me_2$ and I^iPr_2 resulted in degradation of the cluster. The formation of mononuclear $Ru(NHC)_2(CO)_3$ complexes from these reactions was observed through crystallographic analysis to display both *trans*- and *cis*-NHC ligand geometries. As all

three NHCs were strong σ-donors of similar basicity, it was unusual that the bulkier N-^{i}Pr NHCs were found to exist in the *cis*- geometry, whereas with less bulky N-Et NHC ligands gave the *trans*- isomer. This was remarkable from comparisons with other literature compounds, where the *trans*- conformer is typically favored on steric and electronic grounds. Data for these complexes through solution NMR spectroscopy was indicative of highly dynamic systems, which appeared to be independent of the *cis*- or *trans*- nature of the NHC ligand geometries in the solid-state. Oxidation of the $Ru(NHC)_2(CO)_3$ complexes under O_2 was found to occur in the solid-state and in solution, leading to the isolation of carbonato complexes, $Ru(NHC)_2(CO)_2(CO_3)$ with retention of stereochemistry in each case. Rates of oxidation were found to be significantly higher for the *cis*-NHC complexes compared with the *trans*-NHC conformers.

Potential future directions of this work may be split into two parts. Firstly, the effects of the already isolated compounds $Ru_3(aNHC)(CO)_{11}$ and $Ru_3(\mu\text{-}H)(aNHC)'(CO)_9$ may wish to be explored for their effects in catalytic processes such as the Murai reaction. There are a large number of catalytic procedures in which $Ru_3(CO)_{12}$ is utilised, for example in the intermolecular cyclocoupling of ketones, alkenes and CO[54] and a comparison of catalytic activities between $Ru_3(CO)_{12}$ and the aNHC compounds would be interesting to explore. Lastly, due to the extensive range of NHCs available to the chemist today, the reaction of $Ru_3(CO)_{12}$ with any number of these ligands could lead to potentially more active catalysts for organic transformations, or more examples of unusual complexes or binding modes to append those discovered in this work.

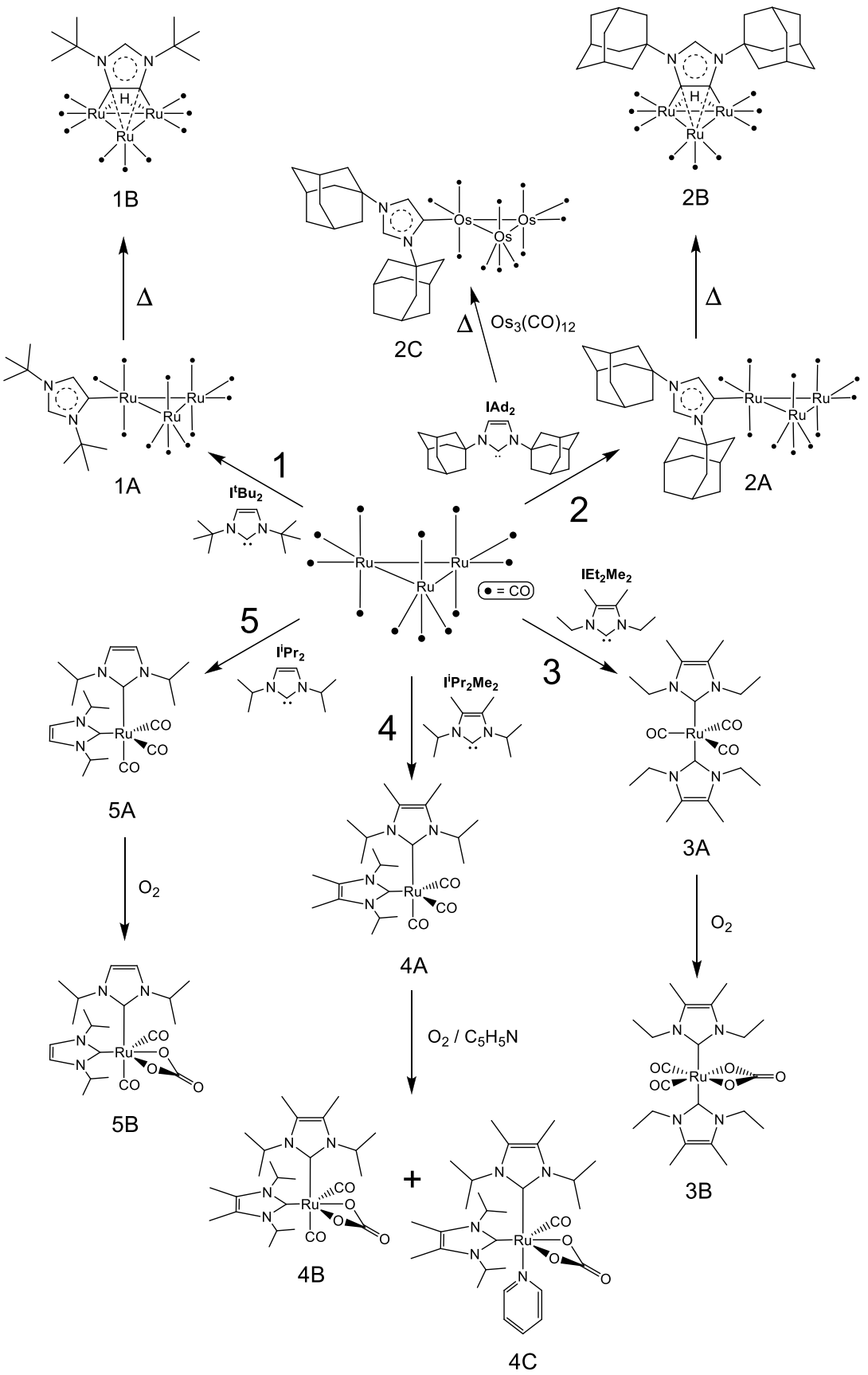

Figure 2.65 Summary of complexes from $Ru_3(CO)_{12}$ + NHC reactions

2.7 References

1 Cabeza, J. A.; Rio, I.; Miguel, D.; Sanchez-Vega, M. G., *Chem. Commun.* **2005**, 3956-3958.

2 Lappert, M. F.; Pye, P. L., *Dalton Trans.* **1977**, 2172-2180.

3 Burling, S.; Paine, B. M.; Nama, D.; Brown, V. S.; Mahon, M. F.; Prior, T. J.; Pregosin, P. S.; Whittlesey, M. K.; Williams, J. M. J., *J. Am. Chem. Soc.* **2007**, *129*, 1987-1995.

4 Burling, S.; Mahon, M. F.; Powell, R. E.; Whittlesey, M. K.; Williams, J. M. J., *J. Am. Chem. Soc.* **2006**, *128*, 13702-13703.

5 Burling, S.; Mahon, M. F.; Paine, B. M.; Whittlesey, M. K.; Williams, J. M. J., *Organometallics* **2004**, *23*, 4537-4539.

6 Leadbeater, N. E., *J. Organomet. Chem.* **1999**, *573*, 211-216.

7 Bruce, M. I.; Shaw, G.; Stone, F. G. A., *Dalton Trans.* **1972**, 2094-2099.

8 Arnold, P. L.; Pearson, S., *Coord. Chem. Rev.* **2007**, *251*, 596-609.

9 Albrecht, M., *Chem. Commun.* **2008**, 3601-3610.

10 Eguillor, B.; Esteruelas, M. A.; Olivan, M.; Puerta, M., *Organometallics* **2008**, *27*, 445-450.

11 Lebel, H.; Janes, M. K.; Charette, A. B.; Nolan, S. P., *J. Am. Chem. Soc.* **2004**, *126*, 5046-5047.

12 Grundemann, S.; Kovacevic, A.; Albrecht, M.; Faller, J. W.; Crabtree, R. H., *J. Am. Chem. Soc.* **2002**, *124*, 10473-10481.

13 Grundemann, S.; Kovacevic, A.; Albrecht, M.; Faller, J. W.; Crabtree, R. H., *Chem. Commun.* **2001**, 2274-2275.

14 Heckenroth, M.; Kluser, E.; Neels, A.; Albrecht, M., *Angew. Chem., Int. Ed.* **2007**, *46*, 1-5.

15 Prades, A.; Viciano, M.; Sanau, M.; Peris, E., *Organometallics* **2008**, *27*, 4254-4259.

16 Graham, T. W.; Udachin, K. A.; Carty, A. J., *Chem. Commun.* **2006**, 2699-2701.

17 Ellis, B. D.; Dyker, A.; Decken, A.; Macdonald, C. L. B., *Chem. Commun.* **2005**, 1965-1967.

18 Hillier, A. C.; Sommer, W. J.; Yong, B. S.; Petersen, J. L.; Cavallo, L.; Nolan, S. P., *Organometallics* **2003**, *22*, 4322-4326.

19 Dorta, R.; Stevens, E. D.; Scott, N. M.; Costabile, C.; Cavallo, L.; Hoff, C. D.; Nolan, S. P., *J. Am. Chem. Soc.* **2005**, *127*, 2485-2495.

20 Dorta, R.; Stevens, E. D.; Hoff, C. D.; Nolan, S. P., *J. Am. Chem. Soc.* **2003**, *125*, 10490-10491.

21 Spectra for **2A** was recorded in d_8-THF and CD_2Cl_2. CD_2Cl_2 is shown here for clarity due to overlap of resonances in d_8-THF.

22 **2C** decomposes in $CHCl_3$/CH_2Cl_2

23 *Comprehensive Organometallic Chemistry III*. Crabtree, R. H.; Mingos, M. P.; Bruce, M., Elsevier, Oxford, UK; **2007**.

24 Crittall, M. R.; Ellul, C. E.; Mahon, M. F.; Saker, O.; Whittlesey, M. K., *Dalton Trans.* **2008**, 4209-4211.

25 Cabeza, J. A.; Rio, I.; Miguel, D.; Perez-Carreno, E.; Sanchez-Vega, M. G., *Organometallics* **2008**, *27*, 211-217.

26 Johnson, B. F. G.; Lewis, J.; Pippard, D. A., *Dalton Trans.* **1981**, 407-412.

27 Baya, M.; Eguillor, B.; Esteruelas, M. A.; Olivan, M.; Onate, E., *Organometallics* **2007**, *26*, 6556-6563.

28 Cooke, C. E.; Jennings, M. C.; Pomeroy, R. K.; Clyburne, J. A. C., *Organometallics* **2007**, *26*, 6059-6062.

29 Churchill, M. R.; Hollander, F. J.; Hutchinson, J. P., *Inorg. Chem.* **1977**, *16*, 2655-2659.

30 Churchill, M. R.; DeBoer, B. G., *Inorg. Chem.* **1977**, *16*, 878-884.

31 Forbes, E. J.; Goodhand, N.; Jones, D. L.; Hamor, T. A., *J. Organomet. Chem.* **1979**, *182*, 143-154.

32 Bruce, M. I.; Liddell, M. J.; Hughes, C. A.; Skelton, B. W.; White, A. H., *J. Organomet. Chem.* **1988**, *347*, 157-180.

33 Crystallisation attempts of **2B** from THF/hexane were unsuccessful due to its high solubility in hexane.

34 Day, M. W.; Hajela, S.; Kabir, S. E.; Irving, M.; McPhillips, T.; Wolf, E.; Hardcastle, K. I.; Rosenberg, E., *Organometallics* **1991**, *10*, 2743-2751.

35 Kabir, S. E.; Rosenberg, E., *Organometallics* **1997**, *16*, 2674-2681.

36 Rosenberg, E., *Organometallics* **1997**, *16*, 2665-2673.

37 Suss-Fink, G.; Jenke, T.; Heitz, H.; Pellinghelli, M. A.; Tiripicchio, A., *J. Organomet. Chem.* **1989**, *379*, 311-323.

38 Rosenberg, E.; Kabir, S. E.; Hardcastle, K. I.; Day, M.; Wolf, E., *Organometallics* **1990**, *9*, 2214-2217.

39 Ellul, C. E.; Mahon, M. F.; Saker, O.; Whittlesey, M. K., *Angew. Chem., Int. Ed.* **2007**, *46*, 6343-6345.

40 Rossi, A. R.; Hoffmann, R., *Inorg. Chem.* **1975**, *14*, 365-374.

41 Burling, S.; Kociok-Kohn, G.; Mahon, M. F.; Whittlesey, M. K.; Williams, J. M. J., *Organometallics* **2005**, *24*, 5868-5878.

42 Jazzar, R. F. R.; Bhatia, P. H.; Mahon, M. F.; Whittlesey, M. K., *Organometallics* **2003**, *22*, 670-683.

43 Bruce, M. I.; Cole, M. L.; Fung, R. S. C.; Forsyth, C. M.; Hilder, M.; Junk, P. C.; Konstas, K., *Dalton Trans.* **2008**, 4118-4128.

44 Shriver, D. F.; Atkins, P. W., Oxford University Press, UK; **1999**.

45 Abdur-Rashid, K.; Fedorkiw, T.; Lough, A. J.; Morris, R. H., *Organometallics* **2004**, *23*, 86-94.

46 Whittlesey, M. K.; Perutz, R. N.; Virrels, I. G.; George, M. W., *Organometallics* **1997**, *16*, 268-274.

47 Gottschalk-Gaudig, T.; Folting, K.; Caulton, K. G., *Inorg. Chem.* **1999**, *38*, 5241-5245.

48 Chatwin, S. L., *Ph.D. Thesis, University of Bath.* **2007**.

49 Ng, S. Y.; Goh, L. Y.; Koh, L. L.; Leong, W. K.; Tan, G. K.; Ye, S.; Zhu, Y., *Eur. J. Inorg. Chem.* **2006**, 663-670.

50 Valentine, J.; Valentine, D.; Collman, J. P., *Inorg. Chem.* **1971**, *10*, 219-225.

51 Ogasawara, M.; Maseras, F.; Gallego-Planas, N.; Kawamura, K.; Ito, K.; Toyota, K.; Streib, W. E.; Komiya, S.; Eisenstein, O.; Caulton, K. G., *Organometallics* **1997**, *16*, 1979-1993.

52 Curtis, M. D.; Han, K. R., *Inorg. Chem.* **1985**, *24*, 378-382.

53 Bunten, K. A.; Farrar, D. H.; Poe, A. J.; Lough, A. J., *Organometallics* **2000**, *19*, 3674-3682.

54 Tobisu, M.; Chatani, N.; Asaumi, T.; Amako, K.; Ie, Y.; Fukumoto, Y.; Murai, S., *J. Am. Chem. Soc.* **2000**, *122*, 12663-12674.

Chapter 3

Ruthenium Hydride Chemistry

3.1 Preface

Over the past few years, one of our group's chief areas of interest has involved the synthesis and investigation of a series of 16-electron coordinatively unsaturated *bis*-NHC ruthenium-hydride complexes of the type $Ru(NHC)_2(CO)HX$ shown in **Figure 3.1**. These complexes are stabilised by bulky N-aryl substituents on the NHC and thus far, our investigations have only encompassed the use of the IMes ligand for this task.[1-3] It is however well documented that variation of the functionality on the NHC ligand can greatly influence the corresponding spectroscopic and catalytic properties of the complex,[4-10] most dramatically demonstrated perhaps by Grubbs' range of metathesis catalysts.[11,12] Previously published $Ru(NHC)_2(CO)HX$ complexes by our group have so far incorporated -OEt, -OH, -F, -SH and -SR moieties as ligand X. One ligand so far neglected prior to this study has been -Cl, which demonstrates potential as a 'universal' X-group that could be simply removed or exchanged for more catalytically useful ligands, as has been shown in many studies with related phosphine complexes.[13-16] In light of the results collated in this work, the analogous hydride-chloride complex $Ru(IMes)_2(CO)HCl$ was prepared for comparative studies by our group.[17]

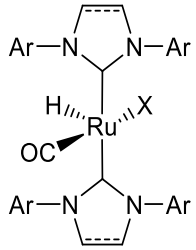

Figure 3.1 Archetypal 16-electron *bis*-NHC ruthenium-hydride complex

Studies by Yi *et al* have shown that the addition of $HBF_4{\cdot}OEt_2$ to $Ru(PCy_3)_2(CO)HCl$ solutions can dramatically increase the activity of this complex in catalytic transformations, through the generation of highly reactive 14-electron intermediates.[18] The removal of a sacrificial ligand from a 16-electron complex has been shown by other groups also through halide extraction[19-23] and protonation[24,25] processes and has been used to generate highly reactive (sometimes catalytically active) complexes or initiate bond activation reactions.[26]

These observations directly lead to the investigations of *bis*-NHC ruthenium hydride complexes presented in this chapter. The potential of an enhanced catalytic and spectroscopic understanding of NHC systems as well as the formation of highly reactive

and/or catalytically active fragments are motives for this work, both of which have been of interest to our group for a number of years.

3.2 Formation of $Ru(NHC)_2(CO)HCl$ complexes

3.2.1 Introduction

The employment of IPr and SIPr ligands in 16-electron *bis*-NHC complexes in this work stemmed from a desire to observe changes through increasing the steric protection afforded to the vacant site of the metal. The $\%V_{Bur}$ values of IPr (29) and SIPr (30) make them sterically bulkier than the mesityl analogues IMes (26) and SIMes (27). The saturated NHCs are bulkier than their unsaturated analogues due to increased C-C backbone bond lengths which force the N-substituents closer to the metal, effectively using the C2 carbon as a pivot (**Figure 3.2**). There are many opportunities for direct comparison of the saturated and unsaturated NHCs through differences in the spectroscopic and catalytic properties of the complexes. In $Ru(L)_2(CO)HCl$ complexes, the steric protection of L as well as the Ru-L bond strength are critical to the stability of the complex. The compounds $Ru(P^tBu_2Me)_2(CO)HCl$,[27] $Ru(P^tBu_2Et)_2(CO)HCl$[27] and $Ru(PCy_3)_2(CO)HCl$[28] contain weaker binding and less sterically bulky phosphine ligands and are all air sensitive. However the analogous *bis*-NHC complex, $Ru(IMes)_2(CO)HF$ remains stable in air for days,[3] and it was envisaged that IPr and SIPr would increase the stability of these 16-electron compounds still further. Preliminary results also indicate that the chloride ligand is very stable in the complex $Ru(IMes)_2(CO)HCl$, with this species being generated rapidly from the dissolution of $Ru(IMes)_2(CO)H(OH)$ in CH_2Cl_2 for example.[3] This trend was expected to continue for the related IPr and SIPr-containing complexes.

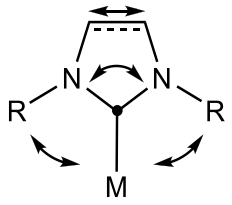

Figure 3.2 Model demonstrating the relationship between the C-C backbone bond length and the proximity of the N-substituents (R-groups) to the metal centre, affecting the NHC $\%V_{Bur}$ value

3.2.2 Ru(IPr)$_2$(CO)HCl (6A)

The addition of d_8-toluene to a J. Youngs NMR tube containing IPr and Ru(AsPh$_3$)$_3$(CO)H$_2$ in 3:1 ratio with heating at 85 ˚C led to the formation of two hydride-containing products after 24 hours, as observed by ^{1}H NMR spectroscopy. The hydride signals located at δ -22.79 and -25.65 indicated formation of Ru(IPr)$_2$(CO)H(OH) and Ru(IPr)$_2$(CO)HCl respectively, as was determined by comparisons with the fully characterised species Ru(IMes)$_2$(CO)H(OH) (δ -23.15) and Ru(IMes)$_2$(CO)HCl (δ -25.38). Traces of chloride were likely to result from contamination of Ru(AsPh$_3$)$_3$(CO)H$_2$ (produced directly from Ru(AsPh$_3$)$_3$(CO)Cl$_2$) whereas it was probable that trace amounts of water in the solvent gave rise to Ru(IPr)$_2$(CO)H(OH), as was also observed during the formation of Ru(IMes)$_2$(CO)H(OH).[1] Doping of the toluene solution with CH_2Cl_2 followed by thermolysis led to the formation of Ru(IPr)$_2$(CO)HCl as the sole hydride-containing product. At no point during the reaction (even with continued heating for 500 hours) was Ru(NHC)$_2$(AsPh$_3$)(CO)H$_2$ observed as for the same reaction with the IMes ligand,[1] possibly resulting from the increased steric shielding of the IPr ligand. Subsequent optimisation of the reaction featured heating of IPr (2.5 excess) at 85 ˚C in a J. Youngs ampoule with Ru(AsPh$_3$)$_3$(CO)H$_2$ for 1.5 hours. The addition of 1.1 equivalents of CH_2Cl_2 was followed by continued heating at 110 ˚C for 18 hours, and then removal of the solvent *in vacuo*. Extraction in toluene and washing with hexanes led to the isolation of Ru(IPr)$_2$(CO)HCl (**6A**) shown in **Figure 3.3**, with X-ray quality crystals recovered from the hexane washings at 5 ˚C to determine its solid-state arrangement.

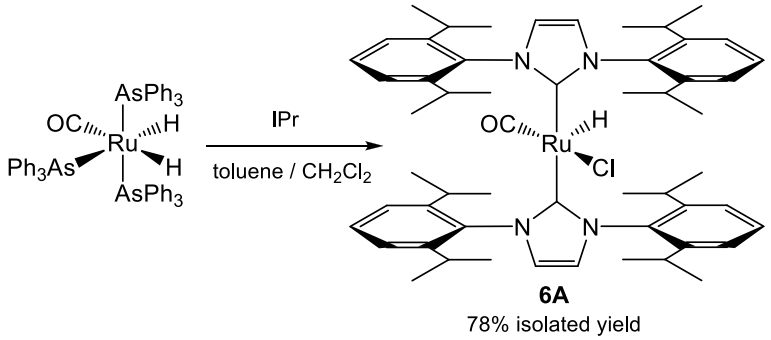

Figure 3.3 Formation of Ru(IPr)$_2$(CO)HCl (6A)

^{1}H NMR spectroscopy of **6A** in d_8-THF at ambient temperature (**Figure 3.4**) shows the isopropyl-C*H*$_3$ groups to be inequivalent resulting in eight doublet resonances (H$_\mathbf{E}$). Only two isopropyl-C*H* septets (H$_\mathbf{D}$) are observed, one of which is very broad. There is one signal for the NC*H* protons (H$_\mathbf{C}$) which overlays one of the two doublet resonances (H$_\mathbf{B}$) for

the *meta*-aryl protons, with the *para*-aryl protons observed as a triplet (H_A). The signal at δ -25.88 (H_F) is characteristic for a hydridic proton opposite a vacant site, as demonstrated in **Table 3.1**, which compares the spectroscopic data of related compounds including $Ru(IMes)_2(CO)HCl$, prepared in parallel with this study by Sarah Chatwin from the Whittlesey group by a similar method to **6A**.[17]

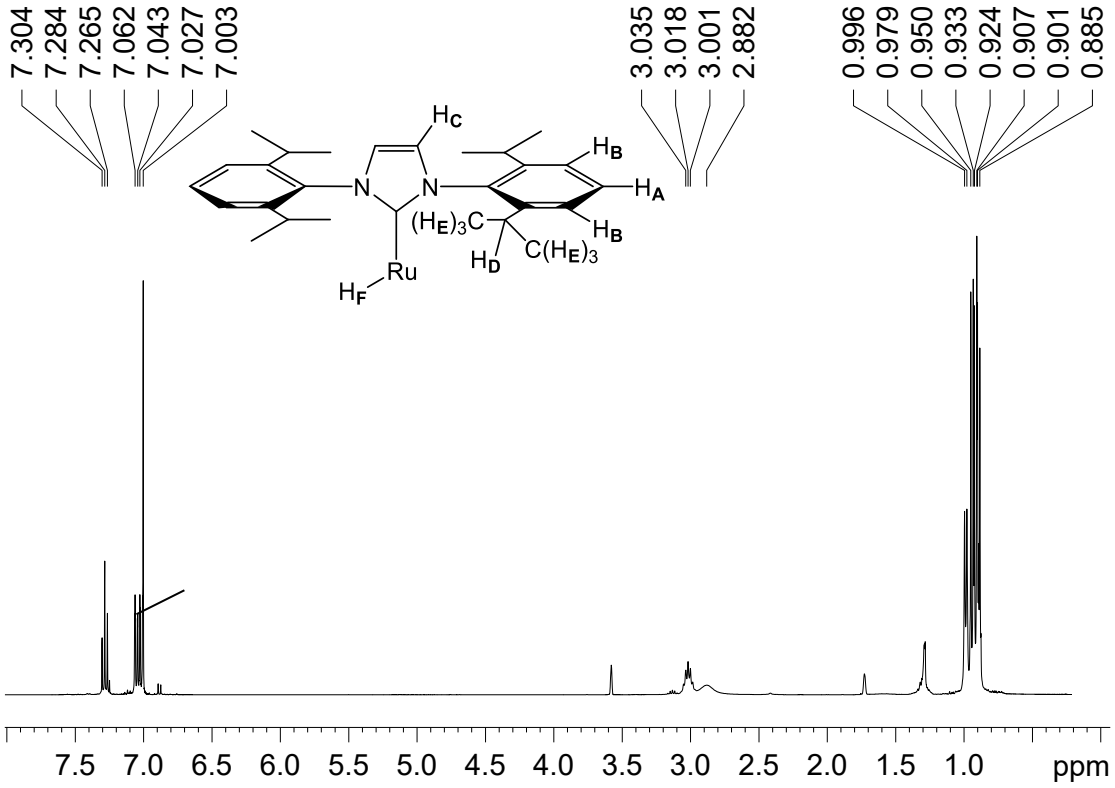

Figure 3.4 ^{1}H NMR spectrum of 6A (d_8-THF, 298 K, 400 MHz)

On dissolution of **6A** in d_8-toluene, H_E resonances were observed as four individual doublets, however signals for H_D protons still remained very broad at 298 K. Cooling to 238 K enabled these H_D signals to be resolved into four distinct septets (**Figure 3.5**). Furthermore, the singlet backbone H_C proton resonance was split into two signals also at 238 K, with these results indicating a number of inequivalencies throughout each of the IPr ligands at this temperature. Assignment of the $^{13}C\{^1H\}$ NMR resonances at room temperature was achieved through ^1H-^{13}C HMQC/HMBC correlation experiments and phase-polarisation from $^{13}C\{^1H\}$ PENDANT NMR data, with pertinent signals at δ 201.8 (*C*O) and δ 195.6 (Ru-C_{NHC}).

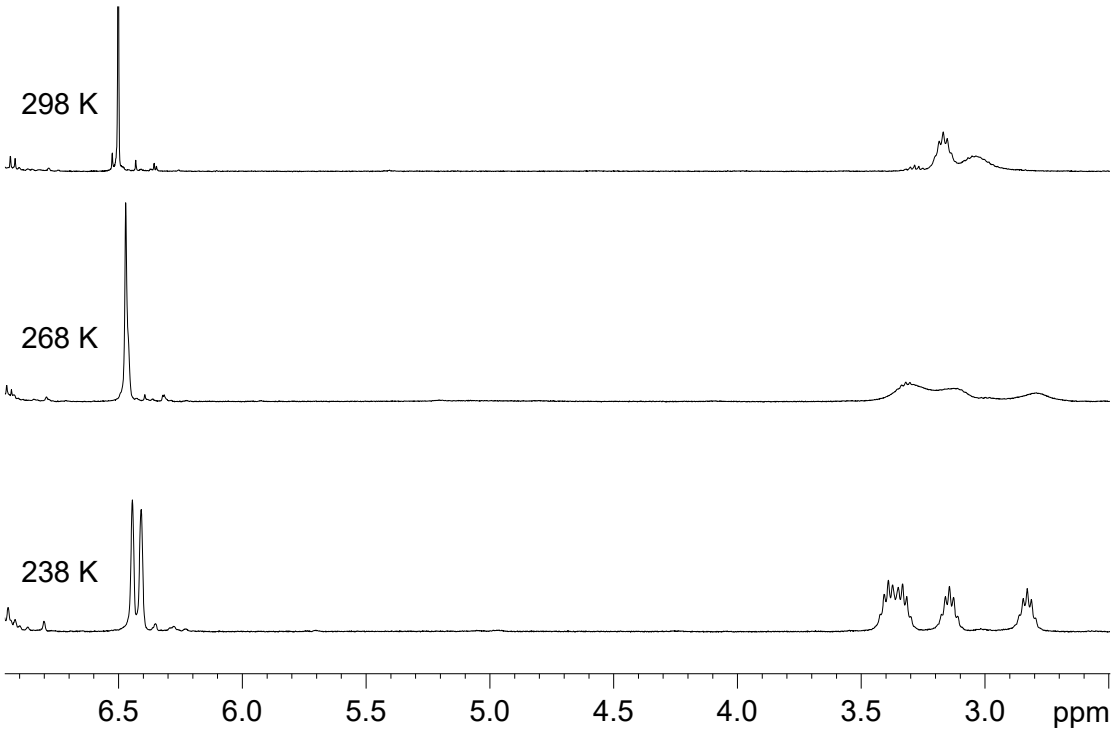

Figure 3.5 Variable temperature ^{1}H NMR spectra of 6A (*d*$_8$-toluene, 400 MHz)

The data in **Table 3.1** compares $^1H_{hydride}$ and M-C_{NHC} NMR resonances and CO IR stretches from related hydride-chloride complexes in the literature, with the data showing **6A** to be comparable to the analogous complexes. Of the three $Ru(IMes)_2(CO)HX$ complexes shown in **Table 3.1**, the chloride ligand enforces the hydride to shift to the lowest frequency of any X-group (δ -25.39 in C_6D_6). This has so far been observed for **6A** also, where the $^1H_{hydride}$ chemical shift was considerably lower than the $Ru(IPr)_2(CO)H(OH)$ complex formed in the initial reaction. The CO band of **6A** (1898 cm^{-1}) is located at a comparable but slightly higher frequency than in the $Ru(IMes)_2(CO)HX$ complexes (1861-1882 cm^{-1}). This implies that the IPr ligand is actually less donating to the metal than IMes, possibly as a result of the increased steric bulk prohibiting a close orbital overlap for this ligand. The IR band of **6A** is lower than most of the phosphine-containing complexes (1896-1913 cm^{-1}), as expected from the increased σ-donation of the NHC ligand.

Compound	$^1H_{hydride}$ (δ)	M-C_{NHC} (δ)	$\nu_{(CO)}$ / cm^{-1}
6A	-25.88 [a]	195.6	1898
Ru(IMes)$_2$(CO)HCl[17]	-25.39 [b]	195.9	1882
Ru(IMes)$_2$(CO)HF[3]	-24.55 [b]	197.0	1873
Ru(IMes)$_2$(CO)H(OH)[1]	-23.15 [b]	198.6	1861
Ru(IMes)(PPh$_3$)(CO)HCl[29]	-23.89 [b]	189.7	1913
Ru(IMes)(PCy$_3$)(CO)HCl[30]	-24.83 [b]	- [c]	1896
Ru(PCy$_3$)$_2$(CO)HCl[28,31]	-24.70 [b]	-	1905
Ru(P^{i}Pr$_3$)$_2$(CO)HCl[32]	-24.90 [b]	-	1910

[a] Recorded in d_8-THF. [b] Recorded in C_6D_6. [c] Value not quoted.

Table 3.1 $^1H_{hydride}$, Ru-C_{NHC} and IR bands for literature complexes, Ru(L)$_2$(CO)HX (L = NHC or PR$_3$, X = -Cl, -F, -OH)

The crystal structure of **6A** is shown in **Figure 3.6** and exhibits a square pyramidal geometry with the hydride ligand in the apical position *trans*- to the vacant site. The Cl-Ru-CO bonds are located on a crystallographic 2-fold rotational axis, and are disordered through molecular symmetry, which precluded accurate determination of these Ru-CO and Ru-Cl bond distances. The related Ru(IMes)$_2$(CO)HX (X = -F, -SH, -OH, -OEt)[1-3] and Ru(P^{i}Pr$_3$)$_2$(CO)HCl complexes[33] also possess the same disorder, showing it to be common in complexes of this type. Pertinent values for **6A** include an average Ru-C_{NHC} bond length of 2.0872(13) Å with a C_{NHC}-Ru-C_{NHC} angle of 178.78(8)˚, which are the same as the values for Ru(IMes)$_2$(CO)HCl (2.075(3) Å and 178.6(11)˚). In **6A** the imidazol ring of one NHC is orientated perpendicular to the Cl-Ru-CO axis, and at an angle of 39.4˚ to the other NHC to minimise steric interactions between the N-substituents. This angle is comparable, but smaller than that of 53.3˚ for Ru(IMes)$_2$(CO)HCl, with the less bulky IMes ligands allowing an increased angle of twist. Complete tables of bond lengths and angles are given in the **Appendices**.

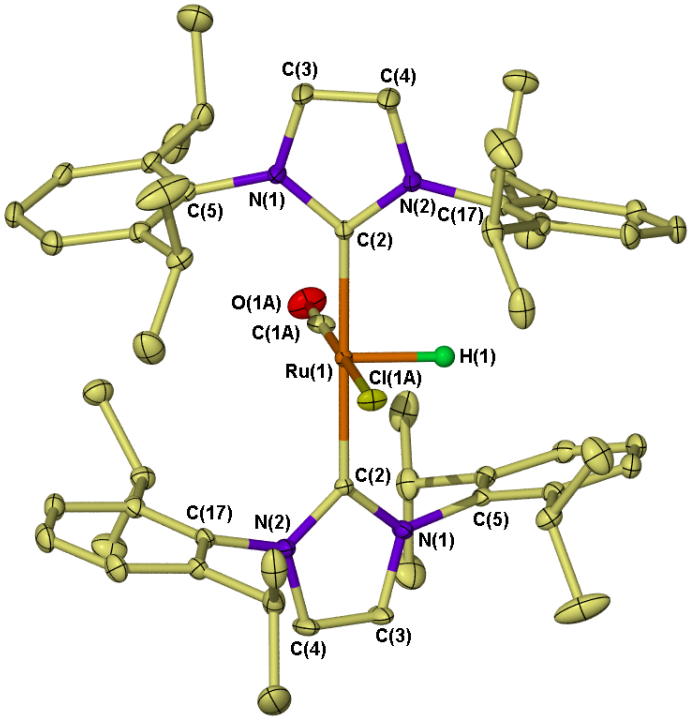

Figure 3.6 Crystal structure of $Ru(IPr)_2(CO)HCl$ (6A) with thermal ellipsoids set to 30% probability and hydrogen atoms (except the hydride) omitted for clarity

3.2.3 $Ru(SIPr)_2(CO)HCl$ (7A)

Initial studies into the generation of **7A** from free SIPr were highly problematic. Studies by Denk *et al* have demonstrated that on contact with air, saturated NHCs such as SI^tBu_2 are hydrolysed instantaneously, whereas unsaturated NHCs such as I^tBu_2 can be handled in air for brief periods of time.[34] This led to the synthesis of SIPr requiring extremely careful and time-consuming procedures to maintain the required inert conditions. Additionally it was possible only to generate small batches (ca. 150 mg, 33% yield) of SIPr under such inert conditions, which led us to investigate the use of the NHC adduct, $SIPr.C_6F_5$-H as an alternative to the free NHC. $SIPr.C_6F_5$-H (also $SIMes.C_6F_5$-H, see **Section 3.2.4**) is air-stable and can be easily generated on a large scale (ca. 4 g) and in reasonable yields (60%). This is achieved in a one-pot condensation reaction (in air) starting from the same *bis*-amine precursor used for synthesising the imidazolinium salt (**Figure 3.7**). Upon heating $SIPr.C_6F_5$-H in solution at over 50 ˚C, pentafluorobenzene is readily eliminated to give the free SIPr *in situ*.

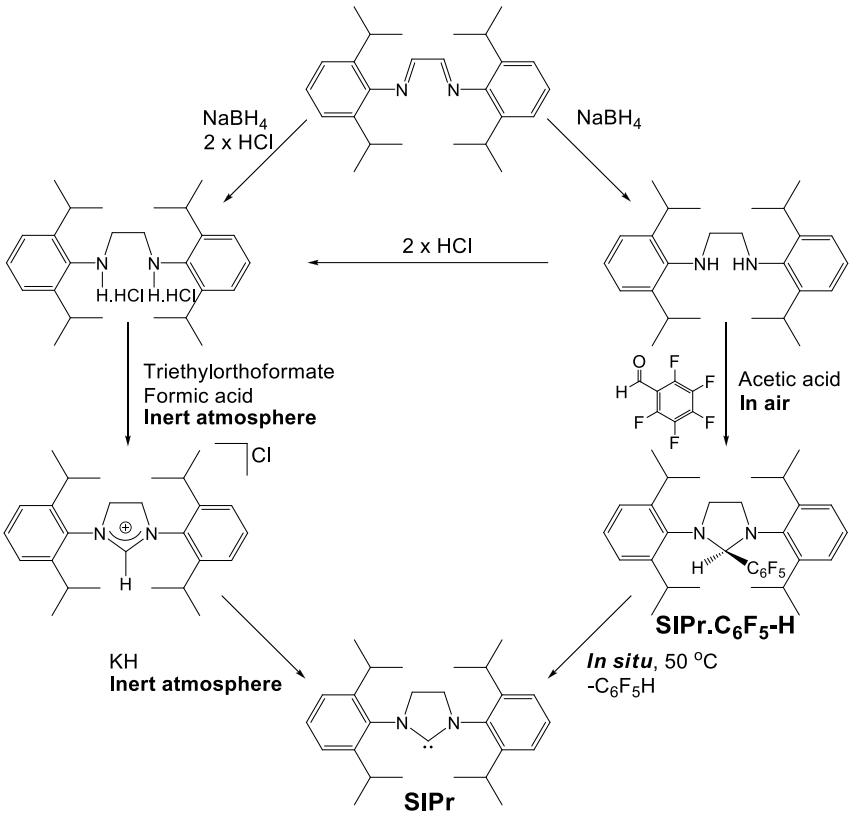

Figure 3.7 Scheme presenting formation of free SIPr and SIPr.C_6F_5-H from the same diazabutadiene precursor

On addition of d_8-toluene to a J. Youngs NMR tube containing SIPr.C_6F_5-H and $Ru(AsPh_3)_3(CO)H_2$ in a 5:1 ratio and heating at 85 ˚C, the formation of two hydride-containing products at δ -25.67 and -24.14 was observed by ^{1}H NMR spectroscopy after 18 hours. These products were assigned as $Ru(SIPr)_2(CO)HCl$ and $Ru(SIPr)_2(CO)HF$ respectively from comparisons of the hydride resonances from $Ru(IMes)_2(CO)HCl$ and $Ru(IMes)_2(CO)HF$. The formation of $Ru(SIPr)_2(CO)HF$ presumably results from defluorination of the C_6F_5H released from SIPr.C_6F_5-H, which has been observed in other reactions within the Whittlesey group.[35] No formation of $Ru(SIPr)_2(CO)H(OH)$ was detected in this reaction. The addition of CH_2Cl_2 to the solution resulted in formation of $Ru(SIPr)_2(CO)HCl$ as the only hydride-containing product upon continued heating of the reaction mixture. Optimisation of the reaction led to thermolysis of SIPr.C_6F_5-H (3-fold excess) with $Ru(AsPh_3)_3(CO)H_2$ in toluene for 5 hours at 85 ˚C. The addition of CH_2Cl_2 (0.5 equivalents) for 24 hours at 110 ˚C and subsequent addition of CH_2Cl_2 (0.5 equivalents) for another 24 hours led to complete removal of resonances attributed to $Ru(AsPh_3)_3(CO)H_2$. Removal of the solvent *in vacuo* followed by extraction in toluene and

washing with a small quantity of hexane[36] yielded $Ru(SIPr)_2(CO)HCl$ (**7A**) (**Figure 3.8**). X-ray quality crystals of **7A** were grown from hexane at 5 ˚C.

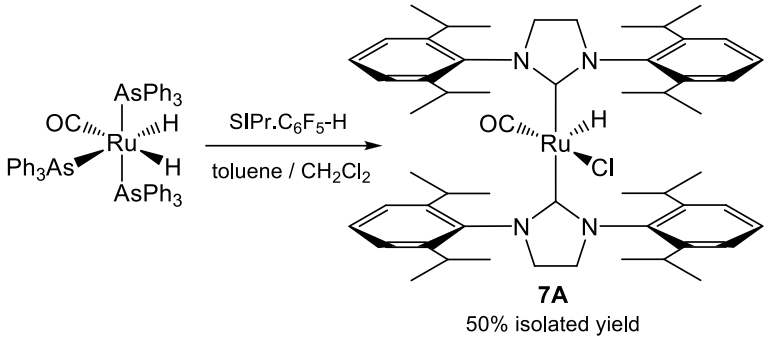

Figure 3.8 Formation of $Ru(SIPr)_2(CO)HCl$ (7A)

At ambient temperature in d_8-THF, **7A** displays a ^1H NMR spectrum (**Figure 3.9**) similar to that of **6A**, with inequivalent environments for isopropyl-C*H*$_3$ groups (H_E) and *meta*-C*H* aryl protons (H_B). In **7A** there is only one septet for the isopropyl-C*H* protons (H_D), although this signal sits atop a very broad resonance which may represent the remainder of the H_D protons. The backbone protons (H_C) are located at δ 3.73 as a broad resonance. At δ -25.77 (H_F), the hydride resonance of **7A** is at a similar frequency to **6A** (δ -25.88) and related complexes (**Table 3.1**). As was observed for **6A**, cooling **7A** below ca. 268 K in d_8-toluene led to splitting of the H_C and H_D protons that demonstrates the inequivalencies present in the SIPr ligands resulting from restricted rotation about the Ru-C_{NHC} and N-C_{Aryl} bonds.

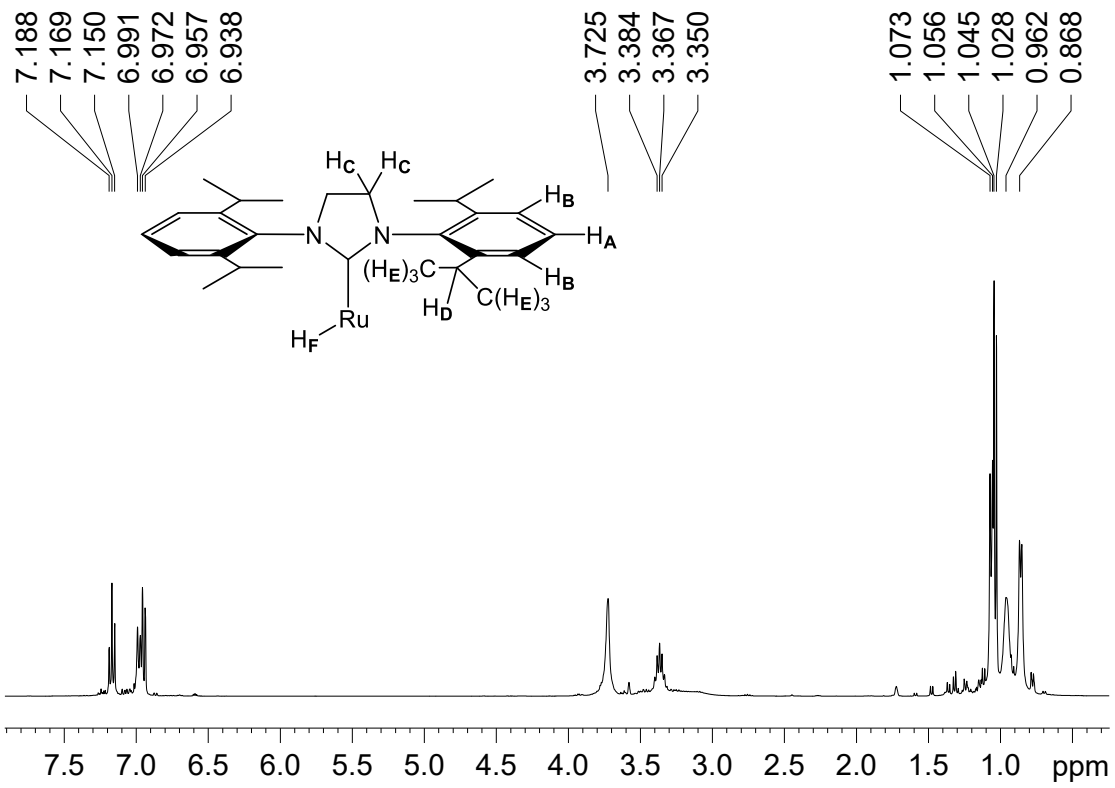

Figure 3.9 ^{1}H NMR spectrum of 7A (d_8-THF, 298 K, 400 MHz)

The $^{13}C\{^{1}H\}$ NMR spectrum of **7A** displayed unremarkable resonances for the SIPr ligands, which were assigned through ^{1}H-^{13}C HMQC/HMBC correlation experiments and phase-polarisation from $^{13}C\{^{1}H\}$ PENDANT NMR data. Resonances for the *C*O and Ru-C_{NHC} atoms were assigned by ^{1}H-^{13}C HMBC correlation to the hydride proton (H_F) (**Figure 3.10**). The ^{13}C NMR signal for *C*O (δ 201.0) was in close correlation with that of **6A** (δ 201.8) and other values from **Table 3.1**. However, the Ru-C_{NHC} resonance for **7A** was at significantly higher frequency (δ 224.4) than in **6A** (δ 195.6) due to the saturated C-C backbone, and this value is located at similar frequency to that found for Ru(SIMes)(PPh_3)(CO)HCl (δ 216.0) by the group of Nolan.[29] The Ru-C_{NHC} assignment was further confirmed by ^{1}H-^{13}C HMBC correlation between the SIPr backbone protons (H_C) with the δ 224.4 signal for the carbenic carbon.

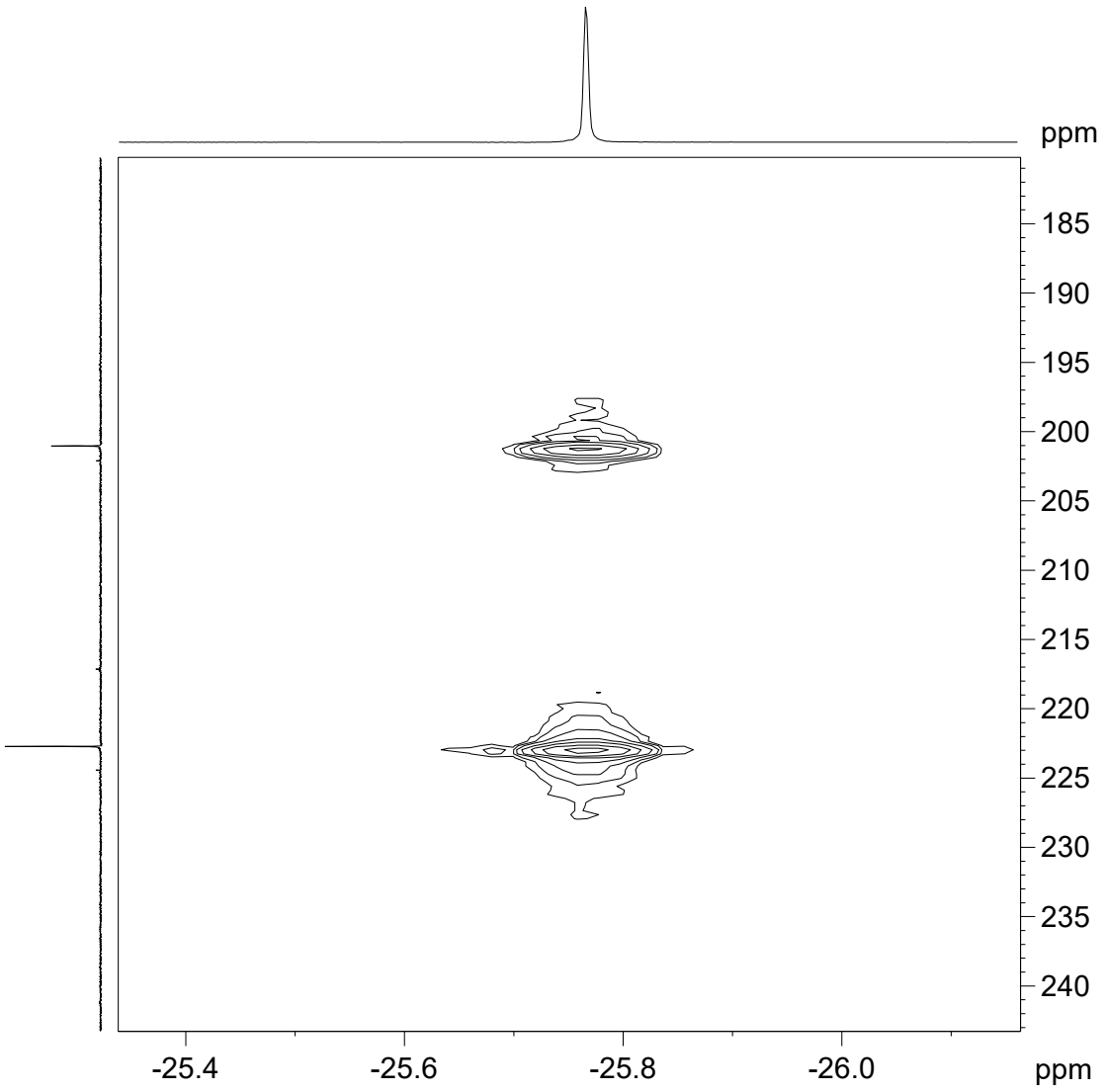

Figure 3.10 ^{1}H-^{13}C HMBC spectrum of 7A correlating the hydride resonance with *C*O and Ru-*C*$_{NHC}$ signals (*d*$_8$-THF, 298 K, 400/101 MHz)

The X-ray crystal structure of **7A** is displayed in **Figure 3.11** and as for **6A**, the structure is observed to exhibit a square pyramidal geometry. The hydride ligand could not be located, although it is envisaged to occupy the apical site in this complex, opposite the vacant site. Positional disorder was again observed due to a 2-fold rotational axis along the Cl-Ru-CO bonds which precluded accurate determination of bond distances between the Ru and the CO and chloride ligands. The Ru-C_{NHC} bond distance of 2.0889(15) Å is the same as that for **6A** (2.0872(13) Å), while the C_{NHC}-Ru-C_{NHC} angle of 177.60(9)˚ is slightly more acute (**6A**, 178.78(8)˚). The dihedral angles between the imidazol rings are marginally larger in **7A** (44.4˚) than in **6A** (39.4˚). This greater degree of twist between the SIPr ligands in **7A** is likely to result from the increased length of the imidazol backbone C-C bond in **7A**

(1.480(3) Å) compared to **6A** (1.347(3) Å), which forces the N-substituents in **7A** closer to the metal and each other, and the NHCs rotate to remove this increased interaction. Complete tables of bond lengths and angles are given in the **Appendices**. The CO absorption band of **7A** (1902 cm^{-1}) is almost identical to that observed for **6A** (1898 cm^{-1}).

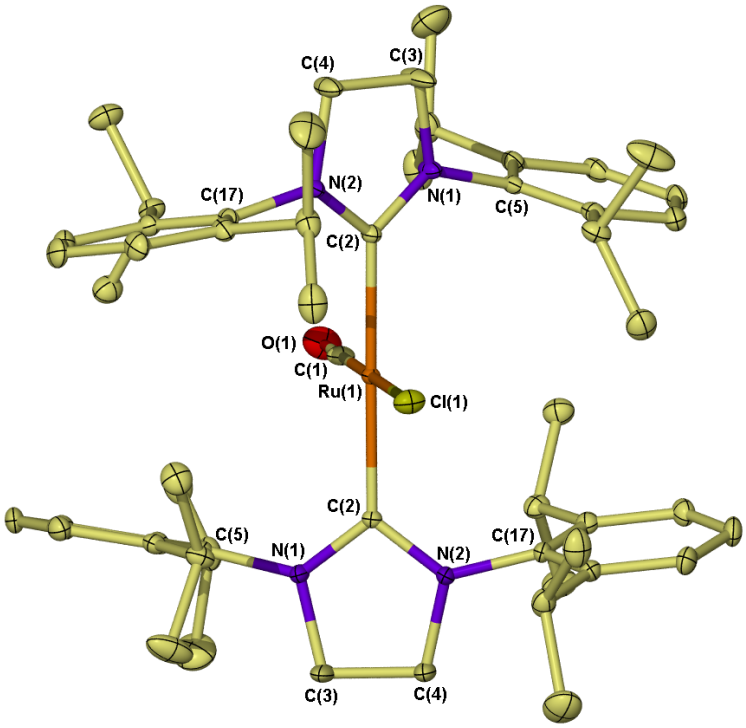

Figure 3.11 Crystal structure of $Ru(SIPr)_2(CO)HCl$ (7A) with thermal ellipsoids set to 30% probability and hydrogen atoms omitted for clarity

3.2.4 $Ru(SIMes)_2(CO)HCl$ (8A)

The synthesis of **8A** from free SIMes was explored in depth, but similar complications were observed as for the use of free SIPr to generate **7A** (see **Section 3.2.3**). Instead, reaction of $Ru(AsPh_3)_3(CO)H_2$ with the SIMes adduct (SIMes.C_6F_5-H,[37] in 3-fold excess) in toluene for 5 hours at 85 ˚C and the addition of 1.1 equivalents of CH_2Cl_2 led to the formation of $Ru(SIMes)_2(CO)HCl$ (**8A**), shown in **Figure 3.12**. Following repeated attempts, **8A** could not be isolated in yields greater than ca. 5% due to its very high solubility in hexane. Repeated recrystallisation attempts from a variety of solvents at ambient temperature and down to 193 K failed. Partial characterisation ($^1H/^{13}C$ NMR, IR and mass spectrometry) was possible on a small quantity of isolated material for comparison with **6A** and **7A**.

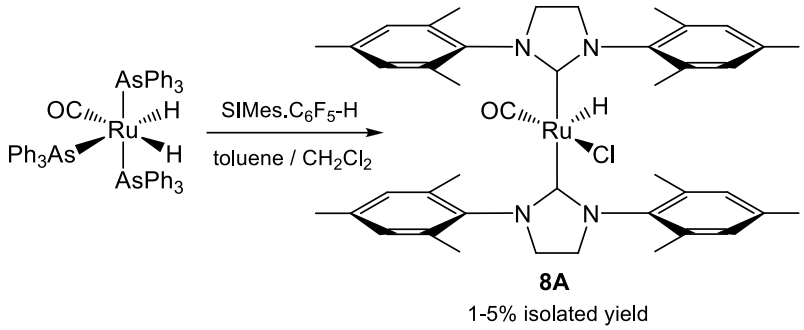

Figure 3.12 Formation of Ru(SIMes)$_2$(CO)HCl (8A)

^{1}H NMR spectroscopy (**Figure 3.13**) revealed the hydride (H_E) resonance for **8A** (δ -25.52) in d_8-toluene to be located at a similar chemical shift to those in **6A** (δ -25.88) and **7A** (δ -25.77). The SIMes ligands display two singlets for the aryl-C*H*s (H_A), and three singlets for aryl-CH_3 groups at the *para*- (H_C) and *ortho*- (H_D) positions in addition to a broad singlet for N-CH_2 backbone protons (H_B). On cooling below 253 K, splitting of all resonances was seen as in both **6A** and **7A**. The ^{13}C{^{1}H} NMR spectrum showed a *C*O resonance at δ 201.5 that was comparable with **6A** and **7A**. The Ru-C_{NHC} signal at δ 221.8 is indicative of a saturated-NHC complex, and is similar to that found in **7A** (δ 224.4). One IR band was observed at 1890 cm^{-1}, consistent with related compounds (**Table 3.1**).

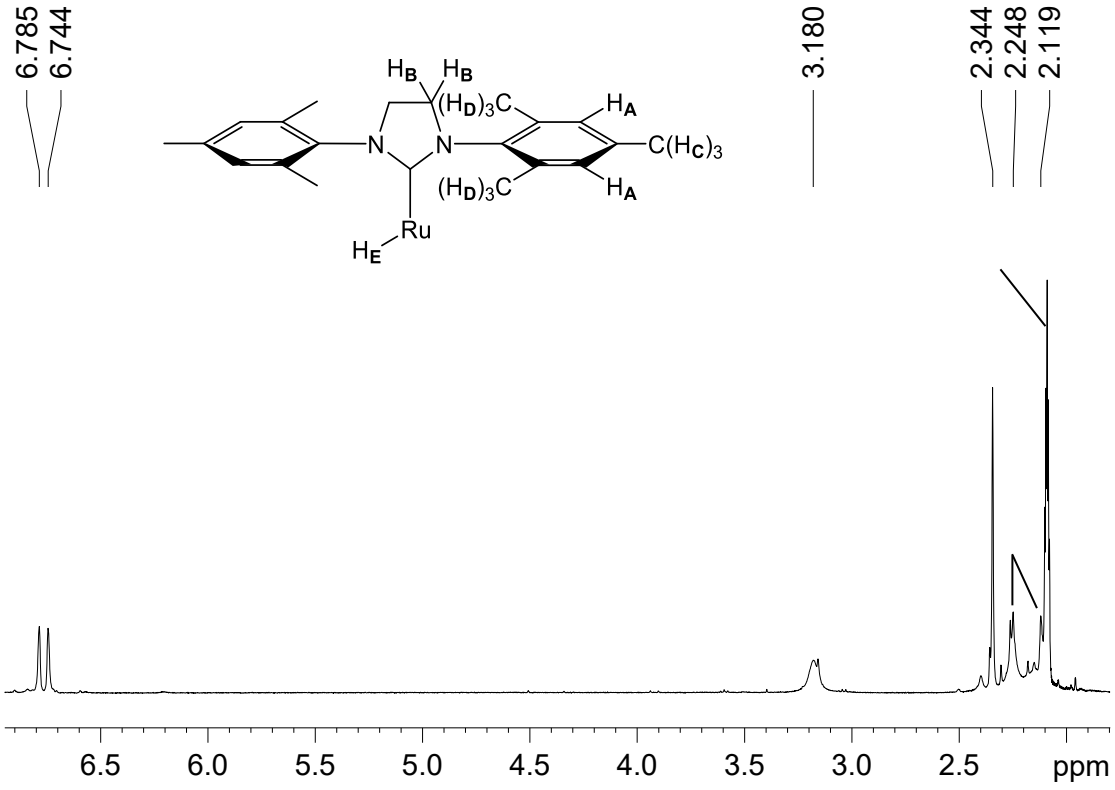

Figure 3.13 ^{1}H NMR spectrum of 8A (d_8-toluene, 298 K, 400 MHz)

3.2.5 Ru(IPr)$_2$(CO)$_2$HCl (6B)

On exposure of a toluene solution of **6A** to CO (1 atm) an instant colour change from pale yellow to colourless was observed. Removal of the solvent *in vacuo* yielded an off-white solid which was recrystallised from toluene/hexane to give the 18-electron *bis*-CO complex, Ru(IPr)$_2$(CO)$_2$HCl (**6B**, **Figure 3.14**) in good yield.

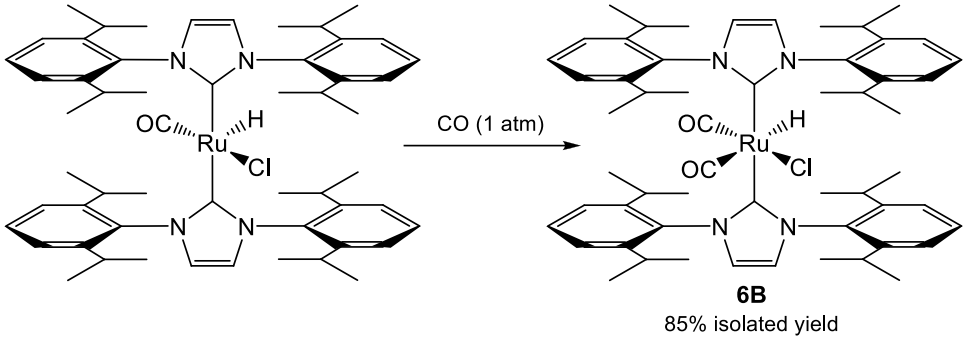

Figure 3.14 Formation of Ru(IPr)$_2$(CO)$_2$HCl (6B)

The ^{1}H NMR spectrum of **6B** in d_8-THF revealed a very large shift in the hydride signal from δ -25.88 (**6A**) to δ -4.59 (H_F), which was consistent with the hydride being *trans*- to the π-accepting CO ligand, as found for other Ru(L)$_2$(CO)$_2$HCl complexes shown in **Table 3.2**. Notable ^{1}H NMR resonances for the IPr ligands (**Figure 3.15**) are two doublets for the isopropyl-C*H*$_3$ groups (H_E), two septets for the isopropyl-C*H* groups (H_D), and one doublet for *meta*-C*H* aryl protons (H_B) instead of the two observed in **6A**. Overall, less broadening of the ^{1}H NMR signals is observed for **6B** than in **6A**, indicating less fluxionality in the IPr ligand groups. ^{13}C NMR resonances in **6B** were assigned by ^{1}H-^{13}C HMQC/HMBC correlation experiments, with pertinent values for *C*O (δ 203.1 and 193.4) and Ru-C_{NHC} (δ 185.9) in excellent agreement with literature values (**Table 3.2**), as are the two CO absorption bands at 2028 and 1934 cm^{-1}.

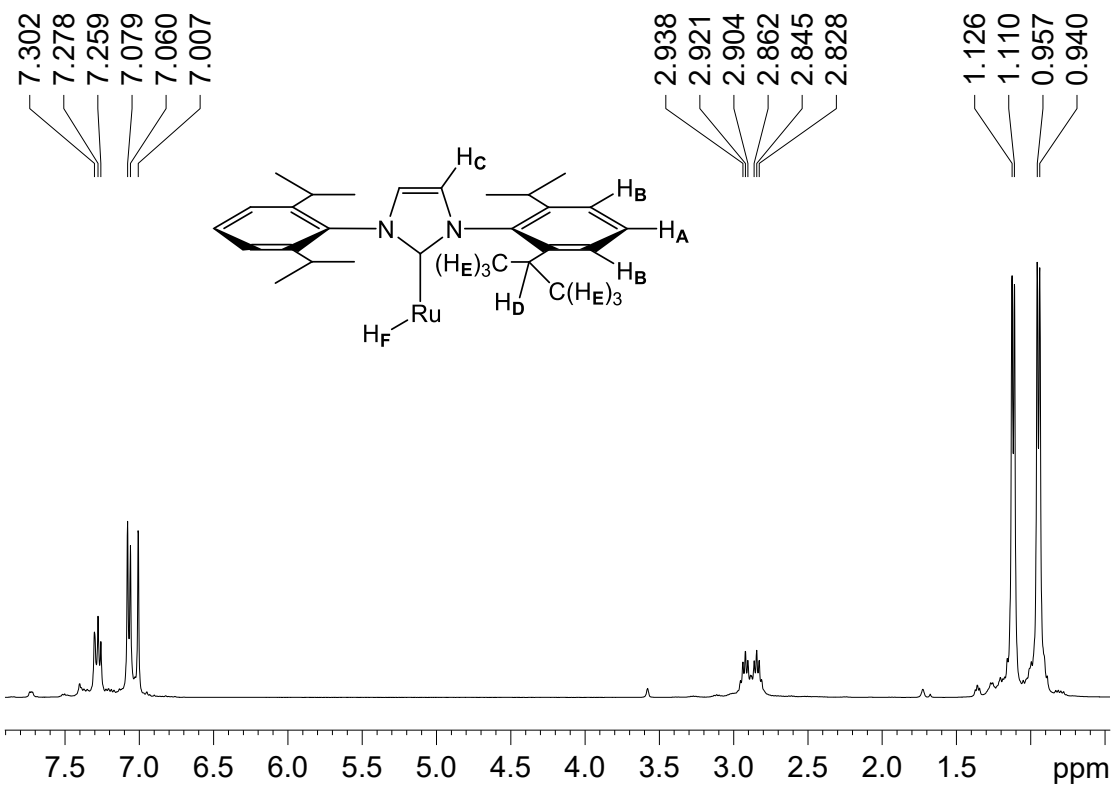

Figure 3.15 ^{1}H NMR spectrum of 6B (d_8-THF, 298 K, 400 MHz)

Compound	$^{1}H_{hydride}$ (δ)	M-C_{NHC} (δ)	M-CO (δ)	$\nu_{(CO)}$ / cm^{-1}
6B	-4.59	185.9	203.1, 193.4	2028, 1934
Ru(IMes)$_2$(CO)$_2$HCl[38]	-4.30	185.7	204.4, 194.6	2037, 1903
Ru(IMes)$_2$(CO)$_2$H(OH)[1]	-4.27	184.8	204.2, 195.4	2019, 1880
Ru(IMes)(PPh$_3$)(CO)$_2$HCl[38]	-4.25	184.9	201.8, 194.5	2044, 1945
Ru(P^{t}Bu$_2$Me)$_2$(CO)$_2$HCl[27]	-5.67	-	- [a]	2042, 1923
Ru(P^{t}Bu$_2$Et)$_2$(CO)$_2$HCl[27]	-5.48	-	- [a]	2045, 1922

[a] Value not quoted.

Table 3.2 $^{1}H_{hydride}$, Ru-C_{NHC} and IR bands of Ru(NHC)(L)(CO)$_2$HX complexes (L = NHC or PR$_3$, X = -Cl, -OH)

The formation of **6B** through the addition of CO to **6A** led to a reduction in the disorder of the crystal structure from reduced symmetry of the complex, and thus allowed accurate determination of all atomic positions. The structure of **6B** (**Figure 3.16**) exhibits a distorted octahedral geometry, and the addition of the CO ligand significantly affects the orientation of the IPr ligands compared with the structure of **6A**. In **6A**, the dihedral angle between the imidazol rings was 39.4˚ which is greatly reduced on formation of **6B** (17.3˚)

resulting from loss of the vacant site into which some N-aryl substituents were located. The imidazol rings of the IPr ligands in **6B** are parallel to the H-Ru-CO axis, with the NHCs tilted away from the CO towards the smaller hydride ligand to give a C_{NHC}-Ru-C_{NHC} bond angle of 170.07(8)˚, which is notably more acute than in **6A** (178.78(8)˚). Ru-C_{NHC} bond lengths are also markedly longer in **6B** (2.126(2), 2.128(2) Å) compared with **6A** (2.0872(13) Å) resulting from an increased steric bulk around the metal centre from the additional CO ligand. These bond lengths and angles are compared to those of **7B** and related compounds in **Section 3.2.6** (data in **Table 3.3**), and complete metrics for **6B** are given in the **Appendices**.

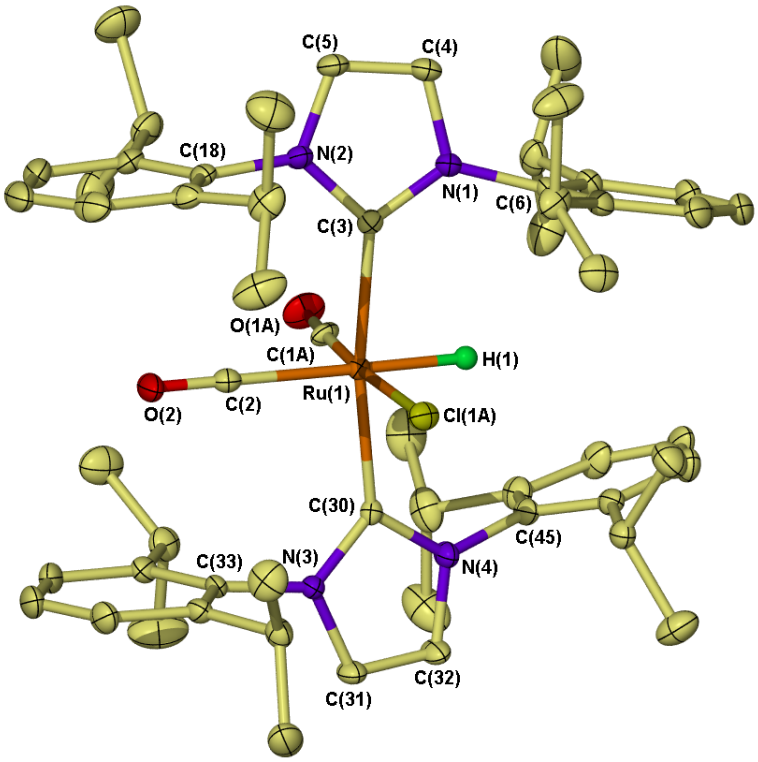

Figure 3.16 Crystal structure of $Ru(IPr)_2(CO)_2HCl$ (6B) with thermal ellipsoids set to 30% probability and hydrogen atoms (except the hydride) omitted for clarity

3.2.6 $Ru(SIPr)_2(CO)_2HCl$ (7B)

As for **6B**, the addition of 1 atm CO to a toluene solution of **7A** resulted in an immediate colour change from pale yellow to colourless. Removal of the solvent afforded an off-white solid that was subsequently recrystallised from toluene/hexane to give microcrystalline $Ru(SIPr)_2(CO)_2HCl$ (**7B**) in high yield, as shown in **Figure 3.17**.

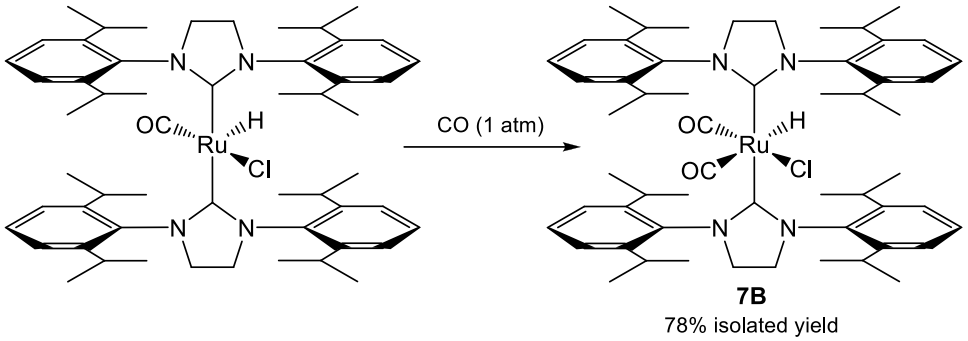

Figure 3.17 Formation of $Ru(SIPr)_2(CO)_2HCl$ (7B)

^1H NMR spectroscopy displayed a shift to higher frequency of the hydride resonance from **7A** (δ -25.77) to **7B** (δ -5.09), as was observed in the formation of **6B**. Resonances for the SIPr ligands were unremarkable and located at similar frequencies to the parent compound **7A**. Notable $^{13}C\{^1H\}$ NMR resonances were situated at δ 202.3 and 193.0 (*C*O) and δ 213.6 (Ru-C_{NHC}), with SIPr resonances assigned by ^1H-^{13}C HMQC/HMBC correlation experiments. All NMR resonances, in addition to the IR bands at 2032 and 1937 cm^{-1} were in good agreement with similar compounds, several of which are presented in **Table 3.2**.

Prolonged exposure of **7B** to vacuum in the solid-state or on heating a freeze-pump-thaw degassed solution led to the re-formation of **7A** through loss of CO. **Figure 3.18** shows the results of heating a C_6D_6 solution of **7B** at 70 ˚C over time, after four freeze-pump-thaw cycles. At room temperature there was 3% conversion from **7B** to **7A**, and this increased rapidly on heating to 20% after 20 minutes, 32% after 80 minutes and 46% re-formation of **7A** after 48 hours. Evolution of CO was so facile that crystals of **7B** could only be grown under a CO atmosphere. Investigation of $Ru(IMes)_2(CO)_2HCl$ showed that removal of CO was not found to occur at all under the same conditions. Further investigation of $Ru(IPr)_2(CO)_2HCl$ (**6B**) by ^1H NMR spectroscopy in a degassed solution revealed that a small amount of CO loss occurs whilst monitoring the sample at 50 ˚C, but cooling of the sample to ambient temperature led to facile and total regeneration of **6B**.

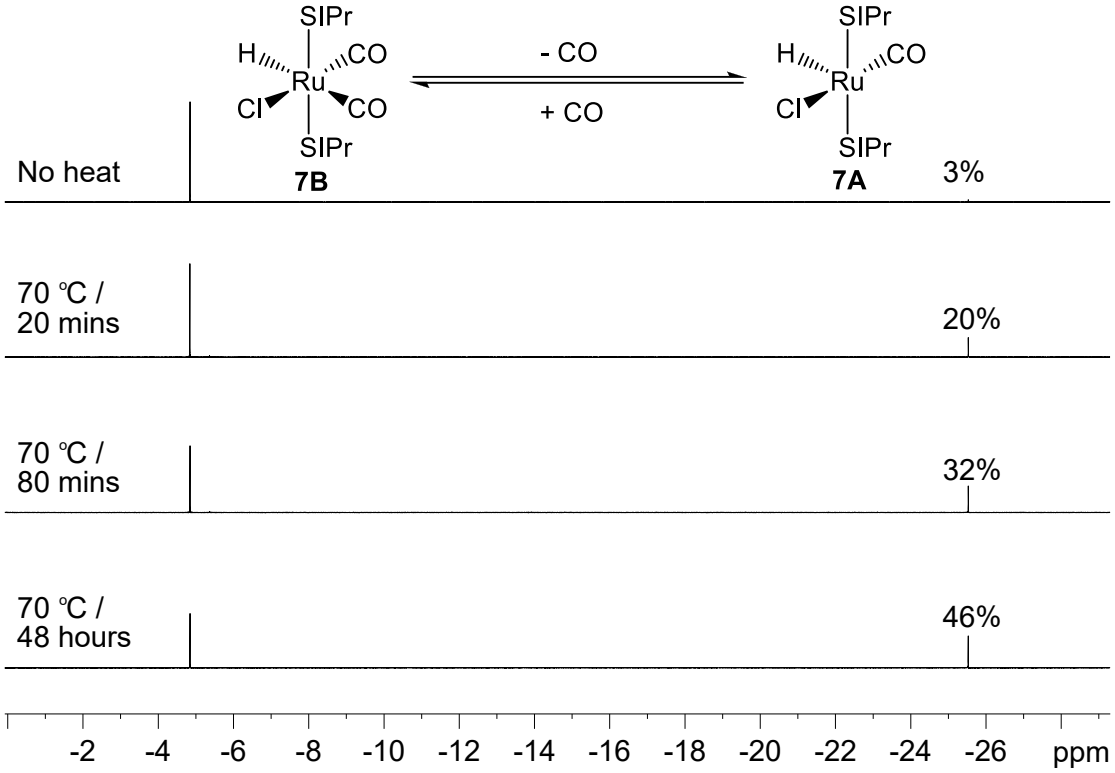

Figure 3.18 ^{1}H NMR spectra demonstrating loss of CO on thermolysis of 7B at 70 ˚C after four freeze-pump-thaw cycles (C_6D_6, 298 K, 400 MHz)

The crystal structure of **7B** is shown in **Figure 3.19** and revealed a distorted octahedral geometry. The NHC ligands lie nearly parallel to the equatorial axis containing the least bulky ligands (the H-Ru-CO axis), as is also observed for **6B**. The C_{NHC}-Ru-C_{NHC} bond angle of 170.39(9)˚ for **7B** is considerably more acute than in **7A** (177.60(9)˚) but identical to the dicarbonyl complex **6B** (170.07(8)˚). This observation sees the NHC ligands tilting away from the additional CO ligand towards the hydride along the H-Ru-CO axis as observed for **6B**. The dicarbonyl **7B** contains notably longer Ru-C_{NHC} bond lengths (2.143(2) and 2.146(2) Å) than in **7A** (2.0889(15) Å) due in part to greater steric congestion around the ruthenium centre, as seen for complexes **6A** and **6B**. Ru-C_{NHC} bond lengths are marginally longer in **7B** (2.143(2)-2.146(2) Å) than in **6B** (2.126(2)-2.128(2) Å) due to the greater steric influence on the metal from the SIPr ligand.

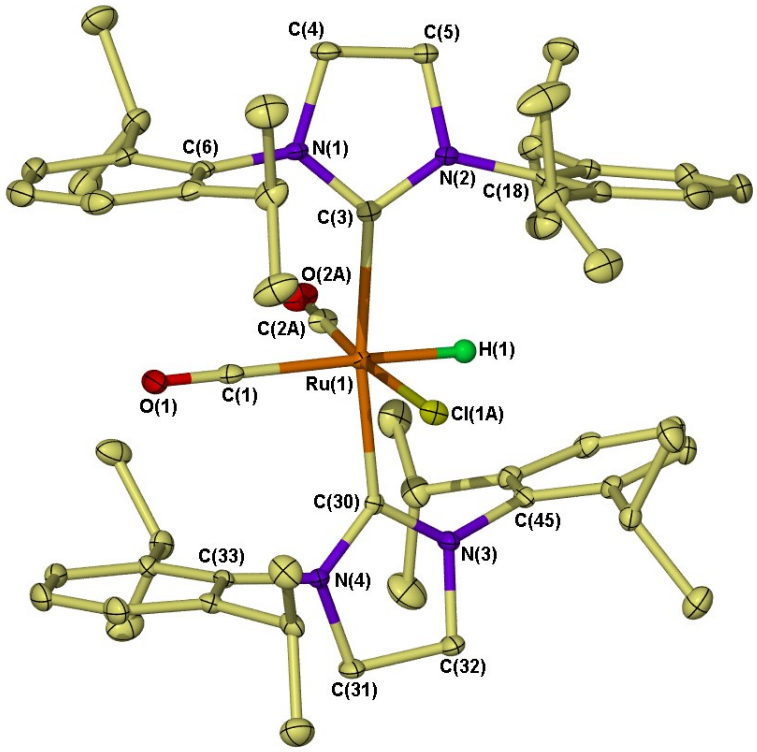

Figure 3.19 Crystal structure of $Ru(SIPr)_2(CO)_2HCl$ (7B) with thermal ellipsoids set to 30% probability and hydrogen atoms (except the hydride) omitted for clarity

The facile evolution of CO in the solid-state from **7B** when compared to the negligible effect in **6B** can be explained in part by comparison of the crystal structures. The longer C-C backbone in the SIPr ligands (**7B** = 1.500(3)-1.503(3) Å) compared to the IPr ligands (**6B** = 1.332(3)-1.332(3) Å) results in the NHC N-substituents in **7B** lying closer to the metal centre. As a consequence, there is a considerably greater interaction of the SIPr N-substituents and the equatorial ligands in **7B** compared with the IPr ligands in **6B**. To reduce this interaction, the NHCs in **7B** are observed to rotate around the Ru-C_{NHC} bond so that they occupy a plane much closer to the H-Ru-CO axis than in **6B**, and this is demonstrated by the dihedral angle (between the imidazol planes) of **7B** (12.2˚) being significantly smaller than in **6B** (17.3˚). Relief of the highly congested ruthenium centre, particularly along the H-Ru-CO bond in **7B** must act as a driving force for the release of CO to generate the 16-electron complex **7A**. In doing so, the SIPr ligands can rotate from the extremely acute angle of 12.2˚ back to the 44.4˚ angle in the 16-electron complex **7A** by utilising the vacant site for the N-substituents.

The bond lengths and angles of **7B** and **6B** can be compared with the related literature compounds[38] $Ru(IMes)_2(CO)_2HCl$ and $Ru(IMes)(PPh_3)(CO)_2HCl$ presented in **Table 3.3**. Both **6B** and **7B** display Ru-C_{NHC} bond lengths (2.126(2)-2.143(2) Å) that are slightly longer than those in the IMes-containing compounds (2.0974(19)-2.1158(15) Å) due to their bulkier N-substituents. Ru-C_{CO} bond lengths in all compounds are longer when CO is *trans*- to hydride as expected by the greater *trans*- influence of this ligand (e.g. **7B**, *trans*- to hydride = 1.982(3) Å, *trans*- to chloride = 1.867(7) Å). Individual Ru-C_{CO} bond distances are the same in all *bis*-NHC complexes, showing them to be essentially independent of the NHC ligands, as are the Ru-Cl bond distances at 2.379(2)-2.3922(19) Å. The L_{ax}-Ru-L_{ax} bond angles are more acute in both IMes compounds (165.42(5)-168.81(2)˚) than for **6B** and **7B** (170.07(8)-170.39(9)˚) due to the reduced steric bulk allowing the IMes/PPh_3 ligands to tilt away from the CO ligands to a greater extent. C_{CO}-Ru-C_{CO} angles are approximately the same for all *bis*-NHC complexes (92.1(7)-96.0(3)˚), and slightly larger for the mixed phosphine/NHC system (98.02(10)˚). The dihedral angle of the least-squares planes of the imidazol rings in $Ru(IMes)_2(CO)_2HCl$ (16.5˚) is shown to be comparable to **6B** (17.3˚) and much larger than in **7B** (12.2˚).

	6B	**7B**	**$Ru(IMes)_2(CO)_2HCl$**	**$Ru(IMes)(PPh_3)(CO)_2HCl$**
Ru-C_{NHC}	2.126(2)	2.143(2)	2.1158(15)	2.0974(19)
	2.128(2)	2.146(2)	2.1064(15)	-
Ru-C_{CO}	1.975(2) [a]	1.982(3) [a]	1.9840(19) [a]	1.973(2) [a]
	1.920(11) [b]	1.867(7) [b]	1.890(8) [b]	1.848(2) [b]
Ru-Cl	2.379(2)	2.3922(19)	2.384(2)	2.4528(5)
L_{ax}-Ru-L_{ax}	170.07(8)	170.39(9)	168.81(2)	165.42(5)
C_{CO}-Ru-C_{CO}	92.1(7)	94.2(5)	96.0(3)	98.02(10)

[a] *Trans*- to hydride. [b] *Trans*- to chloride.

Table 3.3 Bond lengths (Å) and angles (˚) for 6B, 7B, $Ru(IMes)_2(CO)_2HCl$[38] and $Ru(IMes)(PPh_3)(CO)_2HCl$[38]

3.3 Formation of $Ru(NHC)_2(CO)H(\eta^2\text{-}BH_4)$ complexes

3.3.1 Introduction

Complexes containing borohydride ligands have been shown to be active in various catalytic transformations over a number of years.[39,40] Esteruelas has demonstrated that the

catalytic activity of $M(L)_2(CO)HCl$ complexes (M = Ru, Os and L = P^iPr_3, P^tBu_2Me) is significantly enhanced by the addition of $NaBH_4$ into various transfer hydrogenation reactions.[41-43] The synthesis of $Ru(NHC)_2(CO)HCl$ complexes **6A** and **7A** therefore allowed us to investigate replacement of the chloride ligand with the potentially more catalytically active borohydride group through reaction of the complexes with $NaBH_4$.

3.3.2 $Ru(IPr)_2(CO)H(\eta^2\text{-}BH_4)$ (6C)

The reaction of $Ru(IPr)_2(CO)HCl$ (**6A**) and $NaBH_4$ (4-fold excess) in EtOH inside a J. Young's ampoule was complete after 90 minutes at 70 ˚C, as indicated by disappearance of the hydride resonance for **6A** (δ -25.88) in the ^1H NMR spectrum. Removal of the solvent gave a colourless powder, which was then extracted in benzene and recrystallised by layering with hexane to yield $Ru(IPr)_2(CO)H(\eta^2\text{-}BH_4)$ (**6C**), shown in **Figure 3.20**. Interestingly the formation of $Ru(IMes)_2(CO)H(\eta^2\text{-}BH_4)$ by Chatwin in the Whittlesey group was completed using the same quantity of $NaBH_4$ but took only 1 hour at room temperature,[17,38] demonstrating the significant influence of increased steric bulk when moving from IMes to IPr.

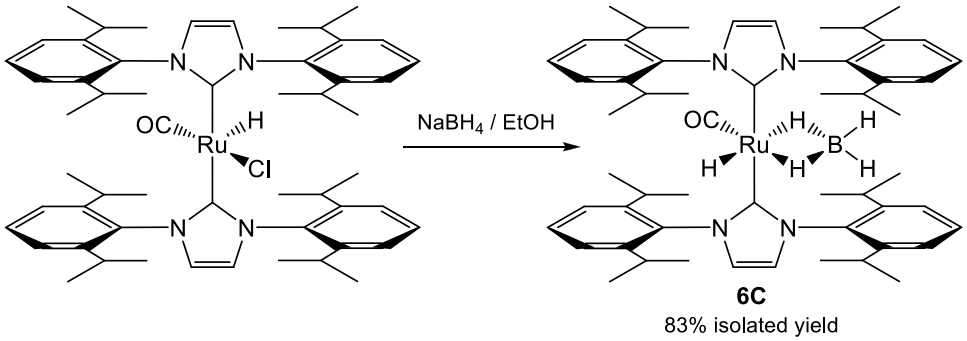

Figure 3.20 Formation of $Ru(IPr)_2(CO)H(\eta^2\text{-}BH_4)$ (6C)

The room temperature ^1H NMR spectrum of **6C** in d_8-THF displayed proton resonances for the IPr ligands that were fairly unremarkable and located at similar chemical shifts to those observed in **6A** and **6B**. Upon cooling a d_8-toluene solution of **6C**, there was splitting of the backbone NC*H* protons and the isopropyl-C*H* septets, clearly demonstrated in **Figure 3.21**, as the two overlapping septets of the isopropyl-C*H* resonances (at 298 K) initially broaden when cooled past 258 K and then split into four which sharpen at around 218 K.

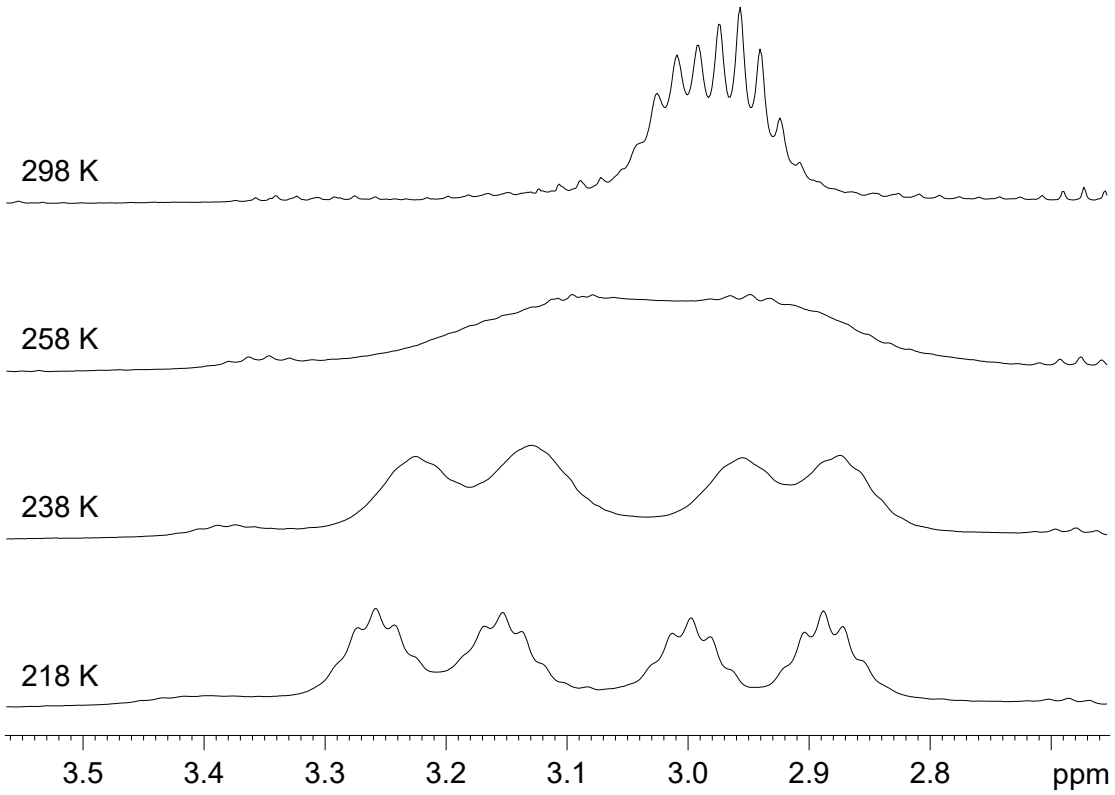

Figure 3.21 Isopropyl-C*H* region of variable temperature ^{1}H NMR spectra of 6C (*d*$_8$-toluene, 400 MHz)

At ambient temperature, **6C** showed a sharply defined hydride signal at δ -16.19 alongside a much broader resonance at δ -7.20 which integrated in a 1:1 ratio. On cooling the solution below 278 K (**Figure 3.22**), a new resonance evolved at ca. δ -5.1 (H_B) that integrated in a 1:1:1 ratio with the two original hydrides, H_C and H_D. This effect was also observed for Ru(IMes)$_2$(CO)H(η^2-BH$_4$), in which the hydrides were fully assigned through ^{1}H ROESY/1D ROE NMR spectroscopy and T_1 measurements.[17,38] The similarities in the -BH$_4$ and hydride resonances for **6C** at 228 K (δ -5.13 (H_B), -6.95 (H_C), -15.90(H_D)) and Ru(IMes)$_2$(CO)H(η^2-BH$_4$) (δ -5.12, -6.98, -16.28) led us to deduce they are effectively independent of the axial ligands, which is also demonstrated for non-NHC BH$_4$-containing compounds, as shown in **Table 3.4**. For Ru(IMes)$_2$(CO)H(η^2-BH$_4$) the signals for H_A are observed at δ 3.13, whereas for **6C** they are located beneath the isopropyl-C*H* signals. ^{13}C{^{1}H} NMR spectroscopy displayed signals for *C*O at δ 205.4 and Ru-C_{NHC} at δ 195.2 which compare to those of Ru(IMes)$_2$(CO)H(η^2-BH$_4$) at δ 205.6 and δ 194.1 respectively. The IR band for **6C** was observed at 1917 cm^{-1} for the CO ligand.

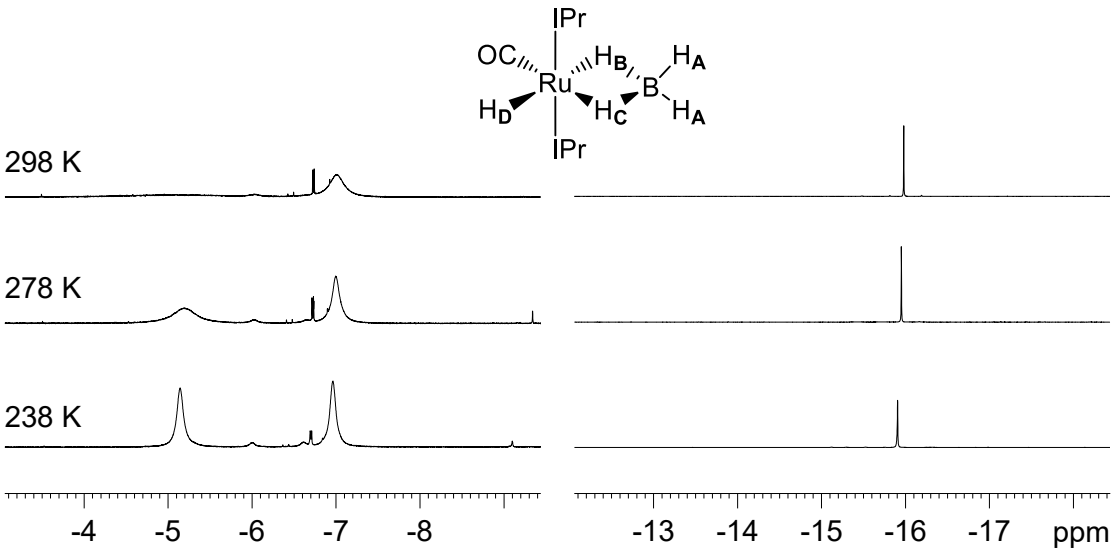

Figure 3.22 Variable temperature ^{1}H NMR spectra of 6C (hydride region) (d_8-toluene, 400 MHz)

^{1}H NMR resonances for the -BH_4 ligand are located at comparable chemical shifts to those observed in Ru(P^tBu_2Me)$_2$(CO)H(η^2-BH_4) and Ru(P^iPr_3)$_2$(CO)H(η^2-BH_4), with the resonances for H_B located at higher chemical shift than for H_C. The classical hydride H_D is typically the sharpest of those observed as a result of reduced fluxional behaviour compared with the bridging hydrides. ^{11}B NMR spectroscopy of **6C** revealed an extremely broad resonance at δ -0.20 which was comparable with those observed for both IMes compounds at δ -2.80 and -2.79, although at a lower chemical shift than the *bis*-phosphine complexes. The IR bands for the -BH_4 ligand in **6C** (2466 and 2394 cm^{-1}) are consistent with literature values for the bidentate coordination mode of the -BH_4 ligand.[39]

Compound	^{1}H (δ) (-40 to -45 °C)				^{11}B (δ)	$\nu_{(BH)}$ / cm^{-1}
	H_A	H_B	H_C	H_D		
6C	- [a]	-5.14	-6.96	-15.91	-0.20	2466, 2394
Ru(IMes)$_2$(CO)H(BH$_4$)[17,38]	3.13	-5.12	-6.98	-16.28	-2.80	2425, 2400
Ru(IMes)(PPh$_3$)(CO)H(BH$_4$)[38]	- [b]	- [b]	- [b]	- [b]	-2.79	2422, 2399
Ru(P^tBu_2Me)$_2$(CO)H(BH$_4$)[41]	4.70	-4.40	-7.20	-14.69	10.00	2400, 2390
Ru(P^iPr_3)$_2$(CO)H(BH$_4$)[41]	4.55	-4.90	-7.78	-14.12	8.90	2420, 2320

[a] Not observed. [b] Not quoted at this temperature.

Table 3.4 Data relevant to -BH_4 ligand in Ru(L)(CO)H(η^2-BH_4) (L = NHC, PR_3) complexes

The crystal structure of **6C** is presented in **Figure 3.23**, with complete data given in the **Appendices**. Atomic positions of the IPr and metal atoms were well defined, although there was significant disorder over the carbonyl and borohydride ligands due to crystallographic symmetry as was seen also in **6A** and **7A**. Hydrogen atoms from the borohydride ligand were unable to be located, as was the hydride on the ruthenium. The orientations of the IPr ligands in **6C** and the parent compound **6A** are very similar. Ru-C_{NHC} bond lengths are identical for both compounds, (**6C** = 2.086(3), **6A** = 2.0872(13) Å), and both the C_{NHC}-Ru-C_{NHC} bond angles (**6C** = 179.58(14)˚, **6A** = 178.78(8)˚) and the dihedral angles between the imidazol rings of the IPr ligands (**6C** = 37.3˚, **6A** = 39.4˚) are comparable also.

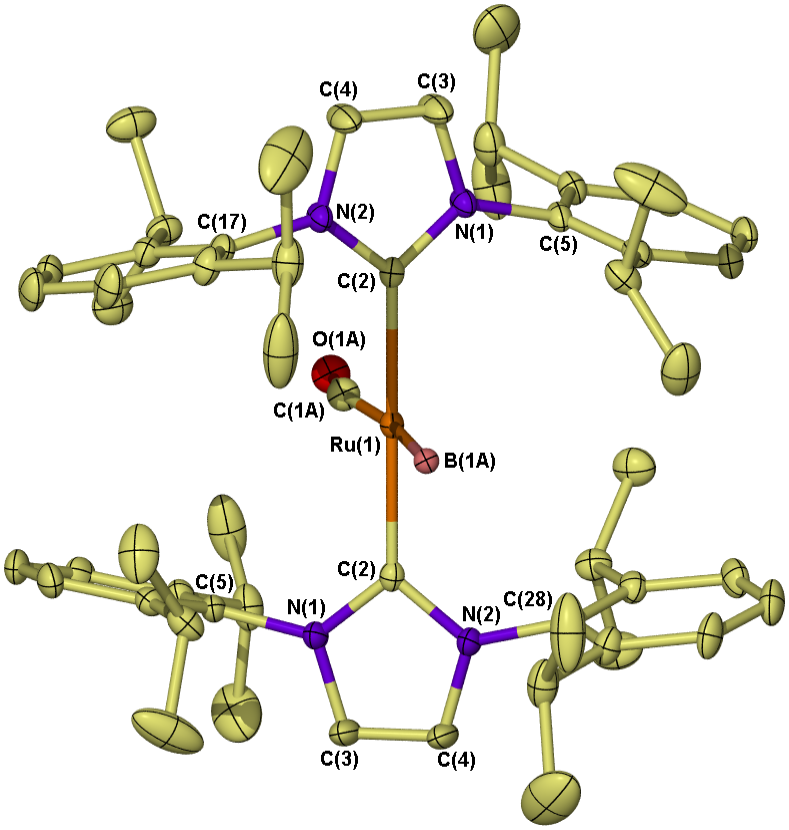

Figure 3.23 Crystal structure of Ru(IPr)$_2$(CO)H(η^2-BH$_4$) (6C) with thermal ellipsoids set to 30% probability and hydrogen atoms omitted for clarity

3.3.3 Ru(SIPr)$_2$(CO)H(η^2-BH$_4$) (7C)

Ru(SIPr)$_2$(CO)HCl and a 4-fold excess of NaBH$_4$ were suspended in EtOH and heated at 70 ˚C for 90 minutes. Extraction in benzene and removal of the solvent *in vacuo* afforded a

grey/white microcrystalline solid that was characterised as $Ru(SIPr)_2(CO)H(\eta^2\text{-}BH_4)$ (**7C**, **Figure 3.24**) by comparison to **6C**.

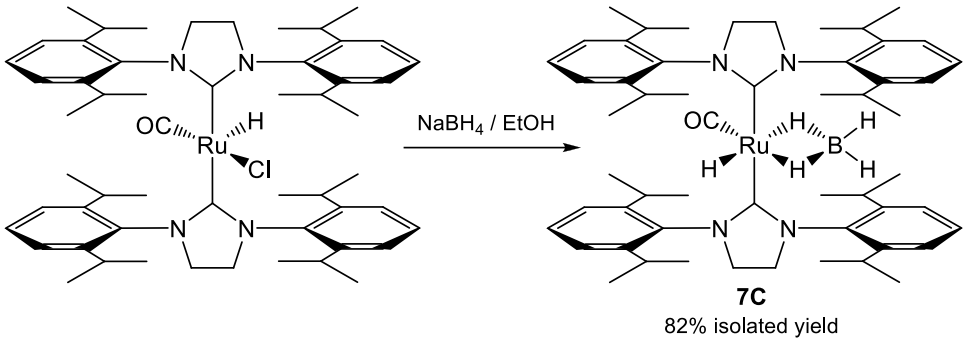

Figure 3.24 Formation of $Ru(SIPr)_2(CO)H(\eta^2\text{-}BH_4)$ (7C)

Thus, at ambient temperature, ^{1}H NMR spectroscopy of **7C** in d_8-THF showed a sharply defined signal at δ -15.40 (H_D) which integrated in a 1:1 ratio with a second broad hydride signal at δ -7.33 (H_C). Cooling of a d_8-toluene solution of **7C** (**Figure 3.25**) resolved an additional hydride resonance at ca. δ -5.4 (H_B) which integrated in a 1:1:1 ratio with H_C and H_D. Additional data for **7C** is in good agreement with related complexes and data in **Table 3.4**.

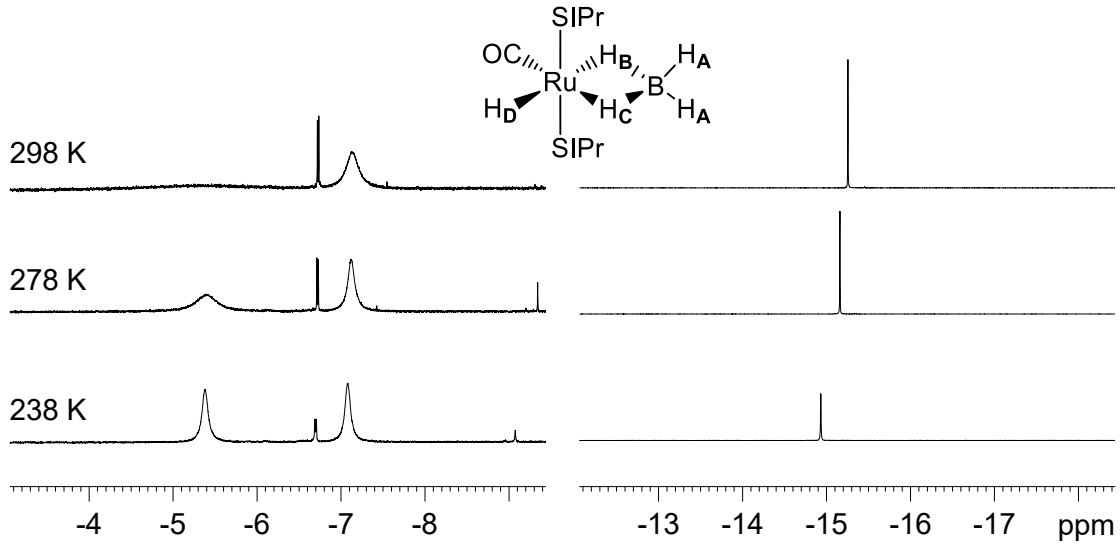

Figure 3.25 Variable temperature ^{1}H NMR spectra of 7C (hydride region) (d_8-toluene, 400 MHz)

3.4 Direct/transfer hydrogenation reactions of $Ru(NHC)_2(CO)HCl$ and $Ru(NHC)_2(CO)H(\eta^2\text{-}BH_4)$ complexes

3.4.1 Introduction

Recently, there have been a number of NHC-containing complexes prepared by our group[44-47] which have displayed activity in the fields of alkene and ketone hydrogenation reactions, and the synthesis of catalytically useful compounds continues to be of great interest to us. So far, 16-electron complexes of the general type $Ru(L)_2(CO)HX$ (L = PR_3 or NHC, X = -Cl or -BH_4) have been shown by Fogg, Nolan, Esteruelas and Yi to display activity in homogenous catalytic transformations such as the hydrogenation of alkenes[29,30,48] and ketones,[42] the coupling of alkenes with cyclic amines[49] and hydrovinylation.[31] In this section the catalytic activity of 16-electron *bis*-NHC ruthenium complexes is investigated for the first time. An exploration into the effects of varying the NHC and X-group ligands on the $Ru(NHC)_2(CO)HX$ scaffold is examined through the representative hydrogenation reactions of acetophenone and 4-methoxyacetophenone to their corresponding alcohols.

3.4.2 Results and discussion

The general procedure for ketone hydrogenation reactions involved addition of the ketone substrate (0.3 M), the ruthenium catalyst (0.4 mol%) and neat IPA (degassed) into an autoclave, which was then charged with 10 atm H_2. The reaction mixture was subsequently heated with stirring at 70 ˚C for 20 hours. On cooling to room temperature the reaction mixtures were analysed directly by GC. Studies showed that exclusion of either the H_2 atmosphere or the IPA solvent leads to extremely poor conversions (less than 5%) of the ketone, suggesting that both direct and transfer hydrogenation processes are operating in these systems. The results for the hydrogenation of acetophenone and 4-methoxyacetophenone with **6A**, **6C**, **7A** and **7C** are shown in **Table 3.5**, along with data for $Ru(IMes)_2(CO)HCl$ and $Ru(IMes)_2(CO)H(\eta^2\text{-}BH_4)$ reported by Chatwin.[17] All results are an average of at least two runs.

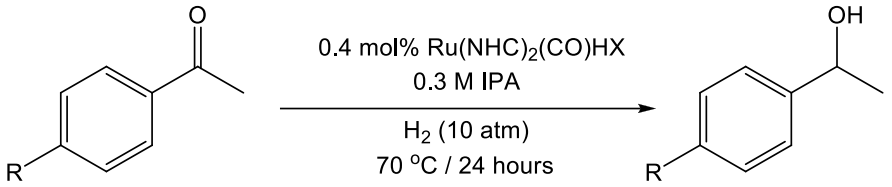

Substrate	Catalyst	Conversion (%)
Acetophenone	$Ru(IPr)_2(CO)HCl$ (**6A**)	96
	$Ru(SIPr)_2(CO)HCl$ (**7A**)	36
	$Ru(IMes)_2(CO)HCl$	84
	$Ru(IPr)_2(CO)H(BH_4)$ (**6C**)	90
	$Ru(SIPr)_2(CO)H(BH_4)$ (**7C**)	45
	$Ru(IMes)_2(CO)H(BH_4)$	85
4-Methoxyacetophenone	$Ru(IPr)_2(CO)HCl$ (**6A**)	68
	$Ru(SIPr)_2(CO)HCl$ (**7A**)	30
	$Ru(IMes)_2(CO)HCl$	33
	$Ru(IPr)_2(CO)H(BH_4)$ (**6C**)	86
	$Ru(SIPr)_2(CO)H(BH_4)$ (**7C**)	76
	$Ru(IMes)_2(CO)H(BH_4)$	44

Table 3.5 Conversions (%) for catalytic hydrogenation reactions of acetophenone and 4-methoxyacetophenone by $Ru(NHC)_2(CO)HX$ complexes

The data in **Table 3.5** demonstrates that the IPr ligand generates the most active complex in all cases. For the reaction of acetophenone, the IMes complex is marginally less active than that of IPr, whereas the SIPr-containing species forms a considerably less active complex, giving around half the percentage conversion as the IPr complex, **6A**. This trend holds true for both chloride and borohydride complexes, and there appears to be no discernible difference between the two X ligands in terms of percentage conversion of acetophenone. For the hydrogenation of 4-methoxyacetophenone, the IMes-BH_4 complex appears considerably less active than the other two NHC-BH_4 complexes, with the lowest conversions of the three. Using this substrate, the -BH_4 ligand shows a marked improvement compared with the chloride, especially in the SIPr complexes **7A** and **7C** where the conversion is increased from 30% to 76%. Overall, it appears that saturation of the NHC backbone reduces the effectiveness of the complex in these catalytic systems, as the IPr complex is always more active than that of SIPr. This trend is echoed by Beller and

co-workers, who observe higher levels of activity for an *in situ* generated ruthenium IPr complex compared with the SIPr analogue for the transfer hydrogenation of acetophenone.[4] However, a difference between saturated and unsaturated NHC ligands in catalytic hydrogenation reactions is not always observed, as Fogg *et al* observe the same level of activity for $Ru(NHC)(PPh_3)(CO)HCl$ (NHC = IMes or SIMes) for the hydrogenation of cyclododecene.[29]

The purpose of this study was to compare the effects of changing the NHC and X-group ligands in the hydrogenation reactions of two ketone substrates. The *bis*-NHC catalysts generated in this study have been shown to remain active in the absence of base, which makes them appealing due to the prevalent requirement for base in numerous reactions throughout the literature to aid in maintaining catalyst activity.[50,51] Clear comparisons between the *bis*-NHC catalysts in this work have been made by observing the percentage conversions of the ketone substrates in the absence of base. The addition of base to any of the reactions undertaken in this study would be expected to generate significant improvements in percentage conversions, via exchange of the chloride ligands to more active hydride groups and in the production of alkoxides from the IPA, which are more nucleophilic than the alcohol alone. Chatwin has previously shown for example that for the hydrogenation of acetophenone under standard conditions, addition of NaOH to the $Ru(IMes)_2(CO)HCl$ catalyst increases conversion of the ketone from 84% to 100%.[17]

3.5 Cationic ruthenium-hydride complexes

3.5.1 Introduction

Hitherto in this chapter, we have shown the 16-electron complexes, $Ru(NHC)_2(CO)HX$ to be active in catalytic transformations. In an endeavour to investigate the creation of yet more active species, the removal of ligands from this moiety has been explored. The groups of both Yi[18] and Connell[52] have shown that for the closely related 16-electron $Ru(PCy_3)_2(CO)HCl$ complex, the removal of the PCy_3 ligand or the chloride can be achieved via the addition of $HBF_4{\cdot}OEt_2$ or $AgSbF_6$ respectively. Besides these observations, Sanchez-Delgado *et al* have shown that solvation of $Ru(PPh_3)_3(CO)HCl$ results in mono-phosphine dissociation in solution, and that the subsequent addition of

HBF_4 leads to generation of H_2 (via removal of the hydride ligand) to leave a 14-electron fragment.[25]

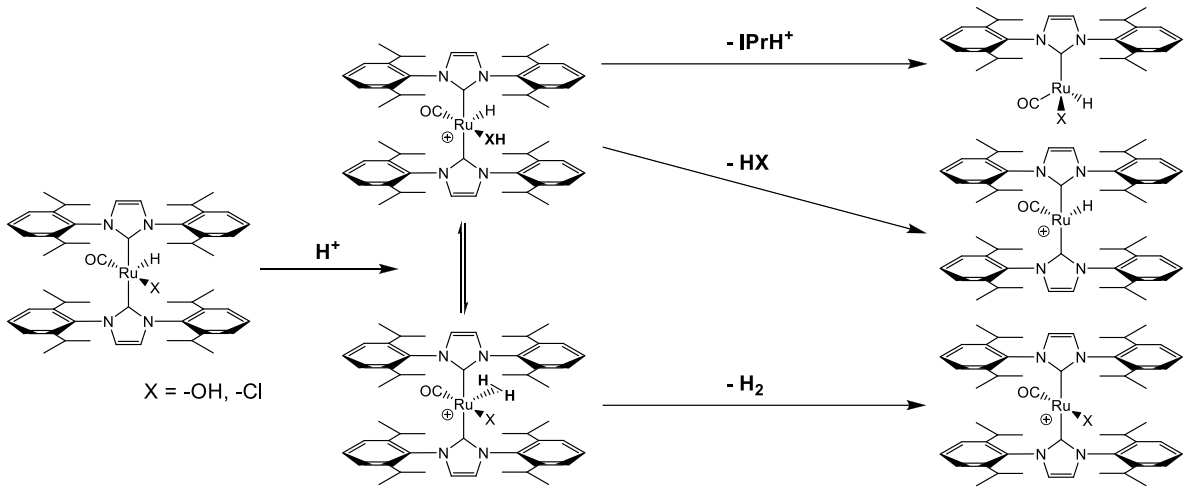

Figure 3.26 Reaction scheme detailing potential products from the protonation of 16-electron complexes

The scheme in **Figure 3.26** therefore introduces the various proposed outcomes of the protonation of $Ru(IPr)_2(CO)HX$. The loss of the bulky ligand L, the X-group or the hydride have been shown to occur in related phosphine-containing complexes, and this work seeks to investigate which outcome is preferential when NHCs are employed. The IPr-containing complex $Ru(IPr)_2(CO)HX$ was investigated in the hope that the bulky N-substituents of the IPr could stabilise the bare 14-electron species through steric shielding. The IMes ligand for example was not chosen for this task, as it has already been shown to undergo C-H activation of one of the *meta*-CH_3 groups in the presence of an electron poor ruthenium.[44,53] In addition, the IPr ligand was shown to yield the most active ketone hydrogenation complexes of those investigated in **Section 3.4**, and this capability may result in enhanced catalytic activity of these complexes in future applications. Additionally in this work we wished to explore the outcome of products upon varying the X-group. By investigating the chloride complex $Ru(IPr)_2(CO)HCl$ (**6A**) and the hydroxide complex $Ru(IPr)_2(CO)H(OH)$, we could modify the nature of the HX-loss pathway shown in **Figure 3.26** (either HCl or H_2O), which may prove decisive to the resultant products.

3.5.2 $Ru(IPr)_2(CO)H(OH)$ (6D)

The isolation of $Ru(IMes)_2(CO)H(OH)$ has previously been described by our group, through the heating of $Ru(AsPh_3)_3(CO)H_2$ with excess IMes followed by the addition of water.[1] It has also been shown by Chatwin that formation can occur from

$Ru(IMes)_2(CO)HCl$ by the addition of KOH in methanol,[17] and a modified version of this route proved most effective in the synthesis of $Ru(IPr)_2(CO)H(OH)$. $Ru(IPr)_2(CO)HCl$ and KOH (15-fold excess) were added to a J. Youngs ampoule under argon, followed by the addition of EtOH with heating of the mixture at 85 ˚C for 16 hours. Interestingly, formation of the related phosphine complex $Ru(P^tBu_2Me)_2(CO)H(OH)$[54,55] by Caulton *et al* from the corresponding hydride-chloride resulted in completion in 2 hours at room temperature. $Ru(IPr)_2(CO)H(OH)$ on the other hand required considerably more forcing conditions. The volatiles were removed *in vacuo* to give a pale yellow residue which was extracted in toluene to yield $Ru(IPr)_2(CO)H(OH)$ (**6D**, **Figure 3.27**). X-ray quality crystals were grown from a toluene/hexane solution at 5 ˚C to unequivocally determine the structure by crystallographic characterisation.

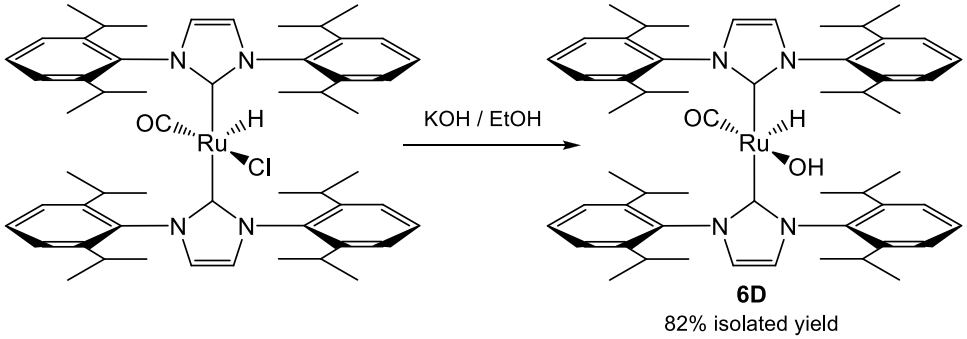

Figure 3.27 Formation of $Ru(IPr)_2(CO)H(OH)$ (6D)

A d_8-THF solution of **6D** at ambient temperature showed a hydride resonance at δ -23.03, comparable to those of the related complexes $Ru(IMes)_2(CO)H(OH)$ (δ -23.15) and $Ru(P^tBu_2Me)_2(CO)H(OH)$ (δ -22.30). Proton resonances for the IPr ligands (**Figure 3.28**) proved to be less broad than those in the parent chloride complex **6A**. Several of the doublet resonances of the aryl *meta*-C*H* protons (H_B) in **6D** display a modicum of splitting into doublets themselves, with J_{HH} values of ca. 1.00-0.50 Hz from coupling of the inequivalent *meta*-C*H* protons on the same ring. There is one signal observed for the NC*H* backbone protons (H_C), two overlapping septets (H_D) and four doublets for the isopropyl-CH_3 protons (H_E). These results indicate restricted rotation along the Ru-C_{NHC} and N-C_{Aryl} bonds as observed for other 16-electron compounds throughout this work. In the $^{13}C\{^1H\}$ NMR spectrum (assigned via ^1H-^{13}C HMQC/HMBC experiments), the *C*O (δ 206.0) and Ru-C_{NHC} (δ 198.1) resonances were almost identical to those of $Ru(IMes)_2(CO)H(OH)$ (*C*O = δ 206.4, Ru-C_{NHC} = δ 198.6). There was one CO band

observed at 1863 cm^{-1} (c.f. $Ru(IMes)_2(CO)H(OH)$, 1861 cm^{-1}) at considerably lower frequency than in the phosphine complex, $Ru(P^tBu_2Me)_2(CO)H(OH)$ (1896 cm^{-1}).

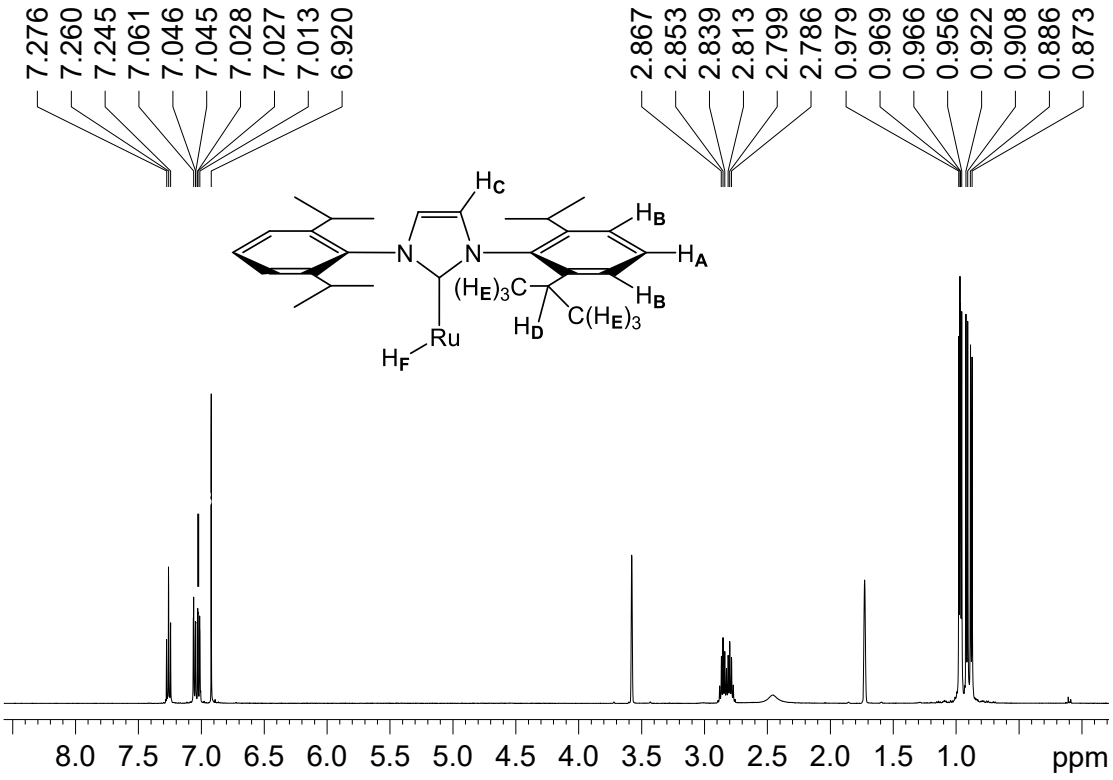

Figure 3.28 ^{1}H NMR spectrum of 6D (d_8-THF, 298 K, 500 MHz)

The crystal structure of **6D** is presented in **Figure 3.29**, with pertinent bond lengths and angles displayed in **Table 3.6** (along with related compounds) and complete data located in the **Appendices**. The structure consists of a distorted square-based pyramid with the hydride occupying the apical position opposite the vacant site. Although this complex is 16-electron, the high symmetry does not lead in this case to disorder as was observed for the 16-electron hydride-chlorides **6A** and **7A**.

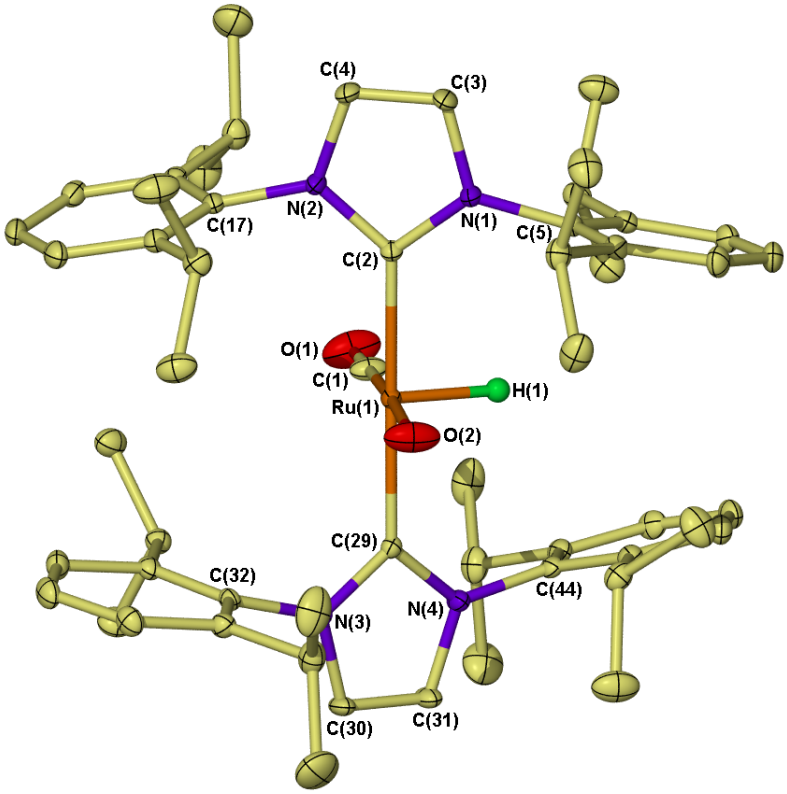

Figure 3.29 Crystal structure of Ru(IPr)$_2$(CO)H(OH) (6D) with thermal ellipsoids set to 30% probability and hydrogen atoms (except the hydride) omitted for clarity

The IPr imidazol rings in **6D** display a least-squares dihedral angle of 39.2˚, which is identical to that found in the parent compound **6A** (39.4˚) and more acute than in Ru(IMes)$_2$(CO)H(OH) (48.3˚). The C_{NHC}-Ru-C_{NHC} angle is marginally distorted from linear (177.34(8)˚) and slightly larger than in Ru(IMes)$_2$(CO)H(OH) (175.43(9)˚), with the C_{CO}-Ru-X angle also slightly larger in **6D** (176.94(10)˚) than in the IMes analogue (174.90(13)˚). Ru-C_{NHC} bond lengths are the same in **6D** (2.0763(19)-2.079(2) Å) and the IMes complex (2.066(2)-2.069(2) Å), and fractionally contracted when compared with the chloride compound **6A** (both 2.0872(13) Å). The Ru-C_{CO} bond distance is notably longer in **6D (**1.838(2) Å**)** than in Ru(IMes)$_2$(CO)H(OH) (1.798(3) Å), possibly resulting from increased steric interactions of the IPr ligand compared with IMes, while the C-O distances are identical for both compounds (1.157(3)-1.165(3) Å).

	6D	Ru(IMes)$_2$(CO)H(OH)	Ru(IPr)$_2$(CO)HCl (6A)
Ru-C$_{NHC}$	2.0763(19)	2.066(2)	2.0872(13)
	2.079(2)	2.069(2)	2.0872(13)
Ru-C$_{CO}$	1.838(2)	1.798(3)	- [b]
Ru-X [a]	1.9958(18)	2.023(2)	- [b]
C$_{NHC}$-Ru-C$_{NHC}$	177.34(8)	175.43(9)	178.78(8)
C$_{CO}$-Ru-X [a]	176.94(10)	174.90(13)	- [b]

[a] X = -OH or -Cl, [b] Disorder precluded accurate value determination.

Table 3.6 Bond lengths (Å) and angles (°) for 6D, Ru(IMes)$_2$(CO)H(OH) and 6A

3.5.3 [Ru(IPr)$_2$(CO)H(OH$_2$)]$^+$BF$_4^-$ (6E)

The slow addition of 1.5 equivalents of $HBF_4{\cdot}OEt_2$ to a d_8-THF solution of Ru(IPr)$_2$(CO)H(OH) (**6D**) in a J. Youngs NMR tube at room temperature led to a slight darkening of the pale yellow solution. After 10 minutes, the hydride signal for **6D** (δ -23.03) was undetectable, and the formation of a new signal at δ -24.97 was revealed by ^{1}H NMR spectroscopy. A new set of proton resonances indicative of two IPr groups was observed and correlated to the new hydride signal through integration. Removal of volatiles *in vacuo* and washing with hexane gave a yellow residue which was recrystallised from THF and hexane to yield X-ray quality crystals of the cationic aqua-hydride complex, [Ru(IPr)$_2$(CO)H(OH$_2$)]$^+$BF$_4^-$ (**6E**), shown in **Figure 3.30**.

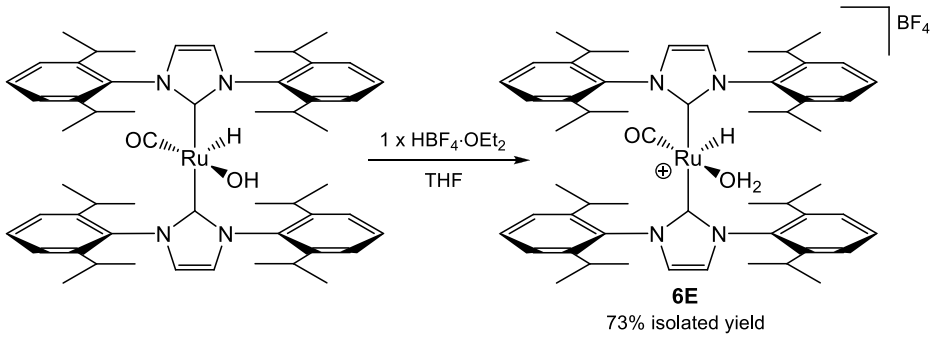

Figure 3.30 Formation of [Ru(IPr)$_2$(CO)H(OH$_2$)]$^+$BF$_4^-$ (6E)

^{1}H NMR spectroscopy of **6E** in d_8-THF (**Figure 3.31**) reveals characteristic resonances for the IPr ligands similar to those observed in **6D**, but at marginally different chemical shifts. Multiple signals are observed for isopropyl (H_E and H_F) and aryl *meta*-C*H* protons (H_C), indicative of inequivalent proton environments resulting from restricted rotation of the N-C$_{Aryl}$ bonds. A very broad signal is detected at δ 4.10 (H_D, see insert in **Figure 3.31**)

which integrates in a 1:4 ratio with the septet resonances for the isopropyl-C*H* protons consistent with a coordinated water molecule. This resonance is comparable with the broad ^{1}H NMR signal observed in $Ru(PEt_3)_2(CO)(H_2O)Cl_2$ at δ 3.99 by the group of Carty *et al*, which is generated from the reaction of $Ru(PEt_3)_2(CO)_2Cl_2$ and MeOH in the presence of water.[56] The hydride signal for **6E** is located at δ -24.97 (H_G), at slightly lower frequency than in **6D** (δ -23.03). In the $^{13}C\{^{1}H\}$ NMR spectrum the *C*O resonance is located at δ 204.3, and is therefore shifted to slightly lower frequency than in **6D** (δ 206.0), with this result mirrored for the Ru-C_{NHC} resonance (**6D**, δ 198.1; **6E**, δ 190.4). In the ^{19}F NMR spectrum, a singlet resonance was detected at δ -151.47, representative of the BF_4 anion. One CO band was observed by IR spectroscopy for **6E** (1923 cm^{-1}) which was at substantially higher wavenumber (+60 cm^{-1}) than for complex **6D** (1863 cm^{-1}). This significant shift in wavenumber corresponds with the change in the X-group *trans*- to the CO ligand from a relatively strong π-donor (-OH) to a much weaker π-donor (OH_2), therefore reducing the available electron density in the metal orbitals for CO backbonding. The formation of $[Ru(P^tBu_2Me)_2(CO)Ph]^+OTf^-$ from $Ru(P^tBu_2Me)_2(CO)PhF$ by Caulton *et al* displayed a similar shift in CO stretching frequency (1921 and 1890 cm^{-1} respectively), although the difference in this example was smaller.

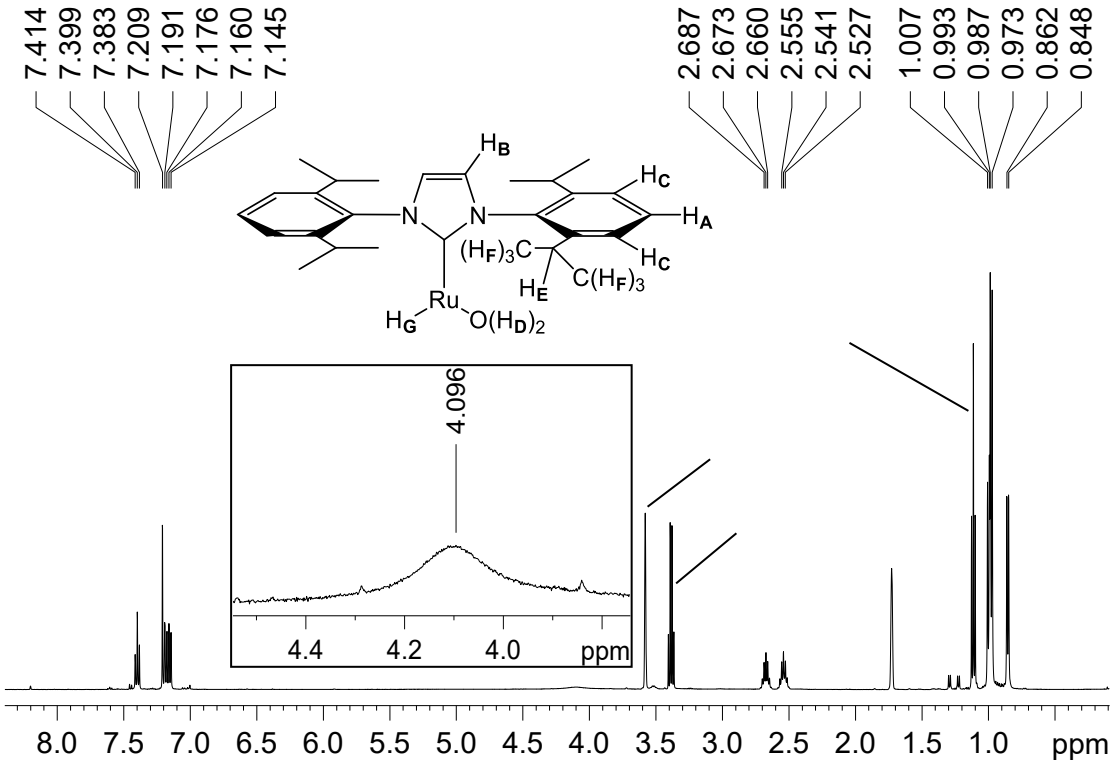

Figure 3.31 ^{1}H NMR spectrum of 6E, with H_2O resonance in insert (d_8-THF, 298 K, 500 MHz)

The crystal structure of **6E** is shown in **Figure 3.32** and complete bond lengths and angles can be found in the **Appendices**. The structure is best described as a distorted square-based pyramid with the hydride occupying the apical position opposite the vacant coordination site. The structure shows the H_2O ligand to interact with the BF_4 moiety through one proton in the form of a hydrogen bond. Structural characterisation of the analogous IMes complex, $[Ru(IMes)_2(CO)H(OH_2)]^+BF_4^-$ was determined by Chatwin from the addition of $AgBF_4$ to $Ru(IMes)_2(CO)HCl$ in the presence of H_2O.[57] Additionally, the aqua-complex $[Ru(PPh_3)_2(CO)_2H(OH_2)]^+BF_4^-$ has been structurally characterised by Clark *et al* from the carbonylation of $[Ru(PPh_3)_3(CO)H(OH_2)]^+BF_4^-$.[58] Pertinent bond lengths and angles for **6E**, $[Ru(IMes)_2(CO)H(OH_2)]^+BF_4^-$ and the parent complex **6D** are presented in **Table 3.7**.

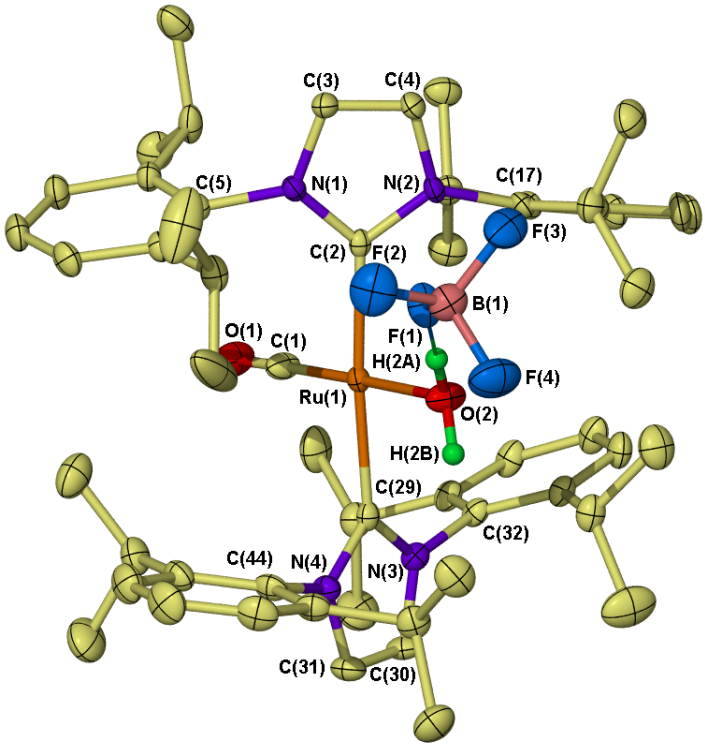

Figure 3.32 Crystal structure of $[Ru(IPr)_2(CO)H(OH_2)]^+BF_4^-$ (6E) with thermal ellipsoids set to 30% probability and hydrogen atoms (except the H_2O protons) omitted for clarity

The Ru-OH_2 bond distances in the IMes complex (2.171(3) Å) and $[Ru(PPh_3)_2(CO)_2H(OH_2)]^+BF_4^-$ (2.15(1) Å) are identical to that observed in **6E** (2.1805(15) Å). All complexes display hydrogen bonding between the coordinated H_2O ligand and the BF_4 anion, although the PPh_3 compound by Clark also shows incorporation of an ethanol solvent molecule into the system. The H···F-BF_3 hydrogen bond distance in **6E** is 1.776 Å, which is notably shorter than in the IMes analogue (1.897 Å). The Ru-C_{NHC}

bond lengths are marginally longer in **6E** (2.0958(18) and 2.1071(19) Å) than in the IMes complex (2.078(4) and 2.084(4) Å), likely due to the larger steric bulk of the IPr ligands. Ru-C_{CO} bond distances are the same in both cationic IPr (1.799(2) Å) and IMes (1.801(4) Å) complexes, although **6D** displays a longer distance of 1.838(2) Å. There are only marginal differences in C_{NHC}-Ru-C_{NHC} and C_{CO}-Ru-OH_2 bond angles for both $[Ru(NHC)_2(CO)H(OH_2)]^+BF_4^-$ compounds. The dihedral angles of the NHC rings however are rather divergent, with **6E** (43.0˚) showing a significantly less acute angle than in the IMes analogue (29.8˚).

	6E	**$[Ru(IMes)_2(CO)H(OH_2)]^+BF_4^-$**	**$Ru(IPr)_2(CO)H(OH)$ (6D)**
Ru-C_{NHC}	2.0958(18)	2.078(4)	2.0763(19)
	2.1071(19)	2.084(4)	2.079(2)
Ru-C_{CO}	1.799(2)	1.801(4)	1.838(2)
Ru-OH_2	2.1805(15)	2.171(3)	-
C_{NHC}-Ru-C_{NHC}	175.04(7)	174.28(13)	177.34(8)
C_{CO}-Ru-OH_2	177.07(10)	175.83(16)	-

Table 3.7 Bond lengths (Å) and angles (˚) for 6E, $[Ru(IMes)_2(CO)H(OH_2)]^+BF_4^-$ and 6D

3.5.4 $[Ru(IPr)(\eta^6\text{-}C_6H_6)(CO)H]^+BF_4^-$ (6F)

The reaction of $Ru(IPr)_2(CO)H(OH)$ (**6D**) with $HBF_4{\cdot}OEt_2$ in THF was shown in **Section 3.5.3** to generate $[Ru(IPr)_2(CO)H(OH_2)]^+BF_4^-$ (**6E**), which remains stable in THF solution even in the presence of a excess of $HBF_4{\cdot}OEt_2$. On repeating this reaction in C_6D_6 with 1.3 equivalents of $HBF_4{\cdot}OEt_2$, the major product initially was once more observed by ^{1}H NMR spectroscopy to be **6E**, although a second hydride resonance was observed at δ -10.08, which gradually increased in intensity over time. After 5 hours at 298 K (**Figure 3.33**), there was no further increase in the hydride signal of the new product (**6F**), even upon thermolysis of the reaction mixture at 50 ˚C for 120 minutes. This observation suggested that **6F** was *not* formed directly via degradation of **6E**.

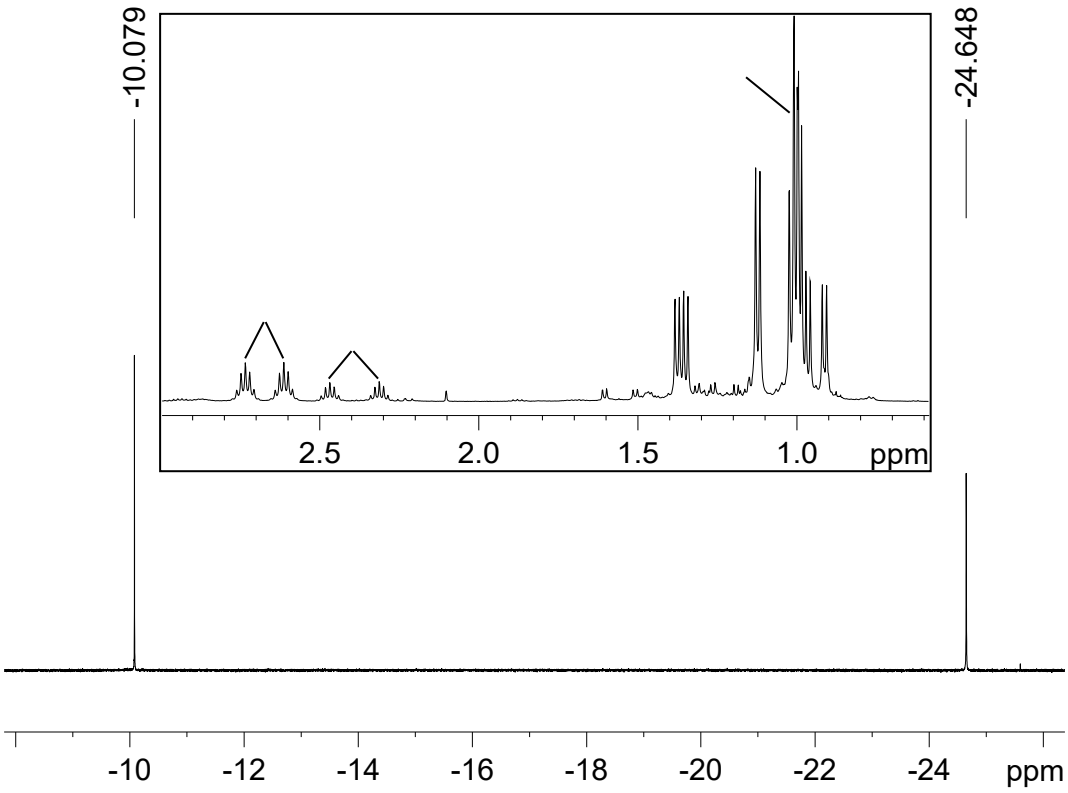

Figure 3.33 ^{1}H NMR spectrum of 6E and a new product 6F, with IPr ligand isopropyl proton region shown in insert (C_6D_6, 298 K, 500 MHz)

The addition of a further 1.3 equivalents of $HBF_4{\cdot}OEt_2$ to the solution of **6E** and **6F** led to the disappearance of the ^{1}H NMR resonances for **6E**, and evolution of **6F** as the exclusive product. The IPr resonances that remained integrated with the **6F** hydride signal in a 1:1 ratio, implying the presence of a single IPr ligand in this complex. A white precipitate was observed in C_6D_6, and subsequent removal of the solvent *in vacuo* with re-dissolution in d_8-THF showed the presence of imidazolium salts that confirmed that one IPr ligand had been protonated. Upon formation of **6F**, the complex was extracted in C_6H_6 to remove the imidazolium salts, and the solvent was then removed *in vacuo*. Washing the residue with Et_2O and hexane yielded a pale brown solid, which upon recrystallisation from CH_2Cl_2 and hexane gave crystals that were crystallographically characterised as the cationic arene-complex $[Ru(IPr)(C_6H_6)(CO)H]^{+}BF_4^{-}$ (**6F**), shown in **Figure 3.34**. Further studies concluded that the synthesis of **6F** was possible via the addition of 1.3 equivalents $HBF_4{\cdot}OEt_2$ to a solution of **6E**, or alternatively the reaction of 2-3 equivalents of $HBF_4{\cdot}OEt_2$ directly to $Ru(IPr)_2(CO)H(OH)$ (**6D**) in benzene.

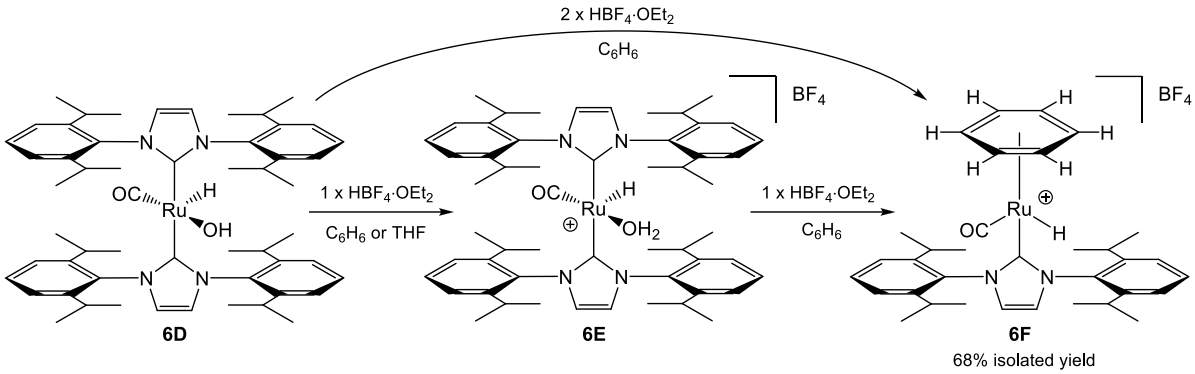

Figure 3.34 Formation of [Ru(IPr)(η^6-C_6H_6)(CO)H]$^+BF_4^-$ (6F)

The initial NMR tube reaction (ca. 10 mg scale) indicated complete formation of **6F** with the addition of a total of 3 equivalents $HBF_4{\cdot}OEt_2$ to $Ru(IPr)_2(CO)H(OH)$ (**6D**) in C_6H_6. On scaling-up the reaction to over 100 mg however, ^1H NMR spectroscopy showed the reaction to terminate approximately 2/3 of the way through, despite a considerable excess of $HBF_4{\cdot}OEt_2$ in solution. The addition of a larger excess of $HBF_4{\cdot}OEt_2$ (over 5 equivalents) eventually led to complete formation of **6F** after 6 hours at room temperature. Further investigation found that the reaction could be completed more efficiently by first the addition of 1.1 equivalents of $HBF_4{\cdot}OEt_2$ to **6E** for 60 minutes, then removal of the volatiles *in vacuo* and subjection of the residue to further vacuum for 30 minutes. On addition of fresh solvent and an additional 1.1 equivalents of $HBF_4{\cdot}OEt_2$ for 10 minutes, reaction was completed. Possible causes for cessation of reaction are discussed later.

The ^1H NMR spectrum of **6F** (**Figure 3.35**) in CD_2Cl_2 reveals inequivalent proton environments in the IPr ligands due to restricted rotation of the N-C_{Aryl} bonds. There is a singlet resonance at δ 5.76 which integrates in a 6:1 ratio with the hydride at δ -9.64 and is assigned to the coordinated η^6-C_6H_6 ring. The resonance is notably shifted to lower frequency from uncoordinated C_6H_6 (ca. δ 7.15), due to the shielding effect on binding to the metal. The $^{13}C\{^1H\}$ NMR spectrum of **6F** displays pertinent resonances at δ 196.1 (*C*O) and δ 172.7 (Ru-C_{NHC}). Crabtree notes that a difference in ^{13}C NMR chemical shift of ca. 25 ppm to lower frequency is typically observed on coordination of an arene,[59] and this is observed for **6F** as the coordinated C_6H_6 signal (δ 98.5) is located at significantly lower frequency than the uncoordinated ring (δ 128.0), again due to shielding effects.

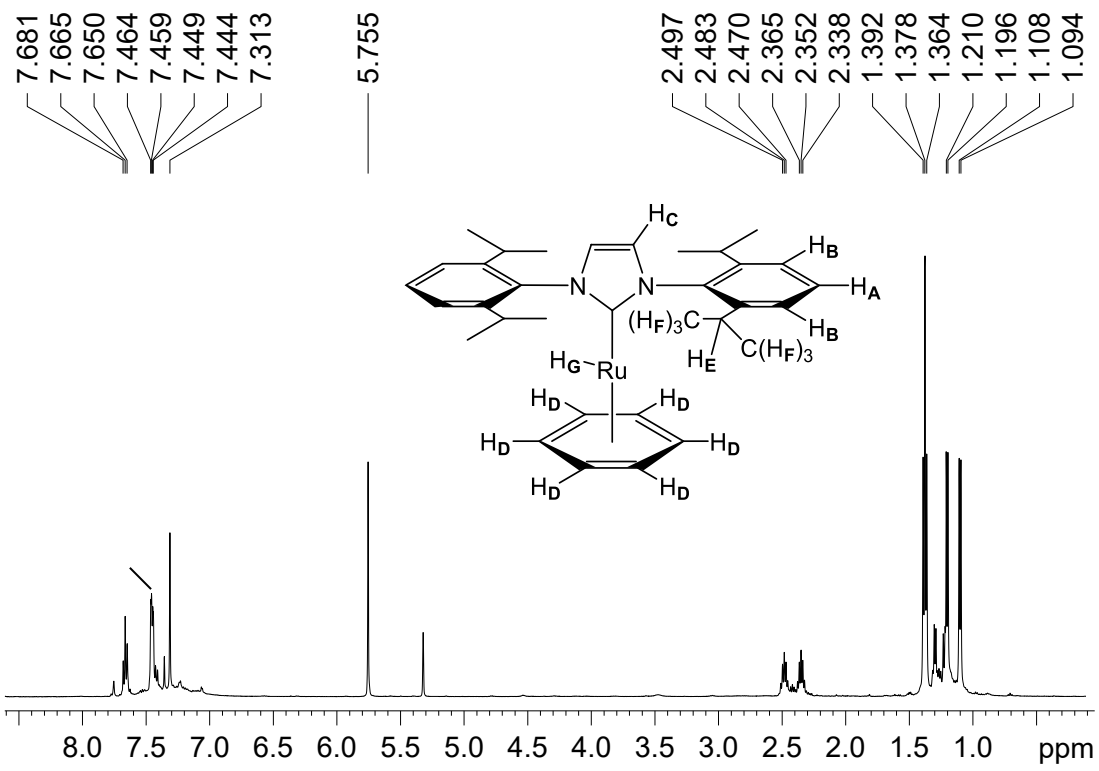

Figure 3.35 ^{1}H NMR spectrum of 6F (CD_2Cl_2, 298 K, 500 MHz)

A selection of related arene-containing complexes are presented in **Table 3.8**, which allow for comparisons of the ^{1}H and ^{13}C NMR data for the hydride, NHC and η^6-C_6H_6 ligands in **6F**. The hydride ligand in η^6-arene complexes is typically located at approximately δ -10, and with resonances for the aromatic C-*H* protons ranging from δ 4.87-6.24 depending upon the arene type. In the ^{13}C NMR spectrum, Ru-C_{NHC} resonances are relatively typical for NHC-containing complexes, at δ 172.1-178.5 and the η^6-carbon atoms of the arenes are located at ca. δ 90-110, with these results showing close relation to the data observed in **6F**. In addition, the ^{13}C NMR resonances for the *C*O ligand in **6F** (δ 196.1) is closely related to those observed in the three $[Ru(C_6Me_6)(PPh_2R)(CO)H]^+BF_4^-$ complexes from the group of Lindner (**Entry 2**, **Table 3.8**; δ 198.7-199.3).[60] There is one CO band observed by IR for **6F** (1986 cm^{-1}) which is at slightly higher wavenumber than those of analogous arene-containing complexes $Ru(C_6Me_6)(CO)H_2$ (1965 cm^{-1}),[61] $[Ru(C_6Me_6)(PMe_3)(CO)H]^+PF_6^-$ (1970 cm^{-1})[62] and the three $[Ru(C_6Me_6)(PPh_2R)(CO)H]^+BF_4^-$ complexes (**Entry 2**, **Table 3.8**; 1973-1974 cm^{-1}),[60] likely to result from the increased electron inducting effects of the six methyl groups in C_6Me_6 compared with C_6H_6.

Entry	Compound	$^1H_{hydride}$ (δ)	η^6-C_6H_n (δ)	Ru-C_{NHC} (δ)	η^6-C_6H_n (δ)
1	6F	-9.64	5.76	172.7	98.5
2	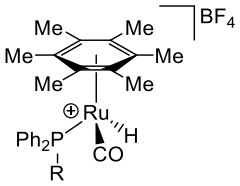	R_A = -11.0,[b] R_B = -11.0,[b] R_C = -11.0[b]	-	-	R_A = 113.3,[b 60] R_B = 113.7,[b 60] R_C = 113.7 [b 60]
3	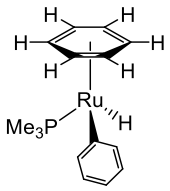	-9.11	4.87	-	-[a 63]
4	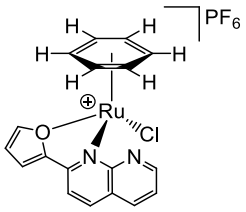	-	5.93	-	-[a 64]
5	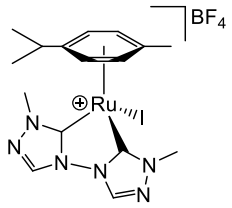	-	6.24, 6.17	178.5	113.2, 108.3, 92.3, 90.1[65]
6	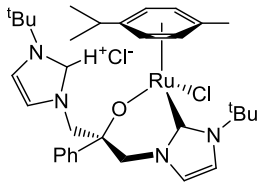	-	-[a]	172.1	-[a 66]

[a] Not quoted. [b] R_A = methoxyethyl, R_B = 1,3-dioxan-2-ylmethyl, R_C = 1,3-dioxolan-2-ylmethyl.

Table 3.8 ^{1}H and ^{13}C NMR data for 6F and related arene-containing complexes

On crystallisation of **6F**, there were found to be two similar but independent structures in the asymmetric unit, only one of which (Ru1) is displayed in **Figure 3.36**. Both cationic structures display the typical three-legged piano stool arrangement, comprising of the three IPr, CO and hydride ligands, with the η^6-C_6H_6 completing the coordination sphere. The complex is chiral due to the presence of four different ligands, with the stereocentre at the ruthenium atom, and both complexes crystallised as the R-enantiomer. Pertinent bond

lengths (Å) and angles (˚) of **6F** are presented in **Table 3.9**, with complete data given in the **Appendices**.

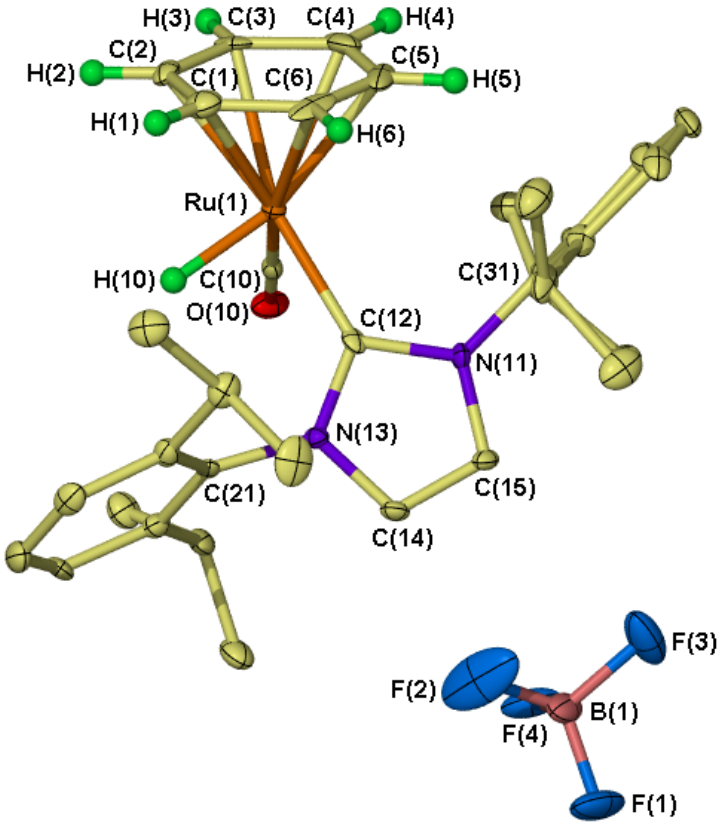

Figure 3.36 Crystal structure of [Ru(IPr)(η^6-C_6H_6)(CO)H]$^+BF_4^-$ (6F) with thermal ellipsoids set to 30% probability and hydrogen atoms (except the hydride and arene protons) omitted for clarity

Both Ru1 and Ru2 structures in the unit cell display bond distances and angles identical to each other. The Ru-centroid distances of 1.818 Å (Ru1) and 1.807 Å (Ru2) in **6F** are found to be significantly longer than those of analogous η^6-C_6H_6 complexes such as $Ru(C_6H_6)(PR_3)Cl_2$ (1.687 Å),[67] $[Ru(C_6H_6)$(2-(2-thiazolyl)-1,8-naphthyridine)Cl$]^+PF_6^-$[64] (1.68 Å) and the η^6-*p*-cymene complex, Ru(*p*-cymene)(1,3-dimethyl-2-phenylimidazol)Cl_2 (1.688 Å).[68] The Ru-C_{NHC} bond lengths of 2.035(9)-2.063(10) Å in **6F** lie inside the expected range, with related NHC-arene complexes such as [Ru(*p*-cymene)(bitriazol)I]$^+BF_4^-$ (**Entry 5**, **Table 3.8**; 2.014(8)-2.019(7) Å)[65] and Ru(*p*-cymene)(1-(oxazolinyl)-3-mesitylimidazol)Cl (2.038(3) Å)[69] showing comparable values.

	6F, Ru(1)	**6F, Ru(2)**
Ru-C_{NHC}	2.035(9)	2.063(10)
Ru-centroid [a]	1.818	1.807
Ru-C_{CO}	1.832(11)	1.808(15)
C-O	1.158(11)	1.205(15)
C_{NHC}-Ru-C_{CO}	85.0(4)	87.0(5)

[a] Calculated centroid of η^6-C_6H_6 ring.

Table 3.9 Bond lengths (Å) and angles (°) in 6F (Ru1 and Ru2)

Formation of the η^6-C_6H_6-complex **6F** occurs from reaction of $HBF_4{\cdot}OEt_2$ and $Ru(IPr)_2(CO)H(OH)$ in benzene, however on varying the solvent to toluene, the η^6-$C_6H_5CH_3$ analogue is produced. The complex displays a slightly lower frequency hydride signal at δ -10.28 instead of δ -10.08 (**6F**) in addition to a series of five multiplets from ca. 5.8-4.8 ppm which integrate in 1:1:1:1:1 ratio with each other (**Figure 3.37**), representative of the toluene aryl protons. Each multiplet integrates with the hydride in a 1:1 ratio, and in a 1:3 ratio with a proton signal at δ 2.08 assigned to the aryl-CH_3 resonance of the coordinated toluene. These multiplet resonances compare with related toluene-coordinated complexes by Dyson *et al*, who report the observation of similar multiplets for $[Ru(\eta^6\text{-}C_6H_5CH_3)(PPh_3)(NCMe)Cl]^+PF_6^-$ (δ 6.01-4.85) and $[Ru(\eta^6\text{-}C_6H_5CH_3)(PPh_3)(PPhMe_2)Cl]^+PF_6^-$ (δ 5.87-4.28) in the ^{1}H NMR spectrum.[70]

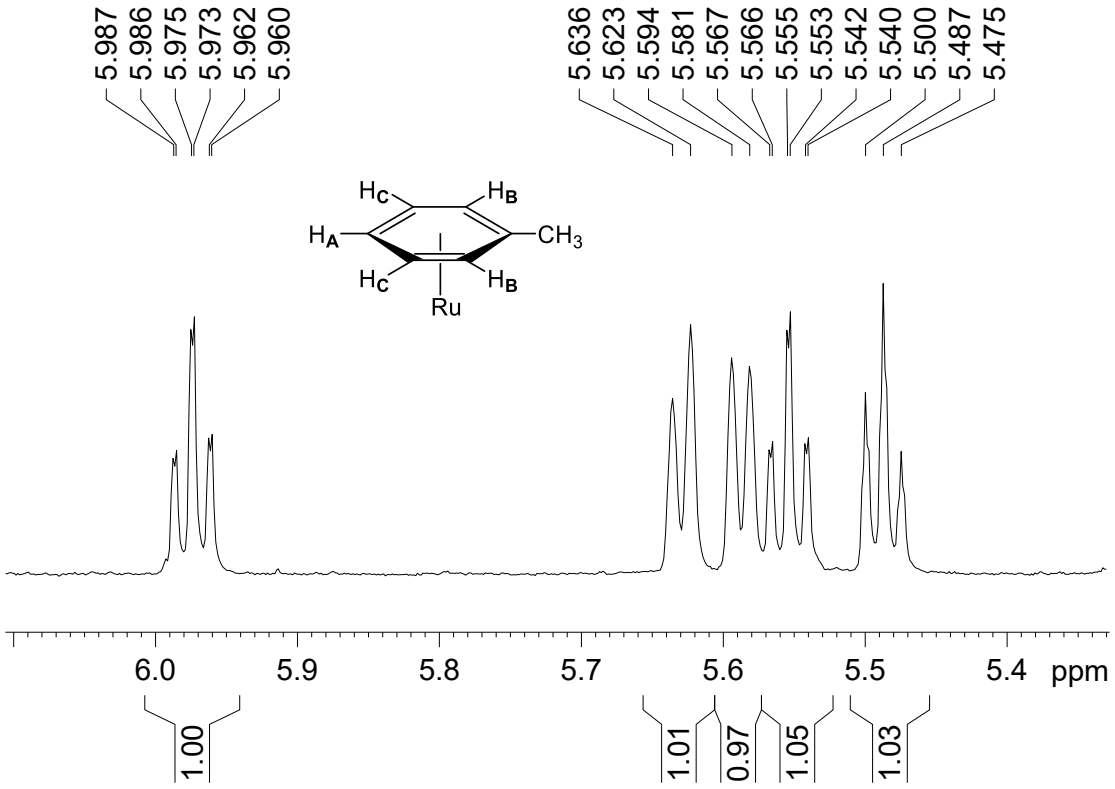

Figure 3.37 ^{1}H NMR spectrum of [Ru(IPr)(η^6-$C_6H_5CH_3$)(CO)H]$^+BF_4^-$, coordinated toluene-C*H* resonances (CD_2Cl_2, 298 K, 500 MHz)

No attempts were made to further characterise [Ru(IPr)(η^6-$C_6H_5CH_3$)(CO)H]$^+BF_4^-$, although interestingly the complex led to the observation of an unexpected reaction. The facile exchange between a free arene and a coordinated arene in η^6-arene-metal(d_6)L_3 complexes is not usually observed, although it may be encouraged in the presence of donor molecules such as a solvent (e.g. ether) or a ketone.[71] In [Ru(IPr)(η^6-$C_6H_5CH_3$)(CO)H]$^+BF_4^-$ and **6F** however, rapid exchange of the coordinated arene occurs whilst devoid of a Lewis base upon dissolution of either complex in a suitable arene-solvent. For example, [Ru(IPr)(η^6-$C_6H_5CH_3$)(CO)H]$^+BF_4^-$ can be dissolved in C_6D_6 and converted to 53% [Ru(IPr)(η^6-C_6D_6)(CO)H]$^+BF_4^-$ in 5 minutes at room temperature, as observed by ^{1}H and ^{2}H NMR spectroscopy, with full conversion to **6F** occurring on standing at room temperature for 15 minutes, or mild heating of the compound for a few minutes at 50 ˚C. In a separate reaction, dissolution of the protio-C_6H_6 complex **6F** in C_6D_6 followed by immediate removal of the solvent *in vacuo*, and dissolution in CD_2Cl_2 yielded **6F** in a roughly 1:1 mixture of both C_6H_6/C_6D_6 products resulting from arene-exchange. The ^{1}H NMR spectrum of this mixture contained two hydride resonances separated by 0.01 ppm at δ -9.65 (C_6D_6) and δ -9.64 (C_6H_6), and the $^{13}C\{^{1}H\}$ PENDANT NMR

spectrum contained resonances for the coordinated C_6H_6 (singlet) and C_6D_6 (triplet, quaternary-phased) moieties (**Figure 3.38**).

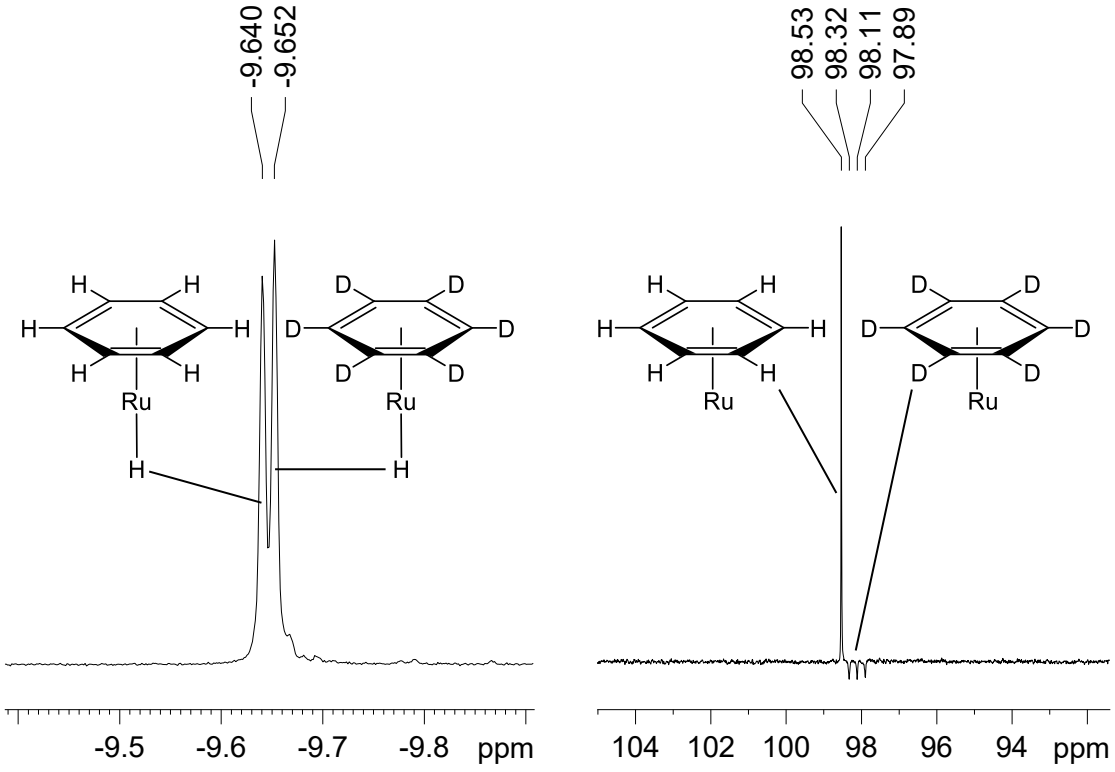

Figure 3.38 ^{1}H NMR (hydride region) and ^{13}C{^{1}H} PENDANT NMR spectra for 6F containing ca. 50% protio and 50% deuterated coordinated benzene rings (CD_2Cl_2, 298 K, 500/126 MHz)

In attempting to generate the C_6Me_6 analogue of **6F**, the addition of 1 equivalent $HBF_4{\cdot}OEt_2$ to a d_8-THF solution of **6E** containing 4 equivalents of C_6Me_6 led to no characteristic arene-hydride signals being observed by ^{1}H NMR spectroscopy, even after 90 minutes at 50 ˚C. Further addition of a large excess of C_6D_6 to the solution led only to traces of **6F** even after prolonged heating at 50 ˚C for 18 hours. Due to the facile initial formation of **6F** in C_6H_6 solvent, this result suggested that generation of the arene C_6Me_6 and C_6H_6 complexes was being hindered, possibly as a result of coordination from the THF solvent. This observation may help to explain the previous observation that in the synthesis of **6F** on large scale, reaction was terminated before completion, as the evolved H_2O from **6E** may coordinate to the ruthenium and inhibit the (normally facile) reaction with the arene. This hypothesis is substantiated by subjecting the residue of **6E** (containing H_2O) to vacuum, after which the addition of fresh solvent and $HBF_4{\cdot}OEt_2$ then permits the rapid formation of **6F**.

In summary, the initial protonation reaction of $Ru(IPr)_2(CO)H(OH)$ (**6D**) by 1 equivalent of $HBF_4{\cdot}OEt_2$ in C_6H_6 did not lead to loss of a ligand from the complex as proposed in **Figure 3.26**, **Section 3.5.1**. However, formation of the aqua-complex was indeed observed, showing that the HX-loss pathway was the initially favoured process for **6D**, although the generated species ($[Ru(IPr)_2(CO)H(OH_2)]^+BF_4^-$, **6E**) was stable enough to be isolated with retention of the H_2O ligand. The subsequent addition of a second equivalent of $HBF_4{\cdot}OEt_2$ in C_6H_6 led to the protonation of an IPr ligand from **6E**, with loss of both the H_2O *and* IPr ligands, therefore involving two of the ligand-loss pathways proposed in **Figure 3.26**. However, the remaining 12-electron fragment was not stabilised sufficiently by the remaining IPr ligand and reacted with the solvent to yield $[Ru(IPr)(\eta^6\text{-}C_6H_6)(CO)H]^+BF_4^-$ (**6F**). The interesting and unusual observation of facile arene-exchange in **6F** demonstrates its behaviour as effectively a 12-electron fragment when dissolved in an arene solvent. The ability of **6F** to undergo such a process may be explained by the somewhat longer Ru-centroid distance of 1.81 Å (shown in **Table 3.9**), when compared with other $\eta^6\text{-}C_6H_6$ complexes (ca. 1.68 Å), indicating that the arene in **6F** is less tightly bonded to the metal.

3.5.5 Reaction of $HBF_4{\cdot}OEt_2$ with $Ru(IPr)_2(CO)HCl$

The reaction of $Ru(IPr)_2(CO)HCl$ (**6A**) with $HBF_4{\cdot}OEt_2$ was commenced to investigate possible variations in ligand-loss processes (see **Figure 3.26**) when changing the X-group from -OH to -Cl. The addition of 1.2 equivalents of $HBF_4{\cdot}OEt_2$ to **6A** in C_6D_6 at room temperature led to a small amount of bubbling in the solution, which was not observed in the equivalent reaction with $Ru(IPr)_2(CO)H(OH)$ (**6D**). ^1H NMR spectroscopy of the solution after 5 minutes showed mainly unreacted **6A** (δ -25.59), with smaller resonances at δ -10.07 (consistent with **6F**) and a broad singlet at δ -24.41. A comparison between this ^1H NMR spectrum and that of **6D** under identical conditions is presented in **Figure 3.39**. In both cases, **6F** is observed, although to a much greater extent in the protonation reaction involving **6A**. A broad hydride signal at δ -24.41 is observed in the **6A** reaction, which is at very similar ^1H NMR chemical shift to that of $[Ru(IPr)_2(CO)H(OH_2)]^+BF_4^-$ (δ -24.51) which was generated by protonation of **6D**. We propose that this δ -24.41 signal may represent a complex such as $Ru(IPr)_2(CO)H(Cl\cdots H\text{-}FBF_3)$, with the HBF_4 hydrogen-bonded to the chloride ligand of **6A**. Although Crabtree *et al* have provided evidence for the existence of an H-F bound species in an iridium system,[72] there are no such examples of

an H-Cl complex in the literature and we therefore do not conclude that the chloride is fully protonated. However, we may propose that the HX-formation pathway is clearly favored in both **6A** and **6D**, although the weaker F_3BF-H···X interaction with the chloride ligand leads to formation of **6F** or retention of **6A** in preference to the $Ru(IPr)_2(CO)H(Cl\cdots H\text{-}FBF_3)$ complex.

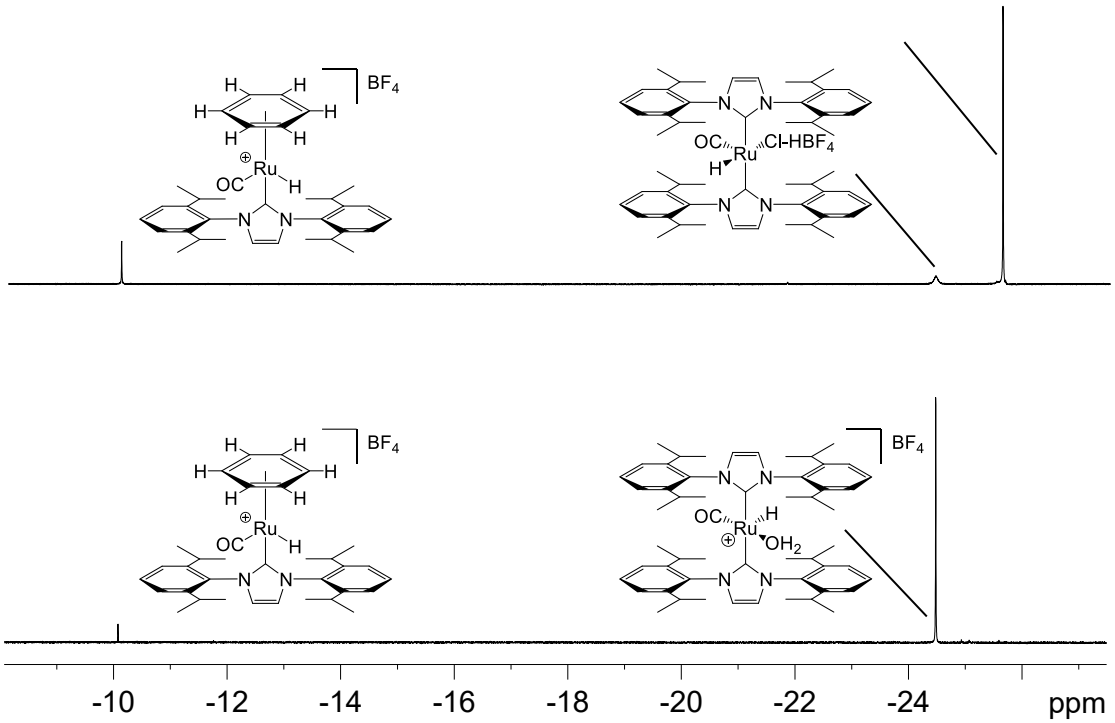

Figure 3.39 ^{1}H NMR (hydride region) of the addition of 1.2 equivalents of $HBF_4{\cdot}OEt_2$ to $Ru(IPr)_2(CO)HCl$ (6A) (top) and $Ru(IPr)_2(CO)H(OH)$ (6D) (bottom) for 5 minutes at 298 K (C_6D_6, 298 K, 500 MHz)

Upon monitoring the reaction of 1.2 equivalents of $HBF_4{\cdot}OEt_2$ with **6A** for a further 24 hours, there was no change in signal intensities observed by ^{1}H NMR spectroscopy. The addition of a further 1.5 equivalents of $HBF_4{\cdot}OEt_2$ in C_6D_6 led to the sole hydride-containing product to be $[Ru(IPr)(\eta^6\text{-}C_6D_6)(CO)H]^+BF_4^-$ (**6F**) after ca. 3 hours at room temperature, as characterised by ^{1}H NMR spectroscopy. Formation of **6F** was confirmed further through ^{2}H NMR spectroscopy which detected a singlet at δ 5.35 for the coordinated $\eta^6\text{-}C_6D_6$ ring. The low temperature addition of $HBF_4{\cdot}OEt_2$ to **6A** in d_8-toluene at -78 ˚C was investigated in an attempt to observe possible intermediates. However, monitoring the ^{1}H NMR spectrum from 215 K to 258 K showed no formation of new species, and above 278 K there was only evolution of signals attributed to $[Ru(IPr)(\eta^6\text{-}C_6D_5CD_3)(CO)H]^+BF_4^-$ and the δ -24.41 product.

On addition of 3 equivalents of $HBF_4{\cdot}OEt_2$ to **6A**, there was vigorous bubbling of the reaction mixture. The formation of **6F** was observed by ^1H NMR spectroscopy, in addition to a new set of IPr resonances for a non-hydride containing product. Extraction of the product in C_6H_6 preceded removal of the solvent *in vacuo*, which was followed by an additional extraction in Et_2O (away from **6F**) and removal of the solvent to afford a yellow solid. Recrystallisation of the solid was achieved from toluene and hexane to give X-ray quality crystals which were crystallographically characterised to be $[Ru_2(IPr)_2(CO)_2(OH_2)_2(\mu\text{-}Cl)_3]^+BF_4^-$ in 32% yield (**Figure 3.40**). This dimeric cationic species contains three bridging chloride atoms between the two ruthenium metals, with two H_2O ligands hydrogen-bonded to a single BF_4 anion. This appears to be generated upon removal of the hydride ligand and η^6-C_6H_6 ring from **6F** in the presence of excess $HBF_4{\cdot}OEt_2$ and residual H_2O from the solvent. Repeating the reaction with isolated **6F** however does not lead to formation of this product, due to the lack of a chloride source, indicating the evolved HCl from the protonation of **6A** to give **6F** must be involved in the formation of this dimer.

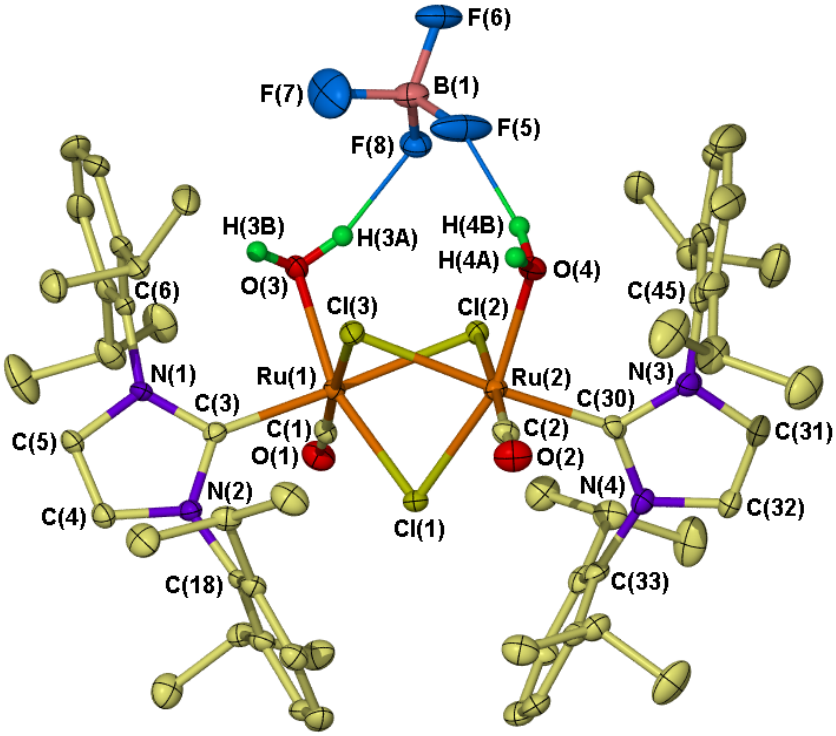

Figure 3.40 Crystal structure of $[Ru_2(IPr)_2(CO)_2(OH_2)_2(\mu\text{-}Cl)_3]^+BF_4^-$ with thermal ellipsoids set to 30% probability and hydrogen atoms (except the H_2O protons) omitted for clarity

The reaction of **6A** with $HBF_4{\cdot}OEt_2$ (3 equivalents) in CD_2Cl_2 in the presence of 4 equivalents of mesitylene ($C_6H_3Me_3$) led to formation of a hydride signal (δ -10.90) characteristic for a $[Ru(IPr)(\eta^6\text{-arene})(CO)H]^+BF_4^-$ complex after 30 minutes at room temperature. ^1H NMR spectroscopy showed the hydride to integrate in a 1:3 ratio with a singlet at δ 5.58 and in a 1:9 ratio with a resonance at δ 1.92, likely to result from the coordinated η^6-mesitylene ring. Although this complex was not characterised further, the method demonstrates that a range of arene-containing complexes may be generated in CD_2Cl_2, whereas reactions in benzene and toluene result in arene-exchange reactions, while THF was shown to inhibit the reaction.

The reaction of $Ru(IPr)_2(CO)HCl$ (**6A**) with *1.2 equivalents* of $HBF_4{\cdot}OEt_2$ is directly comparable to work by Yi *et al* who have reacted the analogous complex $Ru(PCy_3)_2(CO)HCl$ under identical conditions.[18] Their observations are described in **Figure 3.41**. They reported that the main product "$Ru(PCy_3)(CO)HCl$" could not be separated from the protonated phosphine ligand $PCy_3H^+BF_4^-$, and therefore this species was not fully characterised. Spectroscopic data for "$Ru(PCy_3)(CO)HCl$" shows a ^1H NMR hydride signal at δ -10.52, a ^{13}C NMR resonance at δ 196.9 (attributed to *C*O) and a CO band at 1969 cm^{-1}, which they conclude may indicate a cationic species. Given the comparative results in this work (equivalent values for $[Ru(IPr)(\eta^6\text{-}C_6H_6)(CO)H]^+BF_4^-$ are δ -10.07, δ 196.1 and 1986 cm^{-1} respectively), it is highly likely that "$Ru(PCy_3)(CO)HCl$" is actually $[Ru(PCy_3)(\eta^6\text{-}C_6H_6)(CO)H]^+BF_4^-$. They observed that "$Ru(PCy_3)(CO)HCl$" (or $[Ru(PCy_3)(\eta^6\text{-}C_6H_6)(CO)H]^+BF_4^-$) was not stable at room temperature in benzene solution, and quickly decomposed into a variety of products, one of which was isolated as the tetrameric-ruthenium complex shown in **Figure 3.41**. This contrasts with $[Ru(IPr)(\eta^6\text{-}C_6H_6)(CO)H]^+BF_4^-$ which *is stable* indefinitely in benzene and demonstrates the often stabilising nature of the NHC ligands compared with the phosphine analogues.

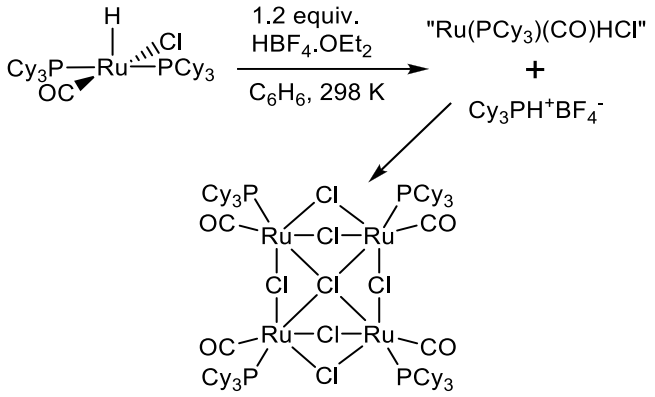

Figure 3.41 Proposed and isolated products from the reaction of $Ru(PCy_3)_2(CO)HCl$ with $HBF_4{\cdot}OEt_2$ by Yi

In summary, the initial protonation reaction of $Ru(IPr)_2(CO)HCl$ (**6A**) by 1 equivalent of $HBF_4{\cdot}OEt_2$ was shown to generate a greater proportion of the arene-complex, $[Ru(IPr)(\eta^6\text{-arene})(CO)H]^+BF_4^-$ (**6F**) than in the same reaction involving $Ru(IPr)_2(CO)H(OH)$ (**6D**). Interaction of HBF_4 with the chloride ligand in **6A** yielded a complex we propose to be $Ru(IPr)_2(CO)H(Cl\cdots H\text{-}FBF_3)$, which was unstable with respect to the starting material and **6F**. Indeed, the addition of another equivalent of $HBF_4{\cdot}OEt_2$ led to the subsequent facile generation of **6F**, which was observed to remain stable in C_6H_6. On the addition of yet another equivalent of $HBF_4{\cdot}OEt_2$, it was observed that the hydride ligand in **6F** was protonated (in the presence of evolved HCl from **6A**) to give H_2 gas and a dimeric complex $[Ru_2(IPr)_2(CO)_2(OH_2)_2(\mu\text{-}Cl)_3]^+BF_4^-$, containing bridging chloride ligands.

3.6 Summary and outlook

This chapter has presented the formation of original 16-electron *bis*-NHC complexes and has investigated their interesting and unusual transformations in a number of stoichiometric and catalytic reactions. A summary of all isolated compounds in this chapter is shown in schematic form in **Figure 3.42**.

Initially, the formation and characterisation of the 16-electron *bis*-NHC complexes was achieved through the use of free NHC and NHC-adduct methodologies. The ability to by-pass the use of free saturated NHCs was found to allow considerable improvements in synthetic processes for the isolation of these $Ru(SIPr)_2(CO)HX$ complexes, and with subsequent incorporation of both IPr and SIPr ligands in these complexes have enabled spectroscopic and catalytic comparisons of these ligands to be made. Through a series of

ketone hydrogenation reactions, it has been elucidated that the IPr ligand forms the most active complexes, with SIPr being notably poorer in this task. This observation was attributed to the considerable steric influence of the SIPr ligand, hindering binding of the organic substrate. It was established that changing the chloride ligand for a η^2-borohydride ligand had minimal influences for the hydrogenation of acetophenone, but proved to increase the catalytic activity for the reduction of *para*-methoxyacetophenone. The addition of CO to the coordinatively unsaturated 16-electron complexes led to the formation of *bis*-CO complexes. It was discovered that facile CO elimination occurred from the SIPr complex and not the IPr complex, again demonstrating how the subtle consequences of manipulating the NHC backbone can affect complex reactivity.

The hydroxide complex $Ru(IPr)_2(CO)H(OH)$ was readily formed via the reaction of $Ru(IPr)_2(CO)HCl$ with KOH and enabled the investigation of protonation reactions of both these complexes with $HBF_4{\cdot}OEt_2$. It was shown that when the X ligand was -OH, the first equivalent of $HBF_4{\cdot}OEt_2$ led to formation of the first example of an isolated NHC-containing aqua-hydride complex, $[Ru(IPr)_2(CO)H(OH_2)]^+BF_4^-$. Contrary to the proposed scheme in **Figure 3.26** (**Section 3.5.1**) however, H_2O dissociation was not observed to occur until the addition of another equivalent of $HBF_4{\cdot}OEt_2$ in the presence of an arene solvent (benzene), which led to the protonation and loss of an IPr ligand to generate the chiral cationic arene-complex $[Ru(IPr)(\eta^6\text{-}C_6H_6)(CO)H]^+BF_4^-$. This species is, to date, only the second ruthenium-NHC arene-hydride complex,[73] and is shown to demonstrate a remarkably facile exchange of the η^6-arene ligand when dissolved in other arene solvents. This observation effectively renders this complex a 12-electron fragment, which may boast applications for catalytic systems in the future. The reaction of $Ru(IPr)_2(CO)HCl$ with $HBF_4{\cdot}OEt_2$ in benzene was observed to proceed rapidly to form $[Ru(IPr)(\eta^6\text{-}C_6H_6)(CO)H]^+BF_4^-$, due to instability of the proposed $Ru(IPr)_2(CO)H(Cl\cdots H\text{-}FBF_3)$ species. The addition of excess $HBF_4{\cdot}OEt_2$ led to the evolution of H_2 through loss of the hydride ligand to give a dimeric complex in the presence of evolved HCl. This work has therefore demonstrated that all three ligand-loss processes outlined in **Figure 3.26** can occur in these NHC systems, depending upon the quantities of $HBF_4{\cdot}OEt_2$ used and the type of ligand X-group in the $Ru(NHC)_2(CO)HX$ precursor.

Future work may encompass the potential applications of $Ru(IPr)_2(CO)H(OH)$, $[Ru(IPr)_2(CO)H(OH_2)]^+BF_4^-$ and $[Ru(IPr)(\eta^6\text{-}C_6H_6)(CO)H]^+BF_4^-$ in catalytic fields such as in the hydrogenation of ketones and alkenes or hydrovinylation reactions. Results by Yi indicate a marked improvement in the catalytic activity of $Ru(PCy_3)_2(CO)HCl$ in these reactions upon the removal of ligands with $HBF_4{\cdot}OEt_2$,[18] indicating that a similar outcome may occur for these NHC-containing systems. Additionally, $[Ru(IPr)(\eta^6\text{-}C_6H_6)(CO)H]^+BF_4^-$ may be utilised for a multitude of tasks such as for example RCM or protonation/deprotonation reactions of the coordinated arene, where it may be compared with other arene-containing examples.

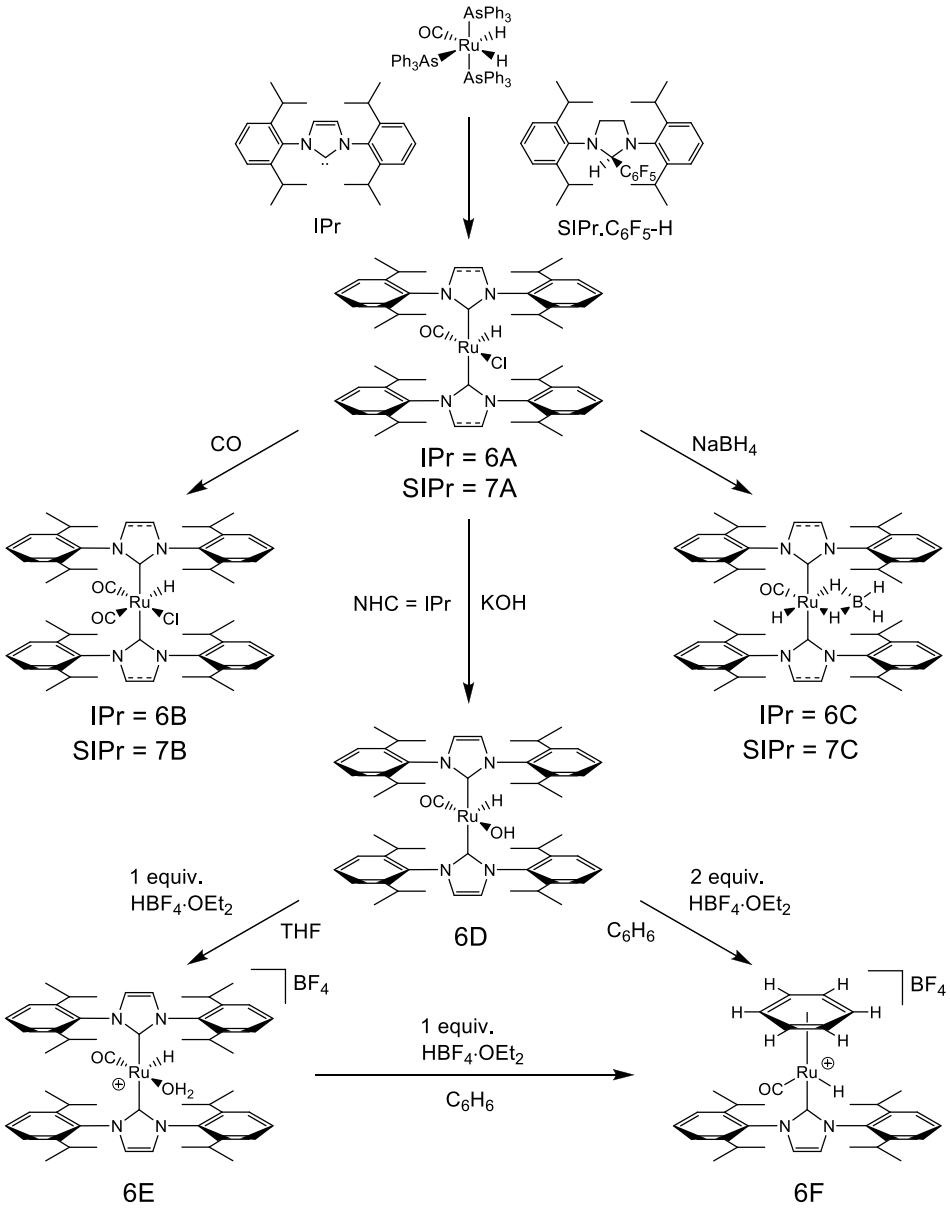

Figure 3.42 Summary of isolated ruthenium hydride complexes

3.7 References

1 Jazzar, R. F. R.; Bhatia, P. H.; Mahon, M. F.; Whittlesey, M. K., *Organometallics* **2003**, *22*, 670-683.

2 Chatwin, S. L.; Diggle, R. A.; Jazzar, R. F. R.; Macgregor, S. A.; Mahon, M. F.; Whittlesey, M. K., *Inorg. Chem.* **2003**, *42*, 7695-7697.

3 Chatwin, S. L.; Davidson, M. G.; Doherty, C.; Donald, S. M.; Jazzar, R. F. R.; Macgregor, S. A.; McIntyre, G.; Mahon, M. F.; Whittlesey, M. K., *Organometallics* **2006**, *25*, 99-110.

4 Enthaler, S.; Jackstell, R.; Hagemann, B.; Junge, K.; Erre, G.; Beller, M., *J. Organomet. Chem.* **2006**, *691*, 4652-4659.

5 Grasa, G. A.; Viciu, M. S.; Huang, J.; Zhang, C.; Trudell, M. L.; Nolan, S. P., *Organometallics* **2002**, *21*, 2866-2873.

6 Dorta, R.; Stevens, E. D.; Scott, N. M.; Costabile, C.; Cavallo, L.; Hoff, C. D.; Nolan, S. P., *J. Am. Chem. Soc.* **2005**, *127*, 2485-2495.

7 Dorta, R.; Stevens, E. D.; Hoff, C. D.; Nolan, S. P., *J. Am. Chem. Soc.* **2003**, *125*, 10490-10491.

8 Huang, J.; Schanz, H.-J.; Stevens, E. D.; Nolan, S. P., *Organometallics* **1999**, *18*, 2370-2375.

9 Viciu, M. S.; Navarro, O.; Germaneau, R. F.; Kelly, R. A.; Sommer, W.; Marion, N.; Stevens, E. D.; Cavallo, L.; Nolan, S. P., *Organometallics* **2004**, *23*, 1629-1635.

10 Ellis, B. D.; Dyker, A.; Decken, A.; Macdonald, C. L. B., *Chem. Commun.* **2005**, 1965-1967.

11 Grubbs, R. H.; Chang, S., *Tetrahedron* **1998**, *54*, 4413-4450.

12 Trnka, T. M.; Grubbs, R. H., *Acc. Chem. Res.* **2001**, *34*, 18-29.

13 Statler, J. A.; Wilkinson, G.; Thornton-Pett, M.; Hursthouse, M. B., *Dalton Trans.* **1984**, 1731-1738.

14 Gusev, D. G.; Dolgushin, F. M.; Antipin, M. Y., *Organometallics* **2000**, *19*, 3429-3434.

15 Chamberlain, B.; Duckett, S. B.; Lowe, J. P.; Mawby, R. J.; Stott, C. J., *Dalton Trans.* **2003**, 2603-2614.

16 Bianchini, C.; Perez, P. J.; Peruzzini, M.; Zanobini, F.; Vacca, A., *Inorg. Chem.* **1991**, *30*, 279-287.

17 Chatwin, S. L., *Ph.D. Thesis, University of Bath.* **2007**.

18 Yi, C. S.; Lee, D. W.; He, Z.; Rheingold, A. L.; Lam, K.-C.; Concolino, T. E., *Organometallics* **2000**, *19*, 2909-2915.

19 Huang, D.; Bollinger, J. C.; Streib, W. E.; Folting, K.; Young, V.; Eisenstein, O.; Caulton, K. G., *Organometallics* **2000**, *19*, 2281-2290.

20 Scott, N. M.; Dorta, R.; Stevens, E. D.; Correa, A.; Cavallo, L.; Nolan, S. P., *J. Am. Chem. Soc.* **2005**, *127*, 3516-3526.

21 Huang, D.; Huffman, J. C.; Bollinger, J. C.; Eisenstein, O.; Caulton, K. G., *J. Am. Chem. Soc.* **1997**, *119*, 7398-7399.

22 Baratta, W.; Mealli, C.; Herdtweck, E.; Lenco, A.; Mason, S. A.; Rigo, P., *J. Am. Chem. Soc.* **2004**, *126*, 5549-5562.

23 Huang, D.; Streib, W. E.; Eisenstein, O.; Caulton, K. G., *Angew. Chem., Int. Ed.* **1997**, *36*, 2004-2006.

24 Kranenburg, M.; Kamer, P. C. J.; van Leeuwen, P. W. N. M.; Chaudret, B., *Chem. Commun.* **1997**, 373-374.

25 Sanchez-Delgado, R. A.; Thewalt, U.; Valencia, N.; Andriollo, A.; Marquez-Silva, R.-L.; Puga, J.; Schollhorn, H.; Klein, H.-P.; Fontal, B., *Inorg. Chem.* **1986**, *25*, 1097-1106.

26 Strauss, S. H., *Chem. Rev.* **1993**, *93*, 927-942.

27 Gill, D. F.; Shaw, B. L., **1979**, *32*, 19-23.

28 Moers, F. G.; Langhout, J. P., *Rec. Trav. Chim.* **1972**, *91*, 591-600.

29 Dharmasena, U. L.; Foucault, H. M.; dos Santos, E. N.; Fogg, D. E.; Nolan, S. P., *Organometallics* **2005**, *24*, 1056-1058.

30 Lee, H. M.; Smith, D. C.; He, Z.; Stevens, E. D.; Yi, C. S.; Nolan, S. P., *Organometallics* **2001**, *20*, 794-797.

31 Yi, C. S.; Lee, D. W.; Chen, Y., *Organometallics* **1999**, *18*, 2043-2045.

32 Esteruelas, M. A.; Werner, H., *J. Organomet. Chem.* **1986**, *303*, 221-231.

33 Huang, D.; Streib, W.; Bollinger, J. C.; Caulton, K. G.; Winter, R. F.; Scheiring, T., *J. Am. Chem. Soc.* **1999**, *121*, 8087-8097.

34 Denk, M. K.; Rodezno, J. M.; Gupta, S.; Lough, A. J., *J. Organomet. Chem.* **2001**, *617*, 242-253.

35 Reade, S., *Unpublished Data*.

36 **7A** is significantly more soluble in hexanes than **6A**, helping to explain the lower yield.

37 Produced via the same method as SIPr.C_6F_5-H

38 Chantler, V. L.; Chatwin, S. L.; Jazzar, R. F. R.; Mahon, M. F.; Saker, O.; Whittlesey, M. K., *Dalton Trans.* **2008**, 2603-2614.

39 Marks, T. J.; Kolb, J. R., *Chem. Rev.* **1977**, *77*, 263-293.

40 Lee, H. M.; Yang, C.; Jia, G., *J. Organomet. Chem.* **2000**, *601*, 330-334.

41 Werner, H.; Esteruelas, M. A.; Meyer, U.; Wrackmeyer, B., *Chem. Ber.* **1987**, *120*, 11-15.

42 Esteruelas, M. A.; Sola, E.; Oro, L. A., *J. Mol. Catal.* **1988**, *45*, 1-5.

43 Esteruelas, M. A.; Valero, C.; Oro, L. A.; Meyer, U.; Werner, H., *Inorg. Chem.* **1991**, *30*, 1159-1160.

44 Burling, S.; Whittlesey, M. K.; Williams, J. M. J., *Adv. Synth. Catal.* **2005**, *347*, 591-594.

45 Burling, S.; Paine, B. M.; Nama, D.; Brown, V. S.; Mahon, M. F.; Prior, T. J.; Pregosin, P. S.; Whittlesey, M. K.; Williams, J. M. J., *J. Am. Chem. Soc.* **2007**, *129*, 1987-1995.

46 Edwards, M. G.; Jazzar, R. F. R.; Paine, B. M.; Shermer, D. J.; Whittlesey, M. K.; Williams, J. M. J.; Edney, D. D., *Chem. Commun.* **2004**, 90-91.

47 Burling, S.; Mahon, M. F.; Paine, B. M.; Whittlesey, M. K.; Williams, J. M. J., *Organometallics* **2004**, *23*, 4537-4539.

48 Yi, C. S.; Lee, D. W., *Organometallics* **1999**, *18*, 5152-5156.

49 Yi, C. S.; Yun, S. Y., *Organometallics* **2004**, *23*, 5392-5395.

50 *N-Heterocyclic Carbenes in Synthesis*. Nolan, S. P., Wiley-VCH, Weinheim, Germany; **2006**.

51 *N-Heterocyclic Carbenes in Transition Metal Catalysis*. Glorius, F., Springer-Verlag Berlin, Heidelberg, Germany; **2007**.

52 Sanchez, R. P.; Connell, B. T., *Organometallics* **2008**, *27*, 2902-2904.

53 Jazzar, R. F. R.; Macgregor, S. A.; Mahon, M. F.; Richards, S. P.; Whittlesey, M. K., *J. Am. Chem. Soc.* **2002**, *124*, 4944-4945.

54 Poulton, J. T.; Sigalas, M. P.; Folting, K.; Streib, W. E.; Eisenstein, O.; Caulton, K. G., *Inorg. Chem.* **1994**, *33*, 1476-1485.

55 Poulton, J. T.; Folting, K.; Streib, W. E.; Caulton, K. G., *Inorg. Chem.* **1992**, *31*, 3190-3191.

56 Sun, Y.; Taylor, J.; Carty, A. J., *Inorg. Chem.* **1993**, *32*, 4457-4459.

57 Chatwin, S. L., *Unpublished Data* **2005**.

58 Boniface, S. M.; Clark, G. R.; Collins, T. J.; Roper, W. R., *J. Organomet. Chem.* **1981**, *206*, 109-117.

59 Crabtree, R. H., *The Organometallic Chemistry of the Transition Metals*. Wiley-Interscience, Hoboken, New Jersey; **2005**.

60 Lindner, E.; Pautz, S.; Fawzi, R.; Steimann, *Organometallics* **1998**, *17*, 3006-3014.

61 Stahl, S.; Werner, H., *Organometallics* **1990**, *9*, 1876-1881.

62 Werner, R.; Werner, H., *Chem. Ber.* **1982**, *117*, 3781-3795.

63 Green, M. L. H.; Joyner, D. S.; Wallis, J. M., *Dalton Trans.* **1987**, 2823-2830.

64 Prasad, K. T.; Therrien, B.; Rao, K. M., *J. Organomet. Chem.* **2008**, *693*, 3049-3056.

65 Poyatos, M.; McNamara, W.; Incarvito, C.; Clot, E.; Peris, E.; Crabtree, R. H., *Organometallics* **2008**, *27*, 2128-2136.

66 Arnold, P. L.; Scarisbrick, A. C., *Organometallics* **2004**, *23*, 2519-2521.

67 Horvath, H.; Laurenczy, G.; Katho, A., *J. Organomet. Chem.* **2004**, *689*, 1036-1045.

68 Prades, A.; Viciano, M.; Sanau, M.; Peris, E., *Organometallics* **2008**, *27*, 4254-4259.

69 Poyatos, M.; Maisse-Francois, A.; Bellemin-Laponnaz, S.; Peris, E.; Gade, L. H., *J. Organomet. Chem.* **2006**, *691*, 2713-2720.

70 Chaplin, A. B.; Dyson, P. J., *Organometallics* **2007**, *26*, 2447-2455.

71 Muetterties, E. L.; Bleeke, J. R.; Wucherer, E. J.; Albright, T. A., *Chem. Rev.* **1982**, *82*, 499-525.

72 Patel, B. P.; Crabtree, R. H., *J. Am. Chem. Soc.* **1996**, *118*, 13105-13106.

73 Hong, S. H.; Day, M. W.; Grubbs, R. H., *J. Am. Chem. Soc.* **2004**, *126*, 7414-7415.

Chapter 4

Experimental

4.1 General Procedures

All manipulations were carried out using standard Schlenk, high vacuum and glovebox techniques under an atmosphere of argon. Solvents (HPLC grade, Fisher Scientific) were purified using an MBraun SPS solvent system (CH_2Cl_2, diethyl ether), Innovative Technologies PS-400-7 solvent system (THF, hexane, $CHCl_3$, methanol), or by refluxing over sodium benzophenone ketyl (toluene, benzene) or Mg/I_2 (ethanol). Pyridine (both C_5H_5N and C_5D_5N) was degassed with argon and dried over molecular sieves (4 Å). Deuterated solvents (Fluorochem) were vacuum transferred from potassium (C_6D_6, d_8-toluene, d_8-THF) or CaH_2 (CD_2Cl_2, $CDCl_3$). d_6-DMSO (Aldrich) was used as received.

Solution NMR spectra were recorded on Bruker Avance 300, 400 and 500 MHz NMR spectrometers at 298 K unless stated otherwise and referenced (^1H; $^{13}C\{^1H\}$) as follows: benzene (δ 7.15; δ 128.0), $CHCl_3$ (δ 7.26; δ 77.4), CH_2Cl_2 (δ 5.32; δ 53.7), DMSO (δ 2.50; δ 39.5) pyridine (δ 8.72; δ 123.5), THF (δ 3.58; δ 67.2), toluene (δ 2.09; δ 21.3). $^{31}P\{^1H\}$, $^{19}F\{^1H\}$ and $^{11}B\{^1H\}$ NMR chemical shifts were referenced externally to 85% H_3PO_4, $CFCl_3$ and $BF_3{\cdot}OEt_2$ respectively (δ 0.0). ^1H-$^{13}C\{^1H\}$ HMQC/HMBC and ^1H COSY/NOESY experiments were performed using standard Bruker pulse sequences.

Solid-state NMR spectra were recorded in Durham under nitrogen on a Varian VNMRS 400 MHz spectrometer (6.0 mm MAS probe) at 303 and 206 K (actual sample temperatures). Temperature calibration was carried out using MeOH, and then lead nitrate at sample spin rates appropriate to the measurements reported here. Chemical shifts were referenced to TMS (^{13}C) by setting the high-frequency signal for adamantane to 38.4 ppm and to nitromethane (^{15}N) by setting the nitrate signal from solid ammonium nitrate to -5.1 ppm.

IR spectra were recorded as nujol mulls (unless otherwise stated) on a Nicolet Nexus FTIR spectrometer. Elemental analyses were performed by Elemental Microanalysis Ltd, Okehampton, Devon, UK. Mass spectra were recorded using a micrOTOF electrospray time-of-flight (ESI-TOF) mass spectrometer (Bruker Daltonik GmbH) coupled to an Agilent 1200 LC system (Agilent Technologies). X-ray crystallography was performed on a Nonius Kappa CCD diffractometer using Mo(Kα) radiation (λ = 0.71073 Å). Structural

work and calculations were solved by use of SHELXS-97[1], refined using full-matrix least squares SHELXL-97[1] and represented as POVray structures.

4.2 Preparation of N-aryl NHCs

The experimental section below shows processes for the generation of the 2,6-diisopropylphenyl variety of aryl substituent, although ratios and methods are identical to those used for the 2,4,6-trimethylphenyl variety, except where stated. NMR characterisation data can be found for both species at the end of each method along with data for the non-aryl 1-adamantyl species which was prepared in the same fashion.

4.2.1 Preparation of N,N'-*bis*(2,6-diisopropylphenyl)diazabutadiene[2]

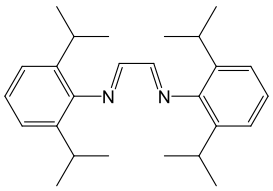

A 1 L round bottomed flask was charged with 2,6-diisopropylaniline (53 mL, 0.28 mol), glyoxal (16 mL, 0.14 mol, 40% aqueous solution), degassed but undried ethanol (250 mL), and a few drops of formic acid catalyst. The solution was stirred at room temperature for two days affording a bright yellow precipitate which was filtered in air over a glass sinter, washed with cold methanol (3 x 50 mL) and dried in air. Yield 39.4 g (75%); ^{1}H NMR ($CDCl_3$, 300 MHz): δ 8.28 (s, 2H, NC*H*), 7.34-7.15 (m, 4H, aryl-C*H*), 3.22 (sept, J_{HH} = 6.90 Hz, 4H, C*H*Me$_2$), 1.27 (d, J_{HH} = 6.90 Hz, 24H, CH*Me*$_2$). ^{13}C{^{1}H} NMR ($CDCl_3$, 75 MHz): δ 163.2 (s, N*C*H), 148.0 (s, *o-C*), 136.8 (s, *i-C*), 125.3 (s, *p-C*H), 123.3 (s, *m-C*H), 28.1 (s, *C*HMe$_2$), 22.5 (s, CH*Me*$_2$). Data for *bis*(2,4,6-trimethylphenyl)diazabutadiene; ^{1}H NMR ($CDCl_3$, 300 MHz): δ 8.10 (s, 2H, NC*H*), 6.92 (s, 4H, aryl-C*H*), 2.30 (s, 6H, *p-Me*), 2.16 (s, 12H, *o-Me*). ^{13}C{^{1}H} NMR ($CDCl_3$, 75 MHz): δ 163.5 (s, N*C*H), 147.5 (s, *o-C*), 134.3 (s, *i-C*), 128.6 (s, *m-C*H), 126.6 (s, *p-C*), 20.8 (s, *p-Me*), 18.3 (s, *o-Me*). Data for *bis*(1-adamantyl)diazabutadiene; ^{1}H NMR ($CDCl_3$, 500 MHz): δ 7.92 (s, 2H, NC*H*), 2.14 (s, 6H, N-Ad), 1.74 (s, 15H, N-Ad), 1.72 (s, 3H, N-Ad), 1.67 (s, 3H, N-Ad), 1.65 (s, 3H, N-Ad).

4.2.2 Preparation of N,N'-*bis*(2,6-diisopropylphenyl)aminoethane[3]

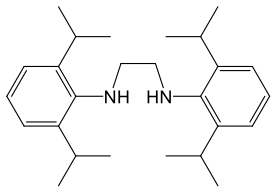

A large Schlenk tube was charged with *bis*(2,6-diisopropylphenyl)diazabutadiene (5.00 g, 13 mmol) and $NaBH_4$ (5.02 g, 0.13 mol) in a glove box, and stirred at room temperature for 1.5 h in a 40:60 mixture of dry methanol (40 mL) and THF (60 mL), at which point the yellow solution had turned clear. Slow addition of a saturated aqueous solution of NH_4Cl (20 mL) by pipette to quench excess $NaBH_4$ was followed by extraction with diethyl ether (3 x 50 mL) into a separating funnel and washing of the extract with de-ionised water (3 x 100 mL), drying with $MgSO_4$ and concentration *in vacuo*. Yield: 4.2 g (85%). ^{1}H NMR ($CDCl_3$, 300 MHz): δ 7.17-7.07 (m, 6H, aryl-C*H*), 3.39 (sept, J_{HH} = 6.90Hz, 4H, C*H*Me$_2$), 3.19 (s, 4H, NC*H*$_2$), 1.28 (d, J_{HH} = 6.90Hz, 24H, CH*Me*$_2$). ^{13}C{^{1}H} NMR ($CDCl_3$, 75 MHz): δ 143.4 (s, *i*-*C*), 142.5 (s, *o*-*C*), 123.9 (s, *p*-*C*H), 123.7 (s, *m*-*C*H), 52.4 (s, N*C*H$_2$), 27.9 (s, *C*HMe$_2$), 24.4 (s, CH*Me*$_2$). Data for N,N'-*bis*(2,4,6-trimethylphenyl)aminoethane; ^{1}H NMR ($CDCl_3$, 400 MHz): δ 6.83 (s, 4H, aryl-C*H*), 3.15 (s, 4H, NC*H*$_2$), 2.28 (s, 12H, *o*-*Me*), 2.23 (s, 6H, *p*-*Me*). ^{13}C{^{1}H}NMR ($CDCl_3$, 75 MHz): δ 143.4 (s, *o*-*C*), 131.5 (s, *i*-*C*), 129.8 (s, *m*-*C*H), 129.6 (s, *p*-*C*), 49.2 (s, N*C*H$_2$), 20.6 (s, *p*-*Me*), 18.5 (s, *o*-*Me*).

4.2.3 Preparation of 1,3-*bis*(2,6-diisopropylphenyl)-2-(pentafluoro-phenyl)imidazolidene (SIPr.C_6F_5-H)

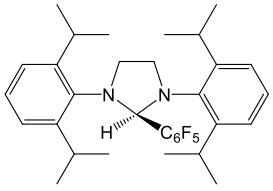

1,3-*bis*(2,6-diisopropylphenyl)-2-(pentafluorophenyl)imidazolidene was prepared by modification of a literature method.[4] A Schlenk tube (not purged) was charged with solid pentafluorobenzaldehyde (4.33 g, 22 mmol), dissolved in the minimum glacial acetic acid (ca. 5 mL) and N,N'-*bis*(2,6-diisopropylphenyl)aminoethane (4.20 g, 11 mmol) was then added. Stirring at room temperature for 1 h was followed by concentration *in vacuo*, washing with cold methanol (3 x 50 mL) and drying to give the white product, which was

stored under argon. Yield: 3.7 g (60%). ^{1}H NMR ($CDCl_3$, 300 MHz): δ 7.22-7.13 (m, 4H, *m*-C*H*), 7.04-7.01 (m, 2H, *p*-C*H*), 6.31 (s, 1H, C_6F_5CH), 3.91-3.87 (m, 2H, NCH_2), 3.69-3.60 (m, 4H, CH_2 + $CHMe_2$), 3.53 (sept, J_{HH} = 9.00 Hz, 2H, $CHMe_2$), 1.41 (d, J_{HH} = 9.00 Hz, 6H, $CHMe_2$), 1.29 (d, J_{HH} = 9.00 Hz, 6H, $CHMe_2$), 1.17 (d, J_{HH} = 9.00 Hz, 6H, $CHMe_2$), 0.79 (d, J_{HH} = 9.00 Hz, 6H, $CHMe_2$). ^{19}F NMR ($CDCl_3$, 376 MHz): δ -135.9 (m, 1F), -148.0 (m, 1F), -156.1, (m, 1F) -161.8 (m, 1F), -163.9 (m, 1F). Data for 1,3-*bis*(2,4,6-trimethylphenyl)-2-(pentafluorophenyl)imidazolidene (SIMes.C_6F_5-H); ^{1}H NMR ($CDCl_3$, 300 MHz): δ 6.80 (s, 4H, meta-C*H*), 6.37 (s, 1H, C_6F_5CH), 3.93-3.89 (m, 2H, NCH_2), 3.57-3.52 (m, 2H, NCH_2), 2.31 (br s, 12H, *o-Me*), 2.21 (s, 6H, *p-Me*). ^{19}F NMR ($CDCl_3$, 376 MHz): δ -136.3 (m, 1F), -148.6 (m, 1F), -155.8 (m, 1F), -163.1 (m, 2F).

4.2.4 Preparation of 1,3-*bis*(2,6-diisopropylphenyl)imidazolium chloride[2]

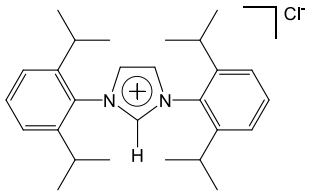

To a solution of *bis*(2,6-diisopropylphenyl)diazabutadiene (25.0 g, 66 mmol) in toluene (500 mL) was added paraformaldehyde (2.0 g, 66 mmol), followed by heating of the mixture to 100 ˚C to dissolve most of the paraformaldehyde. The mixture was then allowed to cool to 40 ˚C, where HCl (16.5 mL, 66 mmol, 4M in dioxane) was added via syringe and the solution heated to 70 ˚C for 5 h. Stirring continued for 36 h at room temperature to leave the reaction mixture dark red/brown in colour and filtration in air then washing with THF (3 x 50 mL) afforded an off-white solid. Yield: 12.7 g (45%). ^{1}H NMR ($CDCl_3$, 400 MHz): δ 10.07 (s, 1H, NC(*H*)N), 8.11 (s, 2H, NC*H*), 7.57 (m, 4H, *m*-C*H*), 7.23 (m, 2H *p*-C*H*), 2.44 (sept, J_{HH} = 6.80 Hz, 4H, $CHMe_2$), 1.27 (d, J_{HH} = 6.80 Hz, 12H, $CHMe_2$), 1.23 (d, J_{HH} = 6.80 Hz, 12H, $CHMe_2$). ^{13}C{^{1}H} NMR (d_6-DMSO, 75 MHz): δ 144.8 (s, *o-C*), 139.4 (s, N*C*(H)N), 131.8 (s, *p-C*H), 130.1 (s, *i-C*), 126.2 (s, NCH), 124.6 (s, *m-C*H), 28.6 (s, $CHMe_2$), 24.2 (s, $CHMe_2$), 23.1 (s, $CHMe_2$). Data for 1,3-*bis*(2,4,6-trimethylphenyl)imidazolium chloride; ^{1}H NMR ($CDCl_3$, 400 MHz): δ 10.60 (s, 1H, NC(*H*)N), 7.65 (s, 2H, NC*H*), 6.98 (s, 4H, *m*-C*H*), 2.30 (s, 6H, *p-Me*), 2.09 (s, 12H, *o-Me*). Data for 1,3-*bis*(1-adamantyl)imidazolium chloride; ^{1}H NMR ($CDCl_3$, 500 MHz):

δ 10.10 (s, 1H, NC(*H*)N), 7.54 (s, 2H, NC*H*), 2.28 (s, 18H, N-Ad), 2.09 (s, 6H, N-Ad), 1.78 (s, 3H, N-Ad), 1.65 (s, 3H, N-Ad).

4.2.5 Preparation of 1,3-*bis*(2,6-diisopropylphenyl)imidazol-2-ylidene (IPr)^2

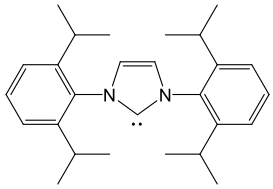

1,3-*bis*(2,6-diisopropylphenyl)imidazolium chloride (6.50 g, 15 mmol) and KO^{t}Bu (1.78 g, 18 mmol) were added to a Schlenk tube, to which THF (40 mL) was added at ambient temperature. The mixture was stirred for 4 h resulting in a brown solution with pale precipitate. Volatiles were removed *in vacuo* to leave a brown residue which was extracted in toluene (100 mL), filtered through celite and concentrated under vacuum to give an off-white solid. Yield: 5.4 g (92%). ^{1}H NMR (C_6D_6, 400 MHz): δ 7.24 (t, J_{HH} = 7.60 Hz, 2H, *p*-C*H*), 7.12 (d, J_{HH} = 6.80 Hz, 4H, *m*-C*H*), 6.57 (s, 2H, NC*H*), 2.92 (sept, J_{HH} = 6.80 Hz, 4H, C*H*Me$_2$), 1.24 (d, J_{HH} = 6.80 Hz, 12H, CH*Me*$_2$), 1.14 (d, J_{HH} = 6.80 Hz, 12H, CH*Me*$_2$). ^{13}C{^{1}H} NMR (C_6D_6, 75 MHz): δ 220.6 (s, N*C*N), 146.3 (s, *o*-*C*), 139.0 (s, *i*-*C*), 129.0 (s, *p*-*C*H), 123.7 (s, *m*-*C*H), 121.6 (s, N*C*H), 28.8 (s, *C*HMe$_2$), 24.8 (s, CH*Me*$_2$), 23.6 (s, CH*Me*$_2$).

4.2.6 Preparation of 1,3-*bis*(2,4,6-trimethylphenyl)imidazol-2-ylidene (IMes)^2

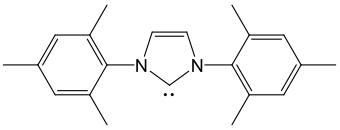

1,3-*bis*(2,4,6-trimethylphenyl)imidazolium chloride (3.80 g, 11 mmol) and KO^{t}Bu (1.40 g, 12 mmol) were added with a stirrer bar to a Schlenk tube, which was then dried overnight *in vacuo*. THF (40 mL) was added at -78 ˚C (dry ice/acetone), and the mixture stirred vigorously for 20 min after which it was allowed to warm to room temperature over 30 min. Volatiles were then removed by vacuum to leave a brown residue which was extensively dried and the product was extracted in toluene (20 mL), filtered through celite and concentrated under vacuum. Washing with hexane (4 x 50 mL) and recrystallisation of

the washings at -20 ˚C gave light brown solid. Yield: 2.1 g (71%). ^{1}H NMR (C_6D_6, 400 MHz): δ 6.80 (s, 4H, aryl-C*H*), 6.47 (s, 2H, NC*H*), 2.15 (s, 18H, aryl-*Me*).

4.2.7 Preparation of 1,3-*bis*(2,6-diisopropylphenyl)imidazolinium chloride[5]

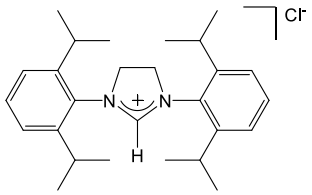

Triethyl orthoformate (25 mL) was distilled to remove water and added to a dried and degassed three-necked round bottom flask containing N,N'-*bis*(2,6-diisopropylphenyl)aminoethane dihydrochloride (900 mg, 2 mmol) via canula. Two drops of formic acid (96%) were added and the mixture was refluxed for 48 h. Upon cooling to room temperature, a white solid precipitated which was filtered in air and washed with diethyl ether (3 x 10 mL). Yield: 310 mg (34%). ^{1}H NMR (d_6-DMSO, 300 MHz): δ 9.49 (s, 1H, NC(*H*)N), 7.55 (t, J_{HH} = 7.50 Hz, 2H, *p*-C*H*), 7.42 (d, J_{HH} = 7.50 Hz, 4H, *m*-C*H*), 4.53 (s, 4H, NCH_2), 3.07 (sept, J_{HH} = 6.80 Hz, 4H, C*H*Me$_2$), 1.34 (d, J_{HH} = 6.80 Hz, 12H, CH*Me*$_2$), 1.19 (d, J_{HH} = 6.80 Hz, 12H, CH*Me*$_2$). ^{13}C{^{1}H} NMR (d_6-DMSO, 75 MHz): δ 160.1 (s, N*C*(H)N), 146.1 (s, *i-C*), 131.0 (s, *p-C*H), 129.9 (s, *o-C*), 124.8 (s, *m-C*H), 53.7 (s, NCH$_2$), 28.2 (s, *C*HMe$_2$), 24.9 (s, CH*Me*$_2$), 23.3 (s, CH*Me*$_2$). Data for 1,3-*bis*(2,4,6-trimethylphenyl)imidazolinium chloride; ^{1}H NMR (d_6-DMSO, 400 MHz): δ 9.13 (s, 1H, NC(*H*)N), 7.09 (s, 4H, *m*-C*H*), 4.47 (s, 4H, NCH_2), 2.36 (s, 12H, *o-Me*), 2.29 (s, 6H, *p-Me*). ^{13}C{^{1}H} NMR (d_6-DMSO, 75 MHz): δ 160.3 (s, N*C*N), 139.6 (s, *i-C*), 135.2 (s, *o-C*), 130.9 (s, *p-C*), 129.4 (s, *m-C*H), 50.9 (s, NCH$_2$), 20.5 (s, *p-Me*), 17.2 (s, *o-Me*).

4.2.8 Preparation of 1,3-*bis*(2,6-diisopropylphenyl)imidazolin-2-ylidene (SIPr)[5]

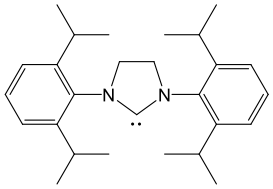

1,3-*bis*(2,6-diisopropylphenyl)imidazolinium chloride (500 mg, 1.08 mmol), potassium hydride (30% in mineral oil, 430 mg, 3.25 mmol) and a crystal of dibenzo-18-crown-6 (< 10 mg) were added to a Schlenk tube equipped with a stirrer bar. THF was added with stirring overnight at room temperature until evolution of H_2 gas had ceased. Celite and filtration apparatus was rigorously and repeatedly flame dried to remove moisture prior to extraction of product in toluene followed by filtration and concentration *in vacuo* to give a light yellow oily solid. Yield: 150 mg (33%). ^{1}H NMR (C_6D_6, 300 MHz): δ 7.13-7.12 (m, 6H, aryl-C*H*), 3.32 (s, 4H, NCH_2), 3.23 (sept, J_{HH} = 6.90 Hz, 4H, C*H*Me$_2$), 1.29 (d, J_{HH} = 6.90 Hz, 12H, CH*Me*$_2$), 1.25 (d, J_{HH} = 6.90 Hz, 12H, CH*Me*$_2$). ^{13}C{^{1}H} NMR (C_6D_6, 75 MHz): δ 244.1 (s, N*C*N), 147.4 (s, *o*-*C*), 139.4 (s, *i*-*C*), 128.4 (s, *p*-*C*H), 124.0 (s, *m*-*C*H), 53.7 (s, NCH$_2$), 29.0 (s, *C*HMe$_2$), 25.5 (s, CH*Me*$_2$), 23.7 (s, CH*Me*$_2$). Data for 1,3-*bis*(2,4,6-trimethylphenyl)imidazolin-2-ylidene; ^{1}H NMR (C_6D_6, 300 MHz): δ 6.57 (s, 4H, aryl-C*H*), 4.00 (s, 4H, NCH_2), 2.00 (s, 6H, *p*-*Me*), 1.93 (s, 12H, *o*-*Me*). ^{13}C{^{1}H} NMR (C_6D_6, 75 MHz): δ 245.2 (s, N*C*N), 138.0 (s, *o*-*C*), 136.6 (s, *i*-*C*), 135.5 (s, *p*-*C*), 129.9 (s, *m*-*C*H), 44.2 (s, N*C*H$_2$), 20.8 (s, *p*-*Me*), 18.3 (s, *o*-*Me*).

4.3 Preparation of N-alkyl NHCs

The section below shows the general preparation of N-alkyl NHCs, firstly with protons and secondly with methyl groups on the backbone C4 and C5 positions. In the first instance the example given is for I^{t}Bu$_2$, although the general method is applicable for I^{i}Pr$_2$ also. In the second case the example reaction is for IEt$_2$Me$_2$, although the method can be used in the cases of IMe$_4$ and I^{i}Pr$_2$Me$_2$. NMR data is described for all relevant NHCs at the end of each method.

4.3.1 Preparation of 1,3-*bis*(*tert*-butyl)imidazolium chloride

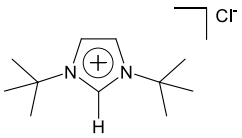

1,3-*bis*(*tert*-butyl)imidazolium chloride was prepared by modification of a literature method.[6] Dry toluene (100 mL) was added to a three-necked 500 mL round-bottomed flask under argon, to which *t*-butylamine (10.51 mL, 100 mmol) was added via syringe. Cooling of the mixture in an ice bath with rigorous stirring facilitated the slow addition of paraformaldehyde (3 g, 100 mmol), and the solution was then allowed to warm to room

temperature with continued stirring over 30 min. Cooling again in an ice bath preceded the addition of another portion of *t*-butylamine (10.51 mL, 100 mmol), followed by 10 min of stirring and then slow addition of HCl (25 mL, 4M in dioxane). The mixture was allowed to warm once again to room temperature where glyoxal (14.5 mL, 100 mmol, 40% w/v in water) was added in three portions and the mixture was stirred for 40 h at 37 ˚C under argon, but with partial vacuum to keep stoppers in place. After cooling to room temperature, a saturated solution of Na_2CO_3 and diethyl ether (100 mL) were added to the solution and the aqueous layer washed with diethyl ether (3 x 100 mL) in air. Note that if a third phase exists between the organic and aqueous layers it should be kept with the organic phase. Due to the hydroscopic nature of the product, the following stages are carried out under inert conditions including concentration of the organic layer *in vacuo*, extraction of the product in (dry) dichloromethane (3 x 50 mL), drying over $MgSO_4$ and filtration. Removal of solvent and drying overnight under reduced pressure gave the product as a pale brown solid. Yield: 13.0 g (60%). (An important note is that the success of this reaction is highly dependent on the quality/age of the acid). ^{1}H NMR ($CDCl_3$, 500 MHz): δ 10.12 (s, 1H, NC(*H*)N), 7.51 (s, 2H, NC*H*), 1.50 (s, 18H, *t-Bu*). $^{13}C\{^1H\}$ NMR ($CDCl_3$, 126 MHz): δ 134.2 (s, N*C*(H)N), 119.7 (s, N*C*H), 60.4 (s, *C*Me$_3$), 30.0 (s, C*Me*$_3$). Data for 1,3-*bis*(isopropyl)imidazolium chloride; ^{1}H NMR ($CDCl_3$, 500 MHz): δ 10.69 (s, 1H, NC(*H*)N), 7.54 (s, 2H, NC*H*), 4.80 (sept, J_{HH} = 7.00 Hz, 2H, C*H*Me$_2$), 1.46 (d, J_{HH} = 7.00 Hz, 12H, CH*Me*$_2$).

4.3.2 Preparation of 1,3-*bis*(*tert*-butyl)imidazol-2-ylidene (I^{t}Bu$_2$)

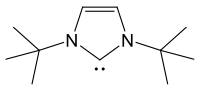

1,3-*bis*(*tert*-butyl)imidazol-2-ylidene was prepared by modification of a literature method.[6] KO^{t}Bu (1.84 g, 16.4 mmol) and 1,3-*bis*(*tert*-butyl)imidazolium chloride (2.96 g, 13.7 mmol) were dried overnight *in vacuo* in a Schlenk tube equipped with a stirrer bar. THF (20 mL) was added at -78 ˚C and the mixture stirred for 1 h after which it was allowed to warm to room temperature with stirring over then next 2 h. Volatiles were then removed to leave a light yellow residue and the product was extracted in toluene (20 mL), filtered through Celite (with an additional 100 mL toluene) and concentrated under vacuum to give a white solid. Yield: 2.01 g (82%). ^{1}H NMR (C_6D_6, 500 MHz): δ 6.78 (s, 2H, NC*H*), 1.49 (s, 18H, *t-Bu*). $^{13}C\{^1H\}$ NMR (C_6D_6, 126 MHz): δ 213.4 (s, N*C*N), 115.7 (s, N*C*H), 56.4

(s, *C*Me$_3$), 32.1 (s, C*Me*$_3$). Data for 1,3-*bis*(isopropyl)imidazol-2-ylidene; ^{1}H NMR (d_8-THF, 300 MHz): δ 6.92 (s, 2H, NC*H*), 4.40 (sept, J_{HH} = 6.75 Hz, 2H, C*H*Me$_2$), 1.38 (d, J_{HH} = 6.75 Hz, 12H, CH*Me*$_2$). I^{i}Pr$_2$ note: Product is a yellow oil at room temperature, so after Celite filtration the compound was transferred to a pre-weighed ampoule for storage and accurate yield determination.

4.3.3 Preparation of 1,3-*bis*(1-adamantyl)imidazol-2-ylidene (IAd$_2$)

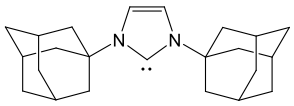

1,3-*bis*(1-adamantyl)imidazol-2-ylidene was prepared by modification of a literature method.[7] 1,3-*bis*(1-adamantyl)imidazolium chloride (500 mg, 1.3 mmol) and potassium *bis*-trimethylsilylamide (670 mg, 3.4 mmol) were dried overnight *in vacuo* in a Schlenk tube with a stirrer bar. THF (10 mL) was added at -78 ˚C (dry ice/acetone) and the mixture stirred for 1 h after which it was allowed to warm to room temperature with stirring over then next 2 h. Volatiles were then removed by vacuum to leave a pale residue and the product was extracted in toluene (10 mL), filtered through celite and concentrated under vacuum to give a white solid. Yield: 160 mg (36%). ^{1}H NMR (C_6D_6, 500 MHz): δ 6.89 (s, 2H, NC*H*), 2.28 (d, J_{HH} = 2.00 Hz, 12H, N-Ad), 2.00 (s, 6H, N-Ad), 1.61-1.54 (m, 12H, N-Ad).

4.3.4 Preparation of 1,3-diethyl-4,5-dimethyl-imidazol-2(3H)-thione

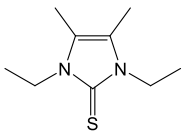

1,3-diethyl-4,5-dimethyl-imidazol-2(3H)-thione was prepared by modification of a literature method.[8] A 1 L 3-necked round-bottomed flask was charged with 3-hydroxy-2-butanone (8.8 g, 100 mmol) and very briefly (due to the volatility of the butanone) purged three times with argon. To this was added dry 1-hexanol (250 mL) and 1,3-diethyl-2-thiourea (13.21 g, 100 mL) and the mixture refluxed for 18 h. The crude reaction mixture was reduced *in vacuo* and washed with water (2 x 50 mL) and diethyl ether (3 x 50 mL). Yield: 9.1 g (49%). ^{1}H NMR ($CDCl_3$, 400 MHz): δ 4.06 (q, J_{HH} = 7.20 Hz, 4H, C*H*$_2$CH$_3$), 2.07 (s, 6H, NC*Me*), 1.24 (t, J_{HH} = 7.20 Hz, 6H, CH$_2$C*H*$_3$). ^{13}C{^{1}H} NMR ($CDCl_3$, 75 MHz): δ 159.5 (s, *C*=S), 120.9 (s, N*C*Me), 40.4 (s, *C*H$_2$CH$_3$),

14.5 (s, CH_2CH_3), 9.5 (s, NC*Me*). Data for 1,3-diisopropyl-4,5-dimethyl-imidazol-2(3H)-thione; ^{1}H NMR ($CDCl_3$, 500 MHz): δ 5.45 (br s, 2H, C*H*Me$_2$), 2.00 (s, 6H, NC*Me*), 1.24 (br s, 12H, CH*Me*$_2$).

4.3.5 Preparation of 1,3-diethyl-4,5-dimethyl-imidazol-2-ylidene (IEt_2Me_2)

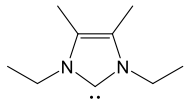

1,3-diethyl-4,5-dimethyl-imidazol-2-ylidene was prepared by modification of a literature method.[8] A 250 mL 3-necked round-bottomed flask was charged with 1,3-diethyl-4,5-dimethyl-imidazol-2(3H)-thione (1.84 g, 10 mmol) and was meticulously purged 3 times with argon. Addition of THF (60 mL) and potassium (1 g, 25.6 mmol) (cut into no more than 6 pieces to increase speed of the filtration stage) preceded refluxing of the mixture for 4 h to give a light blue solution. Upon cooling, the product was separated via filtration through a Teflon canula with a glass-paper filter and concentrated *in vacuo* to give an off-white solid. Yield: 1.15 g (76%). ^{1}H NMR (C_6D_6, 500 MHz): δ 3.78 (q, J_{HH} = 7.00 Hz, 4H, C*H*$_2$CH$_3$), 1.69 (s, 6H, NC*Me*), 1.20 (t, J_{HH} = 7.00 Hz, 6H, CH$_2$C*H*$_3$). ^{13}C{^{1}H} NMR (C_6D_6, 126 MHz): δ 212.1 (s, N*C*N), 122.6 (s, N*C*Me), 43.7 (s, *C*H$_2$CH$_3$), 18.0 (s, CH$_2$*C*H$_3$), 9.5 (s, NC*Me*). Data for 1,3-diisopropyl-4,5-dimethyl-imidazol-2-ylidene; ^{1}H NMR (C_6D_6, 300 MHz): δ 3.94 (sept, J_{HH} = 7.20 Hz, 2H, C*H*Me$_2$), 1.72 (s, 6H, NC*Me*), 1.50 (d, J_{HH} = 7.20 Hz, 12H, CH*Me*$_2$).

4.4 Preparation of metal precursors

4.4.1 Preparation of $Ru(AsPh_3)_3(CO)Cl_2$

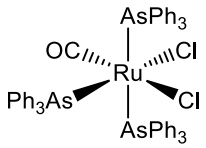

$Ru(AsPh_3)_3(CO)Cl_2$ was prepared using a reported literature method,[9] with slight deviations. A 1 L three-necked round bottomed flask was charged with triphenylarsine (11.81 g, 39 mmol) and flushed three times with argon. 2-methoxyethanol (350 mL) was degassed separately in a 500 mL round bottomed flask and was then added to the 1 L flask, which was then heated and stirred until reflux. Meanwhile, a Schlenk tube containing

rigorously stirred hydrated ruthenium trichloride (2.40 g, 9.2 mmol) in 2-methoxyethanol (50 mL) and a 250 mL round bottomed flask containing formaldehyde (37% w/v solution in water, 180 mL) were both degassed for ca. 15 min. The ruthenium solution then added to the 1 L flask, followed quickly by the formaldehyde, and the solution was left to reflux for 2 h to give a pale orange solution. The solution was then allowed to cool first to room temperature and then to ca. 5 ˚C for 2 h followed by filtering in air and washing with ethanol (3 x 100 mL) and hexane (2 x 100 mL). The compound was dried under vacuum to afford a yellow crystalline solid. Yield: 8.20 g (80%). IR (cm^{-1}): 1938 (ν_{CO}).

4.4.2 Preparation of $Ru(AsPh_3)_3(CO)H_2$

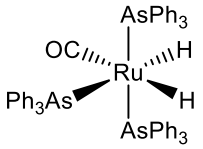

$Ru(AsPh_3)_3(CO)H_2$ was prepared using a reported literature method,[9] with slight deviations. A 1 L three-necked round bottomed flask was flame dried under reduced pressure and flushed with argon. $Ru(AsPh_3)_3(CO)Cl_2$ (8.24 g, 7.4 mmol), $NaBH_4$ (15.60 g, 410 mmol) and dry ethanol (300 mL) were added, followed by reflux for 1.5 h after which the resulting tan slurry was filtered in air and washed with ethanol (3 x 100 mL). To the residue was then added toluene (400 mL) to extract the product through the filter into a 1 L round bottomed flask which was then pumped to dryness. Minimal toluene (ca. 25 mL) was then used to transfer product into a dried and degassed Schlenk tube via pipette, which was reduced *in vacuo* and to which dry ethanol (50 mL) was then added. Stirring took place overnight and the solvent and dissolved impurities were removed via filter cannula and the compound dried under vacuum to give a tan coloured solid. Yield: 5.70 g (74%). ^1H NMR (C_6D_6, 400 MHz): δ -6.61 (d, J_{HH} = 6.80 Hz, 1H, Ru-*H*), -10.11 (d, J_{HH} = 6.80 Hz, 1H, Ru-*H*). IR (cm^{-1}): 1925 (ν_{CO}).

4.4.3 Preparation of $Ru(PPh_3)_2(CO)_3$

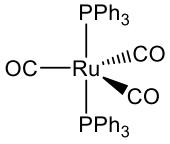

$Ru(PPh_3)_2(CO)_3$ was prepared using a reported literature method,[10] with slight deviations. A 500 mL three-necked round bottomed flask was charged with triphenylphosphine

(4.74 g, 18 mmol) and flushed three times with argon. Degassed 2-methoxyethanol (60 mL) was then added and the mixture refluxed until all triphenylphosphine had dissolved. In the meantime, rigorously stirred hydrated ruthenium trichloride (0.78 g, 3 mmol) in 2-methoxyethanol (60 mL), formaldehyde (37% w/v solution in water, 60 mL) and KOH (1.20 g, 20 mmol) in 2-methoxyethanol (60 mL) were separately degassed in either Schlenk tubes or round bottomed flasks. [Note: KOH was warmed with a heat-gun to aid solvation]. Once refluxing, the three solutions were quickly added to the main 500 mL flask in the order $RuCl_3$, formaldehyde then KOH with refluxing continued for 2 h. Cooling to room temperature and then to 5 ˚C for 2 h gave a fine yellow solid which was washed via filter canula with degassed ethanol (20 mL), water (20 mL) then hexane (20 mL) and dried *in vacuo* to give product. Yield 1.42 g (67%). $^{31}P\{^1H\}$ NMR (d_8-THF, 122 MHz): δ 54.7. IR (cm^{-1}): 1903, 1895 (ν_{CO}).

4.5 Synthesis of tri-ruthenium/osmium NHC complexes

$Ru_3(CO)_{12}$ and $Os_3(CO)_{12}$ were purchased from Aldrich and used as received.

4.5.1 Synthesis of $Ru_3(al^tBu_2)(CO)_{11}$ (1A)

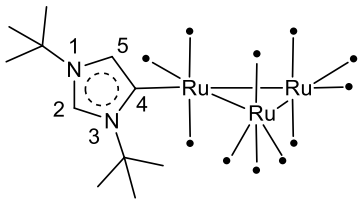

$Ru_3(CO)_{12}$ (532 mg, 0.83 mmol) and I^tBu_2 (150 mg, 0.83 mmol) were added to an ampoule fitted with a J. Youngs PTFE tap in a glove box. THF (5 mL) was then added which facilitated immediate bubbling of the solution. After 2 h, the solvent was removed *in vacuo* and the complex extracted in toluene (3 x 5 mL). Upon removal of the solvent, the product was washed with hexane (3 x 10 mL) to leave an orange-red powder (534 mg, 81%). X-ray quality crystals of **1** were grown from either THF/hexane or $CHCl_3$/hexane. ^1H NMR (d_8-THF, 500 MHz): δ 8.42 (d, J_{HH} = 1.50 Hz, 1H, (C2)*H*), 6.43 (d, J_{HH} = 1.50 Hz, 1H, (C5)*H*), 1.86 (s, 9H, N(3)*t-Bu*), 1.54 (s, 9H, N(1)*t-Bu*). $^{13}C\{^1H\}$ NMR (d_8-THF, 126 MHz): δ 208.0 (s, *C*O), 134.1 (s, Ru-*C*4), 132.5 (s, (*C*2)H), 130.5 (s, (*C*5)H), 60.4 (s, N(3)*C*Me$_3$), 58.1 (s, N(1)*C*Me$_3$), 30.4 (s, N(3)C*Me$_3$*), 29.4 (s, N(1)C*Me$_3$*). IR (KBr, cm^{-1}): 2085, 2034, 2013, 1996, 1984, 1977, 1962, 1943 (ν_{CO}). Anal. calcd for $C_{22}H_{20}N_2O_{11}Ru_3$,%: C, 33.38; H, 2.55; N, 3.54. Found,%: C, 33.51; H, 2.48; N, 3.51.

4.5.2 Synthesis of $Ru_3(alAd_2)(CO)_{11}$ (2A)

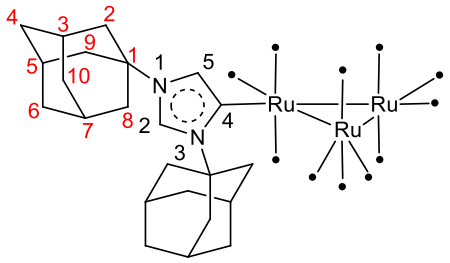

An ampoule fitted with a J. Youngs PTFE tap was charged with $Ru_3(CO)_{12}$ (190 mg, 0.30 mmol) and IAd_2 (100 mg, 0.30 mmol) in a glove box. THF (5 mL) was then added which gave rise to immediate bubbling of the solution. After 2 h, the solvent was removed *in vacuo* and the complex extracted in toluene (5 x 5 mL). Upon removal of the solvent, the product was washed with hexane (3 x 5 mL) to leave an orange-red powder (190 mg, 68%). X-ray quality crystals of **1** were grown from THF/hexane. ^{1}H NMR (d_8-THF, 500 MHz): δ 8.38 (d, J_{HH} = 2.00 Hz, 1H, (C2)*H*), 6.47 (d, J_{HH} = 2.00 Hz, 1H, (C5)*H*), 2.51 (d, J_{HH} = 2.50 Hz, 6H, (N3)$Ad_{2,8,9}$ CH_2), 2.30 (s, 3H, $Ad_{3,5,7}$ C*H*), 2.20 (s, 3H, $Ad_{3,5,7}$ C*H*), 2.07 (d, J_{HH} = 2.50 Hz, 6H, (N1)$Ad_{2,8,9}$ CH_2), 1.95 (s, 1H, $Ad_{4,6,10}$), 1.92 (s, 2H, $Ad_{4,6,10}$), 1.81-1.75 (m, 9H, $Ad_{4,6,10}$). ^{13}C{^{1}H} NMR (d_8-THF, 126 MHz): δ 207.9 (s, *C*O), 132.2 (s, Ru-*C*4), 131.7 (s, (*C*2)H), 129.5 (s, (*C*5)H), 61.6 (s, (N3)AdC_1), 58.3 (s, (N1)AdC_1), 43.1 (s, (N1)Ad$C_{2,8,9}$), 42.5 (s, (N3)Ad$C_{2,8,9}$), 36.3 (s, (N1)Ad$C_{4,6,10}$), 36.1 (s, (N3)Ad$C_{4,6,10}$), 30.9 (s, (N1)Ad$C_{3,5,7}$), 30.5 (s, (N3)Ad$C_{3,5,7}$). IR (cm^{-1}): 2085, 2030, 2019, 1997, 1984, 1988, 1981, 1966, 1947 (ν_{CO}). Anal. calcd for $C_{34}H_{32}N_2O_{11}Ru_3$·THF,%: C, 44.75; H, 3.95; N, 2.75. Found,%: C, 44.39; H, 3.91; N, 2.70.

4.5.3 Synthesis of $Os_3(alAd_2)(CO)_{11}$ (2C)

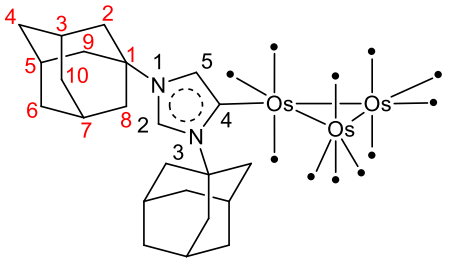

In a glove box, $Os_3(CO)_{12}$ (50 mg, 0.05 mmol) and IAd_2 (200 mg, 0.06 mmol) were added to an ampoule fitted with a PTFE valve. THF (5 mL) was then added and the mixture heated at 70 ˚C for 3 h with an argon purge to remove CO. The solvent was then removed *in vacuo* to leave a red solid which was washed with THF (2 x 1 mL) to remove

imidazolium by-products. The remaining solid was re-dissolved in THF (2 mL) by heating for 30 min at 70 ˚C, and layered with hexane to afford X-ray quality crystals. Yield: 20 mg (35%). ^{1}H NMR (d_8-THF, 500 MHz): δ 8.34 (d, J_{HH} = 2.00 Hz, 1H, (C2)*H*), 6.77 (d, J_{HH} = 2.00 Hz, 1H, (C5)*H*), 2.55 (d, J_{HH} = 2.50 Hz, 6H, (N3)Ad$_{2,8,9}$ CH_2), 2.31 (s, 3H, Ad$_{3,5,7}$ C*H*), 2.21 (s, 3H, Ad$_{3,5,7}$ C*H*), 2.10 (d, J_{HH} = 2.50 Hz, 6H, (N1)Ad$_{2,8,9}$ CH_2), 1.98 (s, 1H, Ad$_{4,6,10}$), 1.95 (s, 2H, Ad$_{4,6,10}$), 1.82-1.76 (m, 9H, Ad$_{4,6,10}$). ^{13}C{^{1}H} NMR (d_8-THF, 126 MHz): δ 212.8 (s, *C*O), 135.8 (s, (*C*5)H), 131.4 (s, (*C*2)H), 111.6 (s, Os-*C*4), 62.3 (s, (N3)Ad*C*$_1$), 58.3 (s, (N1)Ad*C*$_1$), 43.0 (s, (N1)Ad*C*$_{2,8,9}$), 42.5 (s, (N3)Ad*C*$_{2,8,9}$), 36.3 (s, (N1)Ad*C*$_{4,6,10}$), 36.1 (s, (N3)Ad*C*$_{4,6,10}$), 31.0 (s, (N1)Ad*C*$_{3,5,7}$), 30.5 (s, (N3)Ad*C*$_{3,5,7}$). IR (cm^{-1}): 2094, 2068, 2036, 2019, 2000, 1988, 1982, 1967, 1960, 1927. Anal. calcd for $C_{34}H_{32}N_2O_{11}Ru_3$,%: C, 33.60; H, 2.65; N, 2.31. Found,%: C, 33.64; H, 2.84; N, 2.22.

4.5.4 Synthesis of $Ru_3(\mu\text{-}H)(al^tBu_2)'(CO)_9$ (1B)

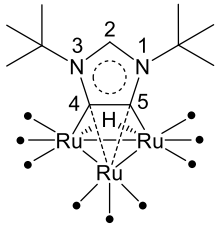

$Ru_3(I^tBu_2)(CO)_{11}$ (100 mg, 0.13 mmol) was dissolved in THF (5 mL) and heated at 70 °C for 5 h with a slow flow of argon passing through to purge the liberated CO. The solvent was removed and the residue extracted in toluene (3 x 5 mL). Upon removal of the solvent *in vacuo*, an yellow-orange solid was left that was washed with hexane (3 x 5 mL) to afford the product (62 mg, 67%). X-ray quality crystals were grown from CH_2Cl_2/hexane. ^{1}H NMR (d_8-THF, 500 MHz): δ 8.59 (s, 1H, (C2)*H*), 1.74 (s, 18H, *t-Bu*), -17.85 (s, 1H, μ-*H*). ^{13}C{^{1}H} NMR (d_8-THF, 126 MHz): δ 210.1 (s, *C*O), 144.0 (s, (*C*2)H), 139.4 (s, Ru$_3$-*C*4/*C*5), 60.9 (s, *C*Me$_3$), 30.2 (s, C*Me$_3$*). IR (KBr, cm^{-1}): 2072, 2042, 2024, 2002, 1981, 1968, 1944, 1932 (ν_{CO}). Anal. calcd for $C_{20}H_{20}N_2O_9Ru_3$,%: C, 32.65; H, 2.74; N, 3.81. Found,%: C, 32.66; H, 2.75; N, 3.71. ESI-TOF MS: $[M + H]^+$ m/z = 735.8254 (theoretical m/z = 735.8240).

4.5.5 Synthesis of $Ru_3(\mu\text{-}H)(alAd_2)'(CO)_9$ (2B)

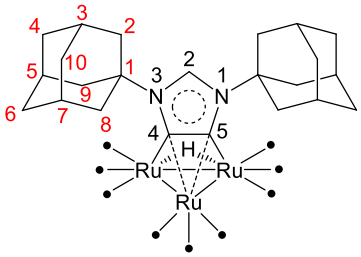

$Ru_3(IAd_2)(CO)_{11}$ (100 mg, 0.13 mmol) was dissolved in THF (5 mL) and heated at 70 °C for 5 h. A slow flow of argon was passed over the headspace of the reaction vessel to aid extraction of the liberated CO. On removal of the solvent, the residue was dissolved in toluene (3 x 5 mL), and the solvent removed *in vacuo* to leave a yellow-orange solid (65 mg, 69%). X-ray quality crystals were obtained by slow evaporation of a concentrated CH_2Cl_2 solution. ^{1}H NMR (d_8-THF, 500 MHz): δ 8.55 (s, 1H, (C2)*H*), 2.39 (s, 12H, $Ad_{2,8,9}$-C*H*$_2$), 2.27 (s, 6H, $Ad_{3,5,7}$-C*H*), 1.81 (s, 12H, $Ad_{4,6,10}$-C*H*$_2$), -17.77 (s, 1H, μ-*H*). ^{13}C{^{1}H} NMR (d_8-THF, 126 MHz): δ 200.1 (s, *C*O), 143.1 (s, (*C*2)H), 137.8 (s, Ru_3-*C*4/*C*5), 61.9 (s, Ad*C*$_1$), 42.9 (s, Ad*C*$_{2,8,9}$), 36.3 (s, Ad*C*$_{4,6,10}$), 30.8 (s, Ad*C*$_{3,5,7}$). IR (cm^{-1}): 2070, 2044, 2013, 1994, 1966, 1944 (ν_{CO}). Anal. calcd for $C_{32}H_{32}N_2O_9Ru_3 \cdot ½DCM$,%: C, 41.78; H, 3.56; N, 3.00. Found,%: C, 42.27; H, 3.53; N, 3.07.

4.6 Synthesis of ruthenium carbonyl and carbonato NHC complexes

4.6.1 Synthesis of $Ru(IEt_2Me_2)_2(CO)_3$ (3A)

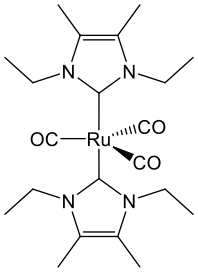

IEt_2Me_2 (100 mg, 0.66 mmol) was added to a THF (10 mL) solution of $Ru_3(CO)_{12}$ (70 mg, 0.11 mmol) and vigorous bubbling of the solution was observed straight away. Removal of the solvent after 1 h afforded an orange-red microcrystalline solid, which was washed with hexane (3 × 5 mL) and then recrystallised from THF and hexane. Yield: 135 mg (83%).

^{1}H NMR (d_8-THF, 500 MHz K): δ 4.43 (q, J_{HH} = 7.20 Hz, 8H, CH_2CH$_3$), 2.17 (s, 12H, NC*Me*), 1.22 (t, J_{HH} = 7.20 Hz, 12H, CH$_2$CH_3). ^{13}C{^{1}H} NMR (d_8-THF, 126 MHz K): δ 218.6 (s, *C*O), 181.6 (s, Ru-*C*), 125.6 (s, N*C*Me), 44.8 (s, *C*H$_2$CH$_3$), 15.7 (s, CH$_2$*C*H$_3$), 9.5 (s, NC*Me*). ^{13}C{^{1}H} NMR (Solid state, recycle time 6.0 s, contact time 1.00 ms, spin rate 6.80 kHz, 303 K): δ 224.3 (s, *C*O), 214.3 (s, *C*O), 212.6 (s, *C*O), 177.3 (s, Ru-*C*), 178.0 (s, Ru-*C*), 126.6 (s, N*C*Me), 124.9 (s, N*C*Me), 45.0 (s, *C*H$_2$CH$_3$), 43.4 (s, *C*H$_2$CH$_3$), 17.7 (s, CH$_2$*C*H$_3$), 16.7 (s, CH$_2$*C*H$_3$), 15.6 (s, CH$_2$*C*H$_3$), 11.9 (s, NC*Me*), 10.1 (s, NC*Me*), 9.0 (s, NC*Me*), 8.1 (s, NC*Me*). ^{15}N NMR (Solid state, recycle time as for carbon, contact time 10.00 ms, spin rate 6.80 kHz, 303 K): δ -183.5, -184.5, -185.1, -185.7. ^{13}C{^{1}H} NMR (Solid state, recycle time 2.0 s, contact time 1.00 ms, spin rate 6.80 kHz, 206 K): δ 224.3 (s, *C*O), 214.2 (s, *C*O), 212.2 (s, *C*O), 176.8 (s, Ru-*C*), 126.4 (s, N*C*Me), 124.8 (s, N*C*Me), 45.0 (s, *C*H$_2$CH$_3$), 43.2 (s, *C*H$_2$CH$_3$), 18.2 (s, CH$_2$*C*H$_3$), 17.4 (s, CH$_2$*C*H$_3$), 16.5 (s, CH$_2$*C*H$_3$), 15.3 (s, CH$_2$*C*H$_3$), 12.3 (s, NC*Me*), 10.0 (s, NC*Me*), 9.2 (s, NC*Me*), 7.9 (s, NC*Me*). ^{15}N NMR (Solid state, recycle time as for carbon, contact time 10.00 ms, spin rate 6.80 kHz, 206 K): δ -184.0, -184.9, -185.6, -186.2. IR (C_6D_6, cm^{-1}): 1967, 1937, 1849, 1836 (ν_{CO}). Anal. calcd for $C_{21}H_{32}N_4O_3Ru$,%: C, 51.52; H, 6.59; N, 11.44. Found,%: C, 51.43; H, 6.63; N, 11.19.

4.6.2 Synthesis of Ru(I^{i}Pr$_2$Me$_2$)$_2$(CO)$_3$ (4A)

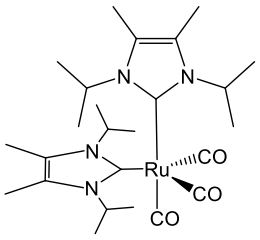

I^{i}Pr$_2$Me$_2$ (336 mg, 1.86 mmol) and Ru$_3$(CO)$_{12}$ (195 mg, 0.31 mmol) were added to a flame-dried ampoule under argon. THF (10 mL) was added and vigorous bubbling of the solution was observed straight away. After 1 h, removal of the solvent afforded an orange-red microcrystalline solid, which was washed with hexane (3 × 5 mL) and THF (1 × 3 mL) and recrystallised from THF and hexane. Yield: 456 mg (91%). ^{1}H NMR (d_8-THF, 500 MHz): δ 6.00 (sept, J_{HH} = 7.20 Hz, 4H, C*H*Me$_2$), 2.23 (s, 12H, NC*Me*), 1.26 (d, J_{HH} = 7.20 Hz, 24H, CH*Me*$_2$). ^{13}C{^{1}H} NMR (d_8-THF, 126 MHz): δ 217.7 (s, *C*O), 187.3 (s, Ru-*C*), 126.4 (s, N*C*Me), 55.0 (s, *C*HMe$_2$), 21.3 (s, CH*Me*$_2$), 10.7 (s, NC*Me*). IR (C_6D_6, cm^{-1}): 1967,

1867, 1845, 1836 (ν_{CO}). Anal. calcd for $C_{25}H_{40}N_4O_3Ru$,%: C, 55.05; H, 7.39; N, 10.27. Found,%: C, 54.39; H, 7.13; N, 9.99.

4.6.3 Synthesis of $Ru(I^iPr_2)_2(CO)_3$ (5A)

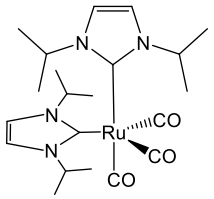

I^iPr_2 (100 mg, 0.66 mmol) was dissolved in THF and transferred by cannula to a weighed and dried ampoule under argon, and the THF removed *in vacuo*. $Ru_3(CO)_{12}$ (70 mg, 0.11 mmol) was then added, followed by the addition of THF (10 mL) that provoked vigorous bubbling of the solution, which was left at room temperature for 1 h. Removal of the solvent afforded an orange-red microcrystalline solid, which was washed with hexane (3 × 5 mL) and then recrystallised from THF and hexane. Yield: 154 mg (95%). ^{1}H NMR (d_8-THF, 500 MHz): δ 7.24 (s, 4H, NC*H*), 5.58 (sept, J_{HH} = 7.00 Hz, 4H, C*H*Me$_2$), 1.26 (d, J_{HH} = 7.00 Hz, 24H, CH*Me*$_2$). ^{13}C{^{1}H} NMR (d_8-THF, 126 MHz): δ 217.8 (s, *C*O), 184.4 (s, Ru-*C*), 118.2 (s, N*C*H), 53.2 (s, *C*HMe$_2$), 23.1 (s, CH*Me*$_2$). ^{13}C{^{1}H} NMR (Solid state, recycle time 1.5 s, contact time 10.00 ms, spin rate 6.80 kHz, 303 K): δ 227.5 (s, *C*O), 216.0 (s, *C*O), 213.6 (s, *C*O), 184.5 (s, Ru-*C*), 181.1 (s, Ru-*C*), 121.0 (s, N*C*H), 119.4 (s, N*C*H), 118.1 (s, N*C*H), 117.0 (s, N*C*H), 53.7 (s, *C*HMe$_2$), 53.2 (s, *C*HMe$_2$), 52.4 (s, *C*HMe$_2$), 25.3 (s, CH*Me*$_2$), 24.4 (s, CH*Me*$_2$), 23.9 (s, CH*Me*$_2$), 23.4 (s, CH*Me*$_2$), 21.3 (s, CH*Me*$_2$). ^{15}N NMR (Solid state, recycle time as for carbon, contact time 10.00 ms, spin rate 5.20 kHz, 303 K): δ -173.5, -174.4, -174.9, -176.7. ^{13}C{^{1}H} NMR (Solid state, recycle time 1.0 s, contact time 10.00 ms, spin rate 5.20 kHz, 206 K): δ 228.1 (s, *C*O), 216.1 (s, *C*O), 213.2 (s, *C*O), 183.8 (s, Ru-*C*), 180.1 (s, Ru-*C*), 121.2 (s, N*C*H), 119.5 (s, N*C*H), 118.0 (s, N*C*H), 116.7 (s, N*C*H), 53.5 (s, *C*HMe$_2$), 52.3 (s, *C*HMe$_2$), 26.0 (s, CH*Me*$_2$), 24.8 (s, CH*Me*$_2$), 23.6 (s, CH*Me*$_2$), 20.7 (s, CH*Me*$_2$). ^{15}N NMR (Solid state, recycle time as for carbon, contact time 10.00 ms, spin rate 5.20 kHz, 206 K): δ -173.9, -175.1, -175.7, -177.7. IR (C_6D_6, cm^{-1}): 1970, 1852, 1841 (ν_{CO}). Anal. calcd for $C_{21}H_{32}N_4O_3Ru$,%: C, 51.52; H, 6.59; N, 11.44. Found,%: C, 51.57; H, 6.65; N, 11.10.

4.6.4 Synthesis of $Ru(IEt_2Me_2)_2(CO)_2(CO_3)$ (3B)

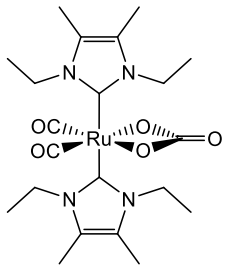

A solid sample of $Ru(IEt_2Me_2)_2(CO)_3$ (100 mg, 0.20 mmol) was heated for 14 h at 70 °C in an ampoule fitted with a J. Youngs PFTE tap under 1 atm O_2. The resulting carbonato complex $Ru(IEt_2Me_2)_2(CO)_2(CO_3)$ was extracted with THF (3 × 5 mL), pumped to dryness and then washed with hexane (3 × 5 mL) to leave a light brown solid. Yield: 50 mg (48%). Crystals for X-ray diffraction were grown from CH_2Cl_2/hexane. ^{1}H NMR (d_8-THF, 500 MHz): δ 4.37 (q, J_{HH} = 7.00 Hz, 8H, C*H*$_2$CH$_3$), 2.20 (s, 12H, NC*Me*), 1.44 (t, J_{HH} = 7.00 Hz, 12H, CH$_2$C*H*$_3$). ^{13}C{^{1}H} NMR (d_8-THF, 126 MHz): δ 201.9 (s, *C*O), 174.5 (s, Ru-*C*), 164.4 (s, *C*O$_3$), 126.0 (s, N*C*Me), 43.6 (s, *C*H$_2$CH$_3$), 16.8 (s, CH$_2$*C*H$_3$), 8.8 (s, NC*Me*). IR (KBr, cm^{-1}): 2024 (ν_{CO}), 1947 (ν_{CO}), 1612 (ν_{OCO}). The molecule of water in the crystal structure resulted from exposure **3B** to air and appeared in the IR spectrum as a broad O–H stretch at 3423 cm^{-1}. Anal. calcd for $C_{21}H_{32}N_4O_5Ru{\cdot}H_2O$,%: C, 46.74; H, 6.35; N, 10.38. Found,%: C, 47.05; H, 6.31; N, 10.17. ESI-TOF MS: $[M + Na]^+$ m/z = 545.1300 (theoretical m/z = 545.1314).

4.6.5 Synthesis of $Ru(I^iPr_2Me_2)_2(CO)_2(CO_3)$ (4B)

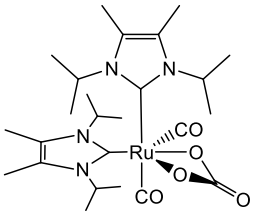

$Ru(I^iPr_2Me_2)_2(CO)_3$ (150 mg, 0.28 mmol) was dissolved in pyridine (2 mL) in an ampoule fitted with a J. Young's re-sealable PTFE valve, freeze–pump–thaw degassed, and then placed under 1 atm O_2. After shaking for 30 s, the gas and solvent were removed quickly under vacuum. The residue was washed with THF (2 × 3 mL) to give the product as a pale yellow solid. X-ray quality crystals were grown by layering from CH_2Cl_2/hexane. Yield: 95 mg (60%). ^{1}H NMR (CD_2Cl_2, 500 MHz): δ 5.95 (sept, J_{HH} = 7.00 Hz, 1H, C*H*Me$_2$), 5.71 (sept, J_{HH} = 7.00 Hz, 1H, C*H*Me$_2$), 4.80 (sept, J_{HH} = 7.00 Hz, 1H, C*H*Me$_2$), 4.67 (sept,

J_{HH} = 7.00 Hz, 1H, C*H*Me$_2$), 2.31 (s, 3H, NC*Me*), 2.26 (s, 3H, NC*Me*), 2.19 (s, 3H, NC*Me*), 2.14 (s, 3H, NC*Me*), 1.62 (d, J_{HH} = 7.00 Hz, 3H, CH*Me*$_2$), 1.60-1.58 (m, 6H, CH*Me*$_2$), 1.56 (d, J_{HH} = 7.00 Hz, 3H, CH*Me*$_2$), 1.33 (d, J_{HH} = 7.00 Hz, 3H, CH*Me*$_2$), 1.32 (d, J_{HH} = 6.90 Hz, 3H, CH*Me*$_2$), 0.85 (d, J_{HH} = 7.00 Hz, 3H, CH*Me*$_2$), 0.72 (d, J_{HH} = 6.90 Hz, 3H, CH*Me*$_2$). $^{13}C\{^1H\}$ NMR (CD_2Cl_2, 126 MHz): δ 200.9 (s, *C*O), 193.1 (s, *C*O), 177.5 (s, Ru-*C*), 168.8 (s, Ru-*C*), 166.7 (*C*O$_3$), 128.0 (s, N*C*Me), 127.1 (s, N*C*Me), 126.4 (s, N*C*Me), 126.1 (s, N*C*Me), 54.0 (s, *C*HMe$_2$), 53.7 (s, *C*HMe$_2$), 52.8 (s, *C*HMe$_2$), 52.6 (s, *C*HMe$_2$), 23.7 (s, CH*Me*$_2$), 22.7 (s, CH*Me*$_2$), 22.5 (s, CH*Me*$_2$), 22.2 (s, CH*Me*$_2$), 21.9 (s, CH*Me*$_2$), 21.5 (s, CH*Me*$_2$), 19.7 (s, CH*Me*$_2$), 19.5 (s, CH*Me*$_2$), 10.8 (s, NC*Me*), 10.7 (s, NC*Me*), 10.6 (s, NC*Me*). IR (KBr, cm^{-1}): 2034 (ν_{CO}), 1945 (ν_{CO}), 1593 (ν_{OCO}). ESI-TOF MS: $[M - CO + H]^+$ m/z = 551.2152 (theoretical m/z = 551.2172).

4.6.6 Synthesis of Ru(I^{i}Pr$_2$Me$_2$)$_2$(CO)(C$_5$H$_5$N)(CO$_3$) (4C)

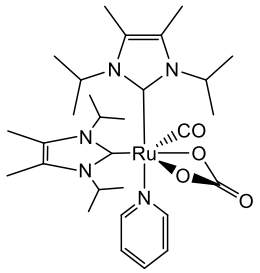

Ru(I^{i}Pr$_2$Me$_2$)$_2$(CO)(C$_5$H$_5$N)(CO$_3$) was isolated in 17% yield (30 mg) from the same reaction as **4B** upon crystallization of the THF washings. ^1H NMR (d_5-pyridine, 500 MHz): δ 6.52 (sept, J_{HH} = 7.00 Hz, 1H, C*H*Me$_2$), 5.85 (sept, J_{HH} = 7.00 Hz, 1H, C*H*Me$_2$), 5.42 (sept, J_{HH} = 7.00 Hz, 1H, C*H*Me$_2$), 5.23 (sept, J_{HH} = 7.00 Hz, 1H, C*H*Me$_2$), 2.15 (s, 3H, NC*Me*), 2.08 (s, 3H, NC*Me*), 2.05 (s, 3H, NC*Me*), 1.99 (s, 3H, NC*Me*), 1.65 (d, J_{HH} = 7.00 Hz, 3H, CH*Me*$_2$), 1.62-1.60 (m, 6H, CH*Me*$_2$), 1.49 (d, J_{HH} = 7.00 Hz, 3H, CH*Me*$_2$), 1.45 (d, J_{HH} = 7.00 Hz, 3H, CH*Me*$_2$), 0.88 (d, J_{HH} = 7.00 Hz, 3H, CH*Me*$_2$), 0.76 (d, J_{HH} = 7.00 Hz, 3H, CH*Me*$_2$), 0.46 (d, J_{HH} = 7.00 Hz, 3H, CH*Me*$_2$). $^{13}C\{^1H\}$ NMR (d_5-pyridine, 126 MHz): δ 208.9 (s, *C*O), 180.9 (s, Ru-*C*), 178.1 (s, Ru-*C*), 169.4 (*C*O$_3$), 127.2 (s, N*C*Me), 126.4 (s, N*C*Me), 126.1 (s, N*C*Me), 126.0 (s, N*C*Me), 53.3 (s, *C*HMe$_2$), 52.8 (s, *C*HMe$_2$), 52.2 (s, *C*HMe$_2$), 50.6 (s, *C*HMe$_2$), 24.1 (s, CH*Me*$_2$), 23.2 [s, CH*Me*$_2$), 23.1 (s, CH*Me*$_2$), 22.2 (s, CH*Me*$_2$), 21.6 (s, CH*Me*$_2$), 21.0 (s, CH*Me*$_2$), 19.8 (s, CH*Me*$_2$), 19.6 (s, CH*Me*$_2$), 10.5 (s, NC*Me*), 10.4 (s, NC*Me*), 10.3 (s, NC*Me*). Spectra were also recorded in CD_2Cl_2 to allow the coordinated pyridine resonances to be observed. ^1H NMR

(CD_2Cl_2, 500 MHz): δ 8.51 (m, 2H, *o*-C*H* (pyr)), 7.70 (m, 1H, *p*-C*H* (pyr)), 7.30 (m, 2H, *m*-C*H* (pyr)), 5.98 (sept, J_{HH} = 7.00 Hz, 1H, C*H*Me_2), 5.43 (sept, J_{HH} = 7.00 Hz, 1H, C*H*Me_2), 5.06 (sept, J_{HH} = 7.00 Hz, 1H, C*H*Me_2), 5.00 (sept, J_{HH} = 7.00 Hz, 1H, C*H*Me_2), 2.25 (s, 3H, NC*Me*), 2.19 (s, 3H, NC*Me*), 2.17 (s, 3H, NC*Me*), 2.15 (s, 3H, NC*Me*), 1.62 (d, J_{HH} = 7.00 Hz, 3H, CH*Me*$_2$), 1.51-1.47 (m, 6H, CH*Me*$_2$), 1.43 (d, J_{HH} = 7.00 Hz, 3H, CH*Me*$_2$), 1.39 (d, J_{HH} = 7.00 Hz, 3H, CH*Me*$_2$), 0.87 (d, J_{HH} = 7.00 Hz, 3H, CH*Me*$_2$), 0.73 (d, J_{HH} = 7.00 Hz, 3H, CH*Me*$_2$), 0.44 (d, J_{HH} = 7.00 Hz, 3H, CH*Me*$_2$). $^{13}C\{^1H\}$ NMR (CD_2Cl_2, 126 MHz): δ 208.3 (s, *C*O), 179.7 (s, Ru-*C*), 176.8 (s, Ru-*C*), 168.7 (*C*O_3), 153.0 (s, *o*-*C*H (pyr)), 137.2 (s, *p*-*C*H (pyr)), 127.4 (s, N*C*Me), 126.4 (s, N*C*Me), 126.2 (s, N*C*Me), 126.1 (s, N*C*Me), 125.2 (s, *m*-*C*H (pyr)), 53.3 (s, *C*HMe_2), 52.8 (s, *C*HMe_2), 52.2 (s, *C*HMe_2), 50.8 (s, *C*HMe_2), 23.6 (s, CH*Me*$_2$), 23.1 (s, CH*Me*$_2$), 22.9 (s, CH*Me*$_2$), 22.1 (s, CH*Me*$_2$), 21.5 (s, CH*Me*$_2$), 20.8 (s, CH*Me*$_2$), 20.0 (s, CH*Me*$_2$), 19.6 (s, CH*Me*$_2$), 10.7 (s, NC*Me*), 10.6 (s, NC*Me*). IR (cm^{-1}): 1905 (ν_{CO}) 1643 (ν_{OCO}). ESI-TOF MS: $[M - C_5H_5N + H]^+$ *m*/*z* = 551.2149 (theoretical *m*/*z* = 551.2172).

4.6.7 Synthesis of Ru(I^{i}Pr$_2$)$_2$(CO)$_2$(CO$_3$) (5B)

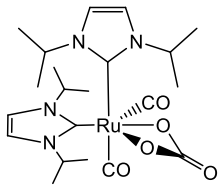

$Ru(I^iPr_2)_2(CO)_3$ (150 mg, 0.31 mmol) was dissolved in pyridine (2 mL) in an ampoule fitted with a J. Young's PTFE valve, freeze–pump–thaw degassed, and then placed under 1 atm O_2. After shaking for ca. 30 s, the gas and solvent were removed quickly under vacuum. The residue was washed with THF (2 × 3 mL) to leave a pale yellow solid that was recrystallised from CH_2Cl_2/hexane. Yield: 85 mg (53%). ^1H NMR (CD_2Cl_2, 500 MHz): δ 7.23 (d, J_{HH} = 2.40 Hz, 2H, NC*H*), 7.11 (br s, 1H, NC*H*), 7.05 (d, J_{HH} = 2.40 Hz, 1H, NC*H*), 6.96 (br s, 1H, NC*H*), 5.72 (sept, J_{HH} = 6.80 Hz, 1H, C*H*Me_2), 5.43 (br sept, 1H, C*H*Me_2), 4.43 (sept, J_{HH} = 6.80 Hz, 1H, C*H*Me_2), 4.37 (br sept, 1H, C*H*Me_2), 1.57 (br d, J_{HH} = 6.80 Hz, 3H, CH*Me*$_2$), 1.54-1.52 (m, 9H, CH*Me*$_2$), 1.32 (d, J_{HH} = 6.80 Hz, 3H, CH*Me*$_2$), 1.28 (br d, J_{HH} = 6.80 Hz, 3H, CH*Me*$_2$), 0.86 (d, J_{HH} = 6.80 Hz, 3H, CH*Me*$_2$), 0.72 (br d, J_{HH} = 6.90 Hz, 3H, CH*Me*$_2$). $^{13}C\{^1H\}$ NMR (CD_2Cl_2, 126 MHz): δ 201.3 (s, *C*O), 192.9 (s, *C*O), 176.5 (s, Ru-*C*), 169.0 (s, Ru-*C*), 166.8 (*C*O_3), 119.6 (s, N*C*H), 119.0

(s, N*C*H), 118.2 (s, N*C*H), 118.0 (s, N*C*H), 53.1 (s, *C*HMe$_2$), 52.8 (s, *C*HMe$_2$), 52.0 (s, *C*HMe$_2$), 51.8 (s, *C*HMe$_2$), 25.9 (s, CH*Me*$_2$), 24.8 (s, CH*Me*$_2$), 24.5 (s, CH*Me*$_2$), 24.3 (s, CH*Me*$_2$), 23.6 (s, CH*Me*$_2$), 23.5 (s, CH*Me*$_2$), 21.9 (s, CH*Me*$_2$), 21.6 (s, CH*Me*$_2$). IR (KBr, cm^{-1}): 2044 (ν_{CO}), 1954, (ν_{CO}) 1586 (ν_{OCO}). Anal. calcd for $C_{21}H_{32}N_4O_5Ru$,%: C, 48.36; H, 6.18; N, 10.74. Found,%: C, 48.94; H, 6.01; N, 10.61. ESI-TOF MS: $[M - CO + H]^+$ m/z = 495.1540 (theoretical m/z = 495.1545).

4.7 Synthesis of ruthenium HCl and H(η^2-BH$_4$) NHC complexes

4.7.1 Synthesis of Ru(IPr)$_2$(CO)HCl (6A)

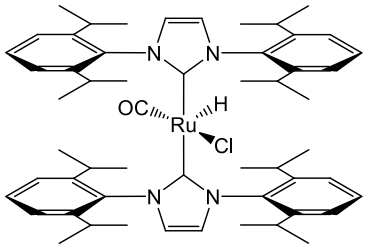

Ru(AsPh$_3$)$_3$(CO)H$_2$ (1.0 g, 0.95 mmol) and IPr (0.93 g, 2.4 mmol) were dissolved in toluene (10 mL) and stirred in an ampoule sealed with a J. Youngs PTFE tap for 1.5 h at 358 K. After addition of 70 μL (1.05 mmol) of CH_2Cl_2, stirring was continued at 393 K for a further 18 h. The solvent was removed under vacuum and the product extracted in toluene (3 × 10 mL), reduced to dryness and then washed with hexane (2 × 5 mL) to give a yellow powder (702 mg, 78%). Recrystallisation was achieved from hexane at 5 ˚C. ^{1}H NMR (d_8-THF, 400 MHz): δ 7.29 (t, J_{HH} = 7.60 Hz, 4H, *p*-C*H*), 7.06-7.03 (m, 8H, *m*-C*H*), 7.00 (s, 4H, NC*H*), 3.02 (sept, J_{HH} = 6.80 Hz, 4H, C*H*Me$_2$), 2.88 (sept (br), J_{HH} = 6.80 Hz, 4H, C*H*Me$_2$), 1.00-0.89 (m, 48H, CH*Me*$_2$), -25.88 (s, 1H, Ru-*H*). ^{13}C{^{1}H} NMR (d_8-THF, 101 MHz): δ 201.8 (s, *C*O), 195.6 (s, Ru-*C*), 147.1 (s, *o*-*C*), 138.2 (s, *i*-*C*), 129.6 (s, *p*-*C*H), 124.8 (s, N*C*H), 124.7 (s, N*C*H), 124.3 (s, *m*-*C*H), 29.1 (s, *C*HMe$_2$), 29.0 (s, *C*HMe$_2$), 26.5 (s, CH*Me*$_2$), 26.4 (s, CH*Me*$_2$), 23.4 (s, CH*Me*$_2$), 23.1 (s, CH*Me*$_2$). IR (cm^{-1}): 1898 (ν_{CO}), 1884 (ν_{Ru-H}). Anal. calcd for $C_{55}H_{73}N_4ClORu$,%: C, 70.07; H, 7.81; N, 5.94. Found,%: C, 70.57; H, 8.06; N, 5.64. ESI-TOF MS: $[M - HCl + H]^+$ m/z = 907.4867 (theoretical m/z = 907.4837).

4.7.2 Synthesis of $Ru(SIPr)_2(CO)HCl$ (7A)

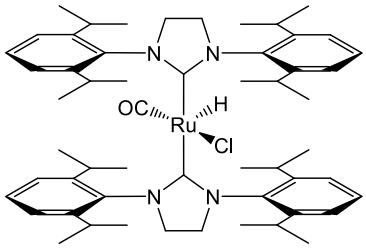

$Ru(AsPh_3)_3(CO)H_2$ (1.0 g, 0.95 mmol) and SIPr.C_6F_5-H (1.62 g, 2.9 mmol) were dissolved in toluene (5 mL) and stirred in an ampoule sealed with a J. Youngs PTFE tap for 5 h at 358 K. Dichloromethane (30 μL, 0.48 mmol) was added and the solution stirred at 393 K for 24 h. Subsequent addition of dichloromethane (30 μL, 0.48 mmol) with continued with thermolysis at 393 K for an additional 24 h. The solvent was removed *in vacuo* and the product washed with hexane (2 × 2 mL) to give a yellow powder (450 mg, 50%). Recrystallisation was from hexane at 5 ˚C. ^{1}H NMR (d_8-THF, 400 MHz): δ 7.17 (t, J_{HH} = 7.60 Hz, 4H, *p*-C*H*), 6.99-6.93 (m, 8H, *m*-C*H*), 3.73 (s, 8H, NCH_2), 3.37 (sept, J_{HH} = 6.80 Hz, 8H, C*H*Me$_2$), 1.06 (d, J_{HH} = 6.80 Hz, 12H, CH*Me*$_2$), 1.03 (d, J_{HH} = 6.80 Hz, 12H, CH*Me*$_2$), 0.96 (br s, 12H, CH*Me*$_2$), 0.86 (d, J_{HH} = 6.80 Hz, 12H, CH*Me*$_2$), -25.77 (s, 1H, Ru-*H*). ^{13}C{^{1}H} NMR (d_8-THF, 101 MHz): δ 224.4 (s, Ru-*C*), 201.0 (s, *C*O), 148.1 (s, *o*- and *i*-*C*), 128.4 (s, *p*-*C*H), 124.7 (s, *m*-*C*H), 54.8 (s, N*C*H$_2$), 28.8 (s, *C*HMe$_2$), 26.8 (s, CH*Me*$_2$), 24.2 (s, CH*Me*$_2$). IR (cm^{-1}): 1902 (ν_{CO}). Anal. calcd for $C_{55}H_{77}N_4ClORu{\cdot}C_6H_{14}$,%: C, 70.92; H, 8.88; N, 5.42. Found,%: C, 70.67; H, 8.84; N, 5.27. ESI-TOF MS: $[M - HCl + H]^+$ *m*/*z* = 911.5127 (theoretical *m*/*z* = 911.5150).

4.7.3 Synthesis of $Ru(SIMes)_2(CO)HCl$ (8A)

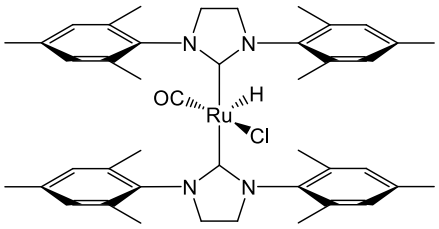

$Ru(AsPh_3)_3(CO)H_2$ (100 mg, 0.095 mmol) and SIMes.C_6F_5-H (136 mg, 0.28 mmol) were dissolved in toluene (5 mL) and stirred in an ampoule sealed with a J. Youngs PTFE tap for 5 h at 358 K. Dichloromethane (6 μL, 0.095 mmol) was added and the solution stirred at the same temperature for an additional 48 h. The solvent was removed *in vacuo* to give the crude product that could not be further purified. ^{1}H NMR (d_8-THF, 500 MHz): δ 6.69

(s, 8H, *m*-C*H*), 3.69 (br s, 8H, NCH_2), 2.37 (s, 12H, aryl-*Me*), 2.08 (s (br), 12H, aryl-*Me*), 2.01 (s, 12H, aryl-*Me*), -25.80 (s, 1H, Ru-*H*). $^{13}C\{^1H\}$ NMR (d_8-THF, 126 MHz): δ 221.8 (s, Ru-*C*), 201.5 (s, *C*O), 140.7 (s, *i, o or m-C*), 136.4 (s, *i, o or m-C*), 136.2 (s, *i, o or m-C*), 134.3 (s, *m*-*C*H), 129.3 (s, *m*-*C*H), 51.2 (s, N*C*H_2), 21.1 (s, *p*-*Me*), 19.8 (s, *o*-*Me*), 18.2 (s, *o*-*Me*). ^1H NMR (d_8-toluene, 400 MHz): δ 6.79 (s, 4H, *m*-C*H*), 6.75 (s, 4H, *m*-C*H*), 3.18 (br s, 8H, NCH_2), 2.35 (s, 12H, *p*-*Me*), 2.25 (br s, 12H, *o*-*Me*), 2.12 (br s, 12H, *o*-*Me*), -25.52 (s, 1H, Ru-*H*). IR (cm^{-1}): 1890 (ν_{CO}). ESI-TOF MS: $[M - HCl + H]^+$ *m*/*z* = 743.3218 (theoretical *m*/*z* = 743.3269).

4.7.4 Synthesis of $Ru(IPr)_2(CO)_2HCl$ (6B)

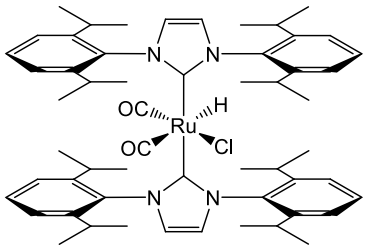

$Ru(IPr)_2(CO)HCl$ (40 mg, 0.04 mmol) was added to a small flame-dried Schlenk tube in a glovebox and was added toluene (3 mL). CO was bubbled through the solution for 5 min, with immediate colour change from pale yellow to clear. The solvent was then removed *in vacuo* to leave an off-white solid. Yield: 35 mg (85%). Recrystallisation took place from toluene/hexane. ^1H NMR (d_8-THF, 400 MHz): δ 7.28 (t, J_{HH} = 7.60 Hz, 4H, *p*-C*H*), 7.07 (d, J_{HH} = 7.60 Hz, 8H, *m*-C*H*), 7.01 (s, 4H, NC*H*), 2.92 (sept, J_{HH} = 6.80 Hz, 4H, C*H*Me_2), 2.85 (sept, J_{HH} = 6.80 Hz, 4H, C*H*Me_2), 1.12 (d, J_{HH} = 6.80 Hz, 24H, CH*Me*$_2$), 0.95 (d, J_{HH} = 6.80 Hz, 24H, CH*Me*$_2$), -4.59 (s, 1H, Ru-*H*). $^{13}C\{^1H\}$ NMR (d_8-THF, 101 MHz): δ 203.1 (s, *C*O), 193.4 (s, *C*O), 185.9 (s, Ru-*C*), 147.2 (s, *o*-*C*), 147.1 (s, *o*-*C*), 140.0 (s, *i*-*C*), 130.2 (s, *p*-*C*), 126.1 (s, N*C*H), 126.0 (s, N*C*H), 125.9 (s, N*C*H), 124.4 (s, *m*-*C*H), 28.9 (s, *C*HMe_2), 26.2 (s, CH*Me*$_2$), 26.1 (s, CH*Me*$_2$), 23.8 (s, CH*Me*$_2$), 23.5 (s, CH*Me*$_2$). IR (C_6D_6, cm^{-1}): 2028, 1934 (ν_{CO}). Anal. calcd for $C_{56}H_{73}N_4O_2ClRu$,%: C, 69.29; H, 7.58; N, 5.77. Found,%: C, 68.97; H, 7.65; N, 5.60. ESI-TOF MS: $[M - HCl + H]^+$ *m*/*z* = 935.4752 (theoretical *m*/*z* = 935.4786).

4.7.5 Synthesis of $Ru(SIPr)_2(CO)_2HCl$ (7B)

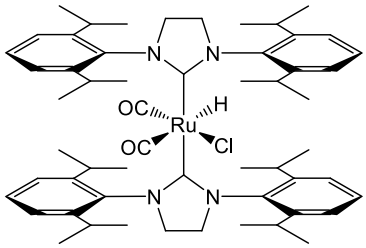

$Ru(SIPr)_2(CO)HCl$ (40 mg, 0.04 mmol) was added to a small flame-dried Schlenk tube in a glovebox and was added toluene (3 mL). CO was bubbled through the solution for 5 min, with immediate colour change from pale yellow to clear. The solvent was then removed *in vacuo* to leave an off-white solid. Yield: 32 mg (78%). Recrystallisation occurred from layering of the original toluene solution with hexane under a CO atmosphere. ^{1}H NMR (d_8-THF, 400 MHz): δ 7.15 (t, J_{HH} = 7.60 Hz, 4H, *p*-C*H*), 7.00 (d, J_{HH} = 7.60 Hz, 8H, *m*-C*H*), 3.73-3.67 (m, 8H, C*H*Me$_2$ + NC*H*$_2$), 3.25-3.23 (m, 8H, C*H*Me$_2$ + NC*H*$_2$), 1.22 (d, J_{HH} = 6.80 Hz, 12H, CH*Me*$_2$), 1.14-1.11 (m, 24H, CH*Me*$_2$), 1.08 (d, J_{HH} = 6.80 Hz, 12H, CH*Me*$_2$), -5.09 (s, 1H, Ru-*H*). ^{13}C{^{1}H} NMR (d_8-THF, 101 MHz): δ 213.6 (s, Ru-*C*), 202.3 (s, *C*O), 193.0 (s, *C*O), 147.9 (s, *o*-*C*), 147.8 (s, *o*-*C*), 140.7 (s, *i*-*C*), 129.4 (s, *p*-*C*H), 129.3 (s, *p*-*C*H), 129.1 (s, *p*-*C*H), 125.1 (s, *m*-*C*H), 125.0 (s, *m*-*C*H), 124.9 (s, *m*-*C*H), 55.3 (s, N*C*H$_2$), 28.8 (s, *C*HMe$_2$), 26.6 (s, CH*Me*$_2$), 26.5 (s, CH*Me*$_2$), 24.7 (s, CH*Me*$_2$), 24.4 (s, CH*Me*$_2$). IR (cm^{-1}): 2032, 1937 (ν_{CO}). Due to the lability of the second CO ligand accurate elemental analysis was not plausible. ESI-TOF MS: $[M - HCl + H]^+$ m/z = 939.5099 (theoretical m/z = 939.5100).

4.7.6 Synthesis of $Ru(IPr)_2(CO)H(\eta^2\text{-}BH_4)$ (6C)

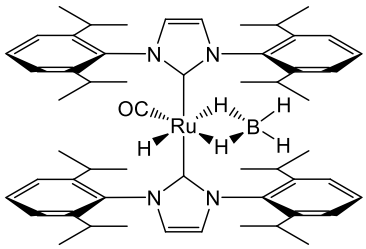

$Ru(IPr)_2(CO)HCl$ (110 mg, 0.12 mmol) and $NaBH_4$ (18 mg, 0.47 mmol) were suspended in ethanol (4 mL) and stirred at 343 K for 1.5 h under argon. Removal of the solvent under vacuum gave a colourless solid, which was extracted with benzene (2 × 5 mL) to give an off-white solid (90 mg, 83%). ^{1}H NMR (d_8-THF, 400 MHz): δ 7.27 (t, J_{HH} = 7.60 Hz, 4H, *p*-C*H*), 7.05 (d, J_{HH} = 7.60 Hz, 8H, *m*-C*H*), 7.02 (s, 4H, NC*H*), 2.89-2.78 (m, 8H, C*H*Me$_2$),

0.97-0.92 (m, 48H, CH*Me*$_2$), -7.20 (br s, 1H, B-*H*), -16.19 (s, 1H, Ru-*H*). [V. T. hydride data: ^{1}H NMR (d_8-toluene, 400 MHz , 238 K): δ -5.14 (br s, 1H, B-H_c), -6.96 (br s, 1H, B-H_b), -15.91 (s, 1H, Ru-H_a)]. ^{13}C{^{1}H} NMR (d_8-THF, 101 MHz): δ 205.4 (s, *C*O), 195.2 (s, Ru-*C*), 146.9 (s, *o*-*C*), 146.8 (s, *o*-*C*), 139.3 (s, *i*-*C*), 129.5 (s, *p*-*C*H), 124.9 (s, N*C*H), 124.8 (s, N*C*H), 124.2 (s, *m*-*C*H), 29.0 (s, *C*HMe$_2$), 26.6 (s, CH*Me*$_2$), 26.5 (s, CH*Me*$_2$), 23.0 (s, CH*Me*$_2$), 22.9 (s, CH*Me*$_2$). ^{11}B NMR (298 K, 128 MHz): δ -0.2 (br s). IR (cm^{-1}): 1917 (ν_{CO}), 2466, 2394 (ν_{BH}). Anal. calcd for $C_{55}H_{77}BN_4ORu$,%: C, 71.64; H, 8.42; N, 6.08. Found,%: C, 71.53; H, 8.50; N, 5.93. ESI-TOF MS: [M - BH_4 + H]$^+$ *m*/*z* = 907.4842 (theoretical *m*/*z* = 907.4837).

4.7.7 Synthesis of Ru(SIPr)$_2$(CO)H(η^2-BH$_4$) (7C)

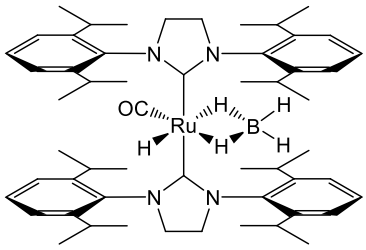

$NaBH_4$ (8 mg, 0.21 mmol) and Ru(SIPr)$_2$(CO)HCl (50 mg, 0.05 mmol) were suspended in ethanol (4 mL) and stirred at 343 K for 1.5 h under argon. Removal of the solvent under vacuum gave a colourless residue, which was extracted with benzene (2 × 5 mL) to give an off-white solid (40 mg, 82%). ^{1}H NMR (d_8-THF, 400 MHz): δ 7.18-7.14 (m, 4H, *p*-C*H*), 7.00-6.99 (m, 8H, *m*-C*H*), 3.74-3.72 (m, 8H, NCH_2), 3.28-3.20 (m, 8H, C*H*Me$_2$), 1.22 (d, J_{HH} = 6.80 Hz, 6H, CH*Me*$_2$), 1.07-1.04 (m, 30H, CH*Me*$_2$), 0.98 (d, J_{HH} = 6.80 Hz, 6H, CH*Me*$_2$), 0.89 (d, J_{HH} = 6.80 Hz, 6H, CH*Me*$_2$), -7.33 (br s, 1H, Ru-*H*), -15.40 (s, 1H, Ru-*H*). [V. T. hydride data: ^{1}H NMR (d_8-toluene, 400 MHz, 234 K): δ -5.38 (br s, 1H, B-H_c), -7.08 (br s, 1H, B-H_b), -14.93 (s, 1H, Ru-H_a)]. ^{13}C{^{1}H} NMR (d_8-THF, 101 MHz): δ 222.6 (s, Ru-*C*), 205.5 (s, *C*O), 147.6 (s, *o*-*C*), 140.1 (s, *i*-*C*), 128.6 (s, *p*-*C*H), 125.1 (s, *m*-*C*H), 124.9 (s, *m*-*C*H), 124.7 (s, *m*-*C*H), 54.8 (s, N*C*H_2), 29.1 (s, *C*HMe$_2$), 29.0 (s, *C*HMe$_2$), 26.6 (s, CH*Me*$_2$), 24.0 (s, CH*Me*$_2$), 23.9 (s, CH*Me*$_2$). ^{11}B NMR (298 K, 96 MHz): δ 0.6 (br s). IR (cm^{-1}): 1922 (ν_{CO}), 2425, 2400 (ν_{B-H}). ESI-TOF MS: [M - BH_4 + H]$^+$ *m*/*z* = 911.5148 (theoretical *m*/*z* = 911.5150).

4.7.8 Catalysis method

The general procedure for catalytic ketone hydrogenation reactions involved the addition of the ketone substrate (0.3 M), the catalyst [Ru] (0.4 mol%) and degassed IPA to a 100 mL Parr 4842 bench top autoclave, which was subsequently charged to 10 atm H_2. The reaction mixture was heated with stirring at 348 K for 20 h. Following cooling to room temperature, volatiles were either removed under vacuum (for NMR analysis) or analysed directly by GC. Percentage conversions were determined by ^{1}H NMR spectroscopy in $CDCl_3$ or by a Fisons Instrument 8000 Series GC, fitted with a 30 m HP-Innowax column.

4.8 Synthesis of ruthenium H(OH) and cationic NHC complexes

4.8.1 Synthesis of Ru(IPr)$_2$(CO)H(OH) (6D)

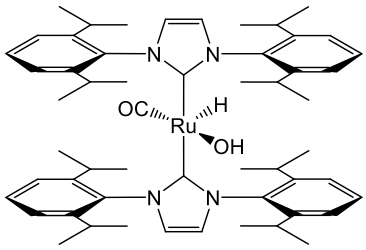

An ampoule fitted with a stirrer bar was charged with Ru(IPr)$_2$(CO)HCl (500 mg, 0.53 mmol) in a glove box. KOH (85%, 446 mg, 8.0 mmol) was then added under argon along with dry ethanol (5 mL) and the mixture was heated to 85 ˚C for 16 h in an oil bath. Upon cooling to ambient temperature, volatiles were removed *in vacuo* and the crude product extracted into a dry/degassed Schlenk tube through a glass filter cannula with benzene (3 x 5 mL). The presence of residual water from the reaction facilitated the addition of hexane (10 mL), vigorous stirring of the suspension and removal of the solvent *in vacuo* to aid its removal. This process was repeated twice and the remaining solid was taken up in benzene (5 mL) and passed under argon through a celite column using benzene as the eluent, removing any residual ionic salts. Concentration of the solvent gave the product as a yellow solid. Yield: 372 mg (82%). Recrystallisation was achieved from dissolution in toluene/hexane (1:3) and cooling to 5 ˚C. ^{1}H NMR (d_8-THF, 500 MHz): δ 7.26 (t, J_{HH} = 7.50 Hz, 4H, *p*-C*H*), 7.06-7.01 (m, 8H, *m*-C*H*), 6.92 (s, 4H, NC*H*), 2.85 (sept, J_{HH} = 7.00 Hz, 4H, C*H*Me$_2$), 2.80 (sept, J_{HH} = 7.00 Hz, 4H, C*H*Me$_2$), 0.98 (d, J_{HH} = 6.50 Hz, 12H, CH*Me*$_2$), 0.96 (d, J_{HH} = 6.50 Hz, 12H, CH*Me*$_2$), 0.91 (d, J_{HH} = 6.50 Hz, 12H,

CH*Me*$_2$), 0.88 (d, J_{HH} = 6.50 Hz, 12H, CH*Me*$_2$), -23.03 (s, 1H, Ru-*H*). $^{13}C\{^1H\}$ NMR (d_8-THF, 126 MHz): δ 206.0 (s, *C*O), 198.1 (s, Ru-*C*), 146.9 (s, *o*-*C*), 138.5 (s, *i*-*C*), 129.2 (s, *p*-*C*H), 124.1 (s, N*C*H), 124.0 (s, *m*-*C*H), 123.9 (s, *m*-*C*H), 29.1 (s, *C*HMe$_2$), 29.0 (s, *C*HMe$_2$), 26.0 (s, CH*Me*$_2$), 25.9 (s, CH*Me*$_2$), 23.4 (s, CH*Me*$_2$), 23.0 (s, CH*Me*$_2$). IR (cm^{-1}): 1863 (ν_{CO}). Anal. calcd for $C_{55}H_{74}N_4O_2Ru$,%: C, 71.47; H, 8.07; N, 6.06. Found,%: C, 71.21; H, 8.19; N, 6.04.

4.8.2 Synthesis of $[Ru(IPr)_2(CO)H(OH_2)]^+BF_4^-$ (6E)

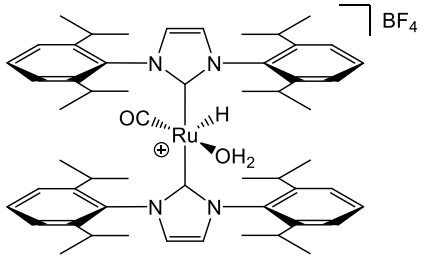

$Ru(IPr)_2(CO)H(OH)$ (100 mg, 0.11 mmol) was dissolved in THF (2 mL) in an ampoule fitted with a J. Youngs valve. $HBF_4{\cdot}OEt_2$ (18 μL, 0.13 mmol) was added slowly via syringe to the solution which was then stirred for 10 min at room temperature. The mixture was reduced *in vacuo* and washed with hexane (3 x 3 mL) to give the product as a pale yellow solid. Formation of X-ray quality crystals was achieved via dissolution in minimal THF and layering with hexane. Yield: 79 mg (73%). ^1H NMR (d_8-THF, 500 MHz): δ 7.41 (t, J_{HH} = 7.50 Hz, 4H, *p*-C*H*), 7.22 (s, 4H, NC*H*), 7.19 (d, J_{HH} = 7.50 Hz, 4H, *m*-C*H*), 7.16 (d, J_{HH} = 7.50 Hz, 4H, *m*-C*H*), 4.10 (s (br), 2H, H_2O), 2.67 (sept, J_{HH} = 6.50 Hz, 4H, C*H*Me$_2$), 2.55 (sept, J_{HH} = 6.50 Hz, 4H, C*H*Me$_2$), 1.01-0.98 (m, 36H, CH*Me*$_2$), 0.86 (d, J_{HH} = 6.50 Hz, 12H, CH*Me*$_2$), -24.93 (s, 1H, Ru-*H*). $^{13}C\{^1H\}$ NMR (d_8-THF, 126 MHz): δ 204.3 (s, *C*O), 190.4 (s, Ru-*C*), 146.8 (s, *o*-*C*), 137.0 (s, *i*-*C*), 130.5 (s, *p*-*C*H), 126.2 (s, N*C*H), 124.9 (s, *m*-*C*H), 124.8 (s, *m*-*C*H), 29.1 (s, *C*HMe$_2$), 26.1 (s, CH*Me*$_2$), 25.9 (s, CH*Me*$_2$), 23.2 (s, CH*Me*$_2$), 23.0 (s, CH*Me*$_2$). $^{19}F\{^1H\}$ NMR (d_8-THF, 471 MHz): δ -151.47. IR (cm^{-1}): 1923 (ν_{CO}). Anal. calcd for $C_{55}H_{75}N_4O_2RuBF_4$,%: C, 65.27; H, 7.47; N, 5.54. Found,%: C, 65.27; H, 7.35; N, 5.35.

4.8.3 Synthesis of [Ru(IPr)(η^6-C_6H_6)(CO)H]$^+BF_4^-$ (6F)

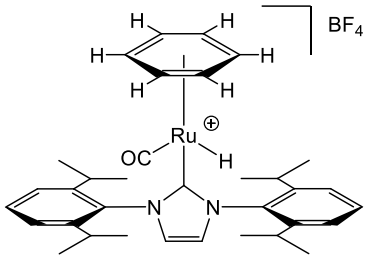

Two methods exist for the synthesis of this compound depending on the starting materials. Workup is the same in both cases. *From Ru(IPr)$_2$(CO)H(OH)*: An ampoule fitted with a J. Youngs PTFE tap and a stirrer bar was charged with Ru(IPr)$_2$(CO)H(OH) (220 mg, 0.22 mmol) and benzene (3 mL), to which $HBF_4{\cdot}OEt_2$ (65 μL, 0.48 mmol) was then slowly added at room temperature with stirring for 1 h. Removal of the volatiles *in vacuo* and drying of the residue for 30 min to remove displaced water from the [Ru(IPr)$_2$(CO)H(OH$_2$)]$^+BF_4^-$ intermediate preceded the addition of fresh benzene (3 mL) and $HBF_4{\cdot}OEt_2$ (33 μL, 0.24 mmol) with stirring for an additional 10 min. At this point the solution became darker brown in colour, with a dark precipitate present. *From [Ru(IPr)$_2$(CO)H(OH$_2$)]$^+BF_4^-$*: [Ru(IPr)$_2$(CO)H(OH$_2$)]$^+BF_4^-$ (10 mg, 0.01 mmol) was added to an NMR tube fitted with a J. Youngs PTFE valve. Benzene (1 mL) and $HBF_4{\cdot}OEt_2$ (2 μL, 0.012 mmol) were then added and the reaction mixture was shaken for 10 min. The formation of water as a by-product of this reaction facilitated the removal of all volatiles from the tube *in vacuo* and the addition of fresh benzene (1 mL) and $HBF_4{\cdot}OEt_2$ (2 μL, 0.012 mmol) to give complete reaction. *Workup*: The solution was reduced *in vacuo* and extracted in benzene (8 x 5 mL) through a glass filter cannula from residual imidazolium salts. The solution was concentrated and washed with diethyl ether (3 x 5 mL) and hexane (3 x 5 mL) to give a pale brown solid. Yield: 99 mg (68%). Small X-ray quality crystals were grown from a saturated dichloromethane solution and layered with hexane. ^{1}H NMR (CD_2Cl_2, 500 MHz): δ 7.67 (t, J_{HH} = 7.50 Hz, 2H, *p*-C*H*), 7.46 (d, J_{HH} = 7.50 Hz, 2H, *m*-C*H*), 7.45 (d, J_{HH} = 7.50 Hz, 2H, *m*-C*H*), 7.31 (s, 2H, NC*H*), 5.76 (s, 6H, C_6H_6), 2.48 (sept, J_{HH} = 6.50 Hz, 2H, C*H*Me$_2$), 2.35 (sept, J_{HH} = 6.50 Hz, 2H, C*H*Me$_2$), 1.39-1.36 (m, 12H, CH*Me*$_2$), 1.20 (d, J_{HH} = 6.50 Hz, 6H, CH*Me*$_2$), 1.10 (d, J_{HH} = 6.50 Hz, 6H, CH*Me*$_2$), -9.64 (s, 1H, Ru-*H* (η^6-C_6H_6 product)) or -9.65 (s, 1H, Ru-*H* (η^6-C_6D_6 product)). ^{13}C{^{1}H} NMR (CD_2Cl_2, 126 MHz): δ 196.1 (s, *C*O), 172.7 (s, Ru-*C*), 146.1 (s, *o*-*C*), 146.0 (s, *o*-*C*), 136.5 (s, *i*-*C*), 131.8 (s, *p*-*C*H), 126.4 (s, NC*H*), 125.1

(s, *m*-*C*H), 125.0 (s, *m*-*C*H), 98.5 (s, C_6H_6), or 98.1 (t, C_6D_6), 29.5 (s, *C*HMe$_2$), 29.1 (s, *C*HMe$_2$), 26.4 (s, CH*Me*$_2$), 25.7 (s, CH*Me*$_2$), 22.7 (s, CH*Me*$_2$), 22.2 (s, CH*Me*$_2$). $^{19}F\{^1H\}$ NMR (CD_2Cl_2, 471 MHz): δ -152.53. IR (cm^{-1}): 1986 (ν_{CO}). ESI-TOF MS: $[M - C_6H_6]^+$ m/z = 519.1966 (theoretical m/z = 519.1951).

4.8.4 Synthesis of $[Ru_2(IPr)_2(CO)_2(OH_2)_2(\mu\text{-}Cl)_3]^+BF_4^-$

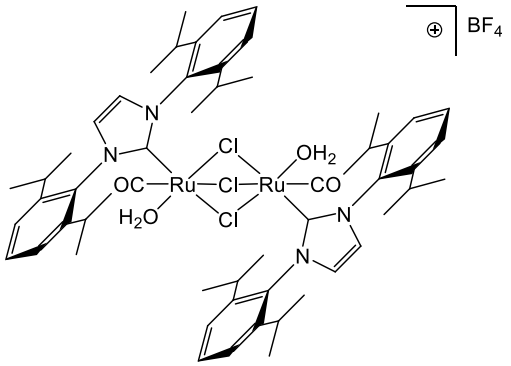

$Ru(IPr)_2(CO)HCl$ (200 mg, 0.21 mmol) was dissolved in C_6H_6 (5 mL) in an ampoule fitted with a J. Youngs valve. $HBF_4{\cdot}OEt_2$ (87 μL, 0.64 mmol) was added via syringe to the solution, with stirring for 10 min at room temperature. The mixture was reduced *in vacuo*, extracted in benzene (6 x 5 mL), reduced again *in vacuo* and then extracted in diethyl ether (4 x 5 mL). Removal of the solvent and washing with hexane (3 x 3 mL) yielded the product as a yellow solid. Formation of X-ray quality crystals was achieved via dissolution in minimal toluene and layering with hexane. Yield: 43 mg (32%). ^1H NMR (CD_2Cl_2, 500 MHz): δ 7.42 (t, J_{HH} = 7.50 Hz, 4H, *p*-C*H*), 7.17 (m, 8H, *m*-C*H*), 6.95 (s, 4H, NC*H*), 2.89 (sept, J_{HH} = 6.50 Hz, 4H, C*H*Me$_2$), 2.70 (sept, J_{HH} = 6.50 Hz, 4H, C*H*Me$_2$), 1.36 (d, J_{HH} = 6.50 Hz, 12H, CH*Me*$_2$), 1.31 (d, J_{HH} = 6.50 Hz, 12H, CH*Me*$_2$), 1.06 (m, 24H, CH*Me*$_2$). $^{13}C\{^1H\}$ NMR (CD_2Cl_2, 126 MHz): δ 200.3 (s, *C*O), 161.7 (s, Ru-*C*), 146.3 (s, *o*-*C*), 145.3 (s, *o*-*C*), 135.4 (s, *i*-*C*), 131.2 (s, *p*-*C*H), 127.1 (s, N*C*H), 124.8 (s, *m*-*C*H), 124.6 (s, *m*-*C*H), 29.0 (s, *C*HMe$_2$), 28.9 (s, *C*HMe$_2$), 26.1 (s, CH*Me*$_2$), 25.9 (s, CH*Me*$_2$), 23.1 (s, CH*Me*$_2$), 22.9 (s, CH*Me*$_2$).

4.9 References

1 Sheldrick, G. M., *Acta Crystallogr. Sect. A* **1990**, *46*, 467-473.

2 Jafarpour, L.; Stevens, E. D.; Nolan, S. P., *J. Organomet. Chem.* **2000**, *606*, 49-54.

3 Grasa, G. A.; Viciu, M. S.; Huang, J.; Nolan, S. P., *J. Org. Chem.* **2001**, *66*, 7729-7737.

4 Bedford, R. B.; Betham, M.; Blake, M. E.; Frost, R. M.; Horton, P. N.; Hursthouse, M. B.; Lopez-Nicolas, R. M., *Dalton Trans.* **2005**, 2774-2779.

5 Arduengo, A. J.; Krafczyk, R.; Schmutzler, R., *Tetrahedron* **1999**, *55*, 14523-14534.

6 Arduengo, A. J., *Patent: 5,077,414* **1991**.

7 Arduengo, A. J.; Harlow, R. L.; Kline, M., *J. Am. Chem. Soc.* **1991**, *113*, 361-363.

8 Kuhn, N.; Kratz, T., *Synthesis* **1993**, 561-562.

9 Harris, A. D.; Robinson, S. D., *Inorg. Chim. Acta.* **1980**, *42*, 25-31.

10 Ahmad, N.; Levison, J. J.; Robinson, S. D.; Uttlky, M. F.; Wonchoba, E. R.; Parshall, G. W., *Inorg. Synth.* **1974**, *15*, 45-64.

Appendices

Appendix 1 Crystallographic data for $Ru_3(al^tBu_2)(CO)_{11}$ (1A)

Identification code	k06mkw22
Empirical formula	C22 H20 N2 O11 Ru3
Formula weight	791.61
Temperature	150(2) K
Wavelength	0.71073 Å
Crystal system	Monoclinic
Space group	P21/n
Unit cell dimensions	a = 12.9520(2)Å α = 90°
	b = 13.4390(2)Å β = 106.861(1)°
	c = 16.7480(2)Å γ = 90°
Volume	2789.87(7) $Å^3$
Z	4
Density (calculated)	1.885 Mg/m^3
Absorption coefficient	1.661 mm^{-1}
F(000)	1544
Crystal size	0.35 x 0.30 x 0.30 mm
Theta range for data collection	3.62 to 30.04°.
Index ranges	-18<=h<=18; -18<=k<=16; -23<=l<=23
Reflections collected	51298
Independent reflections	8154 [R(int) = 0.0565]
Reflections observed (>2σ)	6548
Data Completeness	0.997
Absorption correction	Semi-empirical from equivalents
Max. and min. transmission	0.80 and 0.66
Refinement method	Full-matrix least-squares on F^2
Data / restraints / parameters	8154 / 0 / 354
Goodness-of-fit on F^2	1.081
Final R indices [I>2σ(I)]	R^1 = 0.0312 wR_2 = 0.0677
R indices (all data)	R^1 = 0.0466 wR_2 = 0.0742
Largest diff. peak and hole	1.765 and -1.000 $eÅ^{-3}$

Ru(1)-C(2)	1.869(3)	Ru(1)-C(3)	1.918(3)
Ru(1)-C(1)	1.937(3)	Ru(1)-C(12)	2.151(2)
Ru(1)-Ru(3)	2.8456(3)	Ru(1)-Ru(2)	2.8835(3)
Ru(2)-C(5)	1.898(3)	Ru(2)-C(6)	1.929(3)
Ru(2)-C(7)	1.940(3)	Ru(2)-C(4)	1.941(3)
Ru(2)-Ru(3)	2.8504(3)	Ru(3)-C(11)	1.913(3)
Ru(3)-C(9)	1.928(3)	Ru(3)-C(8)	1.928(3)
Ru(3)-C(10)	1.946(3)	O(1)-C(1)	1.133(3)
O(2)-C(2)	1.139(3)	O(3)-C(3)	1.144(3)
O(4)-C(4)	1.142(4)	O(5)-C(5)	1.137(4)
O(6)-C(6)	1.128(4)	O(7)-C(7)	1.142(4)
O(8)-C(8)	1.140(3)	O(9)-C(9)	1.130(3)
O(10)-C(10)	1.137(3)	O(11)-C(11)	1.145(4)
N(1)-C(14)	1.347(3)	N(1)-C(12)	1.416(3)
N(1)-C(15)	1.507(3)	N(2)-C(14)	1.315(3)

N(2)-C(13)	1.392(3)	N(2)-C(19)	1.502(3)
C(12)-C(13)	1.365(3)	C(15)-C(16)	1.525(4)
C(15)-C(18)	1.526(4)	C(15)-C(17)	1.532(4)
C(19)-C(21)	1.521(4)	C(19)-C(22)	1.522(4)
C(19)-C(20)	1.531(4)		
C(2)-Ru(1)-C(3)	92.93(12)	C(2)-Ru(1)-C(1)	92.33(13)
C(3)-Ru(1)-C(1)	171.70(12)	C(2)-Ru(1)-C(12)	108.12(10)
C(3)-Ru(1)-C(12)	85.10(10)	C(1)-Ru(1)-C(12)	87.17(10)
C(2)-Ru(1)-Ru(3)	88.87(8)	C(3)-Ru(1)-Ru(3)	95.32(7)
C(1)-Ru(1)-Ru(3)	91.20(8)	C(12)-Ru(1)-Ru(3)	162.97(7)
C(2)-Ru(1)-Ru(2)	145.63(8)	C(3)-Ru(1)-Ru(2)	77.89(8)
C(1)-Ru(1)-Ru(2)	101.14(9)	C(12)-Ru(1)-Ru(2)	104.03(7)
Ru(3)-Ru(1)-Ru(2)	59.670(7)	C(5)-Ru(2)-C(6)	101.95(13)
C(5)-Ru(2)-C(7)	91.07(13)	C(6)-Ru(2)-C(7)	94.93(14)
C(5)-Ru(2)-C(4)	89.33(12)	C(6)-Ru(2)-C(4)	95.36(14)
C(7)-Ru(2)-C(4)	169.38(13)	C(5)-Ru(2)-Ru(3)	166.34(10)
C(6)-Ru(2)-Ru(3)	90.53(9)	C(7)-Ru(2)-Ru(3)	82.25(9)
C(4)-Ru(2)-Ru(3)	95.07(8)	C(5)-Ru(2)-Ru(1)	109.89(9)
C(6)-Ru(2)-Ru(1)	145.77(9)	C(7)-Ru(2)-Ru(1)	96.69(9)
C(4)-Ru(2)-Ru(1)	73.24(9)	Ru(3)-Ru(2)-Ru(1)	59.505(7)
C(11)-Ru(3)-C(9)	105.23(12)	C(11)-Ru(3)-C(8)	92.86(12)
C(9)-Ru(3)-C(8)	91.36(12)	C(11)-Ru(3)-C(10)	91.43(12)
C(9)-Ru(3)-C(10)	94.86(12)	C(8)-Ru(3)-C(10)	171.25(11)
C(11)-Ru(3)-Ru(1)	97.14(9)	C(9)-Ru(3)-Ru(1)	157.57(9)
C(8)-Ru(3)-Ru(1)	89.09(8)	C(10)-Ru(3)-Ru(1)	82.81(8)
C(11)-Ru(3)-Ru(2)	156.43(9)	C(9)-Ru(3)-Ru(2)	97.24(9)
C(8)-Ru(3)-Ru(2)	79.40(8)	C(10)-Ru(3)-Ru(2)	93.70(9)
Ru(1)-Ru(3)-Ru(2)	60.825(7)	C(14)-N(1)-C(12)	109.8(2)
C(14)-N(1)-C(15)	121.7(2)	C(12)-N(1)-C(15)	128.35(19)
C(14)-N(2)-C(13)	107.8(2)	C(14)-N(2)-C(19)	127.6(2)
C(13)-N(2)-C(19)	124.6(2)	O(1)-C(1)-Ru(1)	173.6(3)
O(2)-C(2)-Ru(1)	176.0(2)	O(3)-C(3)-Ru(1)	171.6(2)
O(4)-C(4)-Ru(2)	169.3(3)	O(5)-C(5)-Ru(2)	178.2(3)
O(6)-C(6)-Ru(2)	178.2(3)	O(7)-C(7)-Ru(2)	172.8(3)
O(8)-C(8)-Ru(3)	174.7(2)	O(9)-C(9)-Ru(3)	177.9(3)
O(10)-C(10)-Ru(3)	175.3(3)	O(11)-C(11)-Ru(3)	178.3(3)
C(13)-C(12)-N(1)	103.3(2)	C(13)-C(12)-Ru(1)	120.83(18)
N(1)-C(12)-Ru(1)	135.90(17)	C(12)-C(13)-N(2)	110.0(2)
N(2)-C(14)-N(1)	109.0(2)	N(1)-C(15)-C(16)	107.6(2)
N(1)-C(15)-C(18)	110.1(2)	C(16)-C(15)-C(18)	109.0(2)
N(1)-C(15)-C(17)	109.0(2)	C(16)-C(15)-C(17)	113.6(2)
C(18)-C(15)-C(17)	107.5(2)	N(2)-C(19)-C(21)	107.7(2)
N(2)-C(19)-C(22)	109.6(2)	C(21)-C(19)-C(22)	110.9(2)
N(2)-C(19)-C(20)	107.4(2)	C(21)-C(19)-C(20)	111.2(3)
C(22)-C(19)-C(20)	110.0(2)		

Appendix 2 Crystallographic data for $Ru_3(alAd_2)(CO)_{11}$ (2A)

Identification code	k07mkw32
Empirical formula	C38 H40 N2 O12 Ru3
Formula weight	1019.93
Temperature	150(2) K
Wavelength	0.71073 Å
Crystal system	Monoclinic
Space group	$P2_1/c$
Unit cell dimensions	a = 14.7010(1)Å α = 90°
	b = 18.5170(2)Å β = 105.924(1)°
	c = 15.11500(1)Å γ = 90°
Volume	3956.69(6) $Å^3$
Z	4
Density (calculated)	1.712 Mg/m^3
Absorption coefficient	1.194 mm^{-1}
F(000)	2040
Crystal size	0.13 x 0.13 x 0.12 mm
Theta range for data collection	2.99 to 27.48°
Index ranges	-19<=h<=19; -24<=k<=24; -19<=l<=19
Reflections collected	79718
Independent reflections	9050 [R(int) = 0.0440]
Reflections observed (>2σ)	7727
Data Completeness	0.998
Absorption correction	Semi-empirical from equivalents
Max. and min. transmission	0.89 and 0.85
Refinement method	Full-matrix least-squares on F^2
Data / restraints / parameters	9050 / 0 / 496
Goodness-of-fit on F^2	1.078
Final R indices [I>2σ(I)]	R^1 = 0.0290 wR_2 = 0.0650
R indices (all data)	R^1 = 0.0386 wR_2 = 0.0694
Largest diff. peak and hole	0.899 and -0.782 $eÅ^{-3}$

Ru(1)-C(2)	1.862(3)	Ru(2)-C(4)	1.912(3)
Ru(1)-C(1)	1.920(3)	Ru(2)-C(7)	1.928(3)
Ru(1)-C(3)	1.948(3)	Ru(2)-C(6)	1.933(3)
Ru(1)-C(13)	2.150(2)	Ru(2)-C(5)	1.944(3)
Ru(1)-Ru(2)	2.8384(3)	Ru(2)-Ru(3)	2.8613(3)
Ru(1)-Ru(3)	2.8989(3)	Ru(3)-C(10)	1.905(3)
Ru(3)-C(11)	1.936(3)	Ru(3)-C(9)	1.923(3)
Ru(3)-C(8)	1.949(3)	N(1)-C(12)	1.340(3)
O(1)-C(1)	1.141(3)	N(1)-C(13)	1.415(3)
O(2)-C(2)	1.149(3)	N(1)-C(15)	1.502(3)
O(3)-C(3)	1.133(3)	N(2)-C(12)	1.325(3)
O(4)-C(4)	1.138(3)	N(2)-C(14)	1.386(3)
O(5)-C(5)	1.144(3)	N(2)-C(25)	1.486(3)
O(6)-C(6)	1.133(4)	C(13)-C(14)	1.365(3)
O(7)-C(7)	1.142(4)	C(15)-C(24)	1.536(3)

O(8)-C(8)	1.143(4)	C(15)-C(16)	1.537(3)
O(9)-C(9)	1.134(4)	C(15)-C(22)	1.537(3)
O(10)-C(10)	1.137(3)	C(16)-C(17)	1.540(3)
O(11)-C(11)	1.151(3)	C(17)-C(23)	1.533(3)
O(12)-C(38)	1.409(4)	C(17)-C(18)	1.537(4)
O(12)-C(35)	1.417(4)	C(18)-C(19)	1.531(4)
C(26)-C(27)	1.534(3)	C(19)-C(20)	1.534(3)
C(27)-C(28)	1.530(4)	C(19)-C(24)	1.539(3)
C(27)-C(34)	1.531(4)	C(20)-C(21)	1.528(3)
C(28)-C(29)	1.532(4)	C(21)-C(23)	1.523(4)
C(29)-C(30)	1.526(4)	C(21)-C(22)	1.537(3)
C(29)-C(33)	1.535(3)	C(25)-C(32)	1.527(3)
C(30)-C(31)	1.521(4)	C(25)-C(33)	1.530(3)
C(31)-C(34)	1.534(4)	C(25)-C(26)	1.533(3)
C(31)-C(32)	1.540(3)	C(36)-C(37)	1.506(5)
C(35)-C(36)	1.515(5)	C(37)-C(38)	1.484(6)
C(2)-Ru(1)-C(1)	91.81(12)	C(6)-Ru(2)-C(5)	95.71(13)
C(2)-Ru(1)-C(3)	92.69(12)	C(4)-Ru(2)-Ru(1)	101.29(8)
C(1)-Ru(1)-C(3)	171.46(10)	C(7)-Ru(2)-Ru(1)	87.55(8)
C(2)-Ru(1)-C(13)	109.68(10)	C(6)-Ru(2)-Ru(1)	156.80(9)
C(1)-Ru(1)-C(13)	84.27(10)	C(5)-Ru(2)-Ru(1)	81.25(8)
C(3)-Ru(1)-C(13)	87.39(10)	C(4)-Ru(2)-Ru(3)	158.96(8)
C(2)-Ru(1)-Ru(2)	87.56(7)	C(7)-Ru(2)-Ru(3)	78.61(8)
C(1)-Ru(1)-Ru(2)	95.75(7)	C(6)-Ru(2)-Ru(3)	96.64(8)
C(3)-Ru(1)-Ru(2)	91.69(7)	C(5)-Ru(2)-Ru(3)	96.24(8)
C(13)-Ru(1)-Ru(2)	162.76(6)	Ru(1)-Ru(2)-Ru(3)	61.141(6)
C(2)-Ru(1)-Ru(3)	144.34(8)	C(10)-Ru(3)-C(9)	98.58(12)
C(1)-Ru(1)-Ru(3)	78.69(8)	C(10)-Ru(3)-C(11)	89.38(10)
C(3)-Ru(1)-Ru(3)	101.61(8)	C(9)-Ru(3)-C(11)	97.12(12)
C(13)-Ru(1)-Ru(3)	103.51(6)	C(10)-Ru(3)-C(8)	92.22(11)
Ru(2)-Ru(1)-Ru(3)	59.818(6)	C(9)-Ru(3)-C(8)	96.74(13)
C(4)-Ru(2)-C(7)	89.76(12)	C(11)-Ru(3)-C(8)	165.65(11)
C(4)-Ru(2)-C(6)	101.80(12)	C(10)-Ru(3)-Ru(2)	167.99(8)
C(7)-Ru(2)-C(6)	94.77(13)	C(9)-Ru(3)-Ru(2)	91.94(9)
C(4)-Ru(2)-C(5)	91.96(11)	C(11)-Ru(3)-Ru(2)	95.08(7)
C(7)-Ru(2)-C(5)	168.80(11)	C(8)-Ru(3)-Ru(2)	80.74(8)
O(1)-C(1)-Ru(1)	172.2(2)	C(10)-Ru(3)-Ru(1)	112.49(8)
O(2)-C(2)-Ru(1)	174.4(2)	C(9)-Ru(3)-Ru(1)	146.04(9)
O(3)-C(3)-Ru(1)	173.8(2)	C(11)-Ru(3)-Ru(1)	70.81(8)
O(4)-C(4)-Ru(2)	175.8(2)	C(8)-Ru(3)-Ru(1)	95.46(8)
O(5)-C(5)-Ru(2)	175.3(2)	Ru(2)-Ru(3)-Ru(1)	59.041(6)
O(6)-C(6)-Ru(2)	179.0(3)	C(38)-O(12)-C(35)	106.6(3)
O(7)-C(7)-Ru(2)	174.1(2)	C(12)-N(1)-C(13)	109.50(18)
O(8)-C(8)-Ru(3)	173.6(2)	C(12)-N(1)-C(15)	120.76(18)
O(9)-C(9)-Ru(3)	177.6(3)	C(13)-N(1)-C(15)	129.69(18)
O(10)-C(10)-Ru(3)	178.1(2)	C(12)-N(2)-C(14)	106.96(19)
O(11)-C(11)-Ru(3)	167.3(2)	C(12)-N(2)-C(25)	127.75(19)
N(2)-C(12)-N(1)	109.66(19)	C(14)-N(2)-C(25)	125.28(19)
C(14)-C(13)-N(1)	103.40(19)	C(24)-C(15)-C(16)	110.84(18)
C(14)-C(13)-Ru(1)	119.21(17)	N(1)-C(15)-C(22)	110.22(17)

N(1)-C(13)-Ru(1)	137.34(16)	C(24)-C(15)-C(22)	108.25(18)
C(13)-C(14)-N(2)	110.5(2)	C(16)-C(15)-C(22)	108.54(19)
N(1)-C(15)-C(24)	109.83(18)	C(15)-C(16)-C(17)	109.53(19)
N(1)-C(15)-C(16)	109.15(18)	C(23)-C(17)-C(18)	109.1(2)
N(2)-C(25)-C(32)	109.81(18)	C(23)-C(17)-C(16)	109.0(2)
N(2)-C(25)-C(33)	109.04(18)	C(18)-C(17)-C(16)	109.9(2)
C(32)-C(25)-C(33)	109.6(2)	C(19)-C(18)-C(17)	109.82(19)
N(2)-C(25)-C(26)	108.73(18)	C(18)-C(19)-C(20)	109.2(2)
C(32)-C(25)-C(26)	109.55(19)	C(18)-C(19)-C(24)	109.7(2)
C(33)-C(25)-C(26)	110.14(19)	C(20)-C(19)-C(24)	109.5(2)
C(25)-C(26)-C(27)	109.1(2)	C(21)-C(20)-C(19)	109.10(19)
C(28)-C(27)-C(34)	109.9(2)	C(23)-C(21)-C(20)	109.9(2)
C(28)-C(27)-C(26)	109.4(2)	C(23)-C(21)-C(22)	109.9(2)
C(34)-C(27)-C(26)	109.1(2)	C(20)-C(21)-C(22)	109.4(2)
C(27)-C(28)-C(29)	109.8(2)	C(15)-C(22)-C(21)	109.83(18)
C(30)-C(29)-C(28)	109.9(2)	C(21)-C(23)-C(17)	109.4(2)
C(30)-C(29)-C(33)	108.8(2)	C(15)-C(24)-C(19)	109.49(19)
C(28)-C(29)-C(33)	109.1(2)	C(25)-C(32)-C(31)	108.95(19)
C(31)-C(30)-C(29)	110.0(2)	C(25)-C(33)-C(29)	109.4(2)
C(30)-C(31)-C(34)	110.0(2)	C(27)-C(34)-C(31)	109.4(2)
C(30)-C(31)-C(32)	109.5(2)	O(12)-C(35)-C(36)	107.0(3)
C(34)-C(31)-C(32)	108.9(2)	C(37)-C(36)-C(35)	103.3(3)
O(12)-C(38)-C(37)	104.6(3)	C(38)-C(37)-C(36)	104.9(3)

Appendix 3 Crystallographic data for $Os_3(alAd_2)(CO)_{11}$ (2C)

Identification code	k08mkw6
Empirical formula	C34 H32 N2 O11 Os3
Formula weight	1215.22
Temperature	150(2) K
Wavelength	0.71073 Å
Crystal system	Orthorhombic
Space group	P212121
Unit cell dimensions	a = 11.8360(2)Å α = 90°
	b = 12.6320(2)Å β = 90°
	c = 22.3790(4)Å γ = 90°
Volume	3345.94(10) $Å^3$
Z	4
Density (calculated)	2.412 Mg/m^3
Absorption coefficient	11.430 mm^{-1}
F(000)	2264
Crystal size	0.07 x 0.05 x 0.05 mm
Theta range for data collection	3.70 to 27.50°
Index ranges	-15<=h<=15; -16<=k<=16; -28<=l<=29
Reflections collected	7652
Independent reflections	7652 [R(int) = 0.0000]
Reflections observed (>2σ)	6440
Data Completeness	0.956

Absorption correction	None
Refinement method	Full-matrix least-squares on F^2
Data / restraints / parameters	7652 / 0 / 452
Goodness-of-fit on F2	1.032
Final R indices [I>2σ(I)]	R^1 = 0.0454 wR_2 = 0.1015
R indices (all data)	R^1 = 0.0620 wR_2 = 0.1090
Absolute structure parameter	0.499(17)
Largest diff. peak and hole	2.266 and -1.784 e.Å^{-3}

Os(1)-C(2)	1.867(12)	Os(1)-C(1)	1.934(13)
Os(1)-C(3)	1.949(12)	Os(1)-C(12)	2.128(12)
Os(1)-Os(3)	2.8831(8)	Os(1)-Os(2)	2.9051(8)
Os(2)-C(6)	1.886(15)	Os(2)-C(7)	1.926(13)
Os(2)-C(5)	1.931(14)	Os(2)-C(4)	1.949(13)
Os(2)-Os(3)	2.8911(5)	Os(3)-C(9)	1.890(13)
Os(3)-C(10)	1.910(14)	Os(3)-C(8)	1.946(13)
Os(3)-C(11)	1.950(13)	O(1)-C(1)	1.137(15)
O(2)-C(2)	1.168(15)	O(3)-C(3)	1.133(15)
O(4)-C(4)	1.133(15)	O(5)-C(5)	1.128(16)
O(6)-C(6)	1.158(17)	O(7)-C(7)	1.166(17)
O(8)-C(8)	1.143(16)	O(9)-C(9)	1.163(15)
O(10)-C(10)	1.130(17)	O(11)-C(11)	1.135(16)
N(1)-C(14)	1.340(14)	N(1)-C(12)	1.435(16)
N(1)-C(15)	1.529(14)	N(2)-C(14)	1.349(15)
N(2)-C(13)	1.375(16)	N(2)-C(25)	1.511(15)
C(12)-C(13)	1.371(16)	C(15)-C(16)	1.523(19)
C(15)-C(21)	1.546(16)	C(15)-C(20)	1.550(16)
C(16)-C(17)	1.579(19)	C(17)-C(23)	1.506(17)
C(17)-C(18)	1.542(16)	C(18)-C(19)	1.507(18)
C(19)-C(20)	1.537(16)	C(19)-C(24)	1.571(17)
C(21)-C(22)	1.539(18)	C(22)-C(24)	1.526(18)
C(22)-C(23)	1.538(19)	C(25)-C(26)	1.52(2)
C(25)-C(31)	1.53(2)	C(25)-C(30)	1.534(17)
C(26)-C(27)	1.573(19)	C(27)-C(28)	1.51(3)
C(27)-C(33)	1.52(3)	C(28)-C(29)	1.51(3)
C(29)-C(34)	1.51(2)	C(29)-C(30)	1.57(2)
C(31)-C(32)	1.572(17)	C(32)-C(33)	1.49(2)
C(32)-C(34)	1.521(18)		
C(2)-Os(1)-C(1)	93.0(5)	C(2)-Os(1)-C(3)	93.2(6)
C(1)-Os(1)-C(3)	170.4(6)	C(2)-Os(1)-C(12)	107.7(5)
C(1)-Os(1)-C(12)	88.5(5)	C(3)-Os(1)-C(12)	82.6(6)
C(2)-Os(1)-Os(3)	91.4(4)	C(1)-Os(1)-Os(3)	97.8(4)
C(3)-Os(1)-Os(3)	89.4(4)	C(12)-Os(1)-Os(3)	159.6(3)
C(2)-Os(1)-Os(2)	147.9(4)	C(1)-Os(1)-Os(2)	78.4(4)
C(3)-Os(1)-Os(2)	100.0(4)	C(12)-Os(1)-Os(2)	102.9(3)
Os(3)-Os(1)-Os(2)	59.930(13)	C(6)-Os(2)-C(7)	97.4(6)
C(6)-Os(2)-C(5)	103.7(6)	C(7)-Os(2)-C(5)	93.8(6)
C(6)-Os(2)-C(4)	87.3(6)	C(7)-Os(2)-C(4)	172.3(6)
C(5)-Os(2)-C(4)	90.9(5)	C(6)-Os(2)-Os(3)	101.7(4)
C(7)-Os(2)-Os(3)	90.1(4)	C(5)-Os(2)-Os(3)	153.6(5)

C(4)-Os(2)-Os(3)	83.0(4)	C(6)-Os(2)-Os(1)	160.9(4)
C(7)-Os(2)-Os(1)	79.6(4)	C(5)-Os(2)-Os(1)	95.4(4)
C(4)-Os(2)-Os(1)	93.9(4)	Os(3)-Os(2)-Os(1)	59.66(2)
C(9)-Os(3)-C(10)	99.4(7)	C(9)-Os(3)-C(8)	88.3(6)
C(10)-Os(3)-C(8)	97.8(7)	C(9)-Os(3)-C(11)	91.2(6)
C(10)-Os(3)-C(11)	91.7(7)	C(8)-Os(3)-C(11)	170.4(7)
C(9)-Os(3)-Os(1)	102.5(4)	C(10)-Os(3)-Os(1)	157.9(5)
C(8)-Os(3)-Os(1)	79.6(4)	C(11)-Os(3)-Os(1)	91.2(4)
C(9)-Os(3)-Os(2)	162.6(4)	C(10)-Os(3)-Os(2)	97.9(5)
C(8)-Os(3)-Os(2)	91.3(4)	C(11)-Os(3)-Os(2)	86.4(4)
Os(1)-Os(3)-Os(2)	60.41(2)	C(14)-N(1)-C(12)	111.8(9)
C(14)-N(1)-C(15)	118.2(10)	C(12)-N(1)-C(15)	130.0(10)
C(14)-N(2)-C(13)	108.0(9)	C(14)-N(2)-C(25)	124.6(10)
C(13)-N(2)-C(25)	127.3(10)	O(1)-C(1)-Os(1)	172.9(12)
O(2)-C(2)-Os(1)	175.0(12)	O(3)-C(3)-Os(1)	174.8(12)
O(4)-C(4)-Os(2)	175.7(11)	O(5)-C(5)-Os(2)	177.3(14)
O(6)-C(6)-Os(2)	176.7(14)	O(7)-C(7)-Os(2)	174.3(13)
O(8)-C(8)-Os(3)	175.3(13)	O(9)-C(9)-Os(3)	178.4(12)
O(10)-C(10)-Os(3)	178.5(16)	O(11)-C(11)-Os(3)	174.3(13)
C(13)-C(12)-N(1)	101.4(10)	C(13)-C(12)-Os(1)	121.8(9)
N(1)-C(12)-Os(1)	136.6(8)	C(12)-C(13)-N(2)	111.6(11)
N(1)-C(14)-N(2)	107.2(10)	C(16)-C(15)-N(1)	108.8(10)
C(16)-C(15)-C(21)	108.7(11)	N(1)-C(15)-C(21)	109.3(9)
C(16)-C(15)-C(20)	110.0(10)	N(1)-C(15)-C(20)	109.4(10)
C(21)-C(15)-C(20)	110.5(9)	C(15)-C(16)-C(17)	109.7(11)
C(23)-C(17)-C(18)	109.7(10)	C(23)-C(17)-C(16)	107.2(10)
C(18)-C(17)-C(16)	110.1(11)	C(19)-C(18)-C(17)	108.7(10)
C(18)-C(19)-C(20)	113.1(10)	C(18)-C(19)-C(24)	109.6(11)
C(20)-C(19)-C(24)	107.6(10)	C(19)-C(20)-C(15)	108.5(10)
C(22)-C(21)-C(15)	108.3(9)	C(24)-C(22)-C(23)	108.9(11)
C(24)-C(22)-C(21)	110.3(11)	C(23)-C(22)-C(21)	109.0(11)
C(17)-C(23)-C(22)	111.2(12)	C(22)-C(24)-C(19)	109.1(10)
N(2)-C(25)-C(26)	108.3(10)	N(2)-C(25)-C(31)	110.8(11)
C(26)-C(25)-C(31)	111.2(12)	N(2)-C(25)-C(30)	107.7(10)
C(26)-C(25)-C(30)	109.5(11)	C(31)-C(25)-C(30)	109.1(11)
C(25)-C(26)-C(27)	107.4(11)	C(28)-C(27)-C(33)	113.4(14)
C(28)-C(27)-C(26)	108.1(13)	C(33)-C(27)-C(26)	107.6(14)
C(27)-C(28)-C(29)	109.7(13)	C(28)-C(29)-C(34)	112.8(17)
C(28)-C(29)-C(30)	106.8(11)	C(34)-C(29)-C(30)	109.0(11)
C(25)-C(30)-C(29)	108.5(11)	C(25)-C(31)-C(32)	108.8(11)
C(33)-C(32)-C(34)	113.4(12)	C(33)-C(32)-C(31)	107.8(12)
C(34)-C(32)-C(31)	106.9(11)	C(32)-C(33)-C(27)	110.2(14)
C(29)-C(34)-C(32)	109.5(11)		

Appendix 4 Crystallographic data for $Ru_3(\mu\text{-}H)(al^tBu_2)'(CO)_9$ (1B)

Identification code	k07mkw9
Empirical formula	C20 H20 N2 O9 Ru3

Formula weight	735.59
Temperature	150(2) K
Wavelength	0.71073 Å
Crystal system	Orthorhombic
Space group	Pbca
Unit cell dimensions	a = 16.8740(2)Å α = 90°
	b = 15.4110(2)Å β = 90°
	c = 19.4920(2)Å γ = 90°
Volume	5068.80(10)Å^3
Z	8
Density (calculated)	1.928 Mg/m^3
Absorption coefficient	1.814 mm^{-1}
F(000)	2864
Crystal size	0.20 x 0.15 x 0.12 mm
Theta range for data collection	3.58 to 27.47°
Index ranges	-21<=h<=21, -19<=k<=20, -25<=l<=23
Reflections collected	61138
Independent reflections	5788 [R(int) = 0.0619]
Max. and min. transmission	0.70 and 0.63
Data Completeness	0.996
Absorption correction	Semi-empirical from equivalents
Refinement method	Full-matrix least-squares on F^2
Data / restraints / parameters	5788 / 1 / 318
Goodness-of-fit on F2	1.131
Final R indices [I>2σ(I)]	R^1 = 0.0281, wR_2 = 0.0615
R indices (all data)	R^1 = 0.0359, wR_2 = 0.0654
Largest diff. peak and hole	0.765 and -0.924 e.Å^{-3}

Ru(1)-C(2)	1.887(3)	Ru(2)-C(10)	2.102(3)
Ru(1)-C(3)	1.907(3)	Ru(2)-Ru(3)	2.9739(3)
Ru(1)-C(1)	1.908(3)	Ru(3)-H(1)	1.76(2)
Ru(1)-C(11)	2.324(3)	Ru(3)-C(8)	1.902(3)
Ru(1)-C(10)	2.339(2)	Ru(3)-C(7)	1.931(3)
Ru(1)-Ru(2)	2.7183(3)	Ru(3)-C(9)	1.932(3)
Ru(1)-Ru(3)	2.7235(3)	Ru(3)-C(11)	2.109(3)
Ru(2)-H(1)	1.77(2)	O(1)-C(1)	1.137(4)
Ru(2)-C(5)	1.910(3)	O(2)-C(2)	1.145(4)
Ru(2)-C(4)	1.925(3)	O(3)-C(3)	1.144(3)
Ru(2)-C(6)	1.935(3)	O(4)-C(4)	1.137(4)
O(5)-C(5)	1.135(4)	N(2)-C(12)	1.331(4)
O(6)-C(6)	1.132(4)	N(2)-C(11)	1.422(3)
O(7)-C(7)	1.133(4)	N(2)-C(17)	1.507(3)
O(8)-C(8)	1.137(4)	C(10)-C(11)	1.406(4)
O(9)-C(9)	1.132(4)	C(13)-C(15)	1.525(4)
N(1)-C(12)	1.334(3)	C(13)-C(14)	1.527(4)
N(1)-C(10)	1.422(3)	C(13)-C(16)	1.529(4)
N(1)-C(13)	1.503(3)	C(17)-C(18)	1.524(4)
C(17)-C(19)	1.527(4)	C(17)-C(20)	1.525(4)
C(2)-Ru(1)-C(3)	98.30(13)	C(11)-Ru(1)-C(10)	35.11(9)
C(2)-Ru(1)-C(1)	94.67(13)	C(2)-Ru(1)-Ru(2)	86.28(9)

C(3)-Ru(1)-C(1)	91.69(12)	C(3)-Ru(1)-Ru(2)	167.47(9)
C(2)-Ru(1)-C(11)	136.81(11)	C(1)-Ru(1)-Ru(2)	99.59(8)
C(3)-Ru(1)-C(11)	98.64(11)	C(11)-Ru(1)-Ru(2)	70.52(6)
C(1)-Ru(1)-C(11)	124.13(11)	C(10)-Ru(1)-Ru(2)	48.42(6)
C(2)-Ru(1)-C(10)	134.48(11)	C(2)-Ru(1)-Ru(3)	89.03(9)
C(3)-Ru(1)-C(10)	125.08(11)	C(3)-Ru(1)-Ru(3)	102.02(9)
C(1)-Ru(1)-C(10)	96.90(10)	C(1)-Ru(1)-Ru(3)	165.15(8)
C(11)-Ru(1)-Ru(3)	48.61(7)	C(4)-Ru(2)-C(10)	157.29(11)
C(10)-Ru(1)-Ru(3)	70.60(6)	C(6)-Ru(2)-C(10)	98.47(11)
Ru(2)-Ru(1)-Ru(3)	66.254(8)	H(1)-Ru(2)-Ru(1)	89.5(10)
H(1)-Ru(2)-C(5)	176.9(12)	C(5)-Ru(2)-Ru(1)	92.28(9)
H(1)-Ru(2)-C(4)	87.5(12)	C(4)-Ru(2)-Ru(1)	103.02(9)
C(5)-Ru(2)-C(4)	89.56(13)	C(6)-Ru(2)-Ru(1)	154.12(9)
H(1)-Ru(2)-C(6)	81.0(11)	C(10)-Ru(2)-Ru(1)	56.31(7)
C(5)-Ru(2)-C(6)	98.42(12)	H(1)-Ru(2)-Ru(3)	32.6(10)
C(4)-Ru(2)-C(6)	100.57(12)	C(5)-Ru(2)-Ru(3)	148.91(9)
H(1)-Ru(2)-C(10)	83.3(12)	C(4)-Ru(2)-Ru(3)	93.04(9)
C(5)-Ru(2)-C(10)	99.81(12)	C(6)-Ru(2)-Ru(3)	111.48(9)
C(10)-Ru(2)-Ru(3)	68.37(7)	C(9)-Ru(3)-C(11)	100.12(11)
Ru(1)-Ru(2)-Ru(3)	56.957(7)	H(1)-Ru(3)-Ru(1)	89.6(10)
H(1)-Ru(3)-C(8)	177.4(12)	C(8)-Ru(3)-Ru(1)	90.49(9)
H(1)-Ru(3)-C(7)	88.2(12)	C(7)-Ru(3)-Ru(1)	105.53(10)
C(8)-Ru(3)-C(7)	89.34(13)	C(9)-Ru(3)-Ru(1)	155.36(9)
H(1)-Ru(3)-C(9)	81.8(11)	C(11)-Ru(3)-Ru(1)	55.76(7)
C(8)-Ru(3)-C(9)	99.12(13)	H(1)-Ru(3)-Ru(2)	32.9(10)
C(7)-Ru(3)-C(9)	97.27(13)	C(8)-Ru(3)-Ru(2)	146.97(9)
H(1)-Ru(3)-C(11)	83.2(12)	C(7)-Ru(3)-Ru(2)	94.95(9)
C(8)-Ru(3)-C(11)	98.92(12)	C(9)-Ru(3)-Ru(2)	112.72(9)
C(7)-Ru(3)-C(11)	159.27(12)	C(11)-Ru(3)-Ru(2)	67.92(7)
Ru(1)-Ru(3)-Ru(2)	56.789(7)	O(5)-C(5)-Ru(2)	176.4(3)
C(12)-N(1)-C(10)	107.3(2)	O(6)-C(6)-Ru(2)	178.0(3)
C(12)-N(1)-C(13)	122.7(2)	O(7)-C(7)-Ru(3)	178.5(3)
C(10)-N(1)-C(13)	130.0(2)	O(8)-C(8)-Ru(3)	176.0(3)
C(12)-N(2)-C(11)	108.0(2)	O(9)-C(9)-Ru(3)	179.4(3)
C(12)-N(2)-C(17)	121.9(2)	C(11)-C(10)-N(1)	106.9(2)
C(11)-N(2)-C(17)	130.0(2)	C(11)-C(10)-Ru(2)	111.62(18)
O(1)-C(1)-Ru(1)	175.0(2)	N(1)-C(10)-Ru(2)	140.34(18)
O(2)-C(2)-Ru(1)	178.4(3)	C(11)-C(10)-Ru(1)	71.88(14)
O(3)-C(3)-Ru(1)	174.4(3)	N(1)-C(10)-Ru(1)	127.19(17)
O(4)-C(4)-Ru(2)	176.3(3)	Ru(2)-C(10)-Ru(1)	75.27(8)
C(10)-C(11)-N(2)	105.9(2)	C(15)-C(13)-C(16)	109.0(2)
C(10)-C(11)-Ru(3)	112.08(18)	C(14)-C(13)-C(16)	109.6(2)
N(2)-C(11)-Ru(3)	140.6(2)	N(2)-C(17)-C(18)	107.9(2)
C(10)-C(11)-Ru(1)	73.01(15)	N(2)-C(17)-C(20)	109.9(2)
N(2)-C(11)-Ru(1)	126.99(17)	C(18)-C(17)-C(20)	109.6(3)
Ru(3)-C(11)-Ru(1)	75.64(8)	N(2)-C(17)-C(19)	109.6(2)
N(2)-C(12)-N(1)	111.9(2)	C(18)-C(17)-C(19)	111.4(3)
N(1)-C(13)-C(15)	109.6(2)	C(20)-C(17)-C(19)	108.5(3)
N(1)-C(13)-C(14)	108.3(2)	N(1)-C(13)-C(16)	109.4(2)
C(15)-C(13)-C(14)	110.9(2)		

Appendix 5 Crystallographic data for $Ru_3(\mu\text{-}H)(alAd_2)'(CO)_9$ (2B)

Identification code	k07mkw38
Empirical formula	C33 H34 Cl2 N2 O9 Ru3
Formula weight	976.73
Temperature	150(2) K
Wavelength	0.71073 Å
Crystal system	Monoclinic
Space group	P21/n
Unit cell dimensions	a = 11.9540(1)Å α = 90°
	b = 22.9860(2)Å β = 107.636(1)°
	c = 13.3710(1)Å γ = 90°
Volume	3501.33(5) $Å^3$
Z	4
Density (calculated)	1.853 Mg/m^3
Absorption coefficient	1.486 mm^{-1}
F(000)	1936
Crystal size	0.25 x 0.25 x 0.15 mm
Theta range for data collection	3.55 to 30.04°
Index ranges	-16<=h<=16; -32<=k<=32; -18<=l<=18
Reflections collected	73592
Independent reflections	10224 [R(int) = 0.0490]
Reflections observed (>2σ)	8575
Data Completeness	0.998
Absorption correction	Semi-empirical from equivalents
Max. and min. transmission	0.76 and 0.67
Refinement method	Full-matrix least-squares on F^2
Data / restraints / parameters	10224 / 1 / 446
Goodness-of-fit on F^2	1.047
Final R indices [I>2σ(I)]	R^1 = 0.0309 wR_2 = 0.0675
R indices (all data)	R^1 = 0.0424 wR_2 = 0.0728
Largest diff. peak and hole	1.127 and -1.053 $eÅ^{-3}$

Ru(1)-C(2)	1.907(3)	N(2)-C(13)	1.501(3)
Ru(1)-C(1)	1.927(2)	C(10)-C(11)	1.411(3)
Ru(1)-C(3)	1.928(3)	C(13)-C(19)	1.518(3)
Ru(1)-C(11)	2.111(2)	C(13)-C(18)	1.532(3)
Ru(1)-Ru(3)	2.7270(2)	C(13)-C(14)	1.537(3)
Ru(1)-Ru(2)	2.9639(2)	C(14)-C(15)	1.534(3)
Ru(2)-C(5)	1.891(2)	C(15)-C(21)	1.510(5)
Ru(2)-C(6)	1.931(3)	C(15)-C(16)	1.524(4)
Ru(2)-C(4)	1.936(3)	C(16)-C(17)	1.521(4)
Ru(2)-C(10)	2.096(2)	C(17)-C(20)	1.517(4)
Ru(2)-Ru(3)	2.7137(2)	C(17)-C(18)	1.539(3)
Ru(3)-C(7)	1.890(2)	C(19)-C(22)	1.553(4)
Ru(3)-C(9)	1.900(3)	C(20)-C(22)	1.547(5)
Ru(3)-C(8)	1.908(2)	C(21)-C(22)	1.518(5)
Ru(3)-C(10)	2.326(2)	C(23)-C(24)	1.532(3)

Ru(3)-C(11)	2.338(2)	C(23)-C(29)	1.535(3)
Cl(1)-C(34)	1.731(3)	C(23)-C(30)	1.536(3)
Cl(2)-C(34)	1.758(5)	C(24)-C(26)	1.539(3)
O(1)-C(1)	1.134(3)	C(26)-C(31)	1.530(3)
O(2)-C(2)	1.137(3)	C(26)-C(27)	1.532(3)
O(3)-C(3)	1.133(3)	C(27)-C(28)	1.534(3)
O(4)-C(4)	1.136(3)	C(28)-C(32)	1.531(3)
O(5)-C(5)	1.145(3)	C(28)-C(29)	1.542(3)
O(6)-C(6)	1.135(3)	C(30)-C(33)	1.541(3)
O(7)-C(7)	1.145(3)	C(31)-C(33)	1.538(3)
O(8)-C(8)	1.144(3)	C(32)-C(33)	1.528(4)
O(9)-C(9)	1.146(3)	N(1)-C(23)	1.505(3)
N(1)-C(12)	1.329(3)	N(2)-C(12)	1.328(3)
N(1)-C(10)	1.430(3)	N(2)-C(11)	1.425(3)
C(2)-Ru(1)-C(1)	91.58(10)	C(7)-Ru(3)-C(10)	136.89(9)
C(2)-Ru(1)-C(3)	99.81(11)	C(9)-Ru(3)-C(10)	122.38(9)
C(1)-Ru(1)-C(3)	95.95(10)	C(8)-Ru(3)-C(10)	97.02(9)
C(2)-Ru(1)-C(11)	100.47(9)	C(7)-Ru(3)-C(11)	136.44(9)
C(1)-Ru(1)-C(11)	158.76(10)	C(9)-Ru(3)-C(11)	95.08(9)
C(3)-Ru(1)-C(11)	99.10(9)	C(8)-Ru(3)-C(11)	123.80(9)
C(2)-Ru(1)-Ru(3)	91.67(8)	C(10)-Ru(3)-C(11)	35.21(7)
C(1)-Ru(1)-Ru(3)	106.60(8)	C(7)-Ru(3)-Ru(2)	88.95(8)
C(3)-Ru(1)-Ru(3)	154.40(7)	C(9)-Ru(3)-Ru(2)	163.95(7)
C(11)-Ru(1)-Ru(3)	56.06(6)	C(8)-Ru(3)-Ru(2)	100.50(8)
C(2)-Ru(1)-Ru(2)	147.90(8)	C(10)-Ru(3)-Ru(2)	48.41(5)
C(1)-Ru(1)-Ru(2)	92.23(8)	C(11)-Ru(3)-Ru(2)	70.64(5)
C(3)-Ru(1)-Ru(2)	111.45(8)	C(7)-Ru(3)-Ru(1)	88.21(7)
C(11)-Ru(1)-Ru(2)	68.34(6)	C(9)-Ru(3)-Ru(1)	99.21(7)
Ru(3)-Ru(1)-Ru(2)	56.776(6)	C(8)-Ru(3)-Ru(1)	165.56(7)
C(5)-Ru(2)-C(6)	103.40(10)	C(10)-Ru(3)-Ru(1)	70.40(5)
C(5)-Ru(2)-C(4)	88.63(10)	C(11)-Ru(3)-Ru(1)	48.52(5)
C(6)-Ru(2)-C(4)	101.30(11)	Ru(2)-Ru(3)-Ru(1)	66.018(7)
C(5)-Ru(2)-C(10)	98.67(9)	C(12)-N(1)-C(10)	107.37(17)
C(6)-Ru(2)-C(10)	95.65(9)	C(12)-N(1)-C(23)	123.02(18)
C(4)-Ru(2)-C(10)	159.48(10)	C(10)-N(1)-C(23)	129.61(18)
C(5)-Ru(2)-Ru(3)	92.38(8)	C(12)-N(2)-C(11)	107.84(18)
C(6)-Ru(2)-Ru(3)	149.77(7)	C(12)-N(2)-C(13)	123.07(18)
C(4)-Ru(2)-Ru(3)	104.74(8)	C(11)-N(2)-C(13)	129.05(18)
C(10)-Ru(2)-Ru(3)	56.07(6)	O(1)-C(1)-Ru(1)	175.0(2)
C(5)-Ru(2)-Ru(1)	149.43(8)	O(2)-C(2)-Ru(1)	176.0(2)
C(6)-Ru(2)-Ru(1)	105.31(7)	O(3)-C(3)-Ru(1)	179.5(3)
C(4)-Ru(2)-Ru(1)	95.84(8)	O(4)-C(4)-Ru(2)	178.8(3)
C(10)-Ru(2)-Ru(1)	68.32(6)	O(5)-C(5)-Ru(2)	177.1(2)
Ru(3)-Ru(2)-Ru(1)	57.206(6)	O(6)-C(6)-Ru(2)	173.6(2)
C(7)-Ru(3)-C(9)	97.13(11)	O(7)-C(7)-Ru(3)	178.5(2)
C(7)-Ru(3)-C(8)	96.99(11)	O(8)-C(8)-Ru(3)	175.7(2)
C(9)-Ru(3)-C(8)	93.52(11)	O(9)-C(9)-Ru(3)	176.9(2)
C(11)-C(10)-N(1)	106.36(18)	C(19)-C(13)-C(18)	109.6(2)
C(11)-C(10)-Ru(2)	112.25(15)	N(2)-C(13)-C(14)	108.44(18)
N(1)-C(10)-Ru(2)	140.00(15)	C(19)-C(13)-C(14)	108.4(2)

C(11)-C(10)-Ru(3)	72.86(12)	C(18)-C(13)-C(14)	109.66(19)
N(1)-C(10)-Ru(3)	127.34(14)	C(15)-C(14)-C(13)	109.8(2)
Ru(2)-C(10)-Ru(3)	75.52(7)	C(21)-C(15)-C(16)	109.1(2)
C(10)-C(11)-N(2)	106.07(18)	C(21)-C(15)-C(14)	109.4(2)
C(10)-C(11)-Ru(1)	111.09(15)	C(16)-C(15)-C(14)	109.4(2)
N(2)-C(11)-Ru(1)	141.58(15)	C(17)-C(16)-C(15)	110.6(2)
C(10)-C(11)-Ru(3)	71.92(12)	C(20)-C(17)-C(16)	110.0(2)
N(2)-C(11)-Ru(3)	126.78(14)	C(20)-C(17)-C(18)	109.6(2)
Ru(1)-C(11)-Ru(3)	75.42(7)	C(16)-C(17)-C(18)	108.7(2)
N(2)-C(12)-N(1)	112.36(19)	C(13)-C(18)-C(17)	109.7(2)
N(2)-C(13)-C(19)	111.45(18)	C(13)-C(19)-C(22)	109.5(2)
N(2)-C(13)-C(18)	109.28(18)	C(17)-C(20)-C(22)	108.7(2)
C(31)-C(26)-C(24)	109.32(19)	C(15)-C(21)-C(22)	109.7(2)
C(27)-C(26)-C(24)	109.71(19)	C(21)-C(22)-C(20)	110.2(2)
C(26)-C(27)-C(28)	109.41(19)	C(21)-C(22)-C(19)	109.9(3)
C(32)-C(28)-C(27)	109.7(2)	C(20)-C(22)-C(19)	108.5(3)
C(32)-C(28)-C(29)	109.44(19)	N(1)-C(23)-C(24)	109.51(17)
C(27)-C(28)-C(29)	109.40(18)	N(1)-C(23)-C(29)	109.89(17)
C(23)-C(29)-C(28)	109.66(18)	C(24)-C(23)-C(29)	110.65(18)
C(23)-C(30)-C(33)	109.74(18)	N(1)-C(23)-C(30)	109.67(17)
C(26)-C(31)-C(33)	108.9(2)	C(24)-C(23)-C(30)	108.79(18)
C(33)-C(32)-C(28)	109.09(19)	C(29)-C(23)-C(30)	108.30(18)
C(32)-C(33)-C(31)	109.9(2)	C(23)-C(24)-C(26)	109.36(18)
C(32)-C(33)-C(30)	110.1(2)	C(31)-C(26)-C(27)	110.1(2)
C(31)-C(33)-C(30)	109.02(19)	Cl(1)-C(34)-Cl(2)	112.4(2)

Appendix 6 Crystallographic data for $[Ru_4(CO)_{12}(\mu\text{-}H)_3]^-[I^tBu_2]^+$

Identification code	k07mkw13
Empirical formula	C23 H24 N2 O12 Ru4
Formula weight	924.72
Temperature	150(2) K
Wavelength	0.71073 Å
Crystal system	Monoclinic
Space group	P21/n
Unit cell dimensions	a = 13.8140(1)Å α = 90°
	b = 13.9020(1)Å β = 108.075(1)°
	c = 17.0120(2)Å γ = 90°
Volume	3105.80(5) $Å^3$
Z	4
Density (calculated)	1.978 Mg/m^3
Absorption coefficient	1.966 mm^{-1}
F(000)	1792
Crystal size	0.12 x 0.12 x 0.10 mm
Theta range for data collection	3.64 to 30.06°
Index ranges	-19<=h<=18; -19<=k<=17; -22<=l<=23
Reflections collected	71903
Independent reflections	9072 [R(int) = 0.0590]

Reflections observed (>2σ)	6952
Data Completeness	0.996
Absorption correction	Semi-empirical from equivalents
Max. and min. transmission	0.81 and 0.74
Refinement method	Full-matrix least-squares on F^2
Data / restraints / parameters	9072 / 15 / 404
Goodness-of-fit on F^2	1.070
Final R indices [I>2σ(I)]	R^1 = 0.0326 wR_2 = 0.0647
R indices (all data)	R^1 = 0.0536 wR_2 = 0.0725
Largest diff. peak and hole	0.868 and -0.784 eÅ^{-3}

Ru(1)-C(3)	1.891(3)	O(1)-C(1)	1.136(4)
Ru(1)-C(2)	1.894(3)	O(2)-C(2)	1.149(4)
Ru(1)-C(1)	1.910(3)	O(3)-C(3)	1.147(4)
Ru(1)-Ru(4)	2.7610(3)	O(4)-C(4)	1.141(4)
Ru(1)-Ru(3)	2.7943(3)	O(5)-C(5)	1.134(3)
Ru(1)-Ru(2)	2.9107(3)	O(6)-C(6)	1.144(4)
Ru(2)-C(6)	1.889(3)	O(7)-C(7)	1.153(4)
Ru(2)-C(4)	1.904(4)	O(8)-C(8)	1.140(4)
Ru(2)-C(5)	1.918(3)	O(9)-C(9)	1.138(4)
Ru(2)-Ru(4)	2.7969(3)	O(10)-C(10)	1.142(3)
Ru(2)-Ru(3)	2.9391(3)	O(11)-C(11)	1.133(4)
Ru(3)-C(10)	1.886(3)	O(12)-C(12)	1.140(4)
Ru(3)-C(12)	1.903(3)	N(1)-C(13)	1.325(4)
Ru(3)-C(11)	1.920(3)	N(1)-C(14)	1.375(4)
Ru(3)-Ru(4)	2.9104(3)	N(1)-C(16)	1.500(4)
Ru(4)-C(7)	1.877(3)	N(2)-C(13)	1.328(4)
Ru(4)-C(9)	1.905(3)	N(2)-C(15)	1.376(4)
Ru(4)-C(8)	1.910(4)	N(2)-C(20)	1.506(4)
C(16)-C(18A)	1.544(15)	C(14)-C(15)	1.343(4)
C(16)-C(17A)	1.545(15)	C(16)-C(19A)	1.456(16)
C(20)-C(21)	1.523(4)	C(16)-C(17)	1.497(6)
C(20)-C(23)	1.524(4)	C(16)-C(18)	1.531(5)
C(20)-C(22)	1.530(5)	C(16)-C(19)	1.537(5)
C(3)-Ru(1)-C(2)	95.91(13)	C(6)-Ru(2)-C(4)	92.87(15)
C(3)-Ru(1)-C(1)	94.60(14)	C(6)-Ru(2)-C(5)	98.22(13)
C(2)-Ru(1)-C(1)	96.24(13)	C(4)-Ru(2)-C(5)	99.13(14)
C(3)-Ru(1)-Ru(4)	105.29(10)	C(6)-Ru(2)-Ru(4)	88.80(10)
C(2)-Ru(1)-Ru(4)	84.55(10)	C(4)-Ru(2)-Ru(4)	86.23(10)
C(1)-Ru(1)-Ru(4)	159.93(9)	C(5)-Ru(2)-Ru(4)	170.89(9)
C(3)-Ru(1)-Ru(3)	160.52(10)	C(6)-Ru(2)-Ru(1)	93.98(10)
C(2)-Ru(1)-Ru(3)	98.35(9)	C(4)-Ru(2)-Ru(1)	143.17(10)
C(1)-Ru(1)-Ru(3)	96.96(9)	C(5)-Ru(2)-Ru(1)	115.56(9)
Ru(4)-Ru(1)-Ru(3)	63.184(8)	Ru(4)-Ru(2)-Ru(1)	57.819(8)
C(3)-Ru(1)-Ru(2)	98.81(10)	C(6)-Ru(2)-Ru(3)	145.54(10)
C(2)-Ru(1)-Ru(2)	143.14(10)	C(4)-Ru(2)-Ru(3)	100.51(10)
C(1)-Ru(1)-Ru(2)	115.90(9)	C(5)-Ru(2)-Ru(3)	110.60(8)
Ru(4)-Ru(1)-Ru(2)	59.022(8)	Ru(4)-Ru(2)-Ru(3)	60.922(8)
Ru(3)-Ru(1)-Ru(2)	61.978(8)	Ru(1)-Ru(2)-Ru(3)	57.066(7)
C(7)-Ru(4)-C(9)	94.39(14)	C(10)-Ru(3)-C(12)	93.20(13)

C(7)-Ru(4)-C(8)	99.08(15)	C(10)-Ru(3)-C(11)	99.33(12)
C(9)-Ru(4)-C(8)	95.62(14)	C(12)-Ru(3)-C(11)	97.48(13)
C(7)-Ru(4)-Ru(1)	82.47(11)	C(10)-Ru(3)-Ru(1)	86.23(8)
C(9)-Ru(4)-Ru(1)	101.67(10)	C(12)-Ru(3)-Ru(1)	87.15(9)
C(8)-Ru(4)-Ru(1)	162.49(11)	C(11)-Ru(3)-Ru(1)	172.51(9)
C(7)-Ru(4)-Ru(2)	94.92(10)	C(10)-Ru(3)-Ru(4)	92.08(8)
C(9)-Ru(4)-Ru(2)	160.88(9)	C(12)-Ru(3)-Ru(4)	144.14(9)
C(8)-Ru(4)-Ru(2)	99.35(11)	C(11)-Ru(3)-Ru(4)	116.57(10)
Ru(1)-Ru(4)-Ru(2)	63.159(8)	Ru(1)-Ru(3)-Ru(4)	57.849(8)
C(7)-Ru(4)-Ru(3)	140.55(11)	C(10)-Ru(3)-Ru(2)	143.02(8)
C(9)-Ru(4)-Ru(3)	100.82(9)	C(12)-Ru(3)-Ru(2)	101.10(9)
C(8)-Ru(4)-Ru(3)	115.15(11)	C(11)-Ru(3)-Ru(2)	112.16(9)
Ru(1)-Ru(4)-Ru(3)	58.967(8)	Ru(1)-Ru(3)-Ru(2)	60.956(8)
Ru(2)-Ru(4)-Ru(3)	61.952(8)	Ru(4)-Ru(3)-Ru(2)	57.126(7)
C(13)-N(1)-C(14)	107.3(2)	C(19A)-C(16)-C(17)	144.0(7)
C(13)-N(1)-C(16)	126.3(2)	C(19A)-C(16)-N(1)	107.1(7)
C(14)-N(1)-C(16)	126.4(2)	C(17)-C(16)-N(1)	108.3(3)
C(13)-N(2)-C(15)	107.4(2)	C(19A)-C(16)-C(18)	61.7(7)
C(13)-N(2)-C(20)	128.3(2)	C(17)-C(16)-C(18)	111.8(4)
C(15)-N(2)-C(20)	124.2(2)	N(1)-C(16)-C(18)	107.7(3)
O(1)-C(1)-Ru(1)	175.9(3)	C(19A)-C(16)-C(19)	49.3(6)
O(2)-C(2)-Ru(1)	176.5(3)	C(17)-C(16)-C(19)	111.8(4)
O(3)-C(3)-Ru(1)	176.6(3)	N(1)-C(16)-C(19)	109.2(3)
O(4)-C(4)-Ru(2)	176.9(3)	C(18)-C(16)-C(19)	108.0(4)
O(5)-C(5)-Ru(2)	178.9(3)	C(19A)-C(16)-C(18A)	111.9(9)
O(6)-C(6)-Ru(2)	178.1(3)	C(17)-C(16)-C(18A)	61.3(6)
O(7)-C(7)-Ru(4)	177.5(3)	N(1)-C(16)-C(18A)	108.7(6)
O(8)-C(8)-Ru(4)	177.5(3)	C(18)-C(16)-C(18A)	53.1(6)
O(9)-C(9)-Ru(4)	179.4(3)	C(19)-C(16)-C(18A)	141.5(6)
O(10)-C(10)-Ru(3)	178.2(3)	C(19A)-C(16)-C(17A)	112.8(9)
O(11)-C(11)-Ru(3)	177.0(3)	C(17)-C(16)-C(17A)	50.1(6)
O(12)-C(12)-Ru(3)	176.7(3)	N(1)-C(16)-C(17A)	107.0(6)
N(1)-C(13)-N(2)	110.1(2)	C(18)-C(16)-C(17A)	144.8(6)
C(15)-C(14)-N(1)	107.8(3)	C(19)-C(16)-C(17A)	65.4(6)
C(14)-C(15)-N(2)	107.4(3)	C(18A)-C(16)-C(17A)	109.2(8)
N(2)-C(20)-C(22)	107.2(2)	N(2)-C(20)-C(21)	107.1(2)
C(21)-C(20)-C(22)	111.9(3)	N(2)-C(20)-C(23)	108.8(2)
C(23)-C(20)-C(22)	110.7(3)	C(21)-C(20)-C(23)	110.9(3)

Appendix 7 Crystallographic data for $Ru(IEt_2Me_2)_2(CO)_3$ (3A)

Identification code	k06mkw21
Empirical formula	C21 H32 N4 O3 Ru
Formula weight	489.58
Temperature	150(2) K
Wavelength	0.71073 Å
Crystal system	Orthorhombic
Space group	Pbca

Unit cell dimensions	a = 9.2580(1)Å α = 90°
	b = 16.6670(2)Å β = 90°
	c = 29.1940(3)Å γ = 90°
Volume	4504.72(9) $Å^3$
Z	8
Density (calculated)	1.444 Mg/m^3
Absorption coefficient	0.724 mm^{-1}
F(000)	2032
Crystal size	0.35 x 0.30 x 0.30 mm
Theta range for data collection	3.57 to 30.02°
Index ranges	-13<=h<=13; -23<=k<=23; -41<=l<=41
Reflections collected	61789
Independent reflections	6559 [R(int) = 0.0778]
Reflections observed (>2σ)	4295
Data Completeness	0.997
Absorption correction	Semi-empirical from equivalents
Max. and min. transmission	0.82 and 0.75
Refinement method	Full-matrix least-squares on F^2
Data / restraints / parameters	6559 / 0 / 267
Goodness-of-fit on F^2	1.031
Final R indices [I>2σ(I)]	R^1 = 0.0386 wR_2 = 0.0840
R indices (all data)	R^1 = 0.0763 wR_2 = 0.0980
Largest diff. peak and hole	1.445 and -0.791 $eÅ^{-3}$

Ru(1)-C(1)	1.905(3)	Ru(1)-C(3)	1.915(3)
Ru(1)-C(2)	1.916(3)	Ru(1)-C(13)	2.133(2)
Ru(1)-C(4)	2.142(2)	Ru(1)-H(7A)	3.0091
Ru(1)-H(20A)	4.3289	O(1)-C(1)	1.150(4)
O(2)-C(2)	1.158(3)	O(3)-C(3)	1.155(3)
N(1)-C(4)	1.365(3)	N(1)-C(5)	1.407(3)
N(1)-C(7)	1.461(3)	N(2)-C(4)	1.364(3)
N(2)-C(6)	1.392(3)	N(2)-C(11)	1.464(3)
N(3)-C(13)	1.364(3)	N(3)-C(14)	1.396(3)
N(3)-C(16)	1.474(3)	N(4)-C(13)	1.378(3)
N(4)-C(15)	1.395(3)	N(4)-C(20)	1.461(3)
C(5)-C(6)	1.345(4)	C(5)-C(9)	1.490(4)
C(6)-C(10)	1.492(4)	C(7)-C(8)	1.516(4)
C(11)-C(12)	1.522(4)	C(14)-C(15)	1.349(3)
C(14)-C(18)	1.488(4)	C(15)-C(19)	1.491(3)
C(16)-C(17)	1.499(4)	C(20)-C(21)	1.518(4)
C(1)-Ru(1)-C(3)	124.34(13)	C(1)-Ru(1)-C(2)	103.64(14)
C(3)-Ru(1)-C(2)	131.98(13)	C(1)-Ru(1)-C(13)	98.91(11)
C(3)-Ru(1)-C(13)	84.82(10)	C(2)-Ru(1)-C(13)	85.99(11)
C(1)-Ru(1)-C(4)	86.45(11)	C(3)-Ru(1)-C(4)	87.52(10)
C(2)-Ru(1)-C(4)	98.25(11)	C(13)-Ru(1)-C(4)	172.24(9)
C(1)-Ru(1)-H(7A)	56.1	C(3)-Ru(1)-H(7A)	74.2
C(2)-Ru(1)-H(7A)	146.9	C(13)-Ru(1)-H(7A)	120.4
C(4)-Ru(1)-H(7A)	58.2	C(1)-Ru(1)-H(20A)	144.5
C(3)-Ru(1)-H(20A)	60.2	C(2)-Ru(1)-H(20A)	80.3
C(13)-Ru(1)-H(20A)	45.7	C(4)-Ru(1)-H(20A)	128.4

H(7A)-Ru(1)-H(20A)	132.0	C(4)-N(1)-C(5)	111.7(2)
C(4)-N(1)-C(7)	126.0(2)	C(5)-N(1)-C(7)	122.1(2)
C(4)-N(2)-C(6)	112.0(2)	C(4)-N(2)-C(11)	125.7(2)
C(6)-N(2)-C(11)	122.3(2)	C(13)-N(3)-C(14)	112.5(2)
C(13)-N(3)-C(16)	125.7(2)	C(14)-N(3)-C(16)	121.8(2)
C(13)-N(4)-C(15)	111.73(19)	C(13)-N(4)-C(20)	125.9(2)
C(15)-N(4)-C(20)	122.3(2)	O(1)-C(1)-Ru(1)	172.9(3)
O(2)-C(2)-Ru(1)	171.2(3)	O(3)-C(3)-Ru(1)	177.1(2)
N(2)-C(4)-N(1)	103.3(2)	N(2)-C(4)-Ru(1)	129.69(18)
N(1)-C(4)-Ru(1)	127.01(17)	C(6)-C(5)-N(1)	106.1(2)
C(6)-C(5)-C(9)	130.0(2)	N(1)-C(5)-C(9)	123.9(2)
C(5)-C(6)-N(2)	106.9(2)	C(5)-C(6)-C(10)	129.3(3)
N(2)-C(6)-C(10)	123.8(2)	N(1)-C(7)-C(8)	112.9(2)
N(2)-C(11)-C(12)	111.1(2)	N(3)-C(13)-N(4)	102.7(2)
N(3)-C(13)-Ru(1)	131.11(17)	N(4)-C(13)-Ru(1)	126.09(17)
C(15)-C(14)-N(3)	106.3(2)	C(15)-C(14)-C(18)	130.4(2)
N(3)-C(14)-C(18)	123.3(2)	C(14)-C(15)-N(4)	106.7(2)
C(14)-C(15)-C(19)	130.1(2)	N(4)-C(15)-C(19)	123.0(2)
N(3)-C(16)-C(17)	110.4(2)	N(4)-C(20)-C(21)	112.9(2)

Appendix 8 Crystallographic data for $Ru(l^iPr_2Me_2)_2(CO)_3$ (4A)

Identification code	k06mkw18
Empirical formula	C25 H40 N4 O3 Ru
Formula weight	545.68
Temperature	150(2) K
Wavelength	0.71073 Å
Crystal system	Monoclinic
Space group	$P2_1$
Unit cell dimensions	a = 10.6340(1)Å α = 90°
	b = 12.0530(2)Å β = 110.466(1)°
	c = 11.2800(2)Å γ = 90°
Volume	1354.52(4) $Å^3$
Z	2
Density (calculated)	1.338 Mg/m^3
Absorption coefficient	0.610 mm^{-1}
F(000)	572
Crystal size	0.50 x 0.35 x 0.25 mm
Theta range for data collection	3.68 to 30.13°
Index ranges	-14<=h<=14; -16<=k<=16; -15<=l<=15
Reflections collected	27748
Independent reflections	7894 [R(int) = 0.0377]
Reflections observed (>2σ)	7311
Data Completeness	0.992
Absorption correction	Semi-empirical from equivalents
Max. and min. transmission	0.71 and 0.67
Refinement method	Full-matrix least-squares on F^2
Data / restraints / parameters	7894 / 1 / 311

Goodness-of-fit on F^2	1.058
Final R indices [I>2σ(I)]	R^1 = 0.0254 wR_2 = 0.0533
R indices (all data)	R^1 = 0.0304 wR_2 = 0.0551
Absolute structure parameter	-0.036(18)
Largest diff. peak and hole	1.028 and -0.701 eÅ^{-3}

Ru(1)-C(3)	1.880(2)	Ru(1)-C(1)	1.8851(15)
Ru(1)-C(2)	1.9055(19)	Ru(1)-C(4)	2.178(2)
Ru(1)-C(15)	2.2019(17)	O(1)-C(1)	1.1634(19)
O(2)-C(2)	1.161(2)	O(3)-C(3)	1.150(3)
N(1)-C(4)	1.363(3)	N(1)-C(6)	1.401(3)
N(1)-C(12)	1.478(3)	N(2)-C(4)	1.362(3)
N(2)-C(5)	1.403(3)	N(2)-C(7)	1.475(3)
N(3)-C(15)	1.369(2)	N(3)-C(16)	1.398(3)
N(3)-C(18)	1.478(3)	N(4)-C(15)	1.367(2)
N(4)-C(17)	1.404(2)	N(4)-C(23)	1.481(3)
C(5)-C(6)	1.341(3)	C(5)-C(10)	1.498(3)
C(6)-C(11)	1.492(3)	C(7)-C(9)	1.521(3)
C(7)-C(8)	1.530(3)	C(12)-C(14)	1.509(4)
C(12)-C(13)	1.519(4)	C(16)-C(17)	1.349(3)
C(16)-C(21)	1.501(3)	C(17)-C(22)	1.498(3)
C(18)-C(19)	1.519(3)	C(18)-C(20)	1.522(3)
C(23)-C(25)	1.529(3)	C(23)-C(24)	1.530(3)
C(3)-Ru(1)-C(1)	91.80(11)	C(3)-Ru(1)-C(2)	87.00(9)
C(1)-Ru(1)-C(2)	120.57(8)	C(3)-Ru(1)-C(4)	174.02(7)
C(1)-Ru(1)-C(4)	84.11(12)	C(2)-Ru(1)-C(4)	98.83(8)
C(3)-Ru(1)-C(15)	91.18(8)	C(1)-Ru(1)-C(15)	133.70(7)
C(2)-Ru(1)-C(15)	105.73(8)	C(4)-Ru(1)-C(15)	88.52(7)
C(4)-N(1)-C(6)	111.17(18)	C(4)-N(1)-C(12)	123.44(17)
C(6)-N(1)-C(12)	125.39(17)	C(4)-N(2)-C(5)	111.05(18)
C(4)-N(2)-C(7)	122.95(17)	C(5)-N(2)-C(7)	125.60(17)
C(15)-N(3)-C(16)	111.61(16)	C(15)-N(3)-C(18)	121.65(15)
C(16)-N(3)-C(18)	126.41(16)	C(15)-N(4)-C(17)	111.35(16)
C(15)-N(4)-C(23)	122.36(15)	C(17)-N(4)-C(23)	126.25(16)
O(1)-C(1)-Ru(1)	174.55(16)	O(2)-C(2)-Ru(1)	167.24(19)
O(3)-C(3)-Ru(1)	179.5(2)	N(2)-C(4)-N(1)	104.2(2)
N(2)-C(4)-Ru(1)	126.57(15)	N(1)-C(4)-Ru(1)	129.19(15)
C(6)-C(5)-N(2)	106.84(17)	C(6)-C(5)-C(10)	127.6(2)
N(2)-C(5)-C(10)	125.5(2)	C(5)-C(6)-N(1)	106.73(17)
C(5)-C(6)-C(11)	127.8(2)	N(1)-C(6)-C(11)	125.5(2)
N(2)-C(7)-C(9)	111.14(18)	N(2)-C(7)-C(8)	113.06(17)
C(9)-C(7)-C(8)	112.73(18)	N(1)-C(12)-C(14)	113.1(2)
N(1)-C(12)-C(13)	111.76(19)	C(14)-C(12)-C(13)	113.2(2)
N(4)-C(15)-N(3)	103.74(15)	N(4)-C(15)-Ru(1)	129.67(12)
N(3)-C(15)-Ru(1)	126.57(12)	C(17)-C(16)-N(3)	106.63(17)
C(17)-C(16)-C(21)	128.4(2)	N(3)-C(16)-C(21)	124.9(2)
C(16)-C(17)-N(4)	106.67(16)	C(16)-C(17)-C(22)	127.4(2)
N(4)-C(17)-C(22)	125.9(2)	N(3)-C(18)-C(19)	113.29(17)
N(3)-C(18)-C(20)	110.86(17)	C(19)-C(18)-C(20)	114.18(16)
N(4)-C(23)-C(25)	111.54(19)	N(4)-C(23)-C(24)	112.85(18)

C(25)-C(23)-C(24)	112.8(2)		

Appendix 9 Crystallographic data for $Ru(I^iPr_2)_2(CO)_3$ (5A)

Identification code	k07mkw2
Empirical formula	C25 H40 N4 O4 Ru
Formula weight	561.68
Temperature	150(2) K
Wavelength	0.71073 Å
Crystal system	Monoclinic
Space group	P21/a
Unit cell dimensions	a = 16.5190(2)Å α = 90°
	b = 10.7430(2)Å β = 114.699(1)°
	c = 17.3800(2)Å γ = 90°
Volume	2802.15(7) $Å^3$
Z	4
Density (calculated)	1.331 Mg/m^3
Absorption coefficient	0.594 mm^{-1}
F(000)	1176
Crystal size	0.40 x 0.20 x 0.20 mm
Theta range for data collection	3.79 to 30.04°
Index ranges	-23<=h<=23; -15<=k<=14; -18<=l<=24
Reflections collected	53080
Independent reflections	8170 [R(int) = 0.0657]
Reflections observed (>2σ)	5851
Data Completeness	0.997
Absorption correction	Semi-empirical from equivalents
Max. and min. transmission	0.84 and 0.80
Refinement method	Full-matrix least-squares on F^2
Data / restraints / parameters	8170 / 66 / 362
Goodness-of-fit on F^2	1.037
Final R indices [I>2σ(I)]	R^1 = 0.0369 wR_2 = 0.0777
R indices (all data)	R^1 = 0.0692 wR_2 = 0.0895
Largest diff. peak and hole	1.661 and -0.901 $eÅ^{-3}$

Ru(1)-C(1)	1.884(2)	Ru(1)-C(3)	1.888(2)
Ru(1)-C(2)	1.916(2)	Ru(1)-C(4)	2.153(2)
Ru(1)-C(13)	2.177(2)	O(1)-C(1)	1.171(3)
O(2)-C(2)	1.152(3)	O(3)-C(3)	1.155(3)
O(4)-C(22)	1.381(9)	O(4)-C(25)	1.418(8)
O(4A)-C(22A)	1.286(12)	O(4A)-C(25A)	1.401(12)
N(1)-C(4)	1.368(3)	N(1)-C(5)	1.387(3)
N(1)-C(7)	1.468(3)	N(2)-C(4)	1.361(3)
N(2)-C(6)	1.388(3)	N(2)-C(10)	1.476(3)
N(3)-C(13)	1.363(3)	N(3)-C(14)	1.385(3)
N(3)-C(16)	1.473(3)	N(4)-C(13)	1.368(3)
N(4)-C(15)	1.379(3)	N(4)-C(19)	1.479(3)

C(5)-C(6)	1.338(4)	C(5)-H(5)	0.9500
C(6)-H(6)	0.9500	C(7)-C(8)	1.520(4)
C(7)-C(9)	1.521(4)	C(7)-H(7)	1.0000
C(8)-H(8A)	0.9800	C(8)-H(8B)	0.9800
C(8)-H(8C)	0.9800	C(9)-H(9A)	0.9800
C(9)-H(9B)	0.9800	C(9)-H(9C)	0.9800
C(10)-C(12)	1.519(3)	C(10)-C(11)	1.525(3)
C(10)-H(10)	1.0000	C(11)-H(11A)	0.9800
C(11)-H(11B)	0.9800	C(11)-H(11C)	0.9800
C(12)-H(12A)	0.9800	C(12)-H(12B)	0.9800
C(12)-H(12C)	0.9800	C(14)-C(15)	1.336(4)
C(14)-H(14)	0.9500	C(15)-H(15)	0.9500
C(16)-C(18)	1.517(3)	C(16)-C(17)	1.524(3)
C(16)-H(16)	1.0000	C(17)-H(17A)	0.9800
C(17)-H(17B)	0.9800	C(17)-H(17C)	0.9800
C(18)-H(18A)	0.9800	C(18)-H(18B)	0.9800
C(18)-H(18C)	0.9800	C(19)-C(20)	1.508(4)
C(19)-C(21)	1.523(4)	C(19)-H(19)	1.0000
C(20)-H(20A)	0.9800	C(20)-H(20B)	0.9800
C(20)-H(20C)	0.9800	C(21)-H(21A)	0.9800
C(21)-H(21B)	0.9800	C(21)-H(21C)	0.9800
C(22)-C(23)	1.519(11)	C(22)-H(22A)	0.9900
C(22)-H(22B)	0.9900	C(23)-C(24)	1.472(11)
C(23)-H(23A)	0.9900	C(23)-H(23B)	0.9900
C(24)-C(25)	1.561(14)	C(24)-H(24A)	0.9900
C(24)-H(24B)	0.9900	C(25)-H(25A)	0.9900
C(25)-H(25B)	0.9900	C(22A)-C(23A)	1.443(16)
C(22A)-C(25A)	1.995(19)	C(22A)-H(22C)	0.9900
C(22A)-H(22D)	0.9900	C(23A)-C(24A)	1.377(17)
C(23A)-C(25A)	1.88(2)	C(23A)-H(23C)	0.9900
C(23A)-H(23D)	0.9900	C(24A)-C(25A)	1.100(19)
C(24A)-H(24C)	0.9900	C(24A)-H(24D)	0.9900
C(25A)-H(25C)	0.9900	C(25A)-H(25D)	0.9900
C(1)-Ru(1)-C(3)	92.30(10)	C(1)-Ru(1)-C(2)	128.07(9)
C(3)-Ru(1)-C(2)	88.17(10)	C(1)-Ru(1)-C(4)	83.56(9)
C(3)-Ru(1)-C(4)	174.34(9)	C(2)-Ru(1)-C(4)	97.42(9)
C(1)-Ru(1)-C(13)	125.97(9)	C(3)-Ru(1)-C(13)	91.79(9)
C(2)-Ru(1)-C(13)	105.90(9)	C(4)-Ru(1)-C(13)	87.55(8)
C(22)-O(4)-C(25)	115.7(9)	C(22A)-O(4A)-C(25A)	95.8(13)
C(4)-N(1)-C(5)	111.15(19)	C(4)-N(1)-C(7)	126.74(19)
C(5)-N(1)-C(7)	121.89(19)	C(4)-N(2)-C(6)	111.52(19)
C(4)-N(2)-C(10)	126.21(18)	C(6)-N(2)-C(10)	122.09(19)
C(13)-N(3)-C(14)	111.47(19)	C(13)-N(3)-C(16)	125.16(19)
C(14)-N(3)-C(16)	123.31(19)	C(13)-N(4)-C(15)	111.33(19)
C(13)-N(4)-C(19)	125.48(18)	C(15)-N(4)-C(19)	123.17(19)
O(1)-C(1)-Ru(1)	176.90(19)	O(2)-C(2)-Ru(1)	171.6(2)
O(3)-C(3)-Ru(1)	179.5(2)	N(2)-C(4)-N(1)	103.55(18)
N(2)-C(4)-Ru(1)	126.36(16)	N(1)-C(4)-Ru(1)	130.09(15)
C(6)-C(5)-N(1)	107.0(2)	C(6)-C(5)-H(5)	126.5
N(1)-C(5)-H(5)	126.5	C(5)-C(6)-N(2)	106.7(2)

C(5)-C(6)-H(6)	126.6	N(2)-C(6)-H(6)	126.6
N(1)-C(7)-C(8)	110.8(2)	N(1)-C(7)-C(9)	110.2(2)
C(8)-C(7)-C(9)	112.3(2)	N(1)-C(7)-H(7)	107.8
C(8)-C(7)-H(7)	107.8	C(9)-C(7)-H(7)	107.8
C(7)-C(8)-H(8A)	109.5	C(7)-C(8)-H(8B)	109.5
H(8A)-C(8)-H(8B)	109.5	C(7)-C(8)-H(8C)	109.5
H(8A)-C(8)-H(8C)	109.5	H(8B)-C(8)-H(8C)	109.5
C(7)-C(9)-H(9A)	109.5	C(7)-C(9)-H(9B)	109.5
H(9A)-C(9)-H(9B)	109.5	C(7)-C(9)-H(9C)	109.5
H(9A)-C(9)-H(9C)	109.5	H(9B)-C(9)-H(9C)	109.5
N(2)-C(10)-C(12)	110.24(19)	N(2)-C(10)-C(11)	110.68(18)
C(12)-C(10)-C(11)	111.93(19)	N(2)-C(10)-H(10)	108.0
C(12)-C(10)-H(10)	108.0	C(11)-C(10)-H(10)	108.0
C(10)-C(11)-H(11A)	109.5	C(10)-C(11)-H(11B)	109.5
H(11A)-C(11)-H(11B)	109.5	C(10)-C(11)-H(11C)	109.5
H(11A)-C(11)-H(11C)	109.5	H(11B)-C(11)-H(11C)	109.5
C(10)-C(12)-H(12A)	109.5	C(10)-C(12)-H(12B)	109.5
H(12A)-C(12)-H(12B)	109.5	C(10)-C(12)-H(12C)	109.5
H(12A)-C(12)-H(12C)	109.5	H(12B)-C(12)-H(12C)	109.5
N(3)-C(13)-N(4)	103.29(18)	N(3)-C(13)-Ru(1)	127.58(15)
N(4)-C(13)-Ru(1)	129.11(15)	C(15)-C(14)-N(3)	106.7(2)
C(15)-C(14)-H(14)	126.7	N(3)-C(14)-H(14)	126.7
C(14)-C(15)-N(4)	107.2(2)	C(14)-C(15)-H(15)	126.4
N(4)-C(15)-H(15)	126.4	N(3)-C(16)-C(18)	110.3(2)
N(3)-C(16)-C(17)	110.7(2)	C(18)-C(16)-C(17)	112.7(2)
N(3)-C(16)-H(16)	107.6	C(18)-C(16)-H(16)	107.6
C(17)-C(16)-H(16)	107.6	C(16)-C(17)-H(17A)	109.5
C(16)-C(17)-H(17B)	109.5	H(17A)-C(17)-H(17B)	109.5
C(16)-C(17)-H(17C)	109.5	H(17A)-C(17)-H(17C)	109.5
H(17B)-C(17)-H(17C)	109.5	C(16)-C(18)-H(18A)	109.5
C(16)-C(18)-H(18B)	109.5	H(18A)-C(18)-H(18B)	109.5
C(16)-C(18)-H(18C)	109.5	H(18A)-C(18)-H(18C)	109.5
H(18B)-C(18)-H(18C)	109.5	N(4)-C(19)-C(20)	110.0(2)
N(4)-C(19)-C(21)	111.9(2)	C(20)-C(19)-C(21)	111.8(2)
N(4)-C(19)-H(19)	107.6	C(20)-C(19)-H(19)	107.6
C(21)-C(19)-H(19)	107.6	C(19)-C(20)-H(20A)	109.5
C(19)-C(20)-H(20B)	109.5	H(20A)-C(20)-H(20B)	109.5
C(19)-C(20)-H(20C)	109.5	H(20A)-C(20)-H(20C)	109.5
H(20B)-C(20)-H(20C)	109.5	C(19)-C(21)-H(21A)	109.5
C(19)-C(21)-H(21B)	109.5	H(21A)-C(21)-H(21B)	109.5
C(19)-C(21)-H(21C)	109.5	H(21A)-C(21)-H(21C)	109.5
H(21B)-C(21)-H(21C)	109.5	O(4)-C(22)-C(23)	107.6(7)
O(4)-C(22)-H(22A)	110.2	C(23)-C(22)-H(22A)	110.2
O(4)-C(22)-H(22B)	110.2	C(23)-C(22)-H(22B)	110.2
H(22A)-C(22)-H(22B)	108.5	C(24)-C(23)-C(22)	103.7(6)
C(24)-C(23)-H(23A)	111.0	C(22)-C(23)-H(23A)	111.0
C(24)-C(23)-H(23B)	111.0	C(22)-C(23)-H(23B)	111.0
H(23A)-C(23)-H(23B)	109.0	C(23)-C(24)-C(25)	108.7(6)
C(23)-C(24)-H(24A)	109.9	C(25)-C(24)-H(24A)	109.9
C(23)-C(24)-H(24B)	109.9	C(25)-C(24)-H(24B)	109.9
H(24A)-C(24)-H(24B)	108.3	O(4)-C(25)-C(24)	100.5(8)

O(4)-C(25)-H(25A)	111.7	C(24)-C(25)-H(25A)	111.7
O(4)-C(25)-H(25B)	111.7	C(24)-C(25)-H(25B)	111.7
H(25A)-C(25)-H(25B)	109.4	O(4A)-C(22A)-C(23A)	107.1(11)
O(4A)-C(22A)-C(25A)	44.3(8)	C(23A)-C(22A)-C(25A)	63.7(8)
O(4A)-C(22A)-H(22C)	110.3	C(23A)-C(22A)-H(22C)	110.3
C(25A)-C(22A)-H(22C)	133.6	O(4A)-C(22A)-H(22D)	110.3
C(23A)-C(22A)-H(22D)	110.3	C(25A)-C(22A)-H(22D)	116.6
H(22C)-C(22A)-H(22D)	108.6	C(24A)-C(23A)-C(22A)	107.5(11)
C(24A)-C(23A)-C(25A)	35.5(8)	C(22A)-C(23A)-C(25A)	72.6(9)
C(24A)-C(23A)-H(23C)	110.2	C(22A)-C(23A)-H(23C)	110.2
C(25A)-C(23A)-H(23C)	117.3	C(24A)-C(23A)-H(23D)	110.2
C(22A)-C(23A)-H(23D)	110.2	C(25A)-C(23A)-H(23D)	129.9
H(23C)-C(23A)-H(23D)	108.5	C(25A)-C(24A)-C(23A)	97.8(14)
C(25A)-C(24A)-H(24C)	112.2	C(23A)-C(24A)-H(24C)	112.2
C(25A)-C(24A)-H(24D)	112.2	C(23A)-C(24A)-H(24D)	112.2
H(24C)-C(24A)-H(24D)	109.8	C(24A)-C(25A)-O(4A)	126.5(15)
C(24A)-C(25A)-C(23A)	46.7(10)	O(4A)-C(25A)-C(23A)	82.8(10)
C(24A)-C(25A)-C(22A)	89.8(12)	O(4A)-C(25A)-C(22A)	39.9(7)
C(23A)-C(25A)-C(22A)	43.6(6)	C(24A)-C(25A)-H(25C)	105.7
O(4A)-C(25A)-H(25C)	105.7	C(23A)-C(25A)-H(25C)	141.4
C(22A)-C(25A)-H(25C)	138.2	C(24A)-C(25A)-H(25D)	105.7
O(4A)-C(25A)-H(25D)	105.7	C(23A)-C(25A)-H(25D)	107.5
C(22A)-C(25A)-H(25D)	106.5	H(25C)-C(25A)-H(25D)	106.1

Appendix 10 Crystallographic data for $Ru(IEt_2Me_2)_2(CO)_2(CO_3)$ (3B)

Identification code	k07mkw24
Empirical formula	$C_{44}H_{70}Cl_4N_8O_{11}Ru_2$
Formula weight	1231.02
Temperature	150(2) K
Wavelength	0.71073 Å
Crystal system	Monoclinic
Space group	*P*2/c
Unit cell dimensions	a = 15.6640(1)Å α = 90°
	b = 9.6590(1)Å β = 93.325(1)°
	c = 36.0120(3)Å γ = 90°
Volume	5439.39(8) $Å^3$
Z	4
Density (calculated)	1.503 Mg/m^3
Absorption coefficient	0.813 mm^{-1}
F(000)	2536
Crystal size	0.30 x 0.25 x 0.13 mm
Theta range for data collection	3.53 to 30.07°
Index ranges	-22<=h<=22; -13<=k<=13; -50<=l<=50
Reflections collected	94858
Independent reflections	15843 [R(int) = 0.0541]
Reflections observed (>2σ)	12505
Data Completeness	0.991

Absorption correction	Semi-empirical from equivalents
Max. and min. transmission	0.85 and 0.76
Refinement method	Full-matrix least-squares on F^2
Data / restraints / parameters	15843 / 2 / 638
Goodness-of-fit on F^2	1.028
Final R indices [I>2σ(I)]	R^1 = 0.0313 wR_2 = 0.0698
R indices (all data)	R^1 = 0.0496 wR_2 = 0.0764
Largest diff. peak and hole	0.707 and -0.842 eÅ^{-3}

Ru(1)-C(1)	1.8606(19)	O(10)-C(24)	1.228(2)
Ru(1)-C(2)	1.8681(19)	N(1)-C(4)	1.358(2)
Ru(1)-O(4)	2.0945(12)	N(1)-C(5)	1.398(2)
Ru(1)-O(3)	2.1045(12)	N(1)-C(7)	1.470(2)
Ru(1)-C(4)	2.1290(18)	N(2)-C(4)	1.355(2)
Ru(1)-C(13)	2.1318(17)	N(2)-C(6)	1.400(2)
Ru(2)-C(22)	1.864(2)	N(2)-C(11)	1.473(2)
Ru(2)-C(23)	1.866(2)	N(3)-C(13)	1.356(2)
Ru(2)-O(8)	2.0955(12)	N(3)-C(14)	1.402(2)
Ru(2)-O(9)	2.1036(12)	N(3)-C(16)	1.466(2)
Ru(2)-C(25)	2.1213(18)	N(4)-C(13)	1.359(2)
Ru(2)-C(34)	2.1264(19)	N(4)-C(15)	1.404(2)
Ru(2)-C(24)	2.5378(18)	N(4)-C(20)	1.473(2)
Cl(1)-C(43)	1.773(2)	N(5)-C(25)	1.361(2)
Cl(2)-C(43)	1.777(2)	N(5)-C(26)	1.400(2)
Cl(3)-C(44)	1.772(2)	N(5)-C(28)	1.474(2)
Cl(4)-C(44)	1.769(2)	N(6)-C(25)	1.360(2)
O(1)-C(1)	1.150(2)	N(6)-C(27)	1.395(2)
O(2)-C(2)	1.143(2)	N(6)-C(32)	1.468(2)
O(3)-C(3)	1.326(2)	N(7)-C(34)	1.360(3)
O(4)-C(3)	1.326(2)	N(7)-C(36)	1.397(3)
O(5)-C(3)	1.228(2)	N(7)-C(41)	1.468(3)
O(6)-C(22)	1.140(2)	N(8)-C(34)	1.354(3)
O(7)-C(23)	1.146(3)	N(8)-C(35)	1.401(3)
O(8)-C(24)	1.322(2)	N(8)-C(37)	1.466(3)
O(9)-C(24)	1.328(2)	C(5)-C(6)	1.351(3)
C(15)-C(19)	1.495(3)	C(5)-C(9)	1.499(3)
C(16)-C(17)	1.523(3)	C(6)-C(10)	1.493(3)
C(20)-C(21)	1.515(3)	C(7)-C(8)	1.517(3)
C(26)-C(27)	1.346(3)	C(11)-C(12)	1.523(3)
C(26)-C(30)	1.488(3)	C(14)-C(15)	1.343(3)
C(27)-C(31)	1.498(3)	C(14)-C(18)	1.490(3)
C(28)-C(29)	1.522(3)	C(35)-C(39)	1.495(3)
C(32)-C(33)	1.522(3)	C(36)-C(40)	1.494(3)
C(35)-C(36)	1.339(3)	C(37)-C(38)	1.520(3)
C(41)-C(42)	1.520(4)		
C(1)-Ru(1)-C(2)	83.59(8)	C(22)-Ru(2)-C(23)	84.82(9)
C(1)-Ru(1)-O(4)	106.72(7)	C(22)-Ru(2)-O(8)	104.89(7)
C(2)-Ru(1)-O(4)	169.57(6)	C(23)-Ru(2)-O(8)	169.73(7)
C(1)-Ru(1)-O(3)	169.65(7)	C(22)-Ru(2)-O(9)	167.47(7)
C(2)-Ru(1)-O(3)	106.75(7)	C(23)-Ru(2)-O(9)	107.59(7)

O(4)-Ru(1)-O(3)	62.93(5)	O(8)-Ru(2)-O(9)	62.83(5)
C(1)-Ru(1)-C(4)	92.57(7)	C(22)-Ru(2)-C(25)	95.95(8)
C(2)-Ru(1)-C(4)	94.04(7)	C(23)-Ru(2)-C(25)	90.86(8)
O(4)-Ru(1)-C(4)	87.17(6)	O(8)-Ru(2)-C(25)	84.89(6)
O(3)-Ru(1)-C(4)	87.03(6)	O(9)-Ru(2)-C(25)	85.81(6)
C(1)-Ru(1)-C(13)	93.05(7)	C(22)-Ru(2)-C(34)	91.99(8)
C(2)-Ru(1)-C(13)	90.83(7)	C(23)-Ru(2)-C(34)	95.28(8)
O(4)-Ru(1)-C(13)	87.12(6)	O(8)-Ru(2)-C(34)	87.83(6)
O(3)-Ru(1)-C(13)	86.68(6)	O(9)-Ru(2)-C(34)	85.27(6)
C(4)-Ru(1)-C(13)	172.94(6)	C(25)-Ru(2)-C(34)	170.37(7)
C(22)-Ru(2)-C(24)	136.23(8)	C(35)-N(8)-C(37)	123.39(17)
C(23)-Ru(2)-C(24)	138.87(8)	O(1)-C(1)-Ru(1)	176.74(18)
O(8)-Ru(2)-C(24)	31.34(5)	O(2)-C(2)-Ru(1)	176.78(17)
O(9)-Ru(2)-C(24)	31.52(5)	O(5)-C(3)-O(3)	124.62(17)
C(25)-Ru(2)-C(24)	83.51(6)	O(5)-C(3)-O(4)	123.90(17)
C(34)-Ru(2)-C(24)	86.99(6)	O(3)-C(3)-O(4)	111.48(15)
C(3)-O(3)-Ru(1)	92.55(10)	N(2)-C(4)-N(1)	104.40(15)
C(3)-O(4)-Ru(1)	92.98(10)	N(2)-C(4)-Ru(1)	128.09(12)
C(24)-O(8)-Ru(2)	93.12(10)	N(1)-C(4)-Ru(1)	127.44(13)
C(24)-O(9)-Ru(2)	92.58(10)	C(6)-C(5)-N(1)	106.84(15)
C(4)-N(1)-C(5)	111.09(15)	C(6)-C(5)-C(9)	129.38(18)
C(4)-N(1)-C(7)	125.47(16)	N(1)-C(5)-C(9)	123.78(17)
C(5)-N(1)-C(7)	123.37(15)	C(5)-C(6)-N(2)	106.11(16)
C(4)-N(2)-C(6)	111.55(15)	C(5)-C(6)-C(10)	130.57(17)
C(4)-N(2)-C(11)	125.84(15)	N(2)-C(6)-C(10)	123.28(16)
C(6)-N(2)-C(11)	122.57(15)	N(1)-C(7)-C(8)	112.94(16)
C(13)-N(3)-C(14)	110.94(16)	N(2)-C(11)-C(12)	112.45(16)
C(13)-N(3)-C(16)	124.76(16)	N(3)-C(13)-N(4)	104.60(15)
C(14)-N(3)-C(16)	124.22(16)	N(3)-C(13)-Ru(1)	127.71(13)
C(13)-N(4)-C(15)	111.14(16)	N(4)-C(13)-Ru(1)	127.60(13)
C(13)-N(4)-C(20)	125.82(15)	C(15)-C(14)-N(3)	106.97(16)
C(15)-N(4)-C(20)	122.19(16)	C(15)-C(14)-C(18)	129.47(19)
C(25)-N(5)-C(26)	110.89(16)	N(3)-C(14)-C(18)	123.50(19)
C(25)-N(5)-C(28)	125.70(16)	C(14)-C(15)-N(4)	106.33(17)
C(26)-N(5)-C(28)	123.28(16)	C(14)-C(15)-C(19)	130.90(19)
C(25)-N(6)-C(27)	111.19(16)	N(4)-C(15)-C(19)	122.74(19)
C(25)-N(6)-C(32)	124.92(16)	N(3)-C(16)-C(17)	113.21(17)
C(27)-N(6)-C(32)	123.83(16)	N(4)-C(20)-C(21)	111.00(16)
C(34)-N(7)-C(36)	110.98(18)	O(6)-C(22)-Ru(2)	177.9(2)
C(34)-N(7)-C(41)	125.47(18)	O(7)-C(23)-Ru(2)	175.8(2)
C(36)-N(7)-C(41)	123.43(19)	O(10)-C(24)-O(8)	124.35(18)
C(34)-N(8)-C(35)	111.27(18)	O(10)-C(24)-O(9)	124.29(17)
C(34)-N(8)-C(37)	125.33(17)	O(8)-C(24)-O(9)	111.37(15)
N(6)-C(25)-Ru(2)	127.96(13)	O(10)-C(24)-Ru(2)	177.56(14)
N(5)-C(25)-Ru(2)	127.27(13)	O(8)-C(24)-Ru(2)	55.54(8)
C(27)-C(26)-N(5)	106.70(17)	O(9)-C(24)-Ru(2)	55.90(8)
C(27)-C(26)-C(30)	130.07(19)	N(6)-C(25)-N(5)	104.44(15)
N(5)-C(26)-C(30)	123.23(18)	C(36)-C(35)-C(39)	129.9(2)
C(26)-C(27)-N(6)	106.77(17)	N(8)-C(35)-C(39)	123.6(2)
C(26)-C(27)-C(31)	129.87(19)	C(35)-C(36)-N(7)	106.94(19)
N(6)-C(27)-C(31)	123.35(19)	C(35)-C(36)-C(40)	129.6(2)

N(5)-C(28)-C(29)	113.42(16)	N(7)-C(36)-C(40)	123.4(2)
N(6)-C(32)-C(33)	112.86(17)	N(8)-C(37)-C(38)	112.81(16)
N(8)-C(34)-N(7)	104.34(17)	N(7)-C(41)-C(42)	112.5(2)
N(8)-C(34)-Ru(2)	128.54(14)	Cl(1)-C(43)-Cl(2)	111.49(12)
N(7)-C(34)-Ru(2)	126.91(14)	Cl(4)-C(44)-Cl(3)	110.50(12)
C(36)-C(35)-N(8)	106.46(19)		

Appendix 11 Crystallographic data for $Ru(I^iPr_2Me_2)_2(CO)_2(CO_3)$ (4B)

Identification code	k07mkw18
Empirical formula	C50 H80 N8 O10 Ru2
Formula weight	1155.36
Temperature	150(2) K
Wavelength	0.71073 Å
Crystal system	Monoclinic
Space group	P21
Unit cell dimensions	a = 10.6020(2)Å α = 90°
	b = 12.0620(2)Å β = 110.069(1)°
	c = 11.3930(2)Å γ = 90°
Volume	1368.49(4) $Å^3$
Z	1
Density (calculated)	1.402 Mg/m^3
Absorption coefficient	0.613 mm^{-1}
F(000)	604
Crystal size	0.25 x 0.20 x 0.20 mm
Theta range for data collection	3.65 to 27.48°
Index ranges	-13<=h<=13; -15<=k<=15; -14<=l<=14
Reflections collected	26125
Independent reflections	6230 [R(int) = 0.0360]
Reflections observed (>2σ)	5837
Data Completeness	0.997
Absorption correction	Semi-empirical from equivalents
Max. and min. transmission	0.94 and 0.91
Refinement method	Full-matrix least-squares on F^2
Data / restraints / parameters	6230 / 1 / 328
Goodness-of-fit on F^2	1.079
Final R indices [I>2σ(I)]	R^1 = 0.0249 wR_2 = 0.0544
R indices (all data)	R^1 = 0.0291 wR_2 = 0.0560
Absolute structure parameter	-0.027(18)
Largest diff. peak and hole	0.741 and -0.626 $eÅ^{-3}$

Ru(1)-C(1)	1.845(2)	N(2)-C(6)	1.405(3)
Ru(1)-C(2)	1.901(4)	N(2)-C(12)	1.484(3)
Ru(1)-O(3)	2.0975(13)	N(3)-C(15)	1.362(3)
Ru(1)-O(4)	2.1003(12)	N(3)-C(16)	1.406(3)
Ru(1)-C(15)	2.109(2)	N(3)-C(18)	1.478(3)
Ru(1)-C(4)	2.151(3)	N(4)-C(15)	1.358(3)

O(1)-C(1)	1.165(3)	N(4)-C(17)	1.405(3)
O(2)-C(2)	1.148(4)	N(4)-C(23)	1.485(3)
O(3)-C(3)	1.332(2)	C(5)-C(6)	1.353(3)
O(4)-C(3)	1.310(3)	C(5)-C(10)	1.493(3)
O(5)-C(3)	1.233(3)	C(6)-C(11)	1.491(3)
N(1)-C(4)	1.363(3)	C(7)-C(9)	1.485(5)
N(1)-C(5)	1.400(3)	C(7)-C(8)	1.524(5)
N(1)-C(7)	1.492(3)	C(12)-C(14)	1.527(3)
N(2)-C(4)	1.355(4)	C(12)-C(13)	1.528(3)
C(18)-C(19)	1.520(3)	C(16)-C(17)	1.342(4)
C(18)-C(20)	1.523(3)	C(16)-C(21)	1.497(4)
C(23)-C(24)	1.528(4)	C(17)-C(22)	1.509(3)
C(23)-C(25)	1.540(4)		
C(1)-Ru(1)-C(2)	86.01(13)	N(1)-C(4)-Ru(1)	126.95(19)
C(1)-Ru(1)-O(3)	164.13(8)	C(6)-C(5)-N(1)	106.63(19)
C(2)-Ru(1)-O(3)	92.36(10)	C(6)-C(5)-C(10)	127.3(2)
C(1)-Ru(1)-O(4)	101.35(8)	N(1)-C(5)-C(10)	126.0(2)
C(2)-Ru(1)-O(4)	93.82(11)	C(5)-C(6)-N(2)	106.4(2)
O(3)-Ru(1)-O(4)	62.98(5)	C(5)-C(6)-C(11)	127.6(2)
C(1)-Ru(1)-C(15)	94.15(9)	N(2)-C(6)-C(11)	125.9(2)
C(2)-Ru(1)-C(15)	92.07(11)	C(9)-C(7)-N(1)	111.9(3)
O(3)-Ru(1)-C(15)	101.69(7)	C(9)-C(7)-C(8)	113.3(3)
O(4)-Ru(1)-C(15)	163.76(7)	N(1)-C(7)-C(8)	111.1(2)
C(1)-Ru(1)-C(4)	96.63(12)	N(2)-C(12)-C(14)	110.94(18)
C(2)-Ru(1)-C(4)	177.17(8)	N(2)-C(12)-C(13)	112.52(19)
O(3)-Ru(1)-C(4)	84.82(9)	C(14)-C(12)-C(13)	112.6(2)
O(4)-Ru(1)-C(4)	84.68(10)	N(4)-C(15)-N(3)	105.42(18)
C(15)-Ru(1)-C(4)	88.76(10)	N(4)-C(15)-Ru(1)	126.69(15)
C(3)-O(3)-Ru(1)	92.14(12)	N(3)-C(15)-Ru(1)	127.68(17)
C(3)-O(4)-Ru(1)	92.65(11)	C(17)-C(16)-N(3)	106.5(2)
C(4)-N(1)-C(5)	111.1(2)	C(17)-C(16)-C(21)	128.4(2)
C(4)-N(1)-C(7)	123.5(2)	N(3)-C(16)-C(21)	125.0(2)
C(5)-N(1)-C(7)	125.24(19)	C(16)-C(17)-N(4)	107.45(19)
C(4)-N(2)-C(6)	111.3(2)	C(16)-C(17)-C(22)	126.8(2)
C(4)-N(2)-C(12)	123.2(2)	N(4)-C(17)-C(22)	125.7(3)
C(6)-N(2)-C(12)	125.08(19)	N(3)-C(18)-C(19)	113.7(2)
C(15)-N(3)-C(16)	110.50(19)	N(3)-C(18)-C(20)	110.8(2)
C(15)-N(3)-C(18)	123.7(2)	C(19)-C(18)-C(20)	113.4(2)
C(16)-N(3)-C(18)	125.6(2)	N(4)-C(23)-C(24)	112.8(2)
C(15)-N(4)-C(17)	110.09(19)	N(4)-C(23)-C(25)	111.4(2)
C(15)-N(4)-C(23)	123.40(18)	C(24)-C(23)-C(25)	112.3(2)
C(17)-N(4)-C(23)	126.48(19)	O(5)-C(3)-O(3)	123.2(2)
O(1)-C(1)-Ru(1)	173.0(2)	O(4)-C(3)-O(3)	112.17(17)
O(2)-C(2)-Ru(1)	177.4(2)	N(2)-C(4)-N(1)	104.6(3)
O(5)-C(3)-O(4)	124.6(2)	N(2)-C(4)-Ru(1)	128.46(19)

Appendix 12 Crystallographic data for $Ru(I^iPr_2Me_2)_2(CO)(C_5H_5N)(CO_3)$ (4C)

Identification code	k07mkw22
Empirical formula	C33 H53 N5 O5 Ru
Formula weight	700.87
Temperature	150(2) K
Wavelength	0.71073 Å
Crystal system	Monoclinic
Space group	P21/c
Unit cell dimensions	a = 11.3900(2)Å α = 90°
	b = 18.2000(2)Å β = 98.313(1)°
	c = 16.4380(2)Å γ = 90°
Volume	3371.76(8) $Å^3$
Z	4
Density (calculated)	1.381 Mg/m^3
Absorption coefficient	0.512 mm^{-1}
F(000)	1480
Crystal size	0.15 x 0.12 x 0.10 mm
Theta range for data collection	3.58 to 27.51°
Index ranges	-14<=h<=14; -23<=k<=23; -21<=l<=21
Reflections collected	65325
Independent reflections	7717 [R(int) = 0.0617]
Reflections observed (>2σ)	6024
Data Completeness	0.996
Absorption correction	Semi-empirical from equivalents
Max. and min. transmission	0.90 and 0.88
Refinement method	Full-matrix least-squares on F^2
Data / restraints / parameters	7717 / 0 / 409
Goodness-of-fit on F^2	1.046
Final R indices [I>2σ(I)]	R^1 = 0.0371 wR_2 = 0.0819
R indices (all data)	R^1 = 0.0563 wR_2 = 0.0899
Largest diff. peak and hole	0.723 and -0.639 $eÅ^{-3}$

Ru(1)-C(1)	1.820(3)	C(5)-C(10)	1.501(4)
Ru(1)-C(14)	2.066(2)	C(6)-C(8)	1.525(4)
Ru(1)-C(3)	2.081(2)	C(6)-C(7)	1.532(4)
Ru(1)-O(3)	2.1132(16)	C(11)-C(13)	1.525(3)
Ru(1)-O(2)	2.1211(16)	C(11)-C(12)	1.527(4)
Ru(1)-N(5)	2.174(2)	C(15)-C(16)	1.349(4)
O(1)-C(1)	1.160(3)	C(15)-C(20)	1.497(3)
O(2)-C(2)	1.327(3)	C(16)-C(21)	1.489(4)
O(3)-C(2)	1.316(3)	C(17)-C(19)	1.523(4)
O(4)-C(2)	1.236(3)	C(17)-C(18)	1.528(4)
O(5)-C(33)	1.350(5)	C(22)-C(24)	1.516(4)
O(5)-C(30)	1.405(5)	C(22)-C(23)	1.519(4)
N(1)-C(3)	1.370(3)	C(25)-C(26)	1.389(3)
N(1)-C(4)	1.400(3)	C(26)-C(27)	1.376(4)
N(1)-C(6)	1.486(3)	C(27)-C(28)	1.383(4)

N(2)-C(3)	1.373(3)	C(28)-C(29)	1.380(4)
N(2)-C(5)	1.401(3)	C(30)-C(31)	1.475(6)
N(2)-C(11)	1.480(3)	C(31)-C(32)	1.585(6)
N(3)-C(14)	1.363(3)	C(32)-C(33)	1.485(5)
N(3)-C(15)	1.405(3)	N(4)-C(22)	1.488(3)
N(3)-C(17)	1.482(3)	N(5)-C(29)	1.344(3)
N(4)-C(14)	1.363(3)	N(5)-C(25)	1.346(3)
N(4)-C(16)	1.404(3)	C(4)-C(5)	1.358(4)
C(4)-C(9)	1.496(4)		
C(1)-Ru(1)-C(14)	94.47(10)	N(1)-C(6)-C(8)	112.3(2)
C(1)-Ru(1)-C(3)	90.17(11)	N(1)-C(6)-C(7)	112.2(2)
C(14)-Ru(1)-C(3)	92.47(9)	C(8)-C(6)-C(7)	111.8(2)
C(1)-Ru(1)-O(3)	103.51(9)	N(2)-C(11)-C(13)	112.2(2)
C(14)-Ru(1)-O(3)	87.95(8)	N(2)-C(11)-C(12)	112.3(2)
C(3)-Ru(1)-O(3)	166.24(8)	C(13)-C(11)-C(12)	112.8(2)
C(1)-Ru(1)-O(2)	165.46(9)	N(4)-C(14)-N(3)	104.55(18)
C(14)-Ru(1)-O(2)	88.75(8)	N(4)-C(14)-Ru(1)	128.10(16)
C(3)-Ru(1)-O(2)	103.87(8)	N(3)-C(14)-Ru(1)	127.33(17)
O(3)-Ru(1)-O(2)	62.39(7)	C(16)-C(15)-N(3)	106.5(2)
C(1)-Ru(1)-N(5)	87.68(9)	C(16)-C(15)-C(20)	128.3(2)
C(14)-Ru(1)-N(5)	176.24(8)	N(3)-C(15)-C(20)	125.2(2)
C(3)-Ru(1)-N(5)	90.61(8)	C(15)-C(16)-N(4)	106.9(2)
O(3)-Ru(1)-N(5)	88.55(7)	C(15)-C(16)-C(21)	127.6(2)
O(2)-Ru(1)-N(5)	88.41(7)	N(4)-C(16)-C(21)	125.5(2)
C(2)-O(2)-Ru(1)	92.35(14)	N(3)-C(17)-C(19)	113.2(2)
C(2)-O(3)-Ru(1)	93.01(14)	N(3)-C(17)-C(18)	111.4(2)
C(33)-O(5)-C(30)	105.4(3)	C(19)-C(17)-C(18)	113.3(2)
C(3)-N(1)-C(4)	111.5(2)	N(4)-C(22)-C(24)	111.7(2)
C(3)-N(1)-C(6)	123.0(2)	N(4)-C(22)-C(23)	112.1(2)
C(4)-N(1)-C(6)	125.5(2)	C(24)-C(22)-C(23)	113.9(3)
C(3)-N(2)-C(5)	111.0(2)	N(5)-C(25)-C(26)	123.3(2)
C(3)-N(2)-C(11)	124.0(2)	C(27)-C(26)-C(25)	119.8(2)
C(5)-N(2)-C(11)	124.9(2)	C(26)-C(27)-C(28)	117.6(2)
C(14)-N(3)-C(15)	111.1(2)	C(29)-C(28)-C(27)	119.5(2)
C(14)-N(3)-C(17)	122.22(19)	N(5)-C(29)-C(28)	123.9(2)
C(15)-N(3)-C(17)	126.0(2)	O(5)-C(30)-C(31)	106.4(3)
C(14)-N(4)-C(16)	110.9(2)	C(30)-C(31)-C(32)	98.8(3)
C(14)-N(4)-C(22)	122.62(19)	C(33)-C(32)-C(31)	102.2(3)
C(16)-N(4)-C(22)	126.2(2)	O(5)-C(33)-C(32)	110.2(3)
C(29)-N(5)-C(25)	116.0(2)	N(2)-C(3)-Ru(1)	130.56(18)
C(29)-N(5)-Ru(1)	120.68(16)	C(5)-C(4)-N(1)	106.4(2)
C(25)-N(5)-Ru(1)	123.23(16)	C(5)-C(4)-C(9)	127.9(2)
O(1)-C(1)-Ru(1)	175.1(2)	N(1)-C(4)-C(9)	125.6(2)
O(4)-C(2)-O(3)	124.0(2)	C(4)-C(5)-N(2)	107.0(2)
O(4)-C(2)-O(2)	123.8(2)	C(4)-C(5)-C(10)	126.5(2)
O(3)-C(2)-O(2)	112.2(2)	N(2)-C(5)-C(10)	126.3(2)
N(1)-C(3)-N(2)	104.1(2)	N(1)-C(3)-Ru(1)	125.27(17)

Appendix 13 Crystallographic data for $Ru(I^iPr_2Me_2)_2(CO)_2Cl_2$

Identification code	k08mkw24
Empirical formula	C25.44 H42.88 Cl4.88 N4 O2 Ru
Formula weight	710.86
Temperature	150(2) K
Wavelength	0.71073 Å
Crystal system	Tetragonal
Space group	P42nm
Unit cell dimensions	a = 13.0470(2)Å α = 90°
	b = 13.0470(2)Å β = 90°
	c = 9.9420(2)Å γ = 90°
Volume	1692.37(5) $Å^3$
Z	2
Density (calculated)	1.395 Mg/m^3
Absorption coefficient	0.876 mm^{-1}
F(000)	733
Crystal size	0.20 x 0.20 x 0.15 mm
Theta range for data collection	4.05 to 27.48°
Index ranges	-16<=h<=16; -16<=k<=16; -12<=l<=12
Reflections collected	29304
Independent reflections	2045 [R(int) = 0.0566]
Reflections observed (>2σ)	1744
Data Completeness	0.995
Absorption correction	Semi-empirical from equivalents
Max. and min. transmission	0.90 and 0.84
Refinement method	Full-matrix least-squares on F^2
Data / restraints / parameters	2045 / 8 / 113
Goodness-of-fit on F^2	1.059
Final R indices [I>2σ(I)]	R^1 = 0.0549 wR_2 = 0.1502
R indices (all data)	R^1 = 0.0643 wR_2 = 0.1580
Absolute structure parameter	0.09(11)
Largest diff. peak and hole	1.031 and -0.650 $eÅ^{-3}$

Ru(1)-C(1)	1.792(14)	Ru(1)-C(1)#1	1.792(14)
Ru(1)-C(2)#1	2.164(6)	Ru(1)-C(2)	2.164(6)
Ru(1)-Cl(1)#1	2.483(4)	Ru(1)-Cl(1)	2.483(4)
Cl(2)-C(8)	1.732(11)	Cl(3)-C(8)	1.802(11)
O(1)-C(1)	1.020(14)	N(2)-C(2)	1.362(5)
N(2)-C(3)	1.394(5)	N(2)-C(4)	1.479(5)
C(2)-N(2)#2	1.362(5)	C(3)-C(3)#2	1.356(10)
C(3)-C(7)	1.496(6)	C(4)-C(5)	1.508(13)
C(4)-C(6)	1.567(14)	C(4)-H(4)	1.0000
C(5)-H(5A)	0.9800	C(5)-H(5B)	0.9800
C(5)-H(5C)	0.9800	C(6)-H(6A)	0.9800
C(6)-H(6B)	0.9800	C(6)-H(6C)	0.9800
C(7)-H(7A)	0.9800	C(7)-H(7B)	0.9800
C(7)-H(7C)	0.9800	C(8)-H(8A)	0.9900

C(8)-H(8B)	0.9900		
C(1)-Ru(1)-C(1)#1	84.2(8)	C(1)-Ru(1)-C(2)#1	90.59(19)
C(1)#1-Ru(1)-C(2)#1	90.59(19)	C(1)-Ru(1)-C(2)	90.59(19)
C(1)#1-Ru(1)-C(2)	90.59(19)	C(2)#1-Ru(1)-C(2)	178.4(5)
C(1)-Ru(1)-Cl(1)#1	179.0(4)	C(1)#1-Ru(1)-Cl(1)#1	96.8(4)
C(2)#1-Ru(1)-Cl(1)#1	89.40(19)	C(2)-Ru(1)-Cl(1)#1	89.40(19)
C(1)-Ru(1)-Cl(1)	96.8(4)	C(1)#1-Ru(1)-Cl(1)	179.0(4)
C(2)#1-Ru(1)-Cl(1)	89.40(19)	C(2)-Ru(1)-Cl(1)	89.40(19)
Cl(1)#1-Ru(1)-Cl(1)	82.25(13)	C(2)-N(2)-C(3)	111.1(4)
C(2)-N(2)-C(4)	124.8(4)	C(3)-N(2)-C(4)	124.1(3)
O(1)-C(1)-Ru(1)	177.6(12)	N(2)#2-C(2)-N(2)	104.5(5)
N(2)#2-C(2)-Ru(1)	127.7(2)	N(2)-C(2)-Ru(1)	127.7(2)
C(3)#2-C(3)-N(2)	106.6(2)	C(3)#2-C(3)-C(7)	126.2(3)
N(2)-C(3)-C(7)	127.1(4)	N(2)-C(4)-C(5)	112.7(7)
N(2)-C(4)-C(6)	110.5(7)	C(5)-C(4)-C(6)	113.1(5)
N(2)-C(4)-H(4)	106.7	C(5)-C(4)-H(4)	106.7
C(6)-C(4)-H(4)	106.7	C(4)-C(5)-H(5A)	109.5
C(4)-C(5)-H(5B)	109.5	H(5A)-C(5)-H(5B)	109.5
C(4)-C(5)-H(5C)	109.5	H(5A)-C(5)-H(5C)	109.5
H(5B)-C(5)-H(5C)	109.5	C(4)-C(6)-H(6A)	109.5
C(4)-C(6)-H(6B)	109.5	H(6A)-C(6)-H(6B)	109.5
C(4)-C(6)-H(6C)	109.5	H(6A)-C(6)-H(6C)	109.5
H(6B)-C(6)-H(6C)	109.5	C(3)-C(7)-H(7A)	109.5
C(3)-C(7)-H(7B)	109.5	H(7A)-C(7)-H(7B)	109.5
C(3)-C(7)-H(7C)	109.5	H(7A)-C(7)-H(7C)	109.5
H(7B)-C(7)-H(7C)	109.5	Cl(2)-C(8)-Cl(3)	106.5(8)
Cl(2)-C(8)-H(8A)	110.4	Cl(3)-C(8)-H(8A)	110.4
Cl(2)-C(8)-H(8B)	110.4	Cl(3)-C(8)-H(8B)	110.4
H(8A)-C(8)-H(8B)	108.6		

Appendix 14 Crystallographic data for $Ru(I^iPr_2)_2(CO)_2(CO_3)$ (5B)

Identification code	k07mkw6
Empirical formula	C22 H34 Cl2 N4 O5 Ru
Formula weight	606.50
Temperature	150(2) K
Wavelength	0.71073 Å
Crystal system	Monoclinic
Space group	P21/n
Unit cell dimensions	a = 10.2360(1)Å α = 90°
	b = 10.7810(1)Å β = 92.132(1)°
	c = 25.1870(3)Å γ = 90°
Volume	2777.57(5) $Å^3$
Z	4
Density (calculated)	1.450 Mg/m^3
Absorption coefficient	0.794 mm^{-1}
F(000)	1248

Crystal size	0.20 x 0.12 x 0.07 mm
Theta range for data collection	3.62 to 27.54°
Index ranges	-13<=h<=13; -13<=k<=13; -32<=l<=32
Reflections collected	40649
Independent reflections	6352 [R(int) = 0.0348]
Reflections observed (>2σ)	5763
Data Completeness	0.992
Absorption correction	Semi-empirical from equivalents
Max. and min. transmission	0.82 and 0.78
Refinement method	Full-matrix least-squares on F^2
Data / restraints / parameters	6352 / 0 / 325
Goodness-of-fit on F^2	1.174
Final R indices [I>2σ(I)]	R^1 = 0.0390 wR_2 = 0.0870
R indices (all data)	R^1 = 0.0447 wR_2 = 0.0895
Largest diff. peak and hole	1.455 and -1.491 eÅ^{-3}

Ru(1)-C(1)	1.861(3)	Ru(1)-C(2)	1.937(3)
Ru(1)-C(13)	2.083(3)	Ru(1)-O(3)	2.0992(19)
Ru(1)-O(4)	2.1165(19)	Ru(1)-C(4)	2.121(3)
Ru(1)-C(3)	2.536(3)	Cl(1)-C(22)	1.717(6)
Cl(2A)-C(22)	1.649(6)	Cl(2B)-C(22)	2.000(7)
O(1)-C(1)	1.142(4)	O(2)-C(2)	1.130(4)
O(3)-C(3)	1.328(3)	O(4)-C(3)	1.314(3)
O(5)-C(3)	1.231(4)	N(1)-C(4)	1.353(4)
N(1)-C(5)	1.386(4)	N(1)-C(7)	1.476(4)
N(2)-C(4)	1.362(4)	N(2)-C(6)	1.389(4)
N(2)-C(10)	1.478(4)	N(3)-C(13)	1.369(4)
N(3)-C(14)	1.391(4)	N(3)-C(16)	1.479(4)
N(4)-C(13)	1.360(4)	N(4)-C(15)	1.392(4)
N(4)-C(19)	1.480(4)	C(5)-C(6)	1.344(4)
C(7)-C(8)	1.510(5)	C(7)-C(9)	1.527(5)
C(10)-C(11)	1.523(4)	C(10)-C(12)	1.523(4)
C(14)-C(15)	1.334(5)	C(16)-C(18)	1.521(4)
C(16)-C(17)	1.525(5)	C(19)-C(21)	1.523(5)
C(19)-C(20)	1.526(5)		
C(1)-Ru(1)-C(2)	88.90(13)	C(1)-Ru(1)-C(13)	92.10(12)
C(2)-Ru(1)-C(13)	92.58(12)	C(1)-Ru(1)-O(3)	167.48(10)
C(2)-Ru(1)-O(3)	91.43(10)	C(13)-Ru(1)-O(3)	100.38(9)
C(1)-Ru(1)-O(4)	104.82(11)	C(2)-Ru(1)-O(4)	92.94(11)
C(13)-Ru(1)-O(4)	162.28(9)	O(3)-Ru(1)-O(4)	62.66(7)
C(1)-Ru(1)-C(4)	95.20(12)	C(2)-Ru(1)-C(4)	175.46(12)
C(13)-Ru(1)-C(4)	89.21(11)	O(3)-Ru(1)-C(4)	84.14(9)
O(4)-Ru(1)-C(4)	84.15(9)	C(1)-Ru(1)-C(3)	135.96(11)
C(2)-Ru(1)-C(3)	94.15(11)	C(13)-Ru(1)-C(3)	131.49(10)
O(3)-Ru(1)-C(3)	31.55(8)	O(4)-Ru(1)-C(3)	31.19(8)
C(4)-Ru(1)-C(3)	81.55(10)	C(3)-O(3)-Ru(1)	92.67(16)
C(3)-O(4)-Ru(1)	92.31(15)	C(4)-N(1)-C(5)	110.9(2)
C(4)-N(1)-C(7)	125.4(3)	C(5)-N(1)-C(7)	123.1(3)
C(4)-N(2)-C(6)	110.8(2)	C(4)-N(2)-C(10)	126.2(2)
C(6)-N(2)-C(10)	122.6(2)	C(13)-N(3)-C(14)	110.9(3)

C(13)-N(3)-C(16)	127.5(2)	C(14)-N(3)-C(16)	121.6(3)
C(13)-N(4)-C(15)	110.6(3)	C(13)-N(4)-C(19)	127.3(2)
C(15)-N(4)-C(19)	122.1(3)	O(1)-C(1)-Ru(1)	177.2(3)
O(2)-C(2)-Ru(1)	179.3(3)	O(5)-C(3)-O(4)	125.2(3)
O(5)-C(3)-O(3)	122.7(3)	O(4)-C(3)-O(3)	112.1(2)
O(5)-C(3)-Ru(1)	175.8(2)	O(4)-C(3)-Ru(1)	56.50(13)
O(3)-C(3)-Ru(1)	55.78(13)	N(1)-C(4)-N(2)	104.6(2)
N(1)-C(4)-Ru(1)	128.2(2)	N(2)-C(4)-Ru(1)	127.2(2)
C(6)-C(5)-N(1)	107.1(3)	C(5)-C(6)-N(2)	106.6(3)
N(1)-C(7)-C(8)	110.4(3)	N(1)-C(7)-C(9)	109.9(3)
C(8)-C(7)-C(9)	113.3(4)	N(2)-C(10)-C(11)	110.8(2)
N(2)-C(10)-C(12)	109.8(2)	C(11)-C(10)-C(12)	111.6(2)
N(4)-C(13)-N(3)	104.3(2)	N(4)-C(13)-Ru(1)	125.8(2)
N(3)-C(13)-Ru(1)	129.7(2)	C(15)-C(14)-N(3)	106.7(3)
C(14)-C(15)-N(4)	107.6(3)	N(3)-C(16)-C(18)	109.8(3)
N(3)-C(16)-C(17)	111.2(3)	C(18)-C(16)-C(17)	112.1(3)
N(4)-C(19)-C(21)	110.6(3)	N(4)-C(19)-C(20)	110.5(3)
C(21)-C(19)-C(20)	111.5(3)	Cl(2A)-C(22)-Cl(1)	106.8(3)
Cl(2A)-C(22)-Cl(2B)	60.0(2)	Cl(1)-C(22)-Cl(2B)	107.6(3)

Appendix 15 Crystallographic data for $Ru(IPr)_2(CO)HCl$ (6A)

Identification code	k06mkw7
Empirical formula	$C_{61}H_{87}ClN_4ORu$
Formula weight	1028.87
Temperature	150(2) K
Wavelength	0.71073 Å
Crystal system	Orthorhombic
Space group	$P22_12_1$
Unit cell dimensions	a = 10.6270(1)Å α = 90°
	b = 13.0200(1)Å β = 90°
	c = 20.7530(2)Å γ = 90°
Volume	2871.46(4) $Å^3$
Z	2
Density (calculated)	1.190 Mg/m^3
Absorption coefficient	0.361 mm^{-1}
F(000)	1100
Crystal size	0.30 x 0.20 x 0.20 mm
Theta range for data collection	3.51 to 30.03°
Index ranges	-14<=h<=14; -18<=k<=18; -29<=l<=29
Reflections collected	50119
Independent reflections	8385 [R(int) = 0.0376]
Reflections observed (>2σ)	8009
Data Completeness	0.996
Absorption correction	Semi-empirical from equivalents
Max. and min. transmission	0.93 and 0.89
Refinement method	Full-matrix least-squares on F^2
Data / restraints / parameters	8385 / 1 / 333

Goodness-of-fit on F^2	1.050
Final R indices [I>2σ(I)]	R^1 = 0.0272 wR_2 = 0.0683
R indices (all data)	R^1 = 0.0293 wR_2 = 0.0693
Absolute structure parameter	-0.024(17)
Largest diff. peak and hole	0.396 and -0.480 eÅ^{-3}

Ru(1)-H(1)	1.603(10)	Ru(1)-C(1A)	1.870(7)
Ru(1)-C(1)	1.900(7)	Ru(1)-C(2)#1	2.0872(13)
Ru(1)-C(2)	2.0872(13)	Ru(1)-Cl(1)	2.327(2)
Ru(1)-Cl(1A)	2.3314(17)	O(1)-C(1)	1.044(7)
N(1)-C(2)	1.3685(17)	N(1)-C(3)	1.3900(19)
N(1)-C(5)	1.4467(18)	N(2)-C(2)	1.3666(17)
N(2)-C(4)	1.384(2)	N(2)-C(17)	1.4432(18)
C(3)-C(4)	1.347(3)	C(5)-C(10)	1.401(2)
C(5)-C(6)	1.401(2)	C(6)-C(7)	1.398(2)
C(6)-C(11)	1.517(2)	C(7)-C(8)	1.379(3)
C(8)-C(9)	1.388(3)	C(9)-C(10)	1.400(2)
C(10)-C(14)	1.523(2)	C(11)-C(13)	1.516(3)
C(11)-C(12)	1.525(3)	C(14)-C(16)	1.525(3)
C(14)-C(15)	1.544(3)	C(17)-C(18)	1.400(2)
C(17)-C(22)	1.404(2)	C(18)-C(19)	1.395(2)
C(18)-C(23)	1.519(2)	C(19)-C(20)	1.384(3)
C(20)-C(21)	1.384(3)	C(21)-C(22)	1.399(2)
C(22)-C(26)	1.516(2)	C(23)-C(25)	1.526(3)
C(23)-C(24)	1.533(3)	C(26)-C(28)	1.529(2)
C(26)-C(27)	1.532(3)	C(29)-C(30)	1.512(6)
C(30)-C(31)	1.569(6)	O(1A)-C(1A)	1.172(6)
C(29A)-C(30A)	1.540(7)	C(30A)-C(31A)	1.538(6)
C(30A)-C(31A)#2	1.886(6)	C(31A)-C(31A)#2	0.712(6)
C(31A)-C(30A)#2	1.886(6)		
H(1)-Ru(1)-C(1A)	88.7(12)	H(1)-Ru(1)-C(1)	91.3(12)
C(1A)-Ru(1)-C(1)	180.0	H(1)-Ru(1)-C(2)#1	87.2(12)
C(1A)-Ru(1)-C(2)#1	90.61(4)	C(1)-Ru(1)-C(2)#1	89.39(4)
H(1)-Ru(1)-C(2)	92.8(12)	C(1A)-Ru(1)-C(2)	90.61(4)
C(1)-Ru(1)-C(2)	89.39(4)	C(2)#1-Ru(1)-C(2)	178.78(8)
H(1)-Ru(1)-Cl(1)	88.7(12)	C(1A)-Ru(1)-Cl(1)	0.0
C(1)-Ru(1)-Cl(1)	180.0	C(2)#1-Ru(1)-Cl(1)	90.61(4)
C(2)-Ru(1)-Cl(1)	90.61(4)	H(1)-Ru(1)-Cl(1A)	91.3(12)
C(1A)-Ru(1)-Cl(1A)	180.0	C(1)-Ru(1)-Cl(1A)	0.0
C(2)#1-Ru(1)-Cl(1A)	89.39(4)	C(2)-Ru(1)-Cl(1A)	89.39(4)
Cl(1)-Ru(1)-Cl(1A)	180.0	C(2)-N(1)-C(3)	111.88(13)
C(2)-N(1)-C(5)	127.30(12)	C(3)-N(1)-C(5)	120.75(13)
C(2)-N(2)-C(4)	112.20(12)	C(2)-N(2)-C(17)	127.97(12)
C(4)-N(2)-C(17)	119.58(13)	O(1)-C(1)-Ru(1)	180.0
N(2)-C(2)-N(1)	102.79(11)	N(2)-C(2)-Ru(1)	128.15(9)
N(1)-C(2)-Ru(1)	129.06(9)	C(4)-C(3)-N(1)	106.50(13)
C(3)-C(4)-N(2)	106.62(14)	C(10)-C(5)-C(6)	123.14(14)
C(10)-C(5)-N(1)	118.61(14)	C(6)-C(5)-N(1)	118.11(14)
C(7)-C(6)-C(5)	117.36(15)	C(7)-C(6)-C(11)	120.48(16)
C(5)-C(6)-C(11)	122.08(14)	C(8)-C(7)-C(6)	120.99(16)

C(7)-C(8)-C(9)	120.46(15)	C(8)-C(9)-C(10)	121.09(17)
C(9)-C(10)-C(5)	116.96(16)	C(9)-C(10)-C(14)	119.93(16)
C(5)-C(10)-C(14)	123.09(14)	C(13)-C(11)-C(6)	110.66(15)
C(13)-C(11)-C(12)	110.6(2)	C(6)-C(11)-C(12)	112.37(16)
C(10)-C(14)-C(16)	112.35(16)	C(10)-C(14)-C(15)	110.27(17)
C(16)-C(14)-C(15)	110.44(19)	C(18)-C(17)-C(22)	123.07(14)
C(18)-C(17)-N(2)	118.80(14)	C(22)-C(17)-N(2)	117.84(14)
C(19)-C(18)-C(17)	116.89(15)	C(19)-C(18)-C(23)	119.67(15)
C(17)-C(18)-C(23)	123.43(14)	C(20)-C(19)-C(18)	121.70(16)
C(19)-C(20)-C(21)	120.03(15)	C(20)-C(21)-C(22)	121.03(16)
C(21)-C(22)-C(17)	117.26(15)	C(21)-C(22)-C(26)	120.56(15)
C(17)-C(22)-C(26)	122.10(14)	C(18)-C(23)-C(25)	112.54(16)
C(18)-C(23)-C(24)	110.39(17)	C(25)-C(23)-C(24)	109.45(19)
C(22)-C(26)-C(28)	111.97(14)	C(22)-C(26)-C(27)	110.17(15)
C(28)-C(26)-C(27)	111.43(16)	C(29)-C(30)-C(31)	111.8(4)
O(1A)-C(1A)-Ru(1)	180.0	C(31A)-C(30A)-C(29A)	114.5(4)
C(31A)-C(30A)-C(31A)#2	21.0(2)	C(29A)-C(30A)-C(31A)#2	132.0(4)
C(31A)#2-C(31A)-C(30A)	108.2(6)	C(31A)#2-C(31A)-C(30A)#2	50.8(5)
C(30A)-C(31A)-C(30A)#2	126.0(4)		

Appendix 16 Crystallographic data for $Ru(SIPr)_2(CO)HCl$ (7A)

Identification code	k06mkw6
Empirical formula	C62 H93 Cl N4 O Ru
Formula weight	1046.92
Temperature	150(2) K
Wavelength	0.71073 Å
Crystal system	Orthorhombic
Space group	P22121
Unit cell dimensions	a = 10.6170(1)Å α = 90°
	b = 13.0050(1)Å β = 90°
	c = 20.6750(1)Å γ = 90°
Volume	2854.68(4) $Å^3$
Z	2
Density (calculated)	1.218 Mg/m^3
Absorption coefficient	0.364 mm^{-1}
F(000)	1124
Crystal size	0.50 x 0.50 x 0.40 mm
Theta range for data collection	3.52 to 30.03°
Index ranges	-14<=h<=14; -18<=k<=18; -29<=l<=29
Reflections collected	58230
Independent reflections	8352 [R(int) = 0.0438]
Reflections observed (>2σ)	7900
Data Completeness	0.997
Absorption correction	Semi-empirical from equivalents
Max. and min. transmission	0.84 and 0.77
Refinement method	Full-matrix least-squares on F^2
Data / restraints / parameters	8352 / 42 / 361

Goodness-of-fit on F^2	1.035
Final R indices [I>2σ(I)]	R^1 = 0.0305 wR_2 = 0.0754
R indices (all data)	R^1 = 0.0337 wR_2 = 0.0775
Absolute structure parameter	0.00
Largest diff. peak and hole	0.644 and -0.531 eÅ^{-3}

Ru(1)-C(1A)	1.829(12)	Ru(1)-C(1)	1.861(7)
Ru(1)-C(2)	2.0889(15)	Ru(1)-C(2)#1	2.0889(15)
Ru(1)-Cl(1A)	2.346(3)	Ru(1)-Cl(1)	2.3500(19)
O(1)-C(1)	1.146(6)	O(1A)-C(1A)	1.220(10)
N(1)-C(2)	1.356(2)	N(1)-C(5)	1.439(2)
N(1)-C(3)	1.479(2)	N(2)-C(2)	1.352(2)
N(2)-C(17)	1.439(2)	N(2)-C(4)	1.470(2)
C(30A)-C(31A)	1.426(11)	C(30A)-C(29)	1.537(7)
C(31A)-C(32A)	1.427(9)	C(3)-C(4)	1.480(3)
C(5)-C(6)	1.400(3)	C(5)-C(10)	1.406(3)
C(6)-C(7)	1.396(3)	C(6)-C(11)	1.521(3)
C(7)-C(8)	1.382(3)	C(8)-C(9)	1.383(3)
C(9)-C(10)	1.397(3)	C(10)-C(14)	1.524(3)
C(11)-C(13)	1.521(3)	C(11)-C(12)	1.542(3)
C(14)-C(16)	1.527(3)	C(14)-C(15)	1.544(3)
C(17)-C(22)	1.401(3)	C(17)-C(18)	1.404(3)
C(18)-C(19)	1.403(3)	C(18)-C(23)	1.521(3)
C(19)-C(20)	1.380(3)	C(20)-C(21)	1.391(3)
C(21)-C(22)	1.395(3)	C(22)-C(26)	1.525(3)
C(23)-C(24)	1.524(3)	C(23)-C(25)	1.542(3)
C(26)-C(28)	1.532(3)	C(26)-C(27)	1.543(3)
C(29)-C(30)	1.244(4)	C(29)-C(30)#2	1.244(4)
C(29)-C(30A)#2	1.537(7)	C(29)-C(31)	1.878(11)
C(29)-C(31)#2	1.878(11)	C(30)-C(31)	1.268(10)
C(30)-C(32)	1.924(8)	C(31)-C(32)	1.304(13)
C(1A)-Ru(1)-C(1)	180.0	C(1A)-Ru(1)-C(2)	88.80(5)
C(1)-Ru(1)-C(2)	91.20(5)	C(1A)-Ru(1)-C(2)#1	88.80(5)
C(1)-Ru(1)-C(2)#1	91.20(5)	C(2)-Ru(1)-C(2)#1	177.60(9)
C(1A)-Ru(1)-Cl(1A)	180.0	C(1)-Ru(1)-Cl(1A)	0.0
C(2)-Ru(1)-Cl(1A)	91.20(5)	C(2)#1-Ru(1)-Cl(1A)	91.20(5)
C(1A)-Ru(1)-Cl(1)	0.0	C(1)-Ru(1)-Cl(1)	180.0
C(2)-Ru(1)-Cl(1)	88.80(5)	C(2)#1-Ru(1)-Cl(1)	88.80(5)
Cl(1A)-Ru(1)-Cl(1)	180.0	C(2)-N(1)-C(5)	128.03(14)
C(2)-N(1)-C(3)	112.56(15)	C(5)-N(1)-C(3)	117.11(16)
C(2)-N(2)-C(17)	128.84(14)	C(2)-N(2)-C(4)	113.11(14)
C(17)-N(2)-C(4)	115.64(14)	C(31A)-C(30A)-C(29)	113.4(7)
C(30A)-C(31A)-C(32A)	115.9(9)	O(1)-C(1)-Ru(1)	180.0
N(2)-C(2)-N(1)	106.09(14)	N(2)-C(2)-Ru(1)	126.40(11)
N(1)-C(2)-Ru(1)	127.49(11)	N(1)-C(3)-C(4)	102.53(16)
N(2)-C(4)-C(3)	102.72(15)	C(6)-C(5)-C(10)	122.14(16)
C(6)-C(5)-N(1)	119.07(17)	C(10)-C(5)-N(1)	118.48(16)
C(7)-C(6)-C(5)	118.02(18)	C(7)-C(6)-C(11)	119.06(18)
C(5)-C(6)-C(11)	122.87(17)	C(8)-C(7)-C(6)	120.87(19)
C(7)-C(8)-C(9)	120.27(18)	C(8)-C(9)-C(10)	121.2(2)

C(9)-C(10)-C(5)	117.45(19)	C(9)-C(10)-C(14)	119.47(19)
C(5)-C(10)-C(14)	123.07(16)	C(13)-C(11)-C(6)	111.92(18)
C(13)-C(11)-C(12)	108.1(2)	C(6)-C(11)-C(12)	111.04(18)
C(10)-C(14)-C(16)	112.55(19)	C(10)-C(14)-C(15)	109.54(18)
C(16)-C(14)-C(15)	109.0(2)	C(22)-C(17)-C(18)	122.02(16)
C(22)-C(17)-N(2)	118.44(17)	C(18)-C(17)-N(2)	119.03(17)
C(19)-C(18)-C(17)	118.04(18)	C(19)-C(18)-C(23)	119.05(18)
C(17)-C(18)-C(23)	122.86(16)	C(20)-C(19)-C(18)	120.85(19)
C(19)-C(20)-C(21)	120.00(18)	C(20)-C(21)-C(22)	121.4(2)
C(21)-C(22)-C(17)	117.70(18)	C(21)-C(22)-C(26)	118.83(19)
C(17)-C(22)-C(26)	123.46(17)	C(18)-C(23)-C(24)	111.66(17)
C(18)-C(23)-C(25)	110.61(18)	C(24)-C(23)-C(25)	110.96(19)
C(22)-C(26)-C(28)	112.27(18)	C(22)-C(26)-C(27)	110.5(2)
C(28)-C(26)-C(27)	108.7(2)	C(30)-C(29)-C(30)#2	119.2(6)
C(30)-C(29)-C(30A)	20.9(3)	C(30)#2-C(29)-C(30A)	118.9(4)
C(30)-C(29)-C(30A)#2	118.9(4)	C(30)#2-C(29)-C(30A)#2	20.9(3)
C(30A)-C(29)-C(30A)#2	127.1(7)	C(30)-C(29)-C(31)	42.1(4)
C(30)#2-C(29)-C(31)	144.4(6)	C(30A)-C(29)-C(31)	30.6(5)
C(30A)#2-C(29)-C(31)	157.5(6)	C(30)-C(29)-C(31)#2	144.4(6)
C(30)#2-C(29)-C(31)#2	42.1(4)	C(30A)-C(29)-C(31)#2	157.5(6)
C(30A)#2-C(29)-C(31)#2	30.6(5)	C(31)-C(29)-C(31)#2	171.9(9)
C(29)-C(30)-C(31)	96.7(7)	C(29)-C(30)-C(32)	132.9(5)
C(31)-C(30)-C(32)	42.3(6)	C(30)-C(31)-C(32)	96.8(9)
C(30)-C(31)-C(29)	41.2(4)	C(32)-C(31)-C(29)	132.2(8)
C(31)-C(32)-C(30)	40.9(5)	O(1A)-C(1A)-Ru(1)	180.0

Appendix 17 Crystallographic data for $Ru(IPr)_2(CO)_2HCl$ (6B)

Identification code	h06mkw7
Empirical formula	C56 H73 Cl N4 O2 Ru
Formula weight	970.70
Temperature	150(2) K
Wavelength	0.71073 Å
Crystal system	Monoclinic
Space group	C2/c
Unit cell dimensions	a = 19.8060(2)Å α = 90°
	b = 15.1130(2)Å β = 90.646(1)°
	c = 35.3110(4)Å γ = 90°
Volume	10568.9(2) $Å^3$
Z	8
Density (calculated)	1.220 Mg/m^3
Absorption coefficient	0.390 mm^{-1}
F(000)	4112
Crystal size	0.20 x 0.15 x 0.15 mm
Theta range for data collection	3.55 to 27.59°
Index ranges	-25<=h<=25; -19<=k<=19; -45<=l<=45
Reflections collected	54374
Independent reflections	11933 [R(int) = 0.0658]

Reflections observed (>2σ)	8979
Data Completeness	0.974
Absorption correction	Semi-empirical from equivalents
Max. and min. transmission	0.93 and 0.81
Refinement method	Full-matrix least-squares on F^2
Data / restraints / parameters	11933 / 1 / 624
Goodness-of-fit on F^2	1.026
Final R indices [I>2σ(I)]	R^1 = 0.0412 wR_2 = 0.0871
R indices (all data)	R^1 = 0.0663 wR_2 = 0.0956
Largest diff. peak and hole	0.390 and -0.819 eÅ^{-3}

Ru(1)-H(1)	1.601(9)	Ru(1)-C(1A)	1.912(10)
Ru(1)-C(1)	1.920(11)	Ru(1)-C(2)	1.975(2)
Ru(1)-C(3)	2.126(2)	Ru(1)-C(30)	2.128(2)
Ru(1)-Cl(1)	2.379(2)	Ru(1)-Cl(1A)	2.387(3)
O(1)-C(1)	1.134(11)	O(2)-C(2)	1.139(3)
N(1)-C(3)	1.373(3)	N(1)-C(4)	1.389(3)
N(1)-C(6)	1.456(3)	N(2)-C(3)	1.377(3)
N(2)-C(5)	1.380(3)	N(2)-C(18)	1.448(3)
N(3)-C(30)	1.370(3)	N(3)-C(31)	1.385(3)
N(3)-C(33)	1.450(3)	N(4)-C(30)	1.371(3)
N(4)-C(32)	1.384(3)	N(4)-C(45)	1.452(3)
C(4)-C(5)	1.332(3)	C(6)-C(7)	1.390(3)
C(6)-C(11)	1.401(3)	C(7)-C(8)	1.407(3)
C(7)-C(12)	1.518(4)	C(8)-C(9)	1.371(4)
C(9)-C(10)	1.369(4)	C(10)-C(11)	1.401(3)
C(11)-C(15)	1.509(4)	C(12)-C(14)	1.517(4)
C(12)-C(13)	1.528(4)	C(15)-C(17)	1.535(4)
C(15)-C(16)	1.540(4)	C(18)-C(23)	1.397(3)
C(18)-C(19)	1.400(4)	C(19)-C(20)	1.395(4)
C(19)-C(24)	1.514(4)	C(20)-C(21)	1.371(4)
C(21)-C(22)	1.371(4)	C(22)-C(23)	1.402(4)
C(23)-C(27)	1.513(4)	C(24)-C(26)	1.530(4)
C(24)-C(25)	1.535(4)	C(27)-C(29)	1.533(4)
C(27)-C(28)	1.541(4)	C(31)-C(32)	1.332(3)
C(33)-C(34)	1.389(3)	C(33)-C(38)	1.404(3)
C(34)-C(35)	1.401(3)	C(34)-C(39)	1.522(3)
C(35)-C(36)	1.371(4)	C(36)-C(37)	1.367(4)
C(37)-C(38)	1.402(3)	C(38)-C(42)	1.512(4)
C(39)-C(41)	1.526(3)	C(39)-C(40)	1.527(4)
C(42)-C(44)	1.520(4)	C(42)-C(43)	1.525(4)
C(45)-C(46)	1.395(3)	C(45)-C(50)	1.402(4)
C(46)-C(47)	1.398(3)	C(46)-C(51)	1.515(4)
C(47)-C(48)	1.375(4)	C(48)-C(49)	1.384(4)
C(49)-C(50)	1.395(3)	C(50)-C(54)	1.514(4)
C(51)-C(52)	1.516(4)	C(51)-C(53)	1.536(3)
C(54)-C(55)	1.530(4)	C(54)-C(56)	1.548(5)
O(1A)-C(1A)	1.133(10)		
H(1)-Ru(1)-C(1A)	85.1(10)	H(1)-Ru(1)-C(1)	88.5(11)
C(1A)-Ru(1)-C(1)	172.9(8)	H(1)-Ru(1)-C(2)	179.3(9)

C(1A)-Ru(1)-C(2)	94.3(5)	C(1)-Ru(1)-C(2)	92.1(7)
H(1)-Ru(1)-C(3)	84.8(9)	C(1A)-Ru(1)-C(3)	88.7(4)
C(1)-Ru(1)-C(3)	93.8(7)	C(2)-Ru(1)-C(3)	94.80(8)
H(1)-Ru(1)-C(30)	85.3(9)	C(1A)-Ru(1)-C(30)	89.4(4)
C(1)-Ru(1)-C(30)	87.0(7)	C(2)-Ru(1)-C(30)	95.06(8)
C(3)-Ru(1)-C(30)	170.07(8)	H(1)-Ru(1)-Cl(1)	85.8(9)
C(1A)-Ru(1)-Cl(1)	3.2(5)	C(1)-Ru(1)-Cl(1)	174.3(7)
C(2)-Ru(1)-Cl(1)	93.57(12)	C(3)-Ru(1)-Cl(1)	85.65(11)
C(30)-Ru(1)-Cl(1)	92.60(11)	H(1)-Ru(1)-Cl(1A)	87.2(9)
C(1A)-Ru(1)-Cl(1A)	171.9(5)	C(1)-Ru(1)-Cl(1A)	1.5(8)
C(2)-Ru(1)-Cl(1A)	93.42(14)	C(3)-Ru(1)-Cl(1A)	92.90(13)
C(30)-Ru(1)-Cl(1A)	87.65(13)	Cl(1)-Ru(1)-Cl(1A)	172.96(16)
C(3)-N(1)-C(4)	112.13(18)	C(3)-N(1)-C(6)	130.30(18)
C(4)-N(1)-C(6)	117.47(18)	C(3)-N(2)-C(5)	112.30(19)
C(3)-N(2)-C(18)	128.24(18)	C(5)-N(2)-C(18)	118.76(18)
C(30)-N(3)-C(31)	112.37(18)	C(30)-N(3)-C(33)	128.53(17)
C(31)-N(3)-C(33)	118.79(18)	C(30)-N(4)-C(32)	112.20(18)
C(30)-N(4)-C(45)	129.11(19)	C(32)-N(4)-C(45)	118.33(18)
O(1)-C(1)-Ru(1)	174(2)	O(2)-C(2)-Ru(1)	179.8(3)
N(1)-C(3)-N(2)	101.82(17)	N(1)-C(3)-Ru(1)	128.32(15)
N(2)-C(3)-Ru(1)	129.16(15)	C(5)-C(4)-N(1)	106.7(2)
C(4)-C(5)-N(2)	107.0(2)	C(7)-C(6)-C(11)	123.3(2)
C(7)-C(6)-N(1)	118.0(2)	C(11)-C(6)-N(1)	117.9(2)
C(6)-C(7)-C(8)	117.0(2)	C(6)-C(7)-C(12)	123.0(2)
C(8)-C(7)-C(12)	119.9(2)	C(9)-C(8)-C(7)	121.1(3)
C(10)-C(9)-C(8)	120.3(2)	C(9)-C(10)-C(11)	121.8(3)
C(10)-C(11)-C(6)	116.4(2)	C(10)-C(11)-C(15)	121.5(2)
C(6)-C(11)-C(15)	122.0(2)	C(14)-C(12)-C(7)	112.1(2)
C(14)-C(12)-C(13)	111.6(3)	C(7)-C(12)-C(13)	109.7(2)
C(11)-C(15)-C(17)	113.7(2)	C(11)-C(15)-C(16)	110.2(2)
C(17)-C(15)-C(16)	109.6(2)	C(23)-C(18)-C(19)	123.3(2)
C(23)-C(18)-N(2)	118.9(2)	C(19)-C(18)-N(2)	117.5(2)
C(20)-C(19)-C(18)	116.9(3)	C(20)-C(19)-C(24)	120.6(3)
C(18)-C(19)-C(24)	122.4(2)	C(21)-C(20)-C(19)	121.2(3)
C(20)-C(21)-C(22)	120.6(3)	C(21)-C(22)-C(23)	121.4(3)
C(18)-C(23)-C(22)	116.5(3)	C(18)-C(23)-C(27)	123.1(2)
C(22)-C(23)-C(27)	120.3(3)	C(19)-C(24)-C(26)	112.9(3)
C(19)-C(24)-C(25)	110.3(3)	C(26)-C(24)-C(25)	110.3(3)
C(23)-C(27)-C(29)	112.8(3)	C(23)-C(27)-C(28)	109.6(2)
C(29)-C(27)-C(28)	110.4(3)	N(3)-C(30)-N(4)	101.93(17)
N(3)-C(30)-Ru(1)	129.55(14)	N(4)-C(30)-Ru(1)	128.12(15)
C(32)-C(31)-N(3)	106.5(2)	C(31)-C(32)-N(4)	106.9(2)
C(34)-C(33)-C(38)	123.4(2)	C(34)-C(33)-N(3)	118.6(2)
C(38)-C(33)-N(3)	117.7(2)	C(33)-C(34)-C(35)	117.1(2)
C(33)-C(34)-C(39)	122.4(2)	C(35)-C(34)-C(39)	120.5(2)
C(36)-C(35)-C(34)	120.9(3)	C(37)-C(36)-C(35)	120.8(2)
C(36)-C(37)-C(38)	121.4(2)	C(37)-C(38)-C(33)	116.3(2)
C(37)-C(38)-C(42)	121.4(2)	C(33)-C(38)-C(42)	122.3(2)
C(34)-C(39)-C(41)	109.9(2)	C(34)-C(39)-C(40)	112.5(2)
C(41)-C(39)-C(40)	110.7(2)	C(38)-C(42)-C(44)	111.4(2)
C(38)-C(42)-C(43)	113.1(2)	C(44)-C(42)-C(43)	110.2(3)

C(46)-C(45)-C(50)	123.5(2)	C(46)-C(45)-N(4)	118.5(2)
C(50)-C(45)-N(4)	117.5(2)	C(45)-C(46)-C(47)	116.8(2)
C(45)-C(46)-C(51)	122.5(2)	C(47)-C(46)-C(51)	120.6(2)
C(48)-C(47)-C(46)	121.0(3)	C(47)-C(48)-C(49)	120.9(2)
C(48)-C(49)-C(50)	120.6(3)	C(49)-C(50)-C(45)	117.0(2)
C(49)-C(50)-C(54)	120.2(2)	C(45)-C(50)-C(54)	122.8(2)
C(46)-C(51)-C(52)	112.5(2)	C(46)-C(51)-C(53)	110.6(2)
C(52)-C(51)-C(53)	110.8(2)	C(50)-C(54)-C(55)	113.6(3)
C(50)-C(54)-C(56)	110.9(3)	C(55)-C(54)-C(56)	109.8(3)
O(1A)-C(1A)-Ru(1)	177.6(14)		

Appendix 18 Crystallographic data for $Ru(SIPr)_2(CO)_2HCl$ (7B)

Identification code	k07mkw7
Empirical formula	C56 H77 Cl N4 O2 Ru
Formula weight	974.74
Temperature	150(2) K
Wavelength	0.71073 Å
Crystal system	Monoclinic
Space group	C2/c
Unit cell dimensions	a = 19.6590(3)Å α = 90°
	b = 15.1810(2)Å β = 92.022(1)°
	c = 35.1910(6)Å γ = 90°
Volume	10496.0(3) $Å^3$
Z	8
Density (calculated)	1.234 Mg/m^3
Absorption coefficient	0.393 mm^{-1}
F(000)	4144
Crystal size	0.35 x 0.30 x 0.25 mm
Theta range for data collection	3.55 to 29.99°
Index ranges	-27<=h<=27; -21<=k<=21; -39<=l<=49
Reflections collected	33921
Independent reflections	12955 [R(int) = 0.0608]
Reflections observed (>2σ)	8178
Data Completeness	0.847
Absorption correction	Semi-empirical from equivalents
Max. and min. transmission	0.93 and 0.85
Refinement method	Full-matrix least-squares on F^2
Data / restraints / parameters	12955 / 13 / 625
Goodness-of-fit on F^2	0.995
Final R indices [I>2σ(I)]	R^1 = 0.0490 wR_2 = 0.0885
R indices (all data)	R^1 = 0.1030 wR_2 = 0.1028
Largest diff. peak and hole	0.660 and -0.614 $eÅ^{-3}$

Ru(1)-H(1)	1.595(9)	Ru(1)-C(2A)	1.855(7)
Ru(1)-C(2)	1.867(7)	Ru(1)-C(1)	1.982(3)
Ru(1)-C(3)	2.143(2)	Ru(1)-C(30)	2.146(2)

Ru(1)-Cl(1)	2.3922(19)	Ru(1)-Cl(1A)	2.4086(19)
O(1)-C(1)	1.140(3)	O(2)-C(2)	1.179(8)
O(2A)-C(2A)	1.190(8)	N(1)-C(3)	1.361(3)
N(1)-C(6)	1.442(3)	N(1)-C(4)	1.477(3)
N(2)-C(3)	1.362(3)	N(2)-C(18)	1.440(3)
N(2)-C(5)	1.476(3)	N(3)-C(30)	1.356(3)
N(3)-C(45)	1.445(3)	N(3)-C(32)	1.478(3)
N(4)-C(30)	1.356(3)	N(4)-C(33)	1.439(3)
N(4)-C(31)	1.477(3)	C(4)-C(5)	1.503(3)
C(6)-C(7)	1.395(4)	C(6)-C(11)	1.415(4)
C(7)-C(8)	1.402(4)	C(7)-C(12)	1.516(4)
C(8)-C(9)	1.379(4)	C(9)-C(10)	1.365(4)
C(10)-C(11)	1.397(4)	C(11)-C(15)	1.502(4)
C(12)-C(14)	1.534(4)	C(12)-C(13)	1.538(4)
C(15)-C(16)	1.542(4)	C(15)-C(17)	1.548(4)
C(18)-C(23)	1.400(4)	C(18)-C(19)	1.416(3)
C(19)-C(20)	1.403(4)	C(19)-C(24)	1.501(4)
C(20)-C(21)	1.360(4)	C(21)-C(22)	1.385(4)
C(22)-C(23)	1.407(4)	C(23)-C(27)	1.523(4)
C(24)-C(26)	1.521(3)	C(24)-C(25)	1.534(3)
C(27)-C(29)	1.535(4)	C(27)-C(28)	1.538(4)
C(31)-C(32)	1.500(3)	C(33)-C(38)	1.394(4)
C(33)-C(34)	1.416(3)	C(34)-C(35)	1.409(4)
C(34)-C(39)	1.502(4)	C(35)-C(36)	1.362(4)
C(36)-C(37)	1.382(4)	C(37)-C(38)	1.403(3)
C(38)-C(42)	1.519(3)	C(39)-C(41)	1.533(3)
C(39)-C(40)	1.538(3)	C(42)-C(43)	1.529(4)
C(42)-C(44)	1.537(3)	C(45)-C(50)	1.377(4)
C(45)-C(46)	1.416(4)	C(46)-C(47)	1.396(3)
C(46)-C(51)	1.507(4)	C(47)-C(48)	1.369(4)
C(48)-C(49)	1.391(4)	C(49)-C(50)	1.403(3)
C(50)-C(54)	1.529(4)	C(51)-C(52)	1.527(4)
C(51)-C(53)	1.544(4)	C(54)-C(55)	1.526(3)
C(54)-C(56)	1.539(4)		
H(1)-Ru(1)-C(2A)	83.9(9)	H(1)-Ru(1)-C(2)	87.3(10)
C(2A)-Ru(1)-C(2)	171.1(6)	H(1)-Ru(1)-C(1)	177.2(8)
C(2A)-Ru(1)-C(1)	94.6(5)	C(2)-Ru(1)-C(1)	94.2(5)
H(1)-Ru(1)-C(3)	87.8(7)	C(2A)-Ru(1)-C(3)	85.9(4)
C(2)-Ru(1)-C(3)	94.7(4)	C(1)-Ru(1)-C(3)	94.43(9)
H(1)-Ru(1)-C(30)	82.6(7)	C(2A)-Ru(1)-C(30)	92.1(4)
C(2)-Ru(1)-C(30)	85.8(4)	C(1)-Ru(1)-C(30)	95.10(9)
C(3)-Ru(1)-C(30)	170.39(9)	H(1)-Ru(1)-Cl(1)	83.5(8)
C(2A)-Ru(1)-Cl(1)	2.2(4)	C(2)-Ru(1)-Cl(1)	170.7(5)
C(1)-Ru(1)-Cl(1)	95.10(10)	C(3)-Ru(1)-Cl(1)	83.76(9)
C(30)-Ru(1)-Cl(1)	94.17(9)	H(1)-Ru(1)-Cl(1A)	87.2(8)
C(2A)-Ru(1)-Cl(1A)	170.9(4)	C(2)-Ru(1)-Cl(1A)	0.7(5)
C(1)-Ru(1)-Cl(1A)	94.21(10)	C(3)-Ru(1)-Cl(1A)	95.44(9)
C(30)-Ru(1)-Cl(1A)	85.08(9)	Cl(1)-Ru(1)-Cl(1A)	170.69(9)
C(3)-N(1)-C(6)	129.75(18)	C(3)-N(1)-C(4)	113.8(2)
C(6)-N(1)-C(4)	113.91(18)	C(3)-N(2)-C(18)	131.70(19)

C(3)-N(2)-C(5)	113.3(2)	C(18)-N(2)-C(5)	114.91(19)
C(30)-N(3)-C(45)	131.41(18)	C(30)-N(3)-C(32)	112.79(18)
C(45)-N(3)-C(32)	115.76(18)	C(30)-N(4)-C(33)	129.36(19)
C(30)-N(4)-C(31)	113.27(18)	C(33)-N(4)-C(31)	115.17(17)
O(1)-C(1)-Ru(1)	179.6(2)	O(2)-C(2)-Ru(1)	179.3(16)
N(1)-C(3)-N(2)	105.12(18)	N(1)-C(3)-Ru(1)	127.53(18)
N(2)-C(3)-Ru(1)	126.49(17)	N(1)-C(4)-C(5)	101.85(18)
N(2)-C(5)-C(4)	101.95(18)	C(7)-C(6)-C(11)	122.3(3)
C(7)-C(6)-N(1)	118.9(2)	C(11)-C(6)-N(1)	118.4(3)
C(6)-C(7)-C(8)	117.7(3)	C(6)-C(7)-C(12)	122.9(3)
C(8)-C(7)-C(12)	119.2(3)	C(9)-C(8)-C(7)	120.7(3)
C(10)-C(9)-C(8)	120.6(3)	C(9)-C(10)-C(11)	121.9(3)
C(10)-C(11)-C(6)	116.7(3)	C(10)-C(11)-C(15)	120.2(3)
C(6)-C(11)-C(15)	123.1(3)	C(7)-C(12)-C(14)	113.0(2)
C(7)-C(12)-C(13)	110.0(2)	C(14)-C(12)-C(13)	109.5(3)
C(11)-C(15)-C(16)	111.0(3)	C(11)-C(15)-C(17)	112.4(3)
C(16)-C(15)-C(17)	109.5(2)	C(23)-C(18)-C(19)	122.6(3)
C(23)-C(18)-N(2)	118.7(2)	C(19)-C(18)-N(2)	117.8(3)
C(20)-C(19)-C(18)	115.9(3)	C(20)-C(19)-C(24)	121.0(3)
C(18)-C(19)-C(24)	123.0(3)	C(21)-C(20)-C(19)	122.9(3)
C(20)-C(21)-C(22)	120.2(3)	C(21)-C(22)-C(23)	120.5(3)
C(18)-C(23)-C(22)	117.9(3)	C(18)-C(23)-C(27)	121.4(3)
C(22)-C(23)-C(27)	120.7(3)	C(19)-C(24)-C(26)	111.7(2)
C(19)-C(24)-C(25)	110.5(2)	C(26)-C(24)-C(25)	110.6(2)
C(23)-C(27)-C(29)	113.3(3)	C(23)-C(27)-C(28)	111.1(2)
C(29)-C(27)-C(28)	109.9(2)	N(3)-C(30)-N(4)	105.54(18)
N(3)-C(30)-Ru(1)	126.17(16)	N(4)-C(30)-Ru(1)	127.73(16)
N(4)-C(31)-C(32)	101.53(18)	N(3)-C(32)-C(31)	101.59(19)
C(38)-C(33)-C(34)	122.8(2)	C(38)-C(33)-N(4)	119.6(2)
C(34)-C(33)-N(4)	117.2(3)	C(35)-C(34)-C(33)	116.0(3)
C(35)-C(34)-C(39)	121.2(2)	C(33)-C(34)-C(39)	122.7(2)
C(36)-C(35)-C(34)	122.0(3)	C(35)-C(36)-C(37)	120.9(3)
C(36)-C(37)-C(38)	120.4(3)	C(33)-C(38)-C(37)	117.9(2)
C(33)-C(38)-C(42)	123.0(2)	C(37)-C(38)-C(42)	119.1(3)
C(34)-C(39)-C(41)	110.2(2)	C(34)-C(39)-C(40)	112.7(2)
C(41)-C(39)-C(40)	109.4(2)	C(38)-C(42)-C(43)	112.0(2)
C(38)-C(42)-C(44)	111.5(2)	C(43)-C(42)-C(44)	109.6(3)
C(50)-C(45)-C(46)	122.9(2)	C(50)-C(45)-N(3)	119.1(2)
C(46)-C(45)-N(3)	117.5(3)	C(47)-C(46)-C(45)	116.7(3)
C(47)-C(46)-C(51)	120.6(3)	C(45)-C(46)-C(51)	122.7(2)
C(48)-C(47)-C(46)	121.4(3)	C(47)-C(48)-C(49)	120.7(2)
C(48)-C(49)-C(50)	120.1(3)	C(45)-C(50)-C(49)	118.0(3)
C(45)-C(50)-C(54)	123.0(2)	C(49)-C(50)-C(54)	118.9(3)
C(46)-C(51)-C(52)	113.5(2)	C(46)-C(51)-C(53)	111.8(3)
C(52)-C(51)-C(53)	108.9(3)	C(55)-C(54)-C(50)	111.4(2)
C(55)-C(54)-C(56)	109.9(3)	C(50)-C(54)-C(56)	111.1(2)
O(2A)-C(2A)-Ru(1)	178.9(14)		

Appendix 19 Crystallographic data for $Ru(IPr)_2(CO)H(\eta^2\text{-}BH_4)$ (6C)

Identification code	h07mkw3
Empirical formula	C62 H92 B N4 O Ru
Formula weight	1021.28
Temperature	150(2) K
Wavelength	0.71073 Å
Crystal system	Monoclinic
Space group	P22121
Unit cell dimensions	a = 10.6630(2)Å α = 90°
	b = 13.0470(3)Å β = 90°
	c = 20.8400(6)Å γ = 90°
Volume	2899.26(12) $Å^3$
Z	2
Density (calculated)	1.170 Mg/m^3
Absorption coefficient	0.312 mm^{-1}
F(000)	1098
Crystal size	0.35 x 0.30 x 0.30 mm
Theta range for data collection	3.66 to 30.04°
Index ranges	-14<=h<=14; -18<=k<=18; -21<=l<=29
Reflections collected	15736
Independent reflections	6524 [R(int) = 0.0417]
Reflections observed (>2σ)	5389
Data Completeness	0.884
Absorption correction	Semi-empirical from equivalents
Max. and min. transmission	0.92 and 0.88
Refinement method	Full-matrix least-squares on F^2
Data / restraints / parameters	6524 / 5 / 336
Goodness-of-fit on F^2	1.027
Final R indices [I>2σ(I)]	R^1 = 0.0405 wR_2 = 0.0970
R indices (all data)	R^1 = 0.0587 wR_2 = 0.1059
Absolute structure parameter	0.01(3)
Largest diff. peak and hole	0.488 and -0.425 $eÅ^{-3}$

Ru(1)-C(1)#1	1.837(9)	C(11)-C(12)	1.548(7)
Ru(1)-C(1)	1.837(9)	C(11)-H(11)	1.0000
Ru(1)-C(1A)#1	1.840(9)	C(12)-H(12A)	0.9800
Ru(1)-C(1A)	1.840(9)	C(12)-H(12B)	0.9800
Ru(1)-C(2)	2.086(3)	C(12)-H(12C)	0.9800
Ru(1)-C(2)#1	2.086(3)	C(13)-H(13A)	0.9800
Ru(1)-B(1A)#1	2.218(9)	C(13)-H(13B)	0.9800
Ru(1)-B(1A)	2.218(9)	C(13)-H(13C)	0.9800
Ru(1)-B(1)#1	2.219(8)	C(14)-C(15)	1.513(6)
Ru(1)-B(1)	2.219(8)	C(14)-C(16)	1.516(6)
O(1)-C(1)	1.140(11)	C(14)-H(14)	1.0000
O(1)-O(1)#1	1.426(16)	C(15)-H(15A)	0.9800
O(1)-C(1)#1	1.671(11)	C(15)-H(15B)	0.9800
N(1)-C(2)	1.368(3)	C(15)-H(15C)	0.9800

N(1)-C(3)	1.379(4)	C(16)-H(16A)	0.9800
N(1)-C(5)	1.445(3)	C(16)-H(16B)	0.9800
N(2)-C(2)	1.367(3)	C(16)-H(16C)	0.9800
N(2)-C(4)	1.371(4)	C(17)-C(22)	1.387(5)
N(2)-C(17)	1.452(4)	C(17)-C(18)	1.394(4)
C(1)-C(1)#1	1.05(2)	C(18)-C(19)	1.410(4)
C(1)-O(1)#1	1.671(11)	C(18)-C(23)	1.520(4)
C(3)-C(4)	1.349(5)	C(19)-C(20)	1.382(5)
C(3)-H(3)	0.9500	C(19)-H(19)	0.9500
C(4)-H(4)	0.9500	C(20)-C(21)	1.365(5)
C(5)-C(10)	1.386(4)	C(20)-H(20)	0.9500
C(5)-C(6)	1.416(4)	C(21)-C(22)	1.402(4)
C(6)-C(7)	1.397(4)	C(21)-H(21)	0.9500
C(6)-C(11)	1.516(5)	C(22)-C(26)	1.508(5)
C(7)-C(8)	1.372(5)	C(23)-C(25)	1.529(5)
C(7)-H(7)	0.9500	C(23)-C(24)	1.532(5)
C(8)-C(9)	1.363(5)	C(23)-H(23)	1.0000
C(8)-H(8)	0.9500	C(24)-H(24A)	0.9800
C(9)-C(10)	1.395(4)	C(24)-H(24B)	0.9800
C(9)-H(9)	0.9500	C(24)-H(24C)	0.9800
C(10)-C(14)	1.531(5)	C(25)-H(25A)	0.9800
C(11)-C(13)	1.528(6)	C(25)-H(25B)	0.9800
C(27)-H(27C)	0.9800	C(25)-H(25C)	0.9800
C(28)-H(28A)	0.9800	C(26)-C(27)	1.536(7)
C(28)-H(28B)	0.9800	C(26)-C(28)	1.550(6)
C(28)-H(28C)	0.9800	C(26)-H(26)	1.0000
C(29)-C(30)#2	1.371(6)	C(27)-H(27A)	0.9800
C(29)-C(30)	1.371(6)	C(27)-H(27B)	0.9800
C(29)-H(29A)	0.990(3)	C(32)-H(32C)	0.9800
C(30)-C(31)	1.404(8)	B(1)-B(1)#1	0.623(18)
C(30)-H(30A)	0.9900	O(1A)-O(1A)#1	1.09(2)
C(30)-H(30B)	0.9900	O(1A)-C(1A)	1.141(11)
C(31)-C(32)	1.192(11)	O(1A)-C(1A)#1	1.536(14)
C(31)-H(31A)	0.9900	C(1A)-C(1A)#1	0.97(3)
C(31)-H(31B)	0.9900	C(1A)-O(1A)#1	1.536(14)
C(32)-H(32A)	0.9800	B(1A)-B(1A)#1	0.50(2)
C(32)-H(32B)	0.9800		
C(1)#1-Ru(1)-C(1)	33.3(6)	C(1A)-Ru(1)-C(2)#1	91.8(15)
C(1)#1-Ru(1)-C(1A)#1	148.1(6)	C(2)-Ru(1)-C(2)#1	179.58(14)
C(1)-Ru(1)-C(1A)#1	177.6(17)	C(1)#1-Ru(1)-B(1A)#1	10.4(6)
C(1)#1-Ru(1)-C(1A)	177.6(17)	C(1)-Ru(1)-B(1A)#1	23.0(4)
C(1)-Ru(1)-C(1A)	148.1(6)	C(1A)#1-Ru(1)-B(1A)#1	158.3(6)
C(1A)#1-Ru(1)-C(1A)	30.5(9)	C(1A)-Ru(1)-B(1A)#1	171.2(5)
C(1)#1-Ru(1)-C(2)	89.5(6)	C(2)-Ru(1)-B(1A)#1	91.0(11)
C(1)-Ru(1)-C(2)	90.1(6)	C(2)#1-Ru(1)-B(1A)#1	88.6(11)
C(1A)#1-Ru(1)-C(2)	91.8(15)	C(1)#1-Ru(1)-B(1A)	23.0(4)
C(1A)-Ru(1)-C(2)	88.6(15)	C(1)-Ru(1)-B(1A)	10.4(6)
C(1)#1-Ru(1)-C(2)#1	90.1(6)	C(1A)#1-Ru(1)-B(1A)	171.2(5)
C(1)-Ru(1)-C(2)#1	89.5(6)	C(1A)-Ru(1)-B(1A)	158.3(6)
C(1A)#1-Ru(1)-C(2)#1	88.6(15)	C(2)-Ru(1)-B(1A)	88.6(11)

O(1)-C(1)-Ru(1)	171.6(10)	C(2)#1-Ru(1)-B(1A)	91.0(11)
O(1)#1-C(1)-Ru(1)	115.6(6)	B(1A)#1-Ru(1)-B(1A)	12.9(6)
N(2)-C(2)-N(1)	102.3(2)	C(1)#1-Ru(1)-B(1)#1	171.4(4)
N(2)-C(2)-Ru(1)	128.48(19)	C(1)-Ru(1)-B(1)#1	155.3(4)
N(1)-C(2)-Ru(1)	129.23(18)	C(1A)#1-Ru(1)-B(1)#1	23.3(5)
C(4)-C(3)-N(1)	106.6(3)	C(1A)-Ru(1)-B(1)#1	7.3(6)
C(4)-C(3)-H(3)	126.7	C(2)-Ru(1)-B(1)#1	90.3(7)
N(1)-C(3)-H(3)	126.7	C(2)#1-Ru(1)-B(1)#1	90.1(7)
C(3)-C(4)-N(2)	106.4(3)	B(1A)#1-Ru(1)-B(1)#1	177.9(12)
C(3)-C(4)-H(4)	126.8	B(1A)-Ru(1)-B(1)#1	165.5(4)
N(2)-C(4)-H(4)	126.8	C(1)#1-Ru(1)-B(1)	155.3(4)
C(10)-C(5)-C(6)	122.4(3)	C(1)-Ru(1)-B(1)	171.4(4)
C(10)-C(5)-N(1)	119.1(3)	C(1A)#1-Ru(1)-B(1)	7.3(6)
C(6)-C(5)-N(1)	118.4(3)	C(1A)-Ru(1)-B(1)	23.3(5)
C(7)-C(6)-C(5)	116.3(3)	C(2)-Ru(1)-B(1)	90.1(7)
C(7)-C(6)-C(11)	120.6(3)	C(2)#1-Ru(1)-B(1)	90.3(7)
C(5)-C(6)-C(11)	123.1(3)	B(1A)#1-Ru(1)-B(1)	165.5(4)
C(8)-C(7)-C(6)	121.7(3)	B(1A)-Ru(1)-B(1)	177.9(12)
C(8)-C(7)-H(7)	119.1	B(1)#1-Ru(1)-B(1)	16.1(5)
C(6)-C(7)-H(7)	119.1	C(1)-O(1)-O(1)#1	80.4(7)
C(9)-C(8)-C(7)	120.7(3)	C(1)-O(1)-C(1)#1	38.5(8)
C(9)-C(8)-H(8)	119.6	O(1)#1-O(1)-C(1)#1	42.3(4)
C(7)-C(8)-H(8)	119.6	C(2)-N(1)-C(3)	112.1(2)
C(8)-C(9)-C(10)	120.7(3)	C(2)-N(1)-C(5)	128.3(2)
C(8)-C(9)-H(9)	119.6	C(3)-N(1)-C(5)	119.6(3)
C(10)-C(9)-H(9)	119.6	C(2)-N(2)-C(4)	112.6(2)
C(5)-C(10)-C(9)	118.2(3)	C(2)-N(2)-C(17)	128.3(3)
C(5)-C(10)-C(14)	121.4(3)	C(4)-N(2)-C(17)	118.9(3)
C(9)-C(10)-C(14)	120.2(3)	C(1)#1-C(1)-O(1)	99.2(7)
C(6)-C(11)-C(13)	111.5(3)	C(1)#1-C(1)-O(1)#1	42.3(4)
C(6)-C(11)-C(12)	109.6(3)	O(1)-C(1)-O(1)#1	57.3(8)
C(13)-C(11)-C(12)	111.4(4)	C(1)#1-C(1)-Ru(1)	73.4(3)
C(6)-C(11)-H(11)	108.0	C(28)-C(26)-H(26)	107.6
C(13)-C(11)-H(11)	108.0	C(26)-C(27)-H(27A)	109.5
C(12)-C(11)-H(11)	108.0	C(26)-C(27)-H(27B)	109.5
C(11)-C(12)-H(12A)	109.5	H(27A)-C(27)-H(27B)	109.5
C(11)-C(12)-H(12B)	109.5	C(26)-C(27)-H(27C)	109.5
H(12A)-C(12)-H(12B)	109.5	H(27A)-C(27)-H(27C)	109.5
C(11)-C(12)-H(12C)	109.5	H(27B)-C(27)-H(27C)	109.5
H(12A)-C(12)-H(12C)	109.5	C(26)-C(28)-H(28A)	109.5
H(12B)-C(12)-H(12C)	109.5	C(26)-C(28)-H(28B)	109.5
C(11)-C(13)-H(13A)	109.5	H(28A)-C(28)-H(28B)	109.5
C(11)-C(13)-H(13B)	109.5	C(26)-C(28)-H(28C)	109.5
H(13A)-C(13)-H(13B)	109.5	H(28A)-C(28)-H(28C)	109.5
C(11)-C(13)-H(13C)	109.5	H(28B)-C(28)-H(28C)	109.5
H(13A)-C(13)-H(13C)	109.5	C(30)#2-C(29)-C(30)	128.6(5)
H(13B)-C(13)-H(13C)	109.5	C(30)#2-C(29)-H(29A)	107(7)
C(15)-C(14)-C(16)	111.2(4)	C(30)-C(29)-H(29A)	103(7)
C(15)-C(14)-C(10)	110.5(3)	C(29)-C(30)-C(31)	127.8(5)
C(16)-C(14)-C(10)	112.3(4)	C(29)-C(30)-H(30A)	105.4
C(15)-C(14)-H(14)	107.5	C(31)-C(30)-H(30A)	105.4

C(16)-C(14)-H(14)	107.5	C(29)-C(30)-H(30B)	105.4
C(10)-C(14)-H(14)	107.5	C(31)-C(30)-H(30B)	105.4
C(14)-C(15)-H(15A)	109.5	H(30A)-C(30)-H(30B)	106.0
C(14)-C(15)-H(15B)	109.5	C(32)-C(31)-C(30)	130.7(10)
H(15A)-C(15)-H(15B)	109.5	C(32)-C(31)-H(31A)	104.6
C(14)-C(15)-H(15C)	109.5	C(30)-C(31)-H(31A)	104.6
H(15A)-C(15)-H(15C)	109.5	C(32)-C(31)-H(31B)	104.6
H(15B)-C(15)-H(15C)	109.5	C(30)-C(31)-H(31B)	104.6
C(14)-C(16)-H(16A)	109.5	H(31A)-C(31)-H(31B)	105.7
C(14)-C(16)-H(16B)	109.5	C(31)-C(32)-H(32A)	109.5
H(16A)-C(16)-H(16B)	109.5	C(31)-C(32)-H(32B)	109.5
C(14)-C(16)-H(16C)	109.5	H(32A)-C(32)-H(32B)	109.5
H(16A)-C(16)-H(16C)	109.5	C(31)-C(32)-H(32C)	109.5
H(16B)-C(16)-H(16C)	109.5	H(32A)-C(32)-H(32C)	109.5
C(22)-C(17)-C(18)	123.6(3)	H(32B)-C(32)-H(32C)	109.5
C(22)-C(17)-N(2)	118.6(3)	B(1)#1-B(1)-Ru(1)	81.9(2)
C(18)-C(17)-N(2)	117.5(3)	O(1A)#1-O(1A)-C(1A)	86.8(9)
C(17)-C(18)-C(19)	117.5(3)	O(1A)#1-O(1A)-C(1A)#1	47.9(6)
C(17)-C(18)-C(23)	122.9(3)	C(1A)-O(1A)-C(1A)#1	39.0(12)
C(19)-C(18)-C(23)	119.6(3)	C(1A)#1-C(1A)-O(1A)	93.1(9)
C(20)-C(19)-C(18)	120.0(3)	C(1A)#1-C(1A)-O(1A)#1	47.9(6)
C(20)-C(19)-H(19)	120.0	O(1A)-C(1A)-O(1A)#1	45.3(9)
C(18)-C(19)-H(19)	120.0	C(1A)#1-C(1A)-Ru(1)	74.7(5)
C(21)-C(20)-C(19)	120.5(3)	O(1A)-C(1A)-Ru(1)	167.7(15)
C(21)-C(20)-H(20)	119.8	O(1A)#1-C(1A)-Ru(1)	122.6(9)
C(19)-C(20)-H(20)	119.8	B(1A)#1-B(1A)-Ru(1)	83.5(3)
C(20)-C(21)-C(22)	122.2(3)	C(23)-C(25)-H(25B)	109.5
C(20)-C(21)-H(21)	118.9	H(25A)-C(25)-H(25B)	109.5
C(22)-C(21)-H(21)	118.9	C(23)-C(25)-H(25C)	109.5
C(17)-C(22)-C(21)	116.3(3)	H(25A)-C(25)-H(25C)	109.5
C(17)-C(22)-C(26)	124.0(3)	H(25B)-C(25)-H(25C)	109.5
C(21)-C(22)-C(26)	119.7(3)	C(22)-C(26)-C(27)	109.1(4)
C(18)-C(23)-C(25)	109.9(3)	C(22)-C(26)-C(28)	112.2(4)
C(18)-C(23)-C(24)	112.5(3)	C(27)-C(26)-C(28)	112.6(4)
C(25)-C(23)-C(24)	110.7(3)	C(22)-C(26)-H(26)	107.6
C(18)-C(23)-H(23)	107.9	C(27)-C(26)-H(26)	107.6
C(25)-C(23)-H(23)	107.9	C(23)-C(24)-H(24C)	109.5
C(24)-C(23)-H(23)	107.9	H(24A)-C(24)-H(24C)	109.5
C(23)-C(24)-H(24A)	109.5	H(24B)-C(24)-H(24C)	109.5
C(23)-C(24)-H(24B)	109.5	C(23)-C(25)-H(25A)	109.5
H(24A)-C(24)-H(24B)	109.5		

Appendix 20 Crystallographic data for $Ru(IPr)_2(CO)H(OH)$ (6D)

Identification code	k08mkw19
Empirical formula	C61 H88 N4 O2 Ru
Formula weight	1010.42
Temperature	150(2) K

Wavelength	0.71073 Å
Crystal system	Orthorhombic
Space group	P212121
Unit cell dimensions	a = 12.9870(1)Å α = 90°
	b = 20.6070(2)Å β = 90°
	c = 21.2510(2)Å γ = 90°
Volume	5687.26(9) $Å^3$
Z	4
Density (calculated)	1.180 Mg/m^3
Absorption coefficient	0.319 mm^{-1}
F(000)	2168
Crystal size	0.20 x 0.15 x 0.15 mm
Theta range for data collection	3.53 to 27.51°
Index ranges	-16<=h<=16; -26<=k<=26; -27<=l<=27
Reflections collected	109458
Independent reflections	13030 [R(int) = 0.0635]
Reflections observed (>2σ)	10974
Data Completeness	0.995
Absorption correction	None
Refinement method	Full-matrix least-squares on F^2
Data / restraints / parameters	13030 / 2 / 637
Goodness-of-fit on F^2	1.057
Final R indices [I>2σ(I)]	R^1 = 0.0339 wR_2 = 0.0736
R indices (all data)	R^1 = 0.0477 wR_2 = 0.0793
Absolute structure parameter	0.00
Largest diff. peak and hole	0.739 and -0.625 $eÅ^{-3}$

Ru(1)-C(1)	1.838(2)	Ru(1)-O(2)	1.9958(18)
Ru(1)-C(2)	2.0763(19)	Ru(1)-C(29)	2.079(2)
O(1)-C(1)	1.157(3)	N(1)-C(2)	1.372(3)
N(1)-C(3)	1.387(3)	N(1)-C(5)	1.444(3)
N(2)-C(2)	1.375(3)	N(2)-C(4)	1.386(3)
N(2)-C(17)	1.442(3)	N(3)-C(29)	1.363(3)
N(3)-C(30)	1.387(3)	N(3)-C(32)	1.447(3)
N(4)-C(29)	1.373(3)	N(4)-C(31)	1.391(3)
N(4)-C(44)	1.442(3)	C(3)-C(4)	1.341(3)
C(5)-C(6)	1.399(3)	C(5)-C(10)	1.400(3)
C(6)-C(7)	1.397(3)	C(6)-C(11)	1.522(3)
C(7)-C(8)	1.383(4)	C(8)-C(9)	1.376(4)
C(9)-C(10)	1.393(3)	C(10)-C(14)	1.523(3)
C(11)-C(12)	1.523(4)	C(11)-C(13)	1.530(4)
C(14)-C(16)	1.531(4)	C(14)-C(15)	1.537(4)
C(17)-C(18)	1.398(3)	C(17)-C(22)	1.405(3)
C(18)-C(19)	1.398(3)	C(18)-C(23)	1.517(3)
C(19)-C(20)	1.374(4)	C(20)-C(21)	1.383(4)
C(21)-C(22)	1.400(3)	C(22)-C(26)	1.518(3)
C(23)-C(25)	1.523(4)	C(23)-C(24)	1.546(4)
C(26)-C(28)	1.525(4)	C(26)-C(27)	1.535(4)
C(30)-C(31)	1.341(4)	C(32)-C(37)	1.393(3)
C(32)-C(33)	1.400(3)	C(33)-C(34)	1.393(4)
C(33)-C(38)	1.511(4)	C(34)-C(35)	1.376(4)

C(35)-C(36)	1.382(4)	C(36)-C(37)	1.401(3)
C(37)-C(41)	1.518(3)	C(38)-C(39)	1.532(4)
C(38)-C(40)	1.534(5)	C(41)-C(42)	1.523(3)
C(41)-C(43)	1.525(4)	C(44)-C(49)	1.398(3)
C(44)-C(45)	1.412(3)	C(45)-C(46)	1.403(3)
C(45)-C(50)	1.512(3)	C(46)-C(47)	1.374(4)
C(47)-C(48)	1.378(4)	C(48)-C(49)	1.400(3)
C(49)-C(53)	1.523(3)	C(50)-C(51)	1.530(4)
C(50)-C(52)	1.539(4)	C(53)-C(55)	1.527(4)
C(53)-C(54)	1.527(4)	C(56)-C(57)	1.505(4)
C(57)-C(58)	1.513(4)	C(58)-C(59)	1.518(4)
C(59)-C(60)	1.510(4)	C(60)-C(61)	1.530(4)
C(1)-Ru(1)-O(2)	176.94(10)	C(1)-Ru(1)-C(2)	92.09(9)
O(2)-Ru(1)-C(2)	90.64(8)	C(1)-Ru(1)-C(29)	90.57(9)
O(2)-Ru(1)-C(29)	86.70(8)	C(2)-Ru(1)-C(29)	177.34(8)
C(2)-N(1)-C(3)	112.17(18)	C(2)-N(1)-C(5)	127.62(18)
C(3)-N(1)-C(5)	119.96(19)	C(2)-N(2)-C(4)	111.77(18)
C(2)-N(2)-C(17)	126.51(18)	C(4)-N(2)-C(17)	121.60(19)
C(29)-N(3)-C(30)	112.13(18)	C(29)-N(3)-C(32)	127.70(18)
C(30)-N(3)-C(32)	119.91(18)	C(29)-N(4)-C(31)	111.83(19)
C(29)-N(4)-C(44)	126.75(18)	C(31)-N(4)-C(44)	121.38(19)
O(1)-C(1)-Ru(1)	177.9(3)	N(1)-C(2)-N(2)	102.48(16)
N(1)-C(2)-Ru(1)	127.14(15)	N(2)-C(2)-Ru(1)	130.39(14)
C(4)-C(3)-N(1)	106.52(19)	C(3)-C(4)-N(2)	107.06(19)
C(6)-C(5)-C(10)	123.0(2)	C(6)-C(5)-N(1)	118.1(2)
C(10)-C(5)-N(1)	118.7(2)	C(7)-C(6)-C(5)	117.4(2)
C(7)-C(6)-C(11)	120.5(2)	C(5)-C(6)-C(11)	122.0(2)
C(8)-C(7)-C(6)	120.7(2)	C(9)-C(8)-C(7)	120.3(2)
C(8)-C(9)-C(10)	121.7(2)	C(9)-C(10)-C(5)	116.8(2)
C(9)-C(10)-C(14)	120.1(2)	C(5)-C(10)-C(14)	123.2(2)
C(6)-C(11)-C(12)	110.5(2)	C(6)-C(11)-C(13)	112.1(2)
C(12)-C(11)-C(13)	111.2(2)	C(10)-C(14)-C(16)	111.5(2)
C(10)-C(14)-C(15)	110.5(2)	C(16)-C(14)-C(15)	110.3(2)
C(18)-C(17)-C(22)	122.9(2)	C(18)-C(17)-N(2)	118.0(2)
C(22)-C(17)-N(2)	119.0(2)	C(19)-C(18)-C(17)	117.5(2)
C(19)-C(18)-C(23)	119.9(2)	C(17)-C(18)-C(23)	122.6(2)
C(20)-C(19)-C(18)	120.9(2)	C(19)-C(20)-C(21)	120.8(2)
C(20)-C(21)-C(22)	121.0(3)	C(21)-C(22)-C(17)	116.9(2)
C(21)-C(22)-C(26)	120.1(2)	C(17)-C(22)-C(26)	122.9(2)
C(18)-C(23)-C(25)	111.8(2)	C(18)-C(23)-C(24)	110.3(2)
C(25)-C(23)-C(24)	110.7(2)	C(22)-C(26)-C(28)	112.4(2)
C(22)-C(26)-C(27)	110.6(2)	C(28)-C(26)-C(27)	110.0(3)
N(3)-C(29)-N(4)	102.71(17)	N(3)-C(29)-Ru(1)	127.79(14)
N(4)-C(29)-Ru(1)	129.44(15)	C(31)-C(30)-N(3)	106.82(19)
C(30)-C(31)-N(4)	106.45(19)	C(37)-C(32)-C(33)	123.6(2)
C(37)-C(32)-N(3)	117.6(2)	C(33)-C(32)-N(3)	118.5(2)
C(34)-C(33)-C(32)	116.3(2)	C(34)-C(33)-C(38)	121.2(2)
C(32)-C(33)-C(38)	122.6(2)	C(35)-C(34)-C(33)	122.0(2)
C(34)-C(35)-C(36)	120.2(2)	C(35)-C(36)-C(37)	120.7(2)
C(32)-C(37)-C(36)	117.2(2)	C(32)-C(37)-C(41)	122.3(2)

C(36)-C(37)-C(41)	120.4(2)	C(33)-C(38)-C(39)	112.2(2)
C(33)-C(38)-C(40)	110.4(2)	C(39)-C(38)-C(40)	111.2(3)
C(37)-C(41)-C(42)	111.8(2)	C(37)-C(41)-C(43)	110.6(2)
C(42)-C(41)-C(43)	111.2(2)	C(49)-C(44)-C(45)	123.4(2)
C(49)-C(44)-N(4)	118.7(2)	C(45)-C(44)-N(4)	117.8(2)
C(46)-C(45)-C(44)	116.4(2)	C(46)-C(45)-C(50)	120.6(2)
C(44)-C(45)-C(50)	122.9(2)	C(47)-C(46)-C(45)	121.2(2)
C(46)-C(47)-C(48)	121.1(2)	C(47)-C(48)-C(49)	120.9(2)
C(44)-C(49)-C(48)	117.0(2)	C(44)-C(49)-C(53)	121.5(2)
C(48)-C(49)-C(53)	121.5(2)	C(45)-C(50)-C(51)	112.0(2)
C(45)-C(50)-C(52)	110.7(2)	C(51)-C(50)-C(52)	110.0(3)
C(49)-C(53)-C(55)	112.0(2)	C(49)-C(53)-C(54)	113.0(2)
C(55)-C(53)-C(54)	109.9(3)	C(56)-C(57)-C(58)	114.0(2)
C(57)-C(58)-C(59)	115.0(2)	C(60)-C(59)-C(58)	113.6(2)
C(59)-C(60)-C(61)	114.6(2)		

Appendix 21 Crystallographic data for $[Ru(IPr)_2(CO)H(OH_2)]^+BF_4^-$ (6E)

Identification code	h08mkw17
Empirical formula	C55 H75 B F4 N4 O2 Ru
Formula weight	1012.07
Temperature	150(2) K
Wavelength	0.71073 Å
Crystal system	Orthorhombic
Space group	Pbca
Unit cell dimensions	a = 20.7380(1)Å α = 90°
	b = 21.0220(1)Å β = 90°
	c = 24.9520(2)Å γ = 90°
Volume	10877.93(11) $Å^3$
Z	8
Density (calculated)	1.236 Mg/m^3
Absorption coefficient	0.344 mm^{-1}
F(000)	4272
Crystal size	0.40 x 0.25 x 0.15 mm
Theta range for data collection	3.87 to 27.48°
Index ranges	-26<=h<=26; -27<=k<=27; -32<=l<=32
Reflections collected	176301
Independent reflections	12440 [R(int) = 0.0950]
Reflections observed (>2σ)	9490
Data Completeness	0.997
Absorption correction	PSI-Scans
Max. and min. transmission	0.91 and 0.81
Refinement method	Full-matrix least-squares on F^2
Data / restraints / parameters	12440 / 8 / 652
Goodness-of-fit on F^2	1.041
Final R indices [I>2σ(I)]	R^1 = 0.0335 wR_2 = 0.0846
R indices (all data)	R^1 = 0.0531 wR_2 = 0.0945
Largest diff. peak and hole	0.631 and -0.633 $eÅ^{-3}$

Ru(1)-C(1)	1.799(2)	Ru(1)-C(2)	2.0958(18)
Ru(1)-C(29)	2.1071(19)	Ru(1)-O(2)	2.1805(15)
F(1)-B(1)	1.405(3)	F(2)-B(1)	1.371(4)
F(3)-B(1)	1.399(4)	F(4)-B(1)	1.366(4)
O(1)-C(1)	1.154(3)	O(2)-H(2B)	0.897(5)
O(2)-H(2A)	0.898(5)	N(1)-C(2)	1.368(2)
N(1)-C(3)	1.388(2)	N(1)-C(5)	1.455(2)
N(2)-C(2)	1.368(2)	N(2)-C(4)	1.384(2)
N(2)-C(17)	1.450(2)	N(3)-C(29)	1.373(2)
N(3)-C(30)	1.388(3)	N(3)-C(32)	1.443(2)
N(4)-C(29)	1.370(2)	N(4)-C(31)	1.386(3)
N(4)-C(44)	1.445(2)	C(3)-C(4)	1.334(3)
C(3)-H(3)	0.9500	C(4)-H(4)	0.9500
C(5)-C(6)	1.393(3)	C(5)-C(10)	1.399(3)
C(6)-C(7)	1.401(3)	C(6)-C(11)	1.511(3)
C(7)-C(8)	1.378(3)	C(7)-H(7)	0.9500
C(8)-C(9)	1.373(3)	C(8)-H(8)	0.9500
C(9)-C(10)	1.396(3)	C(9)-H(9)	0.9500
C(10)-C(14)	1.518(3)	C(11)-C(12A)	1.446(8)
C(11)-C(13)	1.489(5)	C(11)-C(12)	1.597(5)
C(11)-C(13A)	1.637(8)	C(11)-H(11)	1.0000
C(11)-H(11A)	0.90(7)	C(12)-H(12A)	0.9800
C(12)-H(12B)	0.9800	C(12)-H(12C)	0.9800
C(13)-H(13A)	0.9800	C(13)-H(13B)	0.9800
C(13)-H(13C)	0.9800	C(14)-C(16)	1.530(3)
C(14)-C(15)	1.540(4)	C(14)-H(14)	1.0000
C(15)-H(15A)	0.9800	C(15)-H(15B)	0.9800
C(15)-H(15C)	0.9800	C(16)-H(16A)	0.9800
C(16)-H(16B)	0.9800	C(16)-H(16C)	0.9800
C(17)-C(22)	1.397(3)	C(17)-C(18)	1.403(3)
C(18)-C(19)	1.393(3)	C(18)-C(23)	1.523(3)
C(19)-C(20)	1.383(3)	C(19)-H(19)	0.9500
C(20)-C(21)	1.376(4)	C(20)-H(20)	0.9500
C(21)-C(22)	1.395(3)	C(21)-H(21)	0.9500
C(22)-C(26)	1.520(3)	C(23)-C(25)	1.522(3)
C(23)-C(24)	1.524(3)	C(23)-H(23)	1.0000
C(24)-H(24A)	0.9800	C(24)-H(24B)	0.9800
C(24)-H(24C)	0.9800	C(25)-H(25A)	0.9800
C(25)-H(25B)	0.9800	C(25)-H(25C)	0.9800
C(26)-C(27)	1.526(3)	C(26)-C(28)	1.535(3)
C(26)-H(26)	1.0000	C(27)-H(27A)	0.9800
C(27)-H(27B)	0.9800	C(27)-H(27C)	0.9800
C(28)-H(28A)	0.9800	C(28)-H(28B)	0.9800
C(28)-H(28C)	0.9800	C(30)-C(31)	1.337(3)
C(30)-H(30)	0.9500	C(31)-H(31)	0.9500
C(32)-C(33)	1.398(3)	C(32)-C(37)	1.402(3)
C(33)-C(34)	1.395(3)	C(33)-C(38)	1.518(3)
C(34)-C(35)	1.375(3)	C(34)-H(34)	0.9500
C(35)-C(36)	1.382(3)	C(35)-H(35)	0.9500
C(36)-C(37)	1.395(3)	C(36)-H(36)	0.9500
C(37)-C(41)	1.520(3)	C(38)-C(39)	1.524(3)

C(38)-C(40)	1.532(4)	C(38)-H(38)	1.0000
C(39)-H(39A)	0.9800	C(39)-H(39B)	0.9800
C(39)-H(39C)	0.9800	C(40)-H(40A)	0.9800
C(40)-H(40B)	0.9800	C(40)-H(40C)	0.9800
C(41)-C(42)	1.510(4)	C(41)-C(43)	1.516(4)
C(41)-H(41)	1.0000	C(42)-H(42A)	0.9800
C(42)-H(42B)	0.9800	C(42)-H(42C)	0.9800
C(43)-H(43A)	0.9800	C(43)-H(43B)	0.9800
C(43)-H(43C)	0.9800	C(44)-C(48)	1.395(3)
C(44)-C(45)	1.401(3)	C(45)-C(46)	1.392(3)
C(45)-C(49)	1.519(3)	C(46)-C(47)	1.382(4)
C(46)-H(46)	0.9500	C(47)-C(60)	1.376(4)
C(47)-H(47)	0.9500	C(48)-C(60)	1.393(3)
C(48)-C(52)	1.517(3)	C(49)-C(50)	1.533(3)
C(49)-C(51)	1.538(3)	C(49)-H(49)	1.0000
C(50)-H(50A)	0.9800	C(50)-H(50B)	0.9800
C(50)-H(50C)	0.9800	C(51)-H(51A)	0.9800
C(51)-H(51B)	0.9800	C(51)-H(51C)	0.9800
C(52)-C(53)	1.530(4)	C(52)-C(54)	1.543(4)
C(52)-H(52)	1.0000	C(53)-H(53A)	0.9800
C(53)-H(53B)	0.9800	C(53)-H(53C)	0.9800
C(54)-H(54A)	0.9800	C(54)-H(54B)	0.9800
C(54)-H(54C)	0.9800	C(60)-H(60)	0.9500
C(13A)-H(13D)	0.9800	C(13A)-H(13E)	0.9800
C(13A)-H(13F)	0.9800	C(12A)-H(12D)	0.9800
C(12A)-H(12E)	0.9800	C(12A)-H(12F)	0.9800
C(1)-Ru(1)-C(2)	94.59(8)	C(1)-Ru(1)-C(29)	89.44(8)
C(2)-Ru(1)-C(29)	175.04(7)	C(1)-Ru(1)-O(2)	177.07(10)
C(2)-Ru(1)-O(2)	85.60(6)	C(29)-Ru(1)-O(2)	90.52(6)
Ru(1)-O(2)-H(2B)	121(2)	Ru(1)-O(2)-H(2A)	119(3)
H(2B)-O(2)-H(2A)	109(4)	C(2)-N(1)-C(3)	111.85(15)
C(2)-N(1)-C(5)	127.30(15)	C(3)-N(1)-C(5)	120.61(16)
C(2)-N(2)-C(4)	111.55(15)	C(2)-N(2)-C(17)	127.44(15)
C(4)-N(2)-C(17)	119.95(15)	C(29)-N(3)-C(30)	111.77(17)
C(29)-N(3)-C(32)	126.47(16)	C(30)-N(3)-C(32)	121.62(16)
C(29)-N(4)-C(31)	112.13(16)	C(29)-N(4)-C(44)	126.87(16)
C(31)-N(4)-C(44)	120.82(16)	O(1)-C(1)-Ru(1)	178.2(2)
N(2)-C(2)-N(1)	102.80(15)	N(2)-C(2)-Ru(1)	127.10(13)
N(1)-C(2)-Ru(1)	129.86(13)	C(4)-C(3)-N(1)	106.48(17)
C(4)-C(3)-H(3)	126.8	N(1)-C(3)-H(3)	126.8
C(3)-C(4)-N(2)	107.27(16)	C(3)-C(4)-H(4)	126.4
N(2)-C(4)-H(4)	126.4	C(6)-C(5)-C(10)	123.78(18)
C(6)-C(5)-N(1)	118.05(17)	C(10)-C(5)-N(1)	117.91(17)
C(5)-C(6)-C(7)	116.52(19)	C(5)-C(6)-C(11)	122.36(18)
C(7)-C(6)-C(11)	121.10(19)	C(8)-C(7)-C(6)	121.3(2)
C(8)-C(7)-H(7)	119.4	C(6)-C(7)-H(7)	119.4
C(9)-C(8)-C(7)	120.31(19)	C(9)-C(8)-H(8)	119.8
C(7)-C(8)-H(8)	119.8	C(8)-C(9)-C(10)	121.6(2)
C(8)-C(9)-H(9)	119.2	C(10)-C(9)-H(9)	119.2
C(9)-C(10)-C(5)	116.47(19)	C(9)-C(10)-C(14)	120.36(19)

C(5)-C(10)-C(14)	123.05(17)	C(12A)-C(11)-C(13)	76.8(6)
C(12A)-C(11)-C(6)	116.7(5)	C(13)-C(11)-C(6)	115.9(3)
C(12A)-C(11)-C(12)	32.8(5)	C(13)-C(11)-C(12)	108.6(3)
C(6)-C(11)-C(12)	108.2(3)	C(12A)-C(11)-C(13A)	109.0(7)
C(13)-C(11)-C(13A)	32.2(3)	C(6)-C(11)-C(13A)	101.3(3)
C(12)-C(11)-C(13A)	140.0(4)	C(12A)-C(11)-H(11)	127.3
C(13)-C(11)-H(11)	108.0	C(6)-C(11)-H(11)	108.0
C(12)-C(11)-H(11)	108.0	C(13A)-C(11)-H(11)	87.3
C(12A)-C(11)-H(11A)	112(5)	C(13)-C(11)-H(11A)	122(5)
C(6)-C(11)-H(11A)	110(5)	C(12)-C(11)-H(11A)	88(5)
C(13A)-C(11)-H(11A)	107(5)	H(11)-C(11)-H(11A)	21.2
C(11)-C(12)-H(12A)	109.5	C(11)-C(12)-H(12B)	109.5
C(11)-C(12)-H(12C)	109.5	C(11)-C(13)-H(13A)	109.5
C(11)-C(13)-H(13B)	109.5	C(11)-C(13)-H(13C)	109.5
C(10)-C(14)-C(16)	113.4(2)	C(10)-C(14)-C(15)	109.9(2)
C(16)-C(14)-C(15)	109.5(2)	C(10)-C(14)-H(14)	107.9
C(16)-C(14)-H(14)	107.9	C(15)-C(14)-H(14)	107.9
C(14)-C(15)-H(15A)	109.5	C(14)-C(15)-H(15B)	109.5
H(15A)-C(15)-H(15B)	109.5	C(14)-C(15)-H(15C)	109.5
H(15A)-C(15)-H(15C)	109.5	H(15B)-C(15)-H(15C)	109.5
C(14)-C(16)-H(16A)	109.5	C(14)-C(16)-H(16B)	109.5
H(16A)-C(16)-H(16B)	109.5	C(14)-C(16)-H(16C)	109.5
H(16A)-C(16)-H(16C)	109.5	H(16B)-C(16)-H(16C)	109.5
C(22)-C(17)-C(18)	122.78(18)	C(22)-C(17)-N(2)	119.10(18)
C(18)-C(17)-N(2)	117.62(16)	C(19)-C(18)-C(17)	117.28(19)
C(19)-C(18)-C(23)	120.03(19)	C(17)-C(18)-C(23)	122.46(17)
C(20)-C(19)-C(18)	121.2(2)	C(20)-C(19)-H(19)	119.4
C(18)-C(19)-H(19)	119.4	C(21)-C(20)-C(19)	120.0(2)
C(21)-C(20)-H(20)	120.0	C(19)-C(20)-H(20)	120.0
C(20)-C(21)-C(22)	121.6(2)	C(20)-C(21)-H(21)	119.2
C(22)-C(21)-H(21)	119.2	C(21)-C(22)-C(17)	117.1(2)
C(21)-C(22)-C(26)	119.57(19)	C(17)-C(22)-C(26)	123.34(18)
C(25)-C(23)-C(18)	113.63(18)	C(25)-C(23)-C(24)	110.75(18)
C(18)-C(23)-C(24)	109.77(17)	C(25)-C(23)-H(23)	107.5
C(18)-C(23)-H(23)	107.5	C(24)-C(23)-H(23)	107.5
C(23)-C(24)-H(24A)	109.5	C(23)-C(24)-H(24B)	109.5
H(24A)-C(24)-H(24B)	109.5	C(23)-C(24)-H(24C)	109.5
H(24A)-C(24)-H(24C)	109.5	H(24B)-C(24)-H(24C)	109.5
C(23)-C(25)-H(25A)	109.5	C(23)-C(25)-H(25B)	109.5
H(25A)-C(25)-H(25B)	109.5	C(23)-C(25)-H(25C)	109.5
H(25A)-C(25)-H(25C)	109.5	H(25B)-C(25)-H(25C)	109.5
C(22)-C(26)-C(27)	111.3(2)	C(22)-C(26)-C(28)	111.0(2)
C(27)-C(26)-C(28)	110.37(19)	C(22)-C(26)-H(26)	108.0
C(27)-C(26)-H(26)	108.0	C(28)-C(26)-H(26)	108.0
C(26)-C(27)-H(27A)	109.5	C(26)-C(27)-H(27B)	109.5
H(27A)-C(27)-H(27B)	109.5	C(26)-C(27)-H(27C)	109.5
H(27A)-C(27)-H(27C)	109.5	H(27B)-C(27)-H(27C)	109.5
C(26)-C(28)-H(28A)	109.5	C(26)-C(28)-H(28B)	109.5
H(28A)-C(28)-H(28B)	109.5	C(26)-C(28)-H(28C)	109.5
H(28A)-C(28)-H(28C)	109.5	H(28B)-C(28)-H(28C)	109.5
N(4)-C(29)-N(3)	102.47(16)	N(4)-C(29)-Ru(1)	130.10(13)

N(3)-C(29)-Ru(1)	127.37(14)	C(31)-C(30)-N(3)	106.97(18)
C(31)-C(30)-H(30)	126.5	N(3)-C(30)-H(30)	126.5
C(30)-C(31)-N(4)	106.65(18)	C(30)-C(31)-H(31)	126.7
N(4)-C(31)-H(31)	126.7	C(33)-C(32)-C(37)	123.26(18)
C(33)-C(32)-N(3)	118.76(17)	C(37)-C(32)-N(3)	117.85(17)
C(34)-C(33)-C(32)	117.16(18)	C(34)-C(33)-C(38)	120.53(19)
C(32)-C(33)-C(38)	122.30(18)	C(35)-C(34)-C(33)	121.0(2)
C(35)-C(34)-H(34)	119.5	C(33)-C(34)-H(34)	119.5
C(34)-C(35)-C(36)	120.5(2)	C(34)-C(35)-H(35)	119.7
C(36)-C(35)-H(35)	119.7	C(35)-C(36)-C(37)	121.3(2)
C(35)-C(36)-H(36)	119.4	C(37)-C(36)-H(36)	119.4
C(36)-C(37)-C(32)	116.66(19)	C(36)-C(37)-C(41)	121.68(19)
C(32)-C(37)-C(41)	121.65(19)	C(33)-C(38)-C(39)	112.8(2)
C(33)-C(38)-C(40)	109.6(2)	C(39)-C(38)-C(40)	110.0(2)
C(33)-C(38)-H(38)	108.1	C(39)-C(38)-H(38)	108.1
C(40)-C(38)-H(38)	108.1	C(38)-C(39)-H(39A)	109.5
C(38)-C(39)-H(39B)	109.5	H(39A)-C(39)-H(39B)	109.5
C(38)-C(39)-H(39C)	109.5	H(39A)-C(39)-H(39C)	109.5
H(39B)-C(39)-H(39C)	109.5	C(38)-C(40)-H(40A)	109.5
C(38)-C(40)-H(40B)	109.5	H(40A)-C(40)-H(40B)	109.5
C(38)-C(40)-H(40C)	109.5	H(40A)-C(40)-H(40C)	109.5
H(40B)-C(40)-H(40C)	109.5	C(42)-C(41)-C(43)	110.0(2)
C(42)-C(41)-C(37)	112.9(2)	C(43)-C(41)-C(37)	112.2(2)
C(42)-C(41)-H(41)	107.1	C(43)-C(41)-H(41)	107.1
C(37)-C(41)-H(41)	107.1	C(41)-C(42)-H(42A)	109.5
C(41)-C(42)-H(42B)	109.5	H(42A)-C(42)-H(42B)	109.5
C(41)-C(42)-H(42C)	109.5	H(42A)-C(42)-H(42C)	109.5
H(42B)-C(42)-H(42C)	109.5	C(41)-C(43)-H(43A)	109.5
C(41)-C(43)-H(43B)	109.5	H(43A)-C(43)-H(43B)	109.5
C(41)-C(43)-H(43C)	109.5	H(43A)-C(43)-H(43C)	109.5
H(43B)-C(43)-H(43C)	109.5	C(48)-C(44)-C(45)	123.6(2)
C(48)-C(44)-N(4)	118.68(19)	C(45)-C(44)-N(4)	117.45(18)
C(46)-C(45)-C(44)	116.7(2)	C(46)-C(45)-C(49)	120.9(2)
C(44)-C(45)-C(49)	122.35(19)	C(47)-C(46)-C(45)	121.2(2)
C(47)-C(46)-H(46)	119.4	C(45)-C(46)-H(46)	119.4
C(60)-C(47)-C(46)	120.4(2)	C(60)-C(47)-H(47)	119.8
C(46)-C(47)-H(47)	119.8	C(60)-C(48)-C(44)	116.7(2)
C(60)-C(48)-C(52)	120.7(2)	C(44)-C(48)-C(52)	122.5(2)
C(45)-C(49)-C(50)	112.5(2)	C(45)-C(49)-C(51)	111.1(2)
C(50)-C(49)-C(51)	109.5(2)	C(45)-C(49)-H(49)	107.9
C(50)-C(49)-H(49)	107.9	C(51)-C(49)-H(49)	107.9
C(49)-C(50)-H(50A)	109.5	C(49)-C(50)-H(50B)	109.5
H(50A)-C(50)-H(50B)	109.5	C(49)-C(50)-H(50C)	109.5
H(50A)-C(50)-H(50C)	109.5	H(50B)-C(50)-H(50C)	109.5
C(49)-C(51)-H(51A)	109.5	C(49)-C(51)-H(51B)	109.5
H(51A)-C(51)-H(51B)	109.5	C(49)-C(51)-H(51C)	109.5
H(51A)-C(51)-H(51C)	109.5	H(51B)-C(51)-H(51C)	109.5
C(48)-C(52)-C(53)	112.3(2)	C(48)-C(52)-C(54)	110.9(2)
C(53)-C(52)-C(54)	110.9(2)	C(48)-C(52)-H(52)	107.5
C(53)-C(52)-H(52)	107.5	C(54)-C(52)-H(52)	107.5
C(52)-C(53)-H(53A)	109.5	C(52)-C(53)-H(53B)	109.5

H(53A)-C(53)-H(53B)	109.5	C(52)-C(53)-H(53C)	109.5
H(53A)-C(53)-H(53C)	109.5	H(53B)-C(53)-H(53C)	109.5
C(52)-C(54)-H(54A)	109.5	C(52)-C(54)-H(54B)	109.5
H(54A)-C(54)-H(54B)	109.5	C(52)-C(54)-H(54C)	109.5
H(54A)-C(54)-H(54C)	109.5	H(54B)-C(54)-H(54C)	109.5
C(47)-C(60)-C(48)	121.4(2)	C(47)-C(60)-H(60)	119.3
C(48)-C(60)-H(60)	119.3	F(4)-B(1)-F(2)	112.8(3)
F(4)-B(1)-F(3)	108.2(2)	F(2)-B(1)-F(3)	109.4(2)
F(4)-B(1)-F(1)	109.8(2)	F(2)-B(1)-F(1)	109.5(2)
F(3)-B(1)-F(1)	107.0(2)	C(11)-C(13A)-H(13D)	109.5
C(11)-C(13A)-H(13E)	109.5	H(13D)-C(13A)-H(13E)	109.5
C(11)-C(13A)-H(13F)	109.5	H(13D)-C(13A)-H(13F)	109.5
H(13E)-C(13A)-H(13F)	109.5	C(11)-C(12A)-H(12D)	109.5
C(11)-C(12A)-H(12E)	109.5	H(12D)-C(12A)-H(12E)	109.5
C(11)-C(12A)-H(12F)	109.5	H(12D)-C(12A)-H(12F)	109.5
H(12E)-C(12A)-H(12F)	109.5		

Appendix 22 Crystallographic data for $[Ru(IPr)(\eta^6\text{-}C_6H_6)(CO)H]^+BF_4^-$ (6F)

Identification code	bath853
Empirical formula	C34.25 H43.50 B C10.50 F4 N2 O Ru
Formula weight	704.82
Temperature	120(2) K
Wavelength	0.69430 Å
Crystal system	Triclinic
Space group	P -1
Unit cell dimensions	a = 9.704(4)Å α = 91.981(5)°
	b = 18.093(8)Å β = 96.119(5)°
	c = 19.237(8)Å γ = 93.590(5)°
Volume	3349(2) $Å^3$
Z	4
Density (calculated)	1.398 Mg/m^3
Absorption coefficient	0.560 mm^{-1}
F(000)	1458
Crystal size	0.04 x 0.02 x 0.02 mm
Theta range for data collection	3.98 to 24.41°
Index ranges	-11<=h<=11, -21<=k<=21, -22<=l<=22
Reflections collected	24891
Independent reflections	11455 [R(int) = 0.1058]
Data Completeness	0.967
Max. and min. transmission	0.7459 and 0.5826
Refinement method	Full-matrix least-squares on F^2
Data / restraints / parameters	11455 / 37 / 831
Goodness-of-fit on F^2	1.051
Final R indices [I>2σ(I)]	R^1 = 0.0816 wR_2 = 0.1845
R indices (all data)	R^1 = 0.1551 wR_2 = 0.2112
Largest diff. peak and hole	1.536 and -1.097 $eÅ^{-3}$

Ru(1)-C(10)	1.832(11)	C(2)-C(3)	1.363(14)
Ru(1)-C(12)	2.035(9)	C(3)-C(4)	1.391(16)
Ru(1)-C(2)	2.245(9)	C(4)-C(5)	1.372(19)
Ru(1)-C(3)	2.262(9)	C(5)-C(6)	1.384(19)
Ru(1)-C(6)	2.283(10)	C(10)-O(10)	1.158(11)
Ru(1)-C(1)	2.287(11)	C(12)-N(13)	1.359(11)
Ru(1)-C(5)	2.311(11)	C(12)-N(11)	1.375(11)
Ru(1)-C(4)	2.323(11)	C(14)-C(15)	1.336(12)
Ru(2)-C(110)	1.808(15)	C(14)-N(13)	1.373(10)
Ru(2)-C(112)	2.063(10)	C(15)-N(11)	1.373(11)
Ru(2)-C(103)	2.239(10)	C(21)-C(22)	1.399(13)
Ru(2)-C(104)	2.254(10)	C(21)-C(26)	1.407(13)
Ru(2)-C(102)	2.270(10)	C(21)-N(13)	1.459(11)
Ru(2)-C(101)	2.292(11)	C(22)-C(23)	1.395(13)
Ru(2)-C(105)	2.304(11)	C(22)-C(41)	1.503(14)
Ru(2)-C(106)	2.317(10)	C(23)-C(24)	1.382(15)
C(1)-C(6)	1.394(16)	C(24)-C(25)	1.337(15)
C(1)-C(2)	1.408(15)	C(25)-C(26)	1.393(13)
C(71)-C(73)	1.519(14)	C(26)-C(51)	1.498(14)
C(101)-C(102)	1.364(15)	C(31)-C(36)	1.372(13)
C(101)-C(106)	1.404(15)	C(31)-C(32)	1.396(13)
C(102)-C(103)	1.414(14)	C(31)-N(11)	1.445(11)
C(103)-C(104)	1.384(14)	C(32)-C(33)	1.376(14)
C(104)-C(105)	1.404(16)	C(32)-C(61)	1.523(15)
C(105)-C(106)	1.365(16)	C(33)-C(34)	1.366(15)
C(110)-O(110)	1.205(15)	C(34)-C(35)	1.395(15)
C(112)-N(113)	1.350(11)	C(35)-C(36)	1.390(13)
C(112)-N(111)	1.360(11)	C(36)-C(71)	1.521(13)
C(114)-C(115)	1.323(13)	C(41)-C(43)	1.501(14)
C(114)-N(113)	1.392(12)	C(41)-C(42)	1.539(14)
C(115)-N(111)	1.380(12)	C(51)-C(52)	1.514(13)
C(121)-C(126)	1.373(14)	C(51)-C(53)	1.524(14)
C(121)-C(122)	1.390(13)	C(61)-C(63)	1.530(14)
C(121)-N(111)	1.456(12)	C(61)-C(62)	1.535(14)
C(122)-C(123)	1.409(14)	C(71)-C(72)	1.515(13)
C(122)-C(141)	1.506(14)	C(136)-C(171)	1.510(15)
C(123)-C(124)	1.377(14)	C(141)-C(142)	1.523(14)
C(124)-C(125)	1.368(15)	C(141)-C(143)	1.536(14)
C(125)-C(126)	1.393(14)	C(151)-C(153)	1.506(17)
C(126)-C(151)	1.532(14)	C(151)-C(152)	1.548(16)
C(131)-C(132)	1.381(13)	C(161)-C(162)	1.521(15)
C(131)-C(136)	1.390(13)	C(161)-C(163)	1.524(15)
C(131)-N(113)	1.443(12)	C(171)-C(173)	1.515(15)
C(132)-C(133)	1.393(13)	C(171)-C(172)	1.545(16)
C(132)-C(161)	1.519(14)	B(1)-F(2)	1.340(15)
C(133)-C(134)	1.369(14)	B(1)-F(4B)	1.342(15)
C(134)-C(135)	1.376(14)	B(1)-F(1)	1.347(15)
C(135)-C(136)	1.398(14)	B(1)-F(2B)	1.365(15)
B(2)-F(6)	1.367(18)	B(1)-F(3)	1.367(13)
B(2)-F(8)	1.390(17)	B(1)-F(4)	1.372(14)
C(91)-Cl(1)	1.675(10)	B(1)-F(3B)	1.388(13)

C(91)-Cl(2)	1.701(10)	B(2)-F(7)	1.313(16)
Cl(2)-Cl(2)#1	1.328(18)	B(2)-F(5)	1.364(16)
C(10)-Ru(1)-C(12)	85.0(4)	C(103)-Ru(2)-C(101)	64.1(4)
C(10)-Ru(1)-C(2)	117.2(4)	C(104)-Ru(2)-C(101)	75.6(4)
C(12)-Ru(1)-C(2)	154.2(4)	C(102)-Ru(2)-C(101)	34.8(4)
C(10)-Ru(1)-C(3)	97.8(4)	C(110)-Ru(2)-C(105)	104.9(6)
C(12)-Ru(1)-C(3)	162.5(4)	C(112)-Ru(2)-C(105)	120.2(4)
C(2)-Ru(1)-C(3)	35.2(4)	C(103)-Ru(2)-C(105)	64.1(4)
C(10)-Ru(1)-C(6)	163.6(5)	C(104)-Ru(2)-C(105)	35.9(4)
C(12)-Ru(1)-C(6)	98.5(4)	C(102)-Ru(2)-C(105)	75.1(4)
C(2)-Ru(1)-C(6)	64.0(4)	C(101)-Ru(2)-C(105)	63.4(4)
C(3)-Ru(1)-C(6)	74.1(4)	C(110)-Ru(2)-C(106)	135.2(6)
C(10)-Ru(1)-C(1)	152.1(4)	C(112)-Ru(2)-C(106)	100.0(4)
C(12)-Ru(1)-C(1)	119.1(4)	C(103)-Ru(2)-C(106)	74.6(4)
C(2)-Ru(1)-C(1)	36.2(4)	C(104)-Ru(2)-C(106)	63.1(4)
C(3)-Ru(1)-C(1)	63.7(4)	C(102)-Ru(2)-C(106)	62.9(4)
C(6)-Ru(1)-C(1)	35.5(4)	C(101)-Ru(2)-C(106)	35.5(4)
C(10)-Ru(1)-C(5)	128.6(6)	C(105)-Ru(2)-C(106)	34.4(4)
C(12)-Ru(1)-C(5)	102.0(4)	C(6)-C(1)-C(2)	117.7(11)
C(2)-Ru(1)-C(5)	75.0(4)	C(6)-C(1)-Ru(1)	72.1(6)
C(3)-Ru(1)-C(5)	62.8(5)	C(2)-C(1)-Ru(1)	70.3(6)
C(6)-Ru(1)-C(5)	35.1(5)	C(3)-C(2)-C(1)	120.1(10)
C(1)-Ru(1)-C(5)	63.7(5)	C(3)-C(2)-Ru(1)	73.1(5)
C(10)-Ru(1)-C(4)	102.8(5)	C(1)-C(2)-Ru(1)	73.5(6)
C(12)-Ru(1)-C(4)	127.2(4)	C(2)-C(3)-C(4)	121.6(11)
C(2)-Ru(1)-C(4)	63.5(4)	C(2)-C(3)-Ru(1)	71.7(5)
C(3)-Ru(1)-C(4)	35.3(4)	C(4)-C(3)-Ru(1)	74.7(6)
C(6)-Ru(1)-C(4)	62.4(5)	C(5)-C(4)-C(3)	119.2(12)
C(1)-Ru(1)-C(4)	74.7(4)	C(5)-C(4)-Ru(1)	72.3(7)
C(5)-Ru(1)-C(4)	34.5(5)	C(3)-C(4)-Ru(1)	70.0(6)
C(110)-Ru(2)-C(112)	87.0(5)	C(4)-C(5)-C(6)	119.8(11)
C(110)-Ru(2)-C(103)	108.5(5)	C(4)-C(5)-Ru(1)	73.2(7)
C(112)-Ru(2)-C(103)	162.8(4)	C(6)-C(5)-Ru(1)	71.4(6)
C(110)-Ru(2)-C(104)	92.8(5)	C(5)-C(6)-C(1)	121.6(12)
C(112)-Ru(2)-C(104)	154.8(4)	C(5)-C(6)-Ru(1)	73.6(7)
C(103)-Ru(2)-C(104)	35.9(4)	C(1)-C(6)-Ru(1)	72.4(6)
C(110)-Ru(2)-C(102)	142.3(6)	O(10)-C(10)-Ru(1)	179.1(8)
C(112)-Ru(2)-C(102)	126.4(4)	N(13)-C(12)-N(11)	102.3(7)
C(103)-Ru(2)-C(102)	36.5(4)	N(13)-C(12)-Ru(1)	129.0(6)
C(104)-Ru(2)-C(102)	64.8(4)	N(11)-C(12)-Ru(1)	128.3(7)
C(110)-Ru(2)-C(101)	167.8(5)	C(15)-C(14)-N(13)	106.5(8)
C(112)-Ru(2)-C(101)	101.9(4)	C(14)-C(15)-N(11)	107.1(8)
C(36)-C(35)-C(34)	119.0(11)	C(22)-C(21)-C(26)	124.0(9)
C(31)-C(36)-C(35)	117.8(10)	C(22)-C(21)-N(13)	117.9(8)
C(31)-C(36)-C(71)	123.3(8)	C(26)-C(21)-N(13)	117.5(8)
C(35)-C(36)-C(71)	118.8(10)	C(23)-C(22)-C(21)	116.6(9)
C(43)-C(41)-C(22)	110.4(9)	C(23)-C(22)-C(41)	121.0(9)
C(43)-C(41)-C(42)	110.4(9)	C(21)-C(22)-C(41)	122.3(9)
C(22)-C(41)-C(42)	112.5(9)	C(24)-C(23)-C(22)	120.4(10)
C(26)-C(51)-C(52)	112.2(9)	C(25)-C(24)-C(23)	120.9(10)

C(26)-C(51)-C(53)	111.2(8)	C(24)-C(25)-C(26)	123.3(10)
C(52)-C(51)-C(53)	110.0(9)	C(25)-C(26)-C(21)	114.8(9)
C(32)-C(61)-C(63)	112.9(10)	C(25)-C(26)-C(51)	122.0(9)
C(32)-C(61)-C(62)	110.8(9)	C(21)-C(26)-C(51)	123.2(9)
C(63)-C(61)-C(62)	109.1(9)	C(36)-C(31)-C(32)	123.6(9)
C(72)-C(71)-C(73)	111.7(9)	C(36)-C(31)-N(11)	119.5(8)
C(72)-C(71)-C(36)	109.9(8)	C(32)-C(31)-N(11)	116.9(9)
C(73)-C(71)-C(36)	112.7(8)	C(33)-C(32)-C(31)	117.3(10)
C(102)-C(101)-C(106)	119.6(11)	C(33)-C(32)-C(61)	119.9(9)
C(102)-C(101)-Ru(2)	71.7(7)	C(31)-C(32)-C(61)	122.7(9)
C(106)-C(101)-Ru(2)	73.2(6)	C(34)-C(33)-C(32)	120.3(10)
C(101)-C(102)-C(103)	119.8(11)	C(33)-C(34)-C(35)	121.8(10)
C(101)-C(102)-Ru(2)	73.5(6)	C(104)-C(105)-Ru(2)	70.1(6)
C(103)-C(102)-Ru(2)	70.5(6)	C(105)-C(106)-C(101)	121.3(11)
C(104)-C(103)-C(102)	120.1(11)	C(105)-C(106)-Ru(2)	72.3(6)
C(104)-C(103)-Ru(2)	72.7(6)	C(101)-C(106)-Ru(2)	71.3(6)
C(102)-C(103)-Ru(2)	72.9(6)	O(110)-C(110)-Ru(2)	177.8(14)
C(103)-C(104)-C(105)	119.6(11)	N(113)-C(112)-N(111)	104.1(8)
C(103)-C(104)-Ru(2)	71.4(6)	N(113)-C(112)-Ru(2)	127.7(7)
C(105)-C(104)-Ru(2)	74.0(6)	N(111)-C(112)-Ru(2)	127.7(7)
C(106)-C(105)-C(104)	119.5(10)	C(115)-C(114)-N(113)	108.1(9)
C(106)-C(105)-Ru(2)	73.3(6)	C(114)-C(115)-N(111)	106.0(9)
C(134)-C(135)-C(136)	121.1(10)	C(126)-C(121)-C(122)	123.6(9)
C(131)-C(136)-C(135)	116.2(9)	C(126)-C(121)-N(111)	119.0(9)
C(131)-C(136)-C(171)	123.3(9)	C(122)-C(121)-N(111)	117.3(9)
C(135)-C(136)-C(171)	120.4(9)	C(121)-C(122)-C(123)	116.3(9)
C(122)-C(141)-C(142)	114.0(9)	C(121)-C(122)-C(141)	122.8(9)
C(122)-C(141)-C(143)	109.4(9)	C(123)-C(122)-C(141)	120.9(9)
C(142)-C(141)-C(143)	110.3(9)	C(124)-C(123)-C(122)	120.7(10)
C(153)-C(151)-C(126)	111.7(10)	C(125)-C(124)-C(123)	120.8(10)
C(153)-C(151)-C(152)	111.7(11)	C(124)-C(125)-C(126)	120.4(10)
C(126)-C(151)-C(152)	109.6(10)	C(121)-C(126)-C(125)	118.1(10)
C(132)-C(161)-C(162)	109.5(9)	C(121)-C(126)-C(151)	122.9(10)
C(132)-C(161)-C(163)	114.3(9)	C(125)-C(126)-C(151)	119.0(10)
C(162)-C(161)-C(163)	110.0(10)	C(132)-C(131)-C(136)	123.9(9)
C(136)-C(171)-C(173)	113.7(9)	C(132)-C(131)-N(113)	117.5(9)
C(136)-C(171)-C(172)	107.3(10)	C(136)-C(131)-N(113)	118.7(8)
C(173)-C(171)-C(172)	111.6(10)	C(131)-C(132)-C(133)	117.1(9)
F(2)-B(1)-F(4B)	123(2)	C(131)-C(132)-C(161)	123.4(9)
F(2)-B(1)-F(1)	112.0(18)	C(133)-C(132)-C(161)	119.5(9)
F(4B)-B(1)-F(1)	118.6(16)	C(134)-C(133)-C(132)	121.0(10)
F(2)-B(1)-F(2B)	37(2)	C(133)-C(134)-C(135)	120.4(10)
F(4B)-B(1)-F(2B)	107(2)	F(3)-B(1)-F(4)	104.1(15)
F(1)-B(1)-F(2B)	101.6(13)	F(2)-B(1)-F(3B)	64.8(18)
F(2)-B(1)-F(3)	113(2)	F(4B)-B(1)-F(3B)	114.7(17)
F(4B)-B(1)-F(3)	70.6(15)	F(1)-B(1)-F(3B)	111.2(11)
F(1)-B(1)-F(3)	111.0(12)	F(2B)-B(1)-F(3B)	101.5(16)
F(2B)-B(1)-F(3)	144.2(17)	F(3)-B(1)-F(3B)	53.3(11)
F(2)-B(1)-F(4)	105(2)	F(4)-B(1)-F(3B)	137.0(15)
F(4B)-B(1)-F(4)	34.0(13)	F(7)-B(2)-F(5)	115.4(14)
F(1)-B(1)-F(4)	111.3(13)	F(7)-B(2)-F(6)	106.3(13)

F(2B)-B(1)-F(4)	76.3(18)	F(5)-B(2)-F(6)	107.9(11)
C(112)-N(111)-C(115)	111.7(8)	F(7)-B(2)-F(8)	113.0(13)
C(112)-N(111)-C(121)	126.7(8)	F(5)-B(2)-F(8)	114.8(12)
C(115)-N(111)-C(121)	121.0(8)	F(6)-B(2)-F(8)	97.2(13)
C(112)-N(113)-C(114)	110.1(8)	C(15)-N(11)-C(12)	111.5(7)
C(112)-N(113)-C(131)	124.9(7)	C(15)-N(11)-C(31)	122.4(7)
C(114)-N(113)-C(131)	123.9(8)	C(12)-N(11)-C(31)	125.7(7)
Cl(1)-C(91)-Cl(2)	103.6(10)	C(12)-N(13)-C(14)	112.5(7)
Cl(2)#1-Cl(2)-C(91)	167.2(18)	C(12)-N(13)-C(21)	128.1(7)
C(14)-N(13)-C(21)	119.4(7)		

Appendix 23 Crystallographic data for $[Ru_2(IPr)_2(CO)_2(OH_2)_2(\mu\text{-}Cl)_3]^+BF_4^-$

Identification code	h08mkw19
Empirical formula	C63 H90.50 B Cl3 F4 N4 O5.75 Ru2
Formula weight	1391.19
Temperature	150(2) K
Wavelength	0.71073 Å
Crystal system	Triclinic
Space group	P-1
Unit cell dimensions	a = 17.1620(3)Å α = 75.345(1)°
	b = 19.7600(4)Å β = 85.613(1)°
	c = 22.2710(5)Å γ = 84.148(1)°
Volume	7258.7(3) $Å^3$
Z	4
Density (calculated)	1.273 Mg/m^3
Absorption coefficient	0.583 mm^{-1}
F(000)	2890
Crystal size	0.25 x 0.25 x 0.13 mm
Theta range for data collection	3.58 to 24.99°
Index ranges	-20<=h<=20; -23<=k<=23; -26<=l<=26
Reflections collected	112642
Independent reflections	25471 [R(int) = 0.1297]
Reflections observed (>2σ)	14778
Data Completeness	0.996
Max. and min. transmission	0.938 and 0.797
Refinement method	Full-matrix least-squares on F^2
Data / restraints / parameters	25471 / 12 / 1545
Goodness-of-fit on F^2	1.028
Final R indices [I>2σ(I)]	R^1 = 0.0572 wR_2 = 0.1364
R indices (all data)	R^1 = 0.1253 wR_2 = 0.1697
Largest diff. peak and hole	1.159 and -0.697 $eÅ^{-3}$

Ru(1)-C(1)	1.831(7)	Ru(1)-C(3)	2.068(6)
Ru(1)-O(3)	2.151(4)	Ru(1)-Cl(1)	2.3932(15)
Ru(1)-Cl(3)	2.4501(15)	Ru(1)-Cl(2)	2.4922(15)
Ru(2)-C(2)	1.854(7)	Ru(2)-C(30)	2.040(6)

Ru(2)-O(4)	2.120(4)	Ru(2)-Cl(1)	2.4047(15)
Ru(2)-Cl(2)	2.4375(16)	Ru(2)-Cl(3)	2.4936(15)
Ru(3)-C(57)	1.844(7)	Ru(3)-C(59)	2.049(6)
Ru(3)-O(7)	2.130(4)	Ru(3)-Cl(4)	2.4043(15)
Ru(3)-Cl(5)	2.4390(15)	Ru(3)-Cl(6)	2.5018(16)
Ru(4)-C(58)	1.829(7)	Ru(4)-C(86)	2.052(6)
Ru(4)-O(8)	2.151(4)	Ru(4)-Cl(4)	2.3878(15)
Ru(4)-Cl(6)	2.4628(15)	Ru(4)-Cl(5)	2.4855(16)
F(5)-B(1)	1.368(10)	F(6)-B(1)	1.364(9)
F(7)-B(1)	1.349(10)	F(8)-B(1)	1.393(9)
F(9)-B(2)	1.417(10)	F(10)-B(2)	1.349(10)
F(11)-B(2)	1.380(9)	F(12)-B(2)	1.397(9)
O(1)-C(1)	1.144(7)	O(2)-C(2)	1.113(7)
O(3)-H(3A)	0.900(3)	O(3)-H(3B)	0.900(3)
O(4)-H(4A)	0.900(3)	O(4)-H(4B)	0.900(3)
O(5)-C(57)	1.129(7)	O(6)-C(58)	1.146(7)
O(7)-H(7A)	0.900(3)	O(7)-H(7B)	0.900(3)
O(8)-H(8A)	0.900(3)	O(8)-H(8B)	0.900(3)
O(9)-C(4S)	1.437(10)	O(9)-C(1S)	1.452(9)
O(10)-C(8SA)	1.426(19)	O(10)-C(5SA)	1.44(2)
O(10)-C(5S)	1.455(16)	O(10)-C(8S)	1.457(18)
O(11)-C(12S)	1.292(15)	O(11)-C(9S)	1.531(17)
O(12)-C(114)	1.35(5)	N(1)-C(3)	1.363(7)
N(1)-C(5)	1.400(7)	N(1)-C(6)	1.449(8)
N(2)-C(3)	1.369(7)	N(2)-C(4)	1.386(7)
N(2)-C(18)	1.441(7)	N(3)-C(31)	1.384(8)
N(3)-C(30)	1.386(7)	N(3)-C(45)	1.475(9)
N(4)-C(30)	1.373(7)	N(4)-C(32)	1.389(7)
N(4)-C(33)	1.438(8)	N(5)-C(59)	1.377(7)
N(5)-C(61)	1.381(8)	N(5)-C(62)	1.449(8)
N(6)-C(60)	1.371(8)	N(6)-C(59)	1.384(7)
N(6)-C(74)	1.470(7)	N(7)-C(87)	1.371(8)
N(7)-C(86)	1.375(7)	N(7)-C(101)	1.451(7)
N(8)-C(88)	1.383(7)	N(8)-C(86)	1.384(7)
N(8)-C(89)	1.441(7)	C(1S)-C(2S)	1.449(12)
C(1S)-H(11O)	0.9900	C(1S)-H(11P)	0.9900
C(2S)-C(3S)	1.455(14)	C(2S)-H(11Q)	0.9900
C(2S)-H(11R)	0.9900	C(3S)-C(4S)	1.432(14)
C(3S)-H(11S)	0.9900	C(3S)-H(11T)	0.9900
C(4)-C(5)	1.327(9)	C(4)-H(4)	0.9500
C(4S)-H(12A)	0.9900	C(4S)-H(12B)	0.9900
C(5)-H(5)	0.9500	C(5S)-C(6S)	1.51(2)
C(5S)-H(5S1)	0.9900	C(5S)-H(5S2)	0.9900
C(5SA)-C(6SA)	1.51(3)	C(5SA)-H(5S3)	0.9900
C(5SA)-H(5S4)	0.9900	C(6)-C(7)	1.399(9)
C(6)-C(11)	1.404(9)	C(6S)-C(7S)	1.55(2)
C(6S)-H(6S1)	0.9900	C(6S)-H(6S2)	0.9900
C(6SA)-C(7SA)	1.57(3)	C(6SA)-H(6S3)	0.9900
C(6SA)-H(6S4)	0.9900	C(7)-C(8)	1.412(10)
C(7)-C(15)	1.501(10)	C(7S)-C(8S)	1.42(2)
C(7S)-H(7S1)	0.9900	C(7S)-H(7S2)	0.9900

C(7SA)-C(8SA)	1.46(3)	C(7SA)-H(7S3)	0.9900
C(7SA)-H(7S4)	0.9900	C(8)-C(9)	1.356(12)
C(8)-H(8)	0.9500	C(8S)-H(8S1)	0.9900
C(8S)-H(8S2)	0.9900	C(8SA)-H(8S3)	0.9900
C(8SA)-H(8S4)	0.9900	C(9)-C(10)	1.381(12)
C(9)-H(9)	0.9500	C(9S)-C(10S)	1.505(17)
C(9S)-H(9S1)	0.9900	C(9S)-H(9S2)	0.9900
C(10)-C(11)	1.390(10)	C(10)-H(10)	0.9500
C(10S)-C(11S)	1.391(17)	C(10S)-H(10A)	0.9900
C(10S)-H(10B)	0.9900	C(11)-C(12)	1.505(10)
C(11S)-C(12S)	1.494(17)	C(11S)-H(11A)	0.9900
C(11S)-H(11B)	0.9900	C(12)-C(14)	1.534(10)
C(12)-C(13)	1.534(10)	C(12)-H(12)	1.0000
C(12S)-H(12C)	0.9900	C(12S)-H(12D)	0.9900
C(13)-H(13A)	0.9800	C(13)-H(13B)	0.9800
C(13)-H(13C)	0.9800	C(14)-H(14A)	0.9800
C(14)-H(14B)	0.9800	C(14)-H(14C)	0.9800
C(15)-C(16)	1.532(9)	C(15)-C(17)	1.550(9)
C(15)-H(15)	1.0000	C(16)-H(16A)	0.9800
C(16)-H(16B)	0.9800	C(16)-H(16C)	0.9800
C(17)-H(17A)	0.9800	C(17)-H(17B)	0.9800
C(17)-H(17C)	0.9800	C(18)-C(19)	1.398(8)
C(18)-C(23)	1.402(8)	C(19)-C(20)	1.399(9)
C(19)-C(27)	1.499(9)	C(20)-C(21)	1.385(9)
C(20)-H(20)	0.9500	C(21)-C(22)	1.383(9)
C(21)-H(21)	0.9500	C(22)-C(23)	1.380(9)
C(22)-H(22)	0.9500	C(23)-C(24)	1.524(8)
C(24)-C(26)	1.495(9)	C(24)-C(25)	1.517(9)
C(24)-H(24)	1.0000	C(25)-H(25A)	0.9800
C(25)-H(25B)	0.9800	C(25)-H(25C)	0.9800
C(26)-H(26A)	0.9800	C(26)-H(26B)	0.9800
C(26)-H(26C)	0.9800	C(27)-C(29)	1.540(9)
C(27)-C(28)	1.542(9)	C(27)-H(27)	1.0000
C(28)-H(28A)	0.9800	C(28)-H(28B)	0.9800
C(28)-H(28C)	0.9800	C(29)-H(29A)	0.9800
C(29)-H(29B)	0.9800	C(29)-H(29C)	0.9800
C(31)-C(32)	1.325(9)	C(31)-H(31)	0.9500
C(32)-H(32)	0.9500	C(33)-C(38)	1.391(8)
C(33)-C(34)	1.399(9)	C(34)-C(35)	1.388(9)
C(34)-C(42)	1.507(9)	C(35)-C(36)	1.397(9)
C(35)-H(35)	0.9500	C(36)-C(37)	1.361(10)
C(36)-H(36)	0.9500	C(37)-C(38)	1.397(9)
C(37)-H(37)	0.9500	C(38)-C(39)	1.506(9)
C(39)-C(41)	1.526(10)	C(39)-C(40)	1.535(10)
C(39)-H(39)	1.0000	C(40)-H(40A)	0.9800
C(40)-H(40B)	0.9800	C(40)-H(40C)	0.9800
C(41)-H(41A)	0.9800	C(41)-H(41B)	0.9800
C(41)-H(41C)	0.9800	C(42)-C(43)	1.531(9)
C(42)-C(44)	1.536(9)	C(42)-H(42)	1.0000
C(43)-H(43A)	0.9800	C(43)-H(43B)	0.9800
C(43)-H(43C)	0.9800	C(44)-H(44A)	0.9800

C(44)-H(44B)	0.9800	C(44)-H(44C)	0.9800
C(45)-C(50)	1.389(11)	C(45)-C(46)	1.403(11)
C(46)-C(47)	1.387(12)	C(46)-C(54)	1.515(12)
C(47)-C(48)	1.356(14)	C(47)-H(47)	0.9500
C(48)-C(49)	1.353(14)	C(48)-H(48)	0.9500
C(49)-C(50)	1.398(12)	C(49)-H(49)	0.9500
C(50)-C(51)	1.500(12)	C(51)-C(53)	1.527(12)
C(51)-C(52)	1.574(11)	C(51)-H(51)	1.0000
C(52)-H(52A)	0.9800	C(52)-H(52B)	0.9800
C(52)-H(52C)	0.9800	C(53)-H(53A)	0.9800
C(53)-H(53B)	0.9800	C(53)-H(53C)	0.9800
C(54)-C(55)	1.528(10)	C(54)-C(56)	1.542(11)
C(54)-H(54)	1.0000	C(55)-H(55A)	0.9800
C(55)-H(55B)	0.9800	C(55)-H(55C)	0.9800
C(56)-H(56A)	0.9800	C(56)-H(56B)	0.9800
C(56)-H(56C)	0.9800	C(60)-C(61)	1.330(9)
C(60)-H(60)	0.9500	C(61)-H(61)	0.9500
C(62)-C(67)	1.395(10)	C(62)-C(63)	1.401(9)
C(63)-C(64)	1.394(10)	C(63)-C(71)	1.498(10)
C(64)-C(65)	1.405(11)	C(64)-H(64)	0.9500
C(65)-C(66)	1.375(10)	C(65)-H(65)	0.9500
C(66)-C(67)	1.405(9)	C(66)-H(66)	0.9500
C(67)-C(68)	1.527(9)	C(68)-C(69)	1.508(10)
C(68)-C(70)	1.523(10)	C(68)-H(68)	1.0000
C(69)-H(69A)	0.9800	C(69)-H(69B)	0.9800
C(69)-H(69C)	0.9800	C(70)-H(70A)	0.9800
C(70)-H(70B)	0.9800	C(70)-H(70C)	0.9800
C(71)-C(73)	1.511(10)	C(71)-C(72)	1.545(10)
C(71)-H(71)	1.0000	C(72)-H(72A)	0.9800
C(72)-H(72B)	0.9800	C(72)-H(72C)	0.9800
C(73)-H(73A)	0.9800	C(73)-H(73B)	0.9800
C(73)-H(73C)	0.9800	C(74)-C(79)	1.364(8)
C(74)-C(75)	1.406(8)	C(75)-C(76)	1.377(9)
C(75)-C(83)	1.513(9)	C(76)-C(77)	1.386(10)
C(76)-H(76)	0.9500	C(77)-C(78)	1.371(10)
C(77)-H(77)	0.9500	C(78)-C(79)	1.398(9)
C(78)-H(78)	0.9500	C(79)-C(80)	1.520(9)
C(80)-C(81)	1.542(10)	C(80)-C(82)	1.555(10)
C(80)-H(80)	1.0000	C(81)-H(81A)	0.9800
C(81)-H(81B)	0.9800	C(81)-H(81C)	0.9800
C(82)-H(82A)	0.9800	C(82)-H(82B)	0.9800
C(82)-H(82C)	0.9800	C(83)-C(84)	1.527(9)
C(83)-C(85)	1.552(10)	C(83)-H(83)	1.0000
C(84)-H(84A)	0.9800	C(84)-H(84B)	0.9800
C(84)-H(84C)	0.9800	C(85)-H(85A)	0.9800
C(85)-H(85B)	0.9800	C(85)-H(85C)	0.9800
C(87)-C(88)	1.324(8)	C(87)-H(87)	0.9500
C(88)-H(88)	0.9500	C(89)-C(94)	1.395(9)
C(89)-C(90)	1.411(9)	C(90)-C(91)	1.403(9)
C(90)-C(98)	1.509(10)	C(91)-C(92)	1.380(10)
C(91)-H(91)	0.9500	C(92)-C(93)	1.360(10)

C(92)-H(92)	0.9500	C(93)-C(94)	1.396(8)
C(93)-H(93)	0.9500	C(94)-C(95)	1.516(9)
C(95)-C(96)	1.524(9)	C(95)-C(97)	1.540(8)
C(95)-H(95)	1.0000	C(96)-H(96A)	0.9800
C(96)-H(96B)	0.9800	C(96)-H(96C)	0.9800
C(97)-H(97A)	0.9800	C(97)-H(97B)	0.9800
C(97)-H(97C)	0.9800	C(98)-C(100)	1.530(10)
C(98)-C(99)	1.534(10)	C(98)-H(98)	1.0000
C(99)-H(99A)	0.9800	C(99)-H(99B)	0.9800
C(99)-H(99C)	0.9800	C(100)-H(1)	0.9800
C(100)-H(2)	0.9800	C(100)-H(10C)	0.9800
C(101)-C(102)	1.388(9)	C(101)-C(106)	1.404(9)
C(102)-C(103)	1.379(9)	C(102)-C(110)	1.514(9)
C(103)-C(104)	1.378(10)	C(103)-H(103)	0.9500
C(104)-C(105)	1.376(11)	C(104)-H(104)	0.9500
C(105)-C(106)	1.405(10)	C(105)-H(105)	0.9500
C(106)-C(107)	1.515(10)	C(107)-C(108)	1.539(11)
C(107)-C(109)	1.547(10)	C(107)-H(107)	1.0000
C(108)-H(10D)	0.9800	C(108)-H(10E)	0.9800
C(108)-H(10F)	0.9800	C(109)-H(10G)	0.9800
C(109)-H(10H)	0.9800	C(109)-H(10I)	0.9800
C(110)-C(112)	1.521(9)	C(110)-C(111)	1.539(10)
C(110)-H(110)	1.0000	C(111)-H(6)	0.9800
C(111)-H(11)	0.9800	C(111)-H(11C)	0.9800
C(112)-H(11D)	0.9800	C(112)-H(11E)	0.9800
C(112)-H(11F)	0.9800	C(113)-C(114)	1.46(4)
C(116)-C(117)	1.37(4)		
C(1)-Ru(1)-C(3)	89.2(2)	C(1)-Ru(1)-O(3)	91.9(2)
C(3)-Ru(1)-O(3)	96.10(19)	C(1)-Ru(1)-Cl(1)	96.7(2)
C(3)-Ru(1)-Cl(1)	100.18(17)	O(3)-Ru(1)-Cl(1)	161.67(11)
C(1)-Ru(1)-Cl(3)	177.66(18)	C(3)-Ru(1)-Cl(3)	93.08(16)
O(3)-Ru(1)-Cl(3)	88.58(12)	Cl(1)-Ru(1)-Cl(3)	82.23(5)
C(1)-Ru(1)-Cl(2)	93.64(18)	C(3)-Ru(1)-Cl(2)	177.03(16)
O(3)-Ru(1)-Cl(2)	82.82(11)	Cl(1)-Ru(1)-Cl(2)	80.50(5)
Cl(3)-Ru(1)-Cl(2)	84.13(5)	C(2)-Ru(2)-C(30)	89.9(3)
C(2)-Ru(2)-O(4)	92.5(2)	C(30)-Ru(2)-O(4)	94.4(2)
C(2)-Ru(2)-Cl(1)	97.6(2)	C(30)-Ru(2)-Cl(1)	100.81(17)
O(4)-Ru(2)-Cl(1)	161.76(12)	C(2)-Ru(2)-Cl(2)	178.2(2)
C(30)-Ru(2)-Cl(2)	91.77(18)	O(4)-Ru(2)-Cl(2)	88.14(13)
Cl(1)-Ru(2)-Cl(2)	81.39(5)	C(2)-Ru(2)-Cl(3)	94.0(2)
C(30)-Ru(2)-Cl(3)	175.40(18)	O(4)-Ru(2)-Cl(3)	83.05(12)
Cl(1)-Ru(2)-Cl(3)	81.10(5)	Cl(2)-Ru(2)-Cl(3)	84.36(5)
C(57)-Ru(3)-C(59)	88.4(2)	C(57)-Ru(3)-O(7)	91.3(2)
C(59)-Ru(3)-O(7)	93.6(2)	C(57)-Ru(3)-Cl(4)	98.47(19)
C(59)-Ru(3)-Cl(4)	99.79(17)	O(7)-Ru(3)-Cl(4)	163.56(12)
C(57)-Ru(3)-Cl(5)	176.85(19)	C(59)-Ru(3)-Cl(5)	94.64(16)
O(7)-Ru(3)-Cl(5)	87.56(12)	Cl(4)-Ru(3)-Cl(5)	81.95(5)
C(57)-Ru(3)-Cl(6)	93.39(19)	C(59)-Ru(3)-Cl(6)	178.06(16)
O(7)-Ru(3)-Cl(6)	85.52(12)	Cl(4)-Ru(3)-Cl(6)	80.78(5)
Cl(5)-Ru(3)-Cl(6)	83.59(5)	C(58)-Ru(4)-C(86)	88.3(2)

C(58)-Ru(4)-O(8)	92.5(2)	C(86)-Ru(4)-O(8)	96.47(19)
C(58)-Ru(4)-Cl(4)	96.70(19)	C(86)-Ru(4)-Cl(4)	99.28(16)
O(8)-Ru(4)-Cl(4)	161.97(12)	C(58)-Ru(4)-Cl(6)	176.1(2)
C(86)-Ru(4)-Cl(6)	95.54(16)	O(8)-Ru(4)-Cl(6)	87.89(12)
Cl(4)-Ru(4)-Cl(6)	81.91(5)	C(58)-Ru(4)-Cl(5)	92.77(19)
C(86)-Ru(4)-Cl(5)	178.75(17)	O(8)-Ru(4)-Cl(5)	82.79(12)
Cl(4)-Ru(4)-Cl(5)	81.31(5)	Cl(6)-Ru(4)-Cl(5)	83.45(5)
Ru(1)-Cl(1)-Ru(2)	83.01(5)	Ru(2)-Cl(2)-Ru(1)	80.32(5)
Ru(1)-Cl(3)-Ru(2)	80.05(4)	Ru(4)-Cl(4)-Ru(3)	83.36(5)
Ru(3)-Cl(5)-Ru(4)	80.64(5)	Ru(4)-Cl(6)-Ru(3)	79.86(5)
Ru(1)-O(3)-H(3A)	106(4)	Ru(1)-O(3)-H(3B)	105(4)
H(3A)-O(3)-H(3B)	112(2)	Ru(2)-O(4)-H(4A)	112(4)
Ru(2)-O(4)-H(4B)	115(4)	H(4A)-O(4)-H(4B)	111(2)
Ru(3)-O(7)-H(7A)	101(4)	Ru(3)-O(7)-H(7B)	107(4)
H(7A)-O(7)-H(7B)	112(2)	Ru(4)-O(8)-H(8A)	104(4)
Ru(4)-O(8)-H(8B)	102(4)	H(8A)-O(8)-H(8B)	111(2)
C(4S)-O(9)-C(1S)	109.2(7)	C(8SA)-O(10)-C(5SA)	107.9(12)
C(8SA)-O(10)-C(5S)	119.3(10)	C(5SA)-O(10)-C(5S)	43.9(10)
C(8SA)-O(10)-C(8S)	40.3(9)	C(5SA)-O(10)-C(8S)	73.2(12)
C(5S)-O(10)-C(8S)	105.0(10)	C(12S)-O(11)-C(9S)	102.7(10)
C(3)-N(1)-C(5)	111.6(5)	C(3)-N(1)-C(6)	130.7(5)
C(5)-N(1)-C(6)	117.7(5)	C(3)-N(2)-C(4)	111.1(5)
C(3)-N(2)-C(18)	129.6(5)	C(4)-N(2)-C(18)	118.9(5)
C(31)-N(3)-C(30)	112.5(5)	C(31)-N(3)-C(45)	118.9(5)
C(30)-N(3)-C(45)	128.6(5)	C(30)-N(4)-C(32)	111.7(5)
C(30)-N(4)-C(33)	129.3(5)	C(32)-N(4)-C(33)	119.0(5)
C(59)-N(5)-C(61)	111.8(5)	C(59)-N(5)-C(62)	129.8(5)
C(61)-N(5)-C(62)	118.0(5)	C(60)-N(6)-C(59)	111.7(5)
C(60)-N(6)-C(74)	116.2(5)	C(59)-N(6)-C(74)	131.9(5)
C(87)-N(7)-C(86)	112.1(5)	C(87)-N(7)-C(101)	117.6(5)
C(86)-N(7)-C(101)	129.9(5)	C(88)-N(8)-C(86)	111.9(5)
C(88)-N(8)-C(89)	118.6(5)	C(86)-N(8)-C(89)	129.3(5)
O(1)-C(1)-Ru(1)	178.0(6)	C(2S)-C(1S)-O(9)	105.7(7)
C(2S)-C(1S)-H(11O)	110.6	O(9)-C(1S)-H(11O)	110.6
C(2S)-C(1S)-H(11P)	110.6	O(9)-C(1S)-H(11P)	110.6
H(11O)-C(1S)-H(11P)	108.7	O(2)-C(2)-Ru(2)	177.8(6)
C(1S)-C(2S)-C(3S)	104.4(8)	C(1S)-C(2S)-H(11Q)	110.9
C(3S)-C(2S)-H(11Q)	110.9	C(1S)-C(2S)-H(11R)	110.9
C(3S)-C(2S)-H(11R)	110.9	H(11Q)-C(2S)-H(11R)	108.9
N(1)-C(3)-N(2)	103.2(5)	N(1)-C(3)-Ru(1)	127.5(4)
N(2)-C(3)-Ru(1)	129.1(4)	C(4S)-C(3S)-C(2S)	109.3(9)
C(4S)-C(3S)-H(11S)	109.8	C(2S)-C(3S)-H(11S)	109.8
C(4S)-C(3S)-H(11T)	109.8	C(2S)-C(3S)-H(11T)	109.8
H(11S)-C(3S)-H(11T)	108.3	C(5)-C(4)-N(2)	107.8(5)
C(5)-C(4)-H(4)	126.1	N(2)-C(4)-H(4)	126.1
C(3S)-C(4S)-O(9)	105.4(9)	C(3S)-C(4S)-H(12A)	110.7
O(9)-C(4S)-H(12A)	110.7	C(3S)-C(4S)-H(12B)	110.7
O(9)-C(4S)-H(12B)	110.7	H(12A)-C(4S)-H(12B)	108.8
C(4)-C(5)-N(1)	106.2(5)	C(4)-C(5)-H(5)	126.9
N(1)-C(5)-H(5)	126.9	O(10)-C(5S)-C(6S)	106.9(12)
O(10)-C(5S)-H(5S1)	110.4	C(6S)-C(5S)-H(5S1)	110.4

O(10)-C(5S)-H(5S2)	110.4	C(6S)-C(5S)-H(5S2)	110.4
H(5S1)-C(5S)-H(5S2)	108.6	O(10)-C(5SA)-C(6SA)	105.6(18)
O(10)-C(5SA)-H(5S3)	110.6	C(6SA)-C(5SA)-H(5S3)	110.6
O(10)-C(5SA)-H(5S4)	110.6	C(6SA)-C(5SA)-H(5S4)	110.6
H(5S3)-C(5SA)-H(5S4)	108.7	C(7)-C(6)-C(11)	124.2(6)
C(7)-C(6)-N(1)	118.1(6)	C(11)-C(6)-N(1)	117.4(6)
C(5S)-C(6S)-C(7S)	103.5(13)	C(5S)-C(6S)-H(6S1)	111.1
C(7S)-C(6S)-H(6S1)	111.1	C(5S)-C(6S)-H(6S2)	111.1
C(7S)-C(6S)-H(6S2)	111.1	H(6S1)-C(6S)-H(6S2)	109.0
C(5SA)-C(6SA)-C(7SA)	103.6(19)	C(5SA)-C(6SA)-H(6S3)	111.0
C(7SA)-C(6SA)-H(6S3)	111.0	C(5SA)-C(6SA)-H(6S4)	111.0
C(7SA)-C(6SA)-H(6S4)	111.0	H(6S3)-C(6SA)-H(6S4)	109.0
C(6)-C(7)-C(8)	115.4(7)	C(6)-C(7)-C(15)	123.0(6)
C(8)-C(7)-C(15)	121.6(7)	C(8S)-C(7S)-C(6S)	106.1(14)
C(8S)-C(7S)-H(7S1)	110.5	C(6S)-C(7S)-H(7S1)	110.5
C(8S)-C(7S)-H(7S2)	110.5	C(6S)-C(7S)-H(7S2)	110.5
H(7S1)-C(7S)-H(7S2)	108.7	C(8SA)-C(7SA)-C(6SA)	105.9(18)
C(8SA)-C(7SA)-H(7S3)	110.6	C(6SA)-C(7SA)-H(7S3)	110.6
C(8SA)-C(7SA)-H(7S4)	110.6	C(6SA)-C(7SA)-H(7S4)	110.6
H(7S3)-C(7SA)-H(7S4)	108.7	C(9)-C(8)-C(7)	121.8(8)
C(9)-C(8)-H(8)	119.1	C(7)-C(8)-H(8)	119.1
C(7S)-C(8S)-O(10)	111.0(14)	C(7S)-C(8S)-H(8S1)	109.4
O(10)-C(8S)-H(8S1)	109.4	C(7S)-C(8S)-H(8S2)	109.4
O(10)-C(8S)-H(8S2)	109.4	H(8S1)-C(8S)-H(8S2)	108.0
O(10)-C(8SA)-C(7SA)	106.7(16)	O(10)-C(8SA)-H(8S3)	110.4
C(7SA)-C(8SA)-H(8S3)	110.4	O(10)-C(8SA)-H(8S4)	110.4
C(7SA)-C(8SA)-H(8S4)	110.4	H(8S3)-C(8SA)-H(8S4)	108.6
C(8)-C(9)-C(10)	121.2(7)	C(8)-C(9)-H(9)	119.4
C(10)-C(9)-H(9)	119.4	C(10S)-C(9S)-O(11)	96.3(11)
C(10S)-C(9S)-H(9S1)	112.5	O(11)-C(9S)-H(9S1)	112.5
C(10S)-C(9S)-H(9S2)	112.5	O(11)-C(9S)-H(9S2)	112.5
H(9S1)-C(9S)-H(9S2)	110.0	C(9)-C(10)-C(11)	120.9(8)
C(9)-C(10)-H(10)	119.6	C(11)-C(10)-H(10)	119.6
C(11S)-C(10S)-C(9S)	99.9(12)	C(11S)-C(10S)-H(10A)	111.8
C(9S)-C(10S)-H(10A)	111.8	C(11S)-C(10S)-H(10B)	111.8
C(9S)-C(10S)-H(10B)	111.8	H(10A)-C(10S)-H(10B)	109.5
C(10)-C(11)-C(6)	116.6(7)	C(10)-C(11)-C(12)	120.7(8)
C(6)-C(11)-C(12)	122.7(6)	C(10S)-C(11S)-C(12S)	107.4(13)
C(10S)-C(11S)-H(11A)	110.2	C(12S)-C(11S)-H(11A)	110.2
C(10S)-C(11S)-H(11B)	110.2	C(12S)-C(11S)-H(11B)	110.2
H(11A)-C(11S)-H(11B)	108.5	C(11)-C(12)-C(14)	110.0(7)
C(11)-C(12)-C(13)	111.6(6)	C(14)-C(12)-C(13)	110.3(7)
C(11)-C(12)-H(12)	108.2	C(14)-C(12)-H(12)	108.2
C(13)-C(12)-H(12)	108.2	O(11)-C(12S)-C(11S)	105.6(12)
O(11)-C(12S)-H(12C)	110.6	C(11S)-C(12S)-H(12C)	110.6
O(11)-C(12S)-H(12D)	110.6	C(11S)-C(12S)-H(12D)	110.6
H(12C)-C(12S)-H(12D)	108.8	C(12)-C(13)-H(13A)	109.5
C(12)-C(13)-H(13B)	109.5	H(13A)-C(13)-H(13B)	109.5
C(12)-C(13)-H(13C)	109.5	H(13A)-C(13)-H(13C)	109.5
H(13B)-C(13)-H(13C)	109.5	C(12)-C(14)-H(14A)	109.5
C(12)-C(14)-H(14B)	109.5	H(14A)-C(14)-H(14B)	109.5

C(12)-C(14)-H(14C)	109.5	H(14A)-C(14)-H(14C)	109.5
H(14B)-C(14)-H(14C)	109.5	C(7)-C(15)-C(16)	113.4(6)
C(7)-C(15)-C(17)	109.9(6)	C(16)-C(15)-C(17)	110.2(6)
C(7)-C(15)-H(15)	107.7	C(16)-C(15)-H(15)	107.7
C(17)-C(15)-H(15)	107.7	C(15)-C(16)-H(16A)	109.5
C(15)-C(16)-H(16B)	109.5	H(16A)-C(16)-H(16B)	109.5
C(15)-C(16)-H(16C)	109.5	H(16A)-C(16)-H(16C)	109.5
H(16B)-C(16)-H(16C)	109.5	C(15)-C(17)-H(17A)	109.5
C(15)-C(17)-H(17B)	109.5	H(17A)-C(17)-H(17B)	109.5
C(15)-C(17)-H(17C)	109.5	H(17A)-C(17)-H(17C)	109.5
H(17B)-C(17)-H(17C)	109.5	C(19)-C(18)-C(23)	123.6(6)
C(19)-C(18)-N(2)	118.1(5)	C(23)-C(18)-N(2)	117.8(5)
C(18)-C(19)-C(20)	115.9(6)	C(18)-C(19)-C(27)	122.8(6)
C(20)-C(19)-C(27)	121.3(6)	C(21)-C(20)-C(19)	122.2(6)
C(21)-C(20)-H(20)	118.9	C(19)-C(20)-H(20)	118.9
C(22)-C(21)-C(20)	119.4(6)	C(22)-C(21)-H(21)	120.3
C(20)-C(21)-H(21)	120.3	C(23)-C(22)-C(21)	121.6(6)
C(23)-C(22)-H(22)	119.2	C(21)-C(22)-H(22)	119.2
C(22)-C(23)-C(18)	117.3(6)	C(22)-C(23)-C(24)	121.0(6)
C(18)-C(23)-C(24)	121.7(5)	C(26)-C(24)-C(25)	109.7(6)
C(26)-C(24)-C(23)	114.1(6)	C(25)-C(24)-C(23)	110.8(5)
C(26)-C(24)-H(24)	107.3	C(25)-C(24)-H(24)	107.3
C(23)-C(24)-H(24)	107.3	C(24)-C(25)-H(25A)	109.5
C(24)-C(25)-H(25B)	109.5	H(25A)-C(25)-H(25B)	109.5
C(24)-C(25)-H(25C)	109.5	H(25A)-C(25)-H(25C)	109.5
H(25B)-C(25)-H(25C)	109.5	C(24)-C(26)-H(26A)	109.5
C(24)-C(26)-H(26B)	109.5	H(26A)-C(26)-H(26B)	109.5
C(24)-C(26)-H(26C)	109.5	H(26A)-C(26)-H(26C)	109.5
H(26B)-C(26)-H(26C)	109.5	C(19)-C(27)-C(29)	110.6(6)
C(19)-C(27)-C(28)	112.3(6)	C(29)-C(27)-C(28)	110.5(5)
C(19)-C(27)-H(27)	107.7	C(29)-C(27)-H(27)	107.7
C(28)-C(27)-H(27)	107.7	C(27)-C(28)-H(28A)	109.5
C(27)-C(28)-H(28B)	109.5	H(28A)-C(28)-H(28B)	109.5
C(27)-C(28)-H(28C)	109.5	H(28A)-C(28)-H(28C)	109.5
H(28B)-C(28)-H(28C)	109.5	C(27)-C(29)-H(29A)	109.5
C(27)-C(29)-H(29B)	109.5	H(29A)-C(29)-H(29B)	109.5
C(27)-C(29)-H(29C)	109.5	H(29A)-C(29)-H(29C)	109.5
H(29B)-C(29)-H(29C)	109.5	N(4)-C(30)-N(3)	101.7(5)
N(4)-C(30)-Ru(2)	130.2(4)	N(3)-C(30)-Ru(2)	128.1(4)
C(32)-C(31)-N(3)	106.3(6)	C(32)-C(31)-H(31)	126.8
N(3)-C(31)-H(31)	126.8	C(31)-C(32)-N(4)	107.8(6)
C(31)-C(32)-H(32)	126.1	N(4)-C(32)-H(32)	126.1
C(38)-C(33)-C(34)	123.4(6)	C(38)-C(33)-N(4)	118.0(6)
C(34)-C(33)-N(4)	118.3(6)	C(35)-C(34)-C(33)	117.1(6)
C(35)-C(34)-C(42)	120.1(6)	C(33)-C(34)-C(42)	122.8(6)
C(34)-C(35)-C(36)	120.9(7)	C(34)-C(35)-H(35)	119.5
C(36)-C(35)-H(35)	119.5	C(37)-C(36)-C(35)	119.9(7)
C(37)-C(36)-H(36)	120.0	C(35)-C(36)-H(36)	120.0
C(36)-C(37)-C(38)	122.0(7)	C(36)-C(37)-H(37)	119.0
C(38)-C(37)-H(37)	119.0	C(33)-C(38)-C(37)	116.6(6)
C(33)-C(38)-C(39)	122.7(6)	C(37)-C(38)-C(39)	120.6(6)

C(38)-C(39)-C(41)	111.2(6)	C(38)-C(39)-C(40)	113.0(6)
C(41)-C(39)-C(40)	110.5(6)	C(38)-C(39)-H(39)	107.3
C(41)-C(39)-H(39)	107.3	C(40)-C(39)-H(39)	107.3
C(39)-C(40)-H(40A)	109.5	C(39)-C(40)-H(40B)	109.5
H(40A)-C(40)-H(40B)	109.5	C(39)-C(40)-H(40C)	109.5
H(40A)-C(40)-H(40C)	109.5	H(40B)-C(40)-H(40C)	109.5
C(39)-C(41)-H(41A)	109.5	C(39)-C(41)-H(41B)	109.5
H(41A)-C(41)-H(41B)	109.5	C(39)-C(41)-H(41C)	109.5
H(41A)-C(41)-H(41C)	109.5	H(41B)-C(41)-H(41C)	109.5
C(34)-C(42)-C(43)	111.7(6)	C(34)-C(42)-C(44)	110.1(5)
C(43)-C(42)-C(44)	110.6(6)	C(34)-C(42)-H(42)	108.1
C(43)-C(42)-H(42)	108.1	C(44)-C(42)-H(42)	108.1
C(42)-C(43)-H(43A)	109.5	C(42)-C(43)-H(43B)	109.5
H(43A)-C(43)-H(43B)	109.5	C(42)-C(43)-H(43C)	109.5
H(43A)-C(43)-H(43C)	109.5	H(43B)-C(43)-H(43C)	109.5
C(42)-C(44)-H(44A)	109.5	C(42)-C(44)-H(44B)	109.5
H(44A)-C(44)-H(44B)	109.5	C(42)-C(44)-H(44C)	109.5
H(44A)-C(44)-H(44C)	109.5	H(44B)-C(44)-H(44C)	109.5
C(50)-C(45)-C(46)	125.8(8)	C(50)-C(45)-N(3)	117.0(7)
C(46)-C(45)-N(3)	117.0(7)	C(47)-C(46)-C(45)	112.5(9)
C(47)-C(46)-C(54)	124.5(9)	C(45)-C(46)-C(54)	123.0(7)
C(48)-C(47)-C(46)	125.2(10)	C(48)-C(47)-H(47)	117.4
C(46)-C(47)-H(47)	117.4	C(49)-C(48)-C(47)	119.2(10)
C(49)-C(48)-H(48)	120.4	C(47)-C(48)-H(48)	120.4
C(48)-C(49)-C(50)	121.8(10)	C(48)-C(49)-H(49)	119.1
C(50)-C(49)-H(49)	119.1	C(45)-C(50)-C(49)	115.5(9)
C(45)-C(50)-C(51)	122.6(7)	C(49)-C(50)-C(51)	122.0(9)
C(50)-C(51)-C(53)	114.4(8)	C(50)-C(51)-C(52)	110.3(8)
C(53)-C(51)-C(52)	110.1(7)	C(50)-C(51)-H(51)	107.3
C(53)-C(51)-H(51)	107.3	C(52)-C(51)-H(51)	107.3
C(51)-C(52)-H(52A)	109.5	C(51)-C(52)-H(52B)	109.5
H(52A)-C(52)-H(52B)	109.5	C(51)-C(52)-H(52C)	109.5
H(52A)-C(52)-H(52C)	109.5	H(52B)-C(52)-H(52C)	109.5
C(51)-C(53)-H(53A)	109.5	C(51)-C(53)-H(53B)	109.5
H(53A)-C(53)-H(53B)	109.5	C(51)-C(53)-H(53C)	109.5
H(53A)-C(53)-H(53C)	109.5	H(53B)-C(53)-H(53C)	109.5
C(46)-C(54)-C(55)	112.6(7)	C(46)-C(54)-C(56)	112.0(7)
C(55)-C(54)-C(56)	109.4(7)	C(46)-C(54)-H(54)	107.5
C(55)-C(54)-H(54)	107.5	C(56)-C(54)-H(54)	107.5
C(54)-C(55)-H(55A)	109.5	C(54)-C(55)-H(55B)	109.5
H(55A)-C(55)-H(55B)	109.5	C(54)-C(55)-H(55C)	109.5
H(55A)-C(55)-H(55C)	109.5	H(55B)-C(55)-H(55C)	109.5
C(54)-C(56)-H(56A)	109.5	C(54)-C(56)-H(56B)	109.5
H(56A)-C(56)-H(56B)	109.5	C(54)-C(56)-H(56C)	109.5
H(56A)-C(56)-H(56C)	109.5	H(56B)-C(56)-H(56C)	109.5
O(5)-C(57)-Ru(3)	175.4(6)	O(6)-C(58)-Ru(4)	178.5(6)
N(5)-C(59)-N(6)	102.0(5)	N(5)-C(59)-Ru(3)	129.0(4)
N(6)-C(59)-Ru(3)	128.3(4)	C(61)-C(60)-N(6)	107.5(6)
C(61)-C(60)-H(60)	126.2	N(6)-C(60)-H(60)	126.2
C(60)-C(61)-N(5)	107.0(6)	C(60)-C(61)-H(61)	126.5
N(5)-C(61)-H(61)	126.5	C(67)-C(62)-C(63)	123.6(6)

C(67)-C(62)-N(5)	116.7(6)	C(63)-C(62)-N(5)	119.2(6)
C(64)-C(63)-C(62)	117.2(7)	C(64)-C(63)-C(71)	119.4(6)
C(62)-C(63)-C(71)	123.4(6)	C(63)-C(64)-C(65)	120.6(7)
C(63)-C(64)-H(64)	119.7	C(65)-C(64)-H(64)	119.7
C(66)-C(65)-C(64)	120.4(7)	C(66)-C(65)-H(65)	119.8
C(64)-C(65)-H(65)	119.8	C(65)-C(66)-C(67)	121.2(7)
C(65)-C(66)-H(66)	119.4	C(67)-C(66)-H(66)	119.4
C(62)-C(67)-C(66)	117.0(6)	C(62)-C(67)-C(68)	124.3(6)
C(66)-C(67)-C(68)	118.7(7)	C(69)-C(68)-C(70)	111.5(6)
C(69)-C(68)-C(67)	112.8(6)	C(70)-C(68)-C(67)	110.6(6)
C(69)-C(68)-H(68)	107.2	C(70)-C(68)-H(68)	107.2
C(67)-C(68)-H(68)	107.2	C(68)-C(69)-H(69A)	109.5
C(68)-C(69)-H(69B)	109.5	H(69A)-C(69)-H(69B)	109.5
C(68)-C(69)-H(69C)	109.5	H(69A)-C(69)-H(69C)	109.5
H(69B)-C(69)-H(69C)	109.5	C(68)-C(70)-H(70A)	109.5
C(68)-C(70)-H(70B)	109.5	H(70A)-C(70)-H(70B)	109.5
C(68)-C(70)-H(70C)	109.5	H(70A)-C(70)-H(70C)	109.5
H(70B)-C(70)-H(70C)	109.5	C(63)-C(71)-C(73)	112.5(6)
C(63)-C(71)-C(72)	110.3(6)	C(73)-C(71)-C(72)	109.3(6)
C(63)-C(71)-H(71)	108.2	C(73)-C(71)-H(71)	108.2
C(72)-C(71)-H(71)	108.2	C(71)-C(72)-H(72A)	109.5
C(71)-C(72)-H(72B)	109.5	H(72A)-C(72)-H(72B)	109.5
C(71)-C(72)-H(72C)	109.5	H(72A)-C(72)-H(72C)	109.5
H(72B)-C(72)-H(72C)	109.5	C(71)-C(73)-H(73A)	109.5
C(71)-C(73)-H(73B)	109.5	H(73A)-C(73)-H(73B)	109.5
C(71)-C(73)-H(73C)	109.5	H(73A)-C(73)-H(73C)	109.5
H(73B)-C(73)-H(73C)	109.5	C(79)-C(74)-C(75)	123.3(6)
C(79)-C(74)-N(6)	118.5(5)	C(75)-C(74)-N(6)	117.4(5)
C(76)-C(75)-C(74)	116.9(6)	C(76)-C(75)-C(83)	119.9(6)
C(74)-C(75)-C(83)	123.2(5)	C(75)-C(76)-C(77)	121.2(6)
C(75)-C(76)-H(76)	119.4	C(77)-C(76)-H(76)	119.4
C(78)-C(77)-C(76)	120.3(6)	C(78)-C(77)-H(77)	119.9
C(76)-C(77)-H(77)	119.9	C(77)-C(78)-C(79)	120.5(7)
C(77)-C(78)-H(78)	119.8	C(79)-C(78)-H(78)	119.8
C(74)-C(79)-C(78)	117.9(6)	C(74)-C(79)-C(80)	123.3(6)
C(78)-C(79)-C(80)	118.9(6)	C(79)-C(80)-C(81)	111.0(6)
C(79)-C(80)-C(82)	111.4(6)	C(81)-C(80)-C(82)	110.9(6)
C(79)-C(80)-H(80)	107.8	C(81)-C(80)-H(80)	107.8
C(82)-C(80)-H(80)	107.8	C(80)-C(81)-H(81A)	109.5
C(80)-C(81)-H(81B)	109.5	H(81A)-C(81)-H(81B)	109.5
C(80)-C(81)-H(81C)	109.5	H(81A)-C(81)-H(81C)	109.5
H(81B)-C(81)-H(81C)	109.5	C(80)-C(82)-H(82A)	109.5
C(80)-C(82)-H(82B)	109.5	H(82A)-C(82)-H(82B)	109.5
C(80)-C(82)-H(82C)	109.5	H(82A)-C(82)-H(82C)	109.5
H(82B)-C(82)-H(82C)	109.5	C(75)-C(83)-C(84)	113.4(6)
C(75)-C(83)-C(85)	110.8(6)	C(84)-C(83)-C(85)	110.1(6)
C(75)-C(83)-H(83)	107.4	C(84)-C(83)-H(83)	107.4
C(85)-C(83)-H(83)	107.4	C(83)-C(84)-H(84A)	109.5
C(83)-C(84)-H(84B)	109.5	H(84A)-C(84)-H(84B)	109.5
C(83)-C(84)-H(84C)	109.5	H(84A)-C(84)-H(84C)	109.5
H(84B)-C(84)-H(84C)	109.5	C(83)-C(85)-H(85A)	109.5

C(83)-C(85)-H(85B)	109.5	H(85A)-C(85)-H(85B)	109.5
C(83)-C(85)-H(85C)	109.5	H(85A)-C(85)-H(85C)	109.5
H(85B)-C(85)-H(85C)	109.5	N(7)-C(86)-N(8)	101.6(5)
N(7)-C(86)-Ru(4)	130.1(4)	N(8)-C(86)-Ru(4)	127.8(4)
C(88)-C(87)-N(7)	107.8(5)	C(88)-C(87)-H(87)	126.1
N(7)-C(87)-H(87)	126.1	C(87)-C(88)-N(8)	106.6(6)
C(87)-C(88)-H(88)	126.7	N(8)-C(88)-H(88)	126.7
C(94)-C(89)-C(90)	123.7(6)	C(94)-C(89)-N(8)	118.4(5)
C(90)-C(89)-N(8)	117.4(6)	C(91)-C(90)-C(89)	115.3(7)
C(91)-C(90)-C(98)	122.1(6)	C(89)-C(90)-C(98)	122.6(6)
C(92)-C(91)-C(90)	121.8(7)	C(92)-C(91)-H(91)	119.1
C(90)-C(91)-H(91)	119.1	C(93)-C(92)-C(91)	121.1(6)
C(93)-C(92)-H(92)	119.5	C(91)-C(92)-H(92)	119.5
C(92)-C(93)-C(94)	120.7(7)	C(92)-C(93)-H(93)	119.6
C(94)-C(93)-H(93)	119.6	C(89)-C(94)-C(93)	117.4(6)
C(89)-C(94)-C(95)	121.8(5)	C(93)-C(94)-C(95)	120.8(6)
C(94)-C(95)-C(96)	109.1(5)	C(94)-C(95)-C(97)	113.4(5)
C(96)-C(95)-C(97)	110.1(5)	C(94)-C(95)-H(95)	108.0
C(96)-C(95)-H(95)	108.0	C(97)-C(95)-H(95)	108.0
C(95)-C(96)-H(96A)	109.5	C(95)-C(96)-H(96B)	109.5
H(96A)-C(96)-H(96B)	109.5	C(95)-C(96)-H(96C)	109.5
H(96A)-C(96)-H(96C)	109.5	H(96B)-C(96)-H(96C)	109.5
C(95)-C(97)-H(97A)	109.5	C(95)-C(97)-H(97B)	109.5
H(97A)-C(97)-H(97B)	109.5	C(95)-C(97)-H(97C)	109.5
H(97A)-C(97)-H(97C)	109.5	H(97B)-C(97)-H(97C)	109.5
C(90)-C(98)-C(100)	111.4(6)	C(90)-C(98)-C(99)	111.8(6)
C(100)-C(98)-C(99)	110.6(6)	C(90)-C(98)-H(98)	107.6
C(100)-C(98)-H(98)	107.6	C(99)-C(98)-H(98)	107.6
C(98)-C(99)-H(99A)	109.5	C(98)-C(99)-H(99B)	109.5
H(99A)-C(99)-H(99B)	109.5	C(98)-C(99)-H(99C)	109.5
H(99A)-C(99)-H(99C)	109.5	H(99B)-C(99)-H(99C)	109.5
C(98)-C(100)-H(1)	109.5	C(98)-C(100)-H(2)	109.5
H(1)-C(100)-H(2)	109.5	C(98)-C(100)-H(10C)	109.5
H(1)-C(100)-H(10C)	109.5	H(2)-C(100)-H(10C)	109.5
C(102)-C(101)-C(106)	123.6(6)	C(102)-C(101)-N(7)	117.8(5)
C(106)-C(101)-N(7)	117.9(6)	C(103)-C(102)-C(101)	117.6(6)
C(103)-C(102)-C(110)	120.7(6)	C(101)-C(102)-C(110)	121.6(5)
C(104)-C(103)-C(102)	120.7(7)	C(104)-C(103)-H(103)	119.7
C(102)-C(103)-H(103)	119.7	C(105)-C(104)-C(103)	121.3(7)
C(105)-C(104)-H(104)	119.3	C(103)-C(104)-H(104)	119.3
C(104)-C(105)-C(106)	120.5(7)	C(104)-C(105)-H(105)	119.8
C(106)-C(105)-H(105)	119.8	C(101)-C(106)-C(105)	116.3(7)
C(101)-C(106)-C(107)	122.3(6)	C(105)-C(106)-C(107)	121.3(7)
C(106)-C(107)-C(108)	111.3(7)	C(106)-C(107)-C(109)	110.8(6)
C(108)-C(107)-C(109)	110.7(7)	C(106)-C(107)-H(107)	108.0
C(108)-C(107)-H(107)	108.0	C(109)-C(107)-H(107)	108.0
C(107)-C(108)-H(10D)	109.5	C(107)-C(108)-H(10E)	109.5
H(10D)-C(108)-H(10E)	109.5	C(107)-C(108)-H(10F)	109.5
H(10D)-C(108)-H(10F)	109.5	H(10E)-C(108)-H(10F)	109.5
C(107)-C(109)-H(10G)	109.5	C(107)-C(109)-H(10H)	109.5
H(10G)-C(109)-H(10H)	109.5	C(107)-C(109)-H(10I)	109.5

H(10G)-C(109)-H(10I)	109.5	H(10H)-C(109)-H(10I)	109.5
C(102)-C(110)-C(112)	112.5(6)	C(102)-C(110)-C(111)	111.5(6)
C(112)-C(110)-C(111)	110.0(6)	C(102)-C(110)-H(110)	107.6
C(112)-C(110)-H(110)	107.6	C(111)-C(110)-H(110)	107.6
C(110)-C(111)-H(6)	109.5	C(110)-C(111)-H(11)	109.5
H(6)-C(111)-H(11)	109.5	C(110)-C(111)-H(11C)	109.5
H(6)-C(111)-H(11C)	109.5	H(11)-C(111)-H(11C)	109.5
C(110)-C(112)-H(11D)	109.5	C(110)-C(112)-H(11E)	109.5
H(11D)-C(112)-H(11E)	109.5	C(110)-C(112)-H(11F)	109.5
H(11D)-C(112)-H(11F)	109.5	H(11E)-C(112)-H(11F)	109.5
O(12)-C(114)-C(113)	94(4)	F(7)-B(1)-F(6)	111.0(7)
F(7)-B(1)-F(5)	111.9(7)	F(6)-B(1)-F(5)	108.6(7)
F(7)-B(1)-F(8)	107.0(7)	F(6)-B(1)-F(8)	109.2(7)
F(5)-B(1)-F(8)	109.2(6)	F(10)-B(2)-F(11)	111.7(7)
F(10)-B(2)-F(12)	111.2(7)	F(11)-B(2)-F(12)	110.3(6)
F(10)-B(2)-F(9)	110.7(6)	F(11)-B(2)-F(9)	108.8(7)
F(12)-B(2)-F(9)	103.9(7)		